NASA CR-120882
AiResearch 71-7487

ANALYTICAL INVESTIGATION OF CHORD SIZE AND COOLING METHODS ON TURBINE BLADE COOLING REQUIREMENTS

BOOK 1. SECTIONS 1 THROUGH 8 AND APPENDIXES A THROUGH I

by

F. E. Faulkner

AIRESEARCH MANUFACTURING COMPANY

prepared for

NATIONAL AERONAUTICS AND SPACE ADMINISTRATION

Requests for copies of this report should be referred to

National Aeronautics and Space Administration
Scientific and Technical Information Facility
P. O. Box 33
College Park, Md. 20740

S-65034

1. Report No. NASA CR-120882	2. Government Accession No.	3. Recipient's Catalog No.
4. Title and Subtitle ANALYTICAL INVESTIGATION OF CHORD SIZE AND COOLING METHODS ON TURBINE BLADE COOLING REQUIREMENTS		5. Report Date August 1971
		6. Performing Organization Code
7. Author(s) F. E. Faulkner		8. Performing Organization Report No. AiResearch 71-7487
		10. Work Unit No.
9. Performing Organization Name and Address AiResearch Manufacturing Company Torrance, California 90509		
		11. Contract or Grant No. NAS 3-13205
		13. Type of Report and Period Covered Contractor Report
12. Sponsoring Agency Name and Address National Aeronautics and Space Administration Washington, D.C. 20546		
		14. Sponsoring Agency Code

15. Supplementary Notes

Program Manager, John E. Rohde, Air Breathing Engine Division, NASA Lewis Research Center, Cleveland, Ohio 44135

16. Abstract

This study was conducted to determine the effect of chord size on air cooled turbine blades. In the preliminary design phase, eight turbine blade cooling configurations in 0.75-in. (0.01905-m), 1.0-in. (0.0254-m), and 1.5-in. (0.0381-m) chord sizes were analyzed to determine the maximum turbine inlet temperature capabilities. A pin fin convection cooled configuration and a film-impingement cooled configuration were selected for a final design analysis in which the maximum turbine inlet temperature was determined as a function of the cooling air inlet temperature and the turbine inlet total pressure for each of the three chord sizes. The cooling air flow requirements were also determined for a varying cooling air inlet temperature with a constant turbine inlet temperature.

The conclusions of this study were that allowable turbine inlet temperature increases with increasing chord for the convection cooled and transpiration cooled designs, however, the film-convection cooled designs did not have a significant change in turbine inlet temperature with chord. The film-convection cooled designs allow turbine inlet temperatures about $200^\circ F$ ($111^\circ K$) higher than the convection cooled designs but the transpiration cooled design studied offered an advantage only for the 1.5-in. (0.0381-m) chord size. The turbine inlet pressure range studied had little effect on turbine inlet temperature capability, but a reduction in cooling air inlet temperature produced an increase in turbine inlet temperature capability or a reduction in cooling air flow required.

17. Key Words (Suggested by Author(s)) Turbine blade cooling Chord size Pin fin Film-convection	18. Distribution Statement Unclassified - Unlimited		
19. Security Classif. (of this report) Unclassified	20. Security Classif. (of this page) Unclassified	21. No. of Pages	22. Price*

FOREWORD

This report is published in two books: Book 1 includes Sections 1 through 8 and Appendixes A through I; Book 2 includes Appendixes J through M.

CONTENTS

BOOK I

CONTENTS (Continued)

CONTENTS (Continued)

SECTION I

SUMMARY

The objective of this study was to determine the effects of chord size on the turbine inlet temperature capabilities of several air-cooled turbine blade design concepts. In addition, the effects of varying turbine inlet total pressure and cooling air inlet total temperature on turbine inlet temperature capability and cooling air flow requirements were determined. Eight air-cooled turbine blade designs in 0.75-in. (0.01905m), 1.0-in. (0.0254 m), and 1.5-in. (0.0381 m) chord sizes with convection cooled, film-convection cooled, and transpiration cooled design concepts were investigated. This preliminary study was conducted to determine the turbine inlet temperature capability of each design in the three chord sizes for a constant turbine inlet total pressure and cooling air inlet total temperature. A pin fin convection cooled configuration and a film-impingement cooled configuration were selected for a final design analysis. The selected designs were modified as required, based on the results of the preliminary design analysis. Cooling passage dimensions, flow control orifices, impingement cooling holes, and film cooling holes were adjusted to optimize each configuration at the design point condition. A study was then conducted to determine the allowable turbine inlet temperature as a function of cooling air inlet temperature and turbine inlet total pressure for each final design in each chord size. An estimated life of 1000 hr for each final design was obtained based on a detailed creep relaxation analysis for the stress critical conditions or based on a maximum metal temperature of 1840°F (1277.8°K) for a coating life limit. Cooling passage dimensions, flow control orifice size, impingement hole size, and film cooling hole sizes were not varied in this study. A study was also performed to determine the minimum cooling flow required as a function of cooling air inlet temperature with a constant turbine inlet temperature for each final design in each chord size. Only the flow control orifices were varied in this analysis. An additional analysis was conducted on the effects of varying cooling passage size in each of the previous studies for the 1.0-in. (0.0254 m) chord final designs. A study of the effect of reducing cooling air supply pressure was conducted for each design point condition.

Results of the preliminary analysis indicate that allowable turbine inlet temperature increases with increasing chord for the convection and transpiration cooled designs. Film-convection cooled designs did not have a significant trend of chord size with turbine inlet temperature. Analysis indicates that film-convection cooled designs allow turbine inlet temperatures about 200°F (111°K) higher than the convection cooled designs and that transpiration cooling offers an advantage only for larger chord size blades.

Final design analysis indicates that a variation in cooling air inlet temperature produces a greater change in turbine inlet temperature capability for the film-convection cooled design than for the convection cooled design. Analysis also indicates that turbine inlet total pressure has relatively little effect on turbine inlet temperature capability over the range of turbine inlet total pressures studied. With a constant turbine inlet temperature, a decrease in cooling air inlet temperature or an increase in chord size produced a

1

reduction in cooling air flow required for the convection cooled blade. The trend of cooling air flow reduction with an increase in chord was not apparent in the film-convection cooled design. A detailed description of these trends and other effects in chord size, turbine inlet pressure, and cooling air inlet temperature are brought out in this study.

SECTION 2

INTRODUCTION

The purpose of this investigation was to determine the effects of chord size, cooling configuration, cooling air inlet temperature, and turbine inlet total pressure on the turbine inlet temperature and cooling air flow requirements of cooled turbine blades. The study was conducted in two phases, the Task I preliminary design analysis, and the Task I final design analysis. The Task I preliminary design analysis includes a study of the turbine inlet temperature capabilities of eight cooling configurations in three chord sizes. Convection, film-convection, and transpiration cooled turbine blade configurations were considered in the preliminary design phase. A convection and a film-convection cooled turbine blade configuration were selected from the preliminary designs studied for the Task I final design analysis. These two designs were analyzed to determine the turbine inlet temperature capabilities at three turbine inlet total pressures and three cooling air inlet temperatures for each of the three chord sizes. In addition, the cooling air flow required with a constant turbine inlet total temperature and pressure was determined at three cooling air inlet temperatures for each of the three chord sizes. Additional studies were made on the effects of reducing cooling air inlet pressure and varying flow control orifice sizes for selected conditions.

In the design of gas turbine engines, turbojet engines, and fanjet engines, higher turbine inlet temperatures provide lower engine weight per unit-horsepower or pound of thrust; greater thrust or horsepower output per pound of airflow; and, in the case of high-bypass-ratio fanjet engines, lower specific fuel consumption. Some indications of the effects of increasing turbine inlet temperature on engine thrust with and without the penalties associated with turbine cooling are discussed in Hare and Malley (Reference 1). This reference indicates that an 18 percent increase in thrust may be achieved with $350^\circ F$ $(194.4^\circ K)$ of blade cooling using two percent of the hot gas flow as cooling flow for the blades. In addition, some indications of the tradeoff factors for a high-bypass-ratio turbofan are given in Burggraf and Houchens (Reference 2).

The influence of turbine inlet temperature on a small gas turbine engine is presented in Moskowitz and Schober (Reference 3). This reference indicates that hp/lb of airflow increases substantially, and specific fuel consumption decreases somewhat, with an increase in turbine inlet temperature. Results of an optimization study of small, cooled gas turbines are reported in Helmbrecht, Kirby, and Weber (Reference 4).

The history and trend in turbine inlet temperature capability is summarized in Figure 2-1 from information given in References 1, 2, and 5. This figure shows the history and expected future for turbine blade cooling and design concepts considered applicable for each range of turbine inlet temperatures.

Cooled turbine blade design began during World War II with the first turbine engines developed in Germany. Turbine cooling studies began at NACA in 1946 and air cooled turbine blades were placed in service around 1959. The first cooled turbine blade designs consisted of three-pass, two-pass, and

3
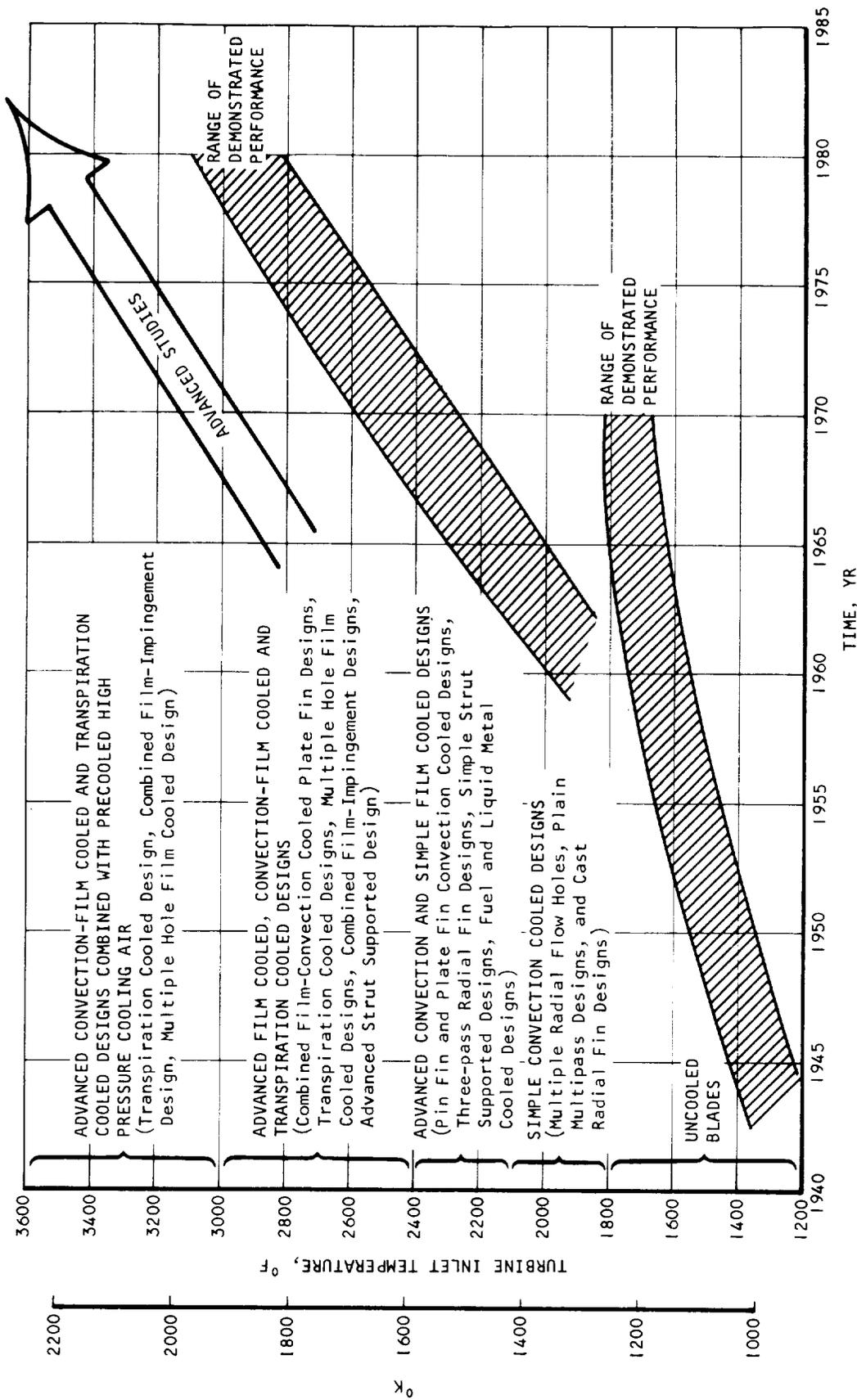
Figure 2-1. Turbine Inlet Temperature Development and Applicable Design Concepts

single-pass blades with plain passages as shown in Reference 1. Simple cast radial fin designs as shown in Helms and Emmerson (Reference 6) were placed in service between 1963 and 1965. Early cast radial fin and simple pin fin designs developed in this same period are shown in Martens and Raabe (Reference 7). Advanced cooled blade designs were studied by General Electric under contract with NASA Lewis and the results are reported in References 8 through 12. Other turbine cooling studies have also been conducted under contract with Wright Patterson and are reported in Anderson, Davis, McLeod, and Nealy (Reference 13).

Short chord cooled turbine blade designs with less than 1.5-in. (0.0381 m) chord are reported in Reference 3 and in Gabel (Reference 14). These references indicate turbine inlet temperature capabilities of $2500^\circ F$ ($1644^\circ K$) for transpiration cooled blades and $2300^\circ F$ ($1533^\circ K$) for liquid cooled blades with heat removed by fuel. Studies conducted at AiResearch Phoenix reported in Reference 4 indicate turbine inlet temperature capabilities of $2400^\circ F$ ($1588^\circ K$) for convection cooled strut supported, and three pass cast radial fin blades of less than 1.5-in. (0.0381 m) chord.

This present study provides information to assess the turbine cooling penalties associated with a variation in cooling design configuration, chord size, turbine inlet pressure, and cooling air inlet temperature. The results of this study may be used to determine the reduction of cooling air flow required for turbine cooling as the cooling air inlet temperature is reduced or the turbine blade chord is increased. The increase in turbine inlet temperature capability with a decrease in cooling air inlet temperature can also be determined. While these results are for a specific design with specific boundary conditions, the trends presented in this study are expected to apply in general.

This study of the effect of chord size on turbine cooling was based on the following assumptions:

- A given external aerodynamic shape with trailing edge modifications allowed

- Constant solidity and corrected velocity triangle

- Turbine blade chords of 0.75-in. (0.01905 m), 1.0 in. (0.0254m) and 1.5 in. (0.0381 m).

- A constant blade span of 1.75 in. (0.04445 m).

- A life of 1000 hr for the IN-100 blade material based on steady-state operating conditions

The metal temperature distribution in each spanwise section was calculated using a three-dimensional thermal analyzer computer program. This calculation considered both spanwise and chordwise conduction and conduction through the blade wall with variable thermal conductivity as a function of temperature. Convection heat transfer was considered on the external surface

with both convection and radiation heat transfer considered in the internal passage. The cooling air temperature rise considered both the effects of heat addition and rotational acceleration.

Stress calculations for the preliminary design phase considered a stress distribution based on centrifugal stresses, thermal stresses, and bending stresses due to thermal distortion. The stress analysis was conducted using an elastic, inelastic, and creep analysis computer program. Using this program the temperature, stress, and stress-to-rupture life of each element at several spanwise sections of each cooled blade design was calculated for the initial conditions before creep relaxation was applied. The minimum life of a tensile stressed element from this analysis was used to determine the life of each preliminary design configuration.

Stress calculations for the final design phase considered the time to one percent creep strain for the critical elements. The analysis accounted for stress redistribution due to creep during the life of the blade.

The specific requirement for SI units on all the figures and tables was waived for this report by the NASA contracting officer. Provisions of NPD2220.4 have been waived under the authority of Paragraph 5.d.

SECTION 3

ANALYTICAL METHODS

Air cooled turbine blades considered in this study were convection cooled, film-convection cooled, and transpiration cooled. The convection cooling techniques considered were flow in (1) a plain passage, (2) a pin fin passage, (3) an offset plate fin passage, (4) a transverse fin passage, and (5) a sharp bend. Other special convection cooling methods considered were leading edge impingement and impingement from an array of holes with crossflow. Film cooling techniques considered were leading edge film cooling from an array of holes, film cooling on each side through a row of holes at an angle to the surface, and tangential injection film cooling at the trailing edge. The transpiration cooling technique utilized a simulated transpiration cooling material.

Aerodynamic, heat transfer, and stress analysis techniques used for these cooling methods are described below.

AERODYNAMIC ANALYSIS

For heat transfer calculations on a turbine blade, the relative total temperatures, the relative total pressure, the freestream critical velocity ratio relative to the leading edge, and the surface critical velocity ratio profile must be determined to provide information for calculating outside heat transfer coefficients and adiabatic wall temperatures. Turbine inlet total temperature and total pressure are used along with turbine velocity diagrams to determine relative total temperature and relative total pressure at each radial section of the blade. These diagrams are presented in the form of critical velocity ratios where the critical velocity is defined in Equation (3-1).

$$V_{CR} = \sqrt{\frac{2\gamma g_c \, RT_T}{\gamma + 1}} \qquad (3-1)$$

From the definition for total temperature given in Equation (3-2), the static to total temperature ratio Equation (3-3) and the static to total pressure ratio Equation (3-4) may be defined based on critical velocity ratios.

$$T_T = T + \frac{\gamma - 1}{\gamma} \, \frac{V^2}{2g_c \, R} \qquad (3-2)$$

$$\frac{T}{T_T} = 1 - \frac{\gamma - 1}{\gamma + 1} \left(\frac{V}{V_{CR}}\right)^2 \qquad (3-3)$$

$$\frac{P}{P_T} = \left[1 - \frac{\gamma - 1}{\gamma + 1} \left(\frac{V}{V_{CR}}\right)^2\right]^{\frac{\gamma}{\gamma - 1}} \qquad (3-4)$$

7

From the inlet velocity triangles, the relative total to absolute total temperature ratio may be calculated from the absolute critical velocity ratio (V/V_{CR}), and the relative critical velocity ratio (W/W_{CR}), at the blade inlet as shown in Equation (3-5).

$$\left(\frac{T_T'}{T_T}\right) = \frac{1 - \frac{\gamma - 1}{\gamma + 1}\left(\frac{V}{V_{CR}}\right)^2}{1 - \frac{\gamma - 1}{\gamma + 1}\left(\frac{W}{W_{CR}}\right)^2} \tag{3-5}$$

where T_T' = relative total temperature

T_T = absolute total temperature

The relative to absolute total pressure ratio at the blade inlet may be calculated as shown in Equation (3-6).

$$\left(\frac{P_T'}{P_T}\right) = \left[\frac{1 - \frac{\gamma - 1}{\gamma + 1}\left(\frac{V}{V_{CR}}\right)^2}{1 - \frac{\gamma - 1}{\gamma + 1}\left(\frac{W}{W_{CR}}\right)^2}\right]^{\frac{\gamma}{\gamma - 1}} \tag{3-6}$$

The turbine airfoil surface critical velocity ratio profile is calculated using the three dimensional blade surface velocity calculation program (TR-1G) described in Appendix A. Input to this program consists of the relative total temperature, relative total pressure, velocity relative to the blade row, and gas flow through the blade stage. The geometry input consists of the number of blades, the mid-channel stream line angle measured from the axial plane, the surface curvatures, and the distance along a potential line in the circumferential direction. The turbine geometry is calculated by a computer program using blade surface coordinate points input as a table.

The calculation method used by the three dimensional blade surface velocity calculation program (TR-1G) is essentially the same as that given in Katsanis and Dellner (Reference 16). The calculations satisfy radial equilibrium and continuity. Channel flow theory is used to determine the velocity distribution across the channel for the continuity calculation. The program iterates on an estimated hub mid-channel velocity until continuity is satisfied.

8

The efficiency of an air cooled turbine rotor is affected by the following factors:

- Power lost by diverting mass flow for the blade cooling

- Power lost in compressing the cooling air in the rotor stage

- Efficiency loss due to a decreased blade aspect ratio for a long chord blade

- Effects of profile shape, such as thicker leading and trailing edges, which may be required for a cooled turbine

- Effects of cooling air discharge at the blade tip on turbine tip clearance losses

- Efficiency loss due to mixing by coolant injection from various areas on the blade

- Efficiency loss due to transpiration cooling of the blades.

Power lost by diverting mass flow for blade cooling may be determined in an engine cycle performance computer program by subtracting total mass flow required for turbine cooling from the compressor discharge flow. Cooling air flow for each stage may be added to the gas flow to determine gas flow into the subsequent stage. Hot gas temperature for each stage may be determined from a simple enthalpy balance between the hot gas and the cooling air discharge from a prior stage. The cooling air discharge temperature is determined from the blade thermal effectiveness. Horsepower is lost because the cooling air is compressed as it passes radially through the blade. The pumping horsepower may be calculated as shown in Equation (3-7) below for a rotational speed (N) in rpm and a cooling air discharge flow rate $(W_{c,o})$ in lb/sec. The radius (r_i) is the distance in inches from the center of rotation to the point of cooling air inlet to the turbine disc and (r_e) is the radius in inches to the point of cooling air discharge from the blade.

$$HP_c = 2.1518 \times 10^{-9} W_{c,o} \left[(N) \ r_e \right]^2 \left[1. - (r_i/r_e)^2 \right] \qquad (3-7)$$

This equation assumes that the coolant enters the blade stage with no tangential velocity. With a preswirl device a portion of this loss may be recovered.

The effects of turbine blade aspect ratio on turbine efficiency are shown in Figure 3-1. The turbine efficiency ratio for 0.75-in. (0.0195 m), 1.0 in. (0.0254 m), and 1.5 in. (0.0381 m) chord blades in this study are also shown in Figure 3-1. The turbine efficiency correction factor from Figure 3-1 is expressed as a ratio of the turbine efficiency (η) for a turbine blade aspect ratio less than 3.0 to the turbine efficiency (η_o) for a turbine blade aspect ratio of 3.0.

Turbine efficiency is not significantly affected by increases in leading edge diameter up to relatively thick leading edges for the subsonic reaction type turbines considered here. No increases in leading edge diameter were required in this study. Increases in trailing edge thickness produce a

9
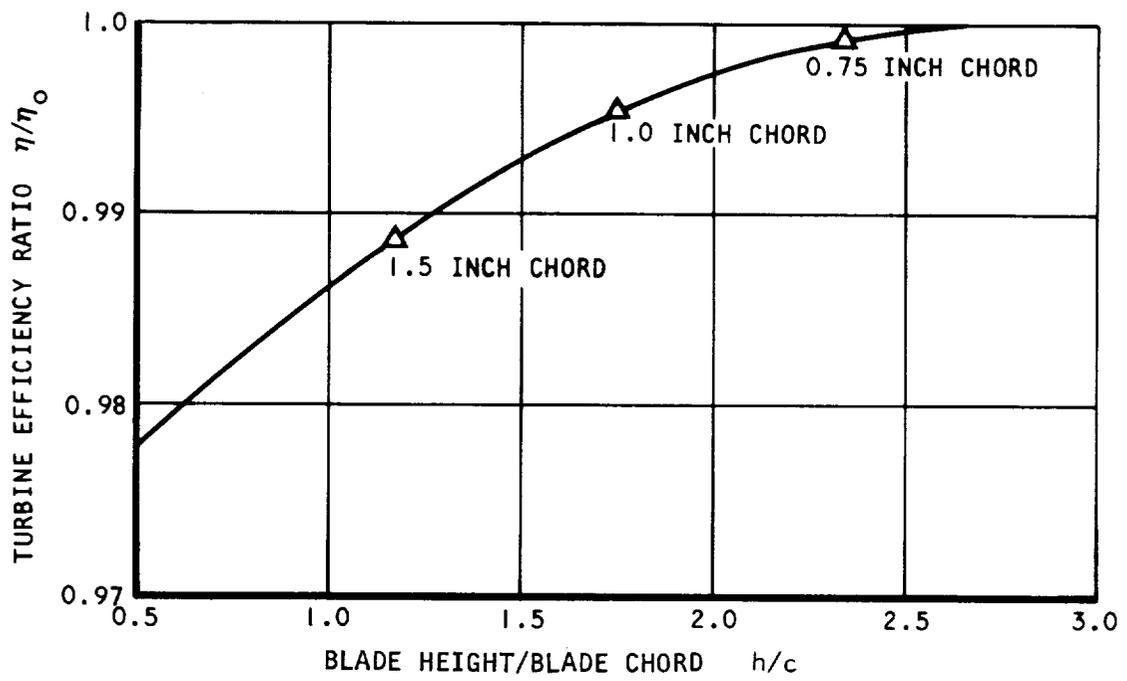
Figure 3-1. Aspect Ratio vs Turbine Efficiency Ratio

10

relatively large loss in efficiency for stator vanes and a somewhat smaller loss for rotor blades. The effects of increases in trailing edge thickness are discussed in Barnes and Came (Reference 17). The turbine stage discussed in Reference 17 has a blade height of 1.75 in. (0.04445 m), a vane chord of 1.3 in. (0.03302 m), a blade chord of 1.0 in. (0.0254 m) and a tip diameter of 13 in. (0.3302 m). Since the size is similar to that in this study, the effects of increasing the trailing edge thickness should apply. The effect of trailing edge thickness on turbine efficiency from Reference 17 is shown in Figure 3-2. The design point turbine blade thickness for the study conducted herein is also shown in Figure 3-2.

Effects of cooling air discharge at the tip of the blade are also discussed in Reference 17. The study was conducted for unshrouded blades with a normal clearance. The results are shown in Figure 3-3 as the effective blade tip clearance as a function of the hot gas incidence angle at the leading edge with and without cooling air ejected from the tip. This figure indicates that the apparent reduction in tip clearance is greatest at negative incidences and relatively poor at positive incidences, when the cooling air would tend to be swept away more easily in a direction perpendicular to the chord line. This effect cannot be fully evaluated for the present study because a tip clearance was not established for the study.

Effects of coolant injection into the gas stream from various areas of the blade and turbine efficiency loss due to transpiration cooling of the blades are discussed in Moffitt, Nosek, and Roelke (Reference 18) and Sucin (Reference 19). Loss in turbine efficiency for coolant injection is a function of location and direction of coolant injection and energy level of coolant flow. Loss in performance is based on calculated momentum exchange between the injected fluid and the main gas stream. Loss in performance may be calculated using the effective kinetic energy and momentum outputs of the coolant and hot gas flows to determine the mixed flow output. High main stream velocities on the suction side of the blade produce a larger difference between the kinetic energy of the injected coolant and the main stream. In addition, the injected coolant must be compressed in passing from a suction side injection point to the blade row exit point. The large velocity difference between the injected coolant and the main stream flow on the suction side may also lead to separation. Other areas, such as the leading edge, require coolant injection in a direction opposite to the direction of hot gas flow and therefore produce large losses. Coolant injection on the pressure side produces lower losses, because the main stream velocity is lower and static pressure may be recovered as the injected coolant flows toward the blade row exit point. Trailing edge injection may actually increase performance by contributing kinetic energy and reducing the momentum deficit region or wake. Effects of coolant injection from each of these areas is shown in Figure 3-4 taken from Reference 19. These data agree with the experimental results shown in Reference 18 for trailing edge injection. A recent analytical study of coolant injection effects is presented in Prust (Reference 72).

Effects of transpiration cooling on turbine efficiency are shown in Figure 3-5, taken from information in Reference 18. These data are based on a transpiration cooled stator with the main gas and coolant at the same temperature and may not be representative of a transpiration cooled rotor blade.
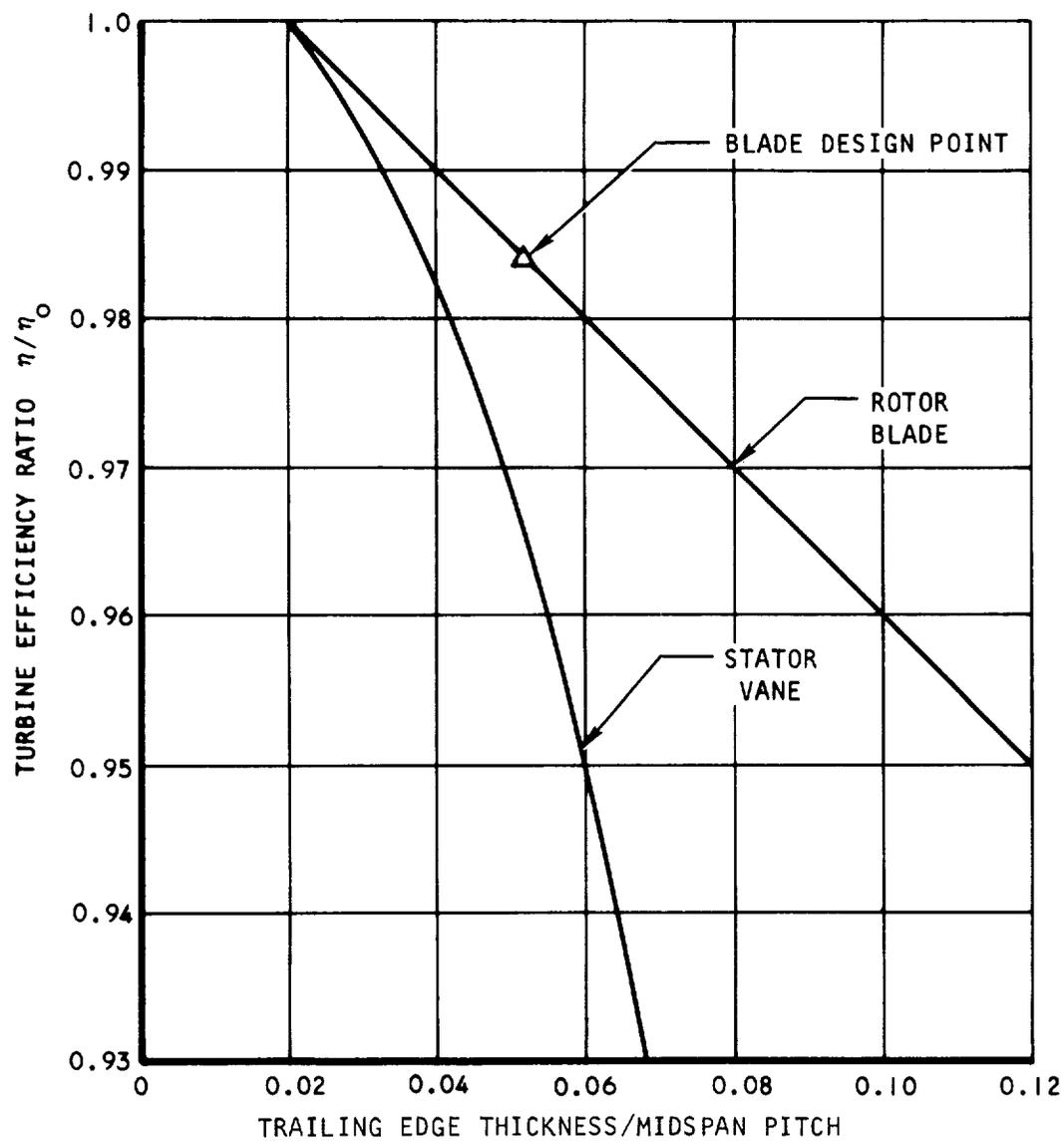
Figure 3-2. Effect of Trailing Edge Thickness on Turbine Efficiency
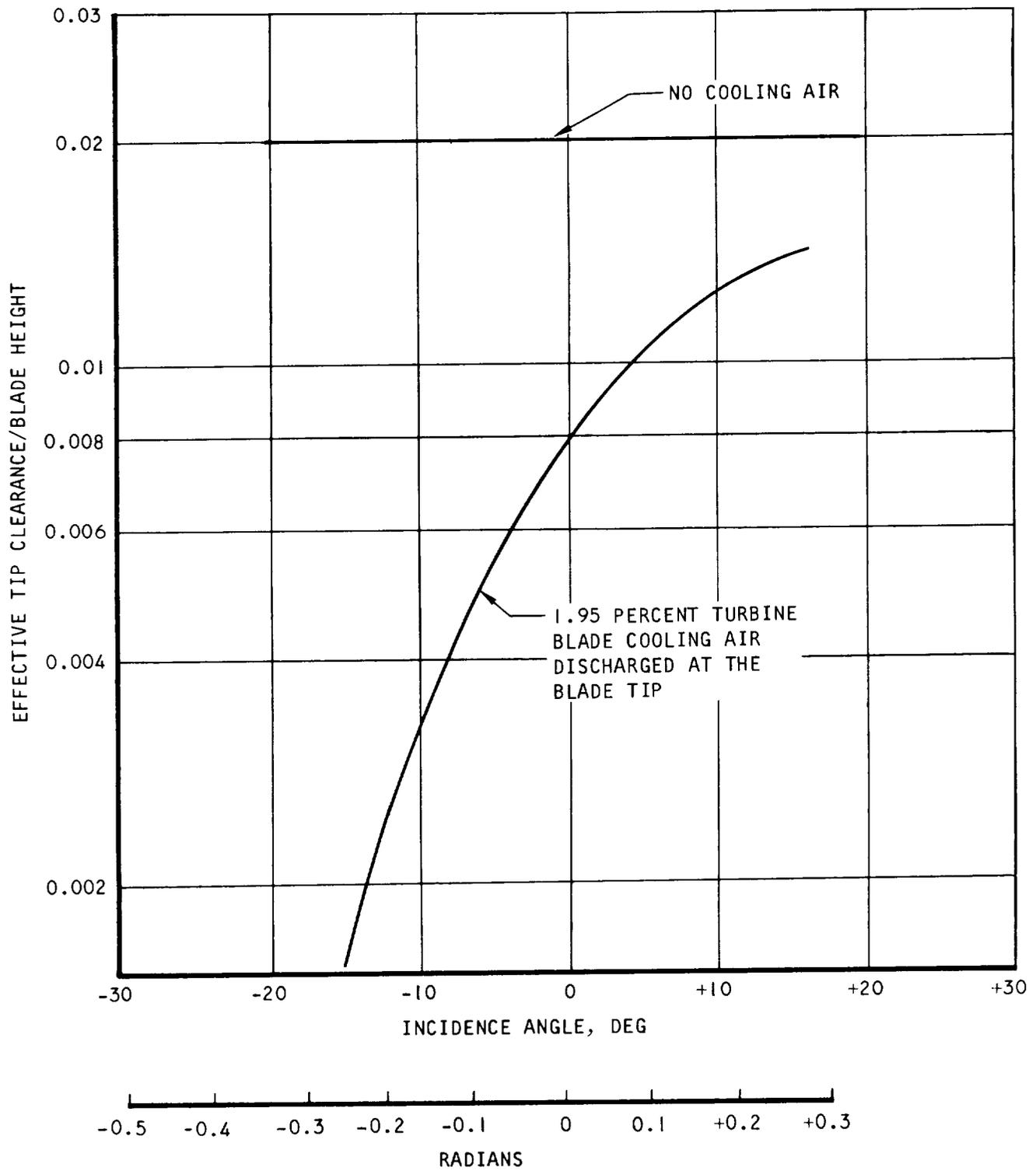
Figure 3-3. Effective Blade Tip Clearance as a Function of Incidence Angle for Cooling Air Discharged at the Blade Tip
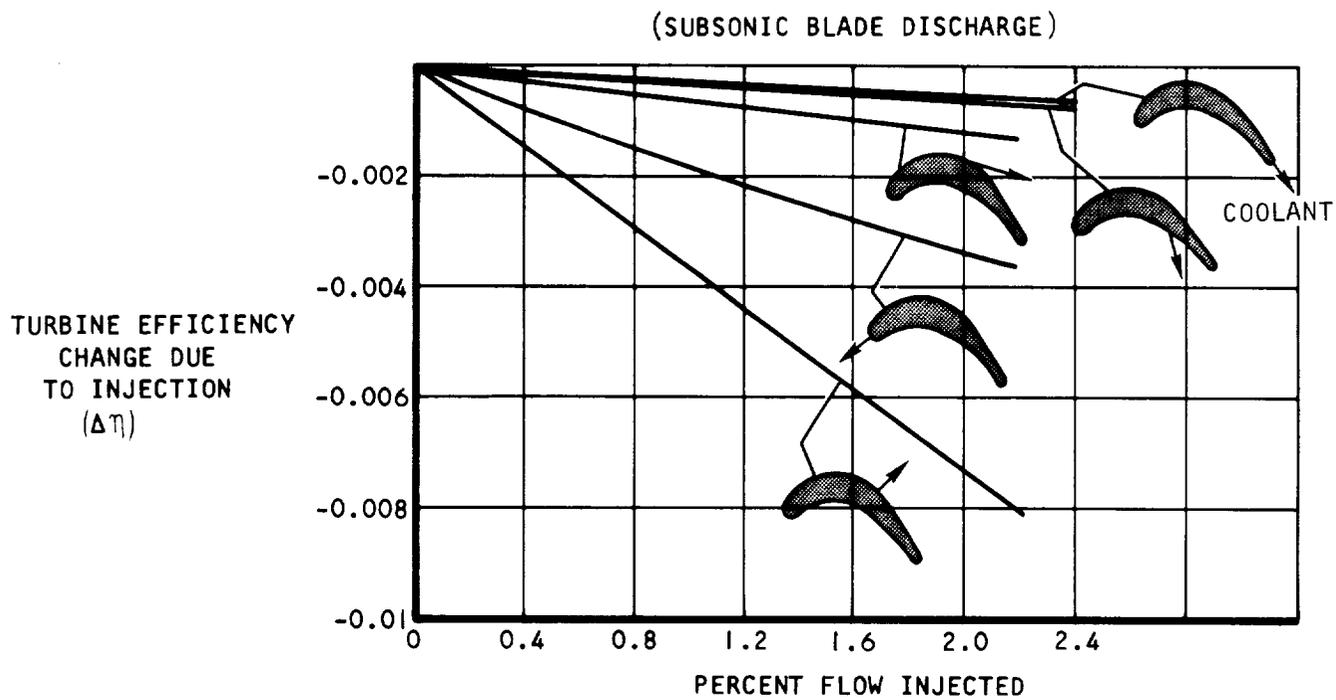
Figure 3-4. Stage I Blade Coolant Injection vs Two Stage Turbine Efficiency
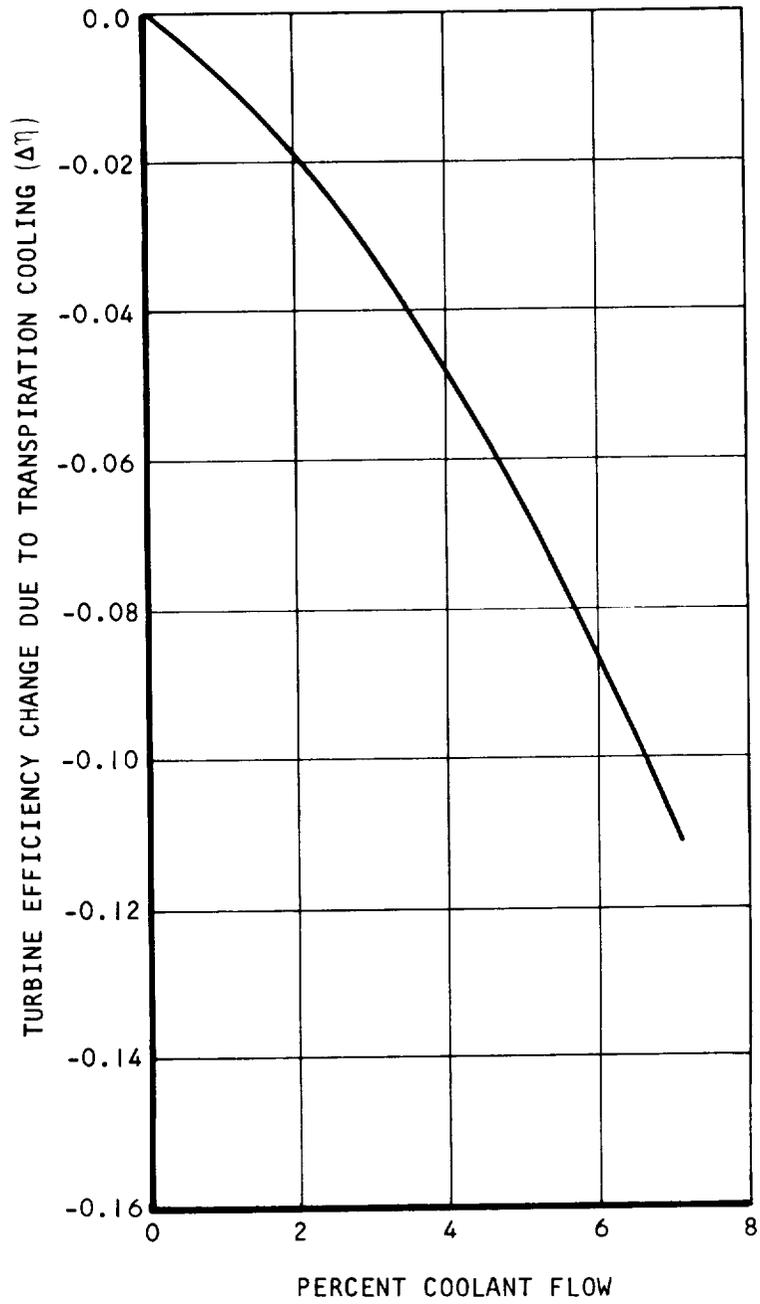
Figure 3-5. Turbine Stage Efficiency Reduction Due to Transpiration Cooling

These data indicate a substantial reduction in turbine efficiency as cooling flow is increased. This trend would be expected based on momentum exchange between the gas and injected coolant; however, it disagrees with the results of Reference 3, which indicate no significant effect of coolant flow on turbine efficiency. For purposes of this study it was assumed that the effects shown in Figure 3-5 would apply to this transpiration cooled blade.

The estimated reduction of turbine efficiency due to trailing edge thickness, coolant injection, and transpiration cooling for each preliminary design is summarized in the analytical results section.

HEAT TRANSFER, COOLING PASSAGE FLOW DISTRIBUTION, AND PRESSURE DROP ANALYSIS

External Blade Heat Transfer

Various methods have been proposed for calculating external heat transfer coefficients on turbine blades and vanes. Ellerbrock (Reference 20) did some of the initial work in turbine cooling which showed the applicability of flat plate relations to hot gas-to-blade heat transfer coefficients. The effects of Euler number and temperature ratio on laminar heat transfer indicated good agreement with the static cascade test data cited.

Wilson and Pope (Reference 21) measured heat transfer in a five-blade cascade by measuring power dissipation from isolated heating strips mounted flush with the surface of the center blade. The results of these tests indicated that the turbulent flow transition point occurred at the minimum pressure point on the suction side of the blade. The results on the pressure side indicated transition at approximately 10 percent chord which correlates adequately with a prediction using the method of Squire and Young (Reference 22) assuming that the effect of pressure gradient on local skin friction coefficient is negligible.

Zysina-Molozhen (Reference 23) derived an expression for the average heat transfer coefficient in a cascade by using the momentum- and thermal-boundary layer thicknesses. The results fit the experimental data cited in Reference 23. Another discussion by Zysina-Molozhen (Reference 24) showed that flat-plate methods were adequate within the range of experimental error.

Walker and Markland (Reference 25) measured heat transfer in the cascade used by Wilson and Pope and investigated the effects of secondary flows set up in boundary layers artificially thickened by spoilers. The results showed an increase in mean heat-transfer rate of about six percent.

Static cascade results generally indicate laminar-to-turbulent transition at about 10 percent chord on the pressure side of the blade and at the minimum pressure point on the suction side of the blade. Schlichting (Reference 26) devotes several chapters to the analytical and experimental work on transition. He shows that negative pressure gradients, smooth surfaces, and minimum free stream turbulence tend to postpone transition.

16

Ainley (Reference 27) indicates that heat transfer on operating turbine blades is about 26 percent higher than on static cascade nozzle vanes. Plotkin and Molchanor (Reference 28) indicate that for operating turbine blades, a more accurate approach is to base heat transfer coefficients on fully developed turbulent flow on each side of the turbine blades.

An AiResearch computer program exists which evaluates the outside local heat transfer coefficients on turbine blades by methods due to Moretti and Kays (Reference 29) and Kays (Reference 30). This program allows the transpiration point to be selected by the user. The program integrates along the blade surface for accelerating and decelerating flow to account for the variation in boundary layer thickness. The computer program of Spalding and Patankar (Reference 31) has also been modified for use at AiResearch. Heat transfer coefficients calculated by the Spalding and Patankar program for the pressure surface of the blades used in this study are 10 to 20 percent higher than the turbulent flat plate results.

Another program has been written which uses the method of Ellerbrock (Reference 20) and Eckert (Reference 32) for outside local heat transfer coefficients on turbine blades. The methods of Bromberg, Fox, and Ackerman (Reference 33), Sasman and Cresci (Reference 34), and Eckert (Reference 32) have also been programmed at AiResearch. For small turbine blades these latter methods give results which are sometimes higher than the simple flat plate relations.

Recent papers presented in AGARD Conference Proceedings No. 73 on High Temperature Turbines indicate some differences from previous results. Dunham and Edwards (Reference 35) performed static cascade tests similar to Wilson and Pope, including the effects of moderate turbulence. The results of these tests indicate a heat transfer coefficient on the pressure surface somewhat less than the turbulent boundary layer value, even in the presence of turbulence. The results on the suction side agreed well with Wilson and Pope. Additional results reported in Bayley and Turner (Reference 36), also indicate a heat transfer coefficient on the pressure side somewhat lower than the turbulent boundary layer value, even with turbulence. This paper also indicates a range of about 2.0 to 2.5 between the lowest and the highest average heat transfer coefficient reported by various investigators for blades operating at similar Reynolds numbers in static cascade rigs.

These results indicate that more experimental work with static cascade and rotating turbine blades is needed for an accurate evaluation of external heat transfer coefficients.

As a result of this literature survey, the turbulent flat plate heat transfer equation given in Appendix B was used for each side of the blades. The data on operating turbine blades indicate that fully developed turbulent flow occurs on both sides of the blade. In addition, a recent paper, Miller and Pucci (Reference 79), indicates that oscillating airfoils produce heat transfer coefficients similar to those predicted by the turbulent flat plate heat transfer equation. The presence of film cooling on an airfoil also produces heat transfer coefficients similar to those predicted by the turbulent

flat plate equation, as indicated in Lander, Fish, and Suo (Reference 80). Recent heat transfer data from static cascade rigs and engine rig tests conducted at NASA Lewis were compared with analytical results reported in Gladden, Gauntner, and Livingood (Reference 81) and Gladden, Livingood, and Gauntner (Reference 82). These results indicate that the turbulent flat plate equation is applicable to the calculation of heat transfer coefficients on each side of the blades.

The leading edge presents special problems, and it is usually handled by assuming a cylinder in crossflow as given by Squire (Reference 37) and Reshotko and Cohen (Reference 38). In addition to these methods, the method of Fay and Riddell (Reference 39) has been programmed at AiResearch. Recent test data taken at AiResearch indicates that leading-edge turbulence could increase the heat transfer coefficient up to 1.8 times the values calculated by the method of Fay and Riddell (Reference 39) for small diameter leading edges at high velocity. The method of Kestin (Reference 40) may be used to estimate this effect, if the turbulence characteristics are known.

Dyban and Kurosh (Reference 41) measured local values of the heat transfer coefficient for the leading edge of a cylinder placed immediately aft of an air turbine in a wind tunnel. This test simulates the conditions on the leading edge of the second stage nozzle vane and approximates the conditions on the leading edge of the first stage blade. The results indicated an increase in the leading edge heat transfer coefficient of from 15 to 50 percent, depending on the Reynolds number.

Based on this information, the heat transfer coefficient on the leading edge used herein was calculated using the equation for local heat transfer coefficients on a cylinder in crossflow as described in Appendix B with a 20 percent multiplying factor to account for free stream turbulence.

The fluid properties for hot gas in the heat transfer correlations of this report are evaluated at Eckert's reference temperature, as defined in Appendix B. The program iterates on the wall temperature at each location and changes the fluid properties as required. The relative total temperature is used for the heat transfer temperature potential to the external blade surface. This relative total temperature is a good approximation of the adiabatic wall temperature for these subsonic turbine blades. If the adiabatic wall temperatures were used, it would require a separate hot gas temperature connected to each external wall element and would result in a minimum wall temperature of $24^\circ F$ ($13.3^\circ K$) cooler than that calculated in this study. On a relative basis, this effect would be uniform over the various designs evaluated.

For film cooling, the external heat transfer coefficient is calculated as if no film cooling were present and the relative total temperature is replaced by the effective film temperature as defined in Appendix C. The fluid properties used for this calculation are evaluated at Eckert's reference temperature with the effective film temperature used as the hot gas temperature.

For transpiration cooling, the external heat transfer coefficient on the turbine blade is reduced using the Stanton number reduction factor as defined in Appendix C.

18

Internal Blade Heat Transfer and Cooling Air Heatup

Internal convection cooling may be applied to the blade using undisturbed or disturbed flow passages. In undisturbed flow passages the heat transfer coefficient may be calculated using a combination of forced convection and natural convection. In a rotating turbine blade the free-convection force is the centrifugal force of rotation and the natural convection heat transfer coefficient is calculated by replacing the gravitational acceleration by the rotational acceleration $(r\omega^2)$ in the Grashof number. For the cooling air flowing radially outward, this free-convection force is in a direction opposite to the direction of forced flow. This counterflow situation has been reported in Eckert, Diaguila, and Curren (Reference 42) and in Brown and Gauvin (Reference 43). Results indicate that the heat transfer coefficient for turbulent flow of air in the passage is up to twice as large as the higher value calculated from either forced convection or natural convection equations for Grashof numbers greater than 10^6. Therefore, a conservative assumption for radial flow in an undisturbed flow passage of a rotating turbine blade would be to add the forced convection to the natural convection heat transfer coefficient.

The forced convection heat transfer coefficient for air flowing through a round, ellipitical, triangular, or rectangular passage may be calculated using the Colburn J-factor relation shown in Figure 3-6. Effects of temperature dependent fluid properties and local heat transfer coefficients in the entrance region are discussed in Appendix B. Natural convection equations for laminar and turbulent flow are also described in Appendix B.

Several disturbed flow heat transfer surfaces which have been considered are: (1) triangular spaced pin fins, (2) transverse fins, and (3) offset plate-fins. A discussion and derivation of the heat transfer coefficient in pin fin passages is presented in Appendix D. The resulting equation for the turbulent flow Colburn J-factor relation for equilateral triangular spaced pin fins is given in Equation (3-8) below.

$$J = \frac{\left[0.023 + \dfrac{4.143 \; \text{EXP} \left\{-3.094\left(\dfrac{D_p}{S_p}\right) -0.89 \left(\dfrac{S_p}{L_p}\right)^{0.5075}\right\}}{(\text{Re})^{0.2946}}\right]}{(\text{Re})^{0.2}} \tag{3-8}$$

Transverse fin heat transfer data was taken from AiResearch data, Nunner (Reference 44) and Koch (Reference 45).

In Koch, data is given on the effects of sets of rings inserted in a round tube with various hole diameter to spacing ratios. The results of these studies were correlated on the basis of $m^* = d/D$ and L'/d.
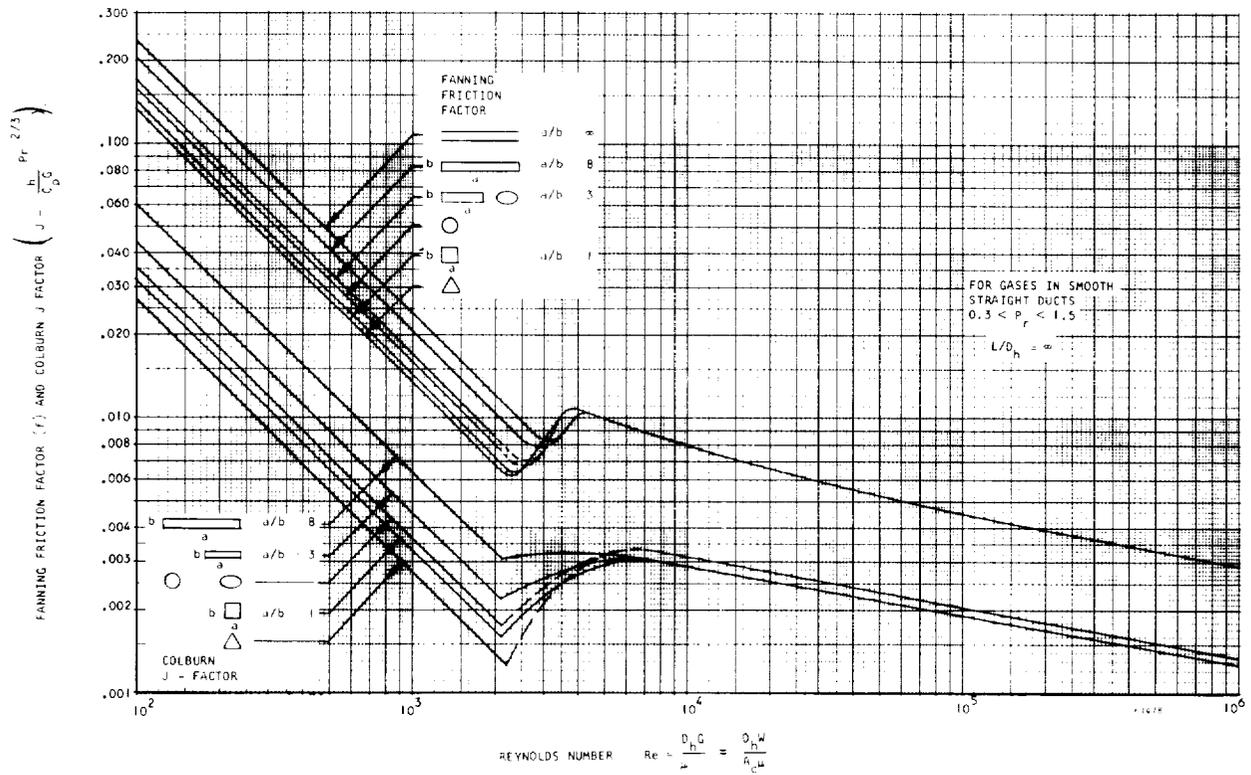
Figure 3-6. Colburn J-Factor and Fanning Friction Factor for Round, Elliptical, Triangular, and Rectangular Smooth Passages with Air

20
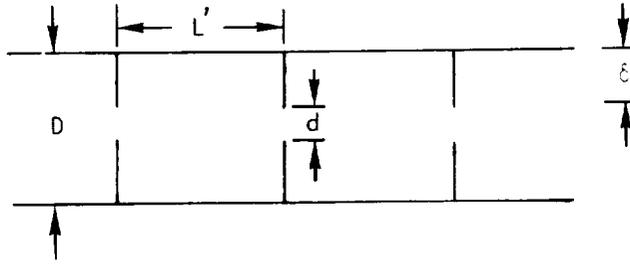
In these studies it was found that friction factor and j-factor (Nusselt No.) reached a maximum at $6 < L'/d < 10$. For L'/d less than 6 and for L'/d greater than 10, friction factor and j-factor decreased.

The transverse finned leading edge used in this study has fins on the inner surface of the leading edge only. These fins have a height varying from 0.02 in. (0.000508 m) to 0.01 in. (0.000254 m), therefore the average fin height (δ) on the leading edge side of the passage is 0.015 (0.000381 m). The center-to-center fin spacing (L') selected is 0.18 in (0.00457 m). Since the leading edge passage diameter (D) is 0.072 in. (0.001829 m) and the fins are on one side of the passage only, the diameter inside the fins (d) is 0.057 in. (0.001448 m) (d = 0.072 - 0.015 = 0.057 in.). This results in $L'/d = 3.16$ and m* d/D = 0.792. For these values, data from Koch indicates that the j-factor or Nusselt No. is 2.3 times the value for a plain tube in the turbulent region, and the friction factor is constant at 0.05 for the turbulent region.

AiResearch data on ring dimpled tubes are correlated as a function of Ψ

where $\Psi = \dfrac{\delta/D}{\sqrt{L'/D}}$

Using the geometry for the transverse finned leading edge of this study:

δ = 0.015 in. (0.00381 m)

D = 0.072 in. (0.001829 m)

L' = 0.18 in. (0.00457 m)

we obtain:

$\Psi = \dfrac{0.015/0.072}{\sqrt{0.018/0.072}} = 0.1318$

No AiResearch data exists for this high value of Ψ; however, an equivalent condition of heat transfer and friction factor at a lower value of Ψ can be found in the data of Koch (Reference 45). Koch shows that the data for L'/d 3.16 is similar to that for L'/d = 15 in both heat transfer and friction factor. For an L'/d value of 15 the equivalent fin spacing (L') is 0.855 in. (0.02172 m) (L' = 15 (0.057) = 0.855 in.). The equivalent value of Ψ may be estimated as shown below.

$$\Psi = \frac{0.015/0.072}{\sqrt{0.855/0.072}} = 0.0605$$

For this value of Ψ the AiResearch data agrees with the data of Koch (Reference 45).

In addition Nunner presents data on heat transfer and pressure drop in rough tubes which shows that the increase in heat transfer due to this type of flow disturbance may be estimated from the increase in friction factor as shown below.

$$\frac{Nu}{Nu_0} = \frac{j}{j_0} = \sqrt{\frac{f}{f_0}}$$

for
$$Re = 10,000$$

$$f = 0.05$$

$$f_0 = 0.0073$$

$$\frac{j}{j_0} = \sqrt{\frac{0.05}{0.0073}} = 2.62$$

Therefore Nunner indicates that the heat transfer coefficient would be 2.62 times the value in a plain tube where the data in Koch and from AiResearch indicates that the heat transfer coefficient would be 2.3 times the value in a plain tube.

The resulting friction factor and Colburn j-factor relation used in the analysis of the transverse finned leading edge of the pin fin blade is shown in Figure 3-7.

The Colburn J-factor for plain and offset plate-fin surfaces may be taken from Kays and London (Reference 46) or from London and Shah (Reference 47). Plain and offset plate-fin surfaces used in this study have 40 fins/in (15.75 fins/cm) with a 0.004 in. (0.0001016 m) fin thickness. The Colburn J-factor for both the plain and offset fins is shown in Figure 3-8.

Colburn J-factor data for the porous simulated transpiration cooled material was developed from the data given in Nealy, Anderson, and Hufford (Reference 48) and Anderson and Nealy (Reference 49).

Impingement heat transfer has been studied by several investigators (References 50 through 61). For impingement heat transfer on the inner surface of the turbine blade leading edge, the method of Chupp, Helms, McFadden, and Brown (Reference 50) was selected. This method is described in Appendix B. The heat transfer coefficient for impingement by an array of jets on the side of a turbine blade was calculated using the method of Kercher and Tabakoff (Reference 51).

22

FANNING FRICTION FACTOR f

COLBURN J-FACTOR

$J = \dfrac{h}{c_p G} \left(\dfrac{c_p \mu}{k}\right)^{2/3}$

TRANSVERSE FIN LEADING EDGE

PIN FIN SURFACE

TRANSVERSE FIN LEADING EDGE

REYNOLDS NUMBER $Re = \dfrac{D_h G}{\mu} = \dfrac{D_h W}{A_c \mu}$
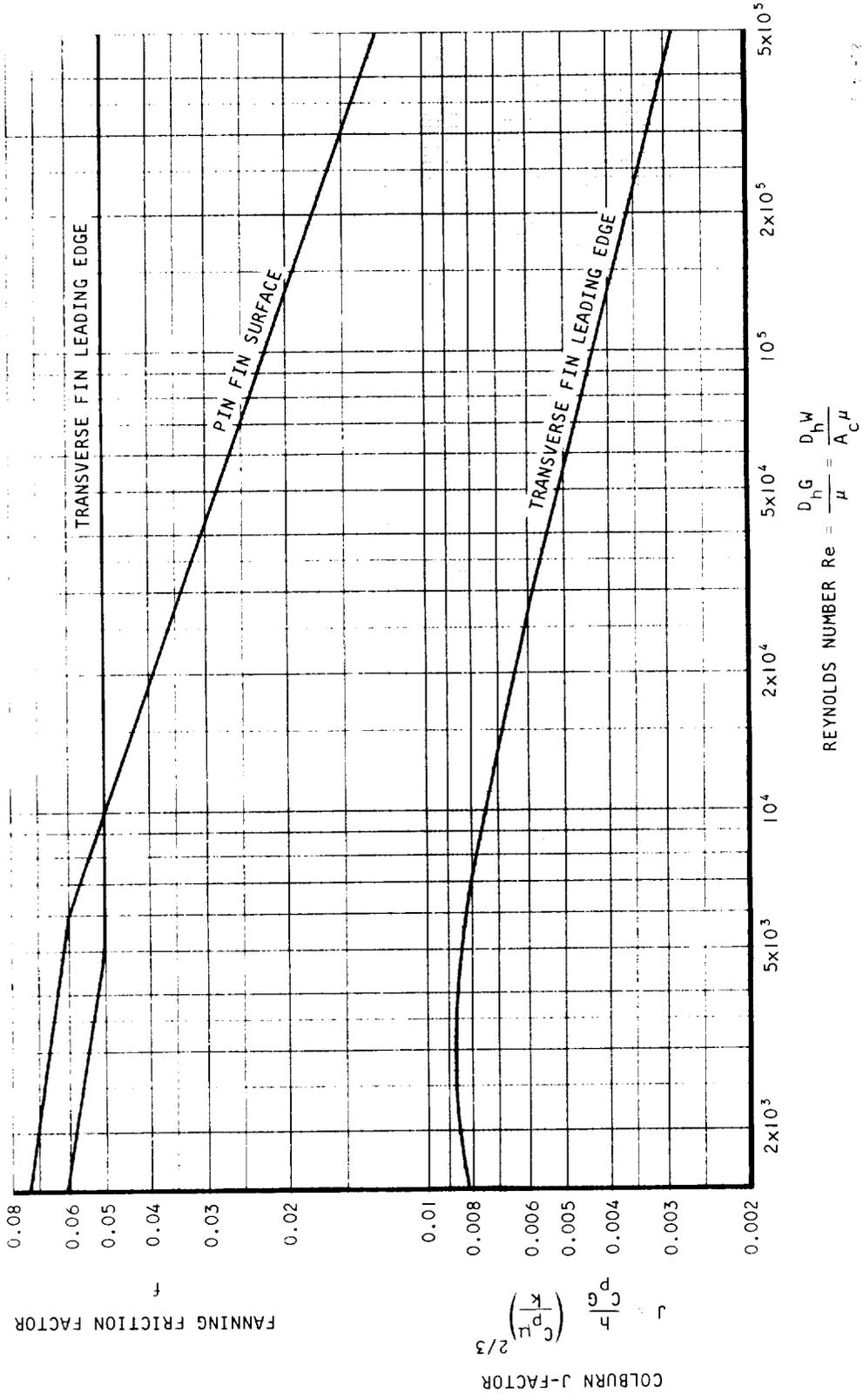
Figure 3-7. Colburn J-Factor and Fanning Function Factor for the Pin Fin Surface and the Transverse Finned Leading Edge

23
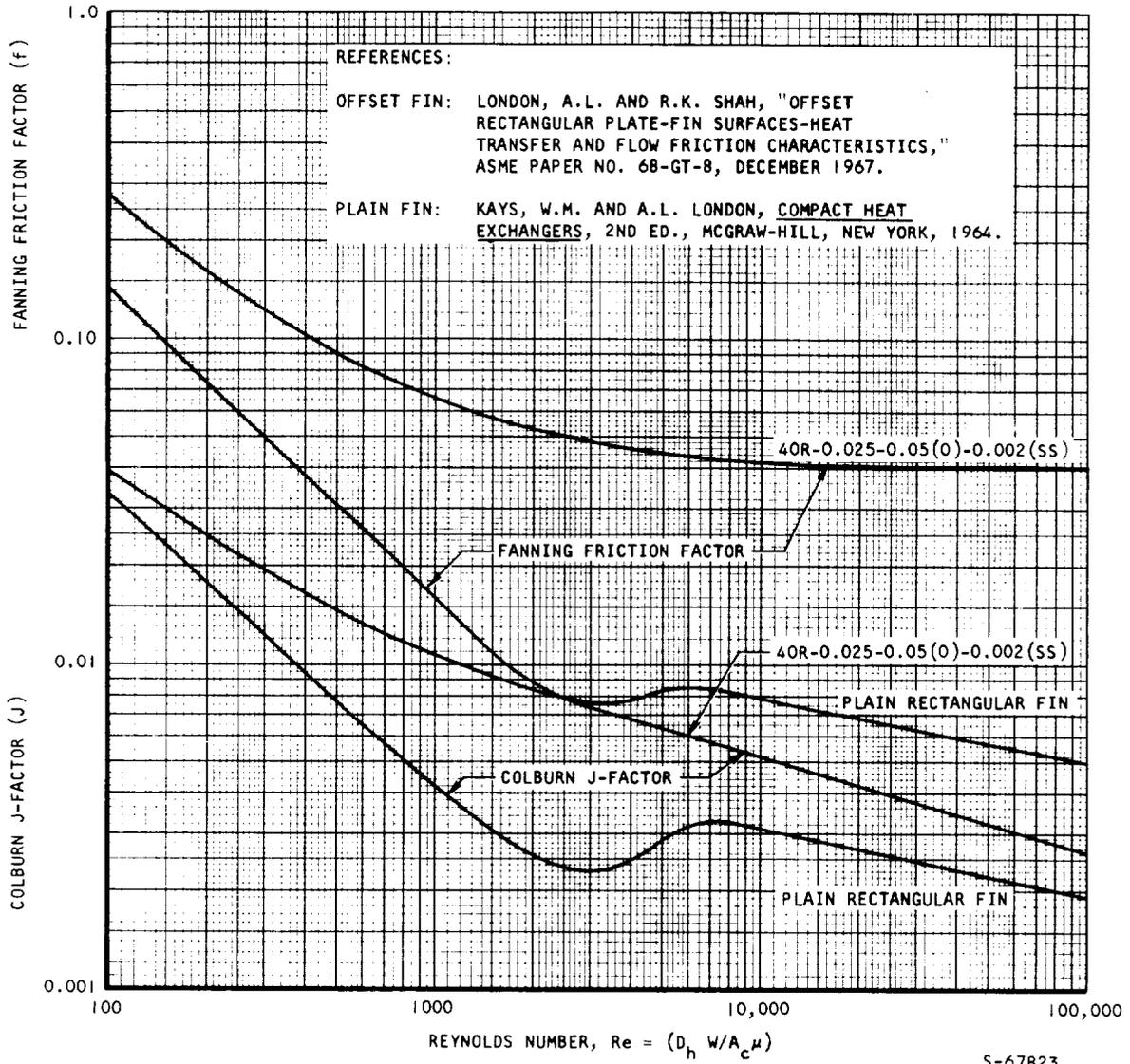
Figure 3-8. Colburn J-Factor and Fanning Friction Factor Data for AiResearch Plate Fin Surfaces

S-67823

24

This method includes the effect of cross-flow of the spent air over subsequent impinging jets in the array. This crossflow deflects the jet and reduces the impingement heat transfer coefficient. The Colburn J-factor relation for an array of jets from round holes in a thin plate is given in Equation (3-9).

$$J = \psi_1 \psi_2 \, Re_o^{(m-1)} \left(\frac{z_o}{d_o}\right)^{0.091} \tag{3-9}$$

The values of ψ_1, ψ_2, and m are given in Figures 3-9, 3-10, and 3-11 taken from Reference 51. The fluid properties for impingement cooling are evaluated at the average between the fluid static temperature in the orifice and the wall temperature.

The heat transfer coefficient for flow in curved pipes has been studied by Mori and Nakayama (Reference 62 and 63). Heat transfer data for flow in a sharp bend of an annular slot has also been obtained from AiResearch testing of the hypersonic research engine leading edge cooling system. The AiResearch data indicates that the sharp bend heat transfer may be correlated with impingement cooling equations. The Colburn J-factor relation based on the AiResearch experimental data for the sharp bend in a slot is given in Equation 3-10 below.

$$J = \frac{0.0584}{Re_b^{.16}} \tag{3-10}$$

Equations for cooling air heatup flowing radially in a turbine blade are derived in Appendix E. The finite increment average temperature difference method was used in this analysis. Equations used are shown in Appendix B.

Cooling Passage Pressure Drop and Flow Distribution

The steady-state compressible flow pressure drop due to (1) flow acceleration caused by area change or heat addition, (2) fluid friction, (3) flow addition or removal, and (4) radial inward or outward flow in a rotating passage is calculated as described in Appendix B. The equation used is based on the method of influence coefficients for constant specific heat and molecular weight as described in Shapiro (Reference 64). The drag component for stationary bodies in the fluid stream is replaced by an equation for rotational flow head.

Fluid friction loss for flow in a cooling passage is calculated using the Fanning friction factor. This friction factor is used as a function of Reynolds number and the variation of friction factor along the passage is considered. Friction factors for air flow through a round, elliptical, triangular, or rectangular passage may be calculated using the Fanning friction factor relation shown in Figure 3-6. Effects of temperature dependent fluid properties on pressure drop are discussed in Appendix B.
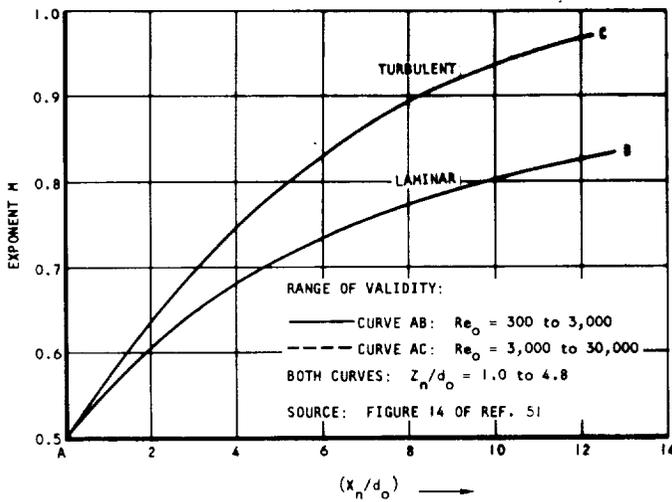
Figure 3-9.   Reynolds Number Exponent
for Equation (3-9)

$$Re_o = \frac{d_o G_o}{\mu_o}$$
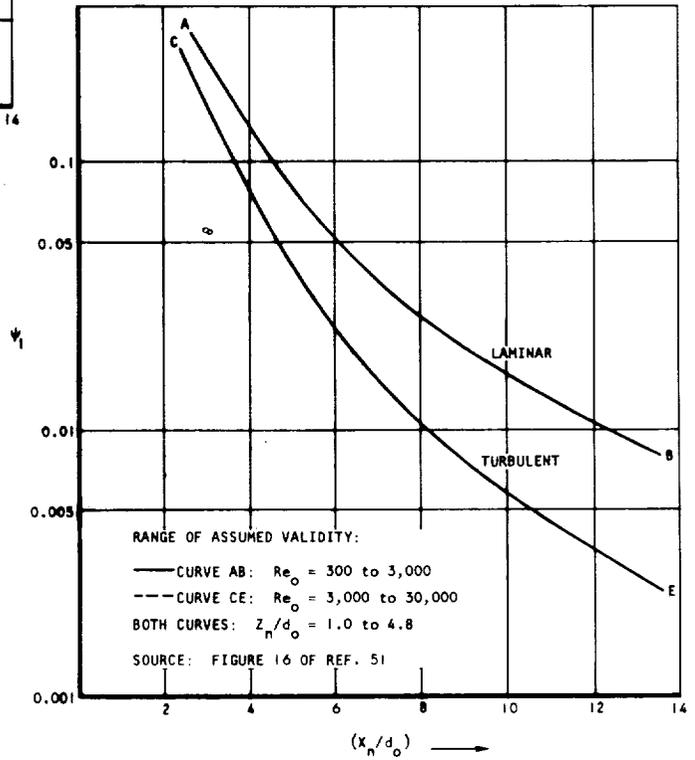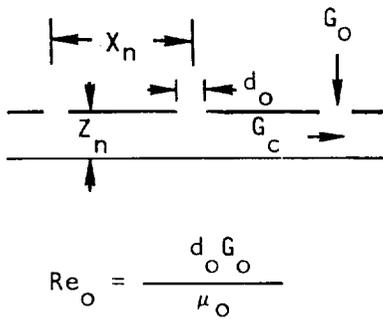
Figure 3-10.   Orifice Spacing Correction
Factor for Equation (3-9)

UNIFORM FLOW SQUARE ARRAY

$$\left[\frac{G_c}{G_o}\right]\left(\frac{Z_n}{d_o}\right) = \left[\frac{\pi}{4}\,(i-1)\left(\frac{d_o}{X_n}\right)\right]$$

S-67824

$$\left[\frac{G_c}{G_o}\right]\left(\frac{Z_n}{d_o}\right) \text{ NONUNIFORM FLOW}$$
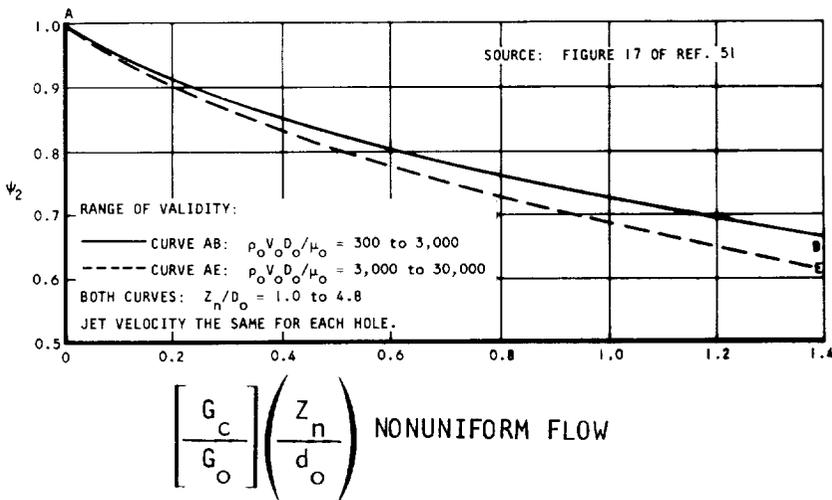
Figure 3-11.   Spent Air Crossflow Correction
Factor for Equation (3-9)

26

Several other cooling passage types which have been considered are: (1) triangular spaced pin fins, (2) transverse fins, and (3) offset plate-fins. The Fanning friction factor for each of these surfaces is presented in Figures 3-7 and 3-8. Triangular spaced pin fin friction factor data is based on cold flow data from pin fin turbine blades measured at AiResearch. The pins were 0.025 in. (0.000635 m) diameter on a 0.075 in. (0.001905 m) center-to-center spacing. The transverse finned leading edge data was taken from AiResearch data, Nunner (Reference 44), and Koch (Reference 45) as described in the internal blade heat transfer section. The offset and plain plate-fin data was taken from Kays and London (Reference 46) and London and Shah (Reference 47). The plain and offset plate-fin surfaces used in this study had 40 fins/in. (15.75 fins/cm) with a 0.004 in. (0.0001016 m) fin thickness.

The Fanning friction factor data for the porous simulated transpiration cooled material was developed from the data given in Nealy, Anderson, and Hufford (Reference 48) and Anderson and Nealy (Reference 49).

The compressible flow pressure drop in bends, sharp expansions and contractions, orifices, and nozzles was calculated from a total head loss coefficient as shown in Appendix B. The total head loss coefficient for bends, diffusers, and branches was determined from Lamb and Holdhusen (Reference 65). The total head loss coefficient for sharp expansions and contractions was taken from information presented in Benedict, Carlucci, and Swetz (Reference 66). This paper presents data for both compressible and incompressible total head loss coefficients. Several sources were investigated for total head loss coefficients in orifices (References 67, 68, 69, 70, and 71) and the resulting total head loss equations used are shown in Appendix F. The total head loss coefficient for an orifice in a fluid stream with the axis parallel to the direction of stream flow or an orifice in a duct wall with the axis perpendicular or inclinded to the direction of stream flow was determined as described in Appendix F. The total head loss coefficient data for orifices in a duct wall was obtained from Metzger and Jenkins (Reference 60), Dittrich (Reference 73), and Rohde, Richards, and Metger (Reference 74). It was necessary to recalculate the data presented in References 73 and 74 to get it in the form of head loss coefficient as used in the computer program described in Appendix B.

The pressure distribution for flow in channels with flow addition and flow removed is derived in Appendix G. The method used in this analysis is based on the Y-factor as defined in Shapiro (Reference 64). For a supply tube with flow leaving the stream, the Y-factor is taken as one $(Y = 1.0)$ This means that the fluid leaves with the full momentum of the main stream. When flow enters the stream perpendicular to the direction of main stream flow, the Y-factor is equal to zero $(Y=0)$. This means that the entering flow must be accelerated to the main stream flow. The Y-factor is defined in Appendix B.

STRESS ANALYSIS AND BLADE LIFE CALCULATIONS

Blade life calculations include the stress distribution based on centrifugal loads, including the effects of the dead weight of the fins and the tip cap where it is used. Gas bending loads were neglected because these loads are small and may be cancelled out by tilting the blades. Bending moments due

to offsetting the line of action of the centrifugal force as a result of thermal distortion is considered in AiResearch program X0850 described in Appendix H. This program was used to predict the thermal stress distribution considering the effects of elastic strain and relaxation of stress due to local instantaneous plastic flow of the material.

Preliminary design analysis included stress distribution based on steady-state temperature distribution at the hub, mean, and tip sections of the blades. Minimum design stress to rupture life at each element was determined for the temperature and stress of the element. If it is assumed that the turbine blade will not fail in stress rupture due to compression, the life at each section may be evaluated by considering only the tensile stress life. Creep relaxation analysis indicates that this assumption is correct because the compressive stressed elements relax rapidly with creep. Therefore only the tensile stressed elements were considered in the calculations of blade life for the preliminary design analysis. This is in accordance with Method 2 of the blade life prediction methods described below.

The final design analysis included the stress distribution based on the steady-state temperature distribution at the hub, mean, and 75 percent span sections of the blades. The blade life was based on the time to one percent creep strain after stress redistribution due to creep. This is in accordance with Method 3 of the blade life prediction methods described below. A creep analysis was not necessary for each condition because the creep analysis for a similar condition could be used in many cases. Also the results indicated that many blades were limited by maximum allowable coating temperature rather than stress. The creep stress analysis was also conducted using AiResearch program X0850 described in Appendix H. This program uses a method of analysis similar to that described in NASA TN D-5282 (Reference 75).

Figure 3-12 through 3-21 show the material properties of IN-100 used in this analysis. Comparing the minimum design curve in Figure 3-13 with the data in Figure 11 of Reference 75 shows that the AiResearch data requires a metal temperature about 70°F lower for the same stress level. This minimum design curve is intended to account for the effects of minimum wall thickness and coating diffusion effects and is somewhat more conservative than the data used in Reference 75.

Several different methods may be employed in the calculation of the useful life of the airfoil section of turbine blades. The predicted life can be greatly extended or reduced depending upon the particular method chosen by the analyst and by the material property curves employed. An attempt to describe the procedures and their accompanying assumptions and conservatism (or lack of it) follows.

Method 1. Equating Average Centrifugal Stress to Material Stress-Rupture Strength Based On Cross-Sectional Average Temperature

In this method of computing blade life the centrifugal force acting at a blade cross section is divided by the cross sectional area to
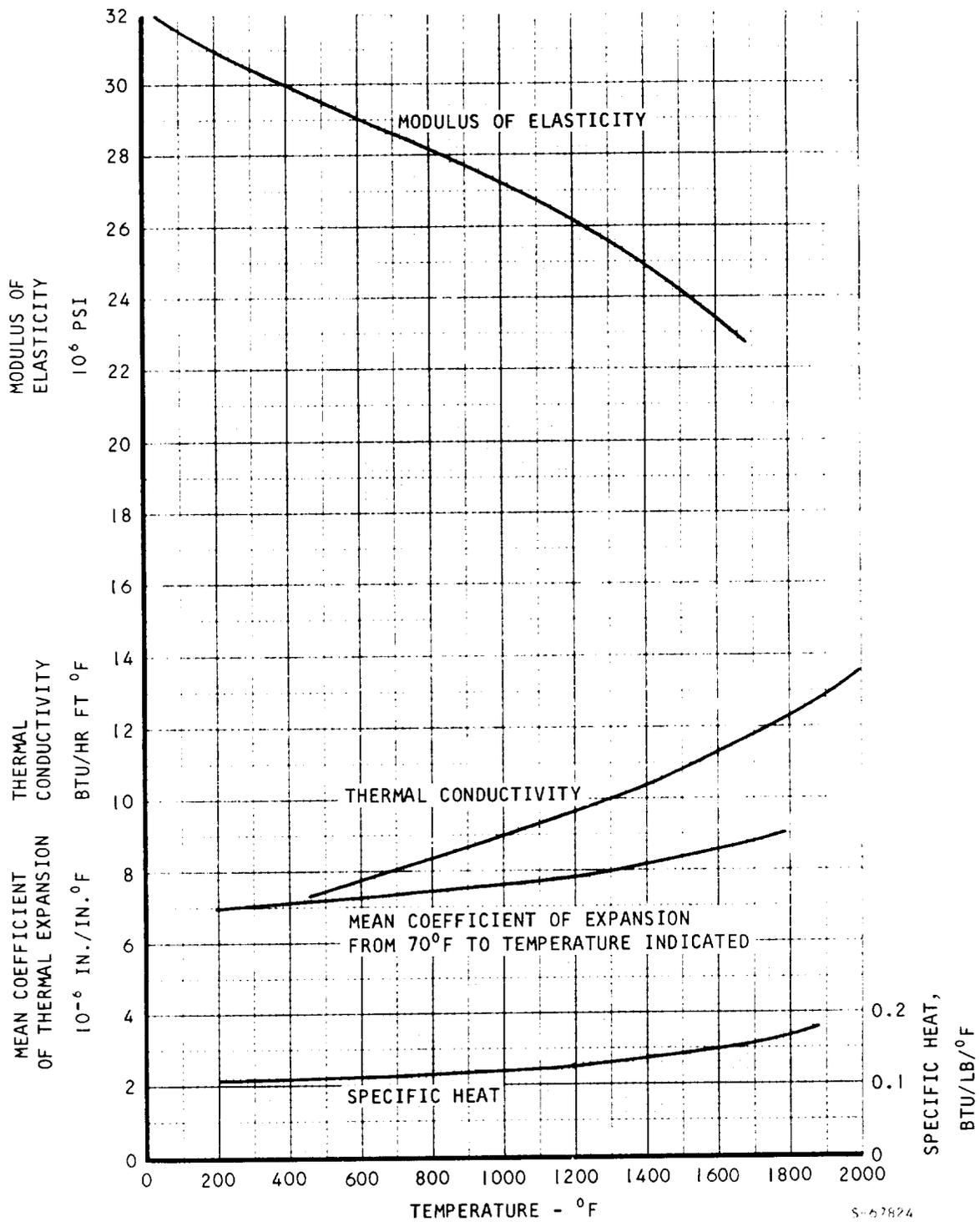
Figure 3-12. Typical Physical Properties of IN-100
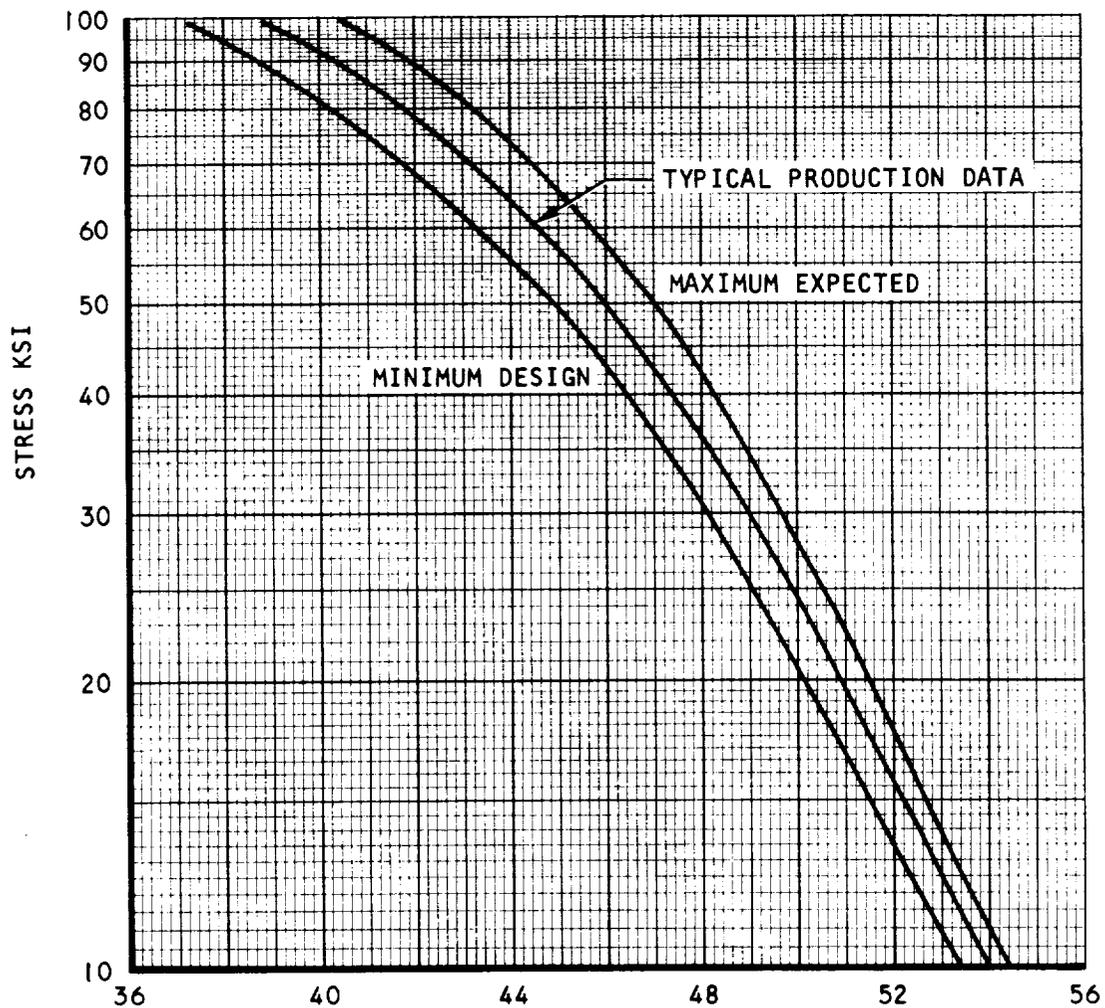
$$\text{LARSON - MILLER PARAMETER}$$
$$(T + 460) (20 + \log_{10}\theta) \times 10^{-3}$$

WHERE T = TEMPERATURE, $^\circ$F

θ = TIME, HOURS

NOTE: THIS CURVE IS NOT TO BE USED FOR TEMPERATURES OVER 2000°F

S-67825

Figure 3-13.   Master Stress-Rupture Curve IN-100,
EMS-589, As-Cast
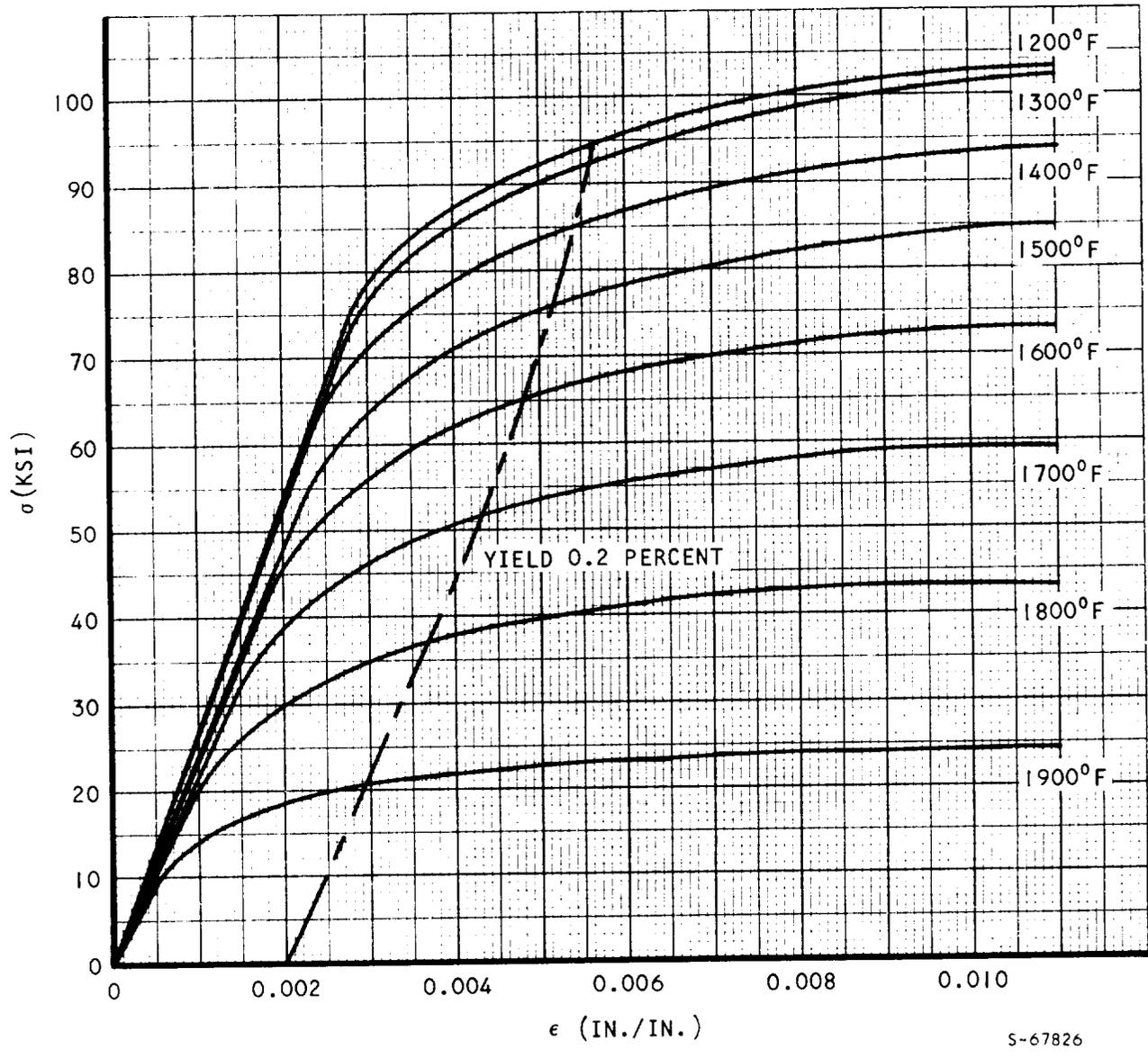
Figure 3-14. Stress-Strain Curves, IN-100

S-67826
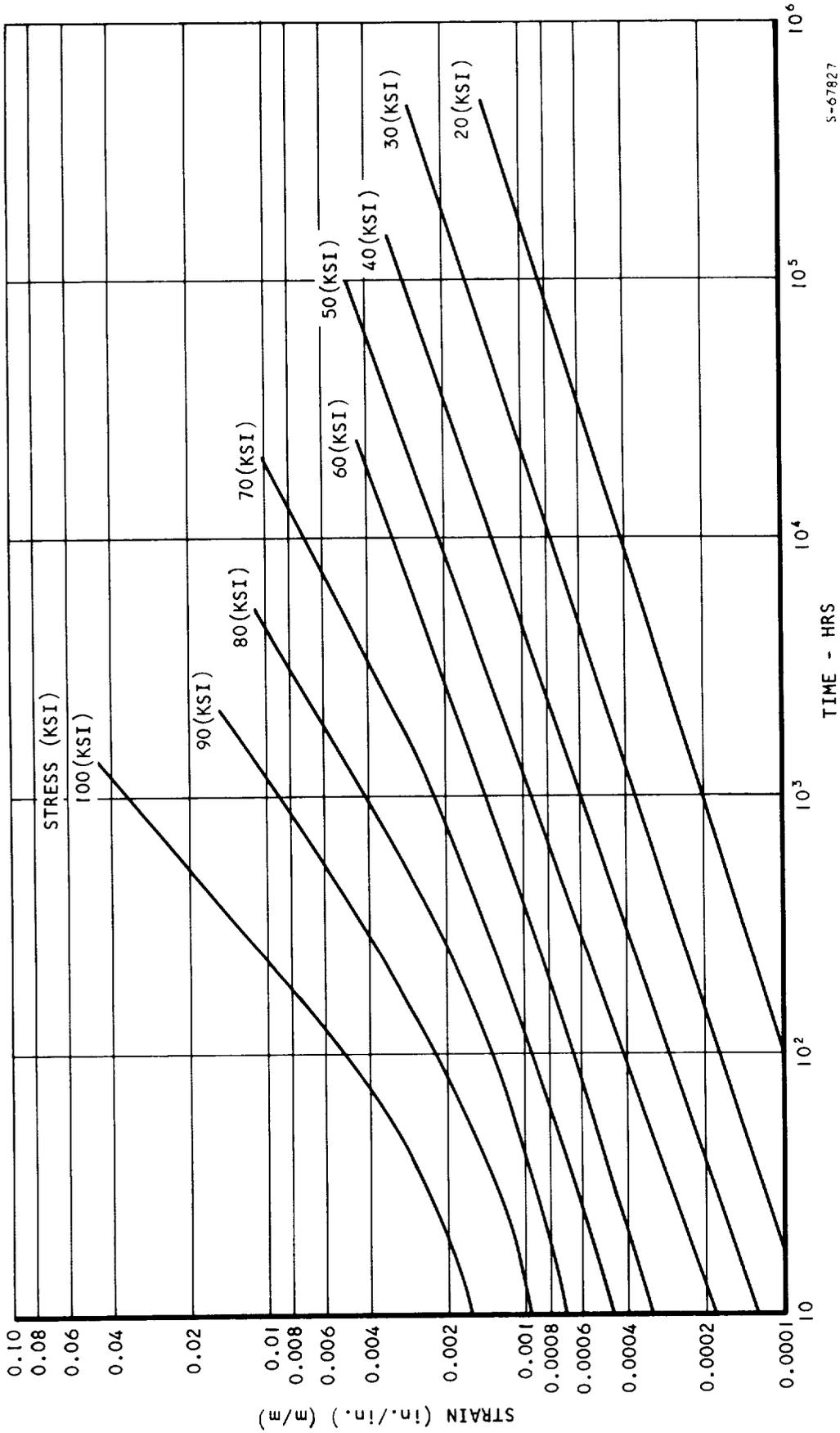
Figure 3-15. Creep Data for IN-100 at 1300°F

S-67827

32
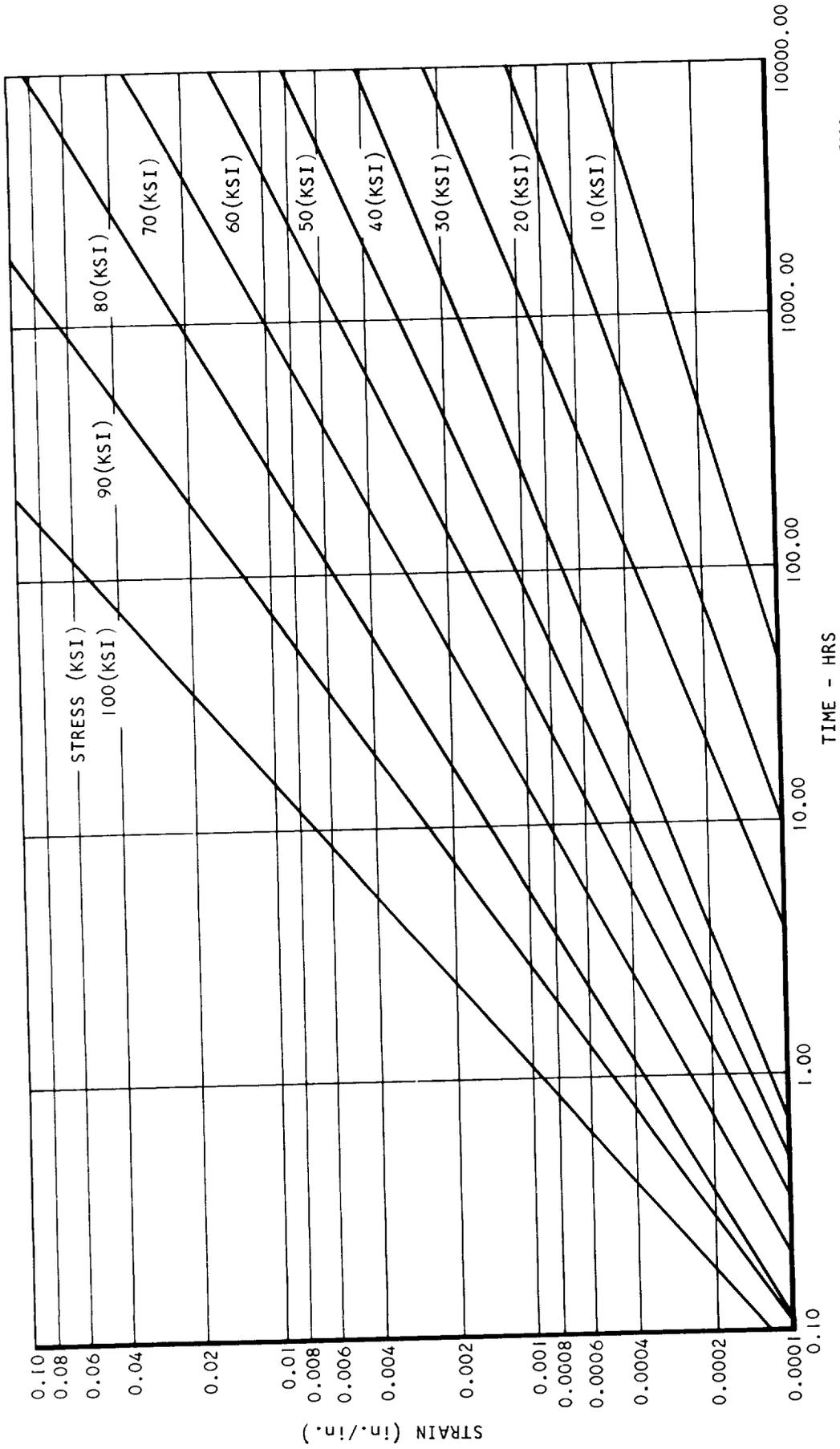
Figure 3-16. Creep Data for IN-100 at 1400°F
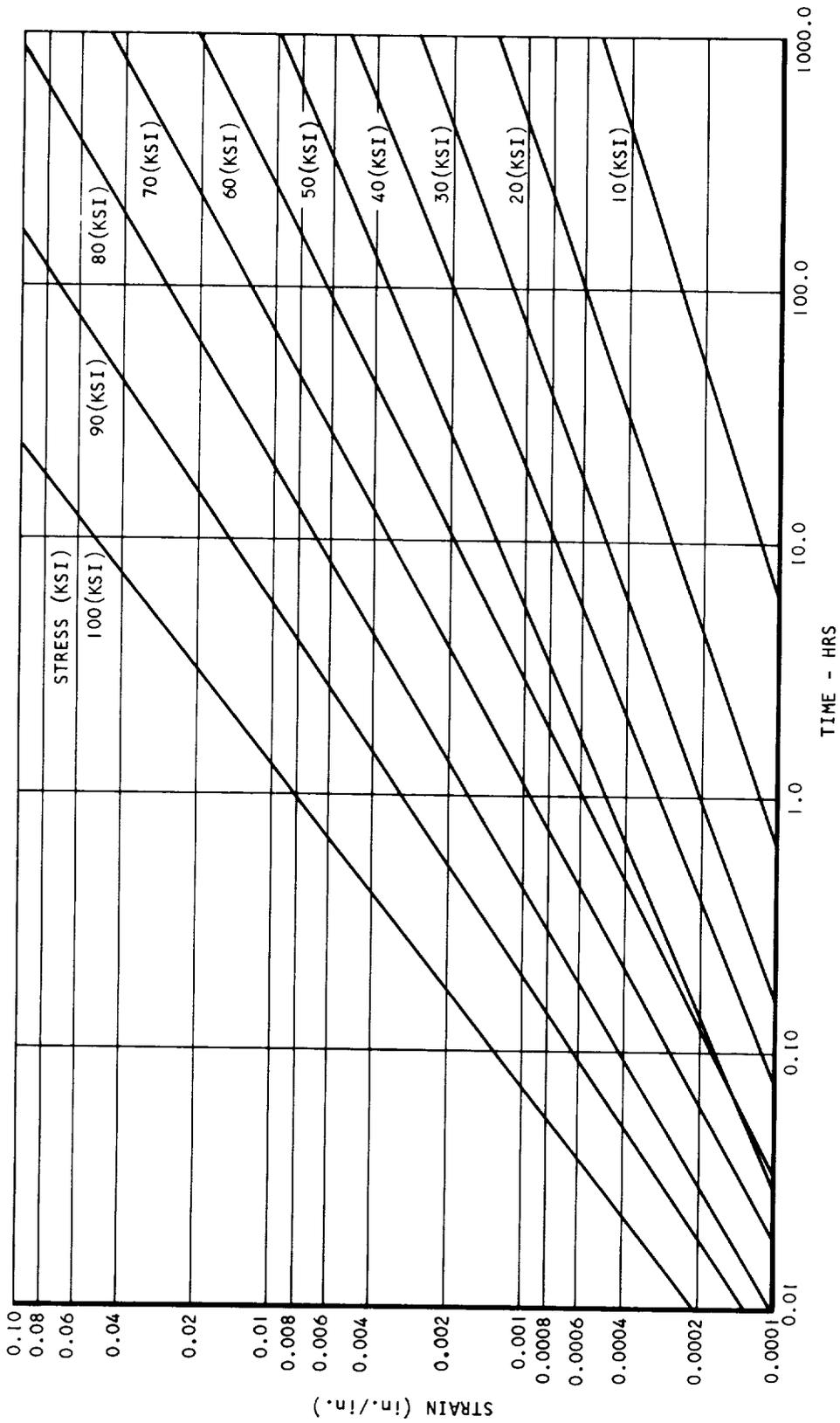
33

Figure 3-17. Creep Data for IN-100 at 1500°F

34
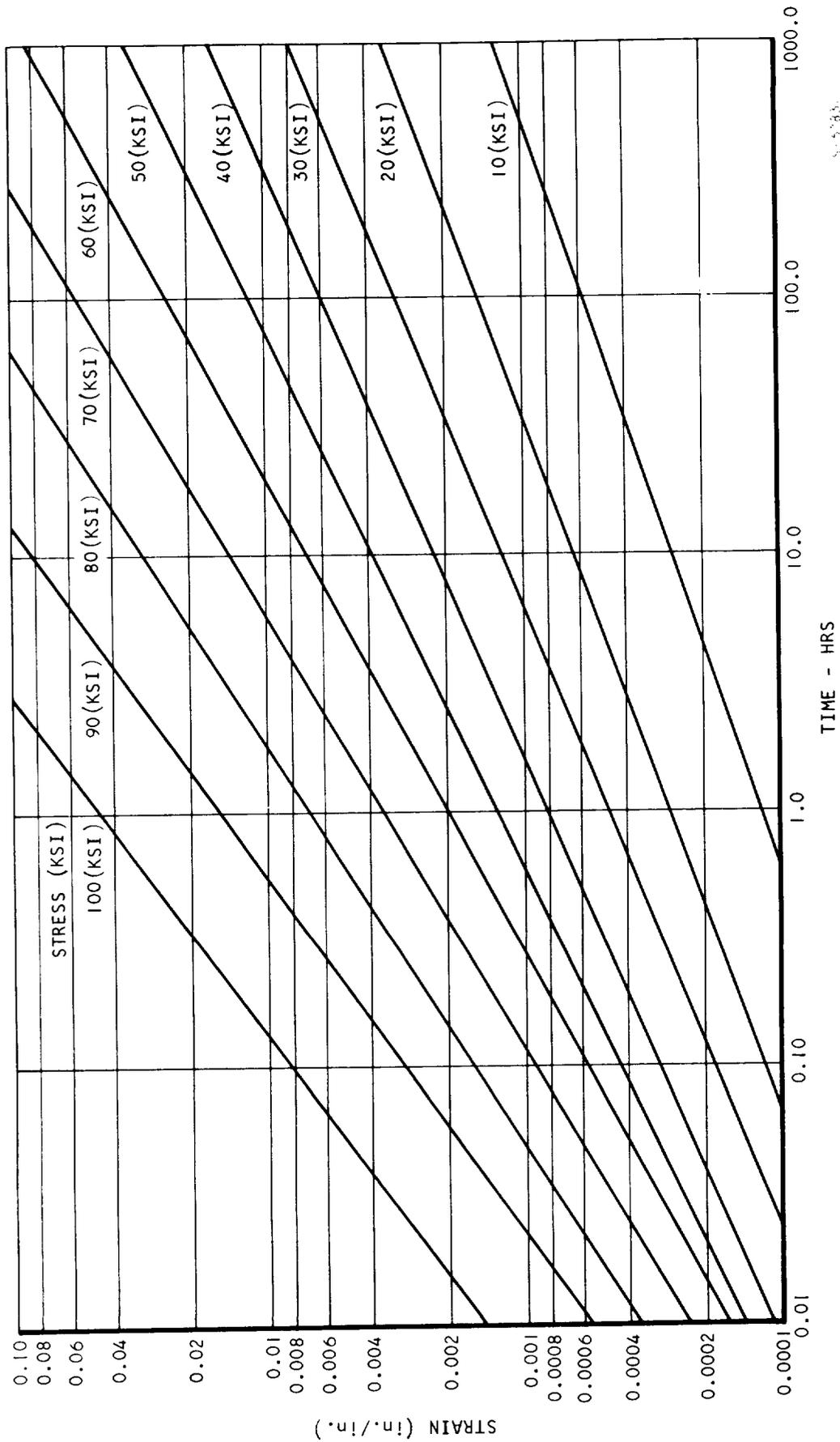
Figure 3-19. Creep Data for IN-100 at 1600°F

35
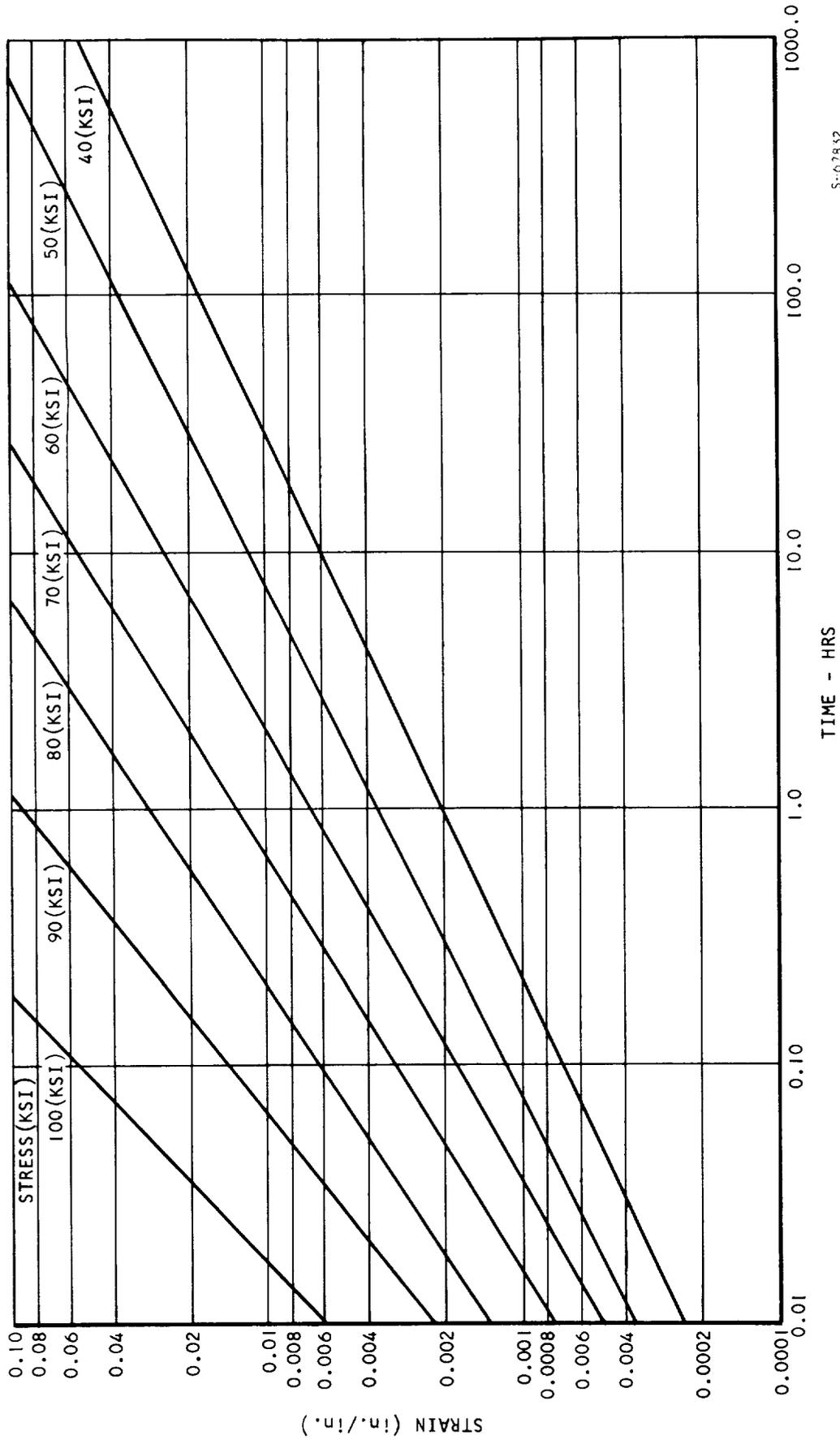
Figure 3-19. Creep Data for IN-100 at 1700°F

S-67852

36
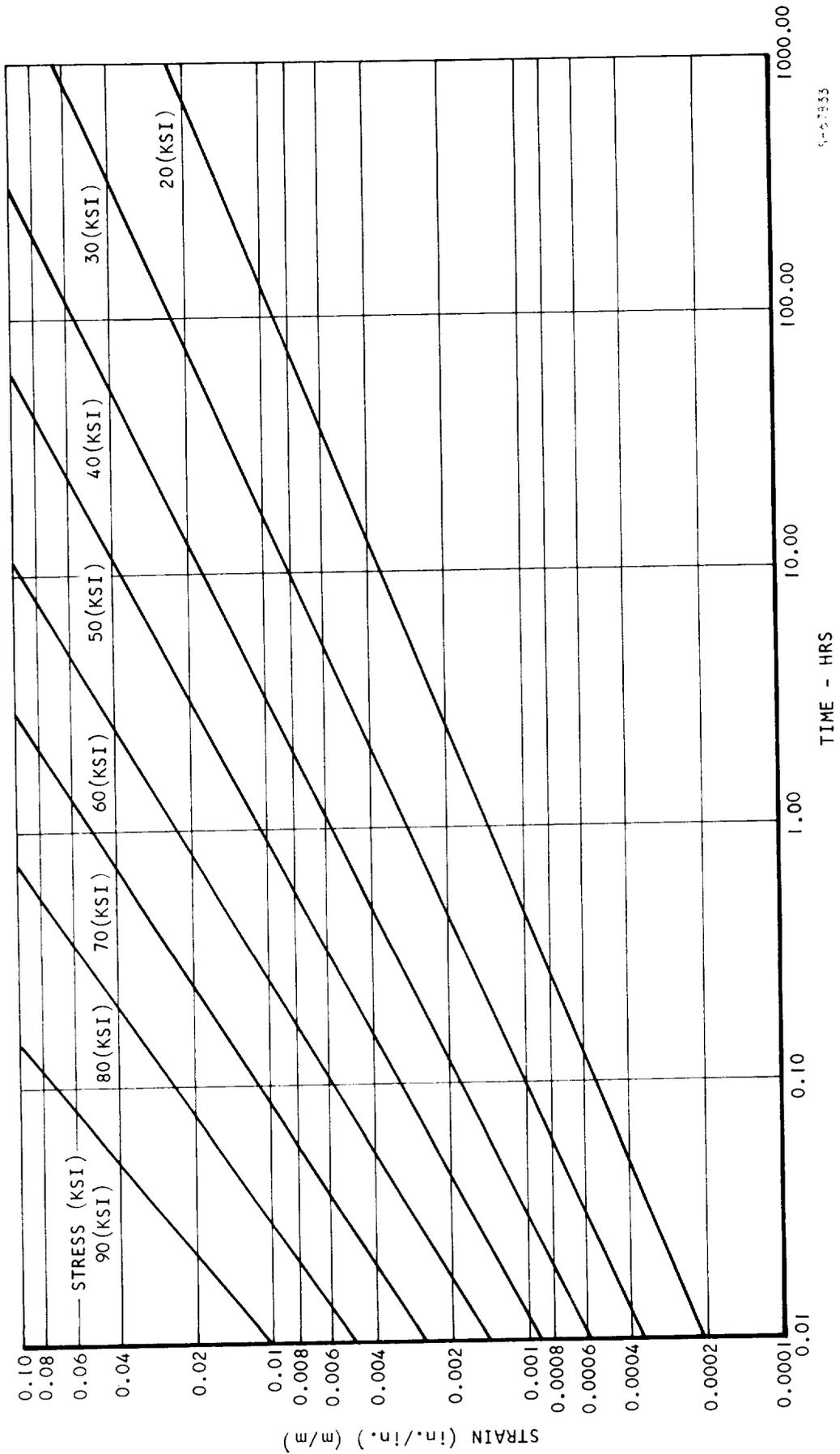
Figure 3-20. Creep Data for IN-100 at 1800°F
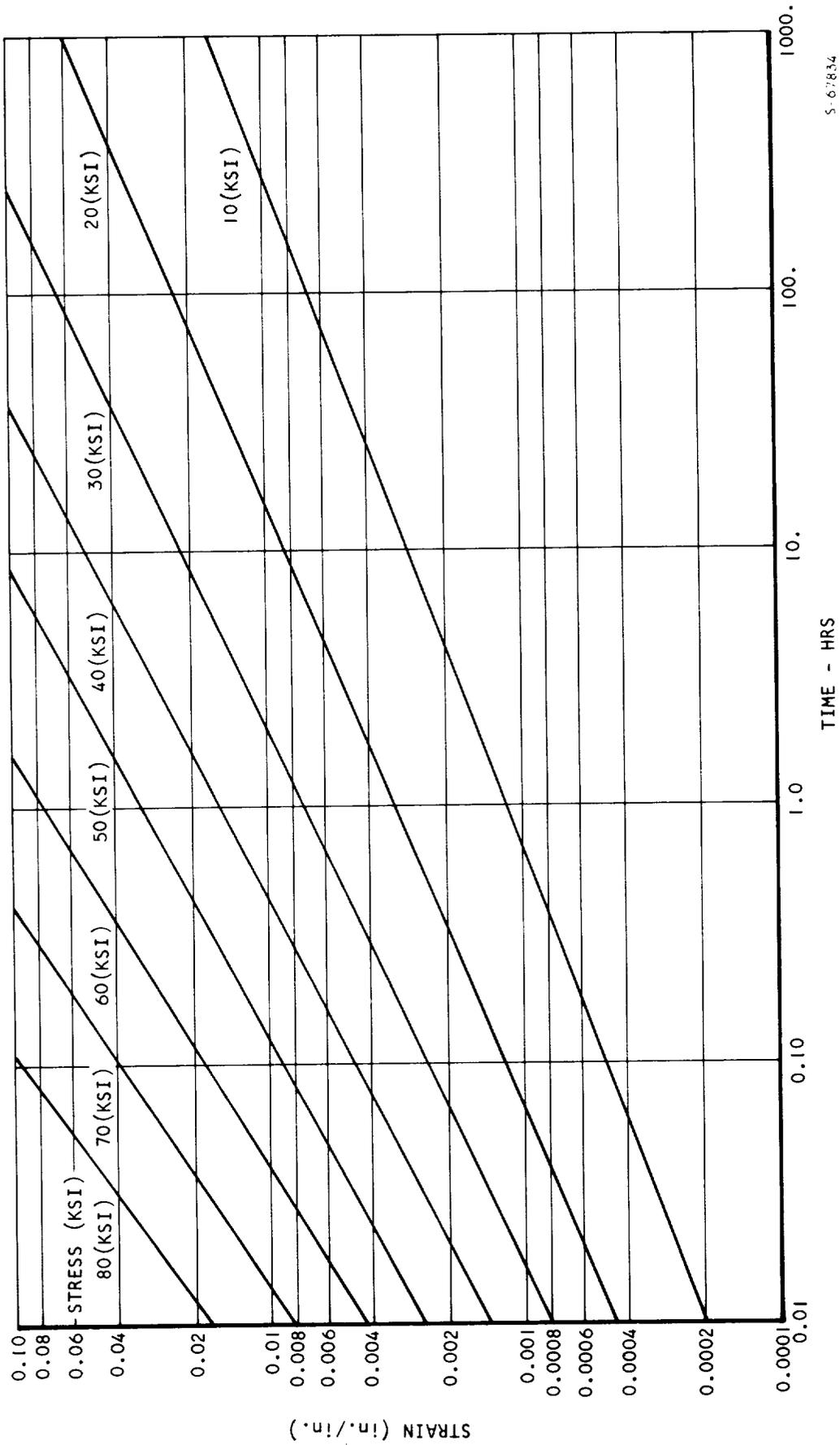
Figure 3-2l. Creep Data for IN-100 at 1900°F

S-67834

38

determine the average stress level. Material strength is determined
by using the weighted average temperature as a reference. The allow-
able stress is usually selected from either creep or stress-rupture
considerations.

Method 2. Equating Short-Time Combined Mechanical and Thermal
           Stresses at Each Element of the Blade Cross-Section to
           Material Stress-Rupture Strength of That Element

In this analysis method, the blade (or vane) cross-section is divided
into elemental areas of sufficient number to describe the cross-
sectional properties and thermal distribution. Mechanical forces
and moments are computed with respect to a selected reference station
of the cross section. Both temperature and corresponding strength
data for each of the elements is used in performing the stress
analysis. The stresses computed for each element are compared to
either the stress rupture or creep strengths of the element. A com-
mon practice is to disregard the elements where compressive stresses
exist and to base the section life on the minimum value obtained from
the tensile stressed elements. Since this is a short time analysis,
the relieving effect of creep is not accounted for.

Method 3. Equating Combined Mechanical and Thermal Stresses at Each
           Element of the Blade Cross-Section to Material Creep and
           Stress-Rupture Strains of That Element

This procedure is quite similar to Method 2 except now the fact that
the cross-section must creep before rupturing is accounted for. The
useful life of the section is assumed to be consumed when the time
to exceed a prescribed strain is exceeded at any element of the
cross-section. It is further required that the prescribed strains
throughout the blade span must be such that neither local fracture
or tip rubbing is permitted.

     Method I represents a rapid means in preliminary design for estimating
the life of a blade or vane. However, it is not dependable for final design
purposes since one cannot evaluate in advance the amount of unconservatism in
the prediction. For example, for sections with only small thermal gradients,
the life predicted can be expected to be reliably estimated by this method.
However, when the peak temperatures deviate by even as much as 100 deg from the
mean temperature, the method will always overestimate the life of the blade.
For the latter case, creep relaxation will not be capable of reducing the peak
stresses to the value estimated by the mean temperature.

     Method 2 estimates stress peak values based on short-time operation. How-
ever, for long time operation these peaks are somewhat flattened through creep
redistribution. Thus, lives based on the short time values are conservative if
both tensile and compressive stress components are considered. Disregarding
the compressive stress components may be unconservative and is not adequately
substantiated by test data.

Method 3 estimates the effects of creep redistribution in smoothing the stress profile. Although this technique is more tedious and time consuming to apply, it does not contain the restrictive assumptions of Methods 1 and 2.

For the creep stress analysis of blades with holes in the blade surface, the area of the hole was subtracted from the cross-sectional area of the element and the metal above the holes was considered as dead weight in determining the loads for the section. Stress concentration effects due to holes in the blade surface are taken into account in a fatigue analysis. A method of combining steady-state creep rupture and fatigue failure is outlined in NASA TM X-1951 (Reference 76). Fatigue data for IN-100 specimens with holes and slots is given in Stewart and Vogel (Reference 77). Since acceleration and deceleration engine transients were not defined for this study, a fatigue failure analysis was not conducted.

The stress analysis of transpiration cooled materials was conducted by determining an equivalent cross-sectional metal area from material properties given in Anderson and Nealy (Reference 49).

SECTION 4

DESIGN CONDITIONS

TASK I   PRELIMINARY DESIGN

The turbine blades in this study were assumed to be first stage rotor blades of 0.75 in. (0.01905 m), 1.0 in. (0.0254 m), and 1.5 in. (0.0381 m) chord. Eight blade cooling configurations in each of the three chord sizes were studied in the preliminary design phase. Blade hub and tip radii for each design were held constant at 4.812 in. (0.1222 m) and 6.562 in. (0.1667 m) respectively. Pitch line blade solidity was held constant at 1.71. Total pressure drop across a stator vane row $\left(\Delta P/P_{ti}\right)_s$ was assumed to be 0.03. For a turbine stator inlet average total pressure of 150 psia (1.034×10^6 Newtons/sq m), the absolute total pressure entering the blades was evaluated as follows:

$$P_{bi} = \left[1. - \left(\frac{\Delta P}{P_{ti}}\right)_s\right] P_{t_i}$$

$$\left(\frac{\Delta P}{P_{ti}}\right)_s = 0.03 \qquad P_{t_i} = 150 \text{ psia } (1.034 \times 10^6 \text{ Newtons/sq m})$$

$$P_{bi} = [1 - 0.03](150) = 145.5 \text{ psia}(1.003 \times 10^6 \text{ Newtons/sq m})$$

From this absolute total pressure, the radial variation in relative total pressure to the blade was evaluated as outlined in the aerodynamics section. The combustor total pressure drop, $\left(\Delta P/P_{co}\right)_c$ was assumed to be 0.06 and total pressure loss in ducting the cooling air from the compressor to the blade base, $\left(\Delta P/P_{co}\right)_{CA}$ was assumed to be 0.08 where P_{co} is the compressor outlet total pressure. For a turbine stator inlet average total pressure of 150 psia (1.034×10^6 Newtons/sq m), the cooling air total pressure at the root of the blade may be evaluated as follows:

$$P_{CA} = P_{ti} \left[\frac{1. - \left(\Delta P/P_{co}\right)_{CA}}{1. - \left(\Delta P/P_{co}\right)_c}\right]$$

$$\left(\Delta P/P_{co}\right)_{CA} = 0.08 \qquad \left(\Delta P/P_{co}\right)_c = 0.06$$

$$P_{ti} = 150 \text{ psia } (1.034 \times 10^6 \text{ Newtons/sq m})$$

$$P_{CA} = 150 \left[\frac{1-0.08}{1-0.06}\right] = 146.8 \text{ psia } (1.012 \times 10^6 \text{ Newtons/sq m})$$

The cooling air inlet temperature used for the preliminary design analysis was 900°F (755.6°K). The circumferentially averaged radial gas temperature profile correction factor for the absolute total inlet temperature is shown in Figure 4-1.

Velocity diagrams for the hub, mean, and tip sections of the turbine blade are shown in Figure 4-2. These velocity diagrams were used to calculate relative total pressure, relative total temperature, and free stream velocity relative to the leading edge.

Thermal analysis design conditions and aerodynamic design conditions are summarized in Table 4-1 and Table 4-2, respectively.

Before starting the preliminary design phase of the contract, a study of the stress limitations and metal area taper ratio of the original design was conducted. Preliminary stress calculations were conducted using Figures 4-3 and 4-4 to calculate the centrifugal root stress of a linearly tapered or a constant stress tapered blade. Based on the IN-100 minimum design stress rupture properties shown in Figure 3-13, a root stress of 30,000 psi (2.068 x 10^8 Newton/sq m) was chosen for this analysis. This stress level is consistent with 1000 hr stress to rupture at 1600°F (1144.4°K) metal temperature or 1000 hr for 0.3 percent creep at 1500°F (1088.9°K) metal temperature for IN-100. Figure 4-5 shows the turbine tip speed as a function of turbine inlet temperature used for this analysis.

Using these conditions, a study of the turbine inlet temperature capabilities of the original blade configuration and of a thickened blade configuration was made. Original and thickened blade configurations are shown in Figures 4-6, 4-7, and 4-8. Table 4-3 shows a comparison of allowable turbine inlet temperatures for the original and thickened blade configuration in the three chord sizes for a stress of 30,000 psi (2.068 x 10^8 Newtons/sq m). The hub-to-tip metal area taper ratio is shown for the solid blade and for a maximum constant cooling air flow area. The maximum cooling air flow area is based on a minimum wall thickness of 0.02 in. (0.000508 m) all the way around the tip section. This minimum wall thickness is consistent with our present casting experience. The results show that the thickened blade configuration allows an increase of from 150°F (83.3°K) to 190°F (105.6°K) in turbine inlet temperature for the linear taper ratio blade. The linear taper ratio condition more nearly represents the true conditions for a cooled turbine blade because it results in a 30,000 psi (2.068 x 10^8 Newtons/sq m) stress at the root and somewhat lower stress over the rest of the blade where the temperature is higher. The constant stress condition assumes the metal area is distributed so that it gives a constant stress over the entire span of the blade. This means that a constant temperature of 1600°F (1144.4°K) for 1000 hr rupture life or 1500°F (1088.9°K) for 100 hr at a 0.3 percent creep limit would be required over the entire span of the blade. This results in an unrealistic requirement for a cooled turbine blade.

TABLE 4-1

THERMAL ANALYSIS PRELIMINARY DESIGN CONDITIONS

		Section		
		Hub	Mean	Tip
Relative Total Temperature Ratio $T_g' = \left(\dfrac{T_g'}{T_g}\right) T_g + \Delta T_{CORR}$	$\left(\dfrac{T_g'}{T_g}\right)$	0.937515	0.0945308	0.954577
Relative Total Pressure Ratio $P_g' = (P_g'/P_g) P_{bi}$	$\left(\dfrac{P_g'}{P_g}\right)$	0.740176	0.769305	0.805116
Critical Velocity Ratio Relative to Leading Edge	$(W/W_{cr})_1$	0.549	0.392	0.318
Trailing Edge Static Pressure Ratio $P_{st} = (P_{st}/P_g) P_{bi}$	$\left(\dfrac{P_{st}}{P_g}\right)$	0.55504	0.55569	0.55663

$\gamma = 1.273$

Cooling air inlet temperature = $900^\circ F$ ($755.6^\circ K$)

Cooling air inlet pressure = 146.8 psia (1.012×10^6 Newtons/sq m)

Blade height = 1.75 in. (0.04445 m)

$N = 433.5\sqrt{T_g}$ rpm

Blade tip speed $(V_{tip}) = 24.8257\sqrt{T_g}$ ft/sec ($10.152\sqrt{t_g}$ m/sec)

Hot gas inlet total pressure $(P_{bi}) = 145.5$ psia (1.00314×10^6 Newtons/sq m)

		Leading Edge	Midchord Pressure Side	Midchord Suction Side
Blade Tip Static Pressure Ratio $P_{so} = (P_{so}/P_g) P_{bi}$	$\left(\dfrac{P_{so}}{P_g}\right)$	0.76052	0.73547	0.47153

TABLE 4-2

AERODYNAMIC ANALYSIS DESIGN CONDITIONS

			Hub	Mean	Tip
Radius	in. (m)		4.81242 (0.12224)	5.68742 (0.14446)	6.56242 (0.16669)
TIT 2200°F (1477.8°K)	T'_g P'_g W	°R (°K) psia (Newtons/ sq m) ft/sec (m/sec)	2484.7 (1380.4) 107.4 (7.4x10⁵) 1201. (366.4)	2506.5 (1392.5) 111.7 (7.7x10⁵) 862. (262.7)	2532.6 (1407.0) 116.97 (8.06x10⁵) 703. (214.3)
TIT 2600°F (1700°K)	T'_g P'_g W	°R (K) psia (Newtons/ sq m) ft/sec (in./sec)	2868.8 (1593.8) 107.7 (7.43x10⁵) 1290 (393.2)	2892.6 (1607.0) 111.93 (7.72x10⁵) 924.9 (281.9)	2921 (1622.8) 117.14 (8.08x10⁵) 754. (229.8)
TIT 3000°F (1722.1°K)	T'_g P'_g W	°R (°K) psia (Newtons/ sq m ft/sec (m/sec)	3255.4 (1808.6) 107.99 (7.45x10⁵) 1372 (418.2)	3280.8 (1822.7) 112.17 (7.73x10⁵) 983 (299.6)	3310.9 (1839.4) 117.3 (8.09x10⁵) 801 (244.1)

Turbine Inlet Temperature		2200°F (1477.8°K)	2600°F (1700°K)	3000°F (1922.2°K)
W_g	lb/sec (k_g/sec)	32.8049 (14.88)	30.4882 (13.829)	28.5835 (12.965)
γ		1.29	1.273	1.257
R $\frac{ft-lb\ f}{lb\ m-°R}$		53.387	53.4	53.413
R $\frac{m\ Newtons}{k_g\ °K}$		(287.2)	(287.3)	(287.4)

Chord - in. (m)	0.75 (0.01905)	1.0 (0.0254)	1.5 (0.0381)
Number of Blades	81	61	41

TABLE 4-3

HUB-TO-TIP AREA RATIO COMPARISON FOR THE ORIGINAL DESIGN
AND THE THICKENED DESIGN IN EACH CHORD SIZE

| | | Original Turbine Blade Configuration Presented by NASA | | | Proposed Turbine Blade Configuration Thickened at the Root and Mean Sections | | |
| | | Chord In. (m) | | | Chord In. (m) | | |
		0.75 (0.01905)	1.0 (0.0254)	1.5 (0.0381)	0.75 (0.01905)	1.0 (0.0254)	1.5 (0.0381)
Hub-to-tip Metal Area Ratio	Solid Blade	1.38	1.38	1.38	1.544	1.544	1.544
A_j/A_b	Maximum Constant Cooling Flow Area	1.83	2.06	2.53	2.19	2.53	3.18
Maximum Turbine Inlet Temperature* °F. (°K) for Constant Cooling Flow Area	Linear Taper Ratio Blade	2200 (1477.8)	2300 (1533.3)	2490 (1638.9)	2350 (1561.1)	2490 (1638.9)	2680 (1744.4)
	Constant Stress Blade	2770 (1794.4)	3040 (1944.4)	-	3100 (1977.8)	-	-

*The maximum turbine inlet temperature is based on the hub-to-tip area ratios and a stress of 30,000 psi (2.068 x 10^8 Newtons/sq m) which are consistent with 1000 hr rupture life at 1600°F (1144.4°K) or 1000 hr for 0.3 percent creep at 1500°F (1088.9°K).
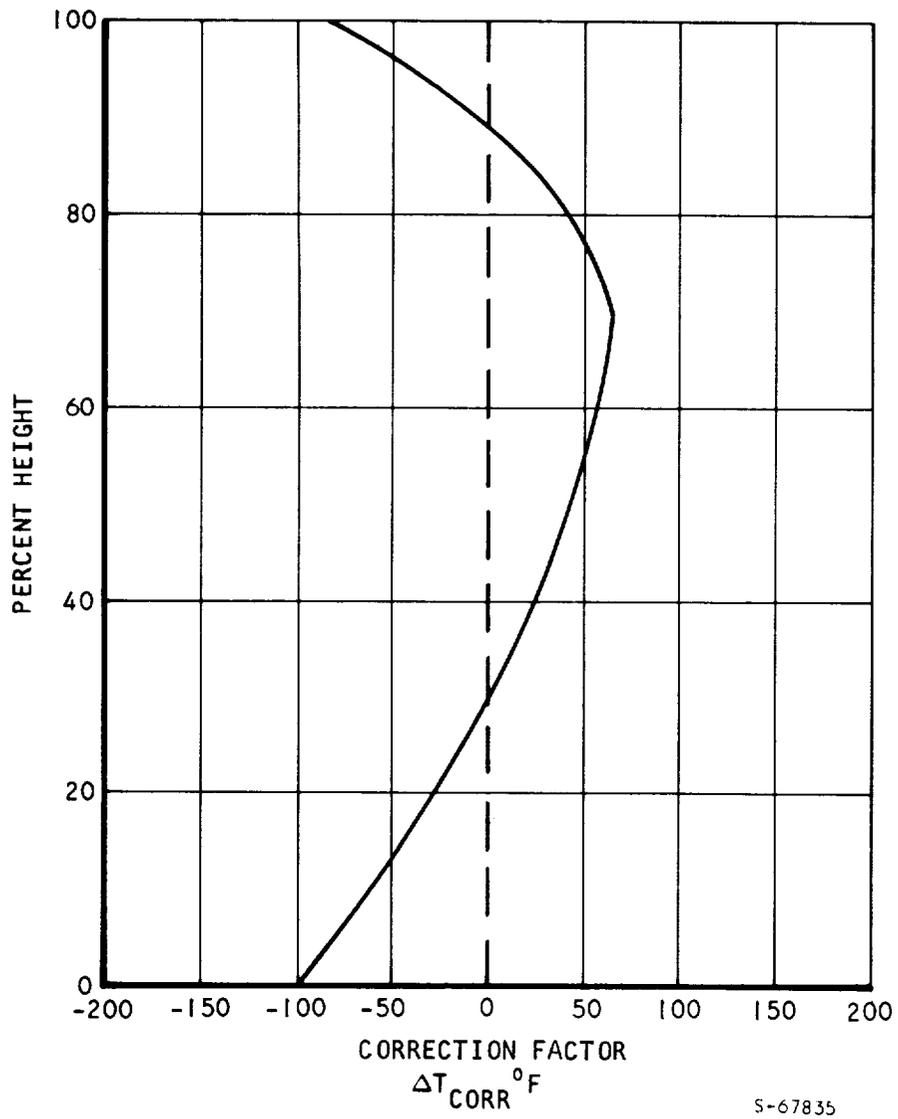
Figure 4-1. Typical AiResearch Radial Temperature
Profile Correction Factor

S-67835

$\left(V/V_{cr}\right)_0 = 0.231$
54.74°
$\left(V/V_{cr}\right)_1 = 0.896$
70.24°
$\left(W/W_{cr}\right)_1 = 0.549$
$U/V_{cr,1} = 0.415$
-20.74°
$\left(W/W_{cr}\right)_2 = 0.706$
-55.87°
$U/V_{cr,2} = 0.447$
$\left(V/V_{cr}\right)_2 = 0.435$
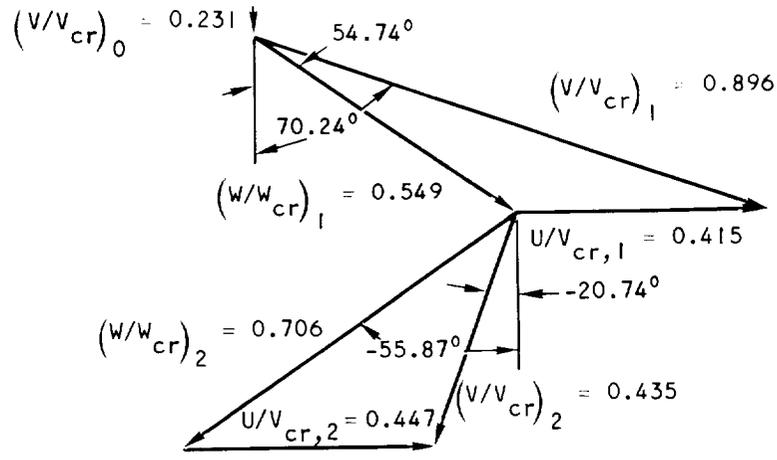
(a) Hub section; radius ratio, r/r_t, 0.733.

$\left(V/V_{cr}\right)_0 = 0.231$
$\left(V/V_{cr}\right)_1 = 0.775$
36.38°
67°
$\left(W/W_{cr}\right)_1 = 0.392$
$U/V_{cr,1} = 0.490$
-17.77°
$\left(W/W_{cr}\right)_2 = 0.749$
-58.26°
$U/V_{cr,2} = 0.528$
$\left(V/V_{cr}\right)_2 = 0.428$
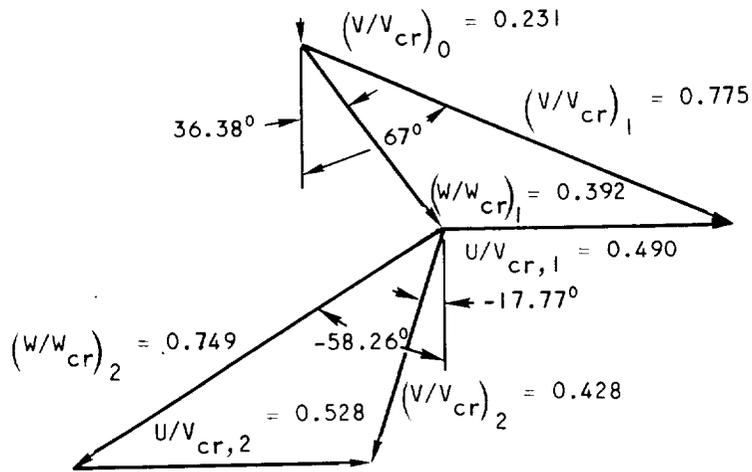
(b) Mean section; radius ratio, r/r_t, 0.8666.

$\left(V/V_{cr}\right)_0 = 0.231$
9.85°
$\left(V/V_{cr}\right)_1 = 0.689$
63.91°
$\left(W/W_{cr}\right)_1 = 0.318$
$U/V_{cr,1} = 0.566$
-15.52°
$\left(W/W_{cr}\right)_2 = 0.796$
-60.58°
$U/V_{cr,2} = 0.609$
$\left(V/V_{cr}\right)_2 = 0.422$
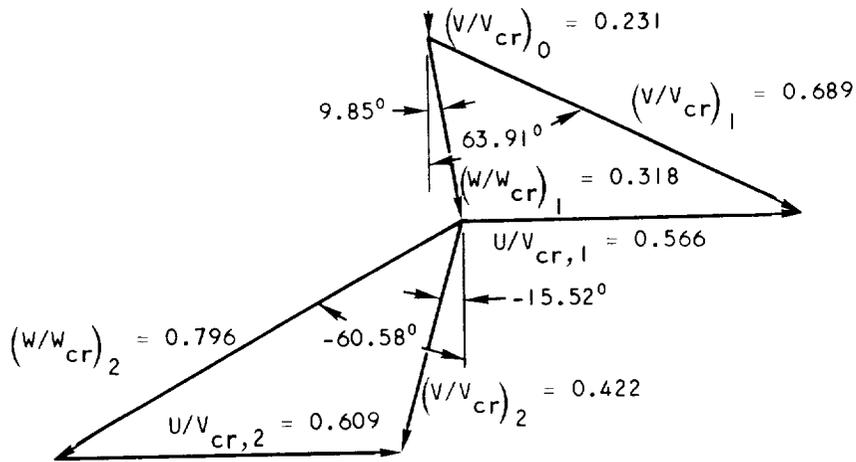
(c) Tip section; radius ratio, r/r_t, 1.000.

S-67836

Figure 4-2. Turbine Design Velocity Diagram
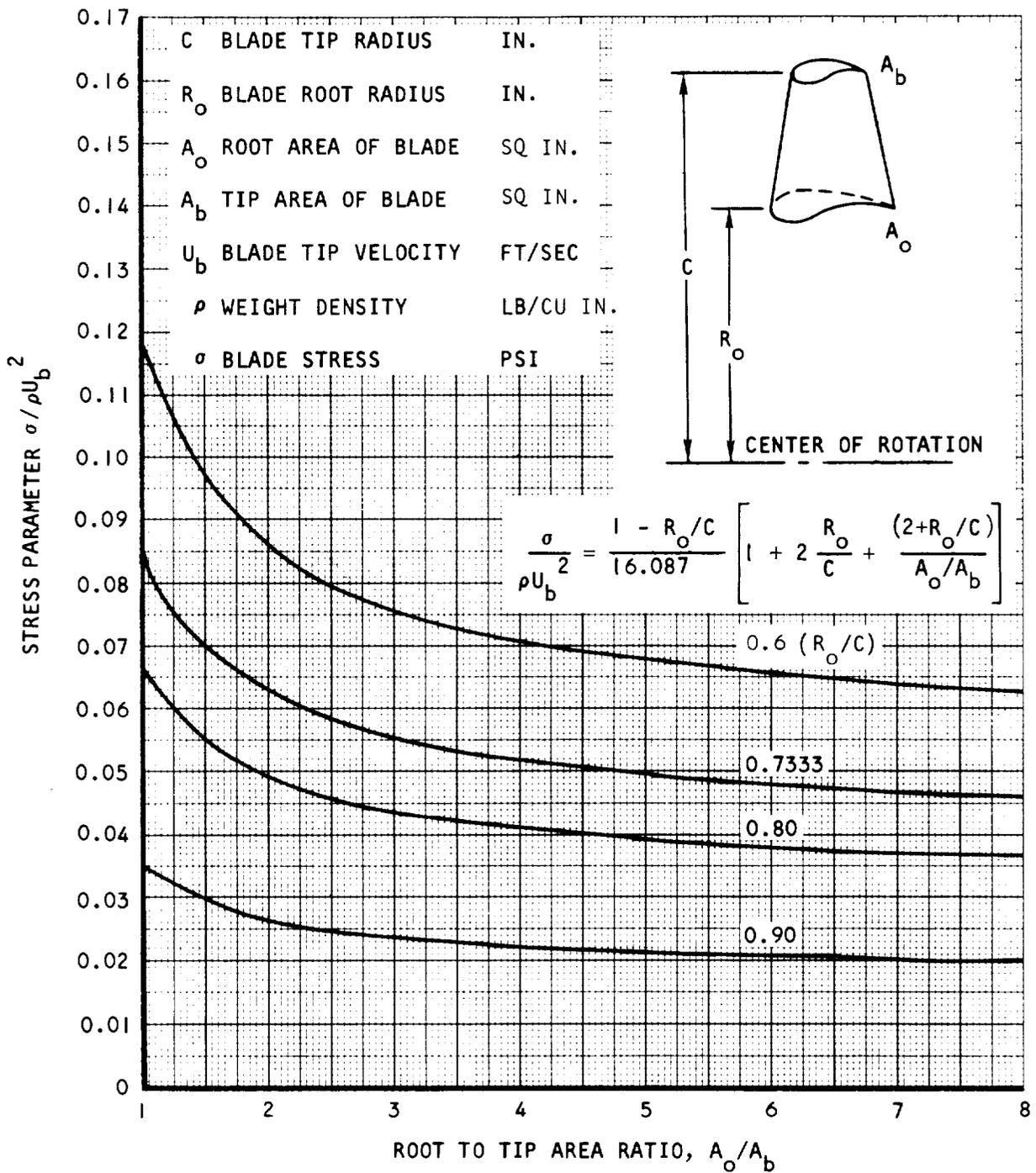
Figure 4-3. Centrifugal Root Stress of a Linearly
Tapered Turbine Blade
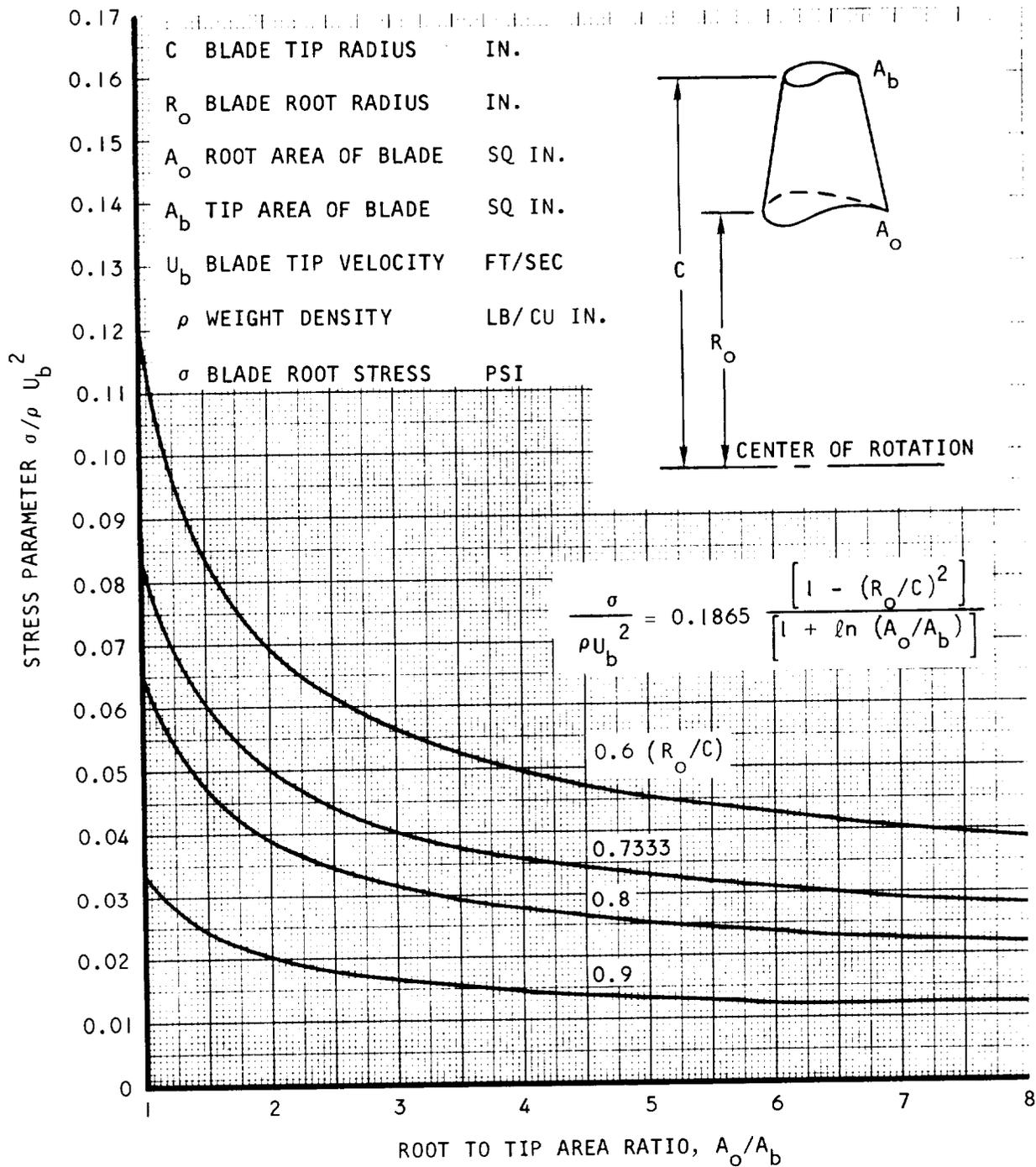
Figure 4-4. Centrifugal Stress in a Constant Stress Turbine Blade
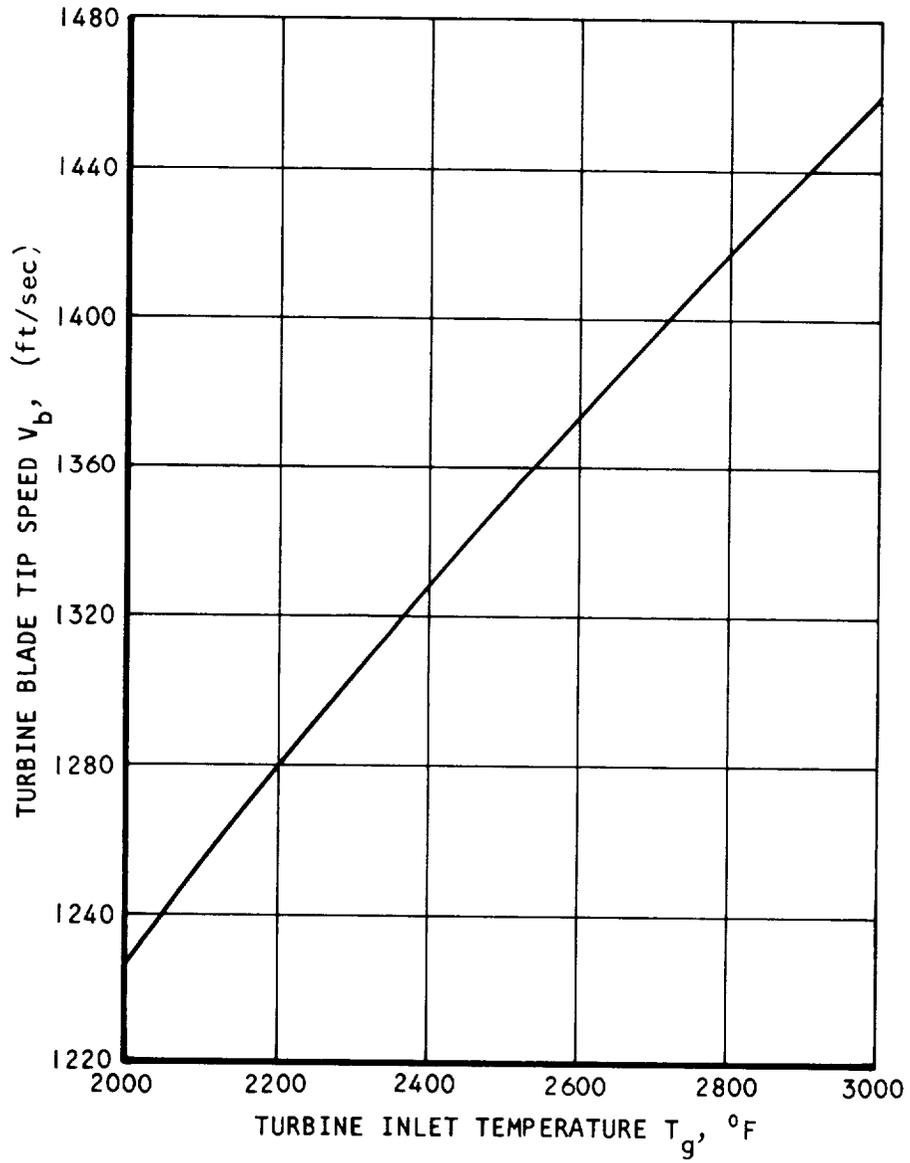
S-67838

Figure 4-5. Turbine Blade Tip Speed as a Function of
Turbine Inlet Temperature

S-67829
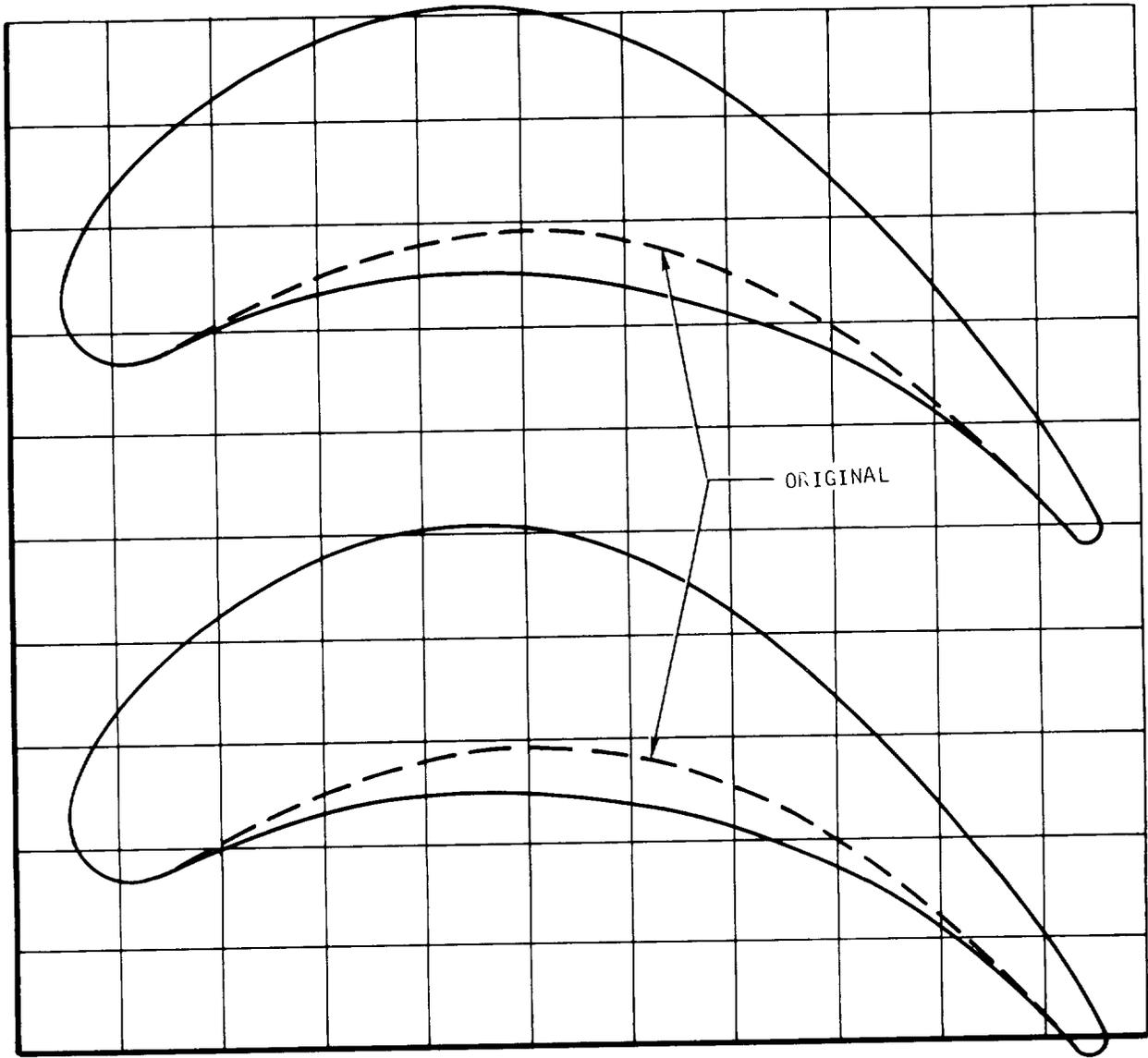
ORIGINAL

Figure 4-6. Comparison of the Original and Thickened Turbine Blade Configuration at the Hub Section (r/r_t = .733)
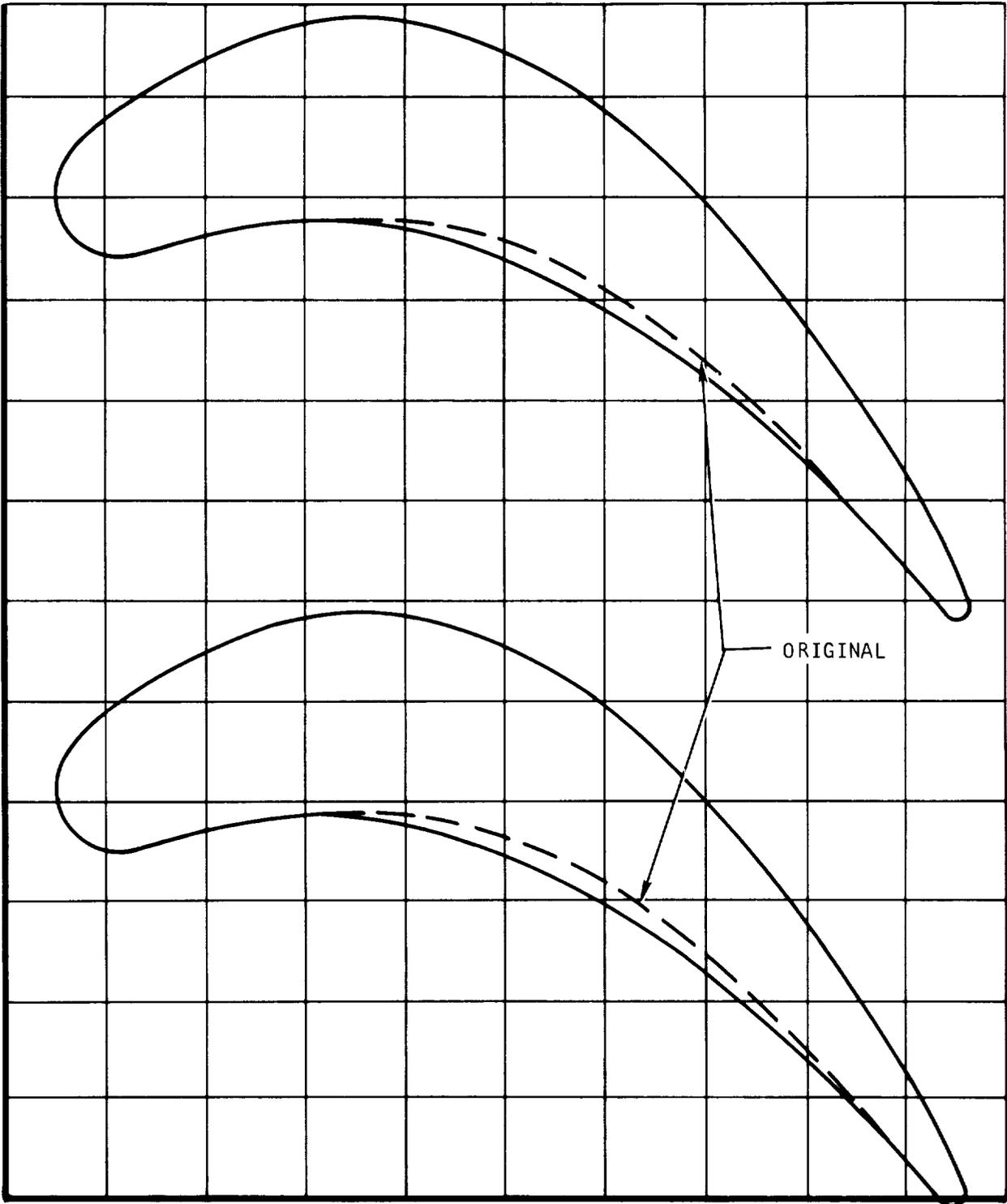
ORIGINAL

S-67840

Figure 4-7. Comparison of the Original and Thickened Turbine Blade
Configuration at the Mean Section (r/r_t = .866)

Figure 4-8. Blade Configuration at the Tip Section (r/r_t = 1.0)

To thicken the rotor hub section, the channels produced by the original blade shapes were laid out to a scale ten times actual size. This was done for the hub and mean sections only, as shown in Figures 4-6 and 4-7; the tip was left unchanged. Figure 4-9 shows the effect this thickening had upon the channel width. In both the hub and mean sections the original channel was diverging-converging as shown in Figure 4-9. In the process of thickening the mean section the channel was made to smoothly converge for the entire channel length. For the hub section it is impossible to avoid a diverging channel. The hub section was thickened by delaying the divergence and eliminating the convergence of the channel. It is felt that thickening of the blades in this manner will cause no decrease in the rotor performance. The critical surface velocity ratio profiles for the hub, mean, and tip sections of the blade are shown in Figures 4-10 through 4-15 for the original and thickened turbine blade configurations. The velocity profiles show that thickening of the rotor blades shifted the profiles up slightly to higher velocities as was expected. The characteristic shape for each of the three sections was not affected. The fact that the tip section profile increases along with the mean and hub indicates that there was some intra-blade shift of the gas flow to the greater radius. Judging from the way these profiles have shifted to higher velocities on both the suction and pressure surfaces the distribution of work for the thickened blade is not expected to be different from the original.

The effect of variation of the inlet total temperature 2200°F (1477.8°K), and 2600°F (1700°K), and 3000°F (1922.2°K) on the velocity profiles was small, and due to the variation of the gas properties.

A variation of the chord length for a constant temperature produced very small changes in the velocity profiles which can be attributed to the rounding off of the number of blades used in each case.

In summary, it can be said that the effects of chord and temperature change on the velocity profiles for a given set of blade shapes is negligible provided the vector diagram is unchanged (i.e., design is analyzed for on-design conditions) as was the condition here. Thickening of the blades did produce a significant change in the velocity profiles of the rotor, therefore, this should be taken into account for heat transfer analysis.

Results of this analysis indicate that the turbine blade configuration thickened at the hub and mean sections provides higher turbine inlet temperature capabilities with no decrease in aerodynamic performance. Therefore, the thickened blade configurations shown in Figures 4-6 through 4-8 were used for this study and the critical surface velocity ratio profiles shown in Figures 4-13 through 4-15 for the thickened blade were also used.

Results also indicated that the optimum metal area taper ratio for these cooled blade designs results from the use of a constant cooling flow area from the hub to the tip of the blade. This provides a large metal area taper ratio without restricting the cooling air flow.

54
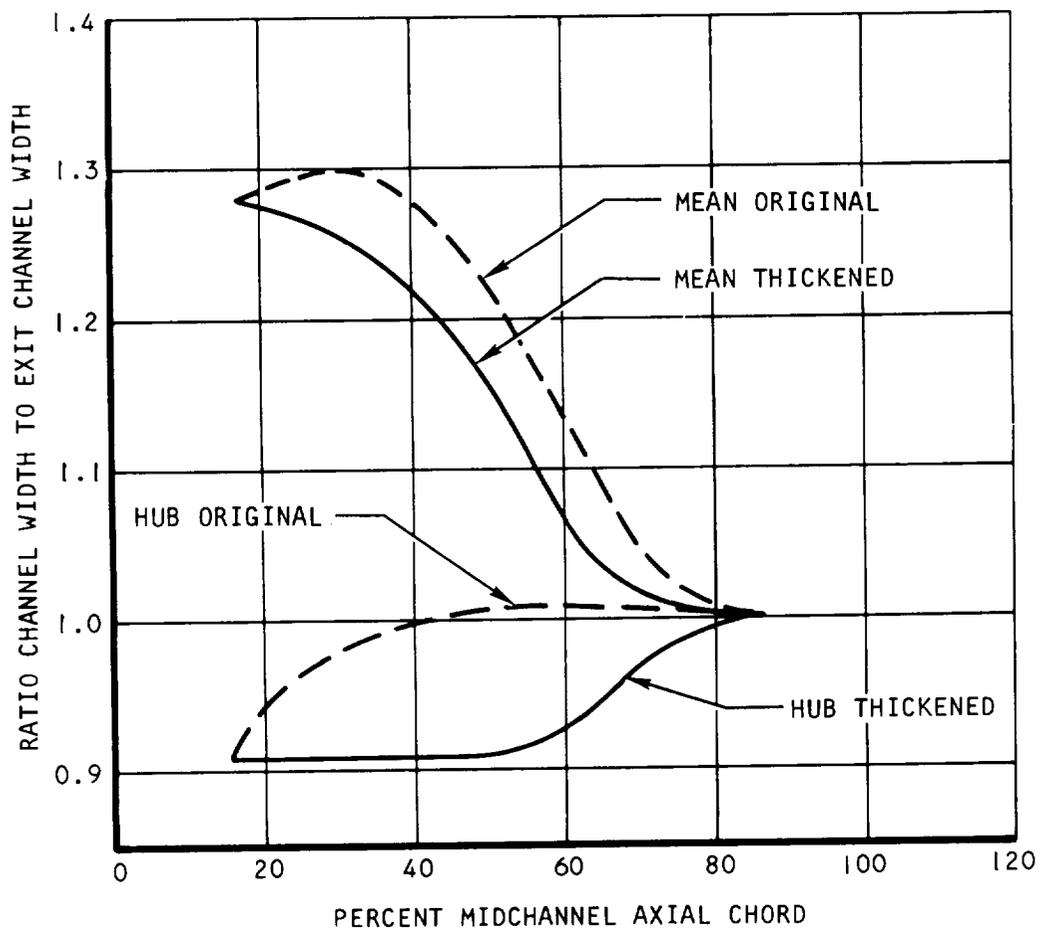
S-67842

Figure 4-9. Comparison of Channel Width Between the Original
and Thickened Blades

RELATIVE CRITICAL VELOCITY RATIO, V/V_{CR}

RATIO OF SURFACE DISTANCE FROM STAGNATION
POINT TO TOTAL SURFACE LENGTH
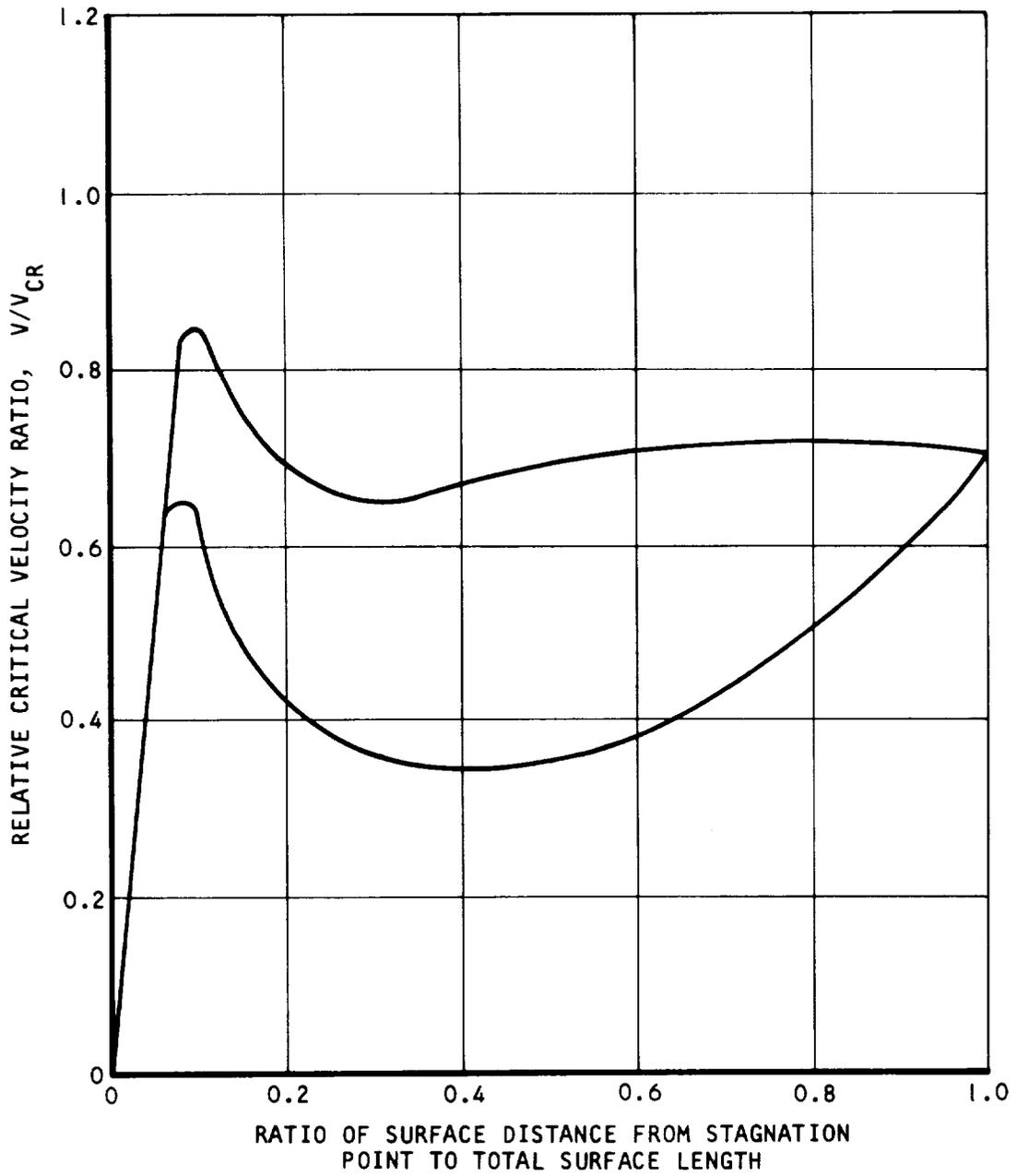
S-67843

Figure 4-10.   Rotor Blade Surface Velocity at the Hub R/R_t = .733 for the NASA
Turbine Blade Study Original Blade
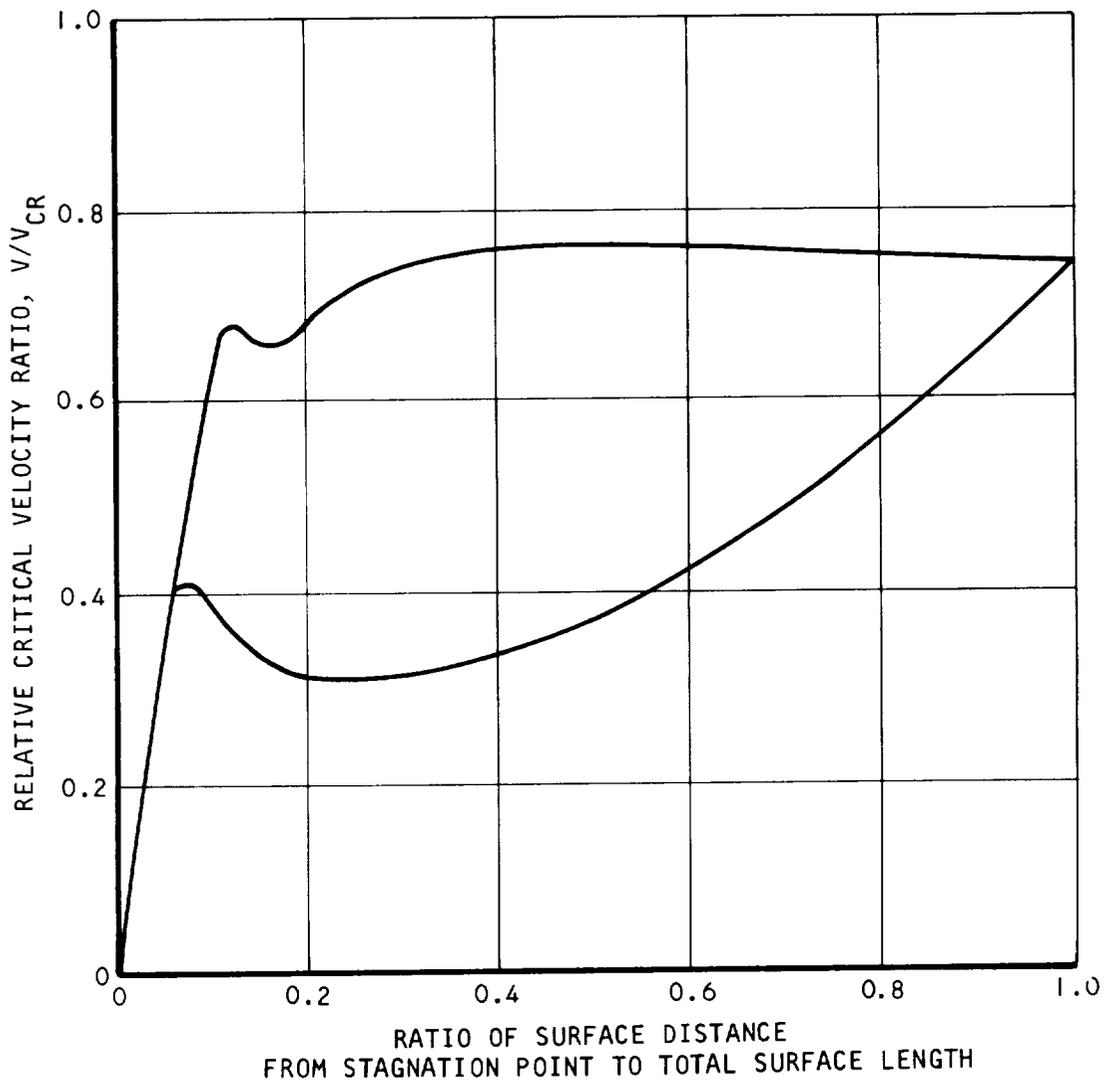
Figure 4-11. Rotor Blade Surface Velocity at the Mean R/R_t = .866 for the NASA Turbine Blade Study Original Blade
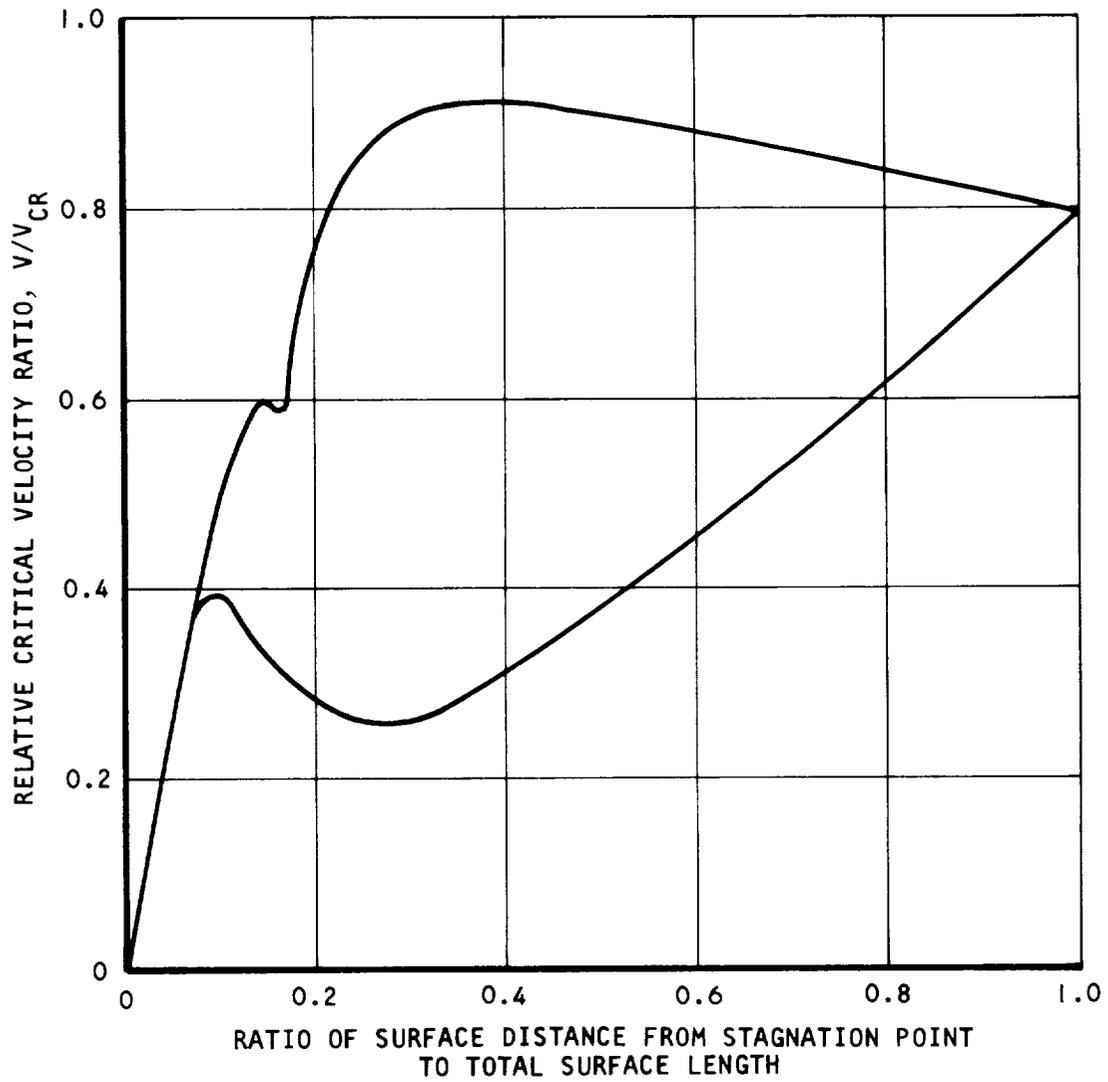
Figure 4-12. Rotor Blade Surface Velocity at the Tip R/R_t = 1.0 for the NASA Turbine Blade Study Original Blade
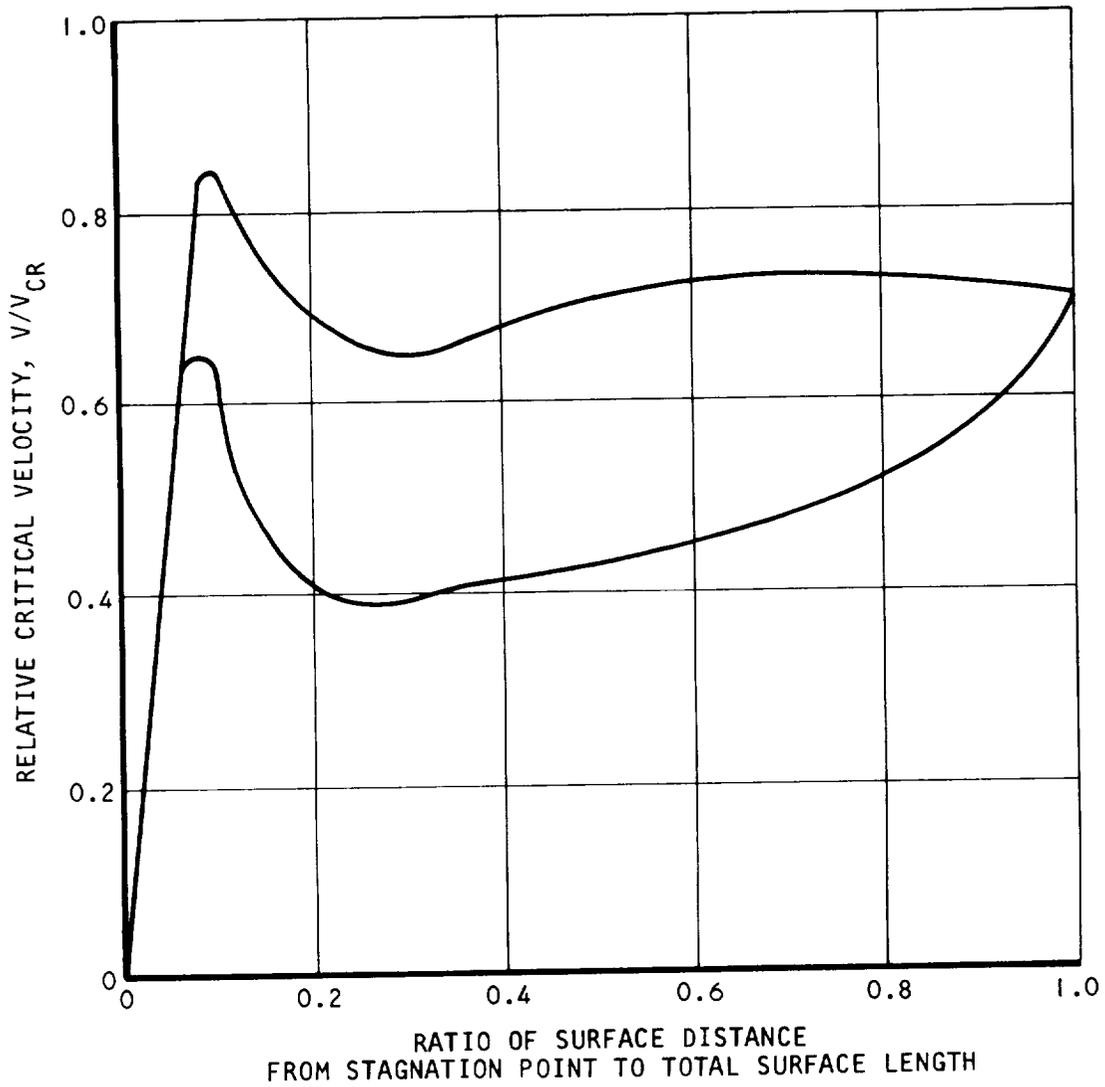
S-67845

Figure 4-13. Rotor Blade Surface Velocity at the Hub $R/R_t = .733$ for the NASA Turbine Blade Study Thickened Blade
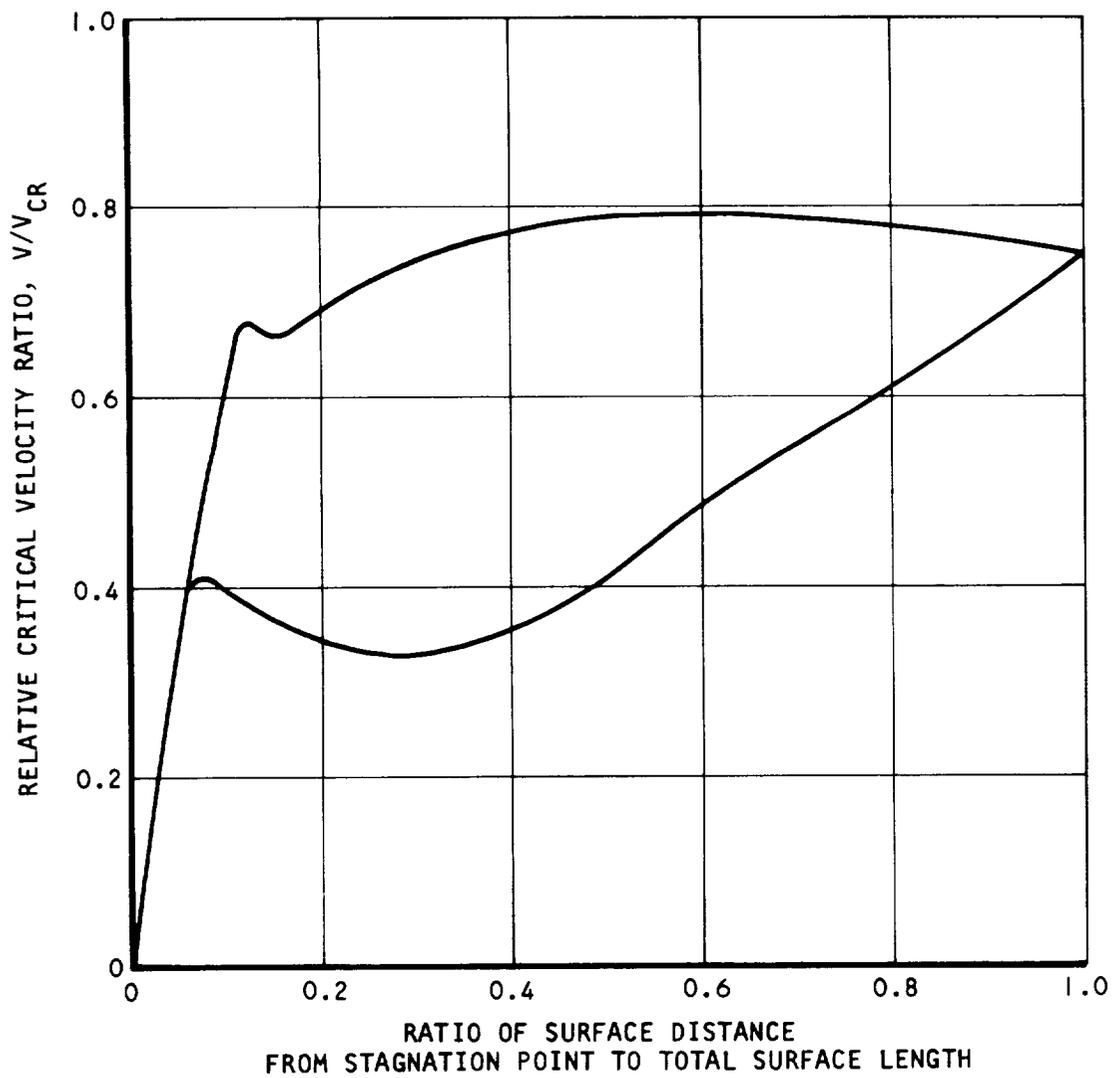
Figure 4-14. Rotor Blade Surface Velocity at the Mean R/R_t = .866 for the NASA Turbine Blade Study Thickened Blade
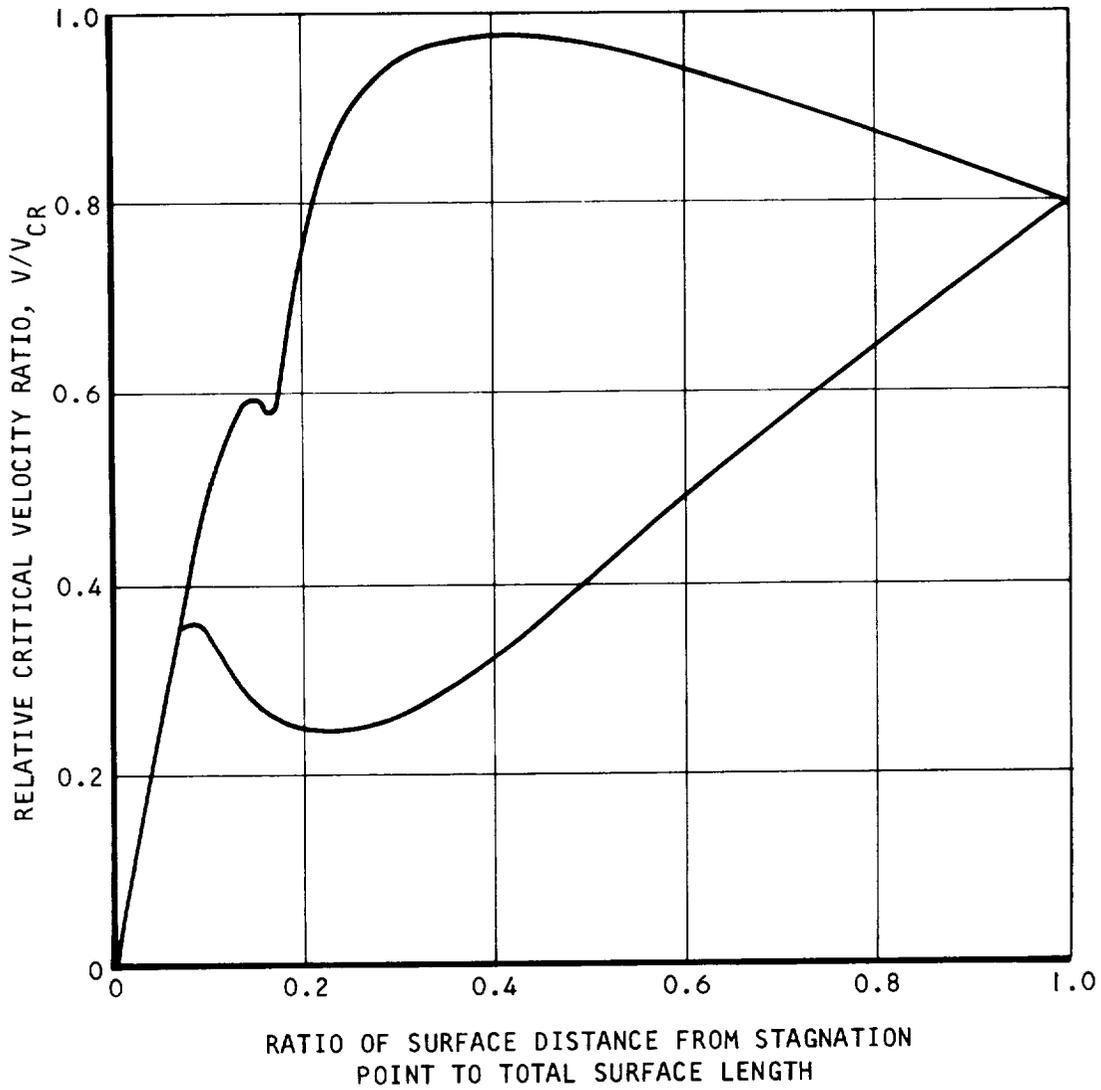
Figure 4-15. Rotor Blade Surface Velocity at the Tip $R/R_t = 1$ for the NASA Turbine Blade Study Thickened Blade

S-67848

TASK I FINAL DESIGN

For the final design analysis, two preliminary design configurations were selected and a detailed analysis was performed to finalize cooling passage dimensions, flow control orifice dimensions, impingement holes, trailing edge discharge holes, and film cooling holes. This analysis was performed for a design point condition as specified in the preliminary design analysis, and the maximum turbine inlet temperature capability for each design in the three chord sizes was determined for 1000 hr life. The blade life in this case was selected as the time to one percent creep strain after stress redistribution due to creep or the maximum coating life for IN-100 material, whichever was limiting.

Based on the design point cooling configuration, the maximum allowable turbine inlet temperature for 1000 hr life at each of the conditions specified in Table 4-4 was determined for each cooling configuration. The required flow control orifices were also determined for each of the design point conditions with a total pressure loss in ducting the cooling air from the compressor to the blade base, $\Delta P/P_{co}$, of 0.10.

Using the turbine inlet temperature determined in Table 4-4 for each cooling configuration using the 0.75 in. (0.01905 m) blade with a cooling air inlet temperature of 1200°F (922.2°K) and a turbine inlet total pressure of 150 psia (1.034 x 10⁶ Newtons/sq m), the cooling air flow required as a function of cooling air inlet temperature and chord size is determined for the conditions shown in Table 4-5. For this analysis, the turbine inlet temperature and turbine inlet pressure are held constant and the cooling air flow for 1000 life is determined at each condition. Cooling passage dimensions, impingement holes, trailing edge discharge holes, and film cooling holes are maintained the same and the flow control orifices are varied to obtain the required cooling air flow.

Three additional conditions from Table 4-4 and two additional conditions from Table 4-5 were selected for the 1.0 in. (0.0254 m) chord design to be analyzed with each condition treated as a design point condition.

TABLE 4-4

COOLING METHOD

Chord, in. (m)	0.75 (0.01905)			1.0 (0.0254)			1.5 (0.0381)		
Cooling air temperature, °F (°K)	1200 (922.1)	900 (755.6)	600 (588.9)	1200 (922.2)	900 (755.6)	600 (588.9)	1200 (922.2)	900 (755.6)	600 (588.9)
Turbine stator inlet total pressure, 450 psia (3.1×10^6 Newtons sq m)		X			X			X	
Turbine stator inlet total pressure, 150 psia (1.03×10^6 Newtons sq m)	X	*X	X	X	*X	X	X	*X	X
Turbine stator inlet total pressure, 50 psia (3.45×10^5 Newtons/sq m)		X			X			X	

*Design point condition

TABLE 4-5

COOLING METHOD

Chord, in. (m)	0.75 (0.01905)			1.0 (0.0254)			1.5 (0.0381)		
Turbine rotor inlet gas temperature, °F (°K)	Allowable turbine inlet temperature of the 0.75-in. (0.01905 m) chord blade determined above at 1200°F (922.1°K) cooling air temperature and 150 psia inlet total pressure								
Cooling air temperature °F (°K)	1200 (922.2)	900 (755.6)	600 (588.9)	1200 (922.2)	900 (755.6)	600 (588.9)	1200 (922.2)	900 (755.6)	600 (588.9)
Turbine stator inlet total pressure – 150 psia (1.03×10^6 Newtons sq m)	X	X	X	X	X	X	X	X	X

SECTION 5

ANALYTICAL RESULTS

TASK I   PRELIMINARY DESIGN

General

Sketches of each of the eight preliminary design turbine blade cooling configurations in each of the three chord sizes are shown in Figures 5-1 through 5-24. A summary of the preliminary design analysis of each configuration is shown in Table 5-1. The results are presented in various ways as described below. The metal cross sectional area weighted average metal temperature was calculated for the hub and mean sections of the blade as shown in equation 5-1.

$$\bar{T} = \frac{\sum\limits_{i=1}^{n} T_i A_i}{\sum\limits_{i=1}^{n} A_i} \qquad (5-1)$$

Using the weighted average metal temperature, the average metal temperature cooling effectiveness at the hub and mean sections of each blade was calculated from equations 5-2 and 5-3.

$$\phi_R = \frac{T_g - \bar{T}_R}{T_g - T_{c,i}} \qquad (5-2)$$

$$\phi_M = \frac{T_g - \bar{T}_M}{T_g - T_{c,i}} \qquad (5-3)$$

From the maximum outer surface temperature at the tip section, the maximum metal temperature effectiveness was calculated as shown in equation 5-4.

$$\phi_{max} = \frac{T_g - T_{max}}{T_g - T_{ci}} \qquad (5-4)$$

64

The weighted average cooling air outlet temperature was calculated from equation 5-5.

$$\bar{T}_{c,o} = \frac{\sum W_{c,o} T_{c,o}}{\sum W_{c,o}} \tag{5-5}$$

Using the weighted average cooling air outlet temperature, the cooling air thermal effectiveness was calculated as shown in equation 5-6.

$$\eta_t = \frac{\bar{T}_{c,o} - T_{c,i}}{\bar{T}_M - T_{c,i}} \tag{5-6}$$

Based on the largest difference between the maximum and minimum metal element temperature at a chordwise section of the blade, the maximum gradient ratio was calculated as shown in equation 5-7.

$$R_g = \frac{T_{max} - T_{min}}{T_g - T_{c,i}} \tag{5-7}$$

The maximum turbine inlet temperature may be limited by either a material strength temperature limit or a maximum oxidation-corrosion protective coating temperature limit. The maximum temperature limit for coated IN-100 with a minimum thickness of 0.02 in. (0.000508 m) is 1840°F (1277.8°K) for 1000 hr life. For thinner sections the temperature limit is somewhat lower. The material strength temperature limit is based on the combined stress of centrifugal load and thermal gradient at each section of the turbine blade. The stress life of each blade was based on the minimum life of a tensile stressed element as described in Method 2 of the stress analysis section of the report.

Detailed temperature, stress, and stress-to-rupture life at each element of each preliminary design cooled blade configuration is shown in Appendix I. The temperature distribution was calculated for the hub, mean, and tip sections using the thermal analyzer computer program (H0910) as described in Appendix B. Heat transfer equations used are presented in the analytical methods section of this report. Stress and stress-to-rupture life at each element was calculated using the stress analysis program described in Appendix H. Stress analysis considerations are also described in the analytical method section of this report.

Since the stress-to-rupture life calculated on this basis was not exactly 1000 hours for each blade configuration, the maximum turbine inlet temperature which would produce a life of 1000 hours at the critical stressed element of the blade was calculated as described below.

The strength of turbine blade materials may be expressed as stress corre-
lated as a function of the Larson-Miller parameter which relates time at tem-
perature. A typical relation between stress and the Larson Miller parameter
is shown in Figure 3-13. This relation indicates that for a given value of
stress, a single value of the Larson-Miller parameter relates the life at a
given metal temperature. Therefore if the stress in the element remained the
same as the metal temperature was reduced, the life would increase. This
method may be used to estimate the required turbine inlet temperature for
1000 hr life if it is assumed that the stress in the element remains the same
as the turbine inlet temperature is changed. For a turbine blade design with
an element having less than 1000 hr stress life, the Larson-Miller parameter
for the minimum life element with a temperature T_{ml} and a life θ_1 may be

equated to a metal temperature T_{m2} which would result in 1000 hr life (θ_2 =
1000) as shown in equations 5-8, 5-9, and 5-10.

$$(T_{m,2} + 460)(20 + \log \theta_2) = (T_{m,1} + 460)(20 + \log \theta_1) \qquad (5\text{-}8)$$

$$T_{m,2} = \frac{(T_{m,1} + 460)(20 + \log \theta_1)}{20 + \log \theta_2} - 460 \qquad (5\text{-}9)$$

If $\theta_2 = 1000$ hr

$$T_{m,2} = \frac{(T_{m,1} + 460)(20 + \log \theta_1)}{23} - 460 \qquad (5\text{-}10)$$

The turbine inlet temperature $(T_{g,1})$ for a metal temperature $(T_{m,1})$ and
a coolant inlet temperature $(T_{c,i})$ may be related to a turbine inlet tempera-
ture $(T_{g,2})$ for a metal temperature $(T_{m,2})$ and a coolant inlet temperature
$(T_{c,i})$ as shown in equations 5-11, 5-12, and 5-13.

$$\phi_1 = \frac{T_{g,1} - T_{m,1}}{T_{g,1} - T_{c,i}} \qquad (5\text{-}11)$$

$$\phi_2 = \frac{T_{g,2} - T_{m,2}}{T_{g,2} - T_{c,i}} \qquad (5\text{-}12)$$

$\phi_1 = \phi_2$ for a constant coolant flow and hot gas flow

Then
$$T_{g2} = \frac{T_{m2} - \phi_1 T_{c,i}}{1 - \phi_1}$$
(5-13)

In the case of an element with less than 1000 hr life initially, this method is conservative because as the turbine inlet temperature is lowered, the thermal gradients and the turbine tip speed is reduced which results in decreased stress in the element and an increase in the Larson-Miller parameter. In the case of an element with greater than 1000 hr life initially, the reverse is true.

Comparing the maximum turbine inlet temperature from oxidation-corrosion considerations and the maximum turbine inlet temperature from stress considerations, the limiting condition is given in Table 5-1 as the maximum turbine inlet temperature for 1000 hr life. The limiting condition and the critical section of the blade is also specified.

A summary of the aerodynamic effects of turbine blade cooling for each of the preliminary design configurations is shown in Table 5-2. This table was generated from information presented in the aerodynamics section. The results indicate that thickening of the trailing edge and transpiration cooling produce the largest losses in turbine efficiency. The effect of increased aspect ratio partially compensates for the effect of increased trailing edge thickness for the small chord blades. The effect of film cooling on turbine efficiency is relatively small, however the method used may not be applicable to these conditions.

A discussion of the effects of chord size on each cooling design from the preliminary design analysis is presented below.

Scheme A-1 Convection Cooled Cast Two-Cavity Pin Fin Blade

The convection cooled cast two-cavity pin fin blade is shown in Figures 5-1, 5-2, and 5-3 for the 0.75 in. (0.01905 m), 1.0 inch (0.0254 m), and 1.5 inch (0.0381 m) chord designs respectively. The cooling air enters the leading edge and center passages at the root and flows radially outward. The leading edge flow discharges at the tip of the blade and the center passage flow discharges at the trailing edge and the blade tip.

The leading-edge cavity uses transverse fins around the inside leading-edge surface. A fin spacing of 0.18 in. (0.004572 m) center-to-center and a fin height of 0.20 in. (0.000508 m), 0.025 in. (0.000635 m), and 0.03 in. (0.000762 m) was selected for the 0.75 in. (0.01905 m), 1.0 in. (0.0254 m), and 1.5 in. (0.0381 m) chord blades respectively. A review of the transverse fin data presented in the heat transfer analysis section indicated that this height and spacing would produce to a value close to the maximum cooling effectiveness for transverse fins.

TABLE 5-1

SUMMARY OF THE RESULTS FOR THE PRELIMINARY DESIGN TASK I ANALYSIS
$P_g = 150$ PSIA $(1.0342 \times 10^6$ NEWTONS/SQ M$)$ $T_{ci} = 900°F$ $(755.6°K)$

Scheme No.	Chord in. (m)	T_g Analysis °F (°K)	$\frac{W_{CA}(100)}{W_g}$	ϕ_R	ϕ_M	q_{max}	η_t	R_g	Stress Critical Section	T_g Maximum °F (K)	Critical Condition	Critical Section
A-1	0.75 (0.01905)	2300 (1533.3)	4.4	0.7043	0.5827	0.3429	0.7899	0.2957	Root	2330 (1550)	1	Tip
A-1	1.0 (0.0254)	2400 (1588.8)	4.98	0.6534	0.545	0.3721	0.6388	0.2267	Root	2397 (1587.2)	1	Tip
A-1	1.5 (0.0381)	2600 (1700)	8.32	0.6727	0.5947	0.4516	0.4738	0.2124	Root	2614 (1707.7)	1	Tip
A-3	0.75 (0.01905)	2300 (1533.3)	4.04	0.6017	0.5252	0.325	0.6964	0.2593	Tip	2393 (1529.4)	1	Tip
A-3	1.0 (0.0254)	2400 (1588.8)	4.25	0.6107	0.5418	0.3619	0.6931	0.228	Tip	2373 (1573.9)	1	Tip
A-3	1.5 (0.0381)	2400 (1588.8)	3.82	0.6003	0.5538	0.4059	0.7381	0.2107	Tip	2410 (1594.4)	3	Mean
A-6	0.75 (0.01905)	2450 (1616.6)	3.9	0.6299	0.5678	0.444	0.7522	0.2690	Root	2447 (1615)	2	Tip
A-6	1.0 (0.0254)	2500 (1644.4)	3.9	0.6528	0.580	0.4675	0.7664	0.3	Root	2515 (1652.8)	2	Tip
A-6	1.5 (0.0381)	2550 (1672.2)	4.16	0.6859	0.626	0.4889	0.8404	0.3291	Root	2552 (1673.3)	3	Mean
A-7	0.75 (0.01905)	2400 (1588.8)	4.77	0.5803	0.4831	0.3887	0.5039	0.194	Root	2221 (1489.4)	3	Mean
A-7	1.0 (0.0254)	2400 (1588.8)	5.07	0.5802	0.5157	0.4203	0.4973	0.2433	Root	2355 (1563.9)	3	Mean
A-7	1.5 (0.0381)	2450 (1616.6)	4.82	0.5666	0.5058	0.4209	0.4675	0.1948	Root	2309 (1538.3)	3	Mean
B-1	0.75 (0.01905)	2450 (1616.6)	5.76	0.7132	0.6369	0.4126	0.4832	0.2284	Root	2457 (1620.5)	3	Mean
B-1	1.0 (0.0254)	2500 (1644.4)	5.53	0.7229	0.6404	0.4902	0.5559	0.2156	Root	2607 (1803.9)	3	Mean
B-1	1.5 (0.0381)	2500 (1644.4)	6.05	0.667	0.6043	0.482	0.3492	0.2069	Root	2605 (1802.8)	3	Mean
B-4	0.75 (0.01905)	2250 (1505.5)	4.27	0.5957	0.5201	0.3979	0.5508	0.1259	Root	2193 (1473.9)	3	Mean
B-4	1.0 (0.0254)	2300 (1533.3)	4.89	0.5945	0.5677	0.418	0.5592	0.3014	Root	2389 (1583.8)	3	Root
B-4	1.5 (0.0381)	2300 (1533.3)	4.06	0.5781	0.5326	0.4439	0.5125	0.2086	Root	2244 (1502.2)	3	Mean
B-5	0.75 (0.01905)	2600 (1700)	6.43	0.6797	0.6587	0.4718	0.4642	0.2241	Tip	2680 (1744.4)	1	Tip
B-5	1.0 (0.0254)	2600 (1700)	5.58	0.6621	0.6278	0.5191	0.4642	0.16706	Root	2770 (1794.4)	3	Root
B-5	1.5 (0.0381)	2600 (1700)	5.4	0.6443	0.5777	0.4689	0.4017	0.1606	Root	2563 (1679.4)	3	Mean
C-1	0.75 (0.01905)	2450 (1616.6)	3.89	0.7094	0.6417	0.3915	0.6197	0.4135	Root	2371 (1572.8)	3	Mean
C-1	1.0 (0.0254)	2500 (1644.4)	4.31	0.8018	0.7251	0.4004	0.7201	0.4913	Root	2468 (1626.7)	1	Tip
C-1	1.5 (0.0381)	2800 (1811.1)	5.29	0.847	0.7802	0.5397	0.7785	0.4079	Root	2942 (1890)	1	Tip

CRITICAL CONDITIONS

1. Turbine inlet temperature limited by maximum coating temperature of 1840°F (1277.8°K) for 1000 hr life with 0.02 in. (0.000508 m) thick IN-100 material.
2. Turbine inlet temperature limited by maximum coating temperature of 1760°F (1233.3°K) for 1000 hr life with 0.008 in. (0.0002032 m) thick IN-100 material.
3. Turbine inlet temperature limited by minimum stress to rupture life of 1000 hr for all tensile stressed elements before creep relaxation of the thermal stresses.

TABLE 5-2

AERODYNAMIC EFFECTS OF TURBINE COOLING
FOR EACH PRELIMINARY DESIGN

Scheme No.	Chord in. (m)	$\dfrac{W_{ca}}{W_g}$ (100)	Cooling Air Pumping Loss hp (kw)	Aspect Ratio Effect (η/η_o)	Trailing Edge Thickness Effect (η/η_o)	Film Cooling Effect ($\Delta\eta$)	Transpiration Cooling Effect ($\Delta\eta$)	Cooling Air Tip Discharge
A-1	0.75 (0.01905)	4.4	61.3 (45.53)	0.999	0.984	-0.0005	-	Yes
A-1	1.0 (0.0254)	4.98	70.7 (52.7)	0.995	0.984	-	-	Yes
A-1	1.5 (0.0381)	8.32	126.8 (94.52)	0.988	0.984	-	-	Yes
A-3	0.75 (0.01905)	4.04	54.1 (40.31)	0.999	0.964	-	-	Yes
A-3	1.0 (0.0254)	4.25	58.1 (43.39)	0.995	0.976	-	-	Yes
A-3	1.5 (0.0381)	3.82	53.2 (39.67)	0.988	0.984	-	-	Yes
A-6	0.75 (0.01905)	3.9	46.3 (34.5)	0.999	0.976	-0.0007	-	No
A-6	1.0 (0.0254)	3.9	47.3 (35.24)	0.995	0.984	-0.0005	-	No
A-6	1.5 (0.0381)	4.16	50.4 (37.55)	0.988	0.984	-0.0007	-	No
A-7	0.75 (0.01905)	4.77	56.4 (42.07)	0.999	0.959	-0.0004	-	No
A-7	1.0 (0.0254)	5.07	59.35 (44.31)	0.995	0.971	-0.0004	-	No
A-7	1.5 (0.0381)	4.82	57.5 (42.88)	0.988	0.984	-0.0003	-	No
B-1	0.75 (0.01905)	5.76	69.3 (51.68)	0.999	0.984	-0.0038	-	Yes
B-1	1.0 (0.0254)	5.53	66.6 (49.63)	0.995	0.984	-0.0037	.-	Yes
B-1	1.5 (0.0381)	6.05	72.8 (54.29)	0.988	0.984	-0.0039	-	Yes
B-4	0.75 (0.01905)	4.27	49.6 (36.99)	0.999	0.959	-0.0006	-	No
B-4	1.0 (0.0254)	4.89	56.9 (42.43)	0.995	0.971	-0.0007	-	No
B-4	1.5 (0.0381)	4.06	47.3 (35.24)	0.988	0.984	-0.0007	-	No
B-5	0.75 (0.01905)	6.43	78.5 (58.5)	0.999	0.976	-0.0029	-	No
B-5	1.0 (0.0254)	5.58	68.1 (50.78)	0.995	0.984	-0.0024	-	No
B-5	1.5 (0.0381)	5.4	65.9 (49.14)	0.988	0.984	-0.0023	-	No
C-1	0.75 (0.01905)	3.89	46.4 (34.56)	0.999	0.984	-	-0.045	No
C-1	1.0 (0.0254)	4.31	51 (38.03)	0.995	0.984	-	-0.052	No
C-1	1.5 (0.0381)	5.29	66.5 (49.6)	0.988	0.984	-	-0.071	No

TIP SECTION
(75 PERCENT SPAN)

MEAN SECTION
(50 PERCENT SPAN)

TRANSVERSE FINS
0.02 IN. HIGH
0.02 IN. THICK
0.18 IN. CENTER-TO-CENTER
SPACING

PIN FINS
0.02 IN. DIAMETER
0.06 IN. TRIANGULAR
CENTER-TO-CENTER
SPACING

HUB SECTION
(5 PERCENT SPAN)

NO PIN FINS

S-67849

WIDE SPACED
PIN FINS
0.12 INCH TRIANGULAR
CENTER-TO-CENTER
SPACING

CLOSE SPACED
PIN FINS

NO PIN FINS

Figure 5-1. Scheme A-I Convection Cooled Cast Two-Cavity Pin Fin Blade
0.75 in. (0.01905 m) Chord

TIP SECTION
75 PERCENT SPAN

MEAN SECTION
50 PERCENT SPAN

PIN FINS

0.025 IN. DIAMETER
0.075 IN. TRIANGULAR CENTER-
TO-CENTER SPACING

HUB SECTION
5 PERCENT SPAN

TRANSVERSE FINS

0.025 IN. HIGH
0.02 IN. THICK
0.18 IN. CENTER-TO-
CENTER SPACING

S-67850

Figure 5-2. Scheme A-1 Convection Cooled Cast Two-Cavity
Pin Fin Blade, 1.0 in. (0.0254 m) Chord

71

PIN FINS
0.03 IN. DIA
0.09 IN. TRIANGULAR CENTER-TO-CENTER SPACING

TIP SECTION
75 PERCENT SPAN

MEAN SECTION
50 PERCENT SPAN

HUB SECTION
5 PERCENT SPAN

TRANSVERSE FINS
0.03 IN. HIGH
0.02 IN. THICK
0.18 IN. CENTER-TO-CENTER SPACING
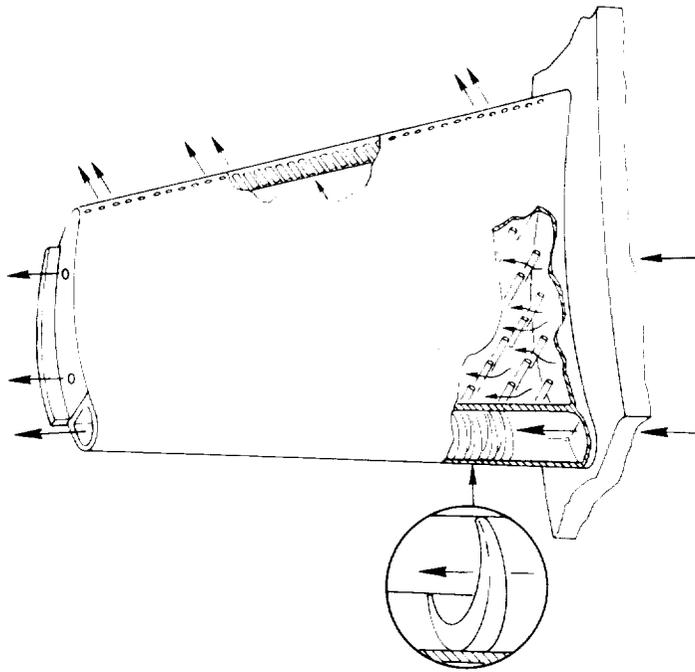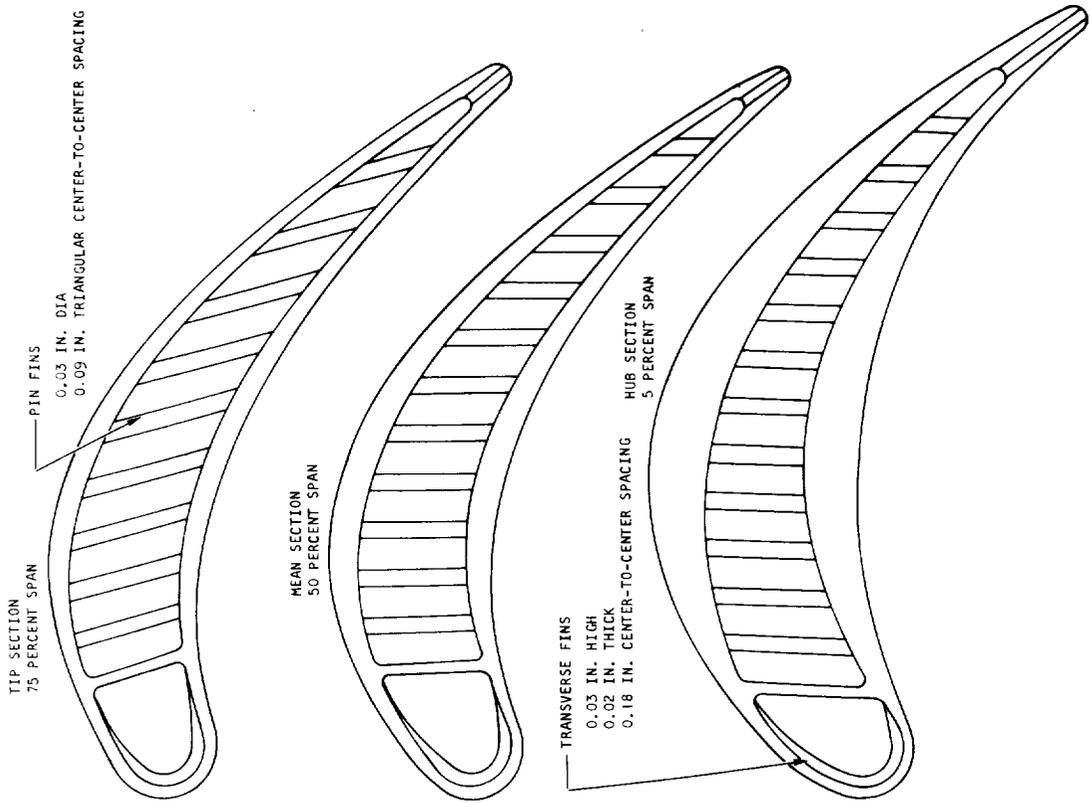
S-67851
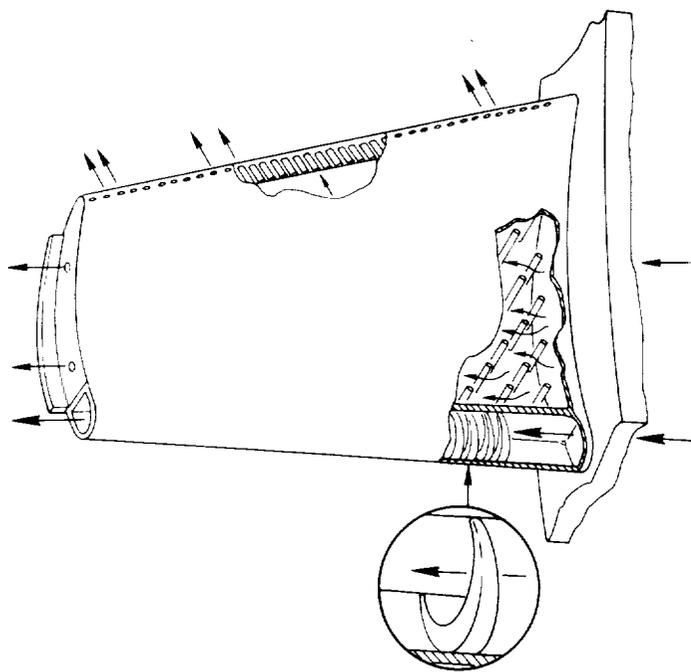
Figure 5-3. Scheme A-1 Convection Cooled Cast Two-Cavity Pin Fin
Blade, 1.5 in. (0.0381 m) Chord

The center passage is cooled by the use of triangular spaced pin fins. The triangular spaced pin fins promote cooling air turbulence and increase the cooling effectiveness of the design. For example, 0.02 in. (0.000508 m) diameter pins on 3-diameter center-to-center spacing will more than triple the basic heat transfer coefficient over that of an unfinned channel. Also, the pin fins increase the surface area, and thus increase the internal cooling potential. The pin fins used in this design were placed on a three-diameter center-to-center equilateral triangular spacing. Pin diameters of 0.02 in. (0.000508 m), 0.025 in. (0.000635 m), and 0.03 in. (0.000762 m) were used for the 0.75 in. (0.01905 m), 1.0 in. (0.0254 m), and 1.5 in. (0.0381 m) chord designs respectively. This pin diameter and spacing is within current casting technology capabilities.

The 0.75 in. (0.01905 m) chord pin fin blade uses a film cooled trailing edge to maintain the design limit on trailing edge thickness. The increased trailing edge thickness of the 1.0 (0.0254 m) and 1.5 in. (0.0381 m) chord blades permits the use of trailing edge discharge through a row of holes in the trailing edge. The film cooling relation of Hatch and Papell (Reference 78 and Appendix C) was used for the 0.75 in. (0.01905 m) chord blade film cooled trailing edge. The heat transfer analysis of the trailing edge discharge holes included the entrance effect multiplying factor of Nunner (Reference 44).

The analytical results for this design indicate that the turbine inlet temperature may be increased substantially by increasing the chord; however the cooling flow required for temperatures above 2400°F (1588.9°K) becomes very large. The radial flow design produces a high cooling effectiveness for the hub and mean sections of the blade, but the maximum metal temperature effectiveness is somewhat restricted. The pin fin heat transfer surface produces a high cooling air thermal effectiveness at low cooling air flow rates, but due to the heat transfer characteristics of this surface, the effectiveness decreases rapidly as the cooling air flow increases.

The limiting element for the 0.75 in. (0.01905 m) chord design is the film cooling trailing edge at the tip section of the blade. Since the film temperature increases about 100°F (55.6°K) from the point of injection to the end of the trailing edge, additional film flow would not significantly increase the allowable turbine inlet temperature. An increase in cooling flow through the center pin fin cavity would produce a lower film injection temperature which could cause an increase in the allowable turbine inlet temperature; however, additional thermal gradients would be imposed on the blades by overcooling the middle cavity.

The limiting element for the 1.0 in. (0.0254 m) chord design is the convection cooled trailing edge at the tip section. The trailing edge holes are pressure drop limited at the tip section so the only way additional cooling can be provided is by additional flow through the center cavity which would reduce the cooling air temperature at the tip section. This additional flow would produce additional thermal gradients by overcooling the middle cavity.

The limiting element for the 1.5 in. (0.0381 m) chord design is also the convection cooled trailing edge at the tip section. This design demonstrates the capability of operation at high turbine inlet temperatures, however the cooling flow required is very large (8.32 percent of the hot gas flow).

Table 5-2 indicates that this design has the minimum aerodynamic penalty due to cooling. No thickening of the trailing edge is required and most of the cooling air discharges from the blade tip, giving a lower effective tip clearance.

This configuration represents the minimum fabrication complexity for present casting technology along with a high turbine inlet temperature capability. It was therefore recommended for a final design analysis.

Scheme A-3 Convection Cooled Fabricated Radial Flow Plate Fin Blade

This concept shown in Figures 5-4, 5-5, and 5-6 for the 0.75 in. (0.01905 m), 1.0 in. (0.0254 m), and 1.5 in. (0.0381 m) chord designs respectively, combines radial and chordwise cooling air flow. The cooling air flows radially through the leading edge finned passage and four additional finned passages on each side of the supply tube. Cooling air also flows radially through the supply tube, discharges from the trailing edge of the supply tube, impinges on each side of the blade, and flows chordwise through the finned passage in the trailing edge of the blade. The fins used in this design were 40 fins/in. (15.75 fins/cm) rectangular plate fins 0.002 in. (0.0000508 m) thick. Plain fins were used at the leading edge of each design because the offset fins provided too much flow restriction for adequate cooling air flow. Offset fins were used for the four finned passages on each side of the blade because less cooling air flow was required and a higher heat transfer coefficient was desirable. The fin height used in each of these areas was 0.02 in. (0.000508 m).

The trailing edge fin passage was 0.02 in. (0.000508 m) high throughout for the 0.75 in. (0.01905 m) chord design with a plain fin for the first 0.2 in. (0.00508 m) and an offset fin for the last 0.15 in. (0.00381 m) of length. A 0.04 in. (0.001016 m) high offset fin was used for the first 0.2 in. (0.00508 m) with a 0.02 in. (0.000508 m) high offset fin for the last 0.2 in. (0.00508 m) in the trailing edge of the 1.0 in. (0.0254 m) chord design. A 0.04 in. (0.001016 m) high fin combined with a 0.02 in. (0.000508 m) high fin was also used in the trailing edge of the 1.5 inch (0.0381 m) chord design. The trailing edge of the 0.75 in.(0.01905 m) chord design was thickened from the design point thickness of 0.0225 in. (0.0005715 m) to 0.04 in. (0.001016 m). The trailing edge of the 1.0 in. (0.0254 m) chord design was also thickened from the design point thickness of 0.03 in. (0.000762 m) to 0.04 in. (0.001016 m). No thickening was required for the 1.5 in. (0.0381 m)

74

TIP SECTION
95 PERCENT SPAN

MEAN SECTION
50 PERCENT SPAN

HUB SECTION
5 PERCENT SPAN

OFFSET FINS
40 FINS/IN.
0.02 IN. HIGH
0.002 IN. THICK FIN

IMPINGEMENT HOLES
44-.015 INCH DIA

RECTANGULAR FINS
PLAIN OFFSET
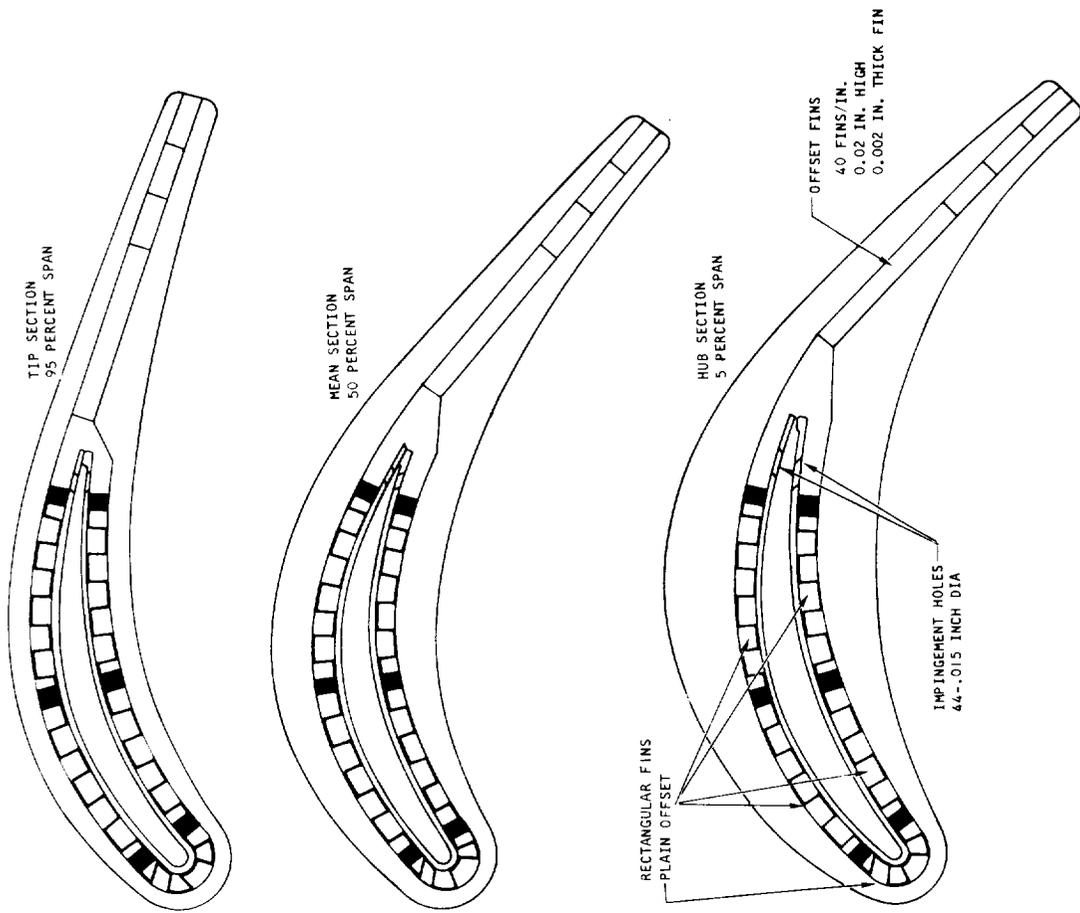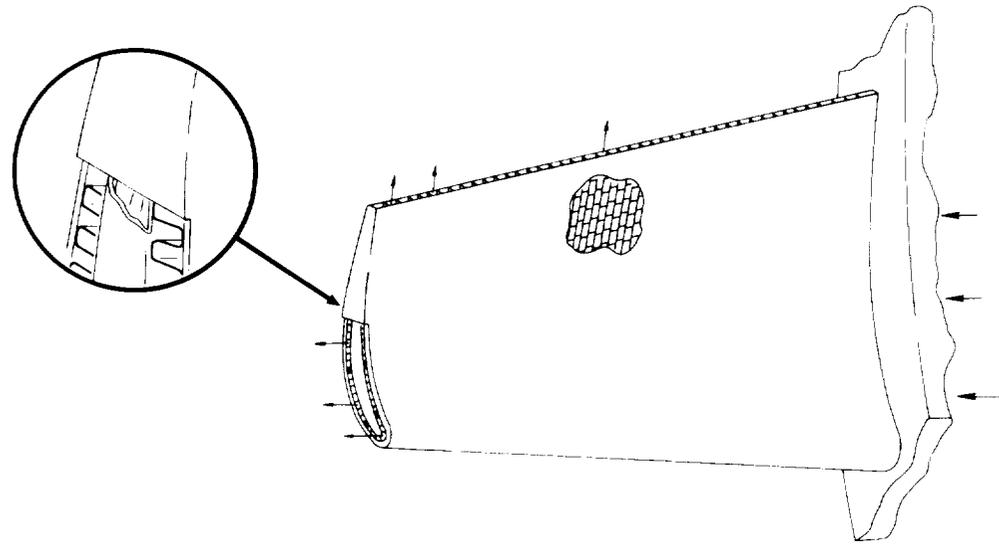
S-67852

Figure 5-4.   Scheme A-3 Convection Cooled Fabricated Radial Flow
Plate Fin Blade 0.75 in. (0.01905 m) Chord

TIP SECTION
75 PERCENT SPAN

MEAN SECTION
50 PERCENT SPAN

HUB SECTION
5 PERCENT SPAN

IMPINGEMENT HOLES
.118-.015 INCH DIA

RECTANGULAR FINS OFFSET
40 FINS/IN.
0.02 IN. HIGH
0.002 IN. THICK FIN

0.04 IN. HIGH

RECTANGULAR FINS PLAIN

RECTANGULAR FINS
PLAIN (HUB AND MEAN)
OFFSET (TIP ONLY)
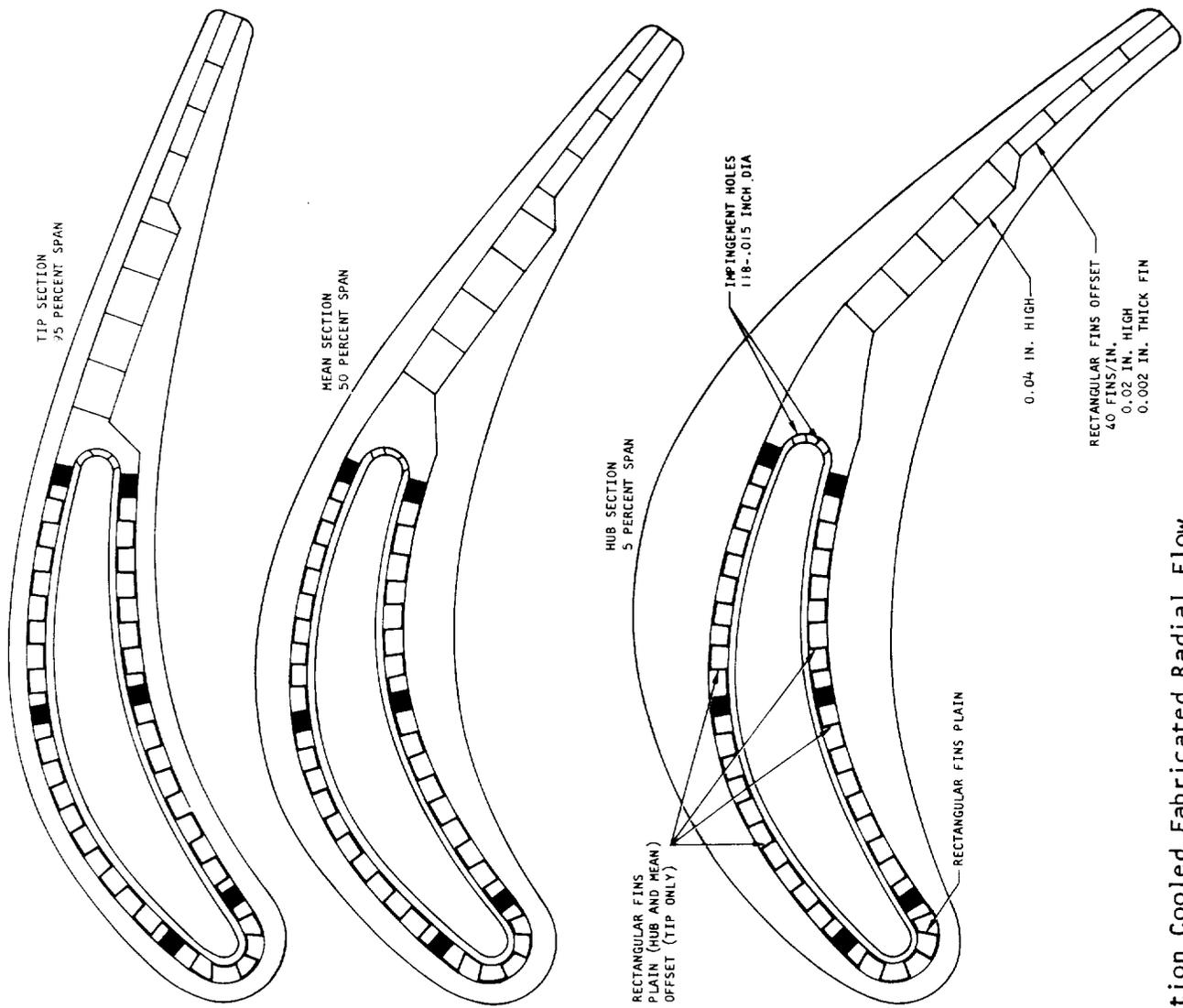
S-67853

Figure 5-5. Scheme A-3 Convection Cooled Fabricated Radial Flow
Plate Fin Blade 1.0 in. (0.0254 m) Chord

76

TIP SECTION
95 PERCENT SPAN

MEAN SECTION
50 PERCENT SPAN

HUB SECTION
5 PERCENT SPAN

IMPINGEMENT HOLES
.030-.035 INCH DIA

RECTANGULAR FINS-OFFSET

RECTANGULAR FINS OFFSET
40 FINS/IN.

0.04 IN. HIGH

0.02 IN. HIGH
0.002 IN. FIN THICKNESS

RECTANGULAR FINS
PLAIN (HUB AND MEAN)
OFFSET (TIP ONLY)

RECTANGULAR FINS PLAIN
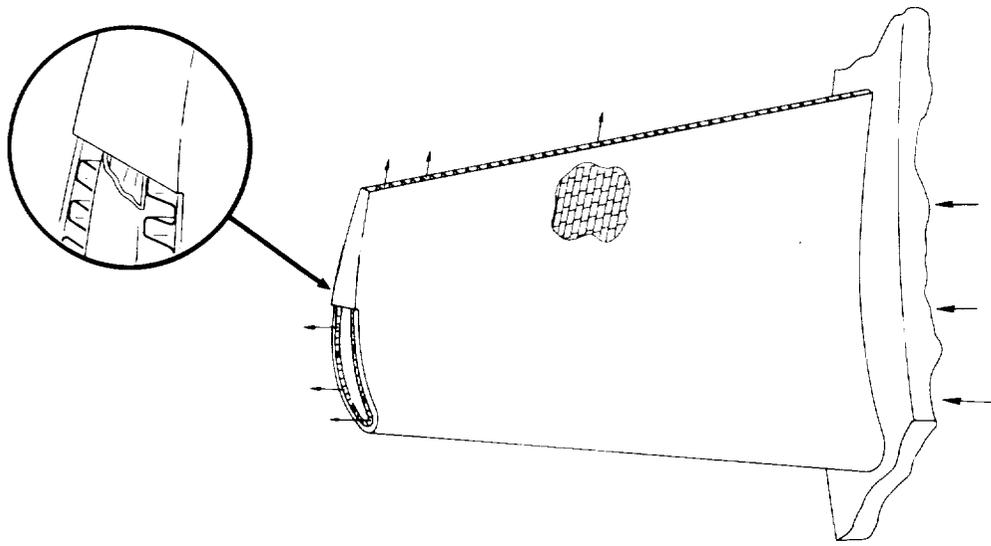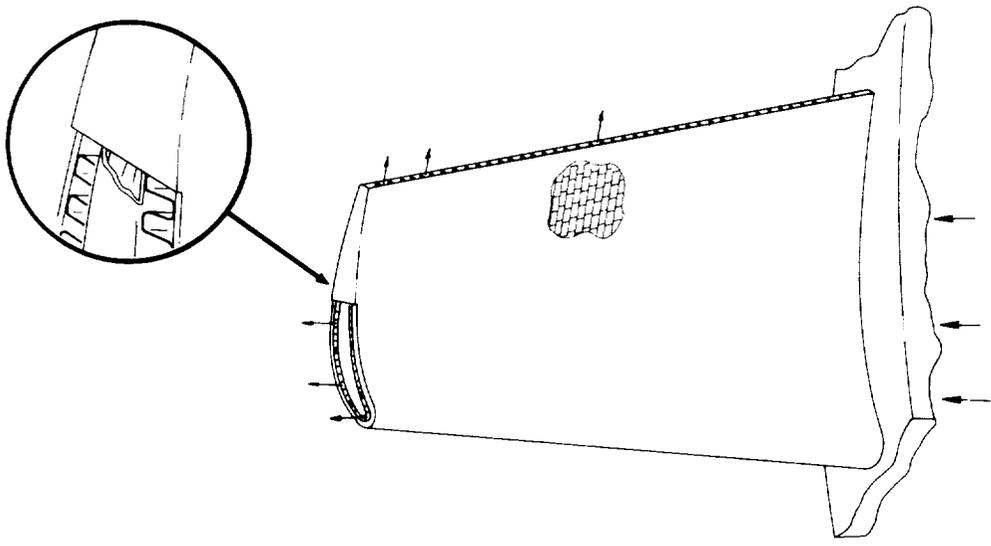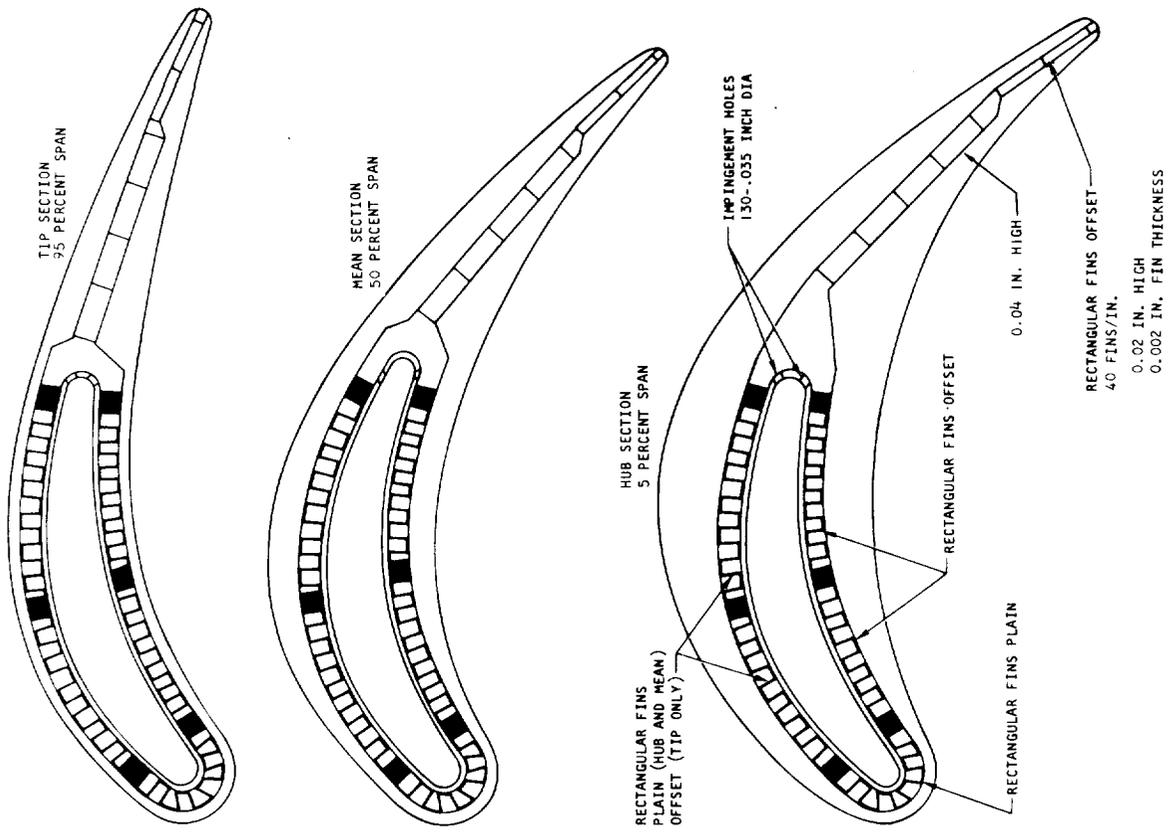
S-67854

Figure 5-6.   Scheme A-3 Convection Cooled Fabricated Radial Flow
Plate Fin Blade 1.5 in. (0.0381 m) Chord

77

chord design. Since trailing edge discharge of the cooling air was used, the adverse effects of thickening the trailing edge were reduced somewhat. An estimate of the aerodynamic effects of thickening the trailing edge is shown in Table 5-2.

The Colburn J-factor data and Fanning friction factor data for plain and offset fins shown in Figure 3-8 as well as the impingement heat transfer relation from Chupp, Helms, McFadden, and Brown (Reference 50) was used in the heat transfer analysis of this design.

The results shown in Table 5-1 indicate that the plate fin turbine blade requires less cooling flow for about the same turbine inlet temperature as Scheme A-1. The maximum turbine inlet temperature capability is limited however, by pressure drop in the leading edge plate fin passage for the 0.75 in. (0.01905 m) and the 1.0 in. (0.0254 m) chord designs. The 1.5 in. (0.0381 m) chord design is limited by the mean section stress rather than pressure drop limitations.

As with practically all of the convection cooled designs, Scheme A-3 shows an increase of turbine inlet temperature capability with chord size. The increase from 0.75 in. (0.01905 m) chord to 1.0 in. (0.0254 m) chord is greater than that from 1.0 in. (0.0254 m) chord to 1.5 in. (0.0381 m) chord.

The combined radial and chordwise flow concept provides rather low thermal gradients at the hub and mean because the flow was metered to each radial passage separately. The maximum thermal gradient is produced at the tip section because the chordwise flow leaves the supply tube only slightly hotter than the cooling air supply temperature.

Scheme A-6 Convection Cooled Fabricated Strut Supported Blade

The convection cooled fabricated strut supported blade scheme A-6 is shown in Figures 5-7, 5-8, and 5-9 for the 0.75 in. (0.01905 m), 1.0 in. (0.0254 m), and 1.5 in. (0.0381 m) chord designs respectively. It consists of a cast strut with chordwise fins and a fabricated sheet metal skin brazed, welded, or diffusion bonded to the strut. A center cavity in the strut supplies cooling air radially to each spanwise section of the blade. Cooling air from the center cavity impinges on the leading edge and flows chordwise through fins on each side of the blade. Cooling air on the pressure side is used to film cool the trailing edge and cooling air on the suction side convection cools the trailing edge.

The chordwise fins in this configuration are 0.02 in. (0.000508 m) thick, 0.01 in. (0.000254 m) high, and spaced 0.04 in. (0.001016 m) center-to-center for the 0.75 in. (0.01905 m) chord design. For the 1.0 in. (0.0254 m) chord design the fins are 0.02 in. (0.000508 m) thick, 0.013 in. (0.0003302 m) high, and spaced 0.04 in. (0.001016 m) center-to-center. In the 1.5 in. (0.0381 m) chord design, the fins are 0.02 in. (0.000508 m) thick, 0.018 in. (0.0004572 m) high, and spaced 0.04 in. (0.001016 m) center-to-center.

78

TIP SECTION
95 PERCENT SPAN

MEAN SECTION
50 PERCENT SPAN

HUB SECTION
5 PERCENT SPAN

IMPINGEMENT HOLES
55-.020 INCH DIA
IMPINGEMENT L/D = 2.5

CHORDWISE FINS
.01 INCH DEPTH
.02 INCH THICK
.04 INCH SPACING CENTER TO CENTER
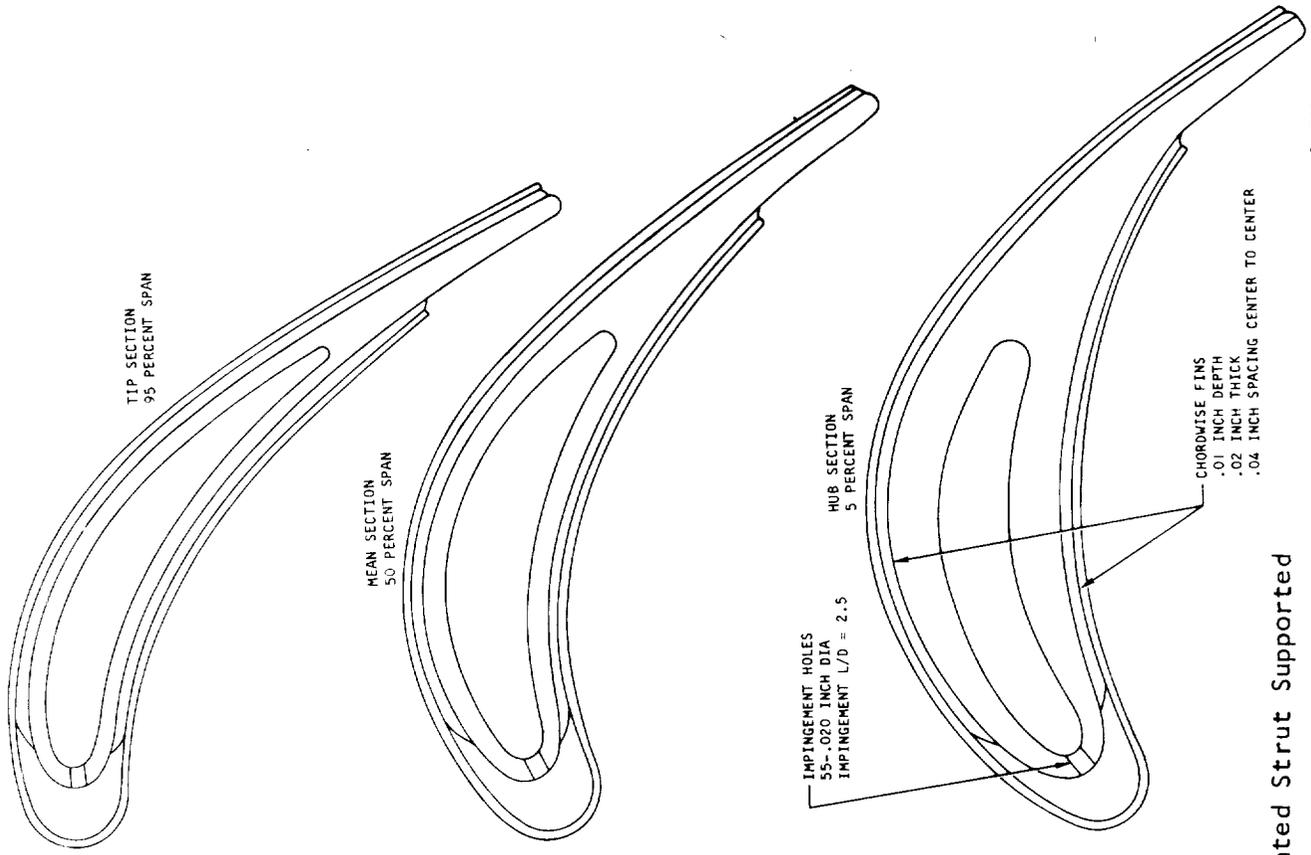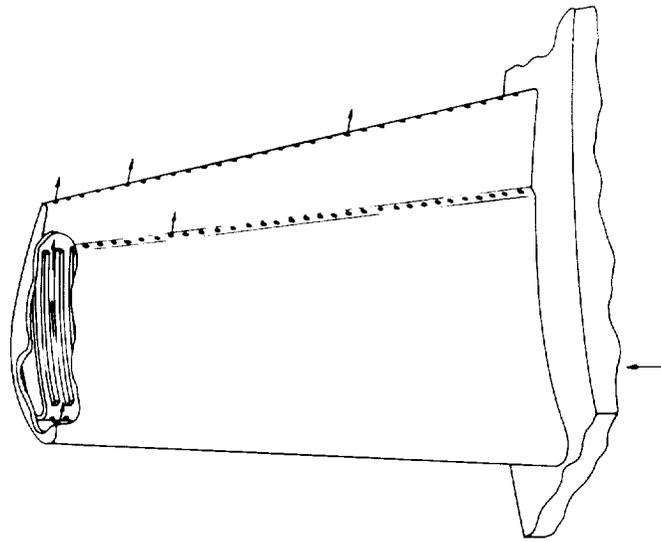
S-67855

Figure 5-7. Scheme A-6 Convection Cooled Fabricated Strut Supported
Blade, 0.75 in. (0.01905 m) Chord

79

TIP SECTION
95 PERCENT SPAN

MEAN SECTION
50 PERCENT SPAN

HUB SECTION
5 PERCENT SPAN

CHORDWISE FINS
.013 INCH DEPTH
.020 INCH THICK
.040 INCH SPACING CENTER TO CENTER

IMPINGEMENT HOLES
51-.025 INCH DIA
IMPINGEMENT L/D = 2.5
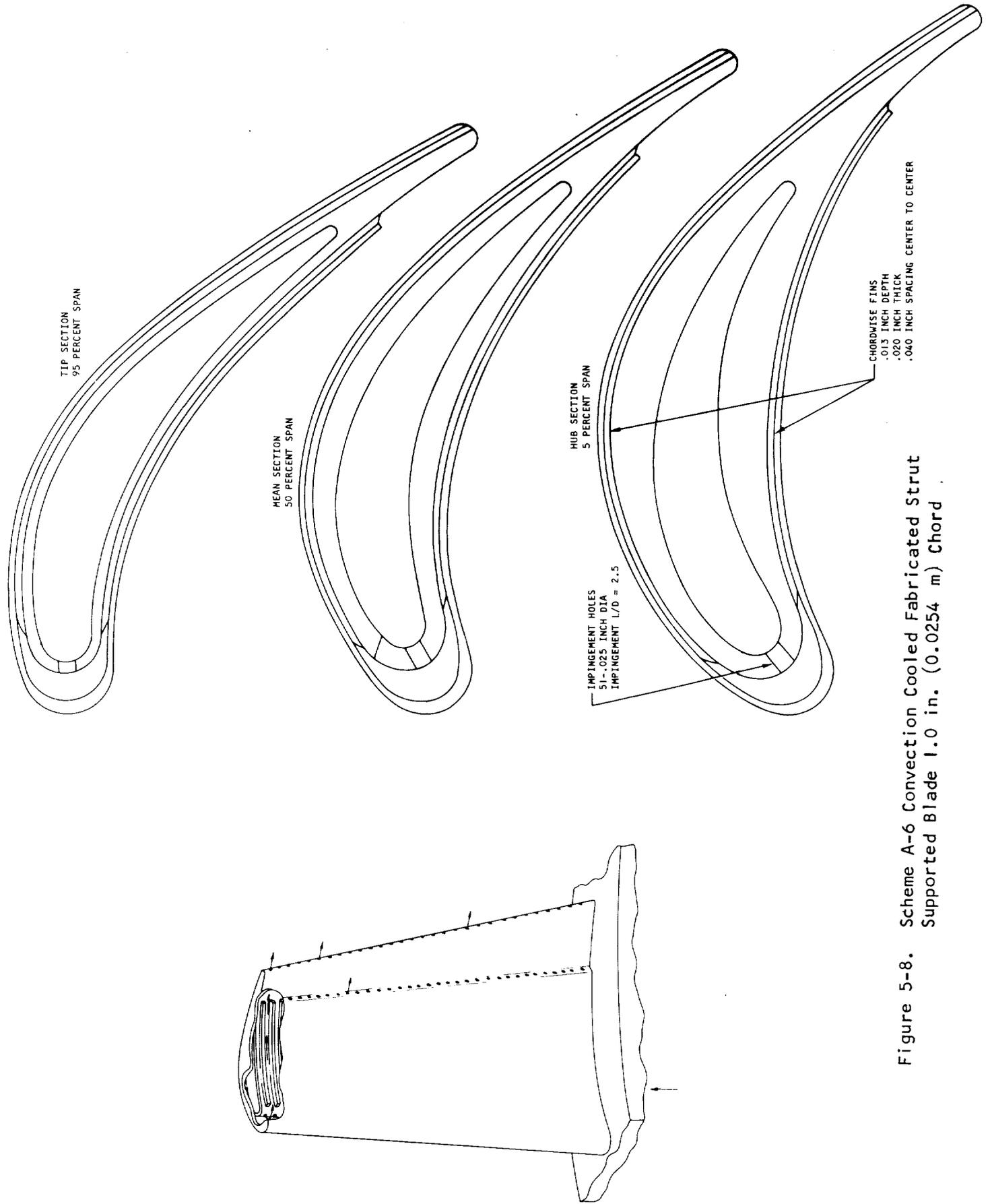
S-67856

Figure 5-8. Scheme A-6 Convection Cooled Fabricated Strut
Supported Blade 1.0 in. (0.0254 m) Chord .

80

TIP SECTION
95 PERCENT SPAN

MEAN SECTION
50 PERCENT SPAN

HUB SECTION
5 PERCENT SPAN

CHORDWISE FINS
.018 INCH DEPTH
.020 INCH THICK
.040 INCH SPACING CENTER TO CENTER

IMPINGEMENT HOLES
29-.040 INCH DIA
IMPINGEMENT L/D = 1.50
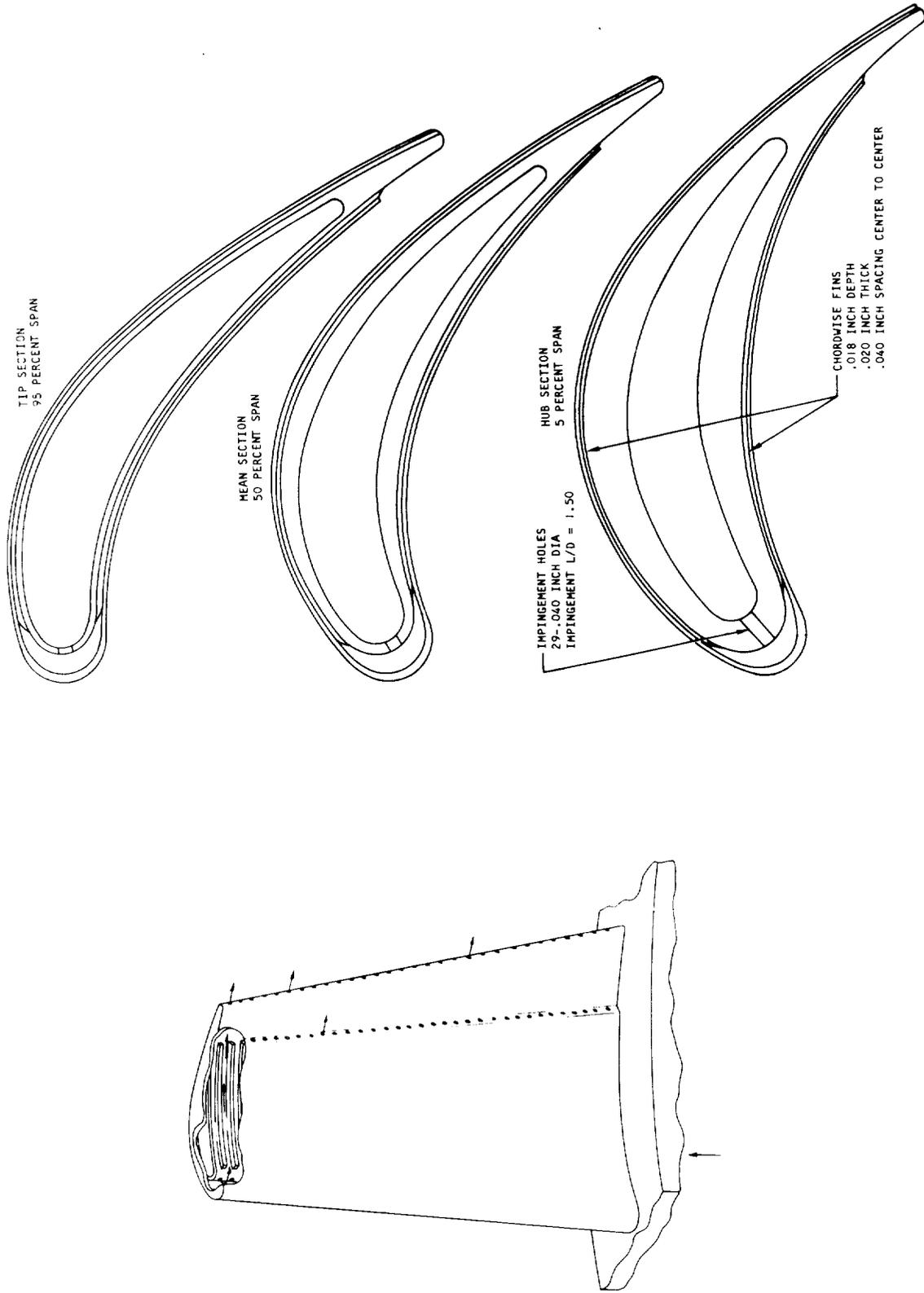
S-67857

Figure 5-9.   Scheme A-6 Convection Cooled Fabricated Strut Supported
Blade 1.5 in. (0.0381 m) Chord

81

The impingement holes for this design are 0.02 in.(0.000508 m) diameter on a 1.75 diameter center-to-center spacing at the root to a 2.25 diameter center-to-center spacing at the tip section of the 0.75 in. (0.01905 m) chord blade. The 1.0 in. (0.0254 m) chord blade has 0.02 in. (0.000762 m) diameter holes on a 1.4 diameter center-to-center spacing. The 1.5 in. (0.0381 m) chord blade has 0.03 in. (0.000762 m) diameter holes on a 1.4 diameter center-to-center spacing. The film cooling relation of Hatch and Papell (Reference 78) was used for the film-cooled trailing edge on the pressure side of the blade. (See Appendix C.)

The results shown in Table 5-1 indicate that the strut supported blade permits turbine inlet temperatures greater than 2400°F (1589°K) for cooling air flows less than 4.0 percent of the hot gas flow. It also gives a high cooling effectiveness at the hub and mean sections of the blade and the highest maximum metal temperature effectiveness of the convection cooled designs. The thermal effectiveness was the highest of any design studied. The gradient ratio was also the highest of the convection cooled designs studies, and for this reason the life may be limited due to low cycle fatigue.

The turbine inlet temperature capability for this design also increases with chord size. The increase from the 0.75 in. (0.01905 m) to the 1.0 in. (0.0254 m) chord design is greater than that from the 1.0 in. (0.0254 m) to the 1.5 in. (0.0381 m) chord design.

The limiting element of the 0.75 in. (0.01905 m) and 1.0 in. (0.0254 m) chord design is the trailing edge outer skin at the tip section of the blade. A maximum metal temperature limit of 1760°F (1233.3°K) for 1000 hr life was selected to account for the reduced thickness of the outer skin and the joining capabilities where the skin attaches to the strut. The cooling flow in this area is limited by pressure drop considerations in the suction side cooling passage.

The limiting element of the 1.5 in. (0.0381 m) chord design is the stress life at the mean section of the blade. This design is also pressure drop limited in the suction side cooling passage.

Table 5-2 indicates a rather high aerodynamic efficiency for this design. Only the 0.75 in. (0.01905 m) chord design required an increased trailing edge thickness and the film cooling losses were low. No recovery of turbine efficiency due to tip discharge of the cooling air is obtained in this design.

The stress analysis of this design considered the centrifugal load distributed over both the strut and the outer skin. The analysis also included the thermal stress induced on the strut by the outer skin. The effects of transient thermal gradients on the life of the blade were not included in the scope of the contract, however the leading edge thickness of the outer skin was increased to 0.020 in. (0.000508 m) to reduce the effects of this problem and to help prevent foreign object damage. Internal supports from the strut to the leading edge could also be added to reduce foreign object damage.

In this design concept the structural member of the blade is protected from the hot gas by a thin outer skin which may be a ductile material with good corrosion life capabilities at high temperatures. The inner strut operates from 80°F (44.4°K) to 140°F (77.8°K) cooler than the outer skin. This causes all of the centrifugal load of the outer skin to be transferred to the strut as well as some additional thermal stresses. Since the strut is highly cooled it is capable of supporting this additional stress while still providing a long stress to rupture life.

Scheme A-7 Convection Cooled Cast Impingement Tube Blade

This cooling scheme is shown in Figures 5-10, 5-11, and 5-12 for the 0.75 in. (0.01905 m), 1.0 in. (0.0254 m), and 1.5 in. (0.0381 m) chord designs respectively. Cooling air flows radially through the supply tube and leaves through a row of holes which provide impingement cooling at the leading edge of the blade. After impinging on the leading edge, the cooling air flows through chordwise fins on each side of the supply tube. The cooling air then flows chordwise through a pin fin passage in the aft section of the blade and discharges through slots in the trailing edge of the blade. In order to provide additional cooling flow area at the hub section of the blade, film cooling holes were added just forward of the trailing edge slots on the pressure side of the blade. This was necessary because the trailing edge slots limited the flow at the hub section and further thickening of the trailing edge was undesirable. Chordwise fin dimensions and pin fin dimensions are shown in Figures 5-10, 5-11, and 5-12.

The results shown in Table 5-1 indicate that Scheme A-7 permits turbine inlet temperature of only 2221°F (1489.4°K) to 2355°F (1563.9°K) for 1000 hr life. The average metal temperature cooling effectiveness for the hub and mean sections is the lowest of any design, but the maximum metal temperature cooling effectiveness is relatively high (less than A6 and ≈ A1) for convection cooling. The thermal effectiveness and the metal temperature gradient ratio are both low. These results show that this design does not act as a very effective heat exchanger, however it does provide low thermal gradients and a low maximum metal temperature. These characteristics indicate that this design is more suited to a low tip speed turbine with a high metal area taper ratio blade shape or to a nozzle vane.

The limiting element of each of these designs is the stress life at the mean section of the blade. Many variations of cooling flow were tried in an effort to achieve maximum blade life. In the last effort it was necessary to incorporate a row of holes on the pressure side of the hub section trailing edge to get the required cooling flow at the hub section of the blade. Since the results shown in Table 5-1 were ratioed using the Larson-Miller parameter over a broad range of life and turbine inlet temperature, the only conclusion which can be drawn is that this design would only be capable of 2300°F (1533.3°K) turbine inlet temperature in any chord size for 1000 hr life. This is due to the limited metal area taper ratio and the high tip speed required in this turbine.

LOCATION AND SIZE OF IMPINGEMENT COOLING SLOTS/HOLES

LEADING EDGE IMPINGEMENT, ROOT SECTION

SLOTS--0.025 IN. (0.000635 M) X 0.04 IN.
(0.001016 M)
CENTER-TO-CENTER SPACING 0.05 IN. (0.00127 M)

MEAN AND TIP SECTIONS

HOLES--0.02-IN. (0.000508-M) DIAM
CENTER-TO-CENTER SPACING 1.5 DIAM

TRAILING EDGE (THICKENED TO PROVIDE DISCHARGE SLOTS
FROM 0.0225 IN. (0.0005715 M) to 0.045 IN.
(0.001143 M)

SLOTS--0.015 IN. (0.000381 M) X 0.04 IN.
(0.001016 M)
CENTER-TO-CENTER SPACING 0.05 IN. (0.00127 M)

FILM COOLING HOLES, PRESSURE SIDE (AT HUB SECTION
JUST FORWARD OF TRAILING EDGE DISCHARGE SLOTS)

HOLES (14 EA.)--0.025-IN. (0.000635-M) DIAM

TIP SECTION
(95 PERCENT SPAN)

MEAN SECTION
(50 PERCENT SPAN)

IMPINGEMENT HOLES

CHORDWISE FINS
.01 INCH DEPTH
.02 INCH THICK
.20 INCH CENTER TO CENTER SPACING
(HUB SECTION ONLY)

PIN FINS
.02 INCH DIA.
.06 INCH TRIANGULAR SPACING
CENTER TO CENTER

HUB SECTION
(5 PERCENT SPAN)

CHORDWISE FINS
.01 INCH DEPTH
.02 INCH THICK
.04 INCH CENTER TO
CENTER SPACING

IMPINGEMENT SLOTS

FILM HOLES
14 - .025 INCH DIA.
HUB SECTION ONLY

TRAILING EDGE SLOTS
35-.015x.040

0.045

0.015

S-67858

Figure 5-10. Scheme A-7 Convection Cooled Cast Impingement Tube Blade
0.75 in. (0.01905 m) Chord)

84

LOCATION AND SIZE OF IMPINGEMENT COOLING SLOTS/HOLES

LEADING EDGE IMPINGEMENT, ROOT SECTION

   HOLES--0.04-IN. 0.001016-M DIAM
   CENTER-TO-CENTER SPACING 1.25 DIAM

MEAN AND TIP SECTIONS

   HOLES--0.03-IN. (0.000762-M DIAM
   CENTER-TO-CENTER SPACING 1.5 DIAM

TRAILING EDGE (THICKENED TO PROVIDE DISCHARGE SLOTS
FROM 0.03 IN. (0.0007762 M to 3.045 IN. (0.0001143 M

   SLOTS--0.015-IN. (0.000381 M X 0.04 IN.
             0.0001016 M
   CENTER-TO-CENTER SPACING 0.05 IN. (0.00127 M

FILM COOLING HOLES, PRESSURE SIDE (AT HUB SECTION
JUST FORWARD OF TRAILING EDGE DISCHARGE SLOTS)

   HOLES (9 EA.)--0.035-IN. 0.000889-M DIAM

TIP SECTION
(95 PERCENT SPAN,

MEAN SECTION
(50 PERCENT SPAN)

HUB SECTION
(5 PERCENT SPAN)

CHORDWISE FINS
.015 INCH DEPTH
.020 INCH THICK
.20 INCH CENTER TO CENTER SPACING
(HUB SECTION ONLY)

CHORDWISE FINS
.01 INCH DEPTH
.02 INCH THICK
.0571 INCH CENTER TO
CENTER SPACING

PIN FINS
.025 INCH DIA.
.075 INCH CENTER TO CENTER
TRIANGULAR SPACING

FILM HOLES
9 - .035 INCH DIA.
(HUB SECTION ONLY)

IMPINGEMENT HOLES

TRAILING EDGE SLOTS
35 - .015 x .040

0.015

S-67859

Figure 5-11. Scheme A-7 Convection Cooled Cast Impingement
Tube Blade 1.0 in. (0.0254 m) Chord

85

TIP SECTION
(95 PERCENT SPAN)

MEAN SECTION
(50 PERCENT SPAN)

CHORDWISE FINS
.018 INCH DEPTH
.020 INCH THICK
.20 INCH CENTER TO CENTER SPACING
(HUB SECTION ONLY)

PIN FINS
.04 INCH DIAMETER
.10 INCH TRIANGULAR
SPACING CENTER TO CENTER

CHORDWISE FINS
.010 INCH DEPTH
.020 INCH THICK
.10 INCH CENTER TO
CENTER SPACING

CHORDWISE FINS
.01 INCH DEPTH
.02 INCH THICK
.10 INCH CENTER TO
CENTER SPACING

FILM HOLES
9 - .045 INCH DIA.
(HUB SECTION ONLY)

0.022

S-67860

HUB SECTION
(5 PERCENT SPAN)

IMPINGEMENT HOLES

LOCATION AND SIZE OF IMPINGEMENT COOLING SLOTS/HOLES

LEADING EDGE IMPINGEMENT, ROOT SECTION

HOLES--0.05-IN. (0.00127-M) DIAM
CENTER-TO-CENTER SPACING 1.3 DIAM

MEAN AND TIP SECTIONS

HOLES--0.05-IN. (0.00127-M) DIAM
CENTER-TO-CENTER SPACING 2 DIAM

TRAILING EDGE (NO THICKENING REQUIRED TO PROVIDE
DISCHARGE SLOTS

SLOTS--0.022 IN. (0.0005588 M) X 0.04 IN.
(0.001016 M)
CENTER-TO-CENTER SPACING - 0.05 IN.
(0.00127 M)

FILM COOLING HOLES, PRESSURE SIDE (AT HUB SECTION
JUST FORWARD OF TRAILING EDGE DISCHARGE SLOTS)

HOLES (9 EA.)--0.045-IN. (0.001143-M) DIAM
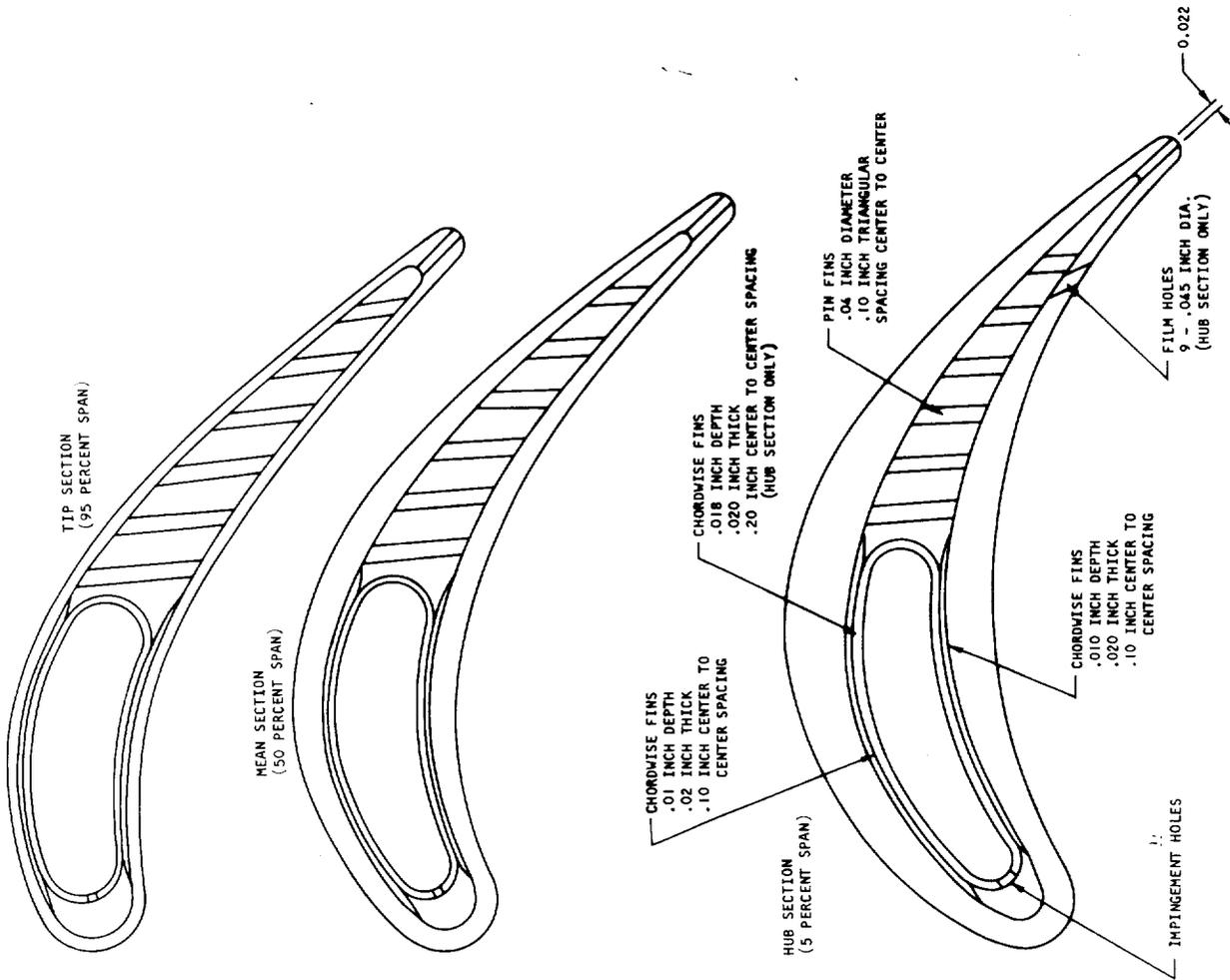
Figure 5-12.   Scheme A-7 Convection Cooled Cast Impingement Tube Blade
1.5 in. (0.0381 m) Chord

86

This design had a large reduction in aerodynamic efficiency due to thickening the trailing edge in the 0.75 in. (0.01905 m) and 1.0 in. (0.0154 m) chord sizes. No recovery of turbine efficiency was obtained due to tip discharge either.

This was the only convection cooled design that did not show a consistent increase in allowable turbine inlet temperature with chord. This trend was probably obscured by the many changes which were applied in an attempt to improve the design.

Scheme B-1 Film-Convection Cooled Cast Three Cavity Blade

This cooling scheme is shown in Figures 5-13, 5-14, and 5-15 for the 0.75 in. (0.01905 m), 1.0 in. (0.0254 m), and 1.5 in. (0.0381 m) chord designs respectively. This design consists of three radial cooling air passages, the leading edge passage, the midchord passage, and the trailing edge passage. The leading edge and midchord passages contain radial fins to provide additional cooled surface area. The trailing edge passage has equilaterial triangular spaced pin fins to provide both increased heat transfer coefficient and additional cooled surface area. The leading edge is cooled by a combination of convection and film cooling via multiple circular holes. Film cooling is also provided for the side walls by a row of holes on each side of the leading edge, a row of holes from the midchord cavity discharging to the suction side, and a row of holes from the trailing edge cavity discharging to the pressure side.

The trailing edge of the 0.75 in. (0.01905 m) chord design is film cooled to maintain the design limit on trailing edge thickness. The increased trailing edge thickness of the 1.0 in. (0.0254 m) and 1.5 in. (0.0381 m) chord blades permits the use of trailing edge discharge through a row of holes in the trailing edge. The film cooling relation of Hatch and Papell (Reference 78 and Appendix C) was used for the trailing edge of the 0.75 in. (0.01905 m) chord blade. For the film cooled leading edge and the film cooling holes in each side of the blade the film cooling data in NASA CR-54513 (Reference 8) was used. The convection heat transfer analysis in the film cooling holes included the entrance effect multiplying factor of Nunner (Reference 44).

The analytical results for this design are summarized in Table 5-1. This table shows that turbine inlet temperatures of 2457°F (1620.6°K) to 2607°F (1703.9°K) for 1000 hr life are possible with this design. This design has the highest average metal temperature cooling effectiveness at the hub section of any film cooling design. The mean section average metal temperature cooling effectiveness, the maximum metal temperature cooling effectiveness, and the thermal effectiveness for this design is comparable to the other advanced film-convection techniques studies. The gradient ratio for this design is somewhat higher than for Scheme B-5 design to be described later. This is caused by the cooling passage separators which are overcooled in this design.

In the 0.75 in. (0.01905 m) chord design the blade is limited to a turbine inlet temperature of 2457°F (1620.6°K) for 1000 hr life by a maximum metal temperature of 1840°F (1277.8°K) at the tip section of the blade. The trailing edge of this blade is similar to that used on Scheme A-1 except that

TIP SECTION
95 PERCENT SPAN

MEAN SECTION
50 PERCENT SPAN

HUB SECTION
5 PERCENT SPAN

FILM HOLES 50-.008 INCH DIA

TRAILING EDGE FILM HOLES
75-.01 INCH DIA

PIN FINS
.02 INCH DIAMETER
.06 INCH TRIANGULAR
SPACING CENTER TO CENTER

FILM HOLES 21-.008 INCH DIA

RADIAL FINS

FILM COOLED LEADING EDGE
192-.008 INCH DIA HOLES

FILM HOLES 20-.008 INCH DIA
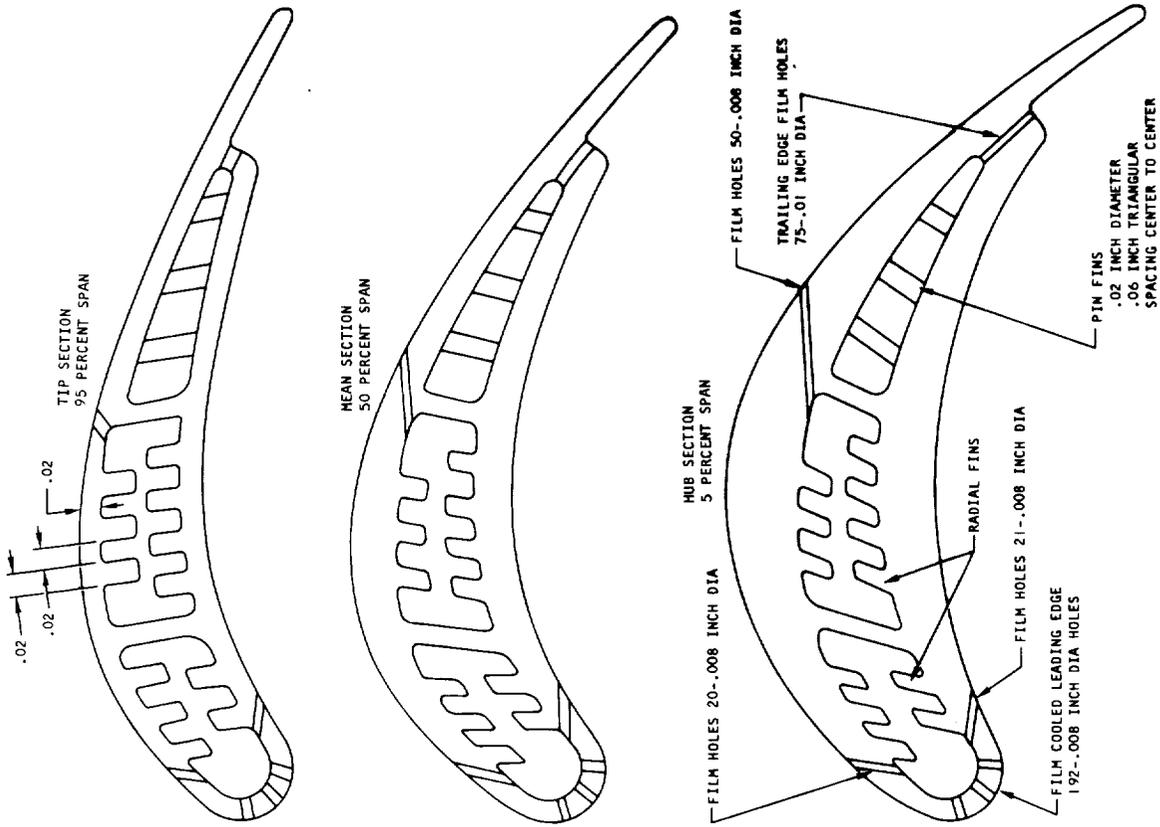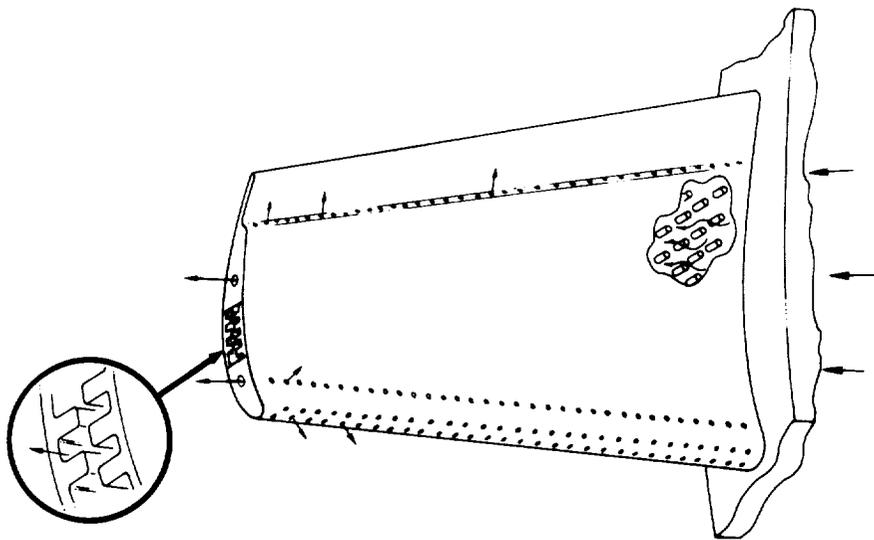
S-67861

Figure 5-13. Scheme B-1 Film Convection Cooled Cast Three
Cavity Blade 0.75 in. (0.01905 m) Chord

TIP SECTION
(95 PERCENT SPAN)

MEAN SECTION
(50 PERCENT SPAN)

HUB SECTION
(5 PERCENT SPAN)

TRAILING EDGE HOLES
113-.010 INCH DIA

FILM HOLES
55-.008 INCH DIA

PIN FINS
.025 INCH DIAMETER
.075 INCH TRIANGULAR
SPACING CENTER TO CENTER

RADIAL FINS

FILM HOLES 51-.008 INCH DIA

FILM HOLES 28-.008 INCH DIA

FILM COOLED LEADING EDGE
192-.008 INCH DIA HOLES

FILM HOLES
26-.008 INCH DIA

.025

.025
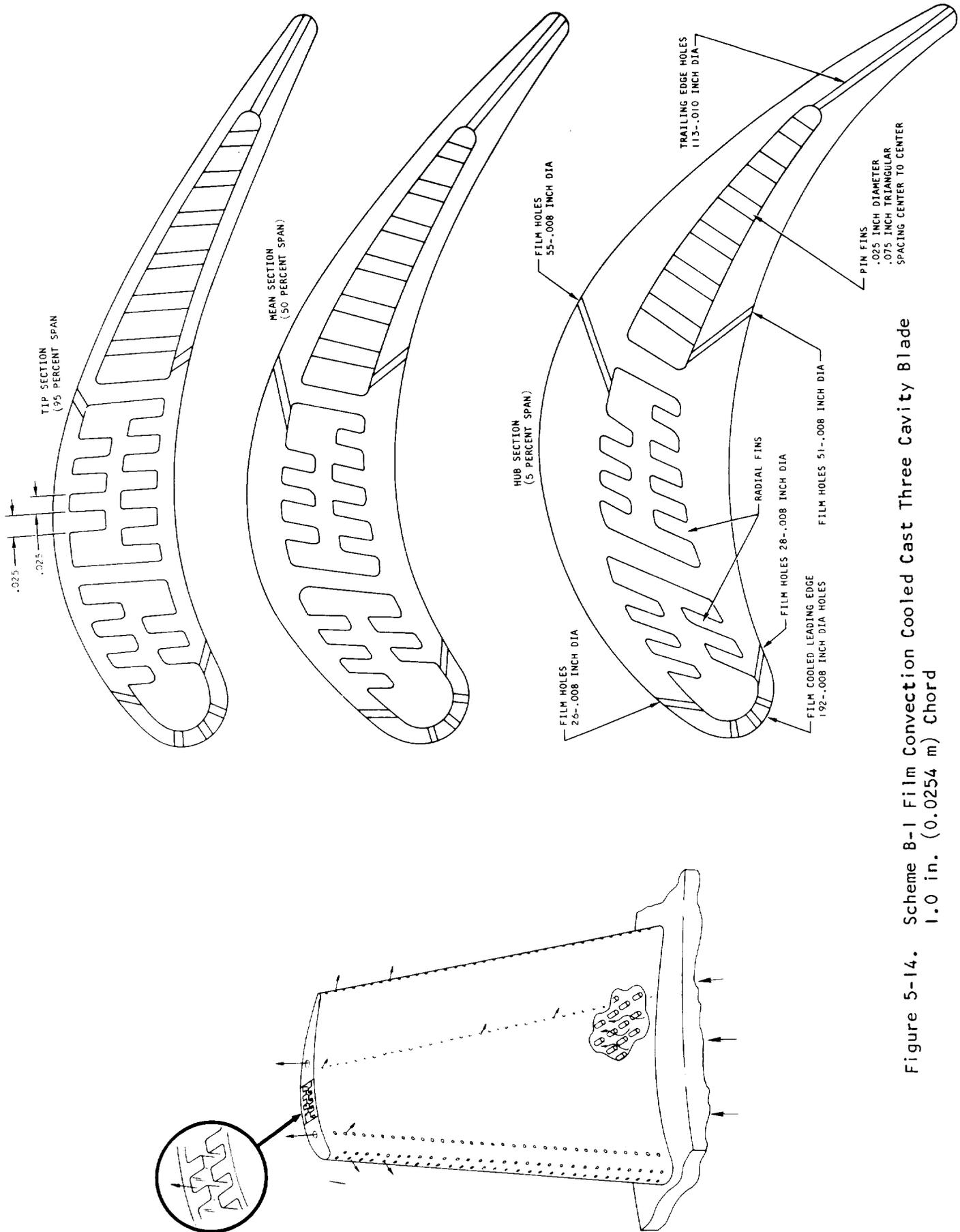
Figure 5-14. Scheme B-1 Film Convection Cooled Cast Three Cavity Blade
1.0 in. (0.0254 m) Chord

S-67862

89

TIP SECTION
(95 PERCENT SPAN)

.02

.03

.03

MEAN SECTION
(50 PERCENT SPAN)

HUB SECTION
(5 PERCENT SPAN)

FILM HOLES 45-.008 INCH DIA

FILM HOLES 47-.008 INCH DIA

FILM COOLED LEADING EDGE
224-.008 INCH DIA

RADIAL FINS

FILM HOLES 120-.010 INCH DIA

TRAILING EDGE HOLES
60-.015 INCH DIA

PIN FINS
.03 INCH DIAMETER
.09 INCH TRIANGULAR
SPACING CENTER TO CENTER
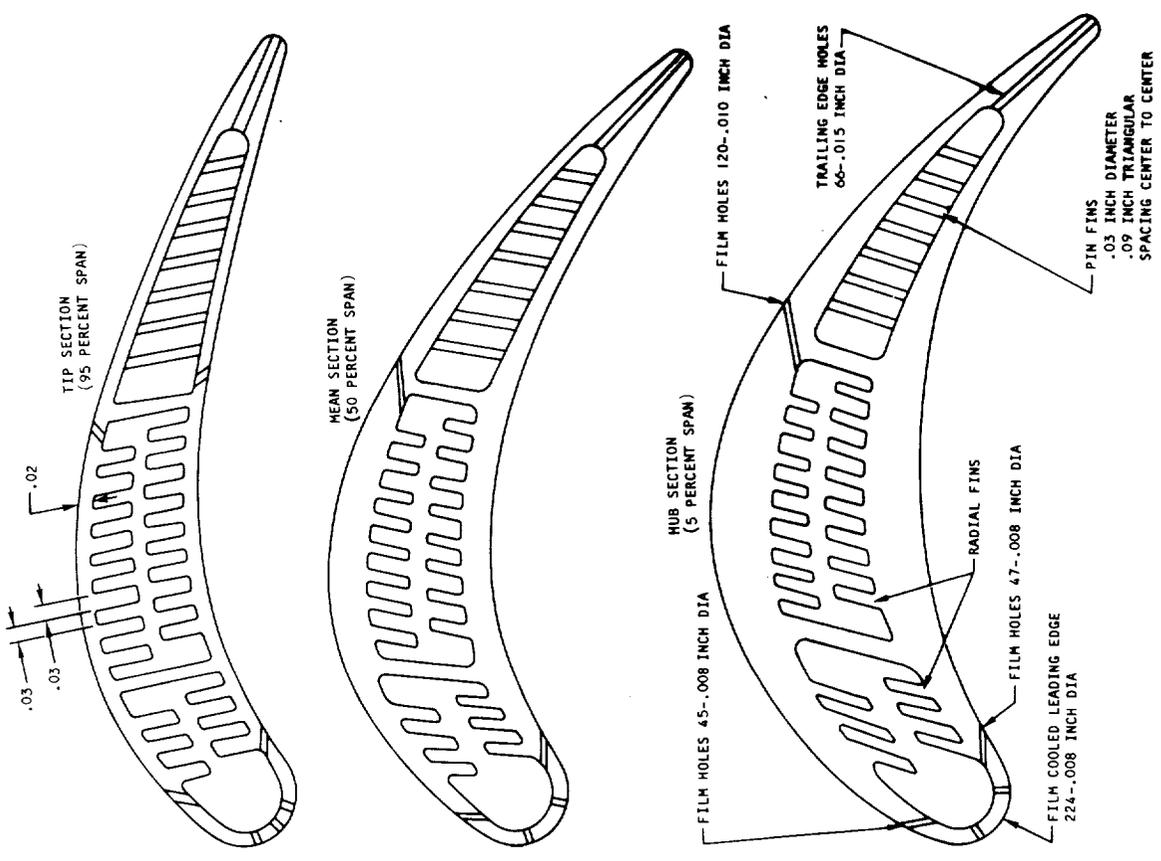
S-67863
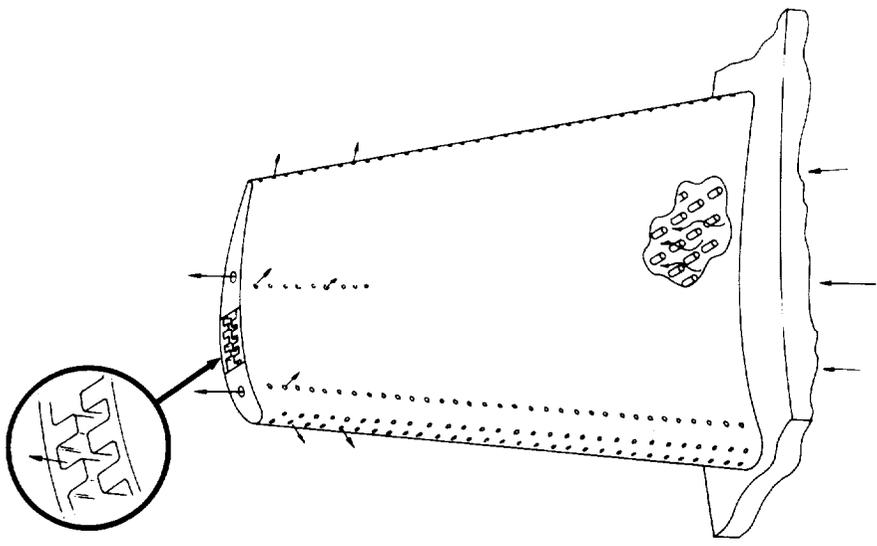
Figure 5-15. Scheme B-I Film-Convection Cooled Cast Three Cavity Blade
1.5 in. (0.0381 m) Chord

90

film cooling is provided on the suction side of the blade. This additional film cooling permits a 170°F (94.4°K) increase in the allowable turbine inlet temperature for 1000 hr life.

In the 1.0 in. (0.0254 m) chord design, the blade is limited to a turbine inlet temperature of 2610°F (1705.6°K) by thermal stress in the cooling passage separators at the tip section of the blade. These separators were thickened as much as possible to increase their temperature and reduce the thermal gradients. Large thermal gradients also occur in the radial fins at the leading edge and center passage. Since the assumptions used in the stress analysis technique do not apply at the tip section of the blade this limit may not be totally valid.

In the 1.5 in. (0.0381 m) chord design, the blade is limited to a turbine inlet temperature of 2610°F (1705.6°K) by thermal stress in the cooling passage separators at the mean section of the blade. These separators were also thickened to reduce thermal stress.

As in most of the film-convection cooled designs, the film cooling permits higher turbine inlet temperatures and obscures the effect of chord size on turbine inlet temperature capability.

The aerodynamic effects for this design shown in Table 5-2 indicate a relatively high turbine efficiency for all three chord sizes. The film cooling gives only a small decrease in turbine efficiency and there is some recovery in turbine efficiency due to tip discharge.

Scheme B-4 Film-Convection Cooled Cast Impingement Tube Blade with Crossflow Impingement and Sharp Corner Flow Leading Edge

This cooling technique is shown in Figure 5-16, 5-17, and 5-18 for the 0.75 in. (0.01905 m), 1.0 in. (0.0254 m), and 1.5 in. (0.0381 m) chord designs respectively. This design is similar to scheme A-7 with the addition of crossflow impingement on the suction side of the supply tube, sharp corner flow around the leading edge rather than impingement, and film cooling over the entire trailing edge pressure side. This design was proposed to eliminate some of the problems associated with cooling flow limitations in the Scheme A-7 design. The leading edge flow metering holes were 0.01 in. (0.000254 m) diameter on a 2.5 diameter center-to-center spacing for the 0.75 in. (0.01905 m) chord blade, 0.015 in. (0.000381 m) diameter on a 2.5 diameter center-to-center spacing for the 1.0 in. (0.0254 m) chord blade, and 0.015 in. (0.000381 m) diameter on a 2.0 diameter center-to-center spacing for the 1.5 in. (0.0381 m) chord blade. The impingement holes on the suction side are 0.005 in. (0.000127 m) diameter holes on a 7.0 diameter triangular center-to-center spacing. The chordwise fins, the pin fins, and the trailing edge slots are the same as in the Scheme A-7 design.

TIP SECTION
(95 PERCENT SPAN)

MEAN SECTION
(50 PERCENT SPAN)

HUB SECTION
(5 PERCENT SPAN)

CHORDWISE FINS
.01 INCH DEPTH
.02 INCH THICK
.20 INCH CENTER TO CENTER SPACING

CHORD WISE FINS
.01 INCH DEPTH
.02 INCH THICK
.04 INCH CENTER TO CENTER SPACING

IMPINGEMENT HOLES
.005 INCH DIA

IMPINGEMENT HOLES
69 - .01 INCH DIA
CENTER-TO-CENTER SPACING = 2.5

TRAILING EDGE SLOTS
30-.015 x .040 INCH

FILM HOLES
88-.01 INCH DIA

PIN FINS
.02 INCH DIA
.06 INCH CENTER TO CENTER
TRIANGULAR SPACING

0.015

S-67864

Figure 5-16.   Scheme B-4 Film-Convection Cooled Cast Impingement
Tube Blade with Crossflow Impingement and Sharp Corner
Flow Leading Edge 0.75 in. (0.0195 m) Chord

TIP SECTION
(95 PERCENT SPAN)

MEAN SECTION
(50 PERCENT SPAN)

HUB SECTION
(5 PERCENT SPAN)

PIN FINS
.025 INCH DIAMETER
.075 INCH CENTER TO CENTER
TRIANGULAR SPACING

TRAILING EDGE SLOTS
35 - .015 x .040 INCH

FILM HOLES
60 - .015 INCH DIA

CHORDWISE FINS

IMPINGEMENT HOLES
46 - .015 INCH DIA
CENTER-TO-CENTER SPACING = 2.50

IMPINGEMENT HOLES
.005 INCH DIA

S-67865
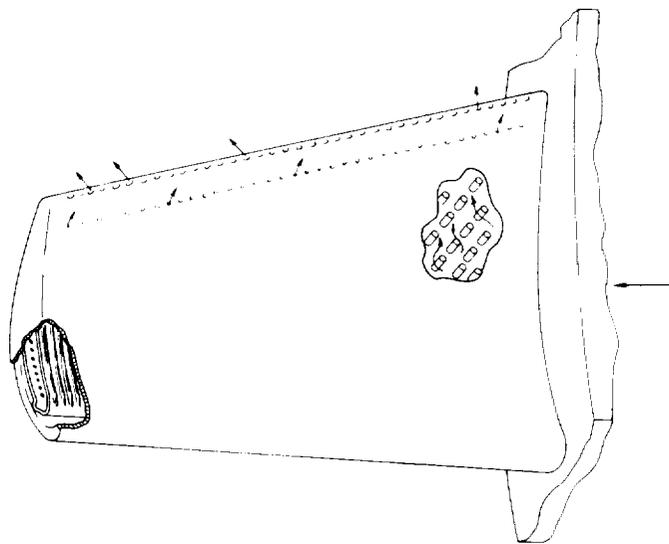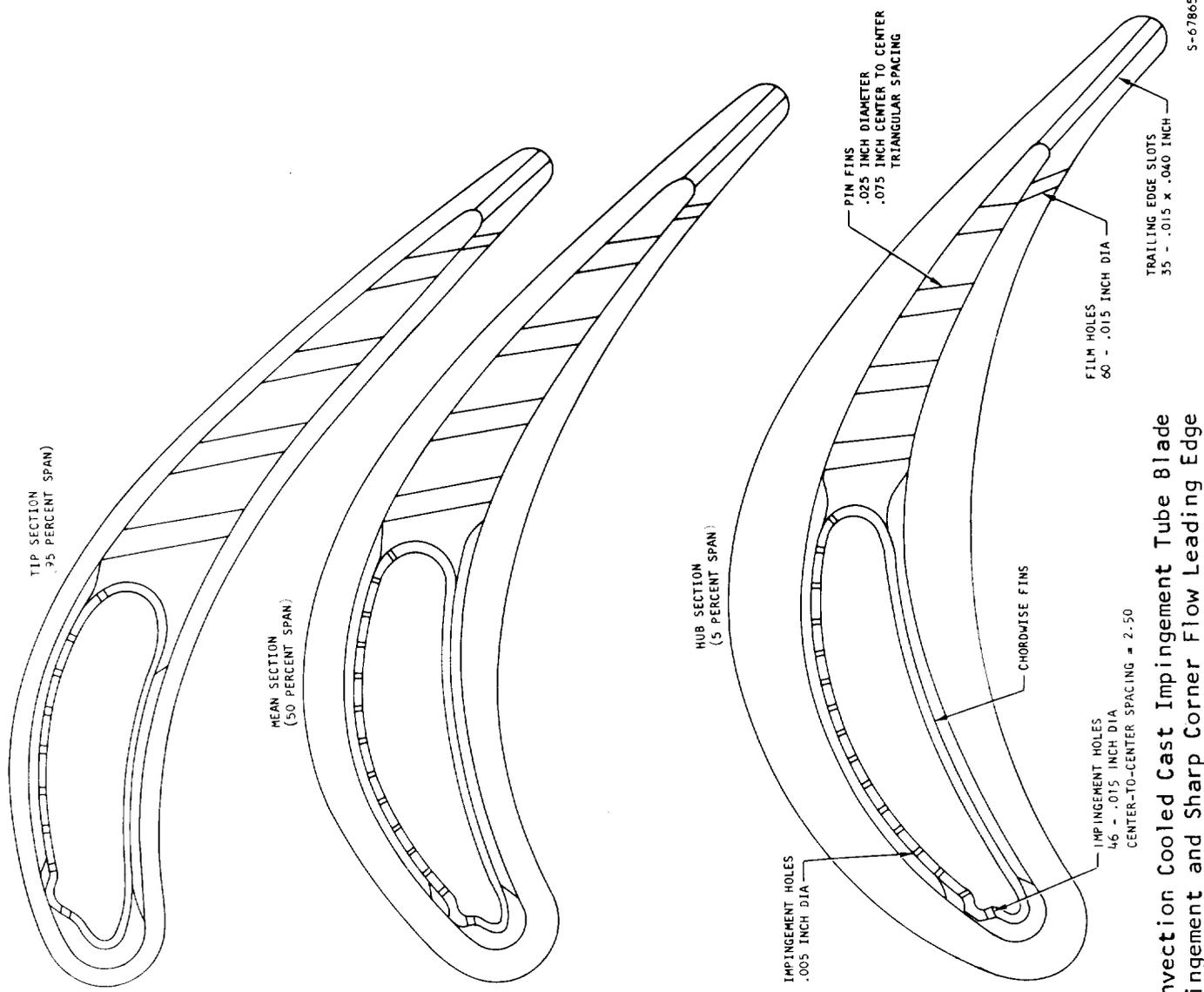
Figure 5-17. Scheme B-4 Film-Convection Cooled Cast Impingement Tube Blade
with Crossflow Impingement and Sharp Corner Flow Leading Edge
1.0 in. (0.0254 m) Chord

93

TIP SECTION
(95 PERCENT SPAN)

MEAN SECTION
(50 PERCENT SPAN)

HUB SECTION
(5 PERCENT SPAN)

CHORDWISE FINS
.020 INCH DEPTH
.020 INCH THICK
.20 INCH CENTER TO CENTER SPACING

IMPINGEMENT HOLES
.005 INCH DIA

IMPINGEMENT HOLES
60 - .015 INCH DIA
IMPINGEMENT
CENTER-TO-CENTER
SPACING =2.0

CHORDWISE FINS

PIN FINS
.04 INCH DIA.
.10 INCH CENTER TO CENTER
TRIANGULAR SPACING

FILM HOLES
33 - .020 INCH DIA

TRAILING EDGE SLOTS
35 - .022 x .040 INCH

0.022

S-67866
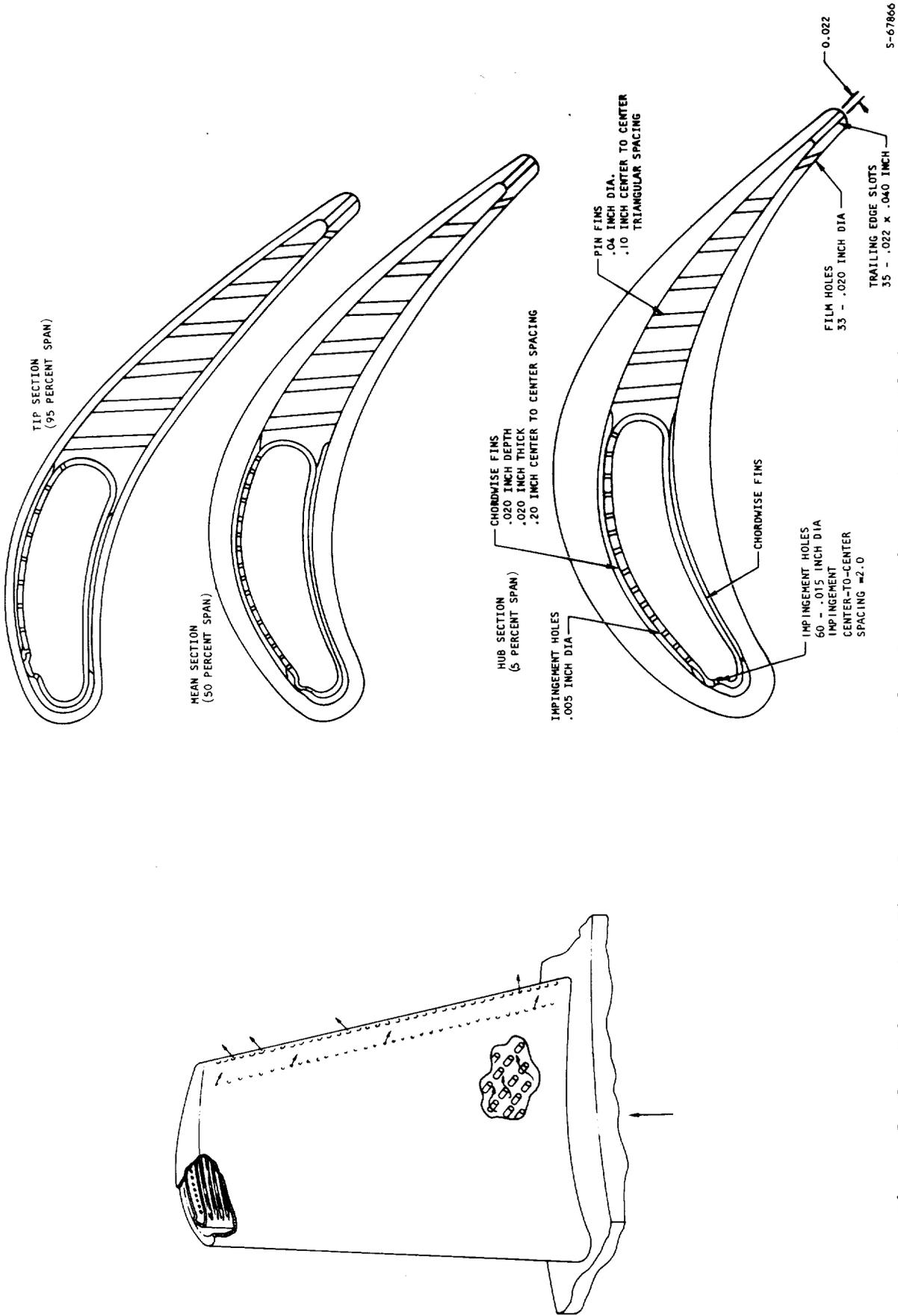
Figure 5-18. Scheme B-4 Film-Convection Cooled Cast Impingement Tube Blade with Crossflow Impingement and Sharp Corner Flow Landing Edge 1.5 in. (0.0381 m) Chord

Table 5-I shows that Scheme B-4 permits turbine inlet temperatures of 2200°F (1477.8°K) to 2390°F (1583.3°K) for 1000 hr life. The average metal temperature cooling effectiveness at the hub and mean sections of the blade were higher than for the Scheme A-7 design. Maximum metal temperature cooling effectiveness and thermal effectiveness were also somewhat higher than the Scheme A-7 design. However, the thermal gradient ratio was generally higher than for the Scheme A-7 design. The combination of slightly higher cooling effectiveness and thermal gradient ratio produced a turbine inlet capability about the same as in the Scheme A-7 design but with lower coolant flow.

The results of this analysis indicate that this design provides rather low average metal temperature cooling effectiveness at the hub and mean sections, but the maximum metal temperature cooling effectiveness is relatively high. The thermal effectiveness and the metal temperature gradient ratio are both about average. These characteristics are similar to those of Scheme A-7 except that the addition of impingement cooling on the suction side and film cooling on the pressure side trailing edge permits higher cooling effectiveness with less coolant flow. Because Scheme B-4 provides low thermal gradients and a low maximum metal temperature, it is more suited to a low tip speed turbine with a high metal area taper ratio or to a nozzle vane.

Scheme B-5 Film-Convection Cooled Fabricated Impingement Tube Blade

The film-convection cooled impingement tube blade is shown in Figures 5-19, 5-20, and 5-21 for the 0.75 in. (0.01905 m), 1.0 in. (0.0254 m), and 1.5 in. (0.0381 m) chord designs respectively. In this design the cooling air flows radially through the supply tube and impinges on the leading edge, the suction side, the pressure side, and the trailing edge of the blade. Film cooling holes are provided on each side of the leading edge and on the pressure and suction sides of the blade near the trailing edge. Cooling holes are also provided in the trailing edge. The impingement hole and film cooling hole patterns used in this design are described in the final design section of this report. The trailing edge was thickened in the 0.75 in. (0.01905 m) chord design from 0.0225 in. (0.0005715 m) to 0.03 in. (0.000762 m) to permit trailing edge discharge. No thickening was required for the 1.0 in. (0.0254 m) and 1.5 in. (0.0381 m) chord designs.

The limiting turbine inlet temperature for 1000 hr life with the Scheme B-5 design is 2560°F (1677.8°K) to 2770°F (1794.4°K) as shown in Table 5-1. This design has a high average metal temperature cooling effectiveness at the hub and mean sections. It also has a high maximum metal temperature cooling effectiveness. The thermal effectiveness is rather low however, and the metal temperature gradient is also low. The low metal temperature gradient along with rather high cooling effectiveness makes this design the best selection for a final design analysis.

The limiting element in the 0.75 in. (0.01905 m) chord design is the maximum metal temperature at the tip section and stress at the hub section. The limiting element of the 1.0 in. (0.0254 m) chord design is the stress at the mean section of the blade. In this design the cooler impingement tube is not attached to the outer shell but is held by pins at the blade root. This eliminates thermal

TIP SECTION
95 PERCENT SPAN

MEAN SECTION
50 PERCENT SPAN

HUB SECTION
5 PERCENT SPAN

FILM HOLES
90-.010 INCH DIA.

FILM HOLES
75-.010 INCH DIA.

IMPINGEMENT HOLES
.005 INCH DIA.

TRAILING EDGE HOLES
70-.008 INCH DIA.

FILM HOLES
24-.010 INCH DIA.

FILM HOLES
25-.010 INCH DIA.

IMPINGEMENT HOLES
53-.010 INCH DIA
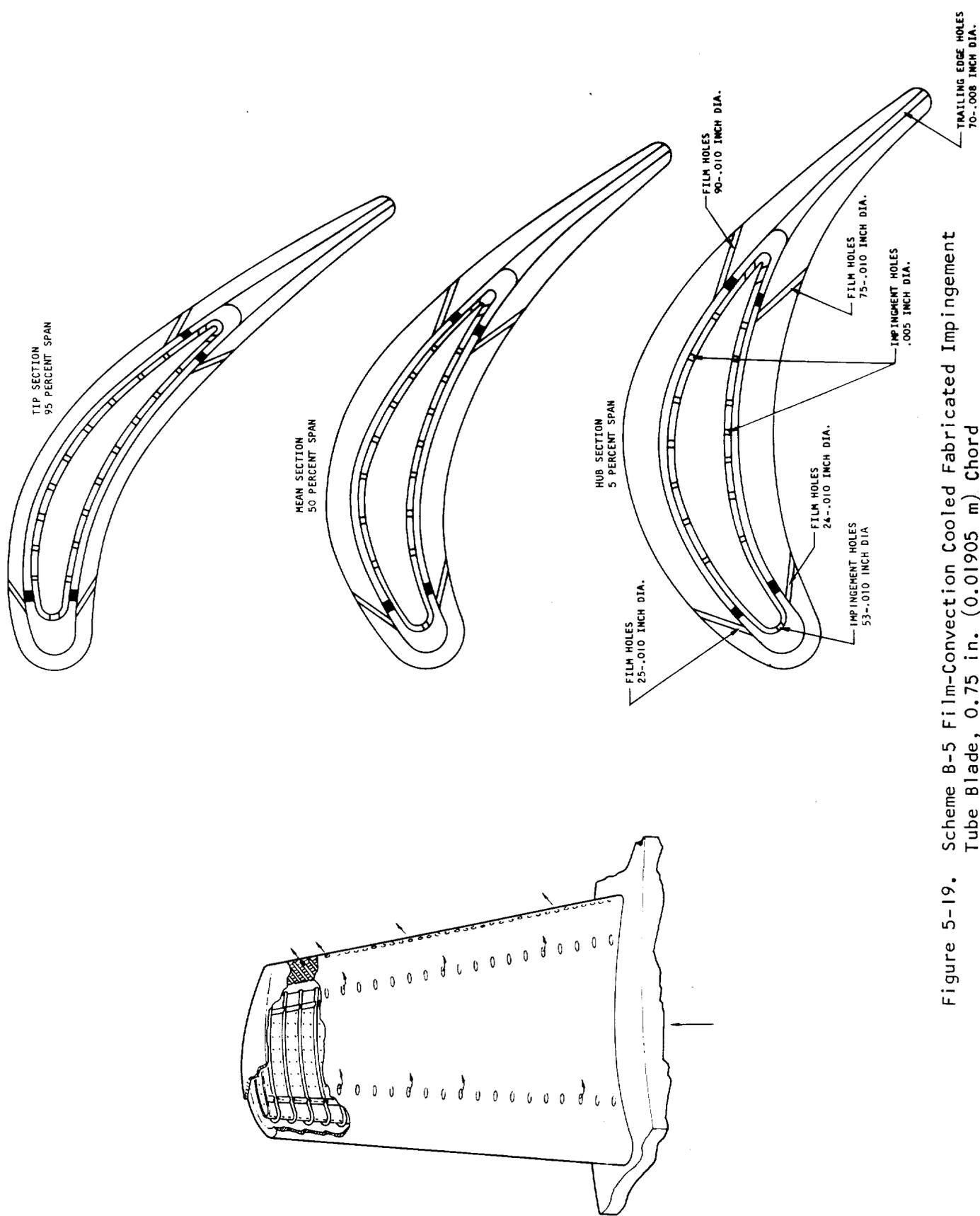
S-67867

Figure 5-19. Scheme B-5 Film-Convection Cooled Fabricated Impingement Tube Blade, 0.75 in. (0.01905 m) Chord

TIP SECTION
95 PERCENT SPAN

MEAN SECTION
50 PERCENT SPAN

HUB SECTION
5 PERCENT SPAN

TRAILING EDGE HOLES
62-.010 INCH DIA.

FILM HOLES
54-.015 INCH DIA.

FILM HOLES
48-.015 INCH DIA.

IMPINGMENT HOLES
.005 INCH DIA.

FILM HOLES
31-.010 INCH DIA.

FILM HOLES
31-.010 INCH DIA.

IMPINGMENT HOLES
54-.010 INCH DIA.
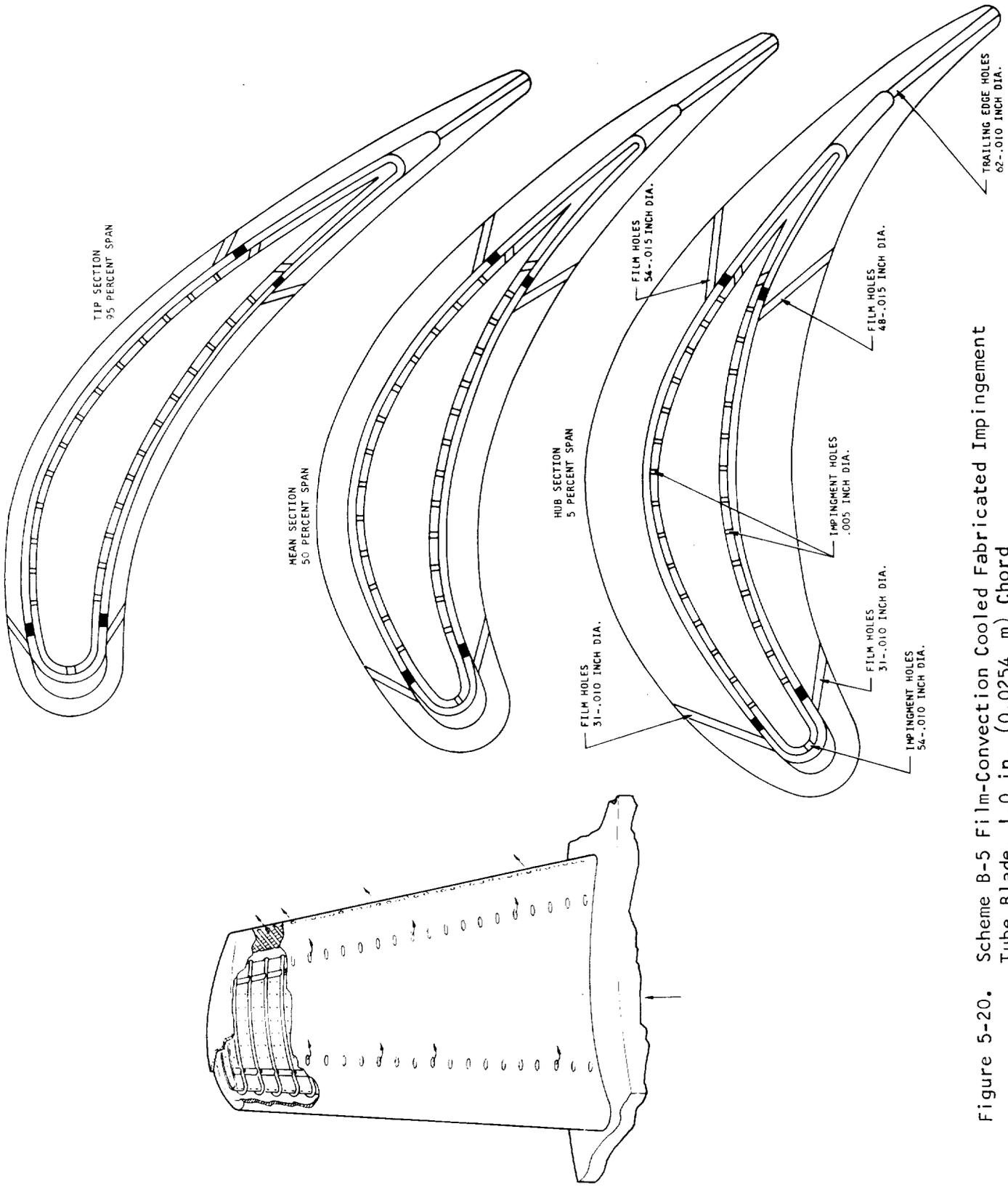
S-67868

Figure 5-20.   Scheme B-5 Film-Convection Cooled Fabricated Impingement
Tube Blade, 1.0 in. (0.0254 m) Chord

97

TIP SECTION
95 PERCENT SPAN

MEAN SECTION
50 PERCENT SPAN

HUB SECTION
5 PERCENT SPAN

TRAILING EDGE HOLES
36-.015 INCH DIA.

FILM HOLES
40-.020 INCH DIA.

FILM HOLES
35-.020 INCH DIA.

IMPINGMENT HOLES
.005 INCH DIA.

FILM HOLES
41-.010 INCH DIA.

IMPINGMENT HOLES
70-.010 INCH DIA.

FILM HOLES
44-.010 INCH DIA.
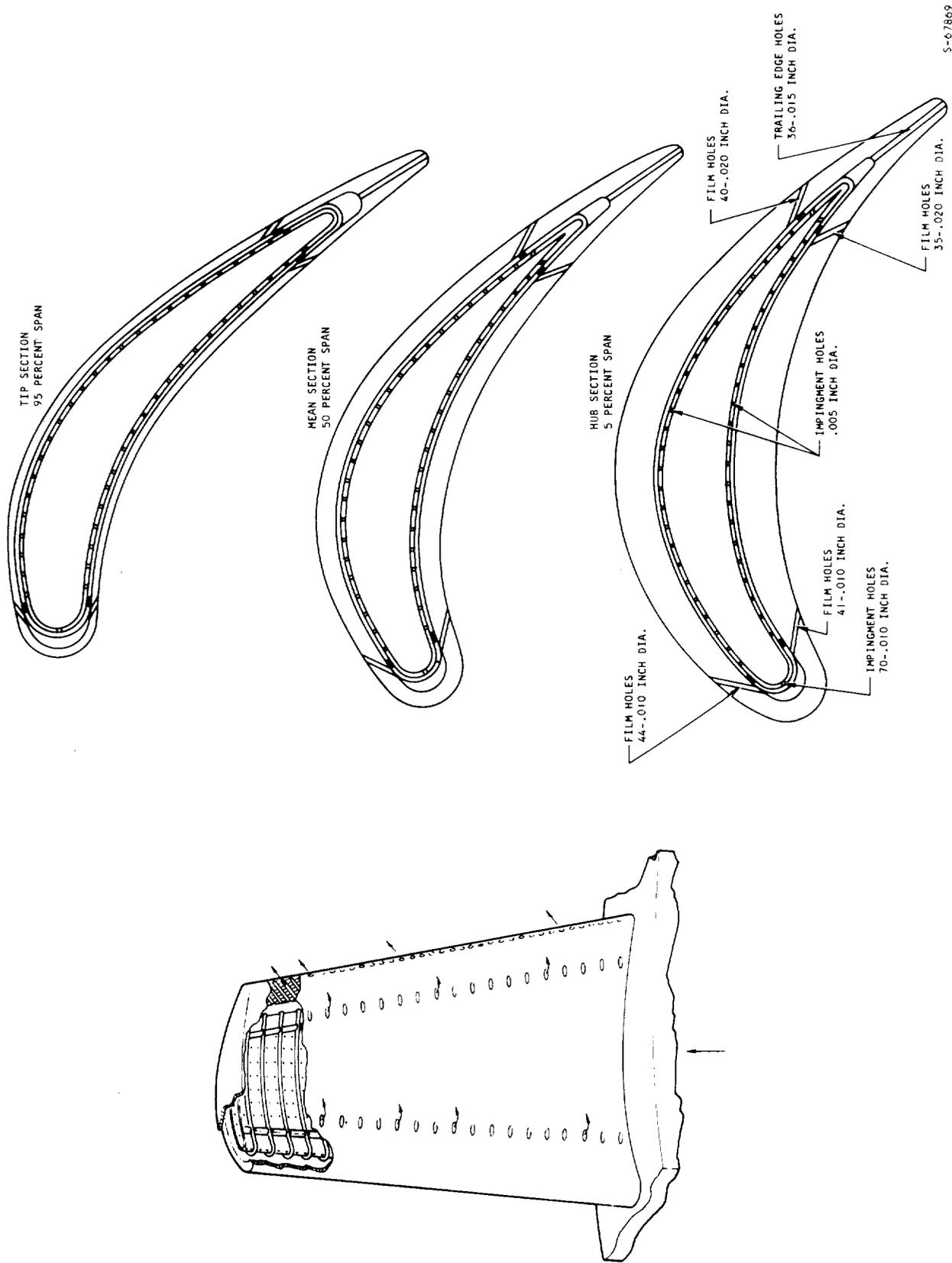
S-67869

Figure 5-21. Scheme B-5 Film-Convection Cooled Fabricated Impingement
Tube Blade, 1.5 in. (0.0381 m) Chord

stress between these parts. However, film cooling produces chordwise thermal gradients in the outer skin and stress concentrations in the areas of film injection. The increased material strength at lower temperatures tends to offset the increased stress and the combination of film and convection cooling produces low metal temperatures.

Table 5-2 indicates that a slight loss in turbine efficiency occurs in the 0.75 in. (0.01905 m) chord blade due to thickening the trailing edge. A small loss in efficiency also occurs due to film cooling.

Scheme C-1 Transpiration Cooled Blade

This concept is shown in Figures 5-22, 5-23, and 5-24 for the 0.75 in. (0.01905 m), 1.0 in. (0.0254 m), and 1.5 in. (0.0381 m) chord designs respectively. The design concept selected consists of a simulated transpiration cooled material wrapped around and welded to a supporting strut. To maintain the design trailing edge thickness with a minimum transpiration cooled material thickness of 0.02 in. (0.000508 m), it was necessary to have a film cooled trailing edge for the 0.75 in. (0.01905 m) and 1.0 in. (0.0254 m) chord blades. In the 0.75 in. (0.01905 m) chord blade each cavity is supplied with cooling air at the hub which flows radially and diffuses out through the porous surface. Additional cooling air is supplied at the two aft cavities to provide film cooling for the trailing edge of the blade. Because of the large cooling air flow required for film cooling, convection cooling was sufficient for the trailing edge cavities and the cooling air in this area was discharged through a row of holes on each side of the blade to provide more effective film cooling for the trailing edge.

In the 1.0 in. (0.0254 m) chord blade, the forward chambers are divided both radially and spanwise, and cooling air is supplied from the center cavity for a more optimum distribution of cooling air to each section. Also in this design, additional cooling air is supplied at the two aft cavities to provide film cooling at the trailing edge. Since the film cooled trailing edge was shorter in this design, less cooling flow was required and transpiration cooling was used for both trailing edge cavities.

In the 1.5 in. (0.0381 m) chord design, cooling air is supplied from the center cavity to the forward chambers which are divided both radially and spanwise. Cooling air flows radially in the two aft cavities and only a small additional flow is required for the short film cooled trailing edge section.

The transpiration cooled material used in the design and analysis was Lamilloy. The heat transfer and pressure drop analysis for the porous surface was based on friction factor and Colburn J-factor data developed from the data given in References 48 and 49. The reduction in the effective heat transfer coefficient from the hot gas to the blade was determined from equation 5-14 below taken from Friedman as described in Appendix C.

$$\frac{h}{h_o} = \frac{r\varphi}{e^{r\varphi} - 1} \qquad (5-14)$$

TIP SECTION
95 PERCENT SPAN

0.015

0.012

0.02

MEAN SECTION
50 PERCENT SPAN

FILM HOLES
55 - 0.010 INCH DIA.

HUB SECTION
5 PERCENT SPAN

FILM HOLES
46 - 0.01 INCH DIA.
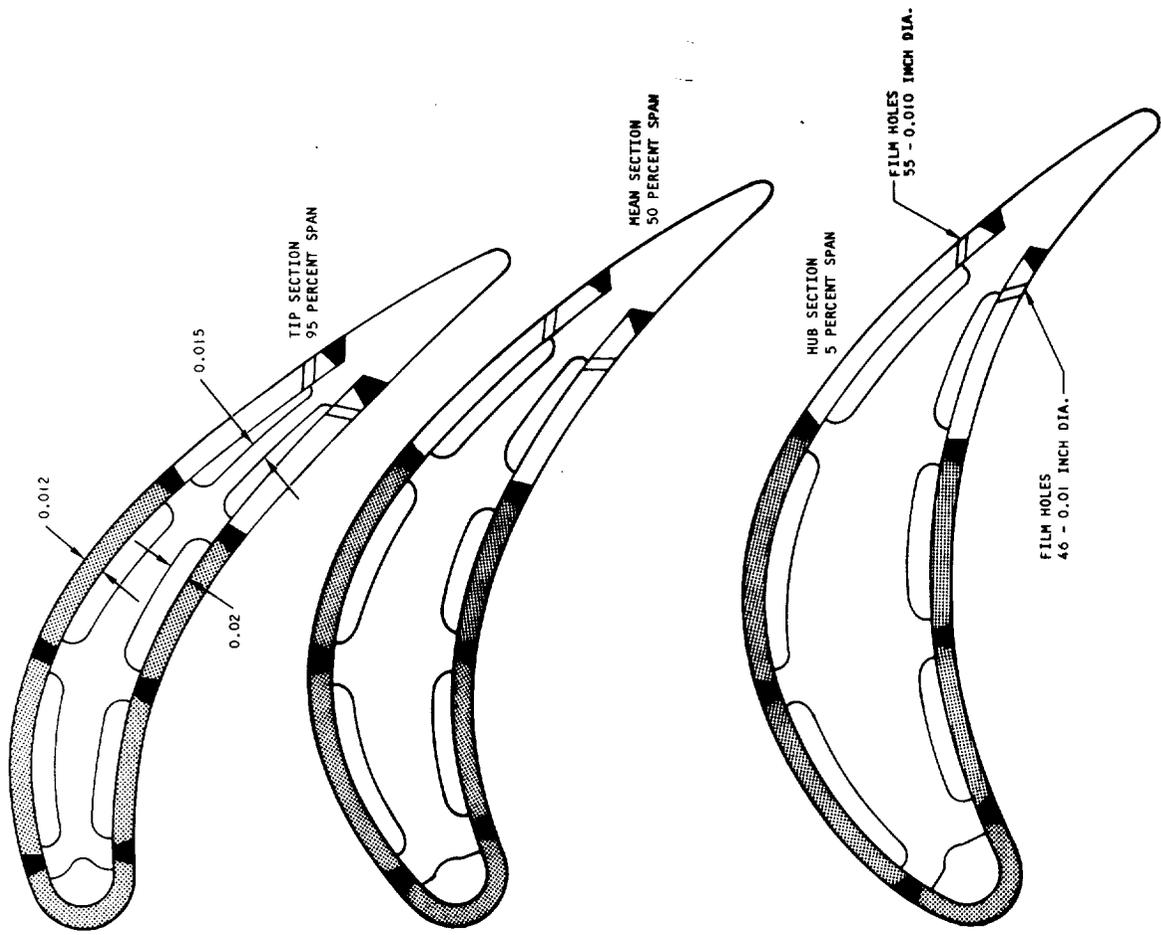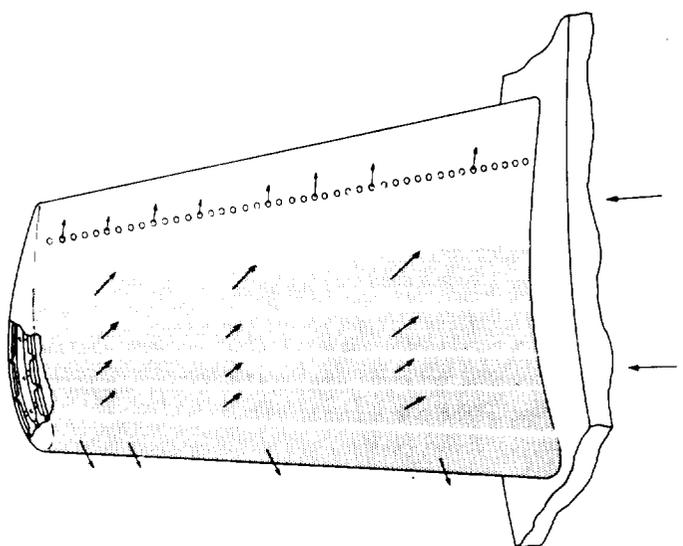
5-67870

Figure 5-22.   Scheme C-1 Transpiration Cooled Blade 0.75 in. (0.01905 m) Chord

TIP SECTION
(95 PERCENT SPAN)

MEAN SECTION
(50 PERCENT SPAN)

HUB SECTION
(5 PERCENT SPAN)

0.015

0.020

0.020
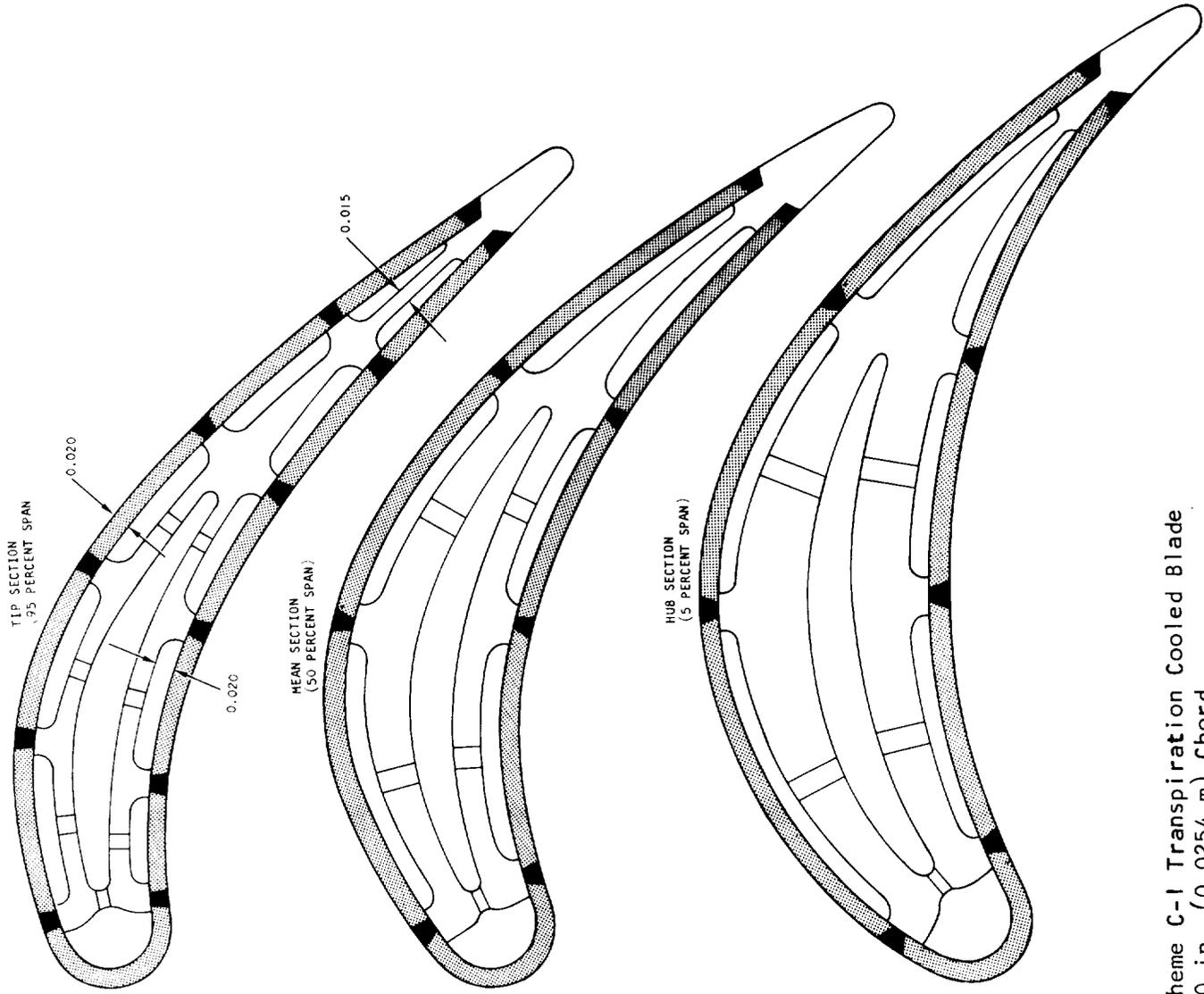
S-67871

Figure 5-23. Scheme C-1 Transpiration Cooled Blade
1.0 in. (0.0254 m) Chord

TIP SECTION
(95 PERCENT SPAN)

0.020

0.020

MEAN SECTION
(50 PERCENT SPAN)

HUB SECTION
(5 PERCENT SPAN)
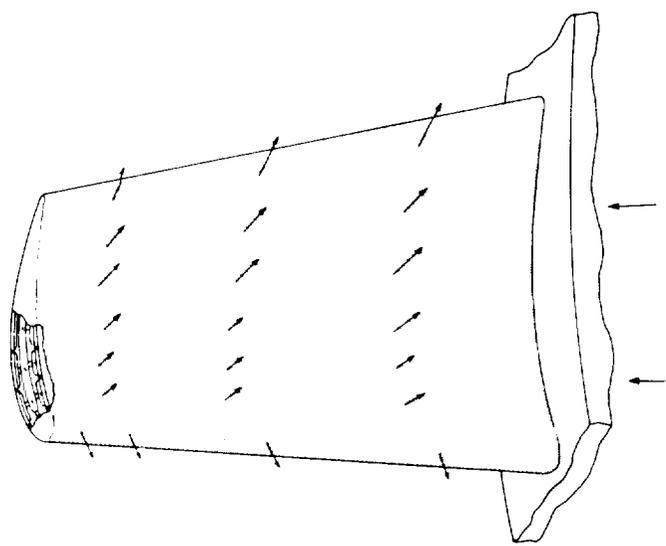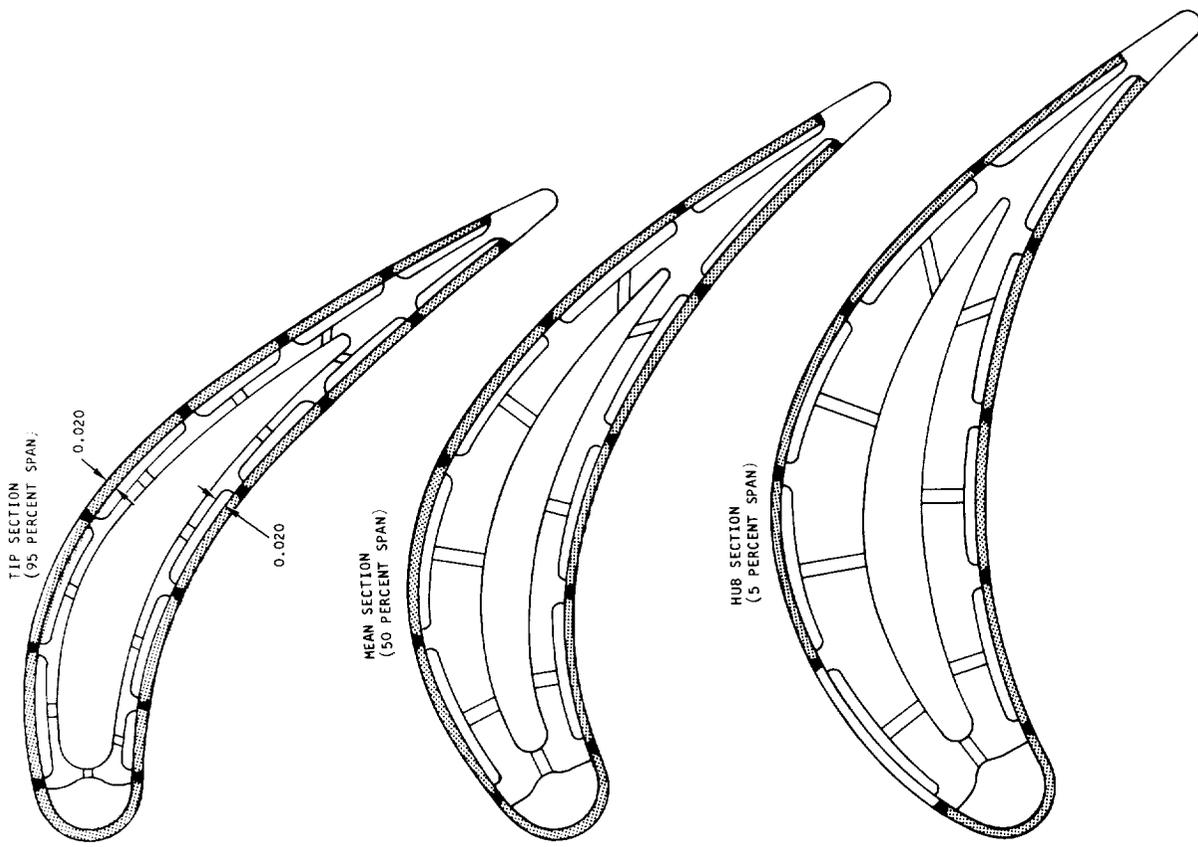
S-67872
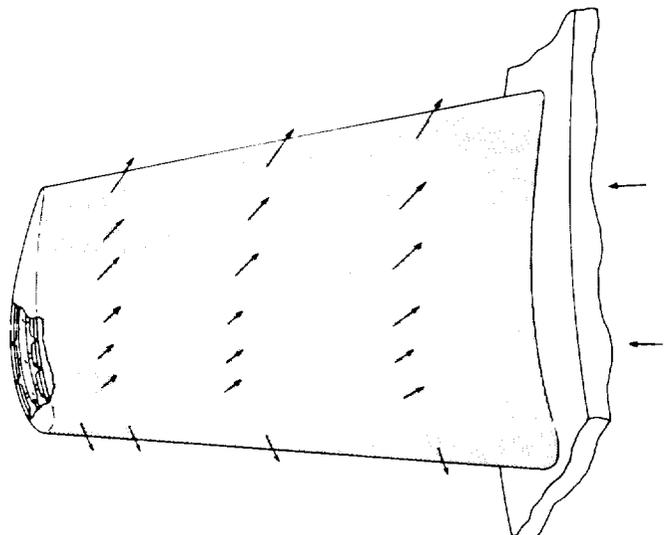
Figure 5-24. Scheme C-1 Transpiration Cooled Blade
1.5 in. (0.0381 m) Chord

102

where

$$r = \frac{2.11}{Re_g^{0.1}}$$

$$\varphi = \frac{C_p \rho_a V_a}{h_o}$$

$$h_o = 0.0296 \frac{k_g}{x} Re_g^{.8} Pr^{1/3}$$

The film cooled trailing edge was evaluated using equation 5-15 below, taken from Librizzi and Crisci as described in Appendix C.

$$\eta = \frac{1}{\left[1 + 0.33 \; \theta^{0.8}\right]} \tag{5-15}$$

where

$$\theta = \frac{X}{MS} \left(Re_a \frac{\mu_a}{\mu_*}\right)^{-0.25} \frac{\rho_*}{\rho_g}$$

The results obtained using this method of analysis were compared with experimental data on Lamilloy expressed in the form of transpiration cooling effectiveness (Ro) as given in Reference 13. This comparison indicated a difference of less than six percent between the calculated and experimental transpiration cooling effectiveness.

The stress calculations for this design were based on assuming that the strut acts as a structural support carrying the transpiration cooled material as a dead weight. The areas where the skin is welded to the strut were considered as part of the strut.

The limiting turbine inlet temperature for 1000 hr life with the Scheme C-1 design is 2370°F (1572.2°K) to 2940°F (1888.9°K). This cooling configuration shows a strong effect of chord size caused by the film cooled trailing edge limitation. In the calculation of the average metal temperature cooling effectiveness only the structural elements were considered and the average metal temperature cooling effectiveness was the highest of any design. If the transpiration cooled skin had been considered, the cooling effectiveness would have been somewhat lower. The maximum metal temperature effectiveness was limited by the film cooled trailing edge in every case. The cooling air thermal effectiveness was very high and the gradient ratio was the highest of any design. The high gradient ratio indicates that this design would have a very short low cycle fatigue life caused by the large thermal gradient between the film cooled trailing edge and the strut. This indicates that a transpiration cooled blade should be designed with a transpiration cooled trailing edge using either a thinner transpiration cooled material or a thicker trailing edge.

The aerodynamic effects shown in Table 5-2 indicate that this design would have the largest reduction in turbine efficiency of any design analyzed. Because of the large reduction in turbine efficiency and the difficulties encountered with the film cooled trailing edge for the smaller chord blades, this transpiration cooling concept is considered undesirable for turbine blades of less than 1.5 in. (0.0381 m) chord.

TASK I FINAL DESIGN

Objective

For the final design analysis, two turbine blade cooling configurations in each of the three chord sizes were selected. The maximum turbine inlet temperature for each of these designs was determined with three cooling air inlet temperatures and three turbine inlet total pressures. The cooling air flow requirements for a constant turbine inlet temperature and pressure was determined with three cooling air inlet temperatures for each design. The effects of a lower cooling air supply pressure for each design point were also calculated. Five additional points for the 1.0 in. (0.0254 m) chord blade were selected and the cooling design flow passages were altered in each case to achieve the maximum turbine inlet temperature or the minimum cooling air flow requirements.

The objective of this analysis was to provide information for the turbine designer on the effects on coolant flow requirements of using a heat exchanger to cool the turbine cooling air. In addition, the effects of engine pressure ratio and cooling air inlet pressure were also provided. This study was conducted on the basis of a coating life limit or a time to 1 percent creep strain of 1000 hr for each design in each chord size. The material used was coated IN-100.

A brief summary of the results for the convection cooled cast two-cavity pin fin blade Scheme A-1 and the film-convection cooled fabricated impingement tube blade Scheme B-5 final design analysis is shown in Tables 5-3 through 5-8. A detailed summary and discussion of the final design analysis results in presented below.

Scheme A-1 Convection Cooled Cast Two-Cavity Pin Fin Blade

The final design cooling configurations for the 0.75 in. (0.01905 m), 1.0 in. (0.0254 m), and 1.5 in. (0.0381 m) chord Scheme A-1 blades are shown in Figures 5-1, 5-2, and 5-3. In the final design configuration, the pins were eliminated at the hub section of the 0.75 in. (0.01905 m) chord design to reduce the thermal gradient at this section. For this reason, the cooling effectiveness at the hub section of the 0.75 in. (0.01905 m) is less than the mean section. However, the maximum thermal gradient is shifted to the mean section in almost every case. Pin fins were required at the hub section of the 1.0 in. (0.0254 m) and 1.5 in. (0.0381 m) chord blades to provide adequate cooling for 1000 hr stress life.

The final design analysis results for the convection cooled two-cavity pin fin blade Scheme A-1 are summarized in Table 5-9. These results are presented in the same form as the preliminary design results. The stress life of each blade was based on the minimum time to reach 1 percent creep strain after creep relaxation of the initial stress distribution. This is described as Method 3 in the stress analysis section. The maximum coating temperature limit is 1840°F (1277.8°K), the same as that used in the preliminary design analysis. The cooling passage flow area, the flow control orifices, the film cooling holes, and the trailing edge discharge holes are summarized in Table 5-10 for each Scheme A-1 final design analyzed.

TABLE 5-3

SUMMARY OF MAXIMUM TURBINE INLET TEMPERATURES FOR SCHEME A-1

Chord, in. (m)	0.75 (0.01905)			1.0 (0.0254)			1.5 (0.0381)		
Cooling air temperature, °F (°K)	1200 (922.2)	900 (755.6)	600 (588.9)	1200 (922.2)	900 (755.6)	600 (588.9)	1200 (922.2)	900 (755.6)	600 (588.9)
Turbine stator inlet total pressure, 450 psia (3.1 x 10^6 Newtons/sq m)		2290 (1527.8)			2330 (1550)			2280 (1522.2)	
Turbine stator inlet total pressure, 150 psia (1.034 x 10^6 Newtons sq m)	2100 (1422.2)	2300 (1533.3)	2465 (1625)	2220 (1488.9)	2390 (1583.3)	2580 (1688.9)	2175 (1463.9)	2350 (1561.1)	2560 (1677.8)
Turbine stator inlet total pressure, 50 psia (3.45 x 10^5 Newtons/sq m)		2270 (1516.7)			2310 (1538.9)			2340 (1555.6)	

Maximum turbine inlet temperature determined at each off design condition for a blade designed at the 150 psia (1.034 x 10^6 Newtons/sq m) turbine inlet pressure and 900°F (755.6 °K) cooling air inlet temperature condition.

TABLE 5-4

SUMMARY OF MINIMUM COOLING AIR FLOW RATIOS FOR SCHEME A-1
WITH A TURBINE INLET GAS TEMPERATURE OF 2100°F (1422.2°K)
AND A GAS TOTAL PRESSURE OF 150 PSIA (1.034 x 10^6 NEWTONS/SQ M)

Chord, in. (m)	0.75 (0.01905)			1.0 (0.0254)			1.5 (0.0381)		
Cooling air temperature, °F (°K)	1200 (922.2)	900 (755.6)	600 (588.9)	1200 (922.2)	900 (755.6)	600 (588.9)	1200 (922.2)	900 (755.6)	600 (588.9)
Minimum cooling air flow to hot gas flow ratio	0.0352	0.0219	0.0193	0.0249	0.0173	0.0141	0.0141	0.0117	0.0106

Determined for a constant turbine inlet temperature by varying only the flow control orifices.

TABLE 5-5

SUMMARY OF ADDITIONAL CONDITIONS FOR SCHEME A-1

		1.0 (0.0254)		
Maximum turbine inlet temperature determined for each point treated as a design point condition	Chord, in. (m)			
	Cooling air temperature, °F (°K)	1200 (922.2)	900 (755.6)	600 (588.9)
	Turbine stator inlet total pressure, 450 psia (3.1 x 10^6 Newtons/sq m)		2400 (1588.9)	
	Turbine stator inlet total pressure, 150 psia (1.034 x 10^6 Newtons/sq m)	2260 (1511.1)		2675 (1741.7)
	Turbine stator inlet total pressure, 50 psia (3.45 x 10^5 Newtons/sq m)			
Turbine rotor inlet gas temperature 2100°F (1422.2°K); turbine stator inlet total pressure 150 psia (1.034 x 10^6 newtons/sq m) Minimum cooling air flow ratio determined for a constant turbine inlet temperature by varying the flow control orifices, film cooling holes, and trailing edge discharge holes.	Chord, in. (m)		1.0	(0.0254)
	Cooling air temperature, °F (°K)	1200 (922.2)	900 (755.6)	600 (588.9)
	Minimum cooling air flow to hot gas flow ratio	0.023		0.0109

TABLE 5-6

SUMMARY OF MAXIMUM TURBINE INLET TEMPERATURES FOR SCHEME B-5

Chord, in. (m)	0.75 (0.01905)			1.0 (0.00254)			1.5 (0.0381)		
Cooling air temperature, °F (°K)	1200 (922.2)	900 (755.6)	600 (588.9)	1200 (922.2)	900 (755.6)	600 (588.9)	1200 (927.2)	900 (755.6)	600 (588.9)
Turbine stator inlet total pressure, 450 psia (3.1 x 10⁶ Newtons/ sq m)		2600 (1700)			2620 (1711.1)			2600 (1700)	
Turbine stator inlet total pressure, 150 psia (1.034 x 10⁶ Newtons/sq m)	2320 (1544.4)	2590 (1694.4)	2900 (1866.7)	2320 (1544.4)	2620 (1711.1)	2910 (1872.2)	2320 (1544.4)	2620 (1711.1)	2920 (1877.8)
Turbine stator inlet total pressure, 50 psia (3.45 x 10⁵ Newtons/sq m)		2570 (1683.3)			2570 (1683.3)			2570 (1677.8)	

Maximum turbine inlet temperature determined at each off design condition for a blade designed at the 150 psia (1.034 x 10⁶ Newtons/sq m) turbine inlet pressure and 900°F (755.6°K) cooling air inlet temperature condition.

TABLE 5-7

SUMMARY OF MINIMUM COOLING AIR FLOW RATIOS FOR SCHEME B-5

Chord, in. (m)	0.75 (0.01905)			1.0 (0.0254)			1.5 (0.0381)		
Turbine rotor inlet gas temperature, °F (°K)	2320 (1544.4)			2320 (1544.4)			2320 (1544.4)		
Cooling air temperature °F (°K)	1200 (922.2)	900 (755.6)	600 (588.9)	1200 (922.2)	900 (755.6)	600 (588.9)	1200 (922.2)	900 (755.6)	600 (588.9)
Minimum cooling air flow to hot gas flow ratio	0.0552	0.0273	0.0196	0.0476	0.0253	0.0187	0.0476	0.0335	0.0234

Determined for a constant turbine inlet temperature by varying only the flow control orifices.

TABLE 5-8

SUMMARY OF ADDITIONAL CONDITIONS FOR SCHEME B-5

		Cooling air temperature, °F (°K)		
Maximum turbine inlet temperature determined for each point treated as a design point condition.	Chord, in. (m)	1.0 (0.0254)		
	Cooling air temperature, °F (°K)	1200 (922.2)	900 (755.6)	600 (588.9)
	Turbine stator inlet total pressure, 450 psia (3.1 x 10⁶ Newtons/sq m)			2990 (1916.7)
	Turbine stator inlet total pressure, 150 psia (1.034 x 10⁶ Newtons/sq m)	2350 (1561.1)		
	Turbine stator inlet total pressure, 50 psia (3.45 x 10⁵ Newtons/sq m)		2660 (1733.3)	
Turbine rotor inlet gas temperature 2320°F (1544.4°K); turbine stator inlet total pressure 150 psia (1.034 x 10⁶ newtons/ sq m)	Chord, in. (m)	1.0 (0.0254)		
Minimum cooling air flow ratio determined for a constant turbine inlet temperature by varying the flow control orifices, film cooling holes, and trailing edge discharge holes.	Cooling air temperature, °F (°K)	1200 (922.2)	900 (755.6)	600 (588.9)
	Minimum cooling air flow to hot gas flow ratio	0.0444		0.0176

The maximum turbine inlet temperature which will produce a life of 1000 hr at the critical stressed element of the blade was calculated as described in the preliminary design analysis section.

The first five conditions in the summary chart, Table 5-9, for each chord size represent the performance of cooling configuration with fixed flow control orifices, cooling passage dimensions, and film cooling holes. The next three conditions represent the cooling flow required for a constant turbine inlet temperature and a variable cooling air inlet temperature. These results were obtained by varying the flow control orifice sizes only and maintaining a constant cooling passage dimension and film cooling hole size. The five additional conditions for the 1.0 in. (0.0254 m) chord blade were obtained by varying the film cooling hole sizes and the flow control orifice sizes to obtain the maximum turbine inlet temperature for the first three additional conditions and to obtain the minimum cooling air flow required for the last two additional conditions.

The results of this analysis show that for the convection cooled pin fin blade Scheme A-1, a variation of 300°F (166.7°K) in the cooling air inlet temperature produces a related variation of from 160°F (88.9°K) to 200°F (111.1°K) in the allowable turbine inlet temperature. Therefore the allowable turbine inlet temperature changes only 53.3 to 66.7 percent as much as the cooling air inlet temperature. This indicates that this convection cooled design is not as severely affected by an increase in cooling air inlet temperature, but its capabilities cannot be increased substantially by a decrease in cooling air inlet temperature.

Studies conducted at NASA Lewis on the effect of chord size on weight and cooling of turbine blades are presented in Esgar, Schum, and Curren (Reference 15). These results indicate that required coolant flow for a 0.5-in. (0.0127 m) chord blade is twice that for 1.0-in. (0.0254 m) chord convection cooled blade with a turbine inlet temperature of 2030°F (1388.9°K) and a cooling air inlet temperature of 787°F (692.8°K). This agrees with the results shown in Table 5-9, which indicates that the required coolant flow for a 0.75-in. (0.01905 m) chord blade is about twice that for a 1.5-in. (0.0281 m) chord pin fin convection cooled blade with turbine inlet temperature of 2100°F (1422.2°K) and cooling air inlet temperature of 900°F (755.6°K).

The results also indicate that the effect of pressure on turbine inlet temperature capability is rather small over the range of turbine inlet pressures from 50 psia (3.45 x 10^5 Newtons/sq m) to 450 psia (3.1 x 10^6 Newtons/sq m). The heat transfer analysis showed that when turbine inlet total pressure increased from 150 psia (1.034 x 10^6 Newtons/sq m) to 450 psia (3.1 x 10^6 Newtons/sq m), the leading and trailing edges cool off, or remain about the same temperature, while the midchord region gets slightly hotter. This decreases the chordwise thermal gradients, but the thermal gradient through the blade wall is increased. The overall thermal gradient increases because the wall separating the leading edge and midchord passage is cooled more as the pressure increases. Also, as the pressure increases the cooling fluid capacity rate $(W_c C_p)$ increases faster than the thermal conductance. This accounts for the decreased thermal effectiveness (η_t) as the pressure increases and helps to explain why there is no large change in cooling effectiveness (ϕ) for the blade as the pressure increases.

TABLE 5-9

DETAILED SUMMARY OF THE RESULTS FOR THE
SCHEME A-1 FINAL DESIGN TASK I ANALYSIS

Condition* Number	Chord in. (m)	P_{T_g} Psia (Newtons/sq m)	T_{ci} °F (°K)	T_g Analysis °F (°K)	$\frac{W_{CA}(100)}{W_g}$	σ_R	σ_m	σ_{max}	τ_t	R_g	Stress Critical Section	T_g Maximum °F (°K)	Critical Condition
1	0.75 (0.01905)	150 (1.034 × 10⁶)	1200 (922.2)	2100 (1422.2)	3.52	0.5799	0.5663	0.3233	0.6989	0.29	Mean	2100 (1422.2)	2
1	0.75 (0.01905)	150 (1.034 × 10⁶)	900 (755.6)	2300 (1533.3)	4.06	0.5394	0.5596	0.3276	0.6643	0.3036	Mean	2300 (1533.3)	1
1	0.75 (0.01905)	150 (1.034 × 106)	600 (588.9)	2465 (1625)	4.745	0.5262	0.5627	0.3346	0.6335	0.3131	Mean	2465 (1625)	1
1	0.75 (0.01905)	450 (3.1 × 10⁶)	900 (755.6)	2300 (1533.3)	4.07	0.5407	0.5502	0.3239	0.4906	0.3943	Root	2990 (1527.8)	1
1	0.75 (0.01905)	50 (3.45 × 10⁵)	900 (755.6)	2250 (1505.6)	4.03	0.5237	0.5551	0.3096	0.8222	0.2237	Mean	2270 (1516.7)	1
2	0.75 (0.01905)	150 (1.034 × 10⁶)	1200 (922.2)	2100 (1422.2)	3.52	0.5799	0.5663	0.3233	0.6989	0.29	Mean	2100 (1422.2)	2
2	0.75 (0.01905)	150 (1.034 × 10⁶)	900 (755.6)	2100 (1422.2)	2.19	0.4667	0.4683	0.2298	0.7017	0.26	Mean	2100 (1422.2)	2
2	0.75 (0.01905)	150 (1.034 × 10⁶)	600 (588.9)	2100 (1422.2)	1.926	0.4260	0.4302	0.1875	0.6954	0.2593	Mean	2100 (1422.2)	2
2	1.0 (0.0254)	150 (1.034 × 10⁶)	1200 (922.2)	2220 (1488.9)	4.163	0.6775	0.5373	0.3819	0.6297	0.2667	Root	2200 (1488.9)	2
1	1.0 (0.0254)	150 (1.034 × 10⁶)	900 (755.6)	2400 (1588.9)	4.79	0.6421	0.5235	0.3689	0.6035	0.268	Mean	2390 (1583.3)	1
1	1.0 (0.0254)	150 (1.034 × 10⁶)	600 (588.9)	2600 (1700)	5.65	0.6286	0.5281	0.3746	0.5765	0.311	Root	2580 (1688.9)	1
1	1.0 (0.0254)	450 (3.1 × 10⁶)	900 (755.6)	2300 (1573.3)	4.805	0.6177	0.5208	0.3392	0.4494	0.38	Root	2330 (1550)	1
1	1.0 (0.0254)	50 (3.45 × 10⁵)	900 (755.6)	2320 (1544.4)	4.54	0.6625	0.5117	0.3335	0.7593	0.2458	Root	2310 (1538.9)	1
2	1.0 (0.0254)	150 (1.034 × 10⁶)	1200 (922.2)	2100 (1422.2)	2.485	0.6379	0.4648	0.2927	0.7339	0.2411	Root	2100 (1422.2)	2
2	1.0 (0.0254)	150 (1.034 × 10⁶)	900 (755.6)	2100 (1422.2)	1.733	0.5654	0.3898	0.2337	0.7811	0.265	Root	2100 (1422.2)	2
2	1.0 (0.0254)	150 (1.034 × 10⁶)	600 (588.9)	2100 (1422.2)	1.46	0.5156	0.3472	0.1925	0.8016	0.2713	Root	2100 (1422.2)	2
1A	1.0 (0.0254)	150 (1.034 × 10⁶)	1200 (922.2)	2300 (1533.3)	4.9	0.6903	0.5593	0.4075	0.5568	0.2636	Root	2260 (1511.1)	2
1A	1.0 (0.0254)	450 (1.034 × 10⁶)	900 (755.6)	2400 (1588.9)	5.33	0.635	0.5491	0.3717	0.4737	0.324	Root	2400 (1588.9)	1
1A	1.0 (0.0254)	150 (1.034 × 10⁶)	600 (588.9)	2700 (1755.5)	6.01	0.6421	0.5457	0.4021	0.6043	0.2995	Root	2675 (1741.7)	1
2A	1.0 (0.0254)	150 (1.034 × 10⁶)	1200 (922.2)	2100 (1422.2)	2.302	0.6349	0.4601	0.2919	0.7611	0.2456	Root	2100 (1422.2)	2

111

TABLE 5-9 (Continued)

Condition* Number	Chord in. (m)	P_{T_g} Psia (Newtons/sq m)	T_{ci} °F (°K)	T_g Analysis °F (°K)	$\dfrac{W_{CA}(100)}{W_g}$	ϕ_R	ϕ_m	ϕ_{max}	η_t	R_g	Stress Critical Section	T_g Maximum °F (°K)	Critical Condition
2A	1.0 (0.0254)	150 (1.034 × 10⁶)	600 (588.9)	2100 (1422.2)	1.086	0.4807	0.3004	0.1699	0.8330	0.2447	Root	2100 (1422.2)	2
1	1.5 (0.0381)	150 (1.034 × 10⁶)	1200 (922.2)	2220 (1488.9)	4.09	0.6407	0.4974	0.371	0.5153	0.3618	Root	2175 (1463.9)	2
1	1.5 (0.0381)	150 (1.034 × 10⁶)	900 (755.6)	2400 (1588.9)	4.67	0.6093	0.4899	0.3667	0.4875	0.3972	Root	2350 (1561.1)	2
1	1.5 (0.0381)	150 (1.034 × 10⁶)	600 (588.9)	2560 (1677.8)	5.58	0.596	0.4936	0.3722	0.4562	0.4026	Root	2560 (1677.8)	2
1	1.5 (0.0381)	450 (3.1 × 10⁶)	900 (755.6)	2290 (1527.8)	4.7	0.5775	0.4727	0.3181	0.3486	0.4381	Root	2280 (1522.2)	1
1	1.5 (0.0381)	50 (3.45 × 10⁵)	900 (755.6)	2340 (1555.5)	4.51	0.635	0.4913	0.3501	0.6340	0.341	Root	2340 (1555.5)	2
2	1.5 (0.0381)	150 (1.034 × 10⁶)	1200 (922.2)	2100 (1422.2)	1.407	0.7019	0.5153	0.2964	0.6836	0.33	Root	2100 (1422.2)	1
2	1.5 (0.0381)	150 (1.034 × 10⁶)	900 (755.6)	2100 (1422.2)	1.172	0.6522	0.4657	0.2186	0.6926	0.37	Root	2100 (1422.2)	1
2	1.5 (0.0381)	150 (1.034 × 10⁶)	600 (588.9)	2100 (1422.2)	1.06	0.5485	0.4305	0.1764	0.6943	0.4107	Root	2100 (1422.2)	1

CRITICAL CONDITIONS:

1. Turbine inlet temperature limited by maximum coating temperature of 1840°F (1277.8°K) for 1000 hr life with 0.02 in. (0.000508 m) thick IN-100 material.

2. Turbine inlet temperature limited by a minimum time to 1 percent creep strain of 1000 hr after relaxation of the thermal stress distribution due to creep.

*CONDITION NUMBER

1. Maximum turbine inlet temperature determined at each off design condition for a blade designed at the 150 psia (1.034 × 10⁶ Newtons/sq m) turbine inlet pressure and 900°F (755.6°K) cooling air inlet temperature condition.

2. Minimum cooling air flow required determined as a function of cooling air inlet temperature for a constant turbine inlet temperature by varying only the flow control orifices.

1A. Maximum turbine inlet temperature determined for each point treated as a design point condition.

2A. Minimum cooling air flow required determined as a function of cooling air inlet temperature by varying the flow control orifices, film cooling holes, and trailing edge discharge holes.

Condition Number		1	1	2	2	2	1	1	2	2
Blade Chord	in. (m)	0.75 0.01905	0.75 0.01905	0.75 0.01905	0.75 0.01905	0.75 0.01905	1.0 0.0254	1.0 0.0254	1.0 0.0254	1.0 0.0254
Cooling Air Inlet Temperature	°F (°K)	600 to 1200 588.9 to 922.2	900. 755.6	1200. 922.2	900. 755.6	600. 588.9	600. to 1200. 588.9 to 922.2	900. 755.6	1200. 922.2	900. 755.6
Cooling Air Supply Pressure Drop Ratio	(ΔP/Pco)	0.08	0.10	0.08	0.08	0.08	0.08	0.10	0.08	0.08
Leading Edge Flow Area	sq in. (sq m)	0.00556 3.59×10^{-6}	0.00556 3.59×10^{-6}	0.00556 3.59×10^{-6}	0.00556 3.59×10^{-6}	0.00556 3.59×10^{-6}	0.01185 7.65×10^{-6}	0.01185 7.65×10^{-6}	0.01185 7.65×10^{-6}	0.01185 7.65×10^{-6}
Leading Edge Root Orifice	sq in. (sq m)	0.0045 2.9×10^{-6}	0.0045 2.9×10^{-6}	0.0045 2.9×10^{-6}	0.0045 2.9×10^{-6}	0.0045 2.9×10^{-6}	0.01185 7.65×10^{-6}	0.01185 7.65×10^{-6}	0.01185 7.65×10^{-6}	0.01185 7.65×10^{-6}
Leading Edge Tip Orifice	sq in. (sq m)	0.0032 2.06×10^{-6}	0.0036 2.32×10^{-6}	0.0032 2.06×10^{-6}	0.0010 0.645×10^{-6}	0.00075 0.484×10^{-6}	0.00932 6.01×10^{-6}	0.00966 6.23×10^{-6}	0.00336 2.17×10^{-6}	0.0017 1.1×10^{-6}
Midchord Passage Flow Area	sq in. (sq m)	0.0345 22.26×10^{-6}	0.0345 22.26×10^{-6}	0.0345 22.26×10^{-6}	0.0345 22.26×10^{-6}	0.0345 22.26×10^{-6}	0.0657 42.39×10^{-6}	0.0657 42.39×10^{-6}	0.0657 42.39×10^{-6}	0.0657 42.39×10^{-6}
Midchord Passage Root Orifice	sq in. (sq m)	0.0073 4.71×10^{-6}	0.0076 4.9×10^{-6}	0.0073 4.71×10^{-6}	0.0041 2.65×10^{-6}	0.00324 2.09×10^{-6}	0.00957 6.17×10^{-6}	0.01056 6.81×10^{-6}	0.006 3.87×10^{-6}	0.00425 2.74×10^{-6}
Midchord Passage Tip Orifice	sq in. (sq m)	0.023 14.84×10^{-6}	0.023 14.84×10^{-6}	0.023 14.84×10^{-6}	0.023 14.84×10^{-6}	0.023 14.84×10^{-6}	0.00686 4.43×10^{-6}	0.00745 4.81×10^{-6}	0.0447 28.84×10^{-6}	0.0447 28.84×10^{-6}
Trailing Edge Hole Diameter	in. (m)	0.015 0.000381	0.015 0.000381	0.015 0.000381	0.015 0.000381	0.015 0.000381	0.01 0.000254	0.01 0.000254	0.01 0.000254	0.01 0.000254
Trailing Edge Hole Spacing to Diameter Ratio Percent Span										
0.0 to 5.0		3.47	3.47	3.47	3.47	3.47	2.0	2.0	2.0	2.0
5.0 to 47.5		3.78	3.78	3.78	3.78	3.78	2.0	2.0	2.0	2.0
47.5 to 52.5		3.0	3.0	3.0	3.0	3.0	2.0	2.0	2.0	2.0
52.5 to 72.5		2.7	2.7	2.7	2.7	2.7	2.0	2.0	2.0	2.0
72.5 to 77.5		2.45	2.45	2.45	2.45	2.45	2.0	2.0	2.0	2.0
77.5 to 100.0		2.4	2.4	2.4	2.4	2.4	2.0	2.0	2.0	2.0

LED CAST TWO CAVITY PIN
ING PASSAGE DIMENSION SUMMARY

2	1A	1A	1A	2A	2A	1	1	2	2	2
1.0 0.0254	1.0 0.0254	1.0 0.0254	1.0 0.0254	1.0 0.0254	1.0 0.0254	1.5 0.0381	1.5 0.0381	1.5 0.0381	1.5 0.0381	1.5 0.0381
600. 588.9	1200. 922.2	900. 755.6	600. 588.9	1200. 922.2	600. 588.9	600. to 1200 588.9 to 922.2	900. 755.6	1200. 922.2	900. 755.6	600. 588.9
0.08	0.08	0.08	0.08	0.08	0.08	0.08	0.10	0.08	0.08	0.08
0.01185 7.65×10^{-6}	0.01185 7.65×10^{-6}	0.01185 7.65×10^{-6}	0.01185 7.65×10^{-6}	0.01185 7.65×10^{-6}	0.01185 7.65×10^{-6}	0.0358 23.1×10^{-6}	0.0358 23.1×10^{-6}	0.0358 23.1×10^{-6}	0.0358 23.1×10^{-6}	0.0358 23.1×10^{-6}
0.01185 7.65×10^{-6}	0.01185 7.65×10^{-6}	0.01185 7.65×10^{-6}	0.01185 7.65×10^{-6}	0.01185 7.65×10^{-6}	0.01185 7.65×10^{-6}	0.02 12.09×10^{-6}	0.02 12.09×10^{-6}	0.02 12.09×10^{-6}	0.03 19.35×10^{-6}	0.0358 23.1×10^{-6}
0.0012 0.774×10^{-6}	0.0086 5.55×10^{-6}	0.00595 3.84×10^{-6}	0.0076 4.9×10^{-6}	0.00272 1.75×10^{-6}	0.00098 0.632×10^{-6}	0.01 6.45×10^{-6}	0.0106 6.84×10^{-6}	0.00208 1.34×10^{-6}	0.00111 0.716×10^{-6}	0.00072 0.465×10^{-6}
0.0657 42.39×10^{-6}	0.0657 42.39×10^{-6}	0.0657 42.39×10^{-6}	0.0657 42.39×10^{-6}	0.0657 42.39×10^{-6}	0.0657 42.39×10^{-6}	0.181 1.17×10^{-4}	0.181 1.17×10^{-4}	0.181 1.17×10^{-4}	0.181 1.17×10^{-4}	0.181 1.17×10^{-4}
0.00317 2.05×10^{-6}	0.024 15.5×10^{-6}	0.0156 10.1×10^{-6}	0.014 9.03×10^{-6}	0.006 3.87×10^{-6}	0.00227 1.46×10^{-6}	0.0123 7.93×10^{-6}	0.0143 9.23×10^{-6}	0.00576 3.72×10^{-6}	0.00477 3.08×10^{-6}	0.00392 2.53×10^{-6}
0.0447 28.84×10^{-6}	0.0055 3.55×10^{-6}	0.0073 4.71×10^{-6}	0.006 3.87×10^{-6}	0.0447 28.84×10^{-6}	0.0447 28.84×10^{-6}	0.02 12.9×10^{-6}	0.018 11.6×10^{-6}	0.122 78.7×10^{-6}	0.122 78.7×10^{-6}	0.122 78.7×10^{-6}
0.01 0.000254	0.01 0.000254	0.01 0.000254	0.01 0.000254	0.01 0.000254	0.01 0.000254	0.015 0.000381	0.015 0.000381	0.015 0.000381	0.015 0.000381	0.015 0.000381

2	1A	1A	1A	2A	2A	1	1	2	2	2
2.0	2.0	2.0	2.0	2.0	2.8	2.0	2.0	2.0	2.0	2.0
2.0	2.0	2.0	2.0	2.0	2.8	2.56	2.56	2.56	2.56	2.56
2.0	2.0	2.0	2.0	2.0	2.8	2.74	2.74	2.74	2.74	2.74
2.0	2.0	2.0	2.0	2.0	2.8	2.82	2.82	2.82	2.82	2.82
2.0	2.0	2.0	2.0	2.0	2.8	2.84	2.84	2.84	2.84	2.84
2.0	2.1	2.1	2.1	2.0	2.8	2.92	2.92	2.92	2.92	2.92

As the turbine inlet pressure decreases, the leading and trailing edges get hotter while the midchord gets cooler. The temperature of the wall separating the leading edge and midchord passages increases and the overall thermal gradient decreases. The thermal effectiveness (η_t) increases and the cooling effectiveness (ϕ) remains essentially constant.

The leading edge cools down with an increase in pressure because the external heat transfer coefficient is proportional to the square root of the pressure $(H_g \sim (P_g)^{.5})$ while the internal heat transfer coefficient is proportional to the eight-tenths power of the coolant flow rate which is directly proportional to pressure $(H_c \sim (W_c)^{.8})$. The trailing edge cools off as the pressure increases because the temperature rise of the coolant decreases which results in lower film temperatures at the trailing edge. The midchord region heats up as the pressure increases because the external heat transfer coefficient is proportional to the eight-tenths power of the pressure along the sides of the blade and the pin fin heat transfer coefficient is proportional to the seven-tenths power of the coolant flowrate.

The analytical results also indicate that the cooling air flow through a cooled turbine blade with fixed flow control orifices, film cooling hole sizes, and cooling passage dimensions may be determined for the off-design point conditions by equating the off-design flow function based on the cooling air inlet temperature and pressure to the design point flow function.

$$\left(\frac{W_c \sqrt{T_{ci}}}{P_{ci}}\right)_D = \left(\frac{W_c \sqrt{T_{ci}}}{P_{ci}}\right)_{OD}$$

While this relation is not exact because of fluid heating and rotational acceleration effects, it does provide a good rapid approximation.

A study of the effects of cooling air flow requirements as a function of cooling air inlet temperature and chord size for a constant turbine inlet temperature and pressure was also conducted. The results of this study for the Scheme A-I blade are shown in Table 5-10 and Figure 5-25. The results shown in Figure 5-25 indicate that the cooling air flow requirements drop rapidly from a cooling air inlet temperature of 1200°F (922.2°K) to 900°F (755.6°K) but only a small reduction is achieved from 900°F (755.6°K) to 600°F (588.9°K). A substantial reduction in cooling airflow requirements was also obtained by increasing the blade chord, with a greater percentage reduction occurring at the highest cooling air inlet temperature.

The results of a study of the additional conditions for the 1.0 in. (0.0254 m) chord Scheme A-I blade indicates that the turbine inlet temperatures for the off-design conditions may be increased about 100°F (55.6°K) by varying both the flow control orifices and the film cooling holes. These results also indicate that the additional capability of varying film cooling holes produces only a slight reduction in cooling air flow for a constant turbine inlet temperature.
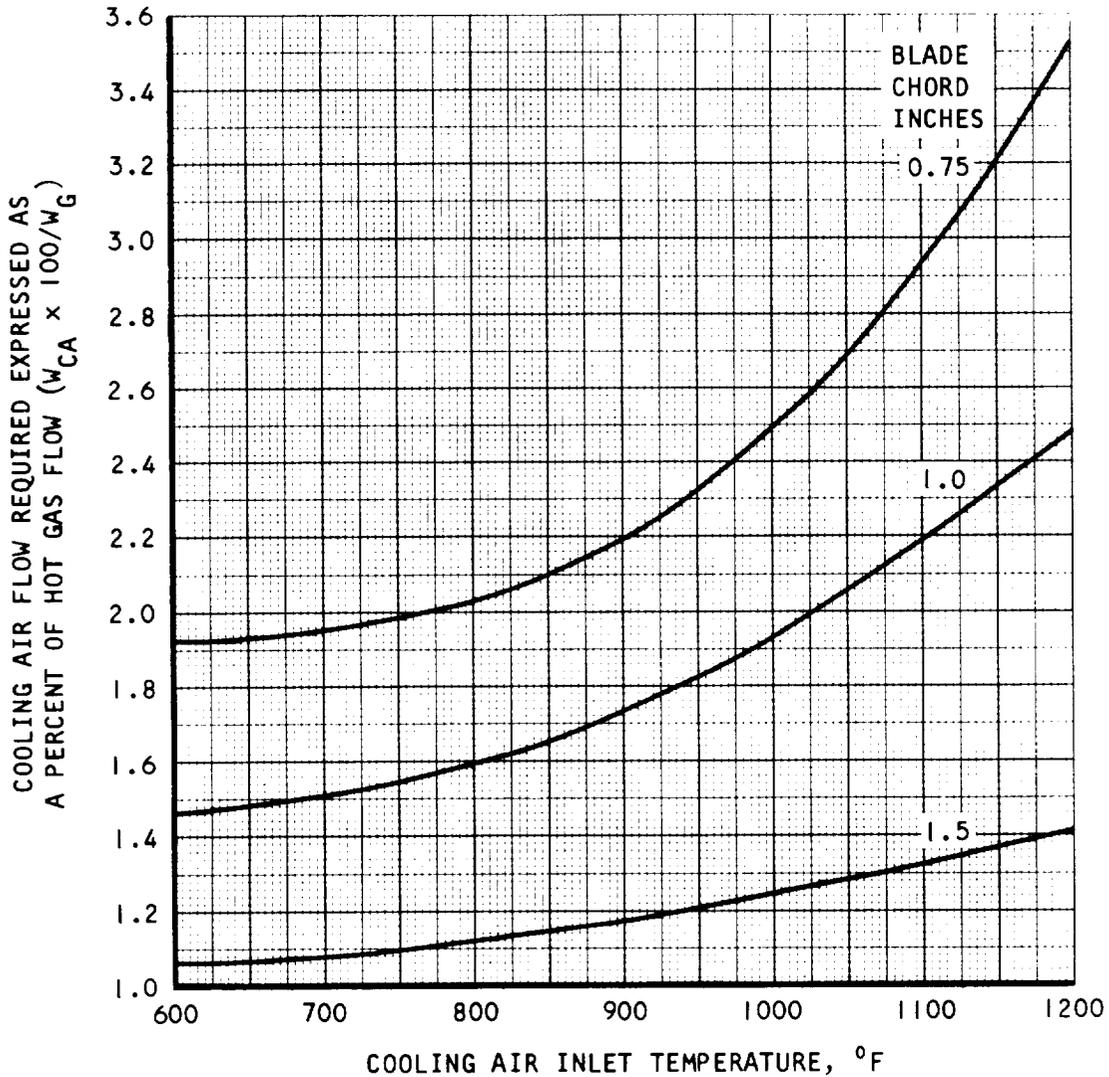
Figure 5-25. Cooling Air Flow Required as a Function of
Cooling Air Inlet Temperature for the
Scheme A-1 Final Design

The detailed boundary conditions for the three turbine inlet total pressure levels and for the 1200°F (922.2°K) cooling air inlet temperature condition in each chord size are shown in Appendix J. The metal temperature distribution for each design point condition in each chord size is also shown in Appendix J. Figures showing the cooling flow distribution for every condition with a turbine inlet total pressure of 150 psia (1.034 x 10⁶ Newtons/ sq m) are given in Appendix J. The effects of increasing the total pressure drop in ducting the cooling air from the compressor to the blade hub ($\Delta P/P_{co}$ = 0.1) are also presented in Appendix J.

The detailed metal temperature and stress analysis results for each chord size at each final design condition are given in Appendix K. Tables showing metal temperatures, stress, and stress-to-rupture life for each element of the hub, mean, and 75 percent span sections at each condition are presented. Figures showing the stress relaxation due to creep and the creep elongation for the critical elements of the stress limited designs are also shown. A creep stress analysis was not performed for every condition since the results for one condition could be used for a similar condition.

Scheme B-5 Film-Convection Cooled Fabricated Impingement Tube Blade

The final design configuration for the 0.75 in. (0.01905 m), 1.0 in. (0.0254 m), and 1.5 in. (0.0381 m) chord Scheme B-5 blades are shown in Figures 5-19, 5-20, and 5-21. In the final design configuration, the impingement holes and the film cooling hole sizes were finalized for the design point condition (P_g = 150 psia (1.034 x 10⁶ Newtons/sq m)) and T_{ci} = 900°F (755.6°K). The cooling passage flow area, the flow control orifices, the impingement holes, and the film cooling holes are summarized in Table 5-11 for each Scheme B-5 final design analyzed.

The final design analysis results for the film-convection cooled fabricated impingement tube blade Scheme B-5 are summarized in Table 5-12. The stress life of each blade was based on the minimum time to reach 1 percent creep strain after creep relaxation of the initial stress distribution. The maximum coating temperature limit is 1840°F (1277.8°K) for 1000 hr life.

In Table 5-12, the first five conditions for each chord size represent the performance of the design point cooling configuration under off-design conditions. The next three conditions represent the cooling flow required for a constant turbine inlet temperature with three different cooling air inlet temperatures. These results were obtained by varying the flow control orifice sizes only. The five additional conditions for the 1.0 in. (0.0254 m) chord blade were obtained by varying the impingement holes, film cooling holes, and flow control orifices to obtain maximum turbine inlet temperature for the first three additional conditions and to obtain minimum cooling air flow required for the last two additional conditions.

The results of this analysis show that a variation of 300°F (166.7°K) in the cooling air inlet temperature produces a related variation of 270°F (150°K) to 320°F (177.8°K) in the allowable turbine inlet temperature. Therefore the allowable turbine inlet temperature varies directly with the cooling air inlet temperature for Scheme B-5.

The results also indicate that the effect of pressure on turbine inlet temperature is small over the range of turbine inlet pressures from 50 psia (3.45 x 10^5 Newtons/sq m) to 450 psia (3.1 x 10^6 Newtons/sq m). The heat transfer analysis results indicate that when the turbine inlet total pressure increased from 150 psia (1.034 x 10^6 Newtons/sq m) to 450 psia (3.1 x 10^6 Newtons/sq m) the leading and trailing edge temperatures drop and the midchord temperatures remain the same. The elements adjacent to the film cooling holes are also further cooled as the pressure increases and this produces a larger thermal gradient. The average metal temperature cooling effectiveness ϕ increases at the hub and mean sections as the pressure increases, however the maximum metal temperature cooling effectiveness remains about the same. The thermal effectiveness η decreases as the pressure increases and this contributes to the increased metal temperature gradient. As the turbine inlet pressure is reduced from 150 psia (1.034 x 10^6 Newtons/ sq m) to 50 psia (3.45 x 10^5 Newtons/sq m), the allowable turbine inlet temperature drops only 20°F (11.1°K) to 40°F (22.2°K). The reduction in turbine inlet pressure also produces a reduction in thermal gradient, a decrease in cooling effectiveness, and an increase in thermal effectiveness. The increased cooling air heatup contributes to the decreased cooling effectiveness and decreased thermal gradient.

These analytical results again indicate that the off-design cooling air flow may be determined by equating the off design flow function based on the cooling air inlet temperature and pressure to the design point flow function.

A study of the effects of cooling air flow requirements as a function of cooling air inlet temperature and chord size for a constant turbine inlet temperature with the Scheme B-5 design did not produce the same results as with the Scheme A-1 design. The results of this study for the Scheme B-5 design are shown in Table 5-12 and Figure 5-26. The results shown in Figure 5-26 indicate the same trend in reduction of cooling air flow with a reduction in cooling air inlet temperature as in the Scheme A-1 design. However the trend in reduction with an increase in chord size is broken with the 1.5 in. (0.0381 m) chord design. This break in the trend is attributed to the detrimental effects of high crossflow velocities on impingement cooling which occurred in the 1.5 in. (0.0381 m) chord Scheme B-5 design.

The results of a study of the additional conditions for the 1.0 in. (0.0254 m) chord Scheme B-5 blade indicates that the turbine inlet temperatures for the off design conditions may be increased 60°F (33.3°K) to 80°F (44.4°K) by varying both the flow control orifices and the film cooling holes. These results also indicate that the additional capability of varying film cooling holes produces only a slight reduction in cooling air flow for a constant turbine inlet temperature.

The detailed boundary conditions for the three turbine inlet total pressure levels and for the 1200°F (922.2°K) cooling air inlet temperature condition in each chord size are shown in Appendix L. The metal temperature distribution for each design point condition in each chord size is also shown in Appendix L. Figures showing the cooling flow distribution for every condition with a turbine inlet total pressure of 150 psia (1.034 x 10^6 Newtons/sq m)

SUMMARY OF THE COOLING PASSAGE DIMENSIONS FOR THE FILM

Condition Number	I	I	2	2
Blade Chord inches (meters)	0.75 (0.01905)	0.75 (0.01905)	0.75 (0.01905)	0.75 (0.01905)
Cooling Air Inlet °F Temperature (°K)	600-1200 (588.9-922.2)	900. (755.6)	1200. (922.2)	900. (755.6)
Cooling Air Supply Pressure Drop Ratio (ΔP/Pco)	0.08	0.10	0.08	0.08
Leading Edge Impingement Holes Diameter inches (meters) Spacing to Root Diameter Mean Ratio Tip	←		0.01 (0.000254) 1.88 1.94 2.16	
Leading Edge Pressure Side Film Cooling Holes* Outside Diameter inches (meters) Inside Diameter Root Inches (meters) Mean Tip	←		0.01 (0.000254) 0.009 (0.000229) 0.009 (0.000229) 0.006 (0.00152)	
Leading Edge Suction Side Film Cooling Holes* Outside Diameter inches (meters) Inside Diameter Root Inches (meters) Mean Tip	←		0.01 (0.000254) 0.007 (0.0001778) 0.007 (0.0001778) 0.0065 (0.000165)	
Midchord Pressure Side Impingement Hole Pattern Diameter inches (meters) Spacing to Diameter Ratio Square Array	←		0.005 (0.000127) 8.84	
Midchord Suction Side Impingement Hole Pattern Diameter inches (meters) Spacing to Diameter Ratio Square Array	←		0.005 (0.000127) 8.85	
Trailing Edge Pressure Side Film Cooling Holes* Outside Diameter inches (meters) Inside Diameter Root Inches (meters) Mean Tip	←		0.015 (0.000381) 0.011 (0.000279) 0.009 (0.000229) 0.009 (0.000229)	
Trailing Edge Suction Side Film Cooling Holes* Outside Diameter inches (meters) Inside Diameter Root Inches (meters) Mean Tip	←		0.015 (0.00381) 0.011 (0.000279) 0.01 (0.000254) 0.0095 (0.000241)	
Trailing Edge Impingement Holes Diameter inches (meters) Spacing to Root Diameter Mean Ratio Tip	←		0.01 (0.000254) 3.52 4.32 4.93	
Trailing Edge Discharge Holes Diameter inches (meters) Spacing to Diameter Ratio	←		0.0095 (0.000241) 2.43	
Supply Tube Inlet Orifice Area sq in. (sq m)	0.014 (9.03×10^{-6})	0.0144 (9.29×10^{-6})	0.014 (9.03×10^{-6})	0.00614 (3.96×10^{-6})
Supply Tube sq in. Flow Area (sq m)	←		0.024 (15.48×10^{-6})	

* The film cooling holes are arranged in a staggered row with a spanwise center to center spacing of 1.5
  The holes are tapered from an outside diameter at the outer surface to an inside diameter at the inner

-CONVECTION COOLED FABRICATED IMPINGEMENT TUBE BLADE SCHEME B-5

2	1	1	2	2	2
0.75 (0.01905)	1.0 (0.0254)	1.0 (0.0254)	1.0 (0.0254)	1.0 (0.0254)	1.0 (0.0254)
600. (588.9)	600-1200 (588.9-922.2)	900. (755.6)	1200. (922.2)	900. (755.6)	600. (588.9)
0.08	0.08	0.10	0.08	0.08	0.08
					0.01 (0.000254)
			2.92 2.92 3.36		
					0.008 (0.0002032)
			0.005 (0.000127) 0.005 (0.000127) 0.004 (0.0001016)		
					0.008 (0.0002032)
			0.005 (0.000127) 0.005 (0.000127) 0.0045 (0.0001143)		
					0.005 (0.000127) 9.86
					0.005 (0.000127) 9.62
					0.022 (0.0005588) 0.015 (0.000381) 0.012 (0.0003048) 0.010 (0.000254)
					0.022 (0.0005988) 0.016 (0.0004064) 0.015 (0.000381) 0.015 (0.000381)
					0.005 (0.000127) 2.44 2.44 2.94
					0.01 (0.000254) 2.91
0.00408 (2.63×10^{-6})	0.01925 (12.42×10^{-6})	0.0204 (13.16×10^{-6})	0.01925 12.42×10^{-6}	0.0081 (5.23×10^{-6})	0.00534 (3.45×10^{-6})
					0.0385 (24.84×10^{-6})

outside diameters between the staggered holes.
surface.

TABLE 5-

Condition Number	IA	IA	IA	2A
Blade Chord — inches (meters)	1.0 (0.0254)	1.0 (0.0254)	1.0 (0.0254)	1.0 (0.0254)
Cooling Air Inlet Temperature — °F (°K)	1200. (922.2)	900. (755.6)	600. (588.9)	1200. (922.2)
Cooling Air Supply Pressure Drop Ratio (ΔP/Pco)	0.08	0.08	0.08	0.08
Leading Edge Impingement Holes				
Diameter — inches (meters)	←		0.01 (0.00254) →	
Spacing to Root	2.34	2.34	2.34	2.34
Diameter Mean	2.55	2.55	2.55	2.55
Ratio Tip	2.92	2.92	2.92	2.92
Leading Edge Pressure Side Film Cooling Holes*				
Outside Diameter — inches (meters)	←		0.008 (0.0002032)	
Inside Diameter Root	0.0065 (0.000165)	0.0055 (0.00014)	0.0055 (0.00014)	0.0055 (0.00...)
Inches (meters) Mean	0.0055 (0.00014)	0.006 (0.000152)	0.006 (0.000152)	0.0055 (0.00...)
Tip	0.005 (0.000127)	0.005 (0.000127)	0.005 (0.000127)	0.005 (0.000...)
Leading Edge Suction Side Film Cooling Holes*				
Outside Diameter — inches (meters)	←		0.008 (0.0002032)	
Inside Diameter Root	0.006 (0.000152)	0.0055 (0.00014)	0.0055 (0.00014)	0.0055 (0.00...)
Inches (meters) Mean	0.005 (0.000127)	0.0055 (0.00014)	0.0055 (0.00014)	0.005 (0.000...)
Tip	0.005 (0.000127)	0.005 (0.000127)	0.005 (0.000127)	0.005 (0.000...)
Midchord Pressure Side Impingement Hole Pattern				
Diameter — inches (meters)	←		0.005 (0.000127)	
Spacing to Diameter Ratio Square Array			9.86	
Midchord Suction Side Impingement Hole Pattern				
Diameter — inches (meters)	←		0.005 (0.000127)	
Spacing to Diameter Ratio Square Array	8.35	8.35	8.35	8.35
Trailing Edge Pressure Side Film Cooling Holes*				
Outside Diameter — inches (meters)	←		0.022 (0.0005588)	
Inside Diameter Root	0.017 (0.0004318)	0.015 (0.000381)	0.015 (0.000381)	0.015 (0.000...)
Inches (meters) Mean	0.012 (0.0003048)	0.012 (0.0003048)	0.012 (0.0003048)	0.012 (0.000...)
Tip	0.010 (0.000254)	0.01 (0.000254)	0.01 (0.000254)	0.01 (0.0002...)
Trailing Edge Suction Side Film Cooling Holes*				
Outside Diameter — inches (meters)	←		0.022 (0.0005588)	
Inside Diameter Root	0.011 (0.0005588)	0.018 (0.000457)	0.018 (0.000457)	0.018 (0.000...)
Inches (meters) Mean	0.018 (0.000457)	0.018 (0.000457)	0.018 (0.000457)	0.016 (0.000...)
Tip	0.017 (0.000432)	0.017 (0.000432)	0.017 (0.000432)	0.016 (0.000...)
Trailing Edge Impingement Holes				
Diameter — inches (meters)	←		0.005 (0.000127)	
Spacing to Root	2.24	2.44	2.44	2.94
Diameter Mean	2.94	2.44	2.44	3.52
Ratio Tip	2.94	2.94	2.94	3.52
Trailing Edge Discharge Holes				
Diameter — inches (meters)	←		0.01 (0.000254)	
Spacing to Diameter Ratio			2.91	
Supply Tube Inlet Orifice Area — sq in. (sq m)	0.0211 (13.61 x 10⁻⁶)	0.0209 (13.48 x 10⁻⁶)	0.0209 (13.48 x 10⁻⁶)	0.01644 (10.61 x 10...)
Supply Tube Flow Area — sq in. (sq m)	←		0.0385 (24.84 x 10⁻⁶)	

	2A	1	1	2	2	2
	1.0 (0.0254)	1.5 (0.0381)	1.5 (0.0381)	1.5 (0.0381)	1.5 (0.0381)	1.5 (0.0381)
	600. (588.9)	600-1200. (588.9-922.2)	900. (755.6)	1200. 922.2)	900. (755.6)	600. (588.9)
	0.08	0.08	0.10	0.08	0.08	0.08
	0.005 (0.000127) 3.23 3.64 4.16			0.012 (0.0003048) 1.94 2.43 3.24		
014) 014) 127)	0.0055 (0.00014) 0.006 (0.000152) 0.005 (0.000127)			0.012 (0.0003048) 0.011 (0.0002794) 0.007 (0.0001778) 0.007 (0.0001778)		
014) 127) 127)	0.0035 (0.0000889) 0.0035 (0.0000889) 0.003 (0.000762)			0.012 (0.0003048) 0.010 (0.000254) 0.007 (0.0001778) 0.007 (0.0001778)		
	12.5			0.005 (0.000127) 10.8		
	13.			0.005 (0.000127) 9.63		
381) 3048) 54)	0.007 (0.0001778) 0.007 (0.0001778) 0.005 (0.000127)			0.030 (0.000762) 0.010 (0.000508) 0.016 (0.0004064) 0.015 (0.000381)		
457) 4064) 4064)	0.009 (0.000229) 0.009 (0.000229) 0.008 (0.000203)			0.030 (0.000762) 0.024 (0.0006096) 0.020 (0.000508) 0.019 (0.000483)		
	5.87 6.95 6.55			0.012 (0.0003048) 3.74 4.43 6.95		
				0.01 (0.000254) 2.53		
6)	0.0055 (3.55×10^{-6})	0.035 (22.58×10^{-6})	0.0374 (24.13×10^{-6})	0.035 (22.58×10^{-6})	0.01854 (11.96×10^{-6})	0.0104 (6.71×10^{-6})
				0.1308 (84.4×10^{-6})		

TABLE 5-12

DETAILED SUMMARY OF THE RESULTS FOR THE
SCHEME B-5 FINAL DESIGN TASK I ANALYSIS

Condition* Number	Chord in. (m)	P_{T_g} Psia (Newtons/sq m)	T_{ci} °F (°K)	T_g Analysis °F (°K)	$\frac{W_{CA}(100)}{W_g}$	ϕ_R	ϕ_m	ϕ_{max}	η_t	R_g	Stress Critical Section	T_g Maximum °F (°K)	Critical Condition
1	0.75 (0.01905)	150 (1.034 × 10⁶)	1200 (922.2)	2320 (1544.4)	5.52	0.6929	0.6236	0.4313	0.5183	0.2536	Tip	2320 (1544.4)	2
1	0.75 (0.01905)	150 (1.034 × 10⁶)	900 (755.6)	2600 (1700)	6.52	0.681	0.6374	0.4429	0.5148	0.2724	Tip	2590 (1694.4)	1
1	0.75 (0.01905)	150 (1.034 × 10⁶)	600 (588.9)	2870 (1850)	7.87	0.688	0.6565	0.4638	0.509	0.2665	Tip	2900 (1866.7)	1
1	0.75 (0.01905)	450 (3.1 × 10⁶)	900 (755.6)	2600 (1700)	6.52	0.7034	0.6617	0.4487	0.4253	0.2888	Tip	2600 (1700)	1
1	0.75 (0.01905)	50 (3.45 × 10⁵)	900 (755.6)	2570 (1683.3)	6.42	0.6009	0.6126	0.4365	0.6312	0.2329	Tip	2570 (1683.3)	1
2	0.75 (0.01905)	150 (1.034 × 10⁶)	1200 (922.2)	2320 (1544.4)	5.52	0.6929	0.6236	0.4313	0.5183	0.2536	Tip	2320 (1544.4)	2
2	0.75 (0.01905)	150 (1.034 × 10⁶)	900 (755.6)	2320 (1544.4)	2.73	0.5641	0.4961	0.3385	0.5843	0.212	Tip	2320 (1544.4)	1
2	0.75 (0.01905)	150 (1.034 × 10⁶)	600 (588.9)	2320 (1544.4)	1.96	0.4556	0.3999	0.2784	0.6032	0.2122	Tip	2320 (1544.4)	1
1	1.0 (0.0254)	150 (1.034 × 10⁶)	1200 (922.2)	2320 (1544.4)	4.76	0.6479	0.5859	0.4594	0.5036	0.1893	Mean	2320 (1544.4)	2
1	1.0 (0.0254)	150 (1.034 × 10⁶)	900 (755.6)	2600 (1700)	5.54	0.6303	0.5877	0.4577	0.4887	0.2041	Root	2620 (1711.1)	1
1	1.0 (0.0254)	150 (1.034 × 10⁶)	600 (588.9)	2910 (1872.2)	6.6	0.6305	0.5997	0.4655	0.4755	0.2177	Root	2910 (1872.2)	1
1	1.0 (0.0254)	450 (3.1 × 10⁶)	900 (755.6)	2620 (1711.1)	5.63	0.6457	0.6155	0.4541	0.4004	0.2512	Root	2620 (1711.1)	1
1	1.0 (0.0254)	50 (3.45 × 10⁵)	900 (755.6)	2560 (1677.8)	5.44	0.6113	0.5689	0.4379	0.608	0.1831	Root	2570 (1683.3)	1
2	1.0 (0.0254)	150 (1.034 × 10⁶)	1200 (922.2)	2320 (1544.4)	4.76	0.6479	0.5839	0.4594	0.5036	0.1893	Mean	2320 (1544.4)	2
2	1.0 (0.0254)	150 (1.034 × 10⁶)	900 (755.6)	2320 (1544.4)	2.53	0.5168	0.4549	0.3585	0.5495	0.1556	Mean	2320 (1544.4)	2
2	1.0 (0.0254)	150 (1.034 × 10⁶)	600 (588.9)	2320 (1544.4)	1.87	0.4446	0.3895	0.3032	0.5859	0.1314	Root	2320 (1544.4)	2
1A	1.0 (0.0254)	150 (1.034 × 10⁶)	1200 (922.2)	2400 (1588.9)	5.76	0.667	0.5928	0.4674	0.4526	0.1817	Root	2350 (1561.1)	1
1A	1.0 (0.0254)	50 (3.45 × 10⁵)	900 (755.6)	2660 (1733.3)	6.26	0.6285	0.5857	0.4658	0.5713	0.1744	Root	2660 (1733.3)	1
1A	1.0 (0.0254)	150 (1.034 × 10⁶)	600 (588.9)	2990 (1916.7)	7.84	0.6457	0.6169	0.4828	0.4332	0.2138	Root	2990 (1916.7)	1

TABLE 5-12 (Continued)

Condition* Number	Chord in. (m)	P_{T_g} Psia (Newtons/sq m)	T_{ci} °F (°K)	T_g Analysis °F (°K)	$\dfrac{W_{CA}(100)}{W_g}$	ϕ_R	ϕ_m	ϕ_{max}	η_t	R_g	Stress Critical Section	T_g Maximum °F (°K)	Critical Condition
2A	1.0 (0.0254)	150 (1.034 × 10⁶)	1200 (922.2)	2320 (1544.4)	4.44	0.6396	0.5554	0.4262	0.4712	0.1670	Root	2320 (1544.4)	2
2A	1.0 (0.0254)	150 (1.034 × 10⁶)	600 (588.9)	2320 (1544.4)	1.76	0.4309	0.3687	0.2841	0.5765	0.1291	Root	2320 (1544.4)	2
1	1.5 (0.0381)	150 (1.034 × 10⁶)	1200 (922.2)	2320 (1544.4)	4.76	0.6553	0.5586	0.4597	0.448	0.1777	Root	2320 (1544.4)	2
1	1.5 (0.0381)	150 (1.034 × 10⁶)	900 (755.6)	2620 (1711.1)	5.56	0.6390	0.5626	0.4569	0.4333	0.1994	Root	2620 (1711.1)	2
1	1.5 (0.0381)	150 (1.034 × 10⁶)	600 (588.9)	2920 (1877.8)	6.61	0.6391	0.5751	0.4656	0.4207	0.2121	Root	2920 (1877.8)	1
1	1.5 (0.0381)	450 (3.1 × 10⁶)	900 (755.6)	2600 (1700)	5.54	0.6525	0.5766	0.4476	0.3383	0.2635	Root	2600 (1700)	1
1	1.5 (0.0381)	50 (3.45 × 10⁵)	900 (755.6)	2620 (1711.1)	5.5	0.6237	0.5455	0.4548	0.5411	0.1599	Root	2560 (1677.8)	2
2	1.5 (0.0381)	150 (1.034 × 10⁶)	1200 (922.2)	2320 (1544.4)	4.76	0.6553	0.5586	0.4597	0.448	0.1982	Root	2560 (1677.8)	2
2	1.5 (0.0381)	150 (1.034 × 10⁶)	900 (755.6)	2320 (1544.4)	3.35	0.5725	0.4796	0.3961	0.4673	0.1641	Root	2320 (1544.4)	2
2	1.5 (0.0381)	150 (1.034 × 10⁶)	600 (588.9)	2320 (1544.4)	2.34	0.4889	0.3993	0.3175	0.497	0.136	Root	2320 (1544.4)	2

CRITICAL CONDITIONS:

1. Turbine inlet temperature limited by maximum coating temperature of 1840°F (1277.8°K) for 1000 hr life with 0.02 in. (0.000508 m) thick IN-100 material.

2. Turbine inlet temperature limited by a minimum time to 1 percent creep strain of 100 hr after relaxation of the thermal stress distribution due to creep.

*CONDITION NUMBER

1. Maximum turbine inlet temperature determined at each off design condition for a blade designed at the 150 psia (1.034 x 10⁶ Newtons/sq m) turbine inlet pressure and 900°F (755.6 °K) cooling air inlet temperature condition.

2. Minimum cooling air flow required determined as a function of cooling air inlet temperature for a constant turbine inlet temperature by varying only the flow control orifices.

1A. Maximum turbine inlet temperature determined for each point treated as a design point condition.

2A. Minimum cooling air flow required determined as a function of cooling air inlet temperature by varying the flow control orifices, impingement holes, film cooling holes, and trailing edge discharge holes.

Figure 5-26. Cooling Air Flow Required as a Function of
Cooling Air Inlet Temperature for the
Scheme B-5 Final Design

are given in Appendix L. The effects of increasing the total pressure drop in ducting the cooling air from the compressor to the blade hub $(\Delta P/P_{co} = 0.1)$ are also presented in Appendix L.

The detailed metal temperature and stress analysis results for each chord size at each final design condition is given in Appendix M. Tables showing metal temperatures, stress, and stress-to-rupture life for each element of the hub, mean, and 75 percent span sections at each condition are presented. Figures showing the stress relaxation due to creep and the creep elongation for the critical elements of the stress limited designs are also shown. A creep stress analysis was not performed for every condition since the results for one condition could be used for a similar condition.

Effects of Tolerance

In cooled turbine blades, tolerances can affect the stress, cooling air, and metal temperature distribution and these effects should be accounted for. Some typical tolerances in turbine blades are ±0.002 in. (0.0000508 m) in blade outside contour, ±0.005 in. (0.000127 m) in stacking tolerance, ±0.005 in. (0.000127 m) in blade inside contour, ±0.005 in. (0.000127 m) in inner passage core shift, and ±0.002 in. (0.0000508 m) in orifice or film cooling hole diameter. The bending moment due to stacking tolerance was evaluated and found to be negligible. The spanwise metal area taper ratio should not be affected more than 10 percent due to tolerances because metal area is added in some areas and removed in other areas of a spanwise section. This effect produces a 4 to 10 percent change in blade stress.

A tolerance of ±0.002 in. (0.0000508 m) for a 0.010 in. (0.0002 m) nominal diameter hole produces a ±44 percent change in flow area. This means that local variations in cooling air flow of ±40 to 50 percent are possible for trailing edge discharge, impingement, and film cooling holes. When these holes are formed in the blade, some of them will be larger than nominal and some smaller. This distribution of hole sizes should reduce the local variation of ±40 to 50 percent in cooling air flow to a variation of ±20 percent in total cooling air flow rate for the blades. A brief study of the effects of a 20 percent increase or decrease in cooling air flow on the turbine inlet temperature capability of the Scheme A-1 and the Scheme B-5, 1 in. (0.0254 m) chord designs is presented below.

Since both the Scheme A-1 and the Scheme B-5 blades are mainly limited by a maximum coating temperature of $1840^\circ F$ ($1277.8^\circ K$) rather than stress for a 1000 hr steady state life, the effects of tolerance can be evaluated as the turbine inlet temperature which produces a maximum metal temperature of $1840^\circ F$ ($1277.8^\circ K$) over the range of cooling airflow variation produced by the cooling passage tolerance.

The effects of a variation in cooling air flow rate on the blade maximum metal temperature can be evaluated from the maximum metal temperature cooling effectiveness curves shown in Figures 5-27 and 5-28 for the Scheme A-1 and the Scheme B-5 cooling configuration respectively. Since the variation in cooling effectiveness as a function of cooling airflow rate is a curve rather than a straight line, the effects of tolerances vary with the level of nominal cooling air flow rates. The effects of tolerances vary with the level of nominal cooling air flow rates. The effects of a ±20 percent change in cooling air flow rate on the turbine inlet temperature of the 1.0 in. (0.0254 m) chord Scheme A-1 and Scheme B-5 designs for a cooling air inlet temperature of $900^\circ F$ ($755.6^\circ K$), a turbine inlet total pressure of 150 psia (1.034×10^6 Newtons sq m) and a nominal cooling air flow rate of 3 percent of the hot gas flow are shown in Table 5-13. The variation in turbine inlet temperature capability of approximately $50^\circ F$ ($27.8^\circ K$) to $80^\circ F$ ($44.4^\circ K$) would be less for a cooling airflow greater than 3 percent and it would be greater for a cooling airflow less than 3 percent.
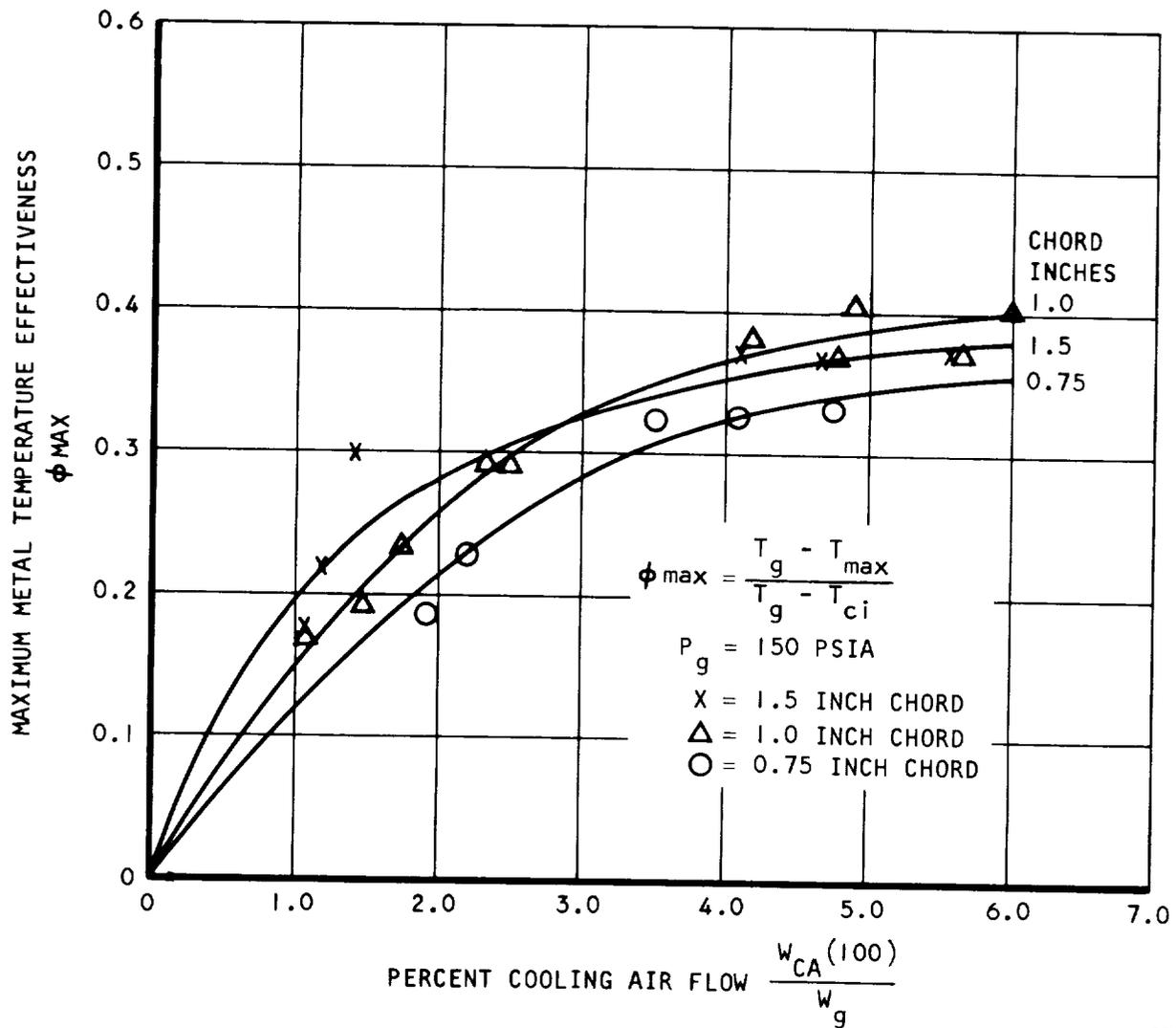
Figure 5-27. Maximum Metal Temperature Cooling Effectiveness
for the Pin Fin Cast Two Cavity Convection
Cooled Blade Scheme A-I
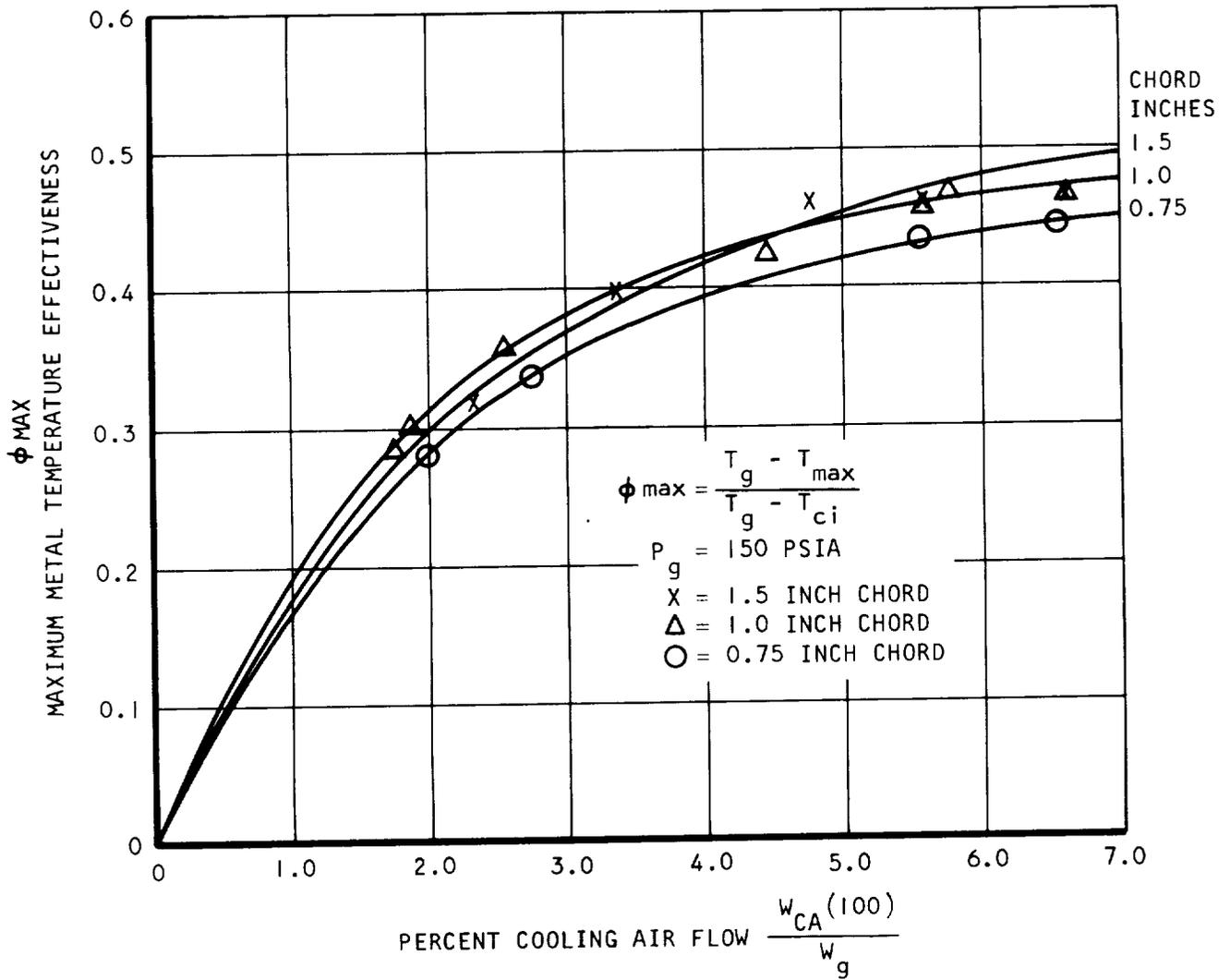
Figure 5-28. Maximum Metal Temperature Cooling Effectiveness for the Film-Convection Cooled Fabricated Impingement Tube Blade Scheme B-5

TABLE 5-13

EFFECT OF TOLERANCE ON TURBINE INLET
TEMPERATURE OF THE 1.0 IN. (0.0254 M) CHORD
SCHEME A-1 AND SCHEME B-5 BLADE DESIGN

$T_{c,i}$ = 900°F (755.6°K), P_g = 150 psia (1.034 × 10⁶ Newtons/sq m)

T_{max} = 1840°F (1277.8°K)

Cooling Air Flow	Scheme A-1				Scheme B-5			
$\frac{W_{ca}(100)}{W_g}$	T_g		ΔT_g		T_g		ΔT_g	
Flow Area	°F	°K	°F	°K	°F	°K	°F	°K
-20 Percent	2224	1491.1	-73	-40.6	2337	1553.9	-82	-45.5
Nominal	2297	1531.7	0	0	2419	1599.4	0	0
+20 Percent	2353	1562.8	+56	+31.1	2488	1637.8	+69	+38.4

SECTION 6

CONCLUSIONS

An investigation of the effect of chord size on the turbine inlet temperature capability of eight turbine blade cooling configurations was conducted. In this preliminary design analysis, four convection cooled designs, three film-convection cooled designs, and one transpiration cooled design were considered in 0.75 in. (0.01905 m), 1.0 in. (0.0254 m), and 1.5 in. (0.0381 m) chord sizes. The Scheme A-1 convection cooled cast two-cavity pin fin blade had a relatively high turbine inlet temperature capability for a simple cast cooling configuration and it provides a moderate increase in turbine inlet temperature capability with chord size at the expense of a substantial increase in cooling air flow. The Scheme A-3 convection cooled fabricated radial flow plate-fin blade requires less cooling air flow for about the same turbine inlet temperature as Scheme A-1. The maximum turbine inlet temperature capability of the Scheme A-3 design is limited primarily by cooling air pressure drop in the leading edge cooling passage. The Scheme A-6 convection cooled fabricated strut supported blade had the highest turbine inlet temperature capability of the convection cooled designs based on the preliminary stress analysis conducted. The thermal gradient was high in the Scheme A-6 design which indicates that the life may be limited due to low cycle fatigue. The Scheme A-7 convection cooled cast impingement tube blade has a relatively high maximum metal temperature cooling effectiveness for a convection cooled design and the thermal gradient is low. This indicates that the Scheme A-7 is more suited to a low tip speed turbine or to a nozzle vane. The Scheme B-1 film-convection cooled cast three cavity blade has large thermal gradients between the outer shell and the cooling passage separators. This large thermal gradient indicates that the life may be limited due to low cycle fatigue. The Scheme B-4 film-convection cooled cast impingement tube blade with crossflow impingement and a sharp corner flow leading edge has the same limitations as Scheme A-7 except that it provides higher cooling effectiveness with less cooling air flow. The Scheme B-4 design is more suited to a low tip speed turbine or to a nozzle vane. The Scheme B-5 film-convection cooled fabricated impingement tube blade provides high turbine inlet temperature capability with low metal temperature gradients. The turbine efficiency losses due to film cooling are minimized by injecting the coolant in the direction of hot gas flow. The Scheme C-1 transpiration cooled blade has a strong effect of chord size on turbine inlet temperature capability caused by the film cooled trailing edge. This indicates that a transpiration cooled blade should be designed with a transpiration cooled trailing edge using either a thinner transpiration cooled material or a thicker trailing edge.

The Scheme A-1 and Scheme B-5 blade designs were selected for a final design analysis in the three chord sizes with a creep relaxation stress analysis and off-design performance considered. The final design analysis included the effects of cooling air inlet temperature on turbine inlet temperature capability and cooling air flow requirements. The effects of turbine inlet total pressure, cooling air inlet pressure, and cooling passage tolerances were also investigated. Additional conclusions relating to the designs studied are summarized below:

(a) Turbine inlet temperature capability increases with an increase in chord for the convection cooled and transpiration cooled designs, but turbine inlet temperature capability for the film cooled designs does not vary significantly with chord size.

(b) Turbine inlet temperature capability of the film cooled designs are 200°F (111.1°K) to 300°F (166.7°K) higher than the convection cooled designs; however, the aerodynamic losses due to film cooling are not expected to be large.

(c) The transpiration cooled design selected had a low turbine inlet temperature for the 0.75 in. (0.01905 m) and 1.0 in. (0.0254 m) chord designs because of the film cooled trailing edge. The 1.5 in. (0.0381 m) chord design had a high turbine inlet temperature capability but all of the designs are expected to have high aerodynamic efficiency losses.

(d) Allowable turbine inlet temperature changes only 53 to 67 percent as much as the cooling air inlet temperature for the pin fin convection cooled turbine blade design.

(e) Allowable turbine inlet temperature increase is essentially the same as the decrease of cooling air inlet temperature for the film-impingement cooled turbine blade design.

(f) Required cooling air flow rate increases with a decrease in chord and an increase in cooling air inlet temperature for the pin fin convection cooled design.

(g) Required cooling air flow rate does not change significantly with a variation in chord and increases with an increase in cooling air inlet temperature for the film-impingement cooled design.

(h) Allowable turbine inlet temperature capability does not change significantly as a function of turbine inlet total pressure over the range studied for either design.

(i) Turbine inlet temperature for the off-design conditions may be increased 60°F (33.3°K) to 100°F (55.6°K) by modifying blade design for these conditions.

(j) A slight reduction in cooling air inlet pressure required only a change in flow control orifice size to produce the same turbine inlet temperature capability for the first stage blade over the range studied.

(k) A method for determining the turbine inlet temperature required for a specified blade life from a condition with a known life is presented based on equating the Larson-Miller parameter for each condition.

(l) A flow area change of ±20 percent due to tolerances produced a change of 56 to -82°F (31.1 to -45.5°K) in the designs for a nominal cooling air flow of 3.0 percent of the hot gas flow.

132

SECTION 7
REFERENCES

1. Hare, Arthur and Harry H. Malley, "Cooling Modern Aero Engine Turbine Blades and Vanes" SAE Paper No. 660053, Automotive Engineering Congress, January 10-14, 1966.

2. Burggraf, H. and W. Houchens, "Air Cooling of Hot Turbine Parts" SAE Paper No. 660054, Automotive Engineering Congress, January 10-14, 1966.

3. Moskowitz, S. A. and T. E. Schober, "Design and Test of a Small Turbine at 2500°F with Transpiration Cooled Blading" SAE Paper No. 690035, Automotive Engineering Congress, January, 1969.

4. Helmbrecht, J. L., R. F. Kirby, and F. Weber, An Investigation of Turbine Blade/Disc Attachment Methods for Small, Cooled Gas Turbines, USAAVLABS TR 69-91, January, 1970.

5. Silverstein, Abe, "Turbine-Engine Development Still Pacemaking in Aviation" Astronautics and Aeronautics, November, 1966, pp. 96-104.

6. Helms, H. E. and C. W. Emmerson, "Analysis and Testing of Air-Cooled Turbine Rotor and Stator Blades," ASME Paper No. 65-WA/GTP-10, November, 1965.

7. Martens, W. R. and W. A. Raabe, "The Materials Challenge of High-Temperature Turbine Vanes and Blades" ASME Paper No. 67-GT-17, March, 1967.

8. Burggraf, F., Murtaugh, J. P., and M. E. Wilton, Design and Analysis of Cooled Turbine Blades. Part I - Leading and Trailing Edge Configurations. General Electric Co. (NASA CR-54513), 1968.

9. Burggraf, F., Murtaugh, J. P., and M. E. Wilton, Design and Analysis of Cooled Turbine Blades. Part II - Convection Cooled Nozzles and Buckets. General Electric Co. (NASA CR-54514), 1968.

10. Burggraf, F., Murtaugh, J. P., and M. E. Wilton, Design and Analysis of Cooled Turbine Blades. Part III - Transpiration and Multiple Small Hole Film Cooled Nozzles and Buckets. General Electric Co. (NASA CR-54515), 1968.

11. Burggraf, F., Murtaugh, J. P., and M. E. Wilton, Design and Analysis of Cooled Turbine Blades. Part IV - Combined Methods of Cooling. General Electric Co. (NASA CR-54512), 1968.

12. Danforth, C.E., and F. Burggraf, Design and Analysis of Cooled Turbine Blades. Part V - Life Prediction of Selected Designs. Rep. R68AEG105, General Electric Co. (NASA CR-72417), August, 1968.

13. Anderson, R. D., Davis, W. C., McLeod, R. N., and D. A. Nealy, High Temperature Cooled Turbine Blades, Wright-Patterson Technical Report AFAPL-TR-69-41 May, 1969.

14. Gabel, R. M. "Feasibility Demonstration of a Small Fluid-Cooled Turbine at 2300°F." SAE Paper No. 690034, Automotive Engineering Congress, January, 1969.

15. Esgar, J. B., E. F. Schum, and A. N. Curren, Effect of Chord Size on Weight and Cooling Characteristics of Air-Cooled Turbine Blades NACA TR 1354, 1958.

16. Katsanis, T. and L. T. Dellner, A Quasi-Three- Dimensional Method for Calculating Blade Surface Velocities for an Axial Flow Turbine, NASA TM X-1394, 1967.

17. Barnes, J. F. and P. M. Came, "Some Aerodynamic Aspects of Turbine Blade Cooling" ASME Paper No. 69-GT-15, March, 1969.

18. Moffitt, T. P., S. M. Nosek, and R. J. Roelke, "Turbine Aerodynamic Considerations for Advanced Turbines," Aircraft Propulsion, NASA SP-259, November, 1970.

19. Sucin, S. N., "High Temperature Turbine Design Considerations," AGARD, High Temperature Turbines, January, 1971.

20. H. Ellerbrock, "Some NACA Investigations of Heat Transfer of Cooled Gas Turbine Blades," Joint Meeting, Inst. Mech. Engineers and ASME, Proc. of the General Discussion of Heat Transfer, 1951.

21. D. G. Wilson, and J. A. Pope, "Convective Heat Transfer to Gas Turbine Blade Surfaces," Proc. Inst. Mech. Engrs., Vol. 168, 1954, pp. 861-876.

22. H. B. Squire, and A. D. Young, "The Calculations of the Profile Drag of Aerofoils," Aero. Res. Council R. and M., No. 1838, 1938.

23. L. M. Zysina-Molozhen, "The Calculation of Heat Transfer in a Cascade of Blades," Zhur. Tekh. Fiz., Vol. 29, 1959, pp. 558-563.

24. L. M. Zysina-Molozhen, "Heat Transfer in Turbine Grids," Trans. as FTD-TT-62-1784/1 + 2, WPAFB, March 8, 1963.

25. Walker, L. A., and E. Markland, "Heat Transfer to Turbine Blading in the Presence of Secondary Flow," Int. J. Heat Mass Transfer, Vol. 8, 1965, pp. 729-748.

26. Schlichting, H., Boundary Layer Theory, Pergammon Press, 1955.

27. Ainley, D. G., "Internal Air Cooling for Turbine Blades," Aeronautical Research Council, Rand M3013, 1957.

28. Plotkin, E. R., and E. I. Molchanor, "Heat Transfer to the Surface of Gas Turbine Blades," Teploenergetika, Vol. 11, No. 11, 1964, pp. 72-74.

29. Moretti, P. M., and W. M. Kays, "Heat Transfer to a Turbulent Boundary Layer with Varying Freestream Velocity an Experimental Study," *Int. J. of Heat and Mass Transfer*, Vol. 8, No. 9, 1965, p. 1197.

30. Kays, W. M., *Convective Heat and Mass Transfer*, McGraw-Hill, New York, 1966.

31. Patankar, S. V. and D. B. Spalding, "A Finite-Difference Procedure for Solving the Equations of the Two-Dimensional Boundary Layer," *International Journal of Heat and Mass Transfer*, Vol. 10, 1967, pp. 1389-1411.

32. Eckert, E. R. G., *Trans. ASME*, Vol. 78, 1956.

33. Bromberg, R., J. L. Fox, and W. D. Ackerman, *A Method of Predicting Convective Heat Input to the Entry Body of a Ballistic Missile*, Ramo-Wooldridge Corporation Report.

34. Sasman, P. K., and R. J. Cresci, *Compressible Turbulent Boundary Layer with Arbitrary Pressure Gradient and Heat Transfer*, AIAA Journal, Vol. 4, No. 1, Jan 1966

35. Dunham, J., and J. P. Edwards, "Heat Transfer Calculations for Turbine Blade Design," AGARD, High Temperature Turbines, January, 1971.

36. Bayley, F. J., and A. B. Turner, "Transpiration-Cooled Turbines" AGARD, High Temperature Turbines, January, 1971.

37. Squire, H. B. *Modern Developments in Fluid Dynamics*, 3rd ed., Vol. 2 Oxford Clarendon Press, 1950.

38. Reshotko, Eli, and C. B. Cohen, "Heat Transfer at the Forward Stagnation Point of Blunt Bodies," NACA TN 3513.

39. Fay, J. A., and F. R. Riddell, "Theory of Stagnation Point Heat Transfer in Dissociated Air," *J. of the Aeronautical Sciences*, Vol. 25, No. 2, February 1958.

40. Kestin, John, *Advances in Heat Transfer*, Vol. III, Academic Press Inc., New York, 1966.

41. Dyban, Ye. P., and V. D. Kurosh, "Heat Transfer at The Leading Edge of a Turbine Blade," *Heat Transfer-Soviet Research*, Vol. 2, No. 1, January, 1970.

42. Eckert, E. R. G., A. J. Diaguila, and A. N. Curren, "Experiments on Mixed-Free-and-Forced-Convective Heat Transfer Connected with Turbulent Flow Through a Short Tube" NACA TN-2974, July 1953.

43. Brown, C. K., and W. H. Gauvin, "Combined Free-and-Forced Convection II. Heat Transfer in Opposing Flow" *Canadian Journal of Chemical Engr.*, December 1965.

44. Nunner, W., "Heat Transfer and Pressure Drop in Rough Tubes," AERE-tr-786, Translated from VDI-Forschungsheft, Series B, 22, No. 459, (1956).

45. Koch, R., "Pressure Loss and Heat Transfer for Turbulent Flow," AEC-tr-3875, Translated from VDI-Forschungsheft, Series B, 24, No. 469, (1958).

46. Kays, W. M. and A. L. London, Compact Heat Exchangers Second Edition, McGraw-Hill Book Co., 1964.

47. London, A. L. and R. K. Shah, "Offset Rectangular Plate-Fin Surfaces-Heat Transfer and Flow Friction Characteristics" ASME Paper No. 68-GT-8, March, 1968.

48. Nealy, D. A., R. D. Anderson and A. A. Hufford, "Periodic Report Design and Experimental Evaluation of a Turbine Vane Fabricated from Laminated Porous Material (U)" NASA CR-72649.

49. Anderson, R. D. and D. A. Nealy, "Final Report-Tasks I and II Evaluation of Laminated Porous Material for High-Temperature Air-Cooled Turbine Blades (U)" NASA CR-72281.

50. Chupp, R. E., H. E. Helms, P. W. McFadden, and T. R. Brown, "Evaluation of Internal Heat Transfer Coefficients for Impingement Cooled Airfoils," AIAA Paper No. 68-564, Joint Propulsion Specialist Conference, Cleveland, Ohio, June 1968.

51. Kercher, D. M., and W. Tabakoff, "Heat Transfer by a Square Array of Round Air Jets Impinging Perpendicular to a Flat Surface Including the Effects of Spent Air," ASME Paper No. 69/GT-4, 1969.

52. Brdlik, P. M., and V. K. Savin, "Heat Transfer Between an Axisymmetric Jet and a Plate Normal to the Flow," Inzhenerno-Fizicheskii Zhurnal, Vol. 8, No. 2, pp. 146-155, A66 25313, 1965.

53. Gardon, R., and J. C. Akfirat, "Heat Transfer Characteristics of Two Dimensional Air Jets," Journal of Heat Transfer, pp. 101-108, February 1966.

54. Gardon, R., and J. E. Akfirat, "The Role of Turbulence in Determining the Heat Transfer Characteristics of Impinging Jets," Int. Journ. of Heat and Mass Transfer, Vol. 8, No. 9, pp. 1261-1272, 1965.

55. Gardon, R., and J. Cobonpue, "Heat Transfer Between a Flat Plate and Jets of Air Impinging on It," International Developments in Heat Transfer, Conference, 1961.

56. Schuh, H., and R. Pettersson, "Heat Transfer by Arrays of Two Dimensional Jets Directed Normal to Surfaces Including the Effects of a Superposed Wall-Parallel Flow," International Heat Transfer Conference, pp. 280-291, 1966.

136

57. Metzger, D. E., and T. Yamashita, "Heat Transfer Characteristics of Single Lines of Circular Jets Impinging on Concave Cylindrical Surfaces," T.R. No. ME-672, Mechancial Engineering Department, Arizona State University, Temper, Arizona, 1967.

58. Metzger, D. E., and C. W. Jenkins, "Impingement Cooling of Concave Surfaces with Slot Jets and Single Lines of Circular Jets," T. R. No. ME-683, Mechanical Engineering Department, Arizona Stage University, Tempe, Arizona, 1968.

59. Metzger, D. E., T. Yamashita, and C. W. Jenkins, "Impingement Cooling of Concave Surfaces with Lines of Circular Air Jets," ASME Paper No. 68-WA/GT-1, 1968.

60. Metzger, D. E., and C. W. Jenkins, "Flow Distributions and Pressure Losses through Impingement Tubes," T.R. No. ME-687, Mechanical Engineering Department, Arizona State University, Tempe, Arizona, 1968.

61. Jenkins, C. W., and D. E. Metzger, "Local Heat Transfer Characteristics of Concave Cylindrical Surfaces Cooled by Impinging Slot Jets and Lines of Circular Jets with Spacing Ratios 1.25 to 6.67," T.R. No. ME-694, Mechanical Engineering Department, Arizona State University, Tempe, Arizona, 1969.

62. Mori, Y. and W. Nakayama, "Study on Forced Convection Heat Transfer in Curved Pipes (First Report, Laminar Region)," Int. J. Heat Mass Transfer Vol. 8, pp. 67-82 (1965).

63. Mori, Y. and W. Nakayama, "Study on Forced Convection Heat Transfer in Curved Pipes (Second Report, Turbulent Region)," Int. J. Heat Mass Transfer, Vol. 10, pp. 37-59 (1967).

64. Shapiro, A. H., The Dynamics and Thermodynamics of Compressible Fluid Flow, Vol. I, Ronald Press Co., New York, 1953.

65. Lamb, O. F. and J. S. Holdhusen, "Investigation of Aircraft Ducting Components at High Subsonic Speeds," WADC Technical Report 56-187, September, 1956.

66. Benedict, R. P., N. A. Carlucci, and S. D. Swetz, "Flow Losses in Abrupt Enlargements and Contractions," ASME Paper No. 65-WA/PTC-1, November 1965.

67. Anon., "Flow of Fluids through Valves, Fittings, and Pipe" Tech Paper 410, Crane Co., 1957.

68. Spink, L. K., "Principles and Practice of Flow Meter Engineering" The Foxboro Company, Foxboro, Mass.

69. Perry, J. A., "Critical Flow Through Sharp-Edged Orifices," Trans. ASME, vol. 71, 1949.

70. Grace, H. P. and C. E. Lapple, "Discharge Coefficients of Small-Diameter Orifices and Flow Nozzles," Tras. ASME, vol. 73, 1951.

71. Weir, A., Jr., J. L. York, and R. B. Morrison "Two-and Three-Dimensional Flow of Air Through Square-Edged Sonic Orifices," Trans. ASME, April, 1956.

72. Prust, H. W., Jr., "An Analytical Study of the Effect of Coolant Flow Variables on the Kinetic Energy Output of a Cooled Turbine Blade Row," NASA TMX-67960, 1971.

73. Dittrich, R.T. "Discharge Coefficients for Combustor - Linear Air-Entry Holes. II - Flush Rectangular Holes, Step Louvers, and Scoops" NACA TN 3924, 1958.

74. Rohde, J. E., H. T. Richards, and G. W. Metger, "Discharge Coefficients for Thick Plate Orifices with Approach Flow Perpendicular and Inclined to the Orifice Axis" NASA TN D-5467, 1969.

75. Kaufman, A., "Steady-State Stress Relaxation Analysis of Turbine Blade Cooling Designs," NASA TN D-5282, 1969.

76. Kaufman, A., "Analytical Study of Cooled Turbine Blades Considering Combined Steady-State and Transient Conditions," NASA TM X-1951, 1970.

77. Stewart, O. L. and W. H. Vogel, "Methods for Predicting Thermal Stress Cracking in Turbine Stator and Rotor Blades," Rep. PWA-3142, Pratt and Whitney Aircraft (NASA CR-54636), July 10, 1967.

78. Hatch, J. E. and S. S. Papell, "Use of a Theoretical Flow Model to Correlate Data for Film Cooling or Heating an Adiabatic Wall by Tangential Injection of Gases of Different Fluid Properties," NASA TN D-130, November 1959.

79. Miller, J. A. and P. F. Pucci, "Heat Transfer to an Airfoil in Oscillating Flow," ASME Paper No. 71-GT-18, April, 1971.

80. Lander, R. D., R. W. Fish, and M. Sud, "The External Heat Transfer Distribution on Film Cooled Turbine Vanes," AIAA Paper No. 72-9, AIAA 10th Aerospace Sciences Meeting, January, 1972.

81. Gladden, H. J., D. J. Gauntner, and J. N. B. Livingood, "Analysis of Heat-Transfer Tests of an Impingement-, Convection-, and Film-Cooled Vane in a Cascade," NASA TMX-2376, December, 1971.

82. Gladden, H. J., J. N. B. Livingood, and D. J. Gauntner, "Comparison of Temperature Data from a Four-Vane Static Cascade and a Research Gas Turbine Engine for a Chordwise-Finned, Impingement-, and Film-Cooled Vane," NASA TMX-2477, February, 1972.

138

SECTION 8

NOMENCLATURE

A	heat transfer area
A_c	cooling air flow area
A_o	blade root metal area
A_b	blade tip metal area
C	blade chord
C_p	specific heat at constant pressure
D	tube diameter
D_h	hydraulic diameter, $D_h = \dfrac{4\,A_c\,L}{A}$
D_P	pin diameter
d	inner ring diameter
d_o	orifice diameter
f	Fanning friction factor
G	gas mass velocity, $G = \rho V = \dfrac{W_c}{A_c}$
G_c	gas mass velocity of crossflow
G_o	gas mass velocity in the impingement holes
g_c	gravitational constant
H	heat transfer coefficient
h_o	hot gas heat transfer coefficient
h	blade height
j	Colburn j-factor, $j = St(Pr)^{2/3}$
k	thermal conductivity
L'	center-to-center spacing of rings

L	cooling passage length
L_p	pin length
M	blowing rate for film cooling $\dfrac{\rho_c V_c}{\rho_g V_g}$
m	impingement hole spacing exponent correction factor
N	rotational speed
P	static pressure
P_{ci}	coolant inlet total pressure
P_{bi}	hot gas total pressure at the blade inlet
P_{co}	coolant outlet total pressure
P_g	hot gas total pressure
P'_g	hot gas relative total pressure
P_{so}	hot gas static pressure at the blade tip
P_{st}	hot gas static pressure at the blade trailing edge
P_T	total pressure
P'_T	total pressure relative to the turbine blade
Pr	Prandtl number, $C_p \, \mu/k$
R	gas constant
Re	Reynolds number $D_h G/\mu$
Re_b	Sharp bend Reynolds number, $D_h G/\mu$
r	radius $\left(r = \dfrac{2.11}{Re_g^{0.1}} \text{ in equations 5-14} \right)$
Re_o	Orifice Reynolds number, $d_o G_o/\mu$
Re_g	hot gas Reynolds number $\dfrac{X \, V_a P_g}{\mu_g}$
r_e	radius of cooling air discharge from the center of rotation
r_i	radius of cooling air inlet from the center of rotation
S_p	pin spacing center to center

St	Stanton number, H/GC_p
T	static temperature
$T_{c,i}$	cooling air inlet temperature to the blade
$T_{c,o}$	cooling air outlet temperature
T_g	hot gas average total temperature
T'_g	hot gas relative total temperature
T_m	metal element temperature
T_{max}	maximum metal temperature in a chordwise section
T_{min}	minimum metal temperature in a chordwise section
T_T	total temperature
T'_T	total temperature relative to the turbine blade
$\overline{T}$	chordwise area weighted average metal temperature (defined in Equation 5-1)
$\overline{T}_{c,o}$	flow rate weighted average air outlet temperature (defined in Equation 5-5)
$\overline{T}_M$	chordwise area weighted average metal temperature at the mean section of the blade
$\overline{T}_R$	chordwise area weighted average metal temperature at the root section of the blade
V	absolute velocity
V_g	hot gas velocity
V_{CR}	critical velocity (defined in Equation 3-1)
W	velocity relative to the turbine blade
W_c	cooling air flow rate
$W_{c,o}$	cooling air outlet flow rate
W_{CR}	critical velocity relative to the turbine blade
W_g	hot gas flow rate
X_n	impingement hole center-to-center spacing

Z_n impingement length

γ specific heat ratio, C_p/C_v

X surface length along the blade

ΔT_{CORR} circumferentially averaged radial gas temperature profile correction factor

δ ring radial height

ϵ strain

η turbine efficiency

ρ density

σ stress

φ $\dfrac{C_p\, \rho_a\, V_a}{h_o}$ in equation 5-14

ϕ cooling effectiveness $\left(\dfrac{T_g - T}{T_g - T_{c,i}}\right)$

ψ ring dimpled tube parameter

ψ_1 impingement hole spacing correction factor

ψ_2 impingement crossflow correction factor

ω rotational speed

SUBSCRIPTS

S   station

C   combustor

1   condition 1

2   condition 2

0   no blowing

g   gas

D   design

0D   off design

142

APPENDIX A

THREE DIMENSIONAL BLADE SURFACE VELOCITY CALCULATION
COMPUTER PROGRAM (TR-IG)

INTRODUCTION

Computer program TR-IG was written to calculate the surface velocities and surface static pressures around a turbine airfoil at the hub, mean, and tip sections. This is accomplished by analyzing the flow through several orthogonal planes at different axial locations. The method used is similar to that described in Katsanis and Dellner (Reference A-1).

INPUT DATA REQUIRED

Orthogonal planes are established from a layout of the hub, mean, and tip section flow channels at approximately ten times scale. Blade surface coord-- inate points for each side of the channel may be input to the turbine geometry calculation program (AI721X). This program then calculates the required geometry input for computer program TR-IG. The geometry is calculated as follows: A mid channel line is constructed, equally distant between the suction and pressure surfaces of the flow channel. Three points of equal mid channel percents, from leading edge to throat, are then selected. A line is then constructed through these points that is perpendicular to the mid channel line and perpendicular to the suction and pressure surfaces of the flow channels. This defines an orthogonal plane at one axial location. Flow through this plane can now be analyzed. In order to completely define the surface velocities of the airfoil, several orthogonal planes must be analyzed. It should be noted that these planes can be analyzed independently of each other.

CALCULATION PROCEDURE

Computer program TR-IG calculates the airfoil surface velocities of flow through both stator rows and rotating blade rows. The calculations satisfy simple radial equilibrium and continuity. Channel flow theory is used to determine the velocity distribution across the channel for the continuity calculation. The program iterates on an estimated hub mid channel velocity until continuity is satisfied. Figure A-I shows a typical flow passage at one axial location.

The first calculation determines the value of mid channel velocities relative to the blade at the mean and tip sections (W_{mm} and W_{mt}) which satisfy radial equilibrium for a specified W_{mh}. The following equation (A-I) expresses the relationship between the estimated mid channel velocity at the hub and the mid channel velocity at any other point, y, along the potential line from hub to tip.

TIP MEAN
CHANNEL LINE

TIP

ORTHOGONAL
PLANE

MEAN

HUB

Y

X

+φ

n

S-67876

Figure A-I. Flow Passage at One Axial Location

144
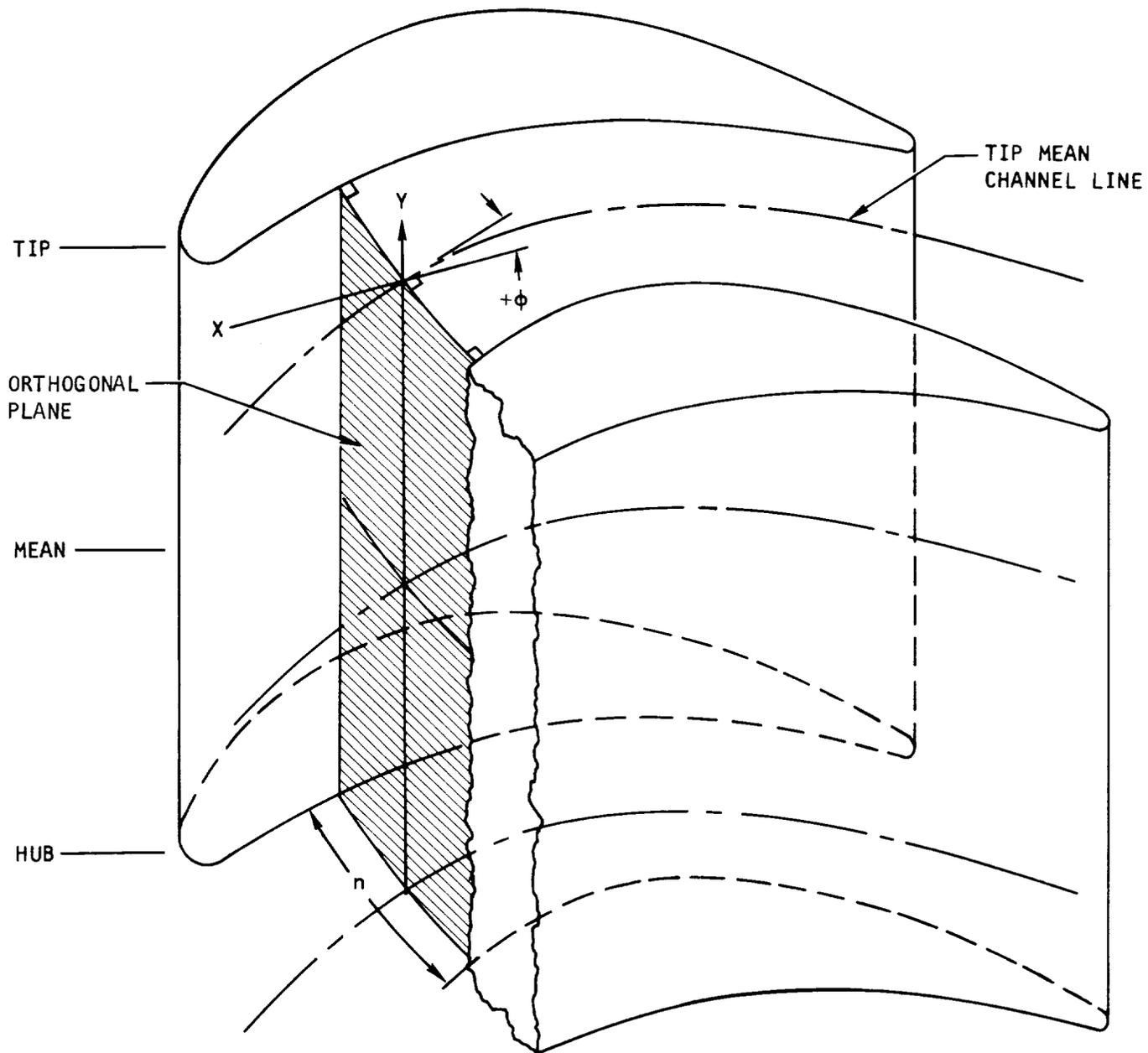
$$W_{my} = \left\{ EXP \int_h^y \left(-\frac{1}{r} \sin^2 \phi \right) dy \right\} \times \left\{ W_{mh} \right.$$

$$\left. - \int_h^y \left[2\omega \sin \phi \, EXP \int_h^y \left(\frac{1}{r} \sin^2 \phi \right) dy \right] \right\} \qquad (A-1)$$

where ω is angular velocity

The preceding equation assumes isentropic flow, constant absolute total enthalpy, neglects the y component of force exerted by the blade on the gas, and assumes that the radial potential lines are radial straight lines perpendicular to the axis of rotation. Due to the assumption of straight radial potential lines, the program is limited to flow paths of little or no divergence.

Next, the velocity is calculated at evenly spaced increments across the hub, mean, and tip circumferential potential lines using the following equation (A2):

$$W = W_{my} \left\{ EXP \left[-\frac{n}{2\Delta c} \left(c^2 - c_m^2 \right) \right] \right\} \qquad (A-2)$$

The mid channel curvature, c_m, is assumed to be the average between the suction surface and pressure surface curvatures. The stream line curvature, c, is assumed to vary linearly with n. Δc is the change in c from the mid channel to the point when the velocity, W, is to be calculated.

By assuming P_{rel} and T_{rel} constant across a given circumferential potential line the flow rate per unit area, ρW (where ρ is static density), can be calculated. The flow rate is determined by integrating ρW over the plane defined by the hub, mean, and tip circumferential potential lines. The calculated flow rate is compared to the desired (input) flow rate. If these two values do not agree within a certain tolerance, W_{mh} is adjusted and the entire calculation is repeated.

The velocity distribution around the leading edge is obtained from the potential flow theory solution for a cylinder in crossflow as shown below,

$$\left(\frac{V}{V_{CR}} \right)_x = 2 \cdot \left(\frac{W}{W_{CR}} \right)_l \sin \left(\frac{X}{R} \right) \qquad (A-3)$$

where

     X   =   the distance from the stagnation point - in.

     R   =   the leading edge radius - in.

$\left(\dfrac{W}{W_{CR}} \right)_l$ =   critical velocity ratio relative to the leading edge

NOMENCLATURE

C	Curvature of streamline on boundary, 1/in.
n	Distance across a potential line in the circumferential direction, in.
W	Velocity relative to the blade row, ft/sec
$\emptyset$	Mid channel stream line angle, measured from axial in the x - n plane, degrees
ω	Rotational speed, rad/sec
a	Radius, in.

SUBSCRIPTS

h	Hub
m	Mean or mid channel
t	Tip
p	Pressure surface
s	Suction surface
x	Axial plane
y	Radial plane
z	Tangential plane

146

REFERENCES

A-1   Katsanis, T. and L. T. Dellner, "A Quasi-Three-Dimensional Method
        for Calculating Blade Surface Velocities for an Axial Flow Turbine
        Blade," NASA TM-1394, June 1967.

STEADY-STATE AND TRANSIENT THERMAL ANALYZER COMPUTER PROGRAM
WITH COMPRESSIBLE AND INCOMPRESSIBLE FLOW AND PRESSURE DROP (HO910)

INTRODUCTION

Computer program HO910 is a network analysis program that includes transient and steady-state heat transfer by conduction, convection, radiation, transpiration, and film cooling. The program performs fluid network pressure drop calculations, including flow area changes, friction, entrance and exit losses, heat addition, and centrifugal pumping for a given flow distribution.

The steady-state and transient thermal analyzer program with pressure drop calculations was developed with AiResearch funds for the analysis of electronic components, electric motor and generator, and gas turbine engine thermal problems.

TRANSIENT AND STEADY-STATE HEAT TRANSFER CALCULATIONS

Transient heat transfer calculations are developed by the explicit finite difference method described by Dusinberre (Reference B-1). This method is based on the transfer of heat along thermal resistance paths by virtue of a temperature difference between heat storage elements that absorb or release heat as a result of a temperature increase or decrease.

A typical energy balance relation around a thermal capacitance element or node is shown below.

$$R_1 = \frac{\ell_1}{k_o A_1} + \frac{1}{H_r A_1}$$

$$R_5 = \frac{\ell_5}{k_o A_5} + \frac{1}{H_o A_5}$$

$$R_2 = \frac{\ell_2}{k_o A_2} + \frac{1}{H_c A_2}$$

$$R_3 = \frac{\ell_0}{k_o A_3} + \frac{\ell_3}{k_3 A_3} + \frac{R_c}{A_3}$$
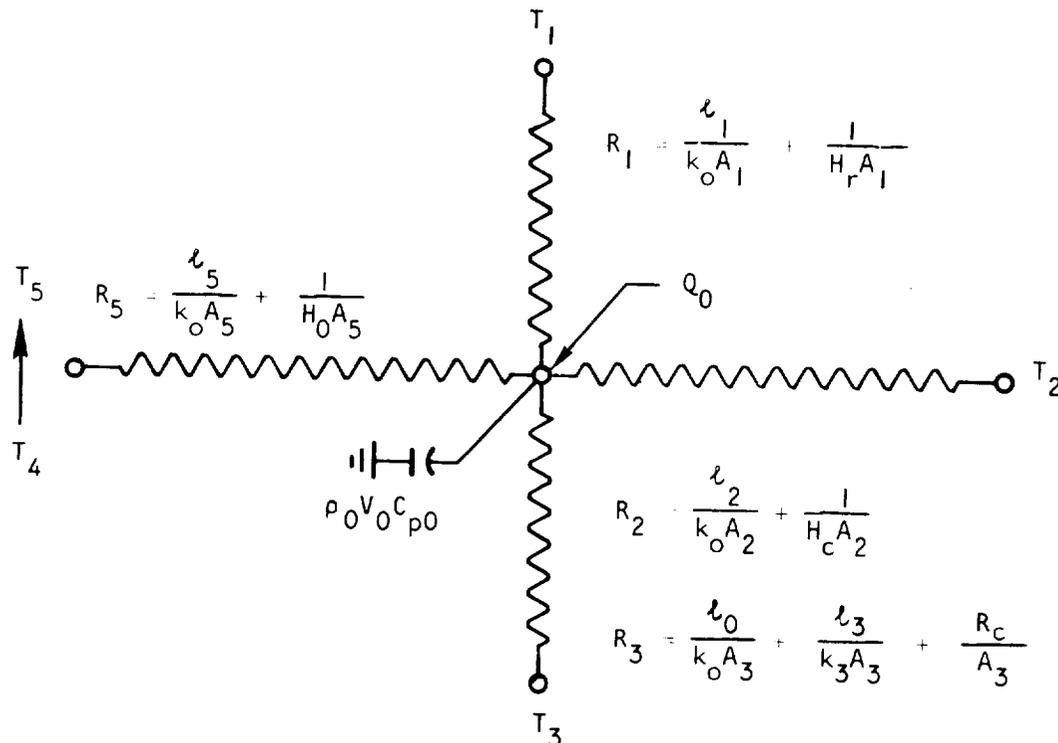
$$\rho_0 V_0 C_{p0} \frac{dT_0}{d\theta} = \frac{T_1 - T_0}{R_1} + \frac{T_2 - T_0}{R_2} + \frac{T_3 - T_0}{R_3} + \frac{\frac{T_4 + T_5}{2} - T_0}{R_5} + Q_0 \quad (B-1)$$

Using the initial-time temperature difference presented by Dusinberre, Equation (B-2) may be written

$$\rho_0 V_0 C_{p0} \frac{T_0(\theta + \Delta\theta) - T_0(\theta)}{\Delta\theta} = \frac{T_1(\theta) - T_0(\theta)}{R_1} + \frac{T_2(\theta) - T_0(\theta)}{R_2}$$

$$+ \frac{T_3(\theta) - T_0(\theta)}{R_3} \quad (B-2)$$

$$+ \frac{\frac{T_4(\theta) + T_5(\theta)}{2} - T_0(\theta)}{R_5} + Q_0$$

Solving for the temperature at time $\theta + \Delta\theta$, Equation (B-3) may be written

$$T_0(\theta + \Delta\theta) = T_0(\theta) + \frac{\Delta\theta}{\rho_0 V_0 C_{p0}} \left[\frac{T_1(\theta) - T_0(\theta)}{R_1} + \frac{T_2(\theta) - T_0(\theta)}{R_2} \right.$$

$$\left. + \frac{T_3(\theta) - T_0(\theta)}{R_3} + \frac{\frac{T_4(\theta) + T_5(\theta)}{2} - T_0(\theta)}{R_5} + Q_0 \right] \quad (B-3)$$

To avoid a physically impossible solution to the above equation, a maximum allowable finite time increment $\Delta\theta$ must be defined as shown in Equation (B-4).

$$\Delta\theta_{max} = \frac{\rho_0 V_0 C_{p0}}{1/R_1 + 1/R_2 + 1/R_3 + 1/R_5} \quad (B-4)$$

If the value of $\Delta\theta$ in Equation (B-3) exceeds $\Delta\theta_{max}$ from Equation (B-4), then the value of $T_0(\theta + \Delta\theta)$ would overshoot its steady-state value relative to the surroundings at time θ and would thereby violate principles of the first law of thermodynamics. When $\Delta\theta$ in Equation (B-3) equals $\Delta\theta_{max}$ in Equation (B-4), then the value of $T_0(\theta + \Delta\theta)$ equals its steady-state value relative to the surroundings at time θ.

149

Steady-state heat transfer calculations are based on the conservation of energy under equilibrium conditions. This means that all the heat flowing into an element plus the heat generated in the element must equal the heat flowing out of the element. The resulting equations in a steady state solution may be solved by elimination, determinants, relaxation, and iteration. The method of elimination is best when the number of unknowns is small, but it becomes quite complex as the number increases. The method of determinants is best for problems with thermal resistances that are not a function of temperature or temperature difference. In these cases a direct solution of the problem is possible with one matrix inversion. When radiation, natural convection, condensation, variable thermal conductivity, or boiling heat transfer is involved, repeated inversions of the matrix are necessary to "iterate" to a solution. In this case the method of determinants or matrix inversion takes more time than other methods and the computer storage requirements for this method are greater. The method of relaxation is difficult to program because the method for reduction of the "residuals" is arbitrary and requires judgment on the part of the user. The method of iteration or successive substitution follows a fixed sequence of operations which, when repeated a sufficient number of times, will give a solution accurate within the limits of the model. In this method the temperature of each element is calculated as the weighted average of the temperatures of its neighbors plus the temperature rise due to heat generation. This process is repeated for each element in the problem and new values of the thermal resistance between elements are calculated, based on the new temperatures when necessary. These new resistances and temperatures are then used to calculate a successive set of values and the process is repeated until the temperature change between successive substitutions is sufficiently small. This method, also known as the Gauss-Seidel method, works best when all the thermal resistances are the same order of magnitude. When two elements are connected together by a resistance that is less than 1/1000 of the average thermal resistance in the problem, and the resistances connecting these elements to the rest of the array are average, then these elements are so controlled by each other that they will move very slowly toward a solution and many iterations will be required to reach steady state. In order to eliminate this problem a mathematical trick called "lumping" is used. In this method the two elements connected by a small resistance are lumped together for one calculation to bring them up to steady state with their environment, and they are then calculated separately up to 100 times. Elements connected by a thermal resistance less than 1/100 of the average thermal resistance are simply calculated separately up to 100 times. This operation is repeated for each successive calculation of the whole array and this brings the element temperatures · more evenly along toward the steady-state solution, thus requiring less iteration steps. When nonlinear thermal resistances such as radiation, natural convection, condensation, and boiling heat transfer coefficients that are a strong function of temperature difference are used, ordinary successive substitution may not be convergent.

To ensure convergence, the method of accelerated step substitution with monotonic deceleration until successive substitutions are convergent is used. In this method the maximum temperature change in each iteration is checked to see if it is less than the temperature change in the previous step. If the latest change is greater than the previous change, this could mean that the temperature has overshot the steady-state solution and is farther away than

150

the previous estimate. In this case the solution would continue to diverge (get farther away). To prevent this, the temperature change is decelerated or reduced by a multiplying factor until the variation in successive approximations is convergent. This acceleration factor may also be input as greater than one to speed up convergence in those cases that are not unstable.

A typical steady-state heat balance relation around a zero thermal capacitance element or node is shown below.
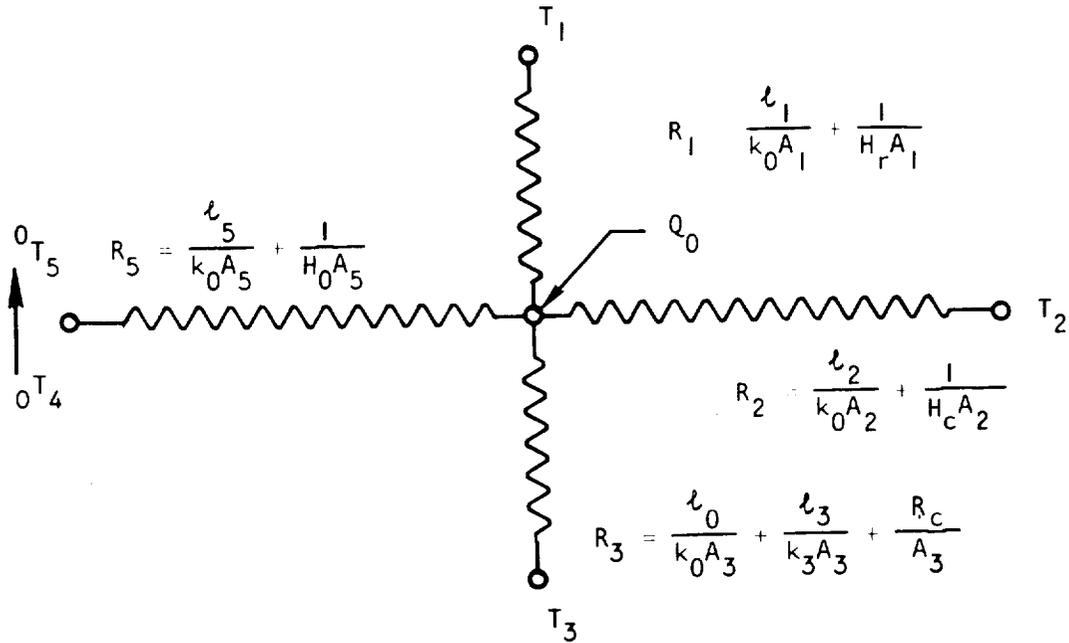
$$Q_0 = \frac{T_0 - T_1}{R_1} + \frac{T_0 - T_2}{R_2} + \frac{T_0 - T_3}{R_3} + \frac{T_0 - \dfrac{T_4 + T_5}{2}}{R_5} \qquad (B-5)$$

Solving this equation for the node temperature (T_0) gives Equation (B-6)

$$T_{0\ new} = \frac{T_1/R_1 + T_2/R_2 + T_3/R_3 + (T_4 + T_5)/2R_5 + Q_0}{1/R_1 + 1/R_2 + 1/R_3 + 1/R_5} \qquad (B-6)$$

Equation (B-6) is used to calculate new temperatures for each node in the array from the previous temperatures for the nodes. The maximum temperature change is determined; if it is greater than the previous temperature change, the value of F_{ac} in Equation (B-7) below is reduced.

$$T_0(n + 1) = (T_{0\ new} - T_0(n)) (F_{ac}) + T_0(n) \qquad (B-7)$$

The $(n + 1)$th value of the temperature distribution calculated from Equation (B-7) is substituted in Equation (B-6) to determine new values of the temperatures. This process is continued until the temperature change in a specified number of increments (NITX) is less than a certain specified value (DTEMP). At this point the solution is accepted as sufficiently accurate and is printed out.

The values of the thermal resistances R_1, R_2, R_3, and R_5 are calculated by the computer program as described below. Thermal resistance R_1 is a typical radiation thermal resistance. The total resistance R_1 is made up of conduction resistance from the center of node (0) to the radiating surface $\frac{\ell_1}{K_o A_1}$ and radiation resistance $\frac{1}{H_r A_1}$ from the radiating surface to the surrounding node (1). The value of H_r is calculated by the program as shown in Equation (B-8).

$$H_r = 0.1713 \times 10^{-8} \; (\mathfrak{F}) \; \left(T_{so}^2 + T_1^2\right) \left(T_{so} + T_1\right) \qquad (B-8)$$

where $T_{so} = \dfrac{\dfrac{K_o A_1}{\ell_1} T_o + \left(H_r A_1\right) T_1}{\dfrac{K_o A_1}{\ell_1} + H_r A_1}$

As shown, the program performs the important and often overlooked task of determining the radiation surface temperature of the node and includes the conduction resistance to this surface. Estimation of the emissivity view factor $\mathfrak{F}$ as obtained from data of Reference B-8, is described in Table B-1.

Thermal resistance R_2 is a typical convection thermal resistance. The total resistance R_2 is made up of conduction resistance $\frac{\ell_2}{K_o A_2}$ from the center of node (0) to the convecting surface, and the convection resistance $\frac{1}{H_c A_2}$ from the surface to the surroundings, node (2). The value of the convection heat transfer coefficient (H_c) is difficult to estimate and often varies as a function of time, fluid bulk temperature, the surface to bulk fluid temperature difference, and the "film" temperature of the fluid. The program provides options for convection heat transfer coefficients input as a function of time, "film" temperature, and surface to bulk temperature difference. The program also provides five different options for calculation of convection heat transfer coefficients from input fluid properties. These options are discussed in the temperature dependent fluid properties section of this appendix.

152

TABLE B-1

EMISSIVITY VIEW FACTORS FOR VARIOUS CONFIGURATIONS
FOR RADIATION THROUGH NONABSORBING GAS

CONFIGURATION	EMISSIVITY VIEW FACTOR $\mathcal{F}$
Radiation from a small surface A_1 to a large surface A_2 $A_1 \leq A_2/20$	ϵ_1
Radiation from a plane surface A_1 to a parallel plane surface A_2 $A_1 = A_2$	$\dfrac{1}{\dfrac{1}{\epsilon_1} + \dfrac{1}{\epsilon_2} - 1}$
Radiation from an inner cylinder A_1 to a concentric outer cylinder A_2	$\dfrac{1}{\dfrac{1}{\epsilon_1} + \dfrac{A_1}{A_2}\left(\dfrac{1}{\epsilon_2} - 1\right)}$
Radiation from an inner sphere A_1 to a concentric outer sphere A_2	$\dfrac{1}{\dfrac{1}{\epsilon_1} + \dfrac{A_1}{A_2}\left(\dfrac{1}{\epsilon_2} - 1\right)}$

$$\mathcal{F} = \frac{1}{\dfrac{1}{\bar{F}_{12}} + \left(\dfrac{1}{\epsilon_1} - 1\right) + \dfrac{A_1}{A_2}\left(\dfrac{1}{\epsilon_2} - 1\right)}$$

A_1 = the radiating area

$\bar{F}_{12} = F_{12}$ where no reradiating surfaces exist
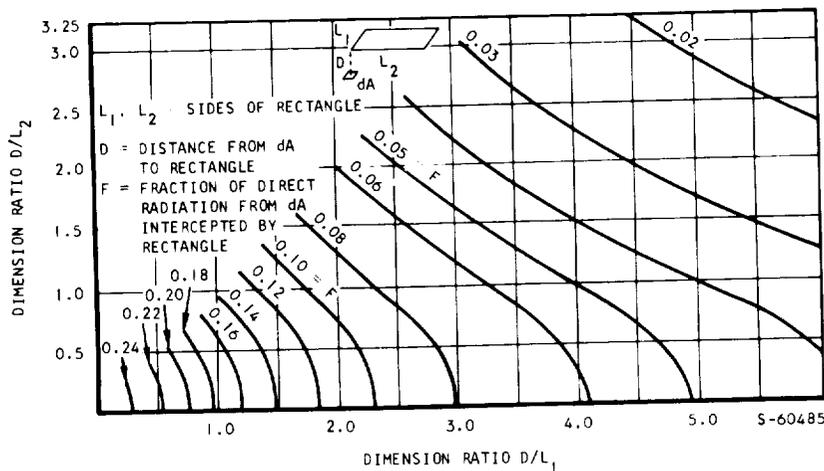
VIEW FACTOR F FOR DIRECT RADIATION BETWEEN AN ELEMENT dA AND
A PARALLEL RECTANGLE WITH ONE CORNER OPPOSITE dA (HOTTEL.)

S-64966

153
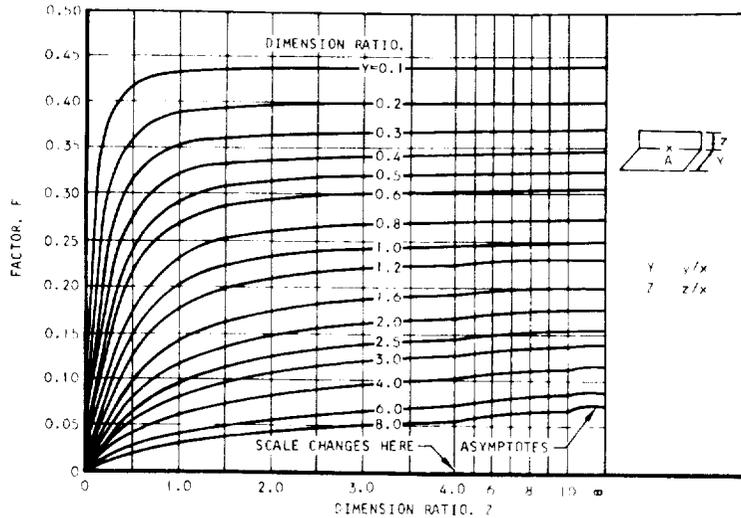
VIEW FACTOR F FOR DIRECT RADIATION BETWEEN ADJACENT RECTANGLES
IN PERPENDICULAR PLANES (HOTTEL)
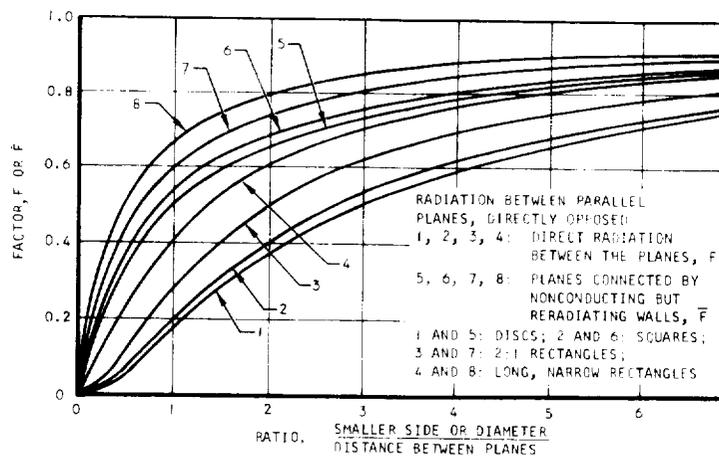
VIEW FACTOR F AND INTERCHANGE FACTOR F̄ FOR RADIATION BETWEEN
PARALLEL PLANES DIRECTLY OPPOSED
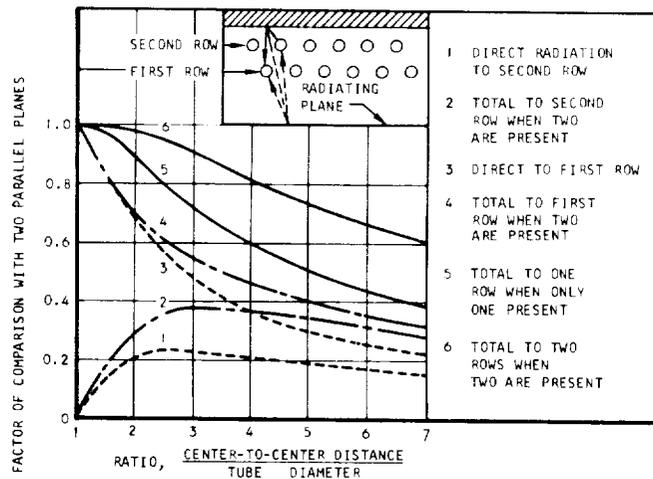
VIEW FACTOR F AND INTERCHANGE FACTOR F̄ FOR RADIATION FROM A
PLANE TO ONE OR TWO ROWS OF TUBES ABOVE AND PARALLEL TO THE PLANE

S-60449

154

Thermal resistance R_3 is a typical conduction thermal resistance. The total resistance R_3 is made up of a conduction thermal resistance from the center of node (0) to the boundary $\dfrac{\ell_0}{K_0 A_3}$, the thermal interface resistance (if any) between the nodes (R_c/A_3), and a conduction thermal resistance from the center of node (3) to the boundary $\dfrac{\ell_3}{K_3 A_3}$. The use of separate thermal resistances from each node to the boundary permits proper estimation of the total thermal resistance where two dissimilar materials are connected or where variable thermal conductivity as a function of node temperature is used. In addition, the thermal interface resistance allows mechanical joint thermal contact resistance to be included. Thermal conductivity of the materials may be input as a function of temperature (if known) and the thermal conductivity will be varied in each iteration step.

CONVECTION HEAT TRANSFER CALCULATIONS

Convection heat transfer coefficients may be input to the program by nine different methods. In method one the film coefficient of heat transfer is input as a constant value. In method two the convection heat transfer coefficient is input as a function of time in a table. In method three the convection heat transfer coefficient is input as a function of the difference between the node surface and the bulk fluid temperature. In this method the node surface temperature is determined by iteration in Equation (B-9) below.

$$T_{s_Q} = \frac{\dfrac{K_0 A_1}{\ell_1} T_0 + (H_c A_1) T_1}{\dfrac{K_0 A_1}{\ell_1} + H_c A_1} \tag{B-9}$$

In method four the convection heat transfer coefficient is input as a function of the "film" temperature of the fluid (the average between the node surface temperature and the bulk fluid temperature). The node surface temperature is determined by iteration in Equation (B-9).

Method five involves natural convection heat transfer coefficients calculated by the program from fluid property tables read into the program. Sets of specific heat (C_p), viscosity (μ), compressibility coefficient (Z), Prandtl number (P_r), and density (ρ) tables may be read into the program. Fluid properties are estimated from these tables by Lagrangian interpolation to the "film" temperature for the natural convection heat transfer coefficient. Equation (B-11) is used for laminar natural convection heat transfer if the product of the Grashof times the Prandtl number is less than the input value of $F_{tn} \times 10^8$.

$$Gr(Pr) = \frac{(L)^3 (\rho)^2 (g_c) (\beta) [T_{so}(NN1) - T(NN2)]}{\mu^2}(Pr) \qquad (B-10)$$

If $Gr(Pr) \leq F_{tn} \times 10^8$, use laminar natural convection.

$$H = 0.55(C_h) \frac{K_f}{L} [Gr(Pr)]^{0.25} \qquad (B-11)$$

Equation (B-12) is used for turbulent natural convection heat transfer if the product of the Grashof time the Prandtl number is greater than the input value of $F_{tn} \times 10^8$.

The value of g_c is normally input as the gravitational force acting on the fluid. When the fluid is enclosed in a rotating chamber or between coaxial rotating disks (as in an axial flow gas turbine compressor), natural convection heat transfer is calculated by replacing g_c by the radius from the center of rotation to the center of the node, in feet, and adding the rotational speed in revolutions per minute for rpm.

Method six involves laminar or turbulent flat plate heat transfer coefficients calculated from fluid property tables read into the program as described above. In this method the fluid properties are determined at Eckert's (Reference B-2) reference temperature as shown in Equation (B-12).

$$T_{ER} = T + 0.5(T_W - T) + 0.22 (T_{adw} - T) \qquad (B-12)$$

where
$$T = T_T - \frac{(V)^2}{2(32.2)(778)C_p}$$

$$T_{adw} = T + (Pr)^{1/2} (T_T - T) \text{ for laminar flow}$$

$$T_{adw} = T + (Pr)^{1/3} (T_T - T) \text{ for turbulent flow}$$

The velocity and pressure may be input to this section of the program as velocity in feet per second and static pressure in psia, or as the velocity divided by the critical velocity and the total pressure in psia. When the critical velocity ratio and total pressure are used, the velocity and static pressure are calculated by the program, as shown in Equations (B-13) and (B-14).

$$V = \left(\frac{V}{V_{CR}}\right)\sqrt{\frac{2\gamma g_c R T_T}{M_W(\gamma + 1)}} \qquad (B-13)$$

$$P_S = P_T \left[1. - \frac{\gamma - 1}{\gamma + 1} \left(\frac{V}{V_{CR}} \right)^2 \right]^{\frac{\gamma}{\gamma - 1}} \qquad (B-14)$$

The advantage of using the critical velocity ratio and total pressure method of input is that the critical velocity ratio distribution on a turbine blade or stator vane surface remains relatively constant during the acceleration and deceleration transients and only the total pressure varies as a function of time.

Equation (B-15) is used for laminar flow heat transfer coefficients and for heat transfer coefficients around the leading edge of a cylinder in cross-flow when $F_t \le 0$.

$$H = 0.332(C_h) \frac{K_f}{L} \left[\frac{L \, (V) \, \rho}{\mu} \right]^{0.5} Pr^{1/3} \qquad (B-15)$$

Equation (B-16) is used for turbulent flow heat transfer coefficients when $F_t > 0$.

$$H = 0.0296(C_h) \frac{K_f}{L} \left[\frac{L \, (V) \, \rho}{\mu} \right]^{0.8} Pr^{1/3} \qquad (B-16)$$

The fluid temperature input with this heat transfer coefficient is the total temperature, and the program uses total temperature for heat transfer calculations.

In the turbine blade analysis, heat transfer coefficients around the leading edge on the hot gas side are calculated using

$$C_h = 1.2(3.43) \left[1 - \left(\frac{\phi}{90} \right)^3 \right]$$

$$0 \le \phi < 80$$

$$L = \text{Diameter of the leading edge, ft.}$$

$$F_t = 0.$$

This yields Equation (B-17) for heat transfer coefficients around the leading edge.

$$H = 1.2(1.14) \frac{K_f}{L} \left[\frac{L \, (V) \, \rho}{\mu} \right]^{0.5} (Pr)^{1/3} \left[1 - \left(\frac{\phi}{90} \right)^3 \right] \qquad (B-17)$$

For heat transfer coefficients along the sides of the blade, the turbulent flat plate equation (B-16) is used with

$$C_h = 1.$$

$$L = \text{Surface length from the stagnation point to the center of the element, ft}$$

$$F_t = 1.$$

Method seven is for laminar or turbulent heat transfer on a rotating disk in an infinite environment. The methods used are described in a paper by Richardson and Saunders (Reference B-3).

Method eight is the heat transfer coefficient for impingement on a concave surface from a row of holes. The equation used is taken from Chupp, Helms, McFadden, and Brown (Reference B-4) as shown in Equation (B-18).

$$H = 0.44 \, (C_h) \, \frac{K_f}{d_o} \left[\frac{d_o \, (W)}{\mu_o \, A_o} \right]^{0.7} \left(\frac{d_o}{X_n} \right)^{0.8}$$

$$\text{EXP} \left[- 0.85 \left(\frac{Z_n}{X_n} \right) \left(\frac{d_o}{D_I} \right)^{0.4} \right] \tag{B-18}$$

Method nine is the heat transfer coefficient calculation for flow in a channel. The fluid properties are taken from input fluid property tables at the film temperature, as described above. (The heat transfer coefficient is given in Equation B-19).

$$H = \frac{C_h \, (J) \, (W) \, C_{pf}}{A_c (Pr)^{2/3}} \tag{B-19}$$

The value of J is taken from Reynolds number $\left(Re = \dfrac{D_h(W)}{A_c\, \mu}\right)$ vs Colburn j-factor (J) tables input to the program. The heat transfer effectiveness of the fin area (A_f) is calculated as shown in Equation (B-21).

$$\eta_f = \frac{\tanh\left[\sqrt{\dfrac{2 \cdot H}{(K_m)\delta_f}}\left(\dfrac{L_f}{12}\right)\right]}{\left[\sqrt{\dfrac{2 \cdot H}{(K_m)\delta_f}}\left(\dfrac{L_f}{12}\right)\right]} \tag{B-20}$$

$$A_T = A + \eta_f\,(A_f) \tag{B-21}$$

C_h may be used to account for entrance-effect heat transfer. Several equations suggested by Nunner (Reference B-5) are given below.

Thermal and Hydrodynamic Entry Region	Thermal Entry Region of Established Flow
Mean value $C_h = 1 + \left(\dfrac{D_h}{L}\right)^{2/3}$	$C_h = 1.0 + 0.1\left(\dfrac{\ell th}{L}\right)$
Local value $C_h = 1 + \dfrac{1}{3}\left(\dfrac{D_h}{\ell}\right)^{2/3}$	$C_h = 1.0 + 0.02\left(\dfrac{\ell th}{\ell}\right)$

For turbulent flow $(2 < L/D_h < 60)$

For pin surfaces, Colburn j-factors (J) from Equation (B-22) based on a computer regression analysis of triangular spaced tube bank data, triangular spaced pin fin data, and continuous finned tube data are used.

$$J = \frac{\left[0.023 + \dfrac{4.143\,\mathrm{EXP}\left\{-3.094\left(\dfrac{D_p}{S_p}\right) - 0.89\left(\dfrac{S_p}{L_p}\right)^{0.5075}\right\}}{(Re)^{0.2946}}\right]}{(Re)^{0.2}} \tag{B-22}$$

FLUID STREAM HEAT TRANSFER AND PRESSURE DROP CALCULATION

Fluid stream heat is normally transferred by conduction, convection, or radiation from a node to the average fluid temperature in the stream section, as previously described. There is no limit to the number of conduction, convection, or radiation thermal resistances that may be connected to each fluid stream section, but at least one conduction, convection, or radiation resistance must be connected to each fluid stream section. If the sum of all conduction, convection, and radiation conductances $(1/R_n)$ connected to a fluid stream section $(UA = \Sigma 1/R_n)$ is greater than or equal to twice the capacity rate in the fluid stream section:

$$2(W)(C_{pf}) \leq UA$$

Then the outlet fluid stream section temperature is used for heat transfer. This eliminates the problem of an outlet fluid temperature overshooting the surrounding surface temperatures, a thermodynamic impossibility.

Steady-state fluid capacity rate calculations in a fluid stream section are handled as shown in Equation (B-23).

$$(W)(C_{pf})(T_o - T_i) = \Sigma \frac{(T_n - \bar{T}_s)}{R_n} \tag{B-23}$$

where
$$\bar{T}_s = \frac{T_o + T_i}{2} \quad \text{if } 2(W)(C_{pf}) > UA$$

$$\bar{T}_s = T_o \quad \text{if } 2(W)(C_{pf}) \leq UA$$

Solving for the outlet fluid stream total temperature (T_o) gives Equations (B-24 and B-25).

$$T_o = \frac{\Sigma \left(\frac{T_n - T_i/2}{R_n} \right) + W(C_{pf}) T_i}{W(C_{pf}) + \Sigma 1/(2R_n)} \quad \text{if } 2(W)(C_{pf}) > UA \tag{B-24}$$

$$T_o = \frac{\Sigma T_n/R_n + W(C_{pf}) T_i}{W(C_{pf}) + \Sigma 1/R_n} \quad \text{if } 2(W)(C_{pf}) \leq UA \tag{B-25}$$

160

To account for fluid stream acceleration in rotational flow, the following term is added:

$$T_{or} = T_o + \frac{(\frac{2\pi}{60})^2 (R1 + R2) (N)^2 \Delta R}{2 J g_c (C_{pf})}$$

In addition to thermal analysis, program H0910 calculates fluid stream pressure drop in both steady-state compressible and incompressible flow. These calculations include pressure losses due to flow disturbances such as elbows, valves, and sudden expansions and contractions, pressure drop due to flow acceleration caused by area change or heat addition, pressure drop due to fluid friction, pressure drop due to flow addition or removal, and pressure change due to radial inward or outward flow in a rotational field.

The compressible flow pressure drop in the fluid stream passage is calculated as described in Shapiro (Reference B-6) with an equation for rotational flow head replacing the drag component for stationary bodies in the fluid stream.

The compressible flow pressure drop in each section of the passage is calculated from influence coefficients as shown in Equation (B-26). The equation is integrated by finite increments in each segment.

$$P_2 = P_1 - P_{avg} \left\{ \frac{\gamma M^2 \left(1 + \frac{\gamma - 1}{2} M^2\right)}{1 - M^2} \frac{\Delta T_o}{T_o} + \frac{\gamma M^2 [1 + (\gamma - 1)M^2]}{2(1 - M^2)} \right.$$
$$\left[4f \frac{\Delta R}{D_h} - \frac{(\frac{2\pi}{60})^2 (Mw)(R2 + R1) N^2 \Delta R}{2 J g_c \gamma T_o M^2} - \frac{2(\gamma)(\Delta W)}{W} \right]$$
$$\left. + \frac{2\gamma M^2 \left(1 + \frac{\gamma - 1}{2} M^2\right)}{1 - M^2} \frac{\Delta W}{W} - \frac{\gamma M^2}{1 - M^2} \frac{\Delta A}{A} \right\} \qquad (B-26)$$

The program allows new streams branching off from any location along a previous stream. This is accomplished by making the inlet temperature node number of the new stream the same as one of the outlet temperatures in a previous stream section. The inlet pressure of the new stream is taken as the outlet static pressure from the previous fluid stream section if it is not the last section in the stream. New streams branching off from the last section of a previous stream use the outlet total pressure of the previous stream as an inlet pressure.

161

The program permits mixing between previous streams to form the inlet temperature of a new stream. To do this, the inlet temperature node number for the new stream is input at NMIX for all the previous streams that mix to form the new stream. Mixing is allowed between the outlet temperature at the end of previously defined streams and the outlet temperature within a new stream section. In this case the outlet temperature node number within the new stream is used as NMIX for the previously defined streams mixing with this stream.

The mixed stream temperature is calculated as shown in Equation (B-27)

$$T_{o2} = \frac{W_1 C_{P1} T_{oi} + W_m C_{Pm} T_{om}}{W_1 C_{P1} + W_m C_{Pm}}$$

(B-27)

The fluid stream section model assumed for Equations (B-26) and (B-27) is shown below.
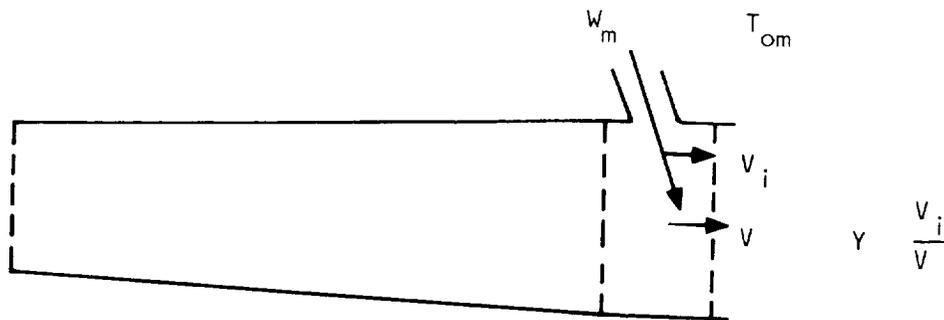
A_1	$\Delta A = A_2 - A_1$	A_2	A_2
T_{o1}	$\Delta T_o = T_{o2} - T_{o1}$	T_{o1}	T_{o2}
W_1	$\Delta W = W_2 - W_1$	W_1	W_2
R_1	$\Delta R = R_2 - R_1$	R_2	R_2

$$A = (A_1 + A_2)/2$$
$$T_o = (T_{o1} + T_{o2})/2$$
$$W = (W_1 + W_2)/2$$
$$M = (M_1 + M_2)/2$$

$$W_2 = W_m + W_1$$

162

The branching or mixing in each fluid stream section is assumed to occur at the exit of the section. The momentum of the exiting or entering stream relative to the main stream is expressed by the Y-factor as defined in the above figure. The Y-factor for turbulent flow in a supply tube with flow removed through holes or slots is usually assumed to be 1 (Y = 1.0) This assumes that the removed flow has the momentum of the main stream. For injected flow perpendicular to the mainstream flow, it is usually assumed that the Y-factor is zero (Y = 0.0). This assumes that the flow enters with no momentum in the direction of the mainstream and must be accelerated from zero velocity. For injection angles other than perpendicular to the mainstream flow, a Y-factor other than zero may be estimated by calculating the vector of inlet velocity in the direction of the mainstream divided by the mainstream velocity.

The friction factor for the flow passages is input as a function of Reynolds number.

The compressible flow pressure drop in elbows, valves, and sudden expansions and contractions is calculated from total head loss coefficients input as a constant for the inlet or exit of each fluid stream, as shown in Equation (B-28).

$$P_{t2} = P_{t1} - \frac{1}{2} (K_t) \, \gamma M^2 P_2 \tag{B-28}$$

The incompressible flow pressure drop in each section of the passage is calculated as shown in Equation (B-29).

$$P_{t2} = P_{t1} - \frac{(W/A_c)^2}{2 g_c \rho} \left[\left(\frac{4 f}{D_h} \Delta R \right) + 2(\Delta W/W)(1 - Y) \right]$$

$$+ \frac{(\frac{2\pi}{60})^2}{2 \cdot gc} \rho (N)^2 (R_2 + R_1) \Delta R \tag{B-29}$$

The incompressible flow pressure drop in elbows, valves, and sudden expansions and contractions is calculated from total head loss coefficients input as a constant.

$$P_{t2} = P_{t1} - (K_t) \frac{(W/A_c)^2}{2 g_c \rho} \tag{B-30}$$

TEMPERATURE DEPENDENT FLUID PROPERTY EFFECTS ON HEAT TRANSFER AND FLUID FRICTION

Conventional methods of predicting single-phase heat transfer and friction coefficients often give values that are in poor agreement with measured values when large temperature differences or large variations of fluid properties are present. Several methods have been proposed for accounting for these differences. Humble, Lowdermilk, and Desmon (Reference B-7) investigated heat transfer and fluid friction coefficients for air flowing in smooth tubes with surface-to-air temperature ratios from 0.46 to 3.5. The results of this study indicate that the fluid properties in the heat transfer and friction coefficient equations should be evaluated at the film temperature with the fluid velocity evaluated at the bulk temperature. Based on this method, the Reynolds number is defined as shown in equation (B-31) below.

$$R_e = \frac{D_h V_b \rho_f}{\mu_f} = \frac{D_h W}{\mu_f A_c} \left(\frac{\rho_f}{\rho_b} \right) \tag{B-31}$$

The Colburn J-factor is defined as shown in equation (B-32) below.

$$J = \frac{H}{C_p \rho_f V_b} \left(\frac{C_p \mu}{k} \right)^{2/3}_f = \frac{H}{C_{pf} \frac{w}{A_c}} \left(\frac{\rho_b}{\rho_f} \right) \left(\frac{C_p \mu}{k} \right)^{2/3}_f \tag{B-32}$$

The Fanning friction factor is defined as shown in equation (B-33) below:

$$f = \frac{\Delta P_{fr}}{\frac{4L}{D_h} \frac{\rho_f V_b^2}{2g_c}} = \frac{\Delta P_{fr}}{\frac{4L}{D_h} \frac{\left(\frac{w}{A_c}\right)^2}{2g_c \rho_b} \left(\frac{\rho_f}{\rho_b}\right)} \tag{B-33}$$

McAdams (Reference B-8) and Kays and London (Reference B-9) indicate that a large amount of data for many types of heat transfer surfaces has been evaluated on the basis of fluid properties evaluated at the bulk temperature of the fluid. This data was evaluated where small temperature differences or small variations in fluid properties were present. Based on this method, the Reynolds number is defined as shown in equation (B-34) below.

$$Re = \frac{D_h V_b \rho_b}{\mu_b} = \frac{D_h W}{\mu_b A_c} \tag{B-34}$$

The Colburn J-factor is defined as shown in equation (B-35) below

$$J = \frac{h}{C_{p_b} \rho_b V_b} \left(\frac{C_p \mu}{k}\right)_b^{2/3} = \frac{h}{C_{pb}\left(\frac{w}{A_c}\right)} \left(\frac{C_p \mu}{k}\right)_b^{2/3} \qquad (B-35)$$

The Fanning friction factor is defined as shown in equation (B-36) below

$$f = \frac{\Delta P_{fr}}{\frac{4L}{D_h} \frac{\rho_b V_b^2}{2g_c}} = \frac{\Delta P_{fr}}{\frac{4L}{D_h} \frac{\left(\frac{w}{A_c}\right)^2}{2g_c \rho_b}} \qquad (B-36)$$

For liquids with large temperature differences or large variations in fluid properties, equations (B-35) and (B-36) above may be modified as shown in equations (B-37) and (B-38) below.

$$\left(\frac{\mu_w}{\mu_b}\right)^n J = \frac{h}{C_p \rho_b V_b} \left(\frac{C_p \mu}{K}\right)_b^{2/3} = \frac{h}{C_{pb}\left(\frac{w}{A_c}\right)} \left(\frac{C_p \mu}{k}\right)_b^{2/3} \qquad (B-37)$$

$$\left(\frac{\mu_w}{\mu_b}\right)^m f = \frac{\Delta P_{fr}}{\frac{4L}{D_h} \frac{\rho_b V_b^2}{2g_c}} = \frac{\Delta P_{fr}}{\frac{4L}{D_h} \frac{\left(\frac{w}{A_c}\right)^2}{2g_c \rho_b}} \qquad (B-38)$$

The coefficients (n) and (m) for equations (B-37) and (B-38) are given in Table B-2.

TABLE B-2

SUGGESTED VALUES OF THE VISCOSITY RATIO
COEFFICIENT FROM VARIOUS REFERENCES

	n				m				Reference
Laminar	Turbulent			Laminar		Turbulent			
-0.14	-0.14			-0.14		-0.14			B-8
	Heating	Cooling	Pr	Heating	Cooling	Heating	Cooling	Pr	
-0.11	-.2	-.19	1	0.58	0.5	0.09	0.12	1	B-9 and B-10
-0.11	-.27	-.21	3	0.58	0.5	.06	.09	3	
-0.11	-.36	-.22	10	0.58	0.5	.03	.05	10	
-0.11	-.39	-.21	30	0.58	0.5	.0	.03	30	
-0.11	-.42	-.2	100	0.58	0.5	-.04	.01	100	
-0.11	-.46	-.2	1000	0.58	0.5	-.12	-.02	1000	

TABLE B-3

SUGGESTED VALUES OF THE TEMPERATURE RATIO COEFFICIENT FROM VARIOUS REFERENCES

n		m		Reference
Laminar	Turbulent	Laminar	Turbulent	Reference
	-0.5 heating 0. cooling $-0.57 + \dfrac{1.59}{x/D}$	.45 heating .3 cooling	-0.1 heating 0. cooling $-0.57 + \dfrac{1.59}{x/D}$	B-9
			(with Reynolds number evaluated at the wall temperature)*	B-11
0.	-0.5 heating 0. cooling	1.	-0.1 heating -0.1 cooling	B-10

$$*Re = \frac{D_h \, V_b \, \rho_b}{\mu_w} = \frac{D_h \, W}{\mu_w \, A_c}$$

For gases with large temperature differences or large variations in fluid properties, equations (B-35) and (B-36) may be modified as shown in equation (B-39) and (B-40) below.

$$\left(\frac{T_w}{T_b}\right)^n J = \frac{h}{C_p \, \rho_b \, V_b} \left(\frac{C_p \, \mu}{k}\right)_b^{2/3} = \frac{h}{C_{pb}\left(\frac{w}{A_c}\right)} \left(\frac{C_p \, \mu}{k}\right)_b^{2/3} \qquad (B-39)$$

$$\left(\frac{T_w}{T_b}\right)^m f = \frac{\Delta P_{fr}}{\frac{4L}{D_h} \frac{\rho_b \, V_b^2}{2g_c}} = \frac{\Delta P_{fr}}{\frac{4L}{D_h} \frac{\left(\frac{w}{A_c}\right)^2}{2g_c \, \rho_b}} \qquad (B-40)$$

These methods of accounting for large temperature differences on convection heat transfer and fluid friction have been included in the program.

FILM COOLING CALCULATIONS

Film cooling calculations have been included in program H0910 as a table of film cooling effectiveness (η) versus the film cooling parameter (X/MS).

Film cooling correlations from several sources may be reduced to this form by the film and transpiration cooling computer program (H0060) described later in this section. In the film cooling relation used, the film coolant mass velocity is defined as:

$$(\rho V)_{CA} = G_{CA} = \frac{W_{CA}}{A_c} = \frac{W_{CA}}{SL}$$

where W_{CA} = weight flow rate of film coolant

S = film slot height

L = film slot length

X = distance downstream from film injection

$M = \rho V_c / \rho V_\infty$

$$\frac{X}{MS} = \frac{X G_{GAS}}{S \frac{W_{CA}}{SL}} = \frac{(LX) G_{GAS}}{W_{CA}}$$

A film-cooled section of width L, length X, hot-gas mass velocity G_{GAS}, and cooling airflow rate W_{CA} is shown below.
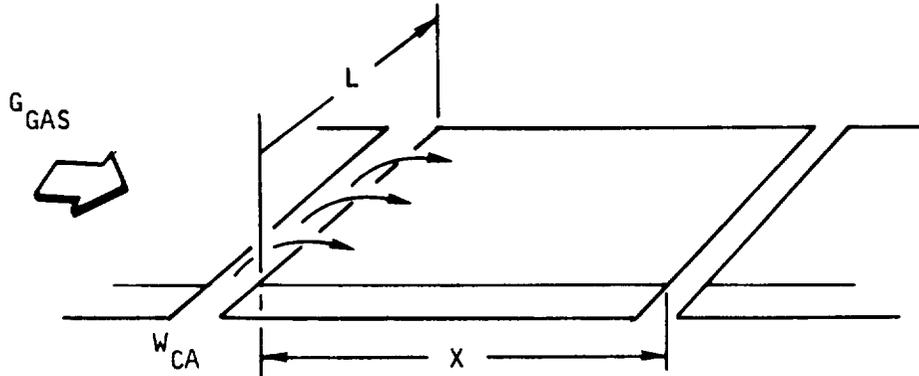
TRANSPIRATION COOLING CALCULATIONS

Transpiration cooling option is available in   program H0910 by using the Stanton number reduction factor calculated by the film and transpiration cooling computer program (H0060) as a reduction factor C_h on the hot gas side heat transfer coefficient. When this method is used, the heat transfer coefficient and the heat transfer area in the transpiration cooling porous media must be known. Since this information is usually not known, the transpiration cooling effectiveness (R_o) may be used to calculate the transpiration cooled surface temperature.

NOMENCLATURE

A_n heat transfer area for resistor (n)

A_c fluid flow area

A_f fin heat transfer area

A_t total heat transfer area

C_h multiplying factor for convection heat transfer

C_{pf} specific heat of fluid stream

C_{pn} specific heat of element n

D_h hydraulic diameter $= \dfrac{4\,A_c\,(L)}{A_t}$

D_1 leading edge inside diameter

d_o impingement hole diameter

D_p pin diameter

F geometrical view factor

f Fanning friction factor

$\mathcal{F}$ radiation emissivity view factor

$\overline{F}$ overall radiation interchange factor

F_{ac} acceleration factor in Equation (B-7)

F_t turbulence factor

F_{tn} natural convection turbulent transition factor

g_c gravitational constant for natural convection

Gr Grashof number

$Gr\,(Pr)$ Grashof number multiplied by Prandtl number

H_c convection heat transfer coefficient

H_r radiation heat transfer coefficient

J Colburn j-factor

K_f	thermal conductivity of fluid at the film temperature
K_n	thermal conductivity
K_t	total head loss coefficient
L	length
ℓn	length from the center of a node to the interface
L_p	pin length
M	Mach number (blowing rate for film cooling)
M_w	molecular weight
N	rotational speed
P_{avg}	average static pressure
Pr	Prandtl number
P_{t1}	total pressure at inlet
P_{t2}	total pressure at outlet
P_1	static pressure at inlet
P_2	static pressure at outlet
Q_n	heat input to node (n)
Q_s	heat input to fluid stream
R	radius
R_c	thermal interface resistance
Re	Reynolds number
R_n	thermal resistance element
R_o	transpiration cooling effectiveness
R_1	Radius at station 1
R_2	Radius at station 2
S_p	pin spacing
T	static temperature

T_{adw}	adiabatic wall temperature
T_{ER}	Eckert's equivalent temperature
T_F	fluid stream temperature
$\overline{T}_F$	average fluid stream temperature
T_I	inlet fluid stream temperature
T_o	node temperature, outlet fluid stream temperature, or stagnation temperature
T_{o_r}	outlet fluid stream temperature with rotation
$T_0(n)$	node temperature for step (n)
$T_0(n+1)$	node temperature for step (n+1)
T_{so}	surface temperature
T_T	total temperature
UA	overall thermal conductance to fluid stream
V	fluid velocity
V_0	volume of solid element
(V/V_{cr})	critical velocity ratio
W	fluid flow rate
X_n	center-to-center spacing of impingement holes
Y	injected fluid to mainstream velocity ratio as defined in Shapiro (Reference 6)
Z	compressibility coefficient
Z_n	impingement length
β	coefficient of volumetric expansion
δ_f	fin thickness
ΔR	Change in radius $(R_2 - R_1)$
η_f	fin effectiveness

γ specific heat ratio C_p/C_v

μ fluid viscosity

μ_o fluid viscosity at fluid temperature in the orifice

ρ density

ρ_0 density of solid element

θ time

REFERENCES

B-1   Dusinberre, G.M., <u>Heat Transfer Calculations by Finite Differences</u>, International Textbook Company, Scranton, Pennsylvania, 1961.

B-2   Eckert, E.R.G., Transactions of the ASME, Vol. 78, 1956, p. 1273.

B-3   Richardson, P.D., and O.A. Saunders, "Studies of Flow and Heat Transfer Associated with a Rotating Disc," <u>Journal Mechanical Engineering Science</u>, Vol. 5, No. 4, 1963.

B-4   Chupp, R.E., H.E. Helms, P.W. McFadden, and T.R. Brown, "Evaluation of Internal Heat Transfer Coefficients for Impingement-Cooled Turbine Airfoils," AIAA 4th Propulsion Joint Specialist Conference, Paper No. 68-584, June 1968.

B-5   Nunner, W., "Heat Transfer and Pressure Drop in Rough Tubes," AERE-TR-786, Translated from VDI-Forschungsheft, Series B, 22, No. 459, 1956.

B-6   Shapiro, A.H., <u>The Dynamics and Thermodynamics of Compressible Fluid Flow, Vol. I</u>, Ronald Press Co., New York, 1953.

B-7   L.V. Humble, W.H. Lowdermilk, and L.G. Desmon, "Measurements of Average Heat-Transfer and Friction Coefficients for Subsonic Flow of Air in Smooth Tubes at High Surface and Fluid Temperature," NACA Report 1020, 1950.

B-8   W.H. McAdams, <u>Heat Transmission</u> Third Ed., McGraw-Hill Book Co., Inc., 1954.

B-9   W. Kays and A.L. London, <u>Compact Heat Exchangers</u> Second Ed., McGraw-Hill Book Co., Inc., 1964.

REFERENCES (Continued)

B-10   W.M. Kays, <u>Convective Heat and Mass Transfer</u>, McGraw-Hill Book Co.,
        Inc., 1966.

B-11   M.F. Taylor, "Prediction of Friction and Heat-Transfer Coefficients
        with Large Variations in Fluid Properties," NASA TM X-2145,
        December, 1970.

174

|

APPENDIX C

FILM AND TRANSPIRATION COOLING COMPUTER PROGRAM (H0060)

INTRODUCTION

The AiResearch film and transpiration cooling computer program reduces the film cooling correlations of several authors to a common basis of film effectiveness (η) as a function of the film cooling parameter (X/MS) for specified hot gas and film injection boundary conditions. Several transpiration cooling effectiveness correlations are also reduced to the form of a Stanton number reduction factor due to mass transfer (St/St_o) and transpiration cooling effectiveness (R_ρ). The results from this program are used to generate the input data for the AiResearch thermal analyzer computer programs for film and transpiration cooling analysis.

CALCULATIONS

The film cooling effectiveness may be defined for both low-speed and high-speed flow as shown in Equations (C-1) and (C-2) described in Reference C-1.

$$\eta = \frac{T_{aw} - T_\infty}{T_f - T_\infty} \text{ (for low-speed flow)} \qquad (C-1)$$

$$\eta = \frac{T_{aw} - T_{awi}}{T_f - T_{fi}} \text{ (for high-speed flow)} \qquad (C-2)$$

The fluid properties for each of the correlations used are determined at the freestream static temperature (T_∞), the reference state (T_*) defined in Equation (C-3), the film injection temperature (T_f), or the freestream recovery temperature (T_r).

$$T_* = T_\infty + 0.72 (T_r - T_\infty) \qquad (C-3)$$

A description of each film cooling relation used is given below. The first film cooling relation is from Tribus and Klein (Reference C-2). The Tribus and Klein film effectiveness (η_{TK}) is utilized in two forms as shown in Equations (C-4) and (C-5).

If SEC = 0

$$\eta_{TK} = \frac{5.76 \, Cp_f (Pr)^{0.667} (Re)^{0.2}}{Cp_\infty (X/MS)^{0.8}} \left(\frac{\rho_\infty}{\rho_*}\right)^{0.8} \qquad (C-4)$$

175

If SEC = 1

$$\eta_{TK} = \frac{5.76 \; Cp_f \; (Pr)^{0.667}}{Cp_\infty \left[\frac{(X/MS)}{(Re)^{0.25}} \left(\frac{\rho_*}{\rho_\infty} \right) + 4.11 \; (Pr)^{0.8333} \right]^{0.8}} \qquad (C-5)$$

These equations are for tangential film injection with an overlapping slot and subsonic freestream flow. The effect of injecting a film cooling fluid that is unlike the mainstream fluid is also included in this correlation. Equation (C-5) gives more conservative results than Equation (C-4) for values of X/MS less than 80; Equation (C-5) is recommended for this region.

The second film cooling relation is from Hartnett, Birkebak, and Eckert (Reference C-3). This relation is also presented in two forms as shown in Equation (C-6) and (C-7).

If SEC = 0

$$\eta_{HBE} = \frac{3.39 \; (Re)^{0.2}}{(X/MS)^{0.8}} \left(\frac{\rho_\infty}{\rho_*} \right)^{0.8} \qquad (C-6)$$

If SEC = 1

$$\eta_{HBE} = \frac{3.39}{\left[\frac{(X/MS)}{(Re)^{0.25}} \left(\frac{\rho_*}{\rho_\infty} \right) + 4 \right]^{0.8}} \qquad (C-7)$$

These equations are also for tangential film injection with subsonic freestream flow, but without an overlapping slot. The effect of foreign gas injection is given in Equation (C-8) where subscript f denotes injected gas and subscript ∞ denotes the free stream.

$$\eta_F = \frac{Cp_f \; (\eta)}{Cp_\infty \left[1 + (\eta) \; (Cp_f - Cp_\infty) \; /Cp_\infty \right]} \qquad (C-8)$$

Equation (C-7) gives more conservative results than Equation (C-6) for values of X/MS less than 80; Equation (C-7) is recommended for this region.

The third film cooling relation is from Stollery and El-Ehwany (Reference C-4). This relation is presented in two forms as shown in Equations (C-9) and (C-10).

176

If SEC = 0

$$\eta_{SE} = \frac{3.09\ (Re)^{0.2}}{(X/MS)^{0.8}} \left(\frac{\rho_\infty}{\rho_*}\right)^{0.8} \tag{C-9}$$

If SEC = 1

$$\eta_{SE} = \frac{3.09}{\left[\dfrac{(X/MS)}{(Re)^{0.25}}\left(\dfrac{\rho_*}{\rho_\infty}\right) + 4.11\right]^{0.8}} \tag{C-10}$$

These equations are for tangential film injection with subsonic free-stream flow and an overlapping slot. Equation (C-10) gives more conservative results than Equation (C-9) for values of X/MS less than 80; Equation (C-10) is recommended for this region. All of the correlations given above for tangential film injection are applicable only for values of the blowing rate (M) less than 1.5. For values of M greater than 1.5, the correlation of Haering (Reference C-5) may be used as shown in Equation (C-11).

$$\eta_{HH} = \frac{1}{1 + 3.6 \left[\dfrac{H_o\ (X/MS)}{\rho_\infty V_\infty C p_f}\left(\dfrac{T_\infty}{T_f}\right)^{0.667} f(V)\right]} \tag{C-11}$$

where

$$f(V) = \left(\frac{V_f}{V_\infty}\right)^{1.5\left(\frac{V_f}{V_\infty} - 1\right)} \quad \text{when } \frac{V_\infty}{V_f} \leq 1$$

$$f(V) = 1 + 0.4\ \arctan\left(\frac{V_\infty}{V_f} - 1\right) \quad \text{when } \frac{V_\infty}{V_f} > 1$$

The film cooling relation of Hatch and Papell (Reference C-6) for tangential film injection has been compared with test data for blowing rates (M) of 0.03 < M < 2.2. The data follows the correlation down to values of film effectiveness below 0.3; the calculated value is somewhat lower than the test data. The film effectiveness equation from Hatch and Papell (Reference C-6) is given in Equation (C-12).

$$\eta_{HP} = EXP\left\{-\left[\frac{H_o\ (X/MS)}{\rho_\infty V_\infty C p_f} - 0.04\right]\left[\frac{S(V_\infty)\ \rho_f\ C p_f}{K_f}\right]^{0.125} f(V)\right\} \tag{C-12}$$

The correlations presented above for tangential film injection are for essentially zero pressure gradient flow over a plane surface. Equation (C-11) correlates reasonably well with film cooling data for accelerating flows. In the application of these equations with surface heat transfer, the heat transfer coefficient calculated without film cooling is used with heat transfer to the effective film temperature (T_{aw}). This method is verified in Hartnett, Birkebak, and Eckert (Reference C-3).

Goldstein and Haji-Sheikh (Reference C-7) present a correlation for film cooling with various injection angles as shown in Equation (C-13).

$$\eta_{GH} = \frac{1.9 \ (Pr)^{2/3}}{\left[1 + 0.33 \ \frac{(X/MS)^{0.8}}{(Re)^{0.2}} \left(\frac{\rho_*}{\rho_\infty} \right)^{0.8} \beta \right]} \qquad (C-13)$$

The effect of injection angle is given in Equation (C-14)

$$\beta = 1 + 0.00015(Re) \sin \alpha \qquad (C-14)$$

Goldstein, Eckert, and Wilson (Reference C-1) present a correlation for film injection through a porous region normal to a supersonic freestream flow as shown in Equation (C-15).

$$\eta_{GEW} = \frac{1}{1 + \frac{Cp_\infty}{Cp_f} \left\{ 0.33 \left[4 + \frac{(X/MS)}{(Re)^{0.25}} \left(\frac{\rho_*}{\rho_\infty} \right) \right]^{0.8} - 1 \right\}} \qquad (C-15)$$

This correlation, which includes the effects of foreign gas injection, was applied to a freestream flow with a Mach number of 2.9 and essentially zero pressure gradient flow.

For normal film injection through a porous region to a subsonic-to-supersonic nozzle, the correlation of Librizzi and Cresci (Reference C-8) was developed as shown in Equation (C-16).

$$\eta_{LC} = \frac{1}{\left[1 + 0.33 \ \frac{(X/MS)^{0.8}}{(Re)^{0.2}} \left(\frac{\rho_*}{\rho_\infty} \right)^{0.8} \right]} \qquad (C-16)$$

The effect of foreign gas injection is given in Equation (C-8). This correlation is applicable for strongly accelerating freestream flow for both subsonic and supersonic freestream conditions.

Heat transfer to or from the film-cooled surface for the correlations shown in Equations (C-13), (C-15), and (C-16) is estimated by using the heat transfer coefficient calculated without film injection with the effective film temperature (T_{aw}) calculated from the film effectiveness. This method is verified in Librizzi and Cresci (Reference C-8).

In addition to the correlations presented above, AiResearch has sponsored research work at Arizona State University on the effects of film cooling with single lines of circular holes, both straight and skewed, with staggered and interrupted slots, and with continuous slots with various angles of film injection. The results for continuous slots at various angles of film injection are presented in Arizona State University Reports ME-671 (Reference C-9) and ME-692 (Reference C-10). These results are summarized by Metzger, Carper, and Swank (Reference C-11) as the heat transfer rate to the total film-cooled surface length divided by the heat transfer rate without film cooling. Correlations are presented for slots with 20-deg, 40-deg, and 60-deg angles of film injection. These correlations have been rearranged and differentiated with respect to the surface length (x) to obtain local values of film effectiveness as a function of the film-cooling parameter (X/MS). The results are given in Equations (C-17), (C-18), and (C-19) for film injection angles of 20 deg, 40 deg, and 60 deg, respectively.

For a 20-deg angle of film injection

$$\eta_{20} = \frac{3.624 \, M^{0.1}}{\sqrt{X/MS}} \qquad\qquad (C-17)$$

For a 40-deg angle of film injection

$$\eta_{40} = \frac{3.178 \, M^{0.1}}{\sqrt{X/MS}} \qquad\qquad (C-18)$$

For a 60-deg angle of film injection

$$\eta_{60} = \frac{2.742 \, M^{0.1}}{\sqrt{X/MS}} \qquad\qquad (C-19)$$

For heat transfer to or from the film-cooled surface, the effective film temperature (T_{aw}) calculated from the film effectiveness may be used. The heat transfer coefficient used is 1.09, 1.18, and 1.24 times the heat transfer coefficient without film cooling for Equations (C-17), (C-18), and (C-19), respectively.

An alternate form of the equation for a 20-deg injection angle for Metzger and Fletcher (Reference C-13) is given in Equation (C-20).

$$\eta_{20N} = \cfrac{1}{1 + \cfrac{0.01238(X/MS)}{M^{0.35}}} \qquad (C-20)$$

The heat transfer coefficient used with this form of equation is the same as the heat transfer coefficient without film cooling. This form of equation has been applied to film cooling with moderate freestream acceleration. The results indicated that this film effectiveness could be applied with a heat transfer coefficient somewhat higher than that without film cooling.

Very little information on film cooling effectiveness is available for rows of holes that are normally used for film injection on turbine blades. Goldstein, Eckert, Eriksen, and Ramsey (Reference C-12) have investigated film cooling through a row of holes spaced at 3-dia intervals across the span with an injection angle of 35 deg to the mainstream flow. They have indicated a good comparison with single-hole data at low blowing rates (M). Additional data on film cooling with a row of holes is presented in Arizona State University Report ME-681 (Reference C-13) and by Metzger and Fletcher (Reference C-14). Data for film cooling with rows of holes on turbine blades is presented in NASA CR-54513 (Reference C-15).

Figure C-1 provides comparative data on film cooling effectiveness for rows of holes. The data from Goldstein, Eckert, Eriksen, and Ramsey (Reference C-12) is presented at a blowing rate (M) of 0.5, which gives the maximum film effectiveness and at a blowing rate (M) of 1, which gives a considerably lower film effectiveness. Curves are presented for both a 3-dia spacing ratio (which was tested) and for a 1.5-dia spacing ratio (which was derived from the single hole data). Data from Arizona State University Report ME-681 (Reference C-13) and Metzger and Fletcher (Reference C-14) is also presented for a 1.53- to 1.71-dia spacing ratio at blowing rates (M) of approximately 0.5 and 0.75 with an injection angle of 20 deg. The General Electric data for film cooling with rows of holes on turbine blades has been applied for an effective 1.5-dia spacing ratio with blowing rates (M) from about 0.5 to 1.2 and injection angles of 30 deg.

The GE data on the suction side of the blade compares very well with the data from Metzger (References C-13 and C-14) over the blowing rate (M) from 0.5 to 0.75. This GE data also compares very well with the maximum value of film effectiveness from Goldstein, Eckert, et al. (Reference C-12) for a blowing rate (M) of 0.5- and a 1.5-dia spacing ratio. Since the blowing rate (M) on the pressure side tends to be larger than the blowing rate (M) on the suction side, the trend of the GE data showing higher effectiveness on the suction side is consistent with the data from Goldstein, Eckert, et al. (Reference C-12). The data from Metzger (References C-13 and C-14), however, shows no significant effect of blowing rate (M), as was assumed in applying the GE data. It may be expected that high values of the blowing rate (M) would cause low values of film effectiveness because of the jet penetration into the mainstream. The data of Metzger (References C-13 and C-14) may not exhibit this effect because of the lower angle of injection (20 deg vs 35 deg).
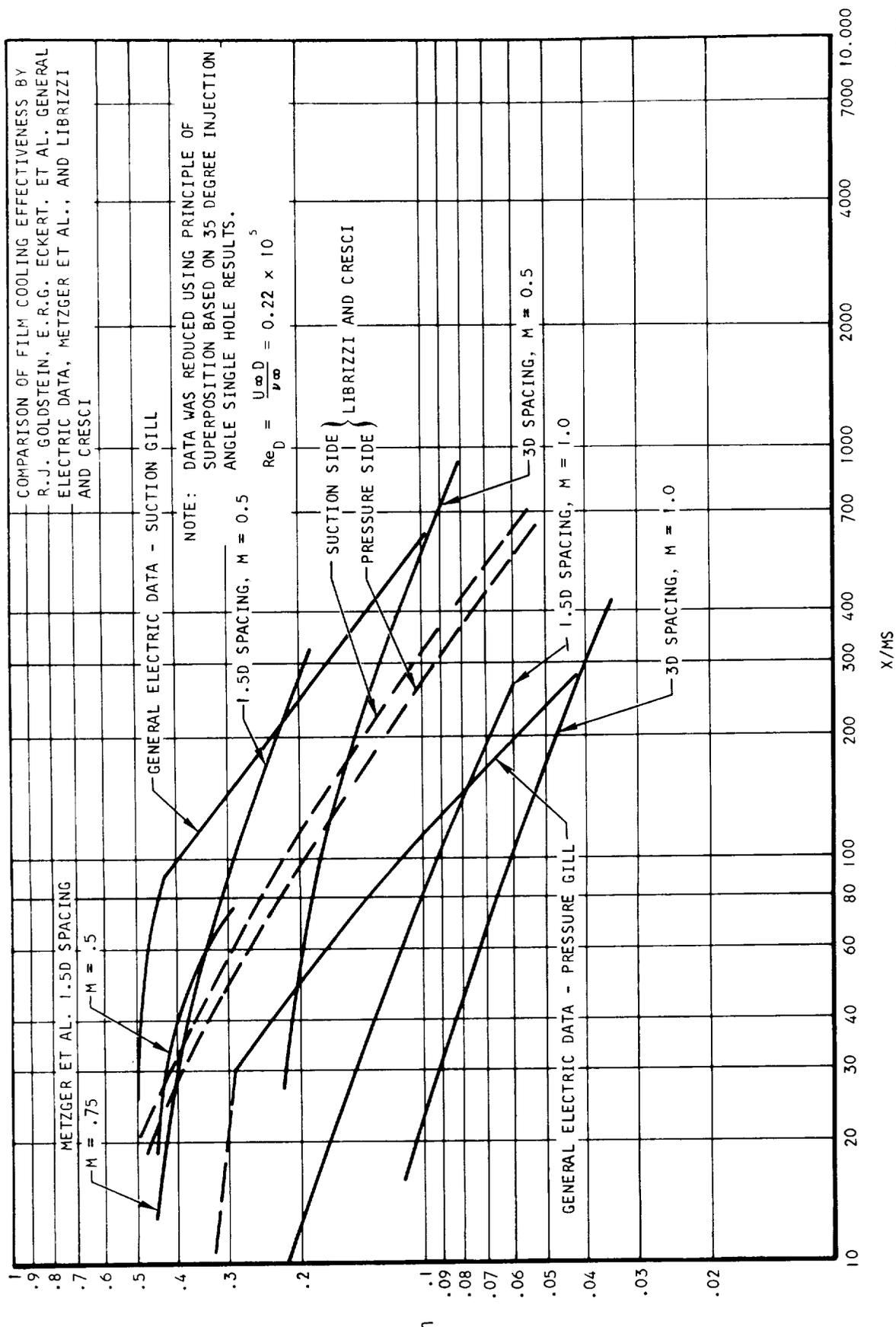
Figure C-I. Film Cooling Effectiveness for Rows of Holes

The data shown in Figure C-1 are correlated as a function of the equivalent slot height (S) for the row of holes. This slot height is calculated as shown below:

$$S = \frac{n\pi d^2}{4}$$

where   n = number of holes per unit width

d = hole diameter

The heat transfer coefficient from the film temperature to the wall is assumed to be the same as that without film injection for the GE data and the data of Goldstein, Eckert, et al. (Reference C-12). The heat transfer coefficient from the data of Metzger (References C-13 and C-14), however, is 1.2 to 1.4 times that without film injection.

The correlation given by Librizzi and Cresci (Reference C-8) for film cooling injection through a porous region of 90 deg to the mainstream flow upstream of a rocket nozzle falls about midway between the GE data for the pressure and suction sides. This correlation does not indicate a strong effect of blowing rate (M) as shown in the correlations for rows of holes; however, it does indicate the effect of large pressure gradients.

Film cooling data in combustors where the turbulence level is high has been investigated by NASA Lewis and is reported in Grobman, Jones, Marek, and Niedzwiecki (Reference C-16). Three film cooling slot configurations with various slot heights and hole sizes were studied within the combustor. The results indicated that the film cooling effectiveness was unaffected by slot geometry and could be represented by a single line. Equation (C-21) was used to predict the film cooling effectiveness for the combustor.

$$\eta_{cm} = \frac{1}{1 + C_M \ (X/MS) \ (Cpo/Cpf)} \tag{C-21}$$

The constant C_M is the mixing coefficient which was set equal to the turbulence level in this case. The turbulence level for the NASA combustor was approximately 15 percent ($C_M = 0.15$).

Transpiration cooling is presented in three correlations described below. They are presented in terms of the reduction of Stanton number at the boundary layer due to mass transfer (St/St_o) and the transpiration cooling effectiveness (R_o) defined in Equations (C-22) and (C-23).

$$R_o = \frac{T_w - T_c}{T_\infty - T_c} \quad \text{(for low-speed flow)} \tag{C-22}$$

$$R_o = \frac{T_w - T_c}{T_{awi} - T_c} \quad \text{(for high-speed flow)} \tag{C-23}$$

The simplified form of transpiration cooling effectiveness (R_o) does not account for the effects of radiation and a reduction of porous wall thickness to the point at which the cooling air effectiveness is substantially less than one $\left(\eta_c = \frac{T_{co} - T_c}{T_w - T_c} < 1 \right)$. The transpiration cooling effectiveness (R_o) correlation is therefore only applicable to the porous wall for which it was tested and for the thermal radiation conditions of the test. To determine the Stanton number reduction factor from measured values of transpiration cooling effectiveness (R_o), Equation (C-25) may be derived from the heat balance relation shown in Equation (C-24).

$$(T_{co} - T_c) w_c Cp_c = HA(T_\infty - T_w) - \sigma FeA \left(T_w^4 - T_{amb}^4 \right) \tag{C-24}$$

$$\left(\frac{St}{St_o} \right) = \frac{\dfrac{Cp_c}{Cp_\infty} \dfrac{M}{St_o} \eta_c (R_o) + \dfrac{\sigma Fe}{\rho_\infty V_\infty Cp_\infty} (St_o) \dfrac{\left(T_w^4 - T_{amb}^4 \right)}{T_\infty - T_c}}{1 - R_o} \tag{C-25}$$

Therefore, measured values of cooling air effectiveness (η_c), transpiration cooling effectiveness (R_o), and ambient temperatures around the test specimen (T_{amb}) are required to determine the effective Stanton number reduction factor due to mass transfer.

The first transpiration cooling relation is based on the film theory as proposed by Mickley and described in Spalding (Reference C-17). The transpiration cooling effectiveness (R_o) correlation by this method is given in Equation (C-26).

$$R_{osp} = EXP - \left(\frac{Cp_c}{Cp_\infty} \frac{M}{St_o} \right) \tag{C-26}$$

Assuming the cooling air effectiveness is equal to one $(\eta_c = 1)$ and the surrounding wall temperatures are equal to the cooled surface temperature $(T_w = T_{amb})$ for the tests in which (R_o) was measured, the Stanton number reduction factor may be calculated as shown in Equation (C-27).

$$\left(\frac{St}{St_o} \right)_{sp} = \frac{\frac{Cp_c}{Cp_\infty} \frac{M}{St_o} (R_{osp})}{1 - R_{osp}} \tag{C-27}$$

The resulting equation for Stanton number reduction factor due to mass transfer from the film theory is given in Equation (C-28).

$$\left(\frac{St}{St_o} \right)_{sp} = \frac{\frac{Cp_c}{Cp_\infty} \frac{M}{St_o}}{EXP \left(\frac{Cp_c}{Cp_\infty} \frac{M}{St_o} \right) - 1} \tag{C-28}$$

The second transpiration cooling relation is taken from Friedman (Reference C-18). The transpiration cooling effectiveness (R_o) correlation by this method is given in Equation (C-29).

$$R_{of} = \frac{\frac{2.11}{(Re_\infty)^{0.1}}}{EXP \left[\frac{2.11}{(Re)^{0.1}} \frac{Cp_c}{Cp_\infty} \frac{M}{St_o} \right] + \frac{2.11}{(Re)^{0.1}} - 1} \tag{C-29}$$

Using the same assumptions as in Equation (C-27), the Stanton number reduction factor may be calculated as shown in Equations (C-30) and (C-31).

$$\left(\frac{St}{St_o}\right)_f = \frac{\frac{Cp_c}{Cp_\infty} \frac{M}{St_o} (R_{of})}{1 - R_{of}}$$

(C-30)

$$\left(\frac{St}{St_o}\right)_f = \frac{\frac{2.11}{(Re\infty)^{0.1}} \frac{Cp_c}{Cp_\infty} \frac{M}{St_o}}{EXP\left[\frac{2.11}{(Re\infty)^{0.1}} \frac{Cp_c}{Cp_\infty} \frac{M}{St_o}\right] - 1}$$

(C-31)

The third transpiration cooling relation is taken from Bartle and Leadon (Reference C-17). The transpiration cooling effectiveness (R_o) correlation by this method is given in Equation (C-32).

$$R_{ob} = \frac{1}{\left[1 + \frac{Cp_c}{3Cp_\infty} \frac{M}{St_o}\right]^3}$$

(C-32)

Using the same assumptions as in Equation (C-27), the Stanton number reduction factor may be calculated as shown in Equation (C-33).

$$\left(\frac{St}{St_o}\right)_b = \frac{\frac{Cp_c}{Cp_\infty} \frac{M}{St_o} (R_{ob})}{1 - R_{ob}}$$

(C-33)

The film theory results are based on transpiration cooling in subsonic flow with essentially zero pressure gradient, using a porous surface with a large, internal, cooled surface area, which should give a cooling air effectiveness near one ($\eta_c \approx 1$). The Friedman (Reference C-18) correlation is based on transpiration cooling with a moderate pressure gradient, using a porous surface with a large, internal, cooled surface area, which should give a cooling air effectiveness near one ($\eta_c \approx 1$). The Bartle and Leadon (Reference C-19) correlation is based on transpiration cooling in supersonic flow using a porous surface with a large, internal, cooled surface area, which should give a cooling air effectiveness near one ($\eta_c \approx 1$).

NOMENCLATURE

C_p	specific heat of the fluid
C_m	mixing coefficient
G_f	mass velocity of film injection, $G_f = W_c/SL$
H_o	heat transfer coefficient from the freestream to the wall without the effects of film cooling or transpiration cooling
L	film slot width
M	blowing rate, $M = \dfrac{\rho_f V_f}{\rho_\infty V_\infty} = \dfrac{G_f}{\rho_\infty V_\infty}$
Pr	Prandtl number
Re	Reynolds number; $Re = \dfrac{SG_f}{\mu_*}$
R_o	transpiration cooling effectiveness defined as shown in Equations (C-20) and (C-21)
S	film slot height
St	Stanton number
$Subscript_\infty$	freestream
T_*	reference temperature defined in Equation (C-3)
T_{aw}	effective gas film temperature or adiabatic wall temperature with film cooling
T_{awi}	adiabatic wall temperature with film cooling air ejected at the gas temperature
T_c	transpiration coolant temperature
T_f	film coolant temperature at the film injection point
T_{fi}	film injection temperature for isoenergetic injection
T_w	wall temperature
T	freestream static temperature
V	fluid velocity
X	distance downstream of film slot

NOMENCLATURE (Continued)

X/MS   film cooling parameter; $X/MS = \dfrac{X\rho_\infty V_\infty}{S\rho_f V_f} = \dfrac{X\rho_\infty V_\infty}{SG_f}$

α angle of film injection into the main stream

η film cooling effectiveness as defined in Equations (C-1) and (C-2)

μ fluid viscosity

ρ fluid density

REFERENCES

C-1   Goldstein, R. J., E. R. G. Eckert, and D. J. Wilson, "Film Cooling with Normal Injection into a Supersonic Flow," ASME J. of Eng. for Industry, November 1968.

C-2   Tribus, M., and J. Klein, "Forced Convection from Non-Isothermal Surfaces," Symposium on Heat Transfer, University of Michigan, 1952.

C-3   Hartnett, J. P., R. C. Birkebak, and E. R. G. Eckert, "Velocity Distributions, Temperature Distributions, Effectiveness, and Heat Transfer for Air Injected through a Tangential Slot into a Turbulent Boundary Layer," Journal of Heat Transfer, Trans. ASME, Series C, Vol. 83, No. 3, August 1961.

C-4   Stollery, J. L., and A. A. M. El-Ehwany, "A Note on the Use of a Boundary Layer Model for Correlating Film Cooling Data," Int. J. of Heat and Mass Transfer, Vol. 8, 1965.

C-5   Haering, G. W., "A Proposed Correlation Scheme for Gas-Film Cooling Data," AFAPL-TR-66-56, Air Force Aero-Propulsion Lab., Wright-Patterson AFB, Ohio, August 1966.

C-6   Hatch, J. E. and S. S. Papell, "Use of a Theoretical Flow Model to Correlate Data for Film Cooling or Heating an Adiabatic Wall by Tangential Injection of Gases of Different Fluid Properties," NASA TN D-140, November 1959.

C-7   Goldstein, R. J., and A. Haji-Sheikh, "Prediction of Film Cooling Effectiveness," Japan Soc. of Mech Eng 1967, Semi-International Symposium, Tokyo, September 1967.

C-8   Librizzi, J., and R. J. Cresci, "Transpiration Cooling of a Turbulent Boundary Layer in an Axisymmetric Nozzle," AIAA Journal, Vol. 2, 1964.

REFERENCES (Continued)

C-9   Metzger, D. E., H. J. Carper, and L. A. Swank, "Heat Transfer with
        Film Cooling near Single-Angled Spanwise Continuous Injection Slots,"
        Arizona State University Report ME-671.

C-10   Hilbun, W. H., and D. E. Metzger, "The Effect of Moderate Freestream
        Acceleration on Film Cooling Performance," Arizona State University
        Report ME-692.

C-11   Metzger, D. E., H. J. Carper, and L. A. Swank, "Heat Transfer with
        Film Cooling Near Nontangential Injection Slots," ASME Paper No.
        67-WA/GT-I, November 1967.

C-12   Goldstein, R. J., E. R. G. Eckert, V. L. Eriksen, J. W. Ramsey,
        "Film Cooling Following Injection through Inclined Circular Tubes,"
        NASA CR-72612.

C-13   Metzger, D. E., and R. W. Smith, "Some Preliminary Results for Film
        Cooling with Injection from Single Lines of Circular Holes,"
        Arizona State University Report ME-681.

C-14   Metzger, D. E., and D. D. Fletcher, "Surface Heat Transfer Immed-
        iately Downstream of Flush, Nontangential Injection Holes and Slots,"
        AIAA Paper No. 69-523, 1969.

C-15   Burggraf, F., J. P. Hurfaugh, and M. E. Wilton, "Design and Analysis
        of Cooled Turbine Blades. Part I - Leading and Trailing Edge Con-
        figurations," NASA CR-54513.

C-16   Grobman, J., R. E. Jones, C. J. Marek, and R. W. Niedzwiecki, (Com-
        bustion) Aircraft Propulsion, NASA SP-259, November 1970.

C-17   Spalding, D. B., Convective Mass Transfer, McGraw-Hill, New York,
        1963.

C-18   Friedman, J., "A Theoretical and Experimental Investigation of
        Rocket-Motor Sweat Cooling," J. American Rocket Society, No. 79,
        December 1949.

C-19   Bartle, E. R., and B. M. Leadon, "The Effectiveness as a Universal
        Measure of Mass Transfer Cooling for a Turbulent Boundary Layer,"
        Proceedings of the 1962 Heat Transfer and Fluid Mechanics Institute,
        June 1962.

APPENDIX D

DERIVATION OF GENERAL EQUATION FOR DETERMINING HEAT TRANSFER COEFFICIENTS FOR ANY GENERAL ARRAY OF TRIANGULARLY SPACED TUBES OR PINS BETWEEN PLATES

A general equation has been derived from a computer regression analysis of heat transfer data for triangularly spaced tube banks, triangularly spaced pin-fin surfaces, and triangularly spaced continuous fin tube surfaces. From an inspection of the heat transfer data for these surfaces, it appeared that the following equation would best fit all this data.

$$\frac{H\,D_h}{k_f} = \left[.023 + \frac{C_1 e^{-C_2\left(\frac{D_p}{S_p}\right) - C_3\left(\frac{S_p}{L_p}\right)^n}}{(Re)^x} \right] (Re)^{0.8}\,(Pr)^{1/3} \qquad (D-1)$$

A computer program was written to determine the constants C_1, C_2, C_3, n, and x in the equation above that would best fit the heat transfer data. The results are shown below and a comparison of the computer-derived equation with data from the literature is shown in Figures D-1 and D-2.

The results of the computer analysis to determine the constants C_1, C_2, C_3, n, and x in Equation (D-1) are shown below.

$$C_1 = 4.143$$

$$C_2 = 3.094$$

$$C_3 = 0.89$$

$$n = 0.5075$$

$$x = 0.2946$$

The constants C_1, C_2, and x were determined from the triangular spaced tube bank array heat transfer data shown in Figure D-1. The constants C_3 and n were eliminated in this study because the plate spacing (L_p) was assumed equal to infinity $L_p = \infty$, therefore $\frac{S_p}{L_p} = 0$.

$$\frac{hD_h}{K} = \left[0.023 + \frac{4.143e^{-3.094\left(\frac{Dp}{Sp}\right)-0.89\left(\frac{Sp}{Lp}\right)^{0.5075}}}{(Re)^{0.2946}} \right] (Re)^{0.8} (Pr)^{1/3}$$

—————— GRIMISON'S DATA FOR TRIANGULAR TUBE BANKS

— —— —— KAYS AND LONDON DATA FOR TRIANGULAR TUBE BANKS
(COMPACT HEAT EXCHANGERS)

COLBURN
J FACTOR

$St(Pr)^{2/3}$

$St = \frac{h}{GC_p}$

$Pr = \frac{C_p \mu}{K}$

ASSUMED TO BE
THE SAME AS A
SINGLE TUBE
IN CROSSFLOW

$\frac{SP}{DP} = 10$

$\frac{SP}{DP} = 3$

$\frac{SP}{DP} = 2$

$\frac{SP}{DP} = 1.5$

REYNOLDS NUMBER, $Re = \frac{D_h G}{\mu}$

S-45231
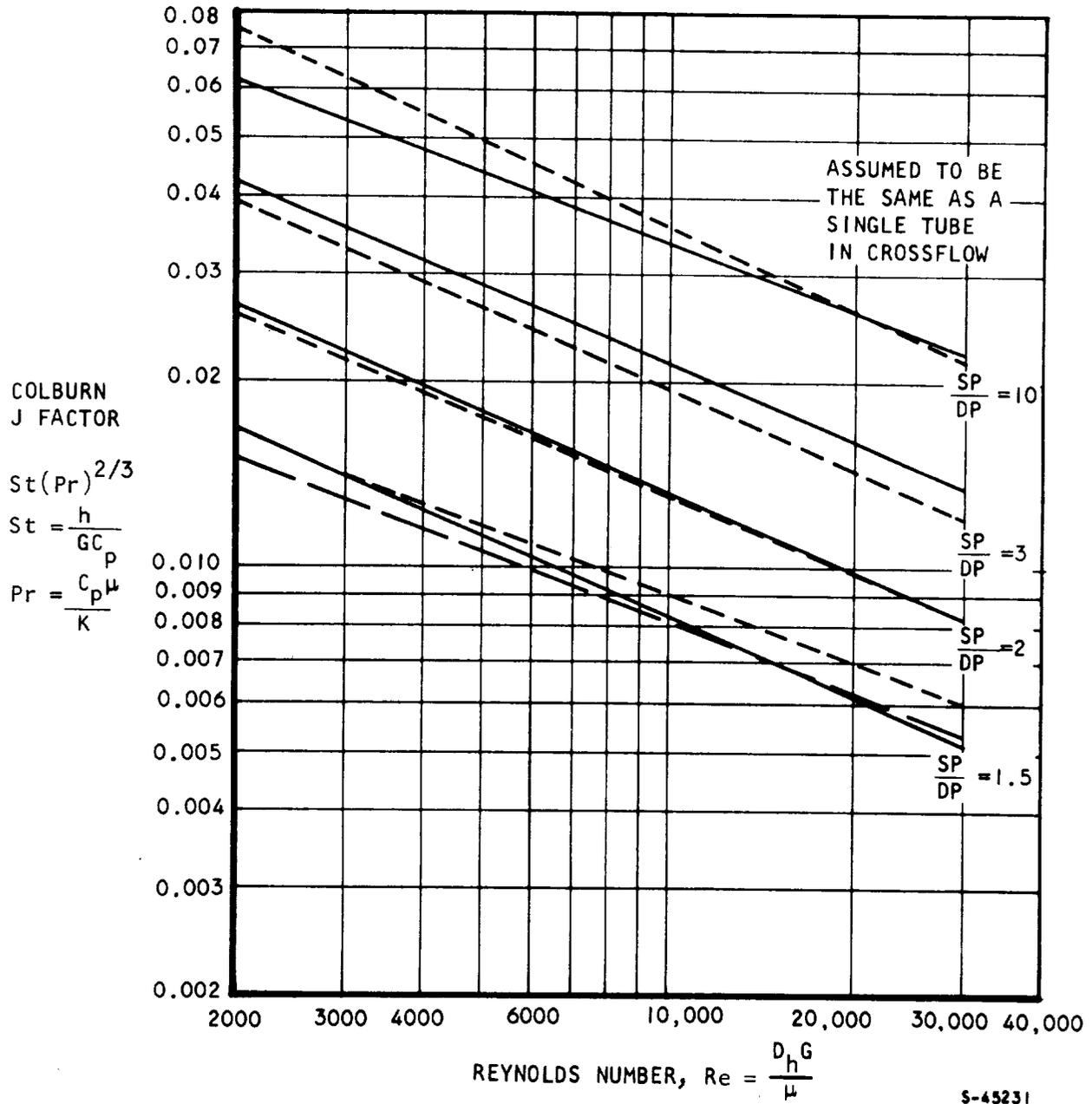
Figure D-1 Comparison of Computer-Derived Equation with
Tube Bank Data from the Literature

- - - - - - COMPUTER-DERIVED EQUATION

$$\frac{HD_h}{K} = \left[0.023 + \frac{4.143e^{-3.094\left(\frac{D_p}{S_p}\right)-0.89\left(\frac{S_p}{L_p}\right)^{0.5075}}}{(Re)^{0.2946}} \right] (Re)^{0.8}(Pr)^{1/3}$$

——————— DATA FROM THE LITERATURE(COMPACT HEAT EXCHANGERS, KAYS AND LONDON)

COLBURN
J FACTOR

$St(Pr)^{2/3}$

$St = \frac{H}{GC_p}$

$Pr = \frac{C_p\mu}{K}$

PIN-FIN SURFACE
PF-4(KAYS AND LONDON)
$\frac{S_p}{D_p} = 2.64$ $\frac{S_p}{L_p} = 0.3435$

8.0-3/8T
$\frac{S_p}{D_p} = 2.49$ $\frac{S_p}{L_p} = 8.93$

CONTINUOUS
FINNED
TUBES
(TRANE CO)

CONTINUOUS FINNED
TUBES (TRANE CO)

7.75-5/8T
$\frac{S_p}{D_p} = 2.59$ $\frac{S_p}{L_p} = 15.5$

FLOW BETWEEN FLAT
PLATES

REYNOLDS NUMBER, $Re = \frac{D_h G}{\mu}$
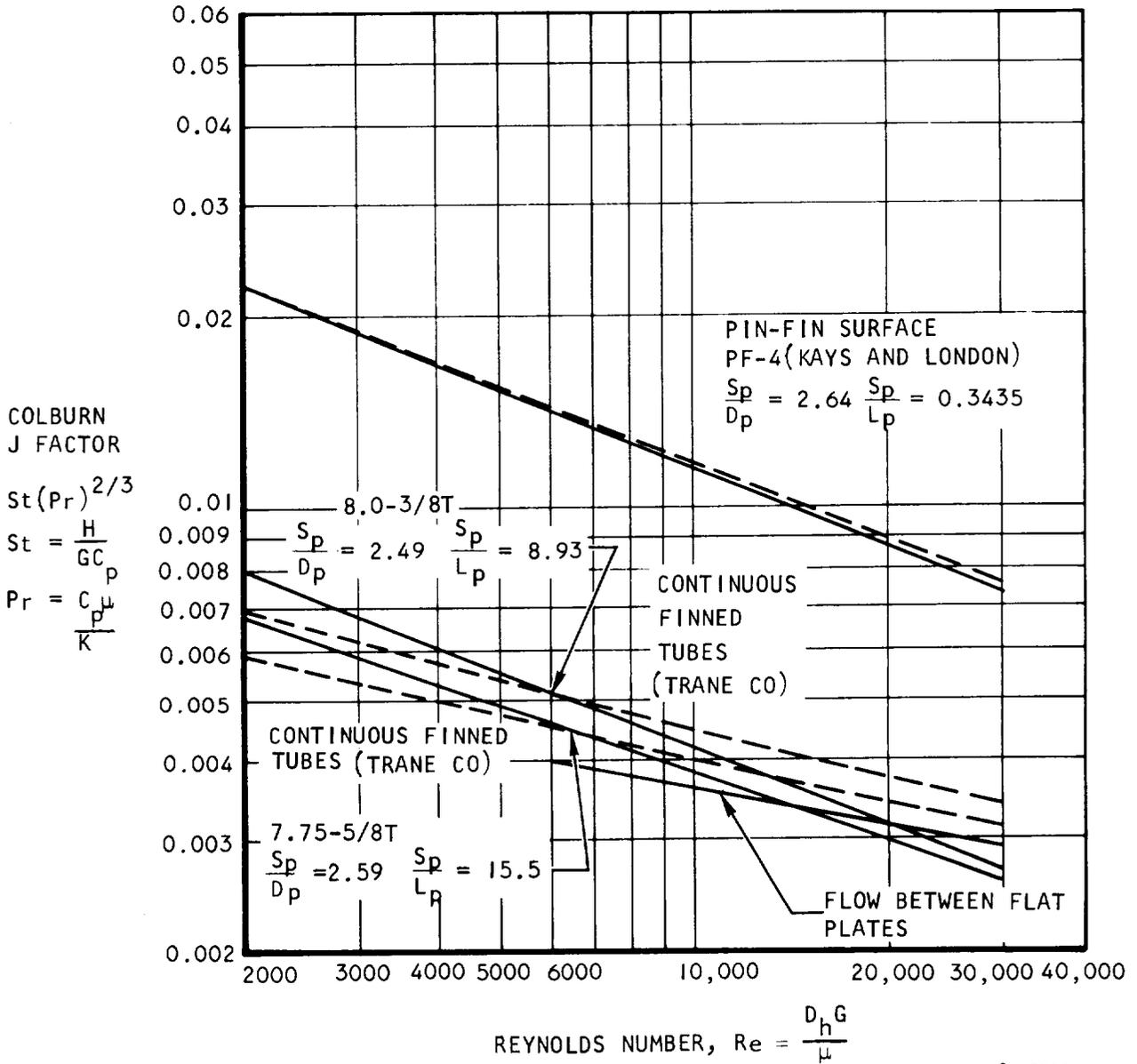
S-45232

Figure D-2. Comparison of Computer-Derived Equation with Pin Fin
and Finned Tube Data from the Literature

The constants C_3 and n were determined from the triangular pin-fin array and the triangular continuous finned tube array data shown in Figure D-2. From a study of the available literature, this represents all the data available for this type of heat transfer surface. Data on rectangular pin-fin arrays are presented in Theoclitus (Reference D-1).

As the pin spacing approaches infinity ($S_p = \infty$) and/or the plate spacing approaches zero $L_p = 0$, it can be seen that this equation approaches the heat transfer equation for flow between flat plates.

$$\frac{H\,D_h}{k_f} = 0.023\,(Re)^{0.8}\,(Pr)^{1/3}$$

The final equation derivied from this analysis is:

$$\frac{H\,D_h}{k_f} = \left[0.023 + \frac{4.143\,e^{-3.094\left(\frac{D_p}{S_p}\right)\,-0.89\left(\frac{S_p}{L_p}\right)^{0.5075}}}{(Re)^{0.2946}}\right](Re)^{0.8}\,(Pr)^{1/3} \qquad (D-2)$$

where
$$Re = \frac{D_h\,G_{min}}{\mu_f}$$

$$Pr = \frac{C_{pf}\,\mu_f}{k_f}$$

From the comparison of the computer-derived equation with Grimson's (Reference D-2) data, it appears that the computer-derived equation gives results that are within the average deviation of ±5 percent. The data from Kays and London (Reference D-3) for a triangular spacing $\frac{S_p}{D_p} = 1.5$ falls below the data of Grimson from which the constants were derived. The slope of the Kays and London (Reference D-3) data is the same as that of the derived equation and for the future it is planned to reevaluate the constants including the Kays and London (Reference D-3) data.

The comparison in Figure D-2 of the computer-derived equation with the pin-fin data shows good agreement. The comparison of the continuous finned tubes with the computer-derived equation showed a large discrepancy in the slope of the data. Extrapolation of the Trane Co. data, however, shows that the (j) factor goes below the (j) factor for flow between parallel plates.

It is evident that the general equation derived herein is useful for predicting heat transfer coefficients on tube banks with close plate spacings, any triangular array pin-fin heat transfer surface, and on continuous finned tube heat transfer surfaces.

NOMENCLATURE

A   - Total heat transfer surface area (pins and wall)

Cpf   - The specific heat of the fluid based on the film temperature

D_h - Hydraulic diameter of the heat transfer surface,

$$D_h = \frac{4A \text{ min } L}{A}$$

D_p - Diameter of the tubes or pins

G_{min} - $\dfrac{W}{A_{min}}$ = The weight flowrate of the heat transfer fluid divided by the minimum flow area between the tubes

h   - Film coefficient of heat transfer

k_f - Thermal conductivity of the heat transfer fluid based on the film temperature

L   - Passage flow length

L_p - Spacing between the plates in the heat transfer surface

Pr   - Prandtl number

Re   - Reynolds number

S_p - Center-to-center spacing of the tubes or pins on equilateral triangles

μ_f - The viscosity of the heat transfer fluid based on the film temperature

REFERENCES

D-1   Theoclitus, G., "Heat Transfer and Flow Friction Characteristics of Nine Pin-Fin Surfaces," J. of Heat Transfer, Vol. 80, No. 4, November 1966.

D-2   Grimson, E. D., "Correlation and Utilization of New Data on Flow Resistance and Heat Transfer for Cross Flow of Gases Over Tube Banks," Trans. ASME, Vol. 59, 1927.

D-3   Kays, W. M. and A. L. London, Compact Heat Exchangers, 2nd Ed., McGraw-Hill, New York, 1964.

APPENDIX E

DERIVATION OF THE FLUID STREAM HEATING EQUATIONS
FOR RADIAL FLOW IN A ROTATIONAL PASSAGE

A derivation of the equation for fluid stream heating with rotational flow in a radial passage is presented below. The equations are based on compressible flow of an ideal fluid with heat transfer from the duct walls, internal heat generation in the fluid, and energy input due to rotational flow. An exact solution and two finite increment solutions are derived. The average temperature difference finite increment form is used only if $\Delta r < \frac{2W\ Cp}{UA}$ and the outlet temperature difference method must be used if $\Delta r \geq \frac{2W\ Cp}{UA}$.
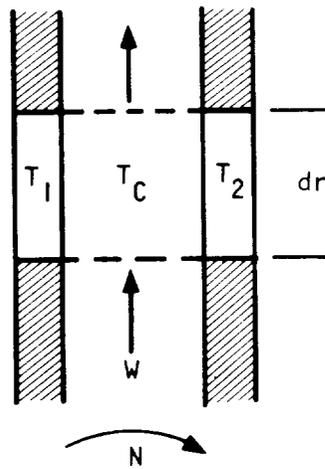
Thermal resistance:

$$R_n = \frac{\ell}{(hA_t)n}$$

Fluid capacity rate:

$$W\ Cp$$

Fluid internal heat generation:

$$\frac{Qs}{\ell}$$

$$\frac{dT_c}{dr} = \frac{r \left(\frac{2\pi}{60}\right)^2 N^2}{Jg_c \, C_p}$$

$$WC_p \frac{dT_c}{dr} = \sum_{i=1}^{m} \frac{(T_i - T_c)}{R_i} + \frac{Q_s}{\ell} + \frac{r \left(\frac{2\pi}{60}\right)^2 N^2}{2 \, Jg_c \, C_p} W \, C_p$$

$$WC_p \frac{dT_c}{dr} = \sum_{i=1}^{m} 1/R_i \left[\frac{\Sigma \, T_i/R_i}{\Sigma \, 1/R_i} - T_c \right] + \frac{Q_s}{\ell} + \frac{r \left(\frac{2\pi}{60}\right)^2 W \, C_p}{2 \, Jg_c \, C_p}$$

Let

$$\overline{T} = \frac{\Sigma \, T_i/R_i}{\Sigma \, 1/R_i}$$

$$UA = \sum_{i=1}^{m} 1/R_i$$

$$\frac{dT_c}{dr} = \frac{UA}{WC_p} (\overline{T} - T_c) + \frac{Q_s}{WC_p \, \ell} + \frac{r \left(\frac{2\pi}{60}\right)^2 N^2}{2 \, Jg_c \, C_p}$$

$$T_c = \left(-\frac{UA}{WC_p} \, r\right) + \frac{WC_p}{UA} \left[\frac{(2\pi/60)^2}{2\,Jg_c} \frac{N^2}{C_p} \left(r - \frac{WC_p}{UA}\right) + \frac{UA}{WC_p} \overline{T} + \frac{Q_s}{WC_p \, \ell} \right]$$

$$+ c_1 \left(-\frac{UA}{WC_p} \, r\right)$$

Boundary conditions:

$$T_c = T_{c1} \text{ at } r = r_1$$

$$T_c = T_{c2} \text{ at } r = r_2$$

196

Exact solution:

$$T_{c2} = T_{c1}\, e^{-\frac{UA}{WC_p}(r_2 - r_1)} + \left(\frac{WC_p}{UA}\right)\left[1. - e^{-\frac{UA}{WC_p}(r_2 - r_1)}\right]$$

$$\left[\frac{UA}{WC_p}\,\overline{T} + \frac{Q_s}{WC_p\,\ell} - \frac{(2\pi/60)^2}{2Jg_c}\,\frac{N^2}{C_p}\,\frac{WC_p}{UA}\right]$$

$$+ \frac{(2\pi/60)^2}{2Jg_c}\,\frac{N^2}{C_p}\left(\frac{WC_p}{UA}\right)\left[r_2 - r_1\, e^{-\frac{UA}{WC_p}(r_2 - r_1)}\right]$$

Finite increment technique:

(Average temperature difference method)

$$\frac{\Delta T_c}{\Delta r} = \frac{UA}{WC_p}\,(\overline{T} - \overline{T}_c) + \frac{Q_s}{WC_p\,\ell} + \frac{(2\pi/60)^2}{2Jg_c}\,\frac{rN^2}{C_p}$$

Let

$$\overline{T}_c = \frac{T_{c2} + T_{c1}}{2.}$$

$$\Delta T_c = T_{c2} - T_{c1}$$

$$T_{c2} - T_{c1} = \frac{UA}{WC_p}\,\Delta r\left[T - \left(\frac{T_{c2} + T_{c1}}{2}\right)\right] + \frac{Q_s\,\Delta r}{WC_p\,\ell} + \frac{(2\pi/60)^2}{2Jg_c}\,\frac{rN^2\Delta r}{C_p}$$

$$T_{c2}\left[1 + \frac{UA\Delta r}{2WC_p}\right] = T_{c1} + \frac{UA}{WC_p}\,\Delta r\left[\overline{T} - T_{c1}/2\right] + \frac{Q_s\Delta r}{WC_p\,\ell} + \frac{(2\pi/60)^2}{2Jg_c}\,\frac{rN^2\Delta r}{C_p}$$

$$T_{c2}\left[1. + \frac{UA\Delta r}{2WC_p}\right] = T_{c1}\left(1. - \frac{UA\Delta r}{2WC_p}\right) + \frac{UA}{WC_p}\,\Delta r\,\overline{T} + \frac{Q_s\Delta r}{WC_p\,\ell} +$$

$$\left(\frac{2\pi/60}{2Jg_c}\right)^2\frac{rN^2\Delta r}{C_p}$$

$$T_{c2} = \frac{T_{c1}\left(1. - \dfrac{UA\,\Delta r}{2WC_p}\right) + \dfrac{UA}{WC_p}\,\Delta r\,\bar{T} + \dfrac{Q_s\,\Delta r}{WC_p\,\ell} + \dfrac{(2\pi/60)^2}{2Jg_c}\dfrac{rN^2\Delta r}{C_p}}{\left[1. + \dfrac{UA\,\Delta r}{2WC_p}\right]}$$

In order not to violate the first law of thermodynamics, the following condition is required.

$$\frac{UA\,\Delta r}{2WC_p} < 1.$$

Therefore:

$$\Delta r < \frac{2WC_p}{UA}$$

(Outlet temperature difference method)

Let

$$\bar{T}_c = T_{c2}$$

$$\Delta T_c = T_{c2} - T_{c1}$$

$$T_{c2} - T_{c1} = \frac{UA}{WC_p}\,\Delta r\,(\bar{T} - T_{c2}) + \frac{Q_s\,\Delta r}{WC_p\,\ell} + \frac{(2\pi/60)^2}{2Jg_c}\frac{rN^2\Delta r}{C_p}$$

$$T_{c2}\left[1 + \frac{UA}{WC_p}\,\Delta r\right] = T_{c1} + \frac{UA}{WC_p}\,\Delta r\,\bar{T} + \frac{Q_s\,\Delta r}{WC_p\,\ell} + \frac{(2\pi/60)^2}{2Jg_c}\frac{rN^2\Delta r}{C_p}$$

$$T_{c2} = \frac{T_{c1} + \dfrac{UA}{WC_p}\,\Delta r\,\bar{T} + \dfrac{Q_s\,\Delta r}{WC_p\,\ell} + \dfrac{(2\pi/60)^2}{2Jg_c}\dfrac{rN^2\Delta r}{C_p}}{1 + \dfrac{UA}{WC_p}\,\Delta r}$$

This form of solution does not violate the first law of thermodynamics under any condition.

Since, in general, the wall temperature in a passage may be assumed constant over only a short increment, the finite increment method is sufficiently accurate for most problems. The average temperature difference method is preferred over the range for which it is applicable, and the outlet temperature method is used outside of this range.

198

APPENDIX F

PRESSURE DROP CALCULATIONS IN ORIFICES

INTRODUCTION

The pressure drop in flow restriction devices such as orifices, nozzles, and long holes may be expressed in terms of the flow coefficient (C_d), the static head loss coefficient (K_s), or the total head loss coefficient (K_T). The flow coefficient is normally used to calculate the flow through an orifice or nozzle for a pressure drop measured across flange taps or pipe taps. The pressure drop measured in this manner does not represent the pressure loss for the orifice or nozzle however because of static pressure recovery which occurs downstream. The pressure drop calculations for the AiResearch thermal analyzer computer program use the total head loss coefficient (K_T) to calculate the pressure loss of an orifice, nozzle, or long hole.

The total head loss coefficient may be expressed in several different forms of equation to predict total head loss in orifices or holes as shown below:

$$P_{t_1} - P_{t_2} = K_T \gamma M_o^2 P_o/2.$$

$$P_{t_1} - P_{t_2} = K_T V_o^2 \rho_o/2 \, g_c$$

$$P_{t_1} - P_{t_2} = K_T \left(\frac{W}{A_o}\right)^2 /2 \, g_c \, \rho_o$$

The total head loss coefficient for orifices or long holes with the axis parallel, perpendicular, or inclined to the direction of main stream flow are presented in this section.

ORIFICE TOTAL HEAD LOSS COEFFICIENT

A thin sharp edge or square edge orifice may be installed in a line as shown below.
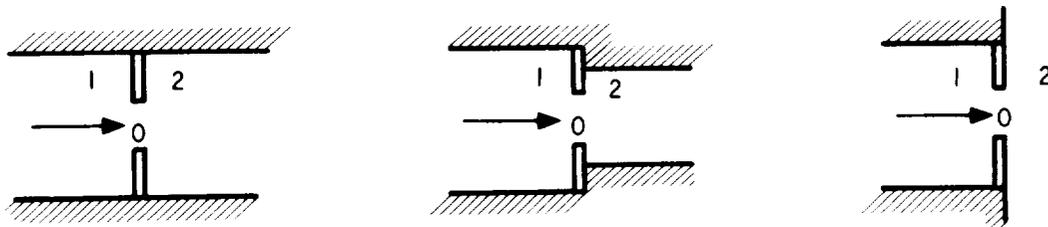
The total head loss coefficient for each of these configurations may be calculated from equations F-1, F-2, F-3, and F-4 below. These equations include the effect of static pressure recovery downstream of the orifice and do not represent the head loss as measured by flange taps on the orifice. The sharp edge or square edge orifice for which these equations are applicable has a thickness less than 30 percent of the orifice diameter $(L/D_o < 0.3)$.

$$K_T = (0.707 \sqrt{1. - A_o/A_1} + 1. - A_o/A_2)^2 \tag{F-1}$$

When $\quad$ $Re > 2.5 \times 10^5$, $A_o/A_1 > 0.1$, and $A_o/A_2 > 0.1$

$$K_T = 2.9 \tag{F-2}$$

When $\quad$ $Re > 2.5 \times 10^5$, $A_o/A_1 < 0.1$, and $A_o/A_2 < 0.1$

$$K_T = \left(\frac{K_B}{X} - \frac{A_o}{A_2}\right)^2 \tag{F-3}$$

When $\quad$ $Re < 2.5 \times 10^5$, $A_o/A_1 > 0.1$, and $A_o/A_2 > 0.1$

$$K_T = \frac{2.9}{X^2} \tag{F-4}$$

When $\quad$ $Re < 2.5 \times 10^5$, $A_o/A_1 < 0.1$, and $A_o/A_2 < 0.1$

The K_B and X factors given in Equation (F-3) are shown in Figures F-1 and F-2.

For a square edge inlet and exit section with a long hole $(L/D_o > 3.0)$, the inlet and exit total head losses may be determined from Figures F-3 and F-4 taken from Benedict, Carlucci, and Swetz (Reference F-1).
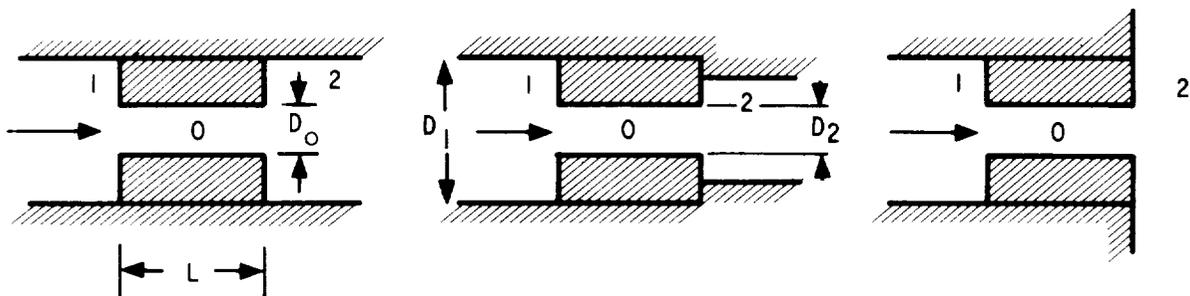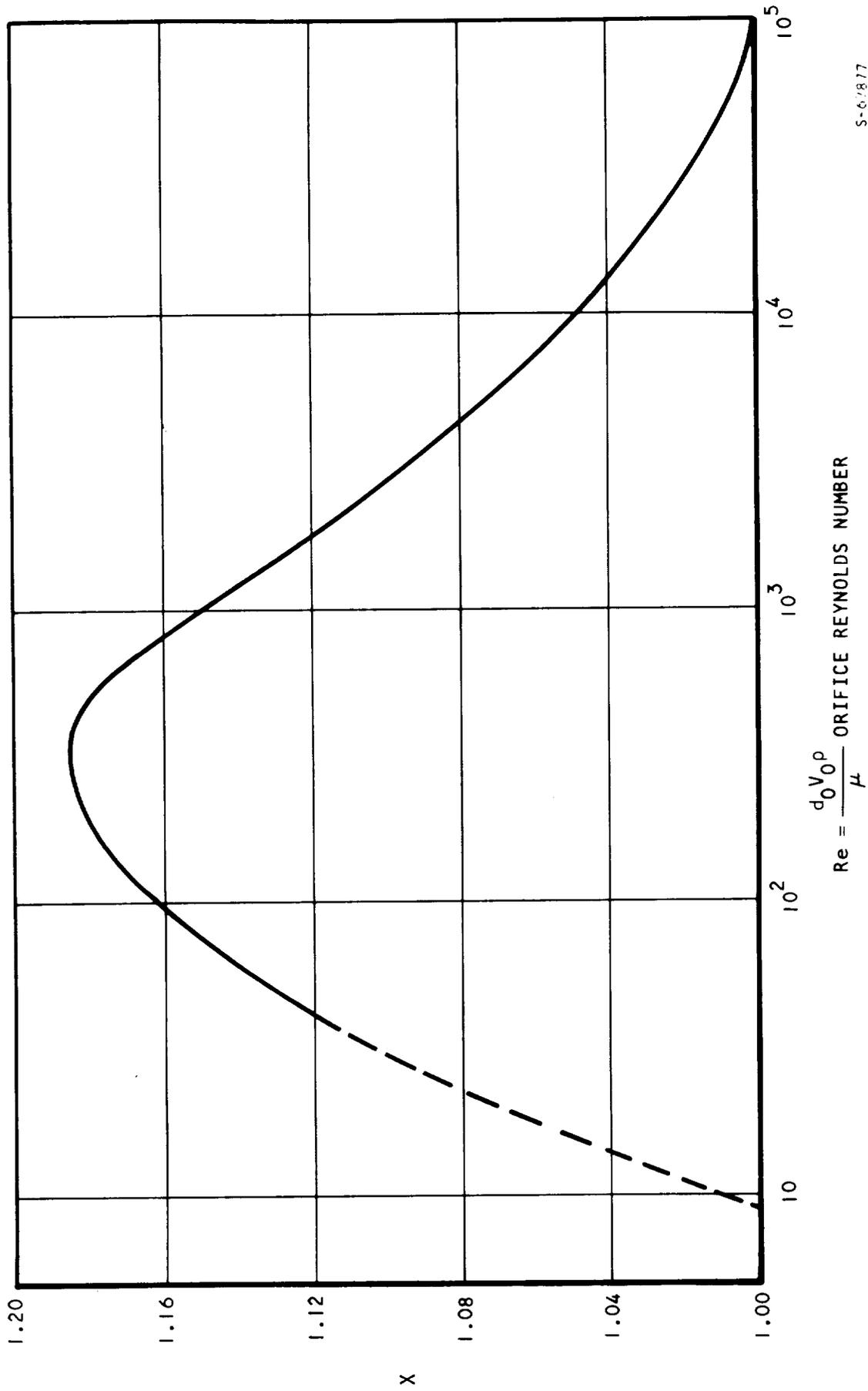
S-6/877

Figure F-1. X-Factor for Reynolds Number Correction for a Sharp Edge Orifice

$$Re = \frac{d_0 V_0 \rho}{\mu} \text{ ORIFICE REYNOLDS NUMBER}$$
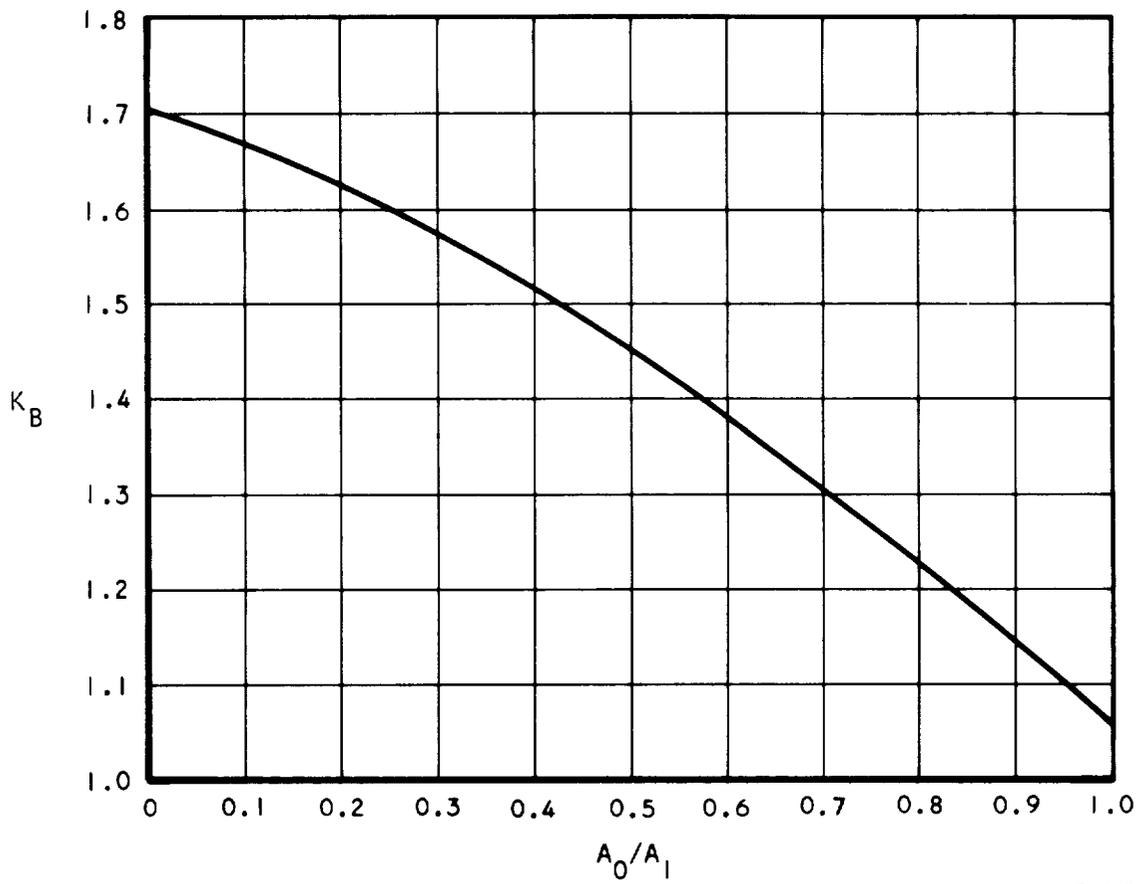
Figure F-2. K_B Factor for a Sharp Edge Orifice

S-67878

If the hole is between 0.3 and 3.0 diameters long $(0.3 < L/D_0 < 3.0)$, a total head loss coefficient in addition to the inlet and exit losses from Figures F-3 and F-4 must be considered. This additional head loss coefficient accounts for the vena contracta which forms downstream of short holes $(0.3 < L/D_0 < 3.0)$. The additional total head loss coefficient for $0.3 < L/D_0 < 3.0$ is presented in Equation F-5 below.

$$K_T = K_L \ (1. - A_o/A_2)\sqrt{1. - A_o/A_1} \tag{F-5}$$

The length factor (K_L) is determined from Figure F-5.

The static head loss coefficient (K_s) for small holes in the side of a larger duct is given below. For this condition the main stream total pressure (P_{TI}) is replaced by the local static pressure in the duct (P_d)

STATIC PRESSURE LOSS COEFFICIENTS FOR SIDE INLETS FOR $V_o > 2\ V_D$

		$L/D_o = 0$	$L/D_o = 3$
Sharp-edged Holes		2.7	1.5
Thimbled Holes		1.8	1.2
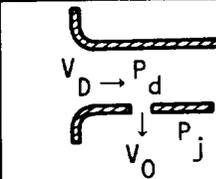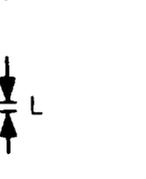
The pressure drop for holes in the side of a duct with the axis perpendicular or inclined to the direction of stream flow has also been studied in NASA TN D-5467 (Reference F-2). The results of this study were presented in terms of the flow coefficient. These results have been change to the head loss coefficient as a function of the ratio of the orifice velocity or Mach number to the duct velocity or Mach number. The head loss coefficient for this case is based on the main duct static pressure to the downstream static pressure difference. The effects of downstream static pressure recovery are not included in this loss coefficient. Figure F-6 shows the loss coefficient for a perpendicular hole with various length to diameter ratios (L/D_0). The loss coefficient for a hole inclined at an angle of 45 degrees in the direction of main duct flow is also shown in Figure F-6.
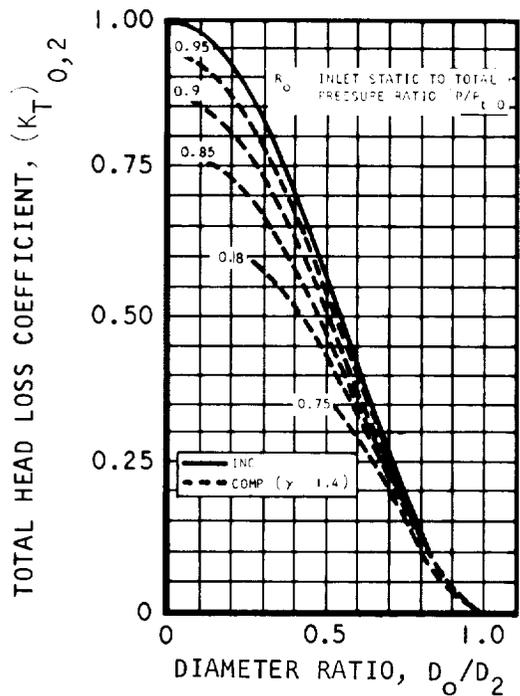
Figure F-3. Compressible and Constant-Density Loss Coefficients for Abrupt Enlargements
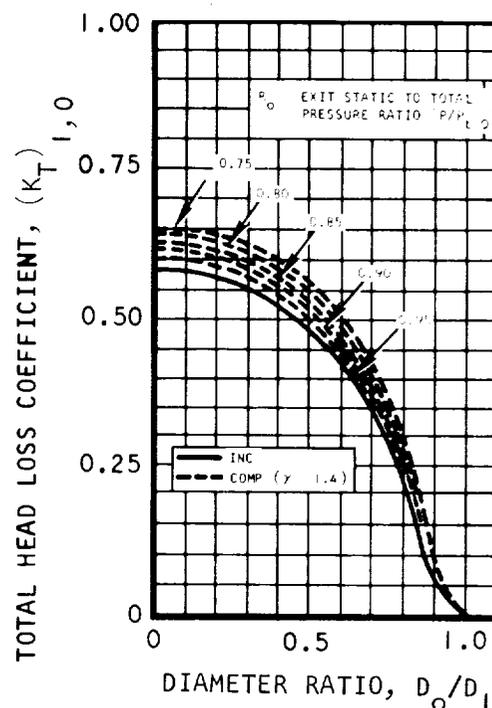
Figure F-4. Compressible and Constant-Density Loss Coefficients for Abrupt Contractions
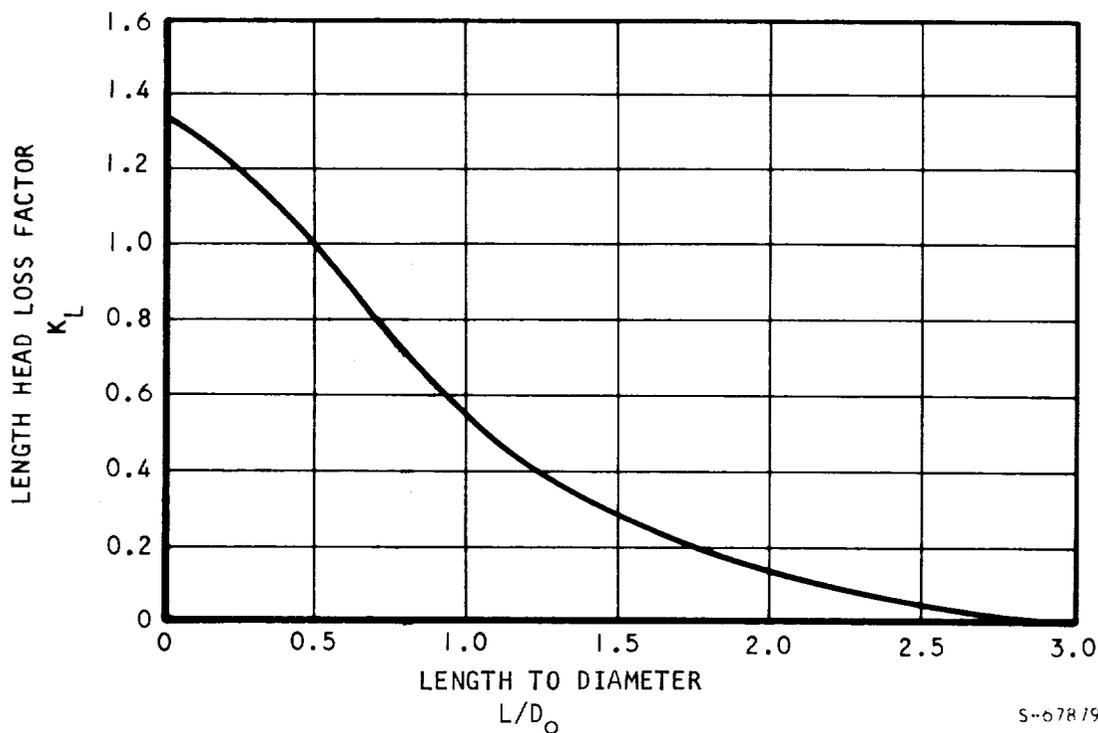
Figure F-5. Length to Diameter Ratio Head Loss Factor for Short Holes

204
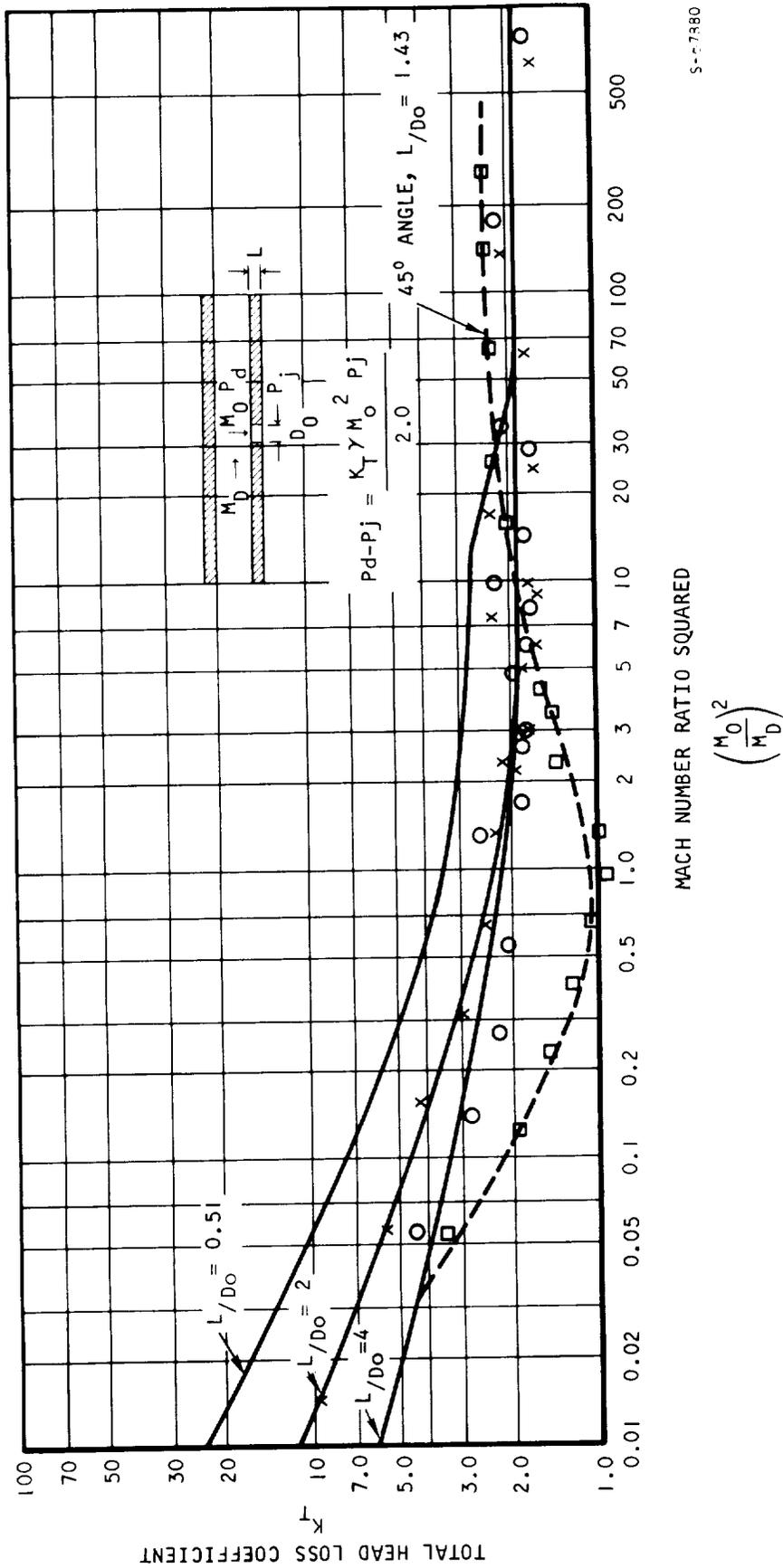
Figure F-6. Head Loss Coefficient for an Orifice in the Side Wall of a Duct from NASA TN D-5467

S-67380

NOMENCLATURE

A_o	Orifice or hole area
A_1	Upstream duct area
A_2	Downstream duct area
C_d	Flow coefficient or discharge coefficient, ratio of measured to ideal flow through the orifice
g_c	Gravitational constant
K_L	Short hole length head loss factor (Figure F-5)
K_S	Static head loss coefficient
K_T	Total head loss coefficient
$(K_T)_{0,2}$	Total head loss coefficient for abrupt enlargements (Figure F-3)
$(K_T)_{1,0}$	Total head loss coefficient for abrupt contractions (Figure F-4)
K_B	Dimensionless orifice loss factor (Figure F-2)
M_D	Mach number in the upstream duct
M_o	Mach number based on the total area of the orifice or hole
P_d	Static pressure in the upstream duct
P_j	Static pressure downstream of the orifice
P_o	Static pressure in the orifice or hole
P_{t_o}	Total pressure in the orifice or hole
P_{t_1}	Total pressure at Station 1
P_{t_2}	Total pressure at Station 2
γ	Specific heat ratio (Cp/C_v)
Re	Orifice or hole Reynolds number $\dfrac{D_o V_o \rho}{\mu}$

206

NOMENCLATURE (Continued)

W   Fluid weight flowrate

X   Reynolds number correction factor for sharp edge orifice (Figure F-1)

ρ_o Fluid density in the orifice or hole

REFERENCES

F-1   Benedict, R. P., N. A. Carlucci, and S. D. Swetz, "Flow Loss in Abrupt Enlargements and Contractions," ASME Paper No. 65-WA/PTC-1, November, 1965.

F-2   Rohde, J. E., H. T. Richards, and G. W. Metger, "Discharge Coefficients for Thick Plate Orifices with Approach Flow Perpendicular and Inclined to the Orifice Axis," NASA TN D-5467, October, 1969.

APPENDIX G

DERIVATION OF FLOW AND PRESSURE DISTRIBUTION EQUATIONS FOR FLOW IN SUPPLY TUBES AND IN CHANNELS WITH CROSSFLOW IMPINGEMENT

INTRODUCTION

Flow distribution in supply tubes and in channels with crossflow impingement have been studied as manifold and "header" problems in heat exchangers, gas burners, distribution pipes for water-filtering systems, and others. Vassonyi (Reference G-1) and Keller (Reference G-2) have indicated that a simple one-dimensional analysis using the Bernoulli equation with the effect of friction loss accounted for is sufficient for incompressible flow in manifolds with flow discharging from holes or slots. In these equations it is assumed that the discharging stream leaves with the full momentum of the main stream. Perlmutter (Reference G-3) and Wolf (Reference G-4) presented a mathematical model for a supply tube as shown in Figure G-1. Perlmutter (Reference G-3) also presented a mathematical model for pressure distribution in a channel with crossflow impingement as shown in Figure G-2.

FLOW DISTRIBUTION THEORY

For the supply tube mathematical model shown in Figure G-1, the solid arrows indicate the pressure forces on the fluid in the control volume; the double arrows indicate the X-momentum convected into the control volume; and the broken arrows indicate the velocities entering and leaving the control volume.

For frictionless, incompressible, steady-state, one-dimensional flow, the X-momentum equation from Figure G-1 is:

$$(p_1 \ y_1) - \left(p_1 + \frac{dp_1}{dx} \ \delta \ x\right) \left(y_1 + \frac{dy_1}{dx} \ \delta \ x\right) - \left(p_1 + \frac{1}{2} \frac{dp_1}{dx} \ \delta \ x\right)\left(-\frac{dy_1}{dx} \ \delta \ x\right)$$

$$= - \left[\frac{\rho_i}{g_c} u_1^2 \ y_1 - \frac{\rho_i}{g_c} \left(u_1 + \frac{du_1}{dx} \ \delta \ x\right)^2 \left(y_1 + \frac{dy_1}{dx} \ \delta \ x\right) \right.$$

$$\left. - \frac{\rho_i}{g_c} \left(u_1 + \frac{1}{2} \frac{du_1}{dx} \ \delta \ x\right)(v_1)(\delta \ x) \right] \qquad \text{(G-1)}$$

The last term in Equation G-1 assumes that the entire X-momentum of the supply tube flow is convected out of the supply tube as the flow enters the orifices. Combining terms and neglecting the higher order terms, Equation G-1 becomes

$$- y_1 \, dp_1 \;=\; \frac{\rho_1}{g_c} \left[d \left(u_1^2 \, y_1 \right) + \left(u_1 \, v_1 \right) dx \right] \tag{G-2}$$

Equation G-2 is in the form used by Wolf in Reference G-4. Note that the direction of fluid flow is in the positive x-direction.

The continuity equation from Figure G-1 is

$$\frac{\rho_i}{g_c} \left(u_1 \, y_1 \right) - \frac{\rho_i}{g_c} \left(u_1 + \frac{du_1}{dx} \, \delta x \right) \left(y_1 + \frac{dy_1}{dx} \, \delta x \right) - \frac{\rho_i}{g_c} \left(v_1 \, \delta x \right) \;=\; 0 \tag{G-3}$$

Combining terms and neglecting the higher order terms, Equation G-3 becomes

$$d \left(u_1 \, y_1 \right) + v_1 \, dx \;=\; 0 \tag{G-4}$$

If the orifice flow is uniform, the following equation also applies

$$u_1 \, y_1 \;=\; u_i \, y_i \left(1 - \frac{x}{L} \right) \tag{G-5}$$

Equation G-4 can be used to eliminate v_1 in Equation G-2 to yield a more convenient form of the momentum equation.

$$- y_1 \, dp_1 \;=\; \frac{\rho_i}{g_c} \left[d \left(u_1^2 \, y_1 \right) - u_1 \, d \left(u_1 \, y_1 \right) \right] \tag{G-6}$$

Equation G-6 is the form used by Perlmutter in Reference G-3.

Further, Equation G-6 can be converted to

$$- y_1 \, dp_1 \;=\; \frac{\rho_i}{g_c} \, u_1 \, d \left(u_1 \, y_1 \right) + \left(u_1 \, y_1 \right) du_1 - u_1 \, d \left(u_1 \, y_1 \right)$$

$$- y_1 \, dp_1 \;=\; \frac{\rho_i}{g_c} \left[\left(u_1 \, y_1 \right) du_1 \right]$$

$$- dp_1 \;=\; \frac{\rho_i}{2 \, g_c} \, d \left(u_1^2 \right) \tag{G-7}$$
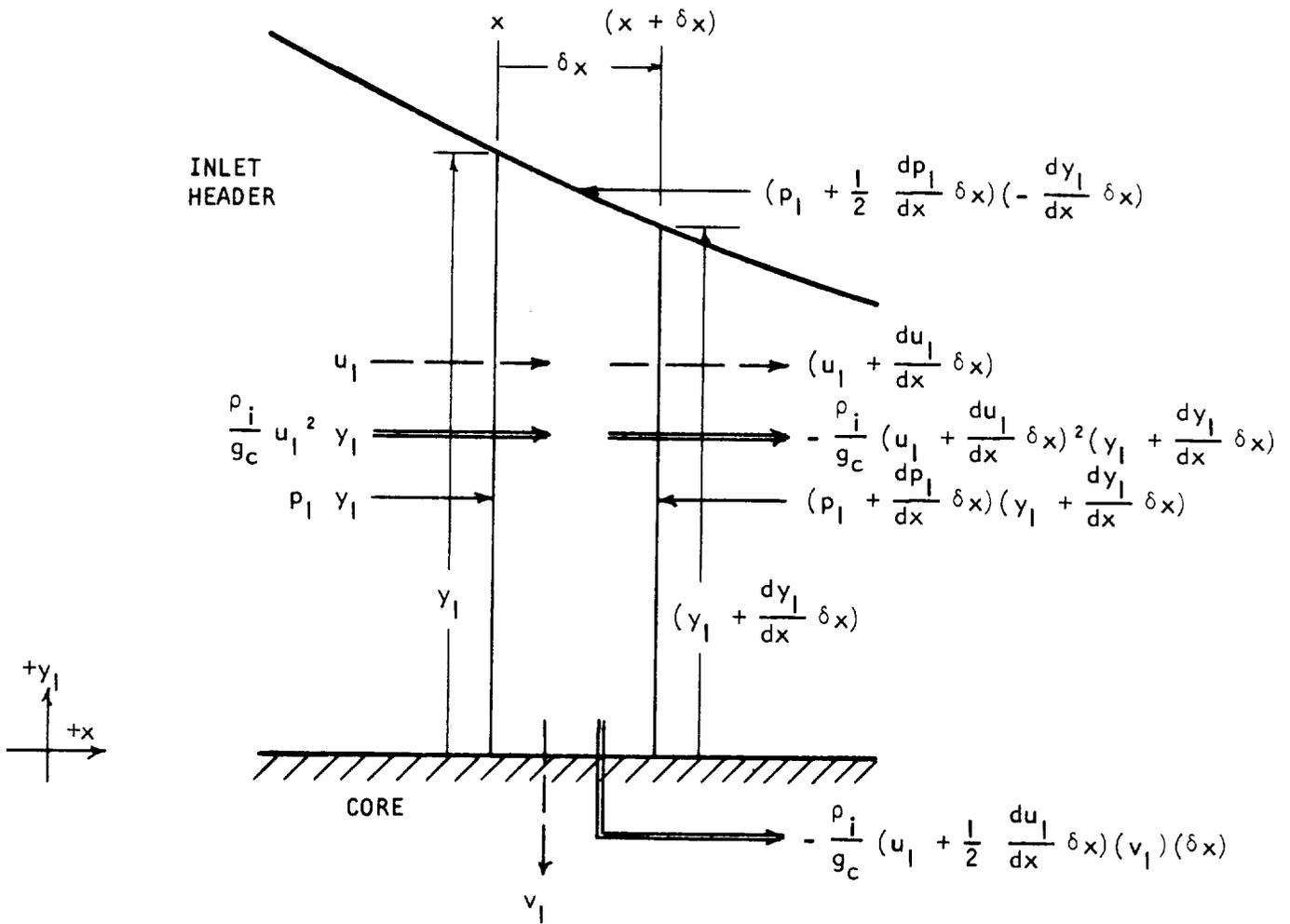
Figure G-1. Supply Tube Control Volume

A-27819

Integrating Equation G-7 from x = 0 (header inlet) to x,

$$P_1 - P_l = \frac{\rho_i}{2 g_c} (u_i^2 - u_l^2) \qquad (G-8)$$

Equation G-8 is in the form used by Wolf in Reference G-4 in his two-dimensional analysis. It is identical to the Bernoulli equation as a result of the assumption that the inlet header flow leaves the heater with its X-momentum. If uniform orifice flow is assumed, Equation G-5 and G-8 can be used with a given supply tube shape to yield a closed form solution for static pressure distribution.

For the crossflow impingement model shown in Figure G-2, the pressure forces on the fluid in the control volume are indicated by solid arrows; the X-momentum convected into the control volume is indicated by double arrows; and the velocities entering and leaving the control volume are indicated by broken arrows.

Assuming a frictionless, steady-state, one-dimensional flow, the X-momentum equation from Figure G-2 is

$$(P_2\, y_2) - (P_2 + \frac{dp_2}{dx} \delta x)(y_2 + \frac{dy_2}{dx}\delta x) - (P_2 + \frac{1}{2}\frac{dp_2}{dx} \delta x)(-\frac{dy_2}{dx} \delta x)$$

$$= - \left\{ - \left[- \frac{\rho_o}{g_c} u_2^2\, y_2 \right] - \left[\frac{\rho_o}{g_c} (u_2 + \frac{du_2}{dx} \delta x)^2 (y_2 + \frac{dy_2}{dx} \delta x) \right] \right\} \qquad (G-9)$$

The flow leaving the core is assumed to contribute no X-momentum to the outlet header flow. Combining terms and neglecting the higher order terms, Equation G-9 becomes

$$- dp_2 = \frac{\rho_o}{g_c} d (u_2^2) \qquad (G-10)$$

Note the differences between the supply tube, Equation G-7, and the crossflow impingement, Equation G-10. The supply tube equation would be identical to Equation G-10 if the flow were assumed to leave the supply tube with no X-component of velocity. If the supply tube flow sign convention is always taken as positive in the positive X-direction, it becomes convenient to allow the same flow sign conventions in the crossflow impingement channel. The sign convention should be taking the positive flow direction to be in the positive X-direction. Equation G-10 remains unchanged for the sign convention.
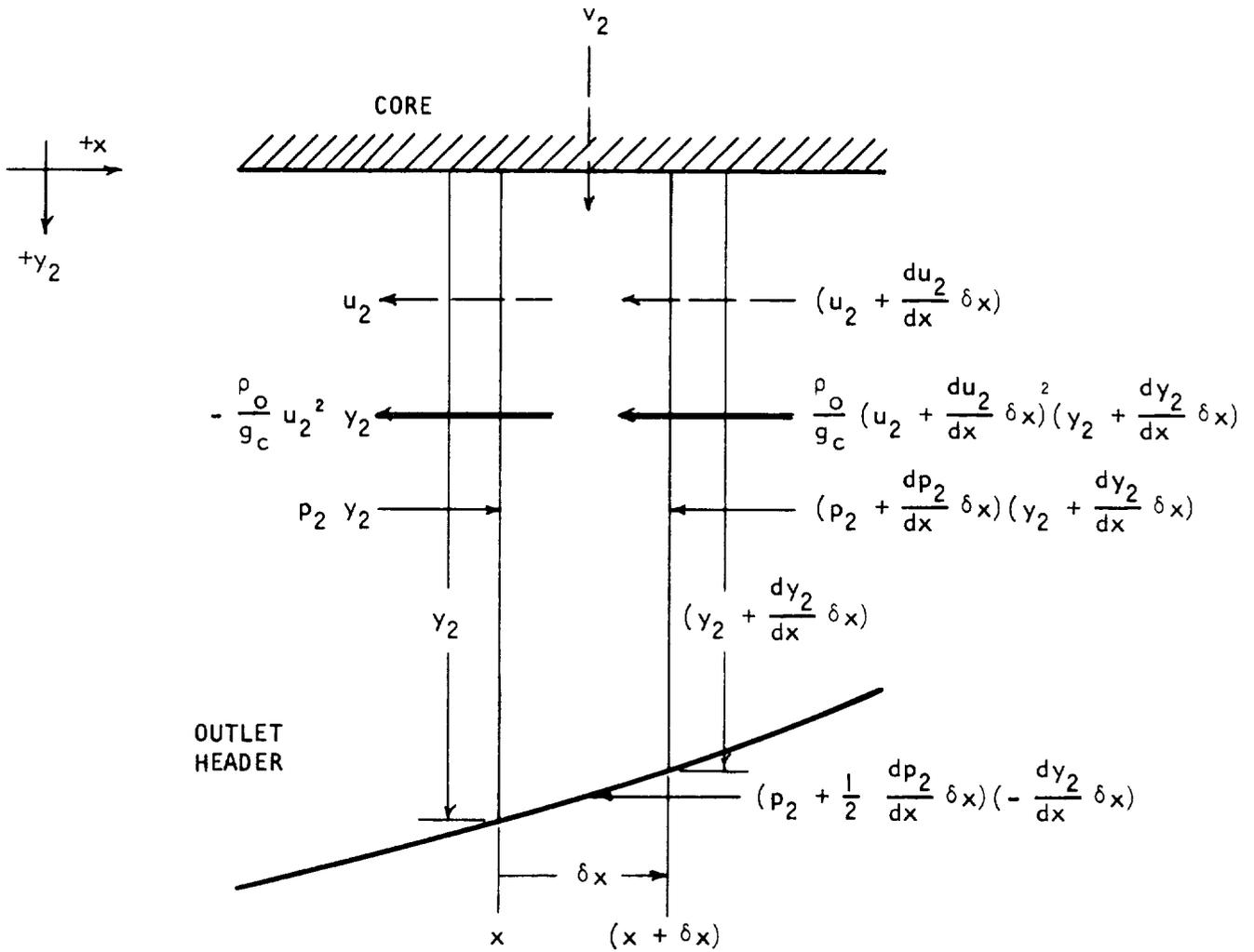
Figure G-2. Crossflow Impingement Control Volume

A-27818

The continuity equation from Figure G-2 is

$$-\frac{\rho_0}{g_c} (u_2 \, y_2) + \frac{\rho_0}{g_c} \left(u_2 + \frac{du_2}{dx} \, \delta \, x \right) \left(y_2 + \frac{dy_2}{dx} \, \delta \, x \right) + \frac{\rho_0}{g_c} (v_2 \, \delta \, x) = 0$$

(G-11)

Combining terms and neglecting the higher order terms, Equation G-11 becomes

$$d \, (u_2 \, y_2) - v_2 \, dx = 0$$

(G-12)

for flow in the positive X direction.

When the impingement flow is uniform, the following equation also applies:

$$u_2 \, y_2 = u_0 \, y_0 \left(\frac{x}{L} \right)$$

(G-13)

for flow in the positive X direction.

The equations derived above assume that the impingement flow entering the channel has no X-component of velocity and must be accelerated from rest to the velocity of the main stream. Herein lies the basic difference between the supply tube where flow exits from the stream along the length of the channel and crossflow impingement where flow enters a channel perpendicular to the direction of stream flow. In the supply tube, the flow leaves the stream with the full momentum of the main stream and in crossflow impingement the flow enters the channel with no X-component of velocity.

The one-dimensional model is applicable to highly turbulent or mixed flow while a two-dimensional model should be used for streamline, stratified, or laminar flow.

Using the influence coefficients from Table 8-2 of Shapiro (Reference G-5), the effects of compressible flow, heat addition, and friction may be included into the simple analysis presented above. To account for the effects of supply tube flow and crossflow impingement a Y-factor is included which is defined in Shapiro (Reference G-5) and given in the computer program writeup discussed in a later section. To meet the requirements for flow leaving the stream with the full momentum of the main stream, the Y-factor should be taken as one (Y = 1.0). To meet the requirement for flow entering the stream with no momentum in the direction of the main stream flow, the Y-factor should be taken as zero (Y = 0.0).

NOMENCLATURE

English Letter Symbols

c	Header y coordinate at $x = L$, $c = y(L)$
G	Header mass velocity, $G = \rho u$
g_c	Gravitational constant
k	Exponent
L	Header length, $0 \leq x \leq L$
m	Slope of header wall
n	Exponent
P	Total pressure
p	Static pressure
q	Uniform flow dynamic head, $q = \dfrac{G^2}{2\,g_c\,\rho}$
t	x Coordinate at which flow streamline in outlet header exits from core
u	Velocity component parallel to core face
v	Velocity component perpendicular to core face
x	Coordinate parallel to core face, $0 \leq x \leq L$
y	Coordinate perpendicular to core face

Greek Letter Symbols

Δ	Indicates a change in a quantity
δ	Indicates infinitesimal change in a quantity
ρ	Density

Subscripts

i	Indicates system inlet
o	Indicates system outlet
1	Indicates inlet header
2	Indicates outlet header

REFERENCES

G-1. Vassonyi, A., "Pressure Losses in Elbows and Duct Branches," Trans.
      ASME, Vol. 66, 1944.

G-2. Keller, J. D., "The Manifold Problem," ASME Paper No. 48-SA-2, May 1948.

G-3. Perlmutter, M., "Inlet and Exist Header Shapes for Uniform Flow Through
      a Resistance Parallel to the Main Stream," Trans. ASME, J. of Basic
      Engr., Vol. 83, September 1961.

G-4. Wolf, S., "Flow for Heat Exchangers with Oblique Flow Headers."
      Supplement to TR No. 60, Dept. of Mechanical Engr., Stanford University,
      September 1964.

G-5. Shapiro, A. H., The Dynamics and Thermodynamics of Compressible Fluid
      Flow, Vol. I, Ronald Press Co., New York, 1953.

APPENDIX H

METHOD AND MODEL DESCRIPTIONS FOR ELASTIC, INELASTIC, AND CREEP ANALYSIS OF BLADE, VANE, AND BEAM STRUCTURES (X0850)

INTRODUCTION

Presented herein are elasticity equations that govern the elastic and inelastic behavior of structural members such as beams, blades, and vanes. The equations, applicable to either thermally or mechanically loaded members, account for elastic, inelastic, or creep effects. The relations have been programmed for the IBM 360 Model 65 computer as AiResearch Program X0850. The mechanics of the analytical method are as follows.

The first step is to solve the elastic and/or inelastic short-time problem. This is accomplished by a series of elastic steps, as illustrated in Figure H-1, until a prescribed permissible convergence criteria is met. Once the short-time stress distribution has been completed, the stress values are used as initial guesses in the creep analysis. The creep analysis is then performed according to the strain-hardening procedure illustrated in Figure H-2. The problem is terminated automatically by the computer when the creep strain at any element exceeds a prescribed value set by the user.

BASIC MATHEMATICAL FORMULATIONS

With the assistance of Figure H-3, the mathematical formulation of the problem can begin. Let ϵ_x and σ_x be the total strain and stress at the middle of the time interval Δt_1 and $\Delta \epsilon_x^c$ the additional increment of creep strain during the interval Δt.

Then
$$\epsilon_x = \epsilon_x^E + \epsilon_x^P + \epsilon_x^C + \frac{\Delta \epsilon_x^c}{2} + \alpha T$$

$$= \frac{\sigma_x}{E_s} + \epsilon_x^C + \frac{\Delta \epsilon_x^c}{2} + \alpha T \tag{H-1}$$

From which

$$\sigma_x = -E_s \left(\epsilon_x - \epsilon_x^C - \frac{\Delta \epsilon_x^c}{2} - \alpha T \right) \tag{H-2}$$

However, from strain deformation we have

$$\epsilon_x = \frac{\partial u}{\partial x} - y \frac{\partial^2 v}{\partial x^2} - z \frac{\partial^2 w}{\partial x^2} \tag{H-3}$$
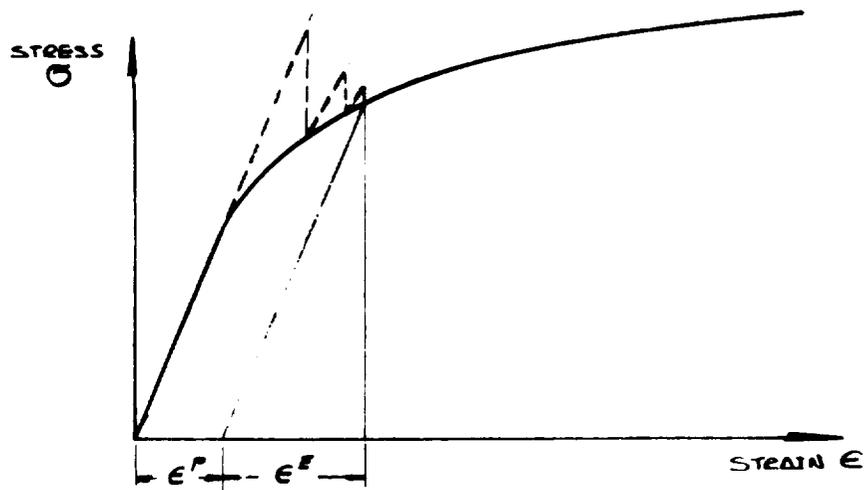
Figure H-I.   Iteration Method for Short-Time Inelastic Analysis
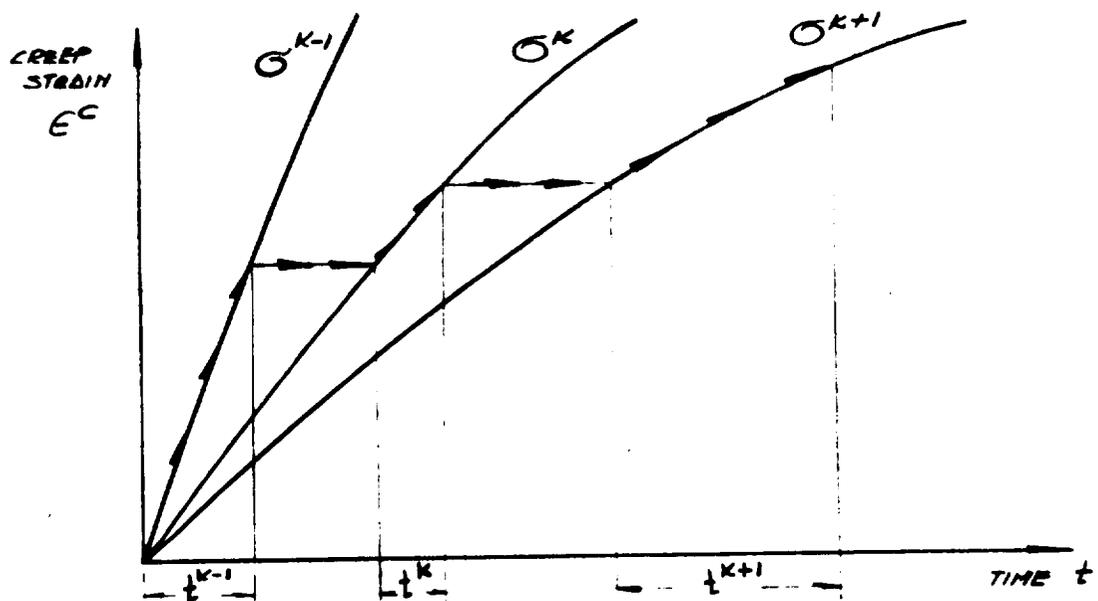
S-67881

Figure H-2.   Strain-Hardening Technique of Creep Analysis
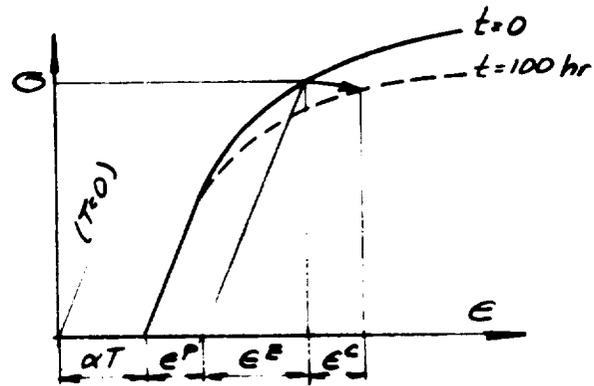
Figure H-3   Strain Components
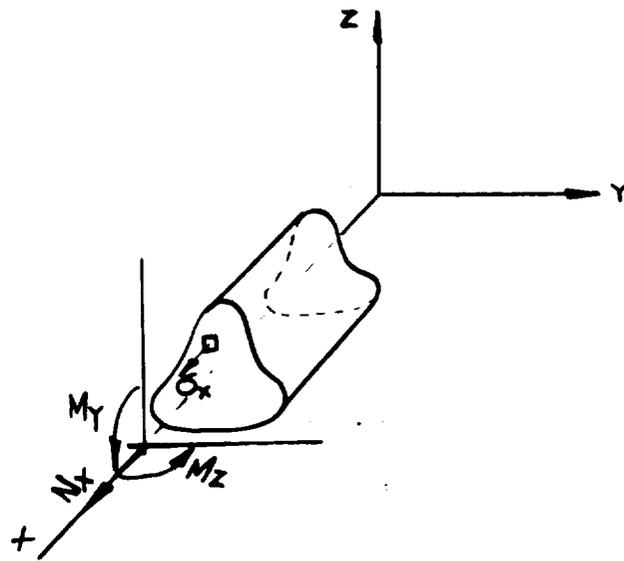
S-o7882

Figure H-4   Coordinate System

218

Substituting Equation (H-3) into (H-2) gives

$$\sigma_x = -E_s \left(\epsilon_x^c + \frac{\Delta\epsilon_x}{2} + \alpha T - \frac{\partial u}{\partial x} + y\,\frac{\partial^2 v}{\partial x^2} + z\,\frac{\partial^2 w}{\partial x^2} \right) \qquad (H-4)$$

Next, with Equation (H-4) and the sign convention of Figures H-4 the stress resultants N_x, M_y, and M_z are computed. First, for the force N_x with the centroid as the origin of the axis system.

$$N_x = \int_A \sigma_x \, dA$$

$$= -\int E_s \left(\epsilon_x^c + \frac{\Delta\epsilon_x^c}{2} \right) dA - \int E_s\,\alpha\,T\,dA + \frac{\partial u}{\partial x}\int E_s\,dA$$

$$- \frac{\partial^2 v}{\partial x^2}\int E_s\,y''^0\,dA - \frac{\partial^2 w}{\partial x^2}\int E_\zeta\,z''^0\,dA \qquad (H-5)$$

Gathering terms permits Equation (H-5) o be written as;

$$N_x = -N_c - N_t + \frac{\partial u}{\partial x}\,\overline{EA} \qquad (H-6)$$

Next, for the moment M_y

$$M_y = \int_A \sigma_x\,z\,dA$$

$$= -\int_A E_s \left(\epsilon_x^c + \frac{\Delta\epsilon_x^c}{2} \right) z\,dA - \int_A E_s\,\alpha T\,z\,dA + \frac{\partial u}{\partial x}\int_A E_s\,z''^0\,dA \qquad (H-7)$$

$$- \frac{\partial^2 v}{\partial x^2}\int_A E_s\,yz\,dA - \frac{\partial^2 w}{\partial x^2}\int_A E_s\,z^2\,dA$$

Equation (H-7) reduces to;

$$M_y = -M_{cy} - M_{ty} - \frac{\partial^2 v}{\partial x^2}\,\overline{EI}_{yz} - \frac{\partial^2 w}{\partial x^2}\,\overline{EI}_{yy} \qquad (H-8)$$

219

Finally, for moment M_z

$$M_z = -\int_A \sigma_x y \, dA$$

$$= -\int_A E_s \left(\epsilon_x^c + \frac{\Delta\epsilon_x^c}{2} \right) y \, dA + \int_A E_s \, \alpha t \, y \, dA - \frac{\partial u}{\partial x} \int_A E_s{}^{{//}^0} y \, dA$$

$$+ \frac{\partial^2 v}{\partial x^2} \int_A E_s \, y^2 \, dA + \frac{\partial^2 w}{\partial x^2} \int_A E_s \, yz \, dA \qquad \text{(H-9)}$$

Equation (H-9) reduces to

$$M_z = M_{cz} + M_{tz} + \frac{\partial^2 v}{\partial x^2} \overline{EI}_{zz} + \frac{\partial^2 w}{\partial x^2} \overline{EI}_{yz} \qquad \text{(H-10)}$$

Solving Equation (H-6) for $\frac{\partial u}{\partial x}$, and Equations (H-8) and (H-10) simultaneously for the curvatures, gives

$$\frac{\partial u}{\partial x} = \frac{N_x + N_t + N_c}{\overline{EA}} \qquad \text{(H-11)}$$

$$\frac{\partial^2 v}{\partial x^2} = \frac{\left(M_y + M_{ty} + M_{cy}\right) \overline{EI}_{yz} + \left(M_z - M_{tz} - M_{cz}\right) \overline{EI}_{yy}}{\left(\overline{EI}_{yy}\right)\left(\overline{EI}_{zz}\right) - \left(\overline{EI}_{yz}\right)^2} \qquad \text{(H-12)}$$

$$\frac{\partial^2 w}{\partial x^2} = \frac{-\left(M_y + M_{ty} + M_{cy}\right) \overline{EI}_{zz} - \left(M_z - M_{tz} - M_{cz}\right) \overline{EI}_{yz}}{\left(\overline{EI}_{yy}\right)\left(\overline{EI}_{zz}\right) - \left(\overline{EI}_{yz}\right)^2} \qquad \text{(H-13)}$$

Substituting Equations (H-11) through (H-13) into Equation (H-14) gives for the stress, σ_x

$$\sigma_x = -E_s\left\{\alpha t + \epsilon_x^c + \frac{\Delta\epsilon_x^c}{2} - \left(\frac{N_x + N_t + N_c}{\overline{EA}}\right)\right. \tag{H-14}$$

$$+ \frac{1}{\left(\overline{EI}_{yy}\right)\left(\overline{EI}_{zz}\right) - \left(\overline{EI}_{yz}\right)^2}\left[\left(\left(M_y + M_{ty} + M_{cy}\right)\overline{EI}_{yz}\right.\right.$$

$$\left.+ \left(M_z - M_{tz} - M_{cz}\right)\overline{EI}_{yy}\right)y$$

$$\left.\left.-\left(\left(M_y + M_{ty} + M_{cy}\right)\overline{EI}_{zz} + \left(M_z - M_{tz} - M_{cz}\right)\overline{EI}_{yz}\right)z\right]\right\}$$

In Equations (H-8) through (H-14), the following symbols have been used:

$$\int_A E_s\, dA = \overline{EA}$$

$$\int_A E_s\, z^2\, da = \overline{EI}_{yy}$$

$$\int_A E_s\, \alpha t\, dA = N_t$$

$$\int_A E_s\, \alpha ty\, dA = M_{tz}$$

$$\int_A E_s\, y^2\, dA = \overline{EI}_{zz}$$

$$\int_A E_s\, \alpha Tz\, dA = M_{ty}$$

$$\int_A E_s\, yz\, dA = \overline{EI}_{yz}$$

$$\int_A E_s\left(\epsilon_x^c + \frac{\Delta\epsilon_x^c}{2}\right)dA = N_c$$

$$\int_A E_s \cdot \left(\epsilon_x^C + \frac{\Delta\epsilon_x^C}{2} \right) y \, dA = M_{cz}$$

$$\int_A E_s \left(\epsilon_x^C + \frac{\Delta\epsilon_x^C}{2} \right) z \, dA = M_{cy}$$

ARBITRARY LOCATION OF CROSS SECTION REFERENCE AXES

The y-z axis system employed in the previous equations is measured from the elastic center of the cross section. However, since that location is unknown at the beginning of a problem it is convenient to employ an axis system chosen by the particular analyst. This is accomplished with the assistance of Figure H-5. Then

$$\left. \begin{array}{l} y = Y - \bar{y} \\ z = Z - \bar{z} \end{array} \right\}$$

(H-15)

From the definition of the elastic axes we have

$$\int_A E_s \, y \, dA = \int_A E_s \, z \, dA = 0$$
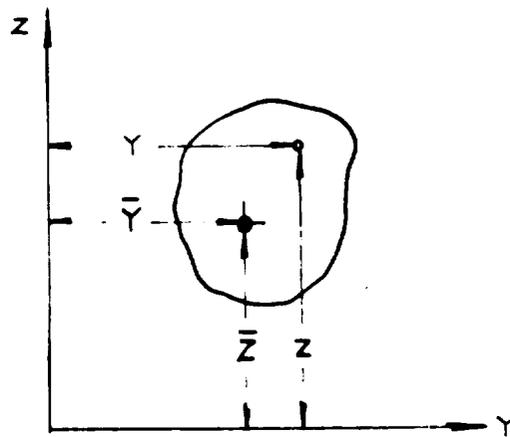
S-67883

Figure H-5. Cross Section Coordinates

222

Inserting Equation (H-15) into the previous expressions gives;

$$\bar{y} = \frac{\int_A E_s \, y \, dA}{\overline{EA}} \qquad (H-16)$$

$$\bar{z} = \frac{\int_A E_s \, z \, dA}{\overline{EA}} \qquad (H-17)$$

Substituting equations (H-16) and (H-17) into Equation (H-14), and the relations immediately following, one obtains

$$\sigma_x = -E_s \left\{ \alpha t + \epsilon_x^c + \frac{\Delta \epsilon_x^c}{2} - \left(\frac{N_x + N_t + N_c}{\overline{EA}} \right) \right.$$

$$+ \frac{1}{\left(\overline{EI}_{yy} \right) \left(\overline{EI}_{zz} \right) - \left(\overline{EI}_{yz} \right)^2} \left[\left(\left(M_y + M_{ty} + M_{cy} \right) \overline{EI}_{yz} \right. \right.$$

$$+ \left(M_z - M_{tz} - M_{cz} \right) \overline{EI}_{yy} \right) \left(y - \bar{y} \right)$$

$$\left. \left. - \left(\left(M_y + M_{ty} + M_{cy} \right) \overline{EI}_{zz} + \left(M_z - M_{tz} - M_{cz} \right) \overline{EI}_{yz} \right) \left(z - \bar{z} \right) \right] \right\} \qquad (H-18)$$

One then obtains for the stiffness and loading parameters

$$\overline{EA} = \int_A E_s \, dA$$

$$\overline{EI}_{yy} = \int_A E_s \, z^2 \, dA - \bar{z}^2 \, \overline{EA}$$

$$N_t = \int_A E_s \, \alpha T \, dA$$

$$M_{tz} = \int_A E_s \, \alpha t y \, dA - \bar{y} N_t$$

$$M_{ty} = \int_A E_s \, \alpha t Z \, dA - \overline{Z} N_t$$

$$\overline{EI}_{yz} = \int_A E_s \, YZ \, dA - \overline{Y} \, \overline{Z} \, \overline{EA}$$

$$\overline{EI}_{zz} = \int_A E_s \, Y^2 \, dA - \overline{Y}^2 \, \overline{EA}$$

$$N_c = \int_A E_s \left(\epsilon_x^C + \frac{\Delta \epsilon_x^C}{2} \right) dA$$

$$M_{cz} = \int_A E_s \left(\epsilon_x^C + \frac{\Delta \epsilon_x^C}{2} \right) Y \, dA - \overline{Y} N_c$$

$$M_{cy} = \int_A E_s \left(\epsilon_x^C + \frac{\Delta \epsilon_x^C}{2} \right) Z \, dA - \overline{Z} N_c$$

It is noted that the change in stress due to creep, $\Delta \sigma_x^C$, is

$$\Delta \sigma_x^C = -E_s \left\{ \epsilon_x^C + \frac{\Delta \epsilon_x^C}{2} - \frac{N_c}{EA} \right. \tag{H-19}$$

$$+ \frac{1}{\overline{EI}_{yy} \, \overline{EI}_{zz} - \overline{EI}_{yz}^2} \left[\left(M_{cy} \times \overline{EI}_{yz} - M_{cz} \times \overline{EI}_{yy} \right)\left(Y - \overline{Y} \right) \right.$$

$$\left. \left. - \left(M_{cy} \times \overline{EI}_{zz} - M_{cz} \times \overline{EI}_{yz} \right)\left(Z - \overline{Z} \right) \right] \right\}$$

RELATION OF LOADING POINT TO ELASTIC CENTROID OF BEAM

The applied loads $(N_x, M_y,$ and $M_z)$ of Equation (H-20) are expressed at the elastic centroid $(\overline{Y}, \overline{Z})$ of the cross section. However, the elastic centroid is usually not known at the time the problem is input, and it must be calculated by the program. Thus the user cannot define the moments at the centroid. The previous problem is overcome by defining the loads at an arbitrary location, P, which is known with respect to the Y-Z axes (see Figure H-6). The following expressions (programmed in the computer) transfer the applied forces at P to the centroid.

$$N_x = N_{x,p} \qquad\qquad\qquad (H\text{-}20)$$

$$\left.\begin{aligned} M_y &= M_{y,p} + N_{x,p}\,(Z_p - \overline{Z}) \\[8pt] M_z &= M_{z,p} - N_{x,p}\,(y_p - \overline{Y}) \end{aligned}\right\}$$
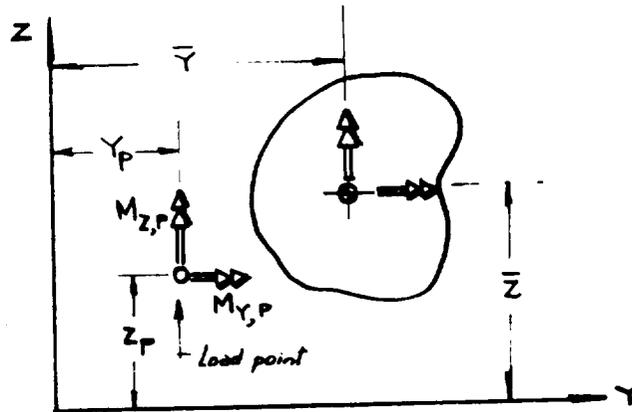
S-67884

Figure H-6. Arbitrary Point of Load Application

225

NOMENCLATURE

A Area

$E_S = \sigma/E$ Secant modulus

$$\overline{EA} = \int_A E_S \, dA$$

$$\overline{EI}_{yy} = \int_A E_S \, z^2 \, dA \; - \; \overline{z}^2 \; \overline{EA}$$

$$\overline{EI}_{zz} = \int_A E_S \, Y^2 \, dA \; - \; \overline{Y}^2 \; \overline{EA}$$

$$\overline{EI}_{yz} = \int_A E_S \, YZ \, dA \; - \; \overline{Y} \; \overline{Z} \; \overline{EA}$$

Extensional and flexural rigidities of cross section

$M_y, \; M_z$ = Moment about y and z axes, respectively

$$M_{ty} = \int_A E_S \, \alpha \, T \, Z \, dA \; - \; \overline{Z} \, N_T$$
Thermal moment vector, y - direction

$$M_{tz} = \int_A E_S \, \alpha \, T \, Y \, dA \; - \; \overline{Y} \, N_T$$
Thermal moment vector, z - direction

$$M_{cy} = \int_A E_S \left(\epsilon_x^c + \frac{\Delta \epsilon_x^c}{2} \right) Z \, dA \\ - \; \overline{Z} \, N_c$$
Creep moment vector, y - direction

$$M_{cz} = \int_A E_S \left(\epsilon_x^c + \frac{\Delta \epsilon_x^c}{2} \right) Y \, da \\ - \; \overline{Y} \, N_c$$
Creep moment vector, z - direction

$M_{y,p}, \; M_{z,p}$ = Applied moments at load point p of cross section

$$N_t = \int_A E_S \, \alpha \, T \, dA$$
Thermal axial force vector

$$N_c = \int_A E_S \left(\epsilon_x^c + \frac{\Delta \epsilon_x^c}{2} \right) dA$$
Creep axial force vector

T = Temperature rise above $70^\circ F$

U, V, W = Displacements in x, y, and z directions, respectively

x, y, z = Centroidal coordinate system, Orthogonal

Y, Z = distances from arbitrarily selected axes to point on cross section

$$\left. \begin{array}{l} \overline{Y} = Y-y = \int_A E_S \, Y \; dA \, / \, \overline{EA} \\[2em] \overline{Z} = Z-z = \int_A E_S \, Z \; dA \, / \, \overline{EA} \end{array} \right\} \quad \text{Elastic center coordinates}$$

$y_p, \; z_p$ = coordinates of load application point

Greek

α = coefficient of thermal expansion

ϵ_x = axial strain, total

σ_x = axial stress

Superscripts

E = elastic

P = plastic

C = creep

APPENDIX I

DETAILED TEMPERATURES, STRESS, AND STRESS-TO-RUPTURE LIFE
FOR EACH ELEMENT IN THE TASK I PRELIMINARY DESIGN ANALYSIS

In the Preliminary Design, Task I phase of the study, eight air cooled turbine blade configurations in each of three chord sizes were studied. A heat transfer analysis was conducted for each preliminary design at the hub section (16.7 percent span), the mean section (50 percent span), and the tip section (83.3 percent span) of the blade. This analysis was performed using the AiResearch transient and steady state thermal analyzer computer program (H0910), described in Appendix B. The analysis includes the effects of the hot gas relative total temperature with a radial gas temperature correction factor; convection heat transfer from the hot gas to the blade surface; span-wise and chordwise conduction as well as conduction through the wall; internal convection heat transfer from the blade surface to the cooling air; and cooling air heatup due to heat addition and rotational acceleration. Film cooling was applied in some cases as a reduction in the effective hot gas temperature calculated from the appropriate film effectiveness curve. Transpiration cooling was applied in some cases as a reduction in the hot gas Stanton number due to mass transfer. Radiation heat transfer was also considered between the inner surface of the blade and the supply tube.

The stress analysis was conducted for each element used in the thermal analysis at the hub, mean, and tip sections of the blade. The analysis was performed using the turbine blade elastic, inelastic, and creep stress analysis computer program (X0850) described in Appendix H. The stress at each element of the blade is determined based on an elastic and plastic stress analysis including the effects of centrifugal loads, bending moments due to thermal distortion, and local plastic flow of the material.

The centrifugal loads for each of the blades include the effects of the dead weight of the fins and the tip cap where it is used. Gas bending loads were neglected because these loads are small and may be cancelled out by tilting the blades. Bending moments due to offsetting the line of action of the centrifugal force as a result of thermal distortion and relaxation of stress due to local instantaneous plastic flow of the material are considered in AiResearch program X0850.

The results shown in Tables I-1 through I-72 indicate very short life for some of the compressive stressed elements of the blades. Creep relaxation analysis has shown that these high compressive stresses are rapidly reduced and that the turbine blade will not fail in stress rupture due to compression. For this reason the compressive stressed elements may be ignored, and only the tensile stressed elements are considred in determining the life of the blade. On the basis of this criteria, the critical element which determines the stress-to-rupture life at each section of the blade is marked by an asterisk (*) in each table. The life of each turbine blade is also limited by a maximum coating temperature limit of 1840°F (1277.8°K) for 1000 hr life. The temperature shown in each table is given in °F and the stress in psi.
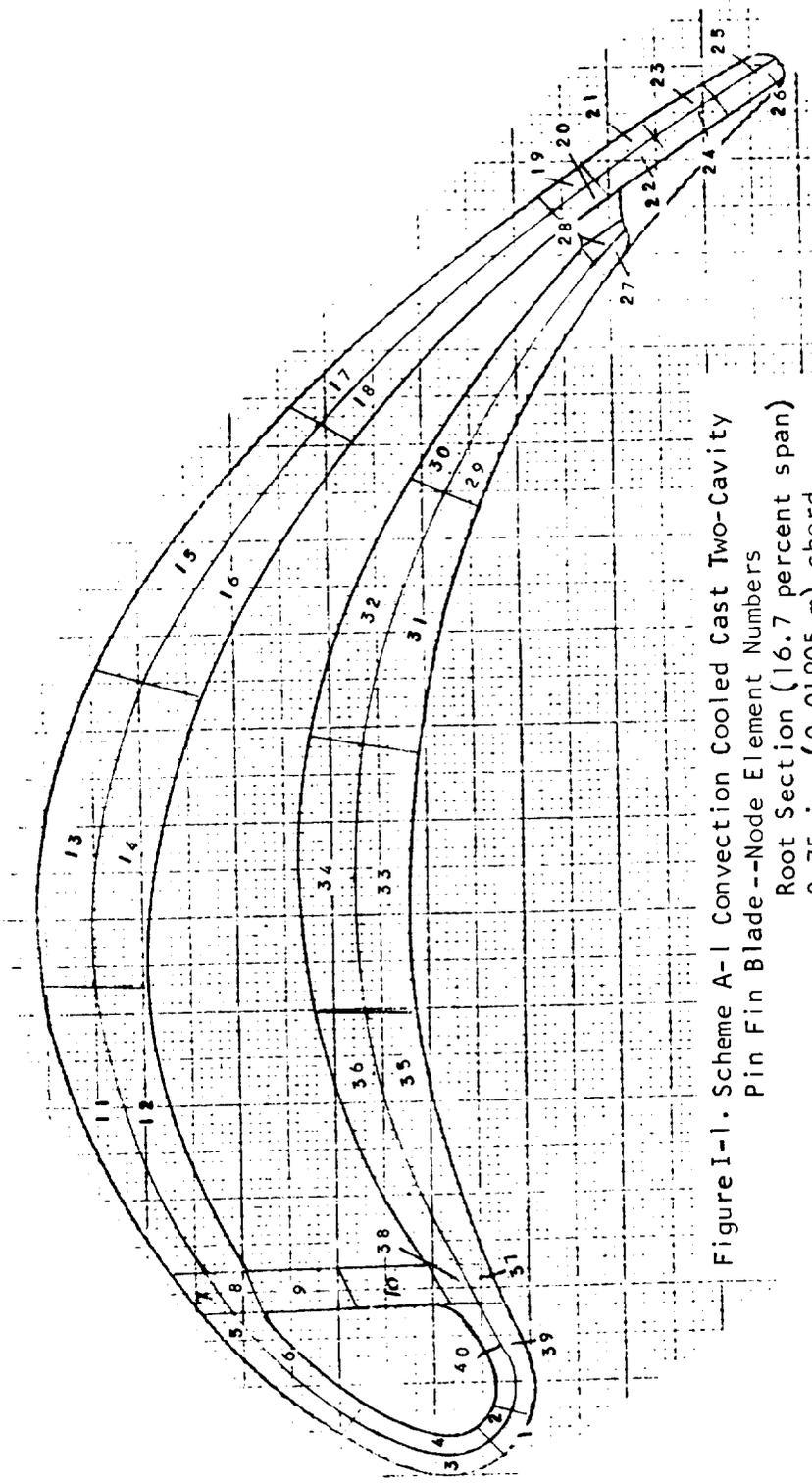
Figure I-I. Scheme A-I Convection Cooled Cast Two-Cavity
Pin Fin Blade--Node Element Numbers
Root Section (16.7 percent span)
0.75 in. (0.01905 m) chord
10 x size

229

TABLE I-I

SCHEME A-I TWO CAVITY PIN FIN BLADE, 0.75 IN. (0.01905 M) CHORD,
HUB SECTION, 22774 RPM, TIT = 2300°F (1533.3°K), WCA = 0.0176 LB/SEC/BLADE
(4.4 PERCENT OF HOT GAS FLOW), TCA = 900°F (755.6°K)

ELEMENT NO.	TEMPERATURE	STRESS	LIFE(HRS)
1	1555.0	-17109.4	10 YRS PLUS
2	1510.0	-5846.1	10 YRS PLUS
3	1514.0	-10060.7	10 YRS PLUS
4	1480.0	-1372.6	10 YRS PLUS
5	1454.0	-2528.2	10 YRS PLUS
6	1422.0	6341.3	10 YRS PLUS
7	1419.0	1356.7	10 YRS PLUS
8	1366.0	16509.0	10 YRS PLUS
9	1242.0	52159.7	10 YRS PLUS
10	1236.0	58439.3	10 YRS PLUS
11	1357.0	10709.9	10 YRS PLUS
12	1267.0	30804.8	10 YRS PLUS
13	1353.0	6011.0	10 YRS PLUS
14	1273.0	29454.1	10 YRS PLUS
15	1318.0	18648.2	10 YRS PLUS
16	1257.0	36892.6	10 YRS PLUS
17	1306.0	31301.4	10 YRS PLUS
18	1268.0	42439.5	10 YRS PLUS
19	1534.0	-21098.5	10 YRS PLUS
20	1518.0	-16155.1	10 YRS PLUS
21	1560.0	-25640.5	20188.5740
22	1544.0	-20225.5	10 YRS PLUS
23	1588.0	-30360.6	3341.9187
24	1573.0	-25466.2	14662.0239
25	1629.0	-36626.8	576.2047
26	1607.0	-31936.9	1442.9712
27	1449.0	4368.3	10 YRS PLUS
28	1439.0	6359.1	10 YRS PLUS
29	1254.0	51219.3	10 YRS PLUS
30	1223.0	57886.9	10 YRS PLUS
31	1266.0	44821.8	10 YRS PLUS
32	1206.0	57984.5	10 YRS PLUS
33	1286.0	40356.3	10 YRS PLUS
34	1218.0	54992.3	10 YRS PLUS
35	1300.0	41953.0	10 YRS PLUS
36	1238.0	55658.9	10 YRS PLUS
37	1406.0	19272.7	10 YRS PLUS
38	1354.0	31149.1	10 YRS PLUS
39	1487.0	909.1	10 YRS PLUS
40	1453.0	8507.5	10 YRS PLUS

Leading Edge W_{CLE} = 0.0035 lb/sec./blade (0.88 percent of hot gas flow)

Middle Cavity W_{CM} = 0.0141 lb/sec./blade (3.54 percent of hot gas flow)

Trailing Edge W_{CTE} = 0.0075 lb/sec./blade (1.88 percent of hot gas flow)
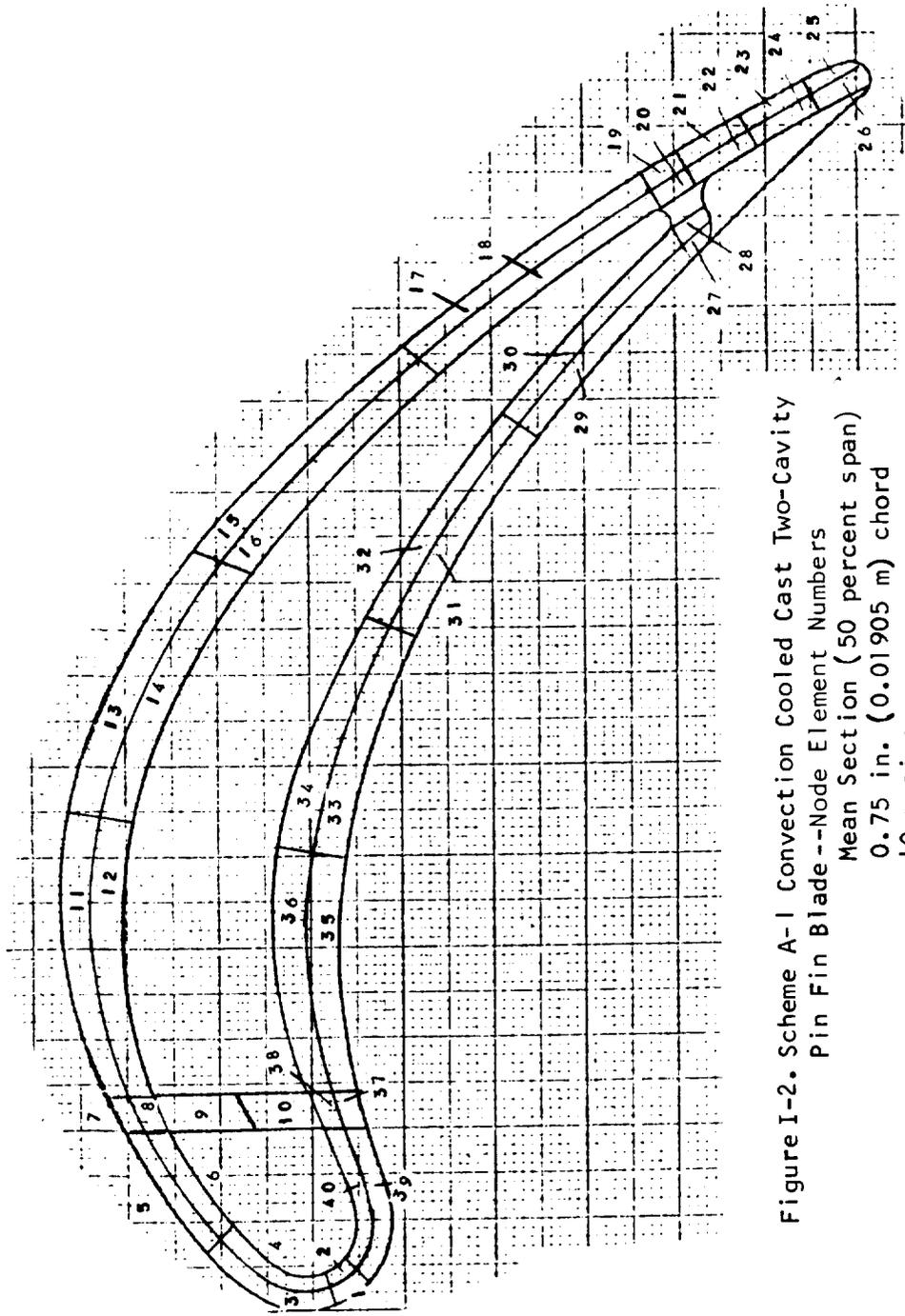
Figure I-2. Scheme A-I Convection Cooled Cast Two-Cavity
Pin Fin Blade--Node Element Numbers
Mean Section (50 percent span)
0.75 in. (0.01905 m) chord
10 x size

S-67885

TABLE I-2

SCHEME A-I TWO CAVITY PIN FIN BLADE, 0.75 IN. (0.01905 M) CHORD, MEAN SECTION

ELEMENT NO.	TEMPERATURE	STRESS	LIFE(HPS)
1	1644.0	-18864.2	11967.8009
2	1604.0	-8930.4	10 YRS PLUS
3	1610.0	-11426.7	10 YRS PLUS
4	1579.0	-2657.1	10 YRS PLUS
5	1579.0	-7629.6	10 YRS PLUS
6	1550.0	787.0	10 YRS PLUS
7	1561.0	-5095.3	10 YRS PLUS
8	1499.0	12319.5	10 YRS PLUS
9	1407.0	38396.0	10 YRS PLUS
10	1394.0	44781.7	39724.6680
11	1528.0	550.7	10 YRS PLUS
12	1434.0	12970.6	10 YRS PLUS
13	1515.0	3784.9	10 YRS PLUS
14	1472.0	16377.6	10 YRS PLUS
15	1486.0	16380.7	10 YRS PLUS
16	1456.0	25260.6	10 YRS PLUS
17	1504.0	19051.3	10 YRS PLUS
18	1475.0	27269.0	10 YRS PLUS
19	1665.0	-22067.5	2701.3807
20	1651.0	-17356.1	16557.2850
21	1636.0	-26552.0	624.2440
22	1673.0	-22311.8	2096.0474
23	1715.0	-32320.4	94.3933
24	1702.0	-28677.0	272.4235
25	1747.0	-32392.2	44.6670
26	1735.0	-31969.8	63.9464
27	1593.0	1393.7	10 YRS PLUS
28	1583.0	3654.0	10 YRS PLUS
29	1456.0	35290.2	44016.5220
30	1431.0	41038.4	25396.4610
31	1420.0	40456.4	39125.1330
32*	1395.0	45968.4	31119.5540
33	1420.0	38077.1	67118.9090
34	1388.0	45225.2	44067.9480
35	1436.0	34460.6	10 YRS PLUS
36	1401.0	42256.7	50496.9230
37	1505.0	18610.7	10 YRS PLUS
38	1473.0	25987.9	10 YRS PLUS
39	1575.0	1757.0	10 YRS PLUS
40	1549.0	7815.9	10 YRS PLUS
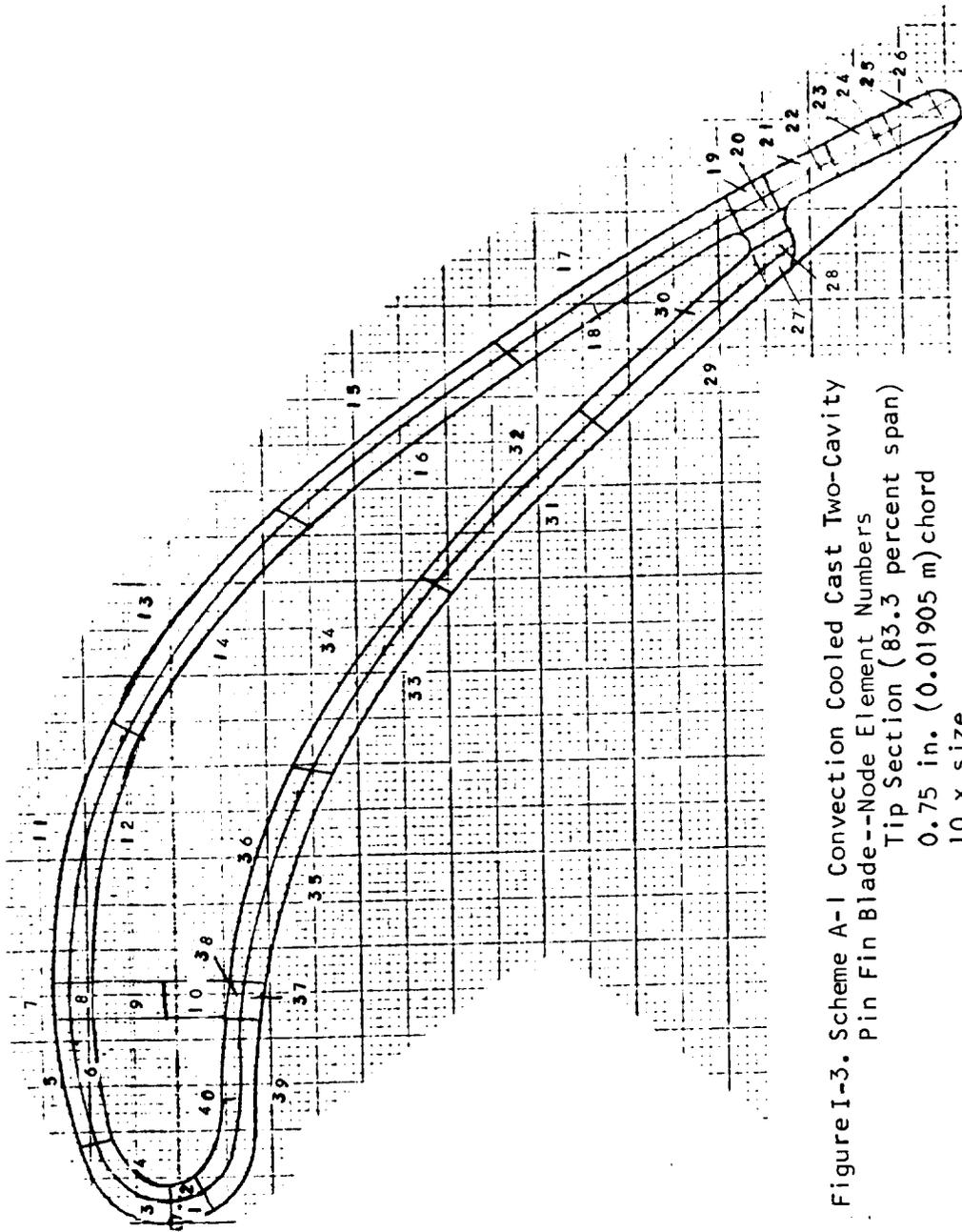
Figure I-3. Scheme A-I Convection Cooled Cast Two-Cavity
Pin Fin Blade--Node Element Numbers
Tip Section (83.3 percent span)
0.75 in. (0.01905 m) chord
10 x size

S-67886

TABLE I-3

SCHEME A-I TWO CAVITY PIN FIN BLADE, 0.75 IN. (0.01905 M) CHORD, TIP SECTION

ELEMENT NO.	TEMPERATURE	STRESS	LIFE(HRS)
1	1717.0	-32523.7	143.8510
2	1685.0	-22100.5	████.████
3	1708.0	-28944.1	███.7725
4	1679.0	-21331.8	2903.1836
5	1648.0	-14223.8	24705.3398
6	1624.0	-8331.4	38567.9102
7	1639.0	-11367.3	54227.7227
8	1614.3	-5306.8	93106.0000
9	1550.0	10483.2	10 YRS PLUS
10	1529.0	16486.1	10 YRS PLUS
11	1651.0	-12392.0	32472.7617
12	1630.0	-7382.7	40145.4570
13	1645.0	-7096.3	28724.3945
14	1626.0	-2604.1	10 YRS PLUS
15	1635.0	-634.9	10 YRS PLUS
16	1616.0	3886.5	10 YRS PLUS
17	1680.0	-7178.5	11483.0586
18	1662.0	-3049.8	42620.8594
19	1711.0	-14161.2	5081.1523
20	1698.0	-9120.2	4928.0117
21	1717.0	-15951.9	3143.1069
22	1706.0	-11207.7	9985.2305
23	1774.0	-29757.7	66.5153
24	1764.0	-29102.6	93.4864
25	1814.0	-31604.1	20.1514
26	1804.0	-31283.5	26.3821
27	1714.0	-15832.7	3457.0913
28	1704.0	-11477.2	9979.9766
29*	1615.0	8162.2	50800.8125
30	1598.0	12325.4	10 YRS PLUS
31	1574.0	14595.9	10 YRS PLUS
32	1558.0	18508.4	10 YRS PLUS
33	1554.0	15947.2	10 YRS PLUS
34	1540.0	19298.1	10 YRS PLUS
35	1541.0	16015.6	10 YRS PLUS
36	1529.0	18776.6	10 YRS PLUS
37	1589.0	2608.9	10 YRS PLUS
38	1573.0	6292.9	10 YRS PLUS
39	1646.0	-11948.9	40305.1953
40	1626.0	-7434.1	44158.9102
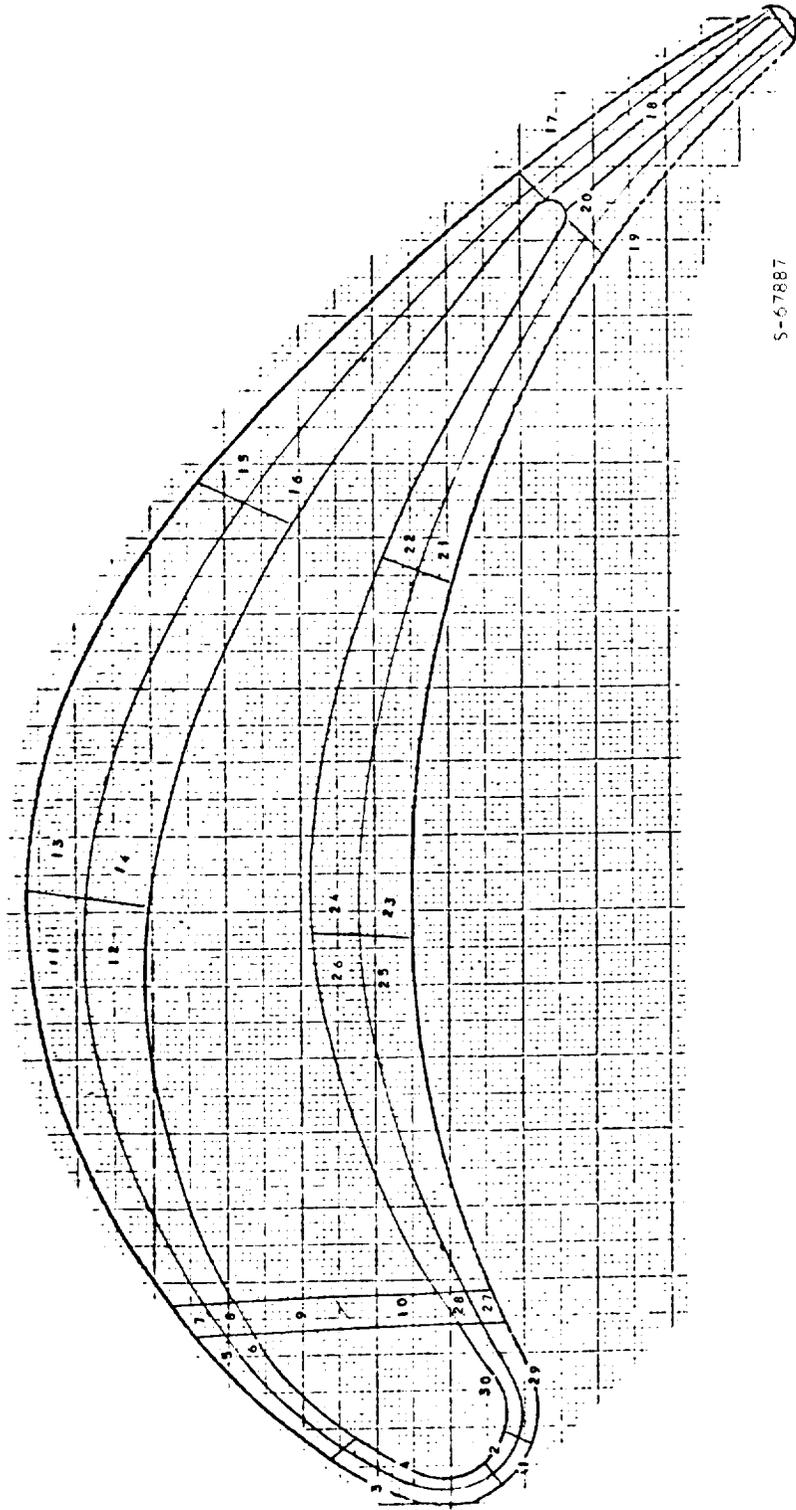
Figure I-4. Scheme A-I Convection Cooled Cast Two-Cavity
Pin Fin Blade--Node Element Numbers
Root Section (16.7 percent span)
1.0 in. (0.0254 m) chord
10 x size

S-67887

235

TABLE I-4

SCHEME A-1 TWO CAVITY PIN FIN BLADE, 1.0 IN. (0.0254 M) CHORD,
HUB SECTION, 23183 RPM, TIT = 2400°F (1588.9°K), WCA = .0258 LB/SEC/BLADE
(4.98 PERCENT OF HOT GAS FLOW), TCA = 900°F (755.6°K)

ELEMENT NO.	TEMPERATURE	STRESS	LIFE(HRS)
1	1583.0	-22435.7	21725.0490
2	1528.0	-7631.8	10 YRS PLUS
3	1528.0	-7532.8	10 YRS PLUS
4	1488.0	3113.5	10 YRS PLUS
5	1447.0	15960.6	10 YRS PLUS
6	1390.0	30674.5	10 YRS PLUS
7	1446.0	17557.1	10 YRS PLUS
8	1379.0	34656.8	10 YRS PLUS
9*	1243.0	70252.3	35814.3700
10	1257.0	65747.5	57455.9500
11	1480.0	12246.0	10 YRS PLUS
12	1403.0	31981.1	10 YRS PLUS
13	1484.0	15626.4	10 YRS PLUS
14	1398.0	37422.7	10 YRS PLUS
15	1465.0	23598.3	10 YRS PLUS
16	1409.0	37228.2	10 YRS PLUS
17	1555.0	98.9	10 YRS PLUS
18	1536.0	4999.2	10 YRS PLUS
19	1548.0	1124.3	10 YRS PLUS
20	1531.0	5849.0	10 YRS PLUS
21	1394.0	39777.7	10 YRS PLUS
22	1350.0	51563.6	45054.8550
23	1388.0	37813.8	10 YRS PLUS
24	1328.0	53956.1	57951.4560
25	1397.0	31062.6	10 YRS PLUS
26	1339.0	46328.0	10 YRS PLUS
27	1465.0	10792.2	10 YRS PLUS
28	1407.0	25958.7	10 YRS PLUS
29	1510.0	-2071.8	10 YRS PLUS
30	1467.0	9272.0	10 YRS PLUS

Leading Edge W_{CLE} = 0.0106 lb/sec/blade (2.05 percent of hot gas flow)

Middle Cavity W_{CM} = 0.0152 lb/sec/blade (2.93 percent of hot gas flow)

Trailing Edge W_{CTE} = 0.0102 lb/sec/blade (1.97 percent of hot gas flow)
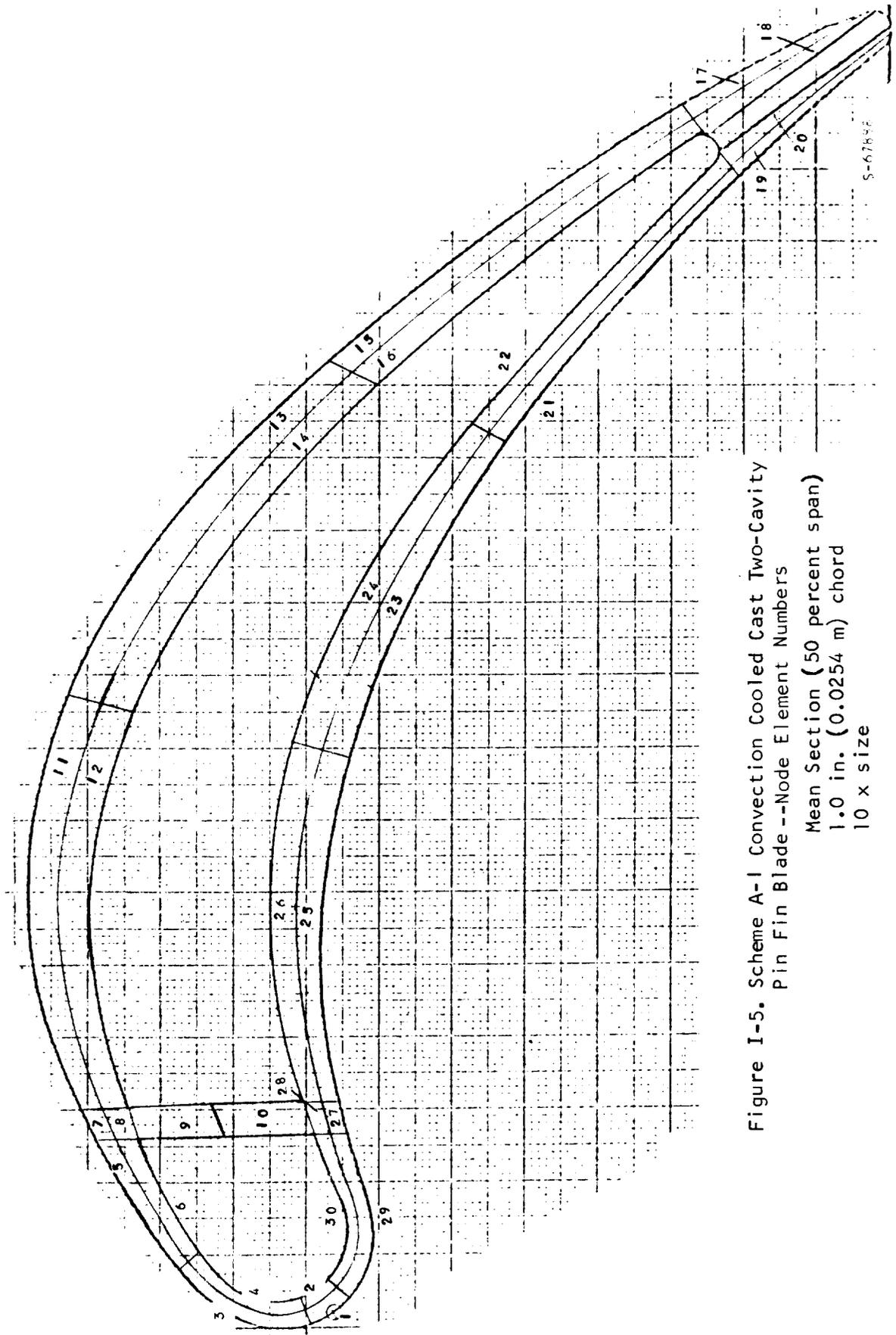
Figure I-5. Scheme A-I Convection Cooled Cast Two-Cavity
Pin Fin Blade--Node Element Numbers

Mean Section (50 percent span)
1.0 in. (0.0254 m) chord
10 x size

S-67898

237

TABLE I-5

SCHEME A-1 TWO CAVITY PIN FIN BLADE, 1.0 IN. (0.0254 M) CHORD, MEAN SECTION

ELEMENT NO.	TEMPERATURE	STRESS	LIFE(HRS)
1	1624.0	-22445.1	7199.2480
2	1571.0	-6583.9	10 YRS PLUS
3	1570.0	-3869.7	10 YRS PLUS
4	1532.0	6596.5	10 YRS PLUS
5	1516.0	20970.4	10 YRS PLUS
6	1478.0	30672.3	67280.1670
7	1556.0	15504.7	10 YRS PLUS
8	1518.0	24838.3	79464.3690
9	1393.0	55085.0	6398.5594
10	1384.0	53801.2	10549.2648
11	1661.0	-1727.1	10 YRS PLUS
12	1615.0	11182.1	10 YRS PLUS
13	1635.0	17611.0	23246.0520
14	1594.0	28439.9	4338.8616
15	1641.0	15927.7	35027.5090
16	1612.0	23686.9	7563.9495
17	1697.0	-4475.0	10 YRS PLUS
18	1681.0	-652.2	10 YRS PLUS
19	1694.0	-7257.0	10 YRS PLUS
20	1680.0	-2295.0	10 YRS PLUS
21	1590.0	23827.7	13232.2805
22	1573.0	29263.6	6348.0896
23	1529.0	35593.4	5122.2889
24*	1507.0	42309.5	2334.1653
25	1525.0	24545.2	69361.6640
26	1502.0	31723.6	26292.8080
27	1526.0	13401.1	10 YRS PLUS
28	1501.0	20760.7	10 YRS PLUS
29	1569.0	-4120.7	10 YRS PLUS
30	1531.0	6480.7	10 YRS PLUS
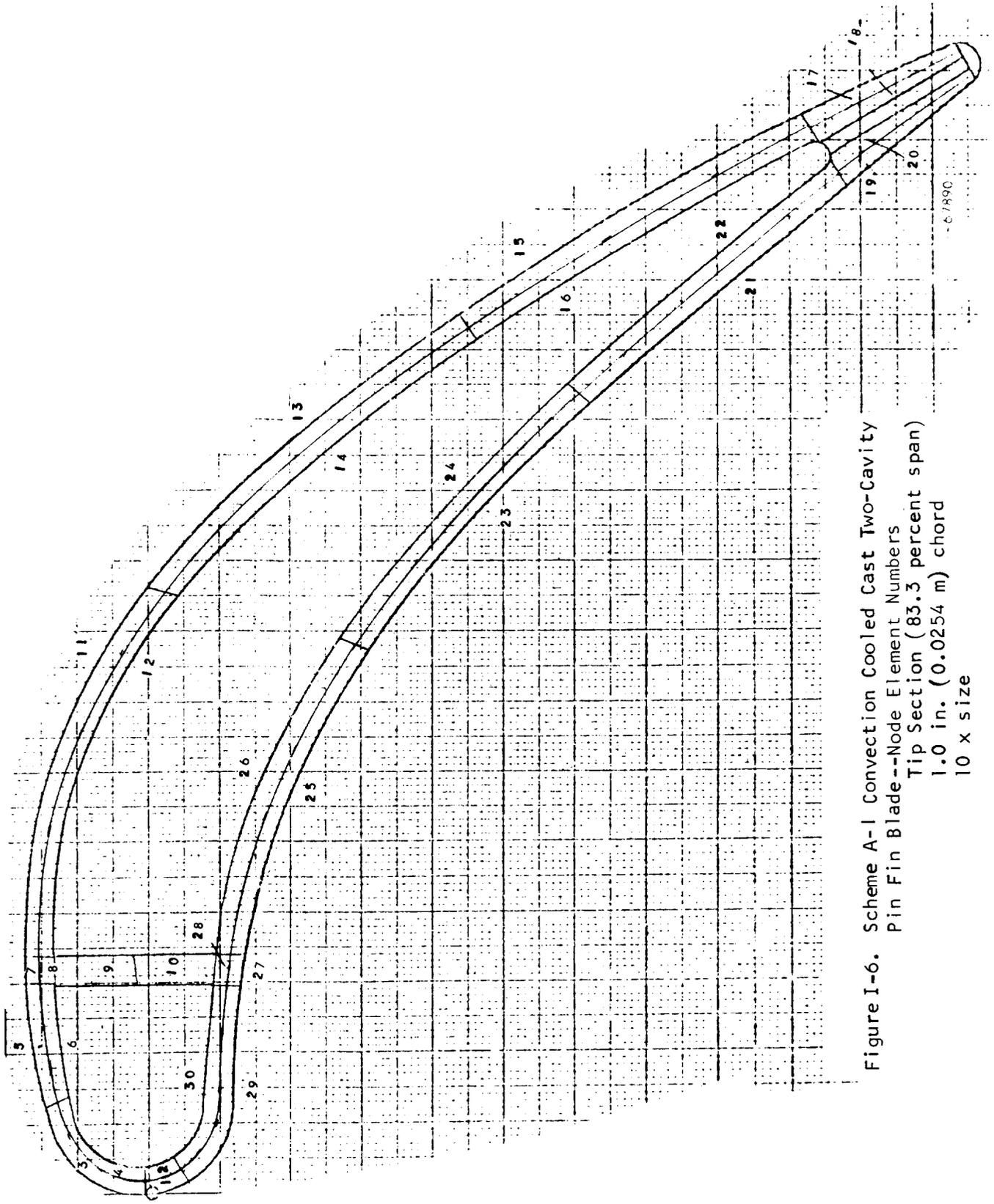
Figure I-6. Scheme A-I Convection Cooled Cast Two-Cavity
Pin Fin Blade--Node Element Numbers
Tip Section (83.3 percent span)
1.0 in. (0.0254 m) chord
10 x size

TABLE I-6

SCHEME A-I TWO CAVITY PIN FIN BLADE, I.O IN. (0.0254 M) CHORD, TIP SECTION

| ELEMENT NO.	TEMPERATURE	STRESS	LIFE(HRS)
1	1657.0	-39719.8	149.1730
2	1610.0	-27222.9	5325.1602
3	1584.0	-12844.4	10 YRS PLUS
4	1549.0	-3743.7	10 YRS PLUS
5	1549.0	21891.9	78576.5625
6	1515.0	29601.0	42465.4258
7	1632.0	13919.3	39865.7617
8	1604.0	19364.8	29024.6797
9	1519.0	34479.0	14019.8320
10	1531.0	23160.1	10 YRS PLUS
11	1807.0	-19030.0	221.5743
12	1792.0	-15212.8	616.0215
13	1810.0	2435.2	1288.2947
14**	1797.0	5493.2	959.6233
15	1818.0	903.8	1441.0889
16	1805.0	3527.5	1169.6021
17	1834.0	-10142.0	589.7180
18	1823.0	-7817.2	340.4058
19	1835.0	-16673.1	181.8077
20	1805.0.	-5135.5	856.6121
21	1794.0	-7173.8	741.3005
22	1781.0	1170.5	3236.3425
23	1743.0	5442.5	3446.0544
24	1731.0	13209.0	3722.8552
25	1675.0	5806.1	17275.3047
26	1665.0	10813.0	30508.4219
27	1644.0	-10883.0	52153.5742
28	1628.0	-4959.4	70366.3750
29	1630.0	-26520.1	3661.8850
30	1597.0	-16478.2	61751.6016
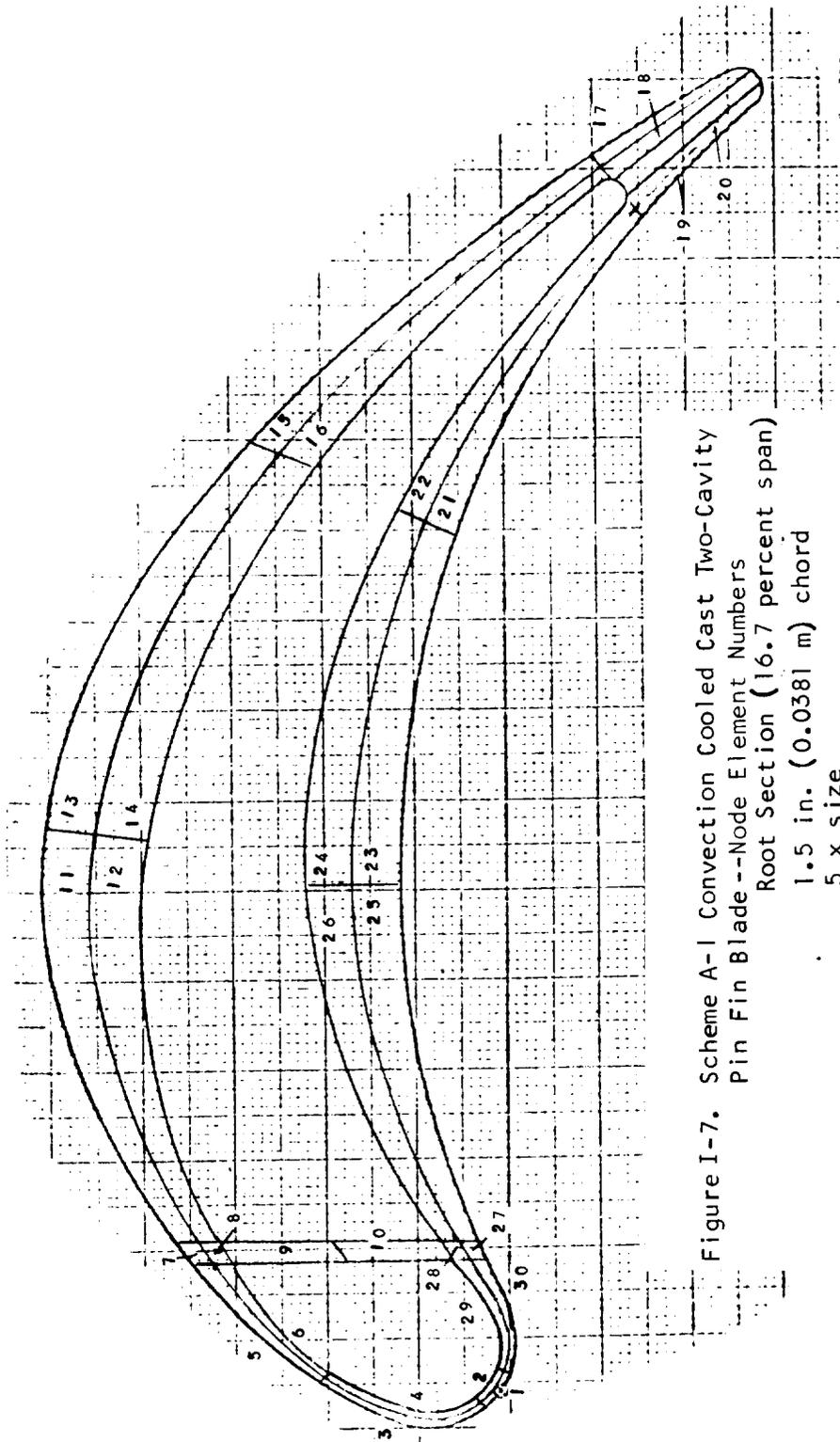
Figure I-7. Scheme A-I Convection Cooled Cast Two-Cavity
Pin Fin Blade--Node Element Numbers
Root Section (16.7 percent span)
1.5 in. (0.0381 m) chord
5 x size

S-67591

TABLE I-7

SCHEME A-I TWO CAVITY PIN FIN BLADE, I.5 IN. (0.0381 M) CHORD, HUB SECTION
23980 RPM, TIT = 2600°F (1700°K), WCA = .0619 LB/SEC/BLADE
(8.32 PERCENT OF HOT GAS FLOW), TCA = 900°F (755.6°K)

ELEMENT NO.	TEMPERATURE	STRESS	LIFE(HRS)
1	1597.0	-21091.2	19888.6890
2	1543.0	-6457.5	10 YRS PLUS
3	1511.0	4609.7	10 YRS PLUS
4	1473.0	14736.4	10 YRS PLUS
5	1455.0	27943.3	10 YRS PLUS
6	1414.0	38263.6	77081.3410
7	1522.0	13657.7	10 YRS PLUS
8	1451.0	31538.8	10 YRS PLUS
9*	1236.0	78880.9	7398.2117
10	1244.0	75752.8	10984.2524
11	1548.0	14509.5	10 YRS PLUS
12	1447.0	39607.1	20849.4510
13	1554.0	15811.5	10 YRS PLUS
14	1442.0	43466.2	11982.5403
15	1507.0	20616.8	10 YRS PLUS
16	1442.0	37040.7	44237.2300
17	1546.0	2635.8	10 YRS PLUS
18	1522.0	8605.9	10 YRS PLUS
19	1545.0	1070.0	10 YRS PLUS
20	1521.0	7844.3	10 YRS PLUS
21	1440.0	33164.4	10 YRS PLUS
22	1381.0	49364.9	25809.3590
23	1463.0	28207.8	10 YRS PLUS
24	1366.0	55388.9	13613.1179
25	1462.0	23097.0	10 YRS PLUS
26	1376.0	46895.3	47129.9400
27	1536.0	-1937.4	10 YRS PLUS
28	1467.0	17024.0	10 YRS PLUS
29	1520.0	78.9	10 YRS PLUS
30	1476.0	12023.5	10 YRS PLUS

Leading Edge W_{CLE} = 0.03   lb/sec/blade (4.03 percent of hot gas flow)

Middle Cavity W_{CM} = 0.0319 lb/sec/blade (4.29 percent of hot gas flow)

Trailing Edge W_{CTE} = 0.0156 lb/sec/blade (2.1 percent of hot gas flow)

-Figure I-8. Scheme A-I Convection Cooled Cast Two-Cavity
Pin Fin Blade--Node Element Numbers
Mean Section (50 percent span)
1.5 in. (0.0381 m) chord
5 x size

243
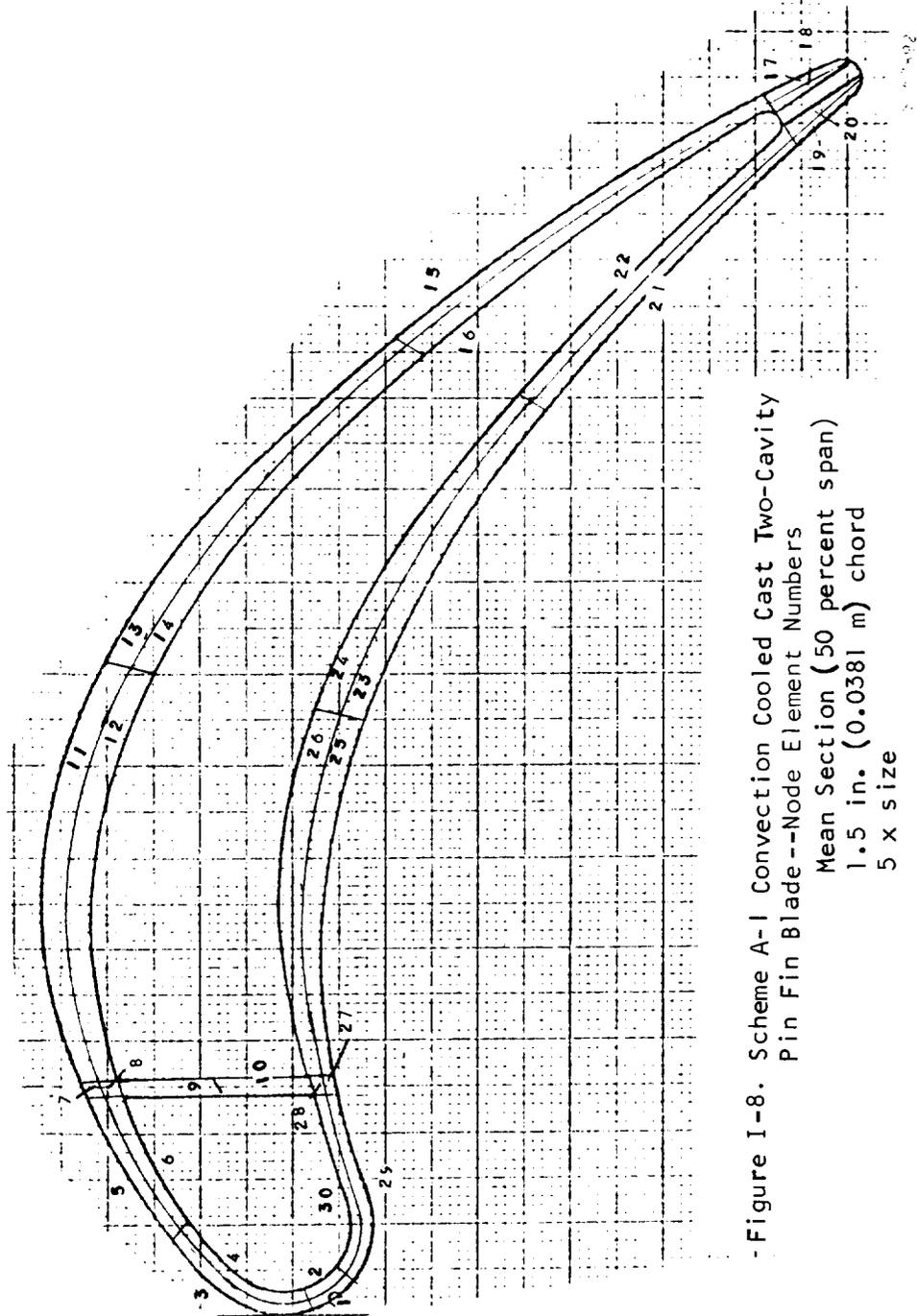
TABLE I-8

SCHEME A-I TWO CAVITY PIN FIN BLADE, I.5 IN.(0.0381 M) CHORD, MEAN SECTION

| ELEMENT NO.	TEMPERATURE	STRESS	LIFE(HRS)
1	1644.0	-30895.9	705.2477
2	1592.0	-14742.5	10 YRS PLUS
3	1541.0	5025.6	10 YRS PLUS
4	1504.0	14903.9	10 YRS PLUS
5	1537.0	20915.5	10 YRS PLUS
6	1479.0	35492.7	21427.0980
7	1598.0	11324.1	10 YRS PLUS
8	1534.0	27388.4	28270.1750
9	1349.0	69067.2	1646.3790
10	1341.0	67493.9	2848.8007
11	1682.0	1405.6	10 YRS PLUS
12	1622.0	17971.4	29173.8150
13	1666.0	14979.1	24757.3640
14*	1610.0	31122.6	1593.3031
15	1644.0	15900.5	32614.5950
16	1607.0	26548.9	4643.8168
17	1702.0	-8931.5	10 YRS PLUS
18	1678.0	-2497.1	10 YRS PLUS
19	1704.0	-13129.5	16963.9410
20	1680.0	-5519.8	10 YRS PLUS
21	1607.0	18269.3	39626.7160
22	1574.0	28760.9	6903.5344
23	1574.0	26078.6	12470.3003
24	1528.0	40478.4	1798.2295
25	1547.0	21958.7	66036.4420
26	1503.0	35466.4	10866.7853
27	1555.0	6632.3	10 YRS PLUS
28	1518.0	17276.3	10 YRS PLUS
29	1584.0	-9328.1	10 YRS PLUS
30	1545.0	1939.1	10 YRS PLUS
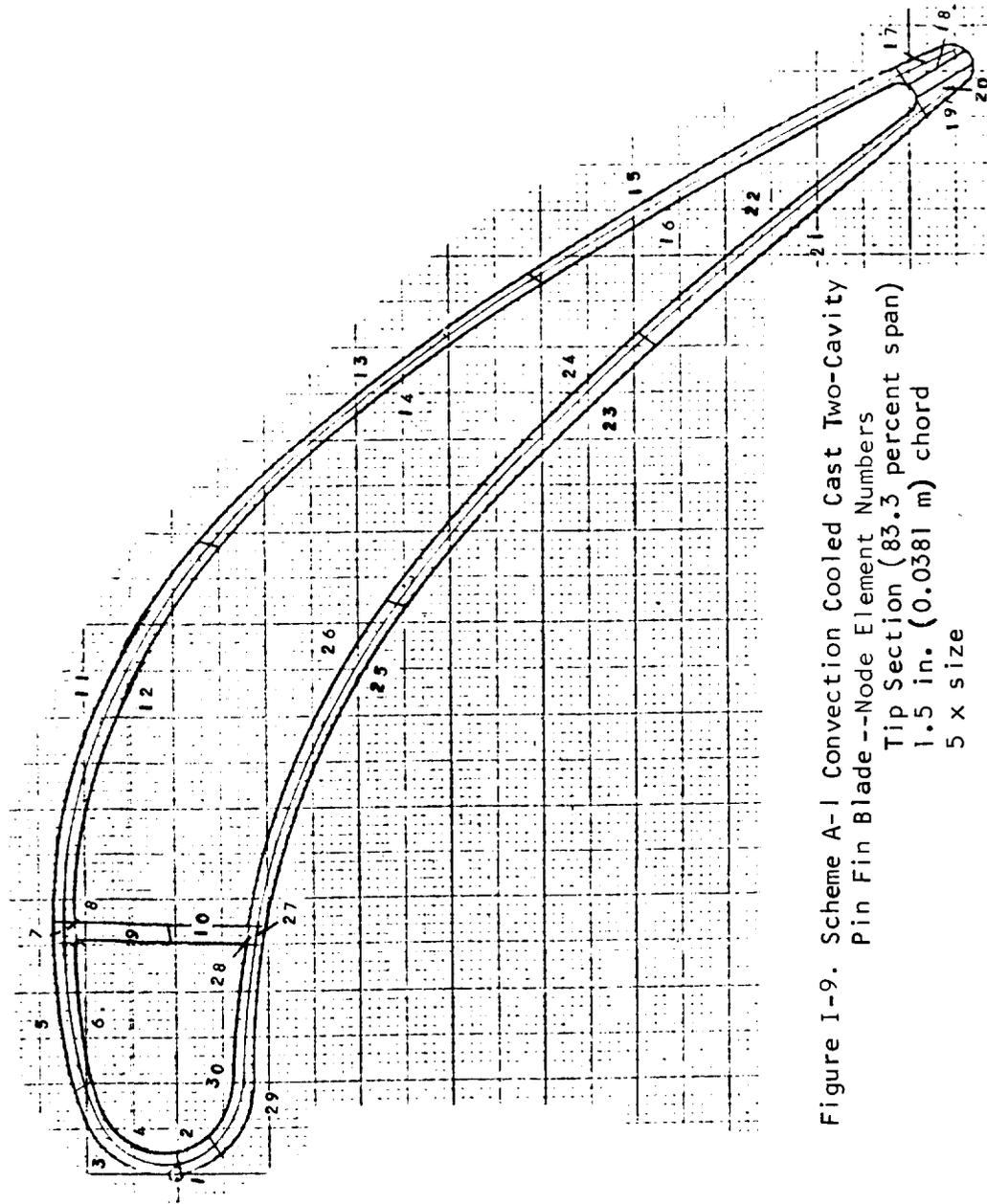
Figure I-9. Scheme A-I Convection Cooled Cast Two-Cavity
Pin Fin Blade--Node Element Numbers
Tip Section (83.3 percent span)
1.5 in. (0.0381 m) chord
5 x size

TABLE I-9

SCHEME A-1   TWO CAVITY PIN FIN BLADE, 1.5 IN. (0.0381 M) CHORD, TIP SECTION

ELEMENT NO.	TEMPERATURE	STRESS	LIFE(HRS)
1	1664.0	-35252.9	296.5767
2	1615.0	-3491.2	10 YRS PLUS
3	1573.0	-15742.6	10 YRS PLUS
4	1538.0	-9322.6	10 YRS PLUS
5	1566.0	11102.1	10 YRS PLUS
6	1527.0	21797.7	10 YRS PLUS
7	1728.0	-20687.2	1002.3198
8	1699.0	-14389.5	6548.3320
9	1503.0	35819.0	16551.6172
10	1433.0	47605.8	9987.3359
11	1797.0	-15721.3	501.7996
12	1775.0	-9700.5	699.5479
13	1790.0	2738.3	1928.8921
14**✗	1770.0	7013.5	1331.6929
15	1787.0	662.9	3102.1870
16	1768.0	4234.2	2411.6165
17	1823.0	-12810.8	470.0059
18	1802.0	-9380.5	402.6985
19	1823.0	-17789.2	194.0857
20	1802.0	-13290.9	692.8699
21	1760.0	-6214.9	1971.4414
22	1741.0	678.1	9341.4062
23	1713.0	-570.8	19130.9766
24	1695.0	6080.1	9848.9961
25	1645.0	474.2	10 YRS PLUS
26	1630.0	5931.2	54412.8203
27	1600.0	-7193.5	93519.1250
28	1559.0	5005.3	10 YRS PLUS
29	1598.0	-22456.1	18553.7539
30	1562.0	-11211.7	10 YRS PLUS

246
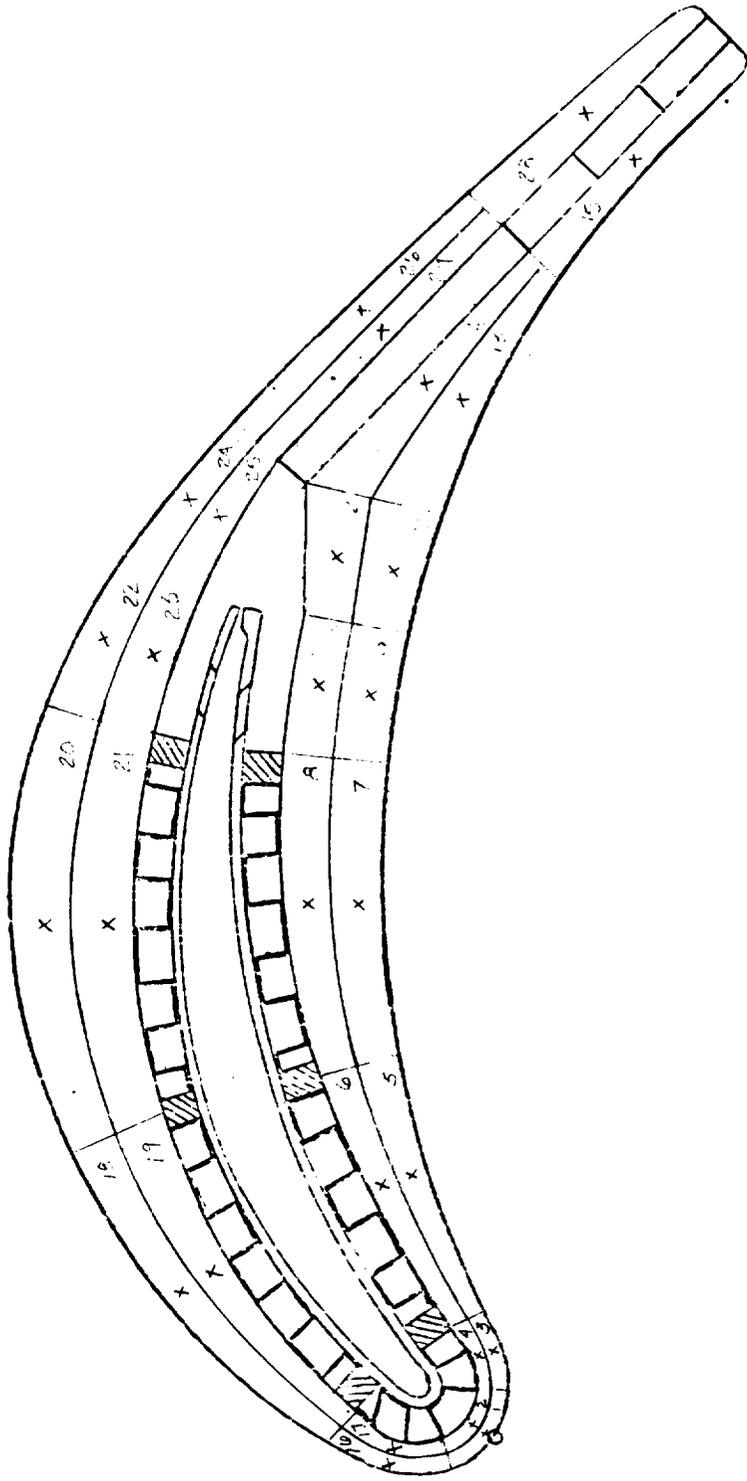
Figure I-10. Scheme A-3 Convection Cooled Fabricated Radial
Flow Plate Fin Blade--Node Element Numbers
Hub Section (16.7 percent span)
0.75 in. (0.01905 m) chord
10 x size

S-67894

247

TABLE I-10

SCHEME A-3 CONVECTION COOLED FABRICATED RADIAL FLOW PLATE FIN BLADE
0.75 IN. (0.01905 M) CHORD, HUB SECTION, 22774 RPM,
TIT = 2300°F (1533.3°K), WCA = 0.01607 LB/SEC/BLADE
(4.04 PERCENT OF HOT GAS FLOW) TCA = 900°F (755.6°K)

ELEMENT NO.	TEMPERATURE	STRESS	LIFE(HRS)
1	1658.0	-15716.3	23892.1820
2	1630.0	-7919.6	10 YRS PLUS
3	1578.0	8507.9	10 YRS PLUS
4	1552.0	14680.8	10 YRS PLUS
5	1442.0	41000.8	18471.2750
6	1412.0	47344.7	14588.3508
7	1444.0	38560.0	29141.2090
8	1405.0	46175.8	22160.6840
9	1437.0	41600.7	19257.7370
10*	1375.0	55321.1	10494.1478
11	1468.0	35022.6	32905.0760
12	1414.0	46290.3	16588.0910
13	1480.0	35787.1	19447.8250
14	1441.0	44267.0	10718.3926
15	1561.0	23502.4	31557.3090
16	1592.0	-877.4	10 YRS PLUS
17	1568.0	5894.6	10 YRS PLUS
18	1468.0	22123.8	10 YRS PLUS
19	1413.0	38135.8	81944.9600
20	1466.0	16869.6	10 YRS PLUS
21	1386.0	40850.3	10 YRS PLUS
22	1446.0	26015.1	10 YRS PLUS
23	1383.0	44788.9	55629.8810
24	1481.0	21509.9	10 YRS PLUS
25	1443.0	32959.2	10 YRS PLUS
26	1523.0	19539.1	10 YRS PLUS
27	1490.0	29346.9	64189.6950
28	1569.0	18989.4	10 YRS PLUS

Leading Edge W_{CLE} = 0.00119 lb/sec/blade (0.299 percent of hot gas flow)

Pressure Side W_{CAP} = 0.00133 lb/sec/blade (0.334 percent of hot gas flow)

Suction Side W_{CAS} = 0.00476 lb/sec/blade (1.20 percent of hot gas flow)
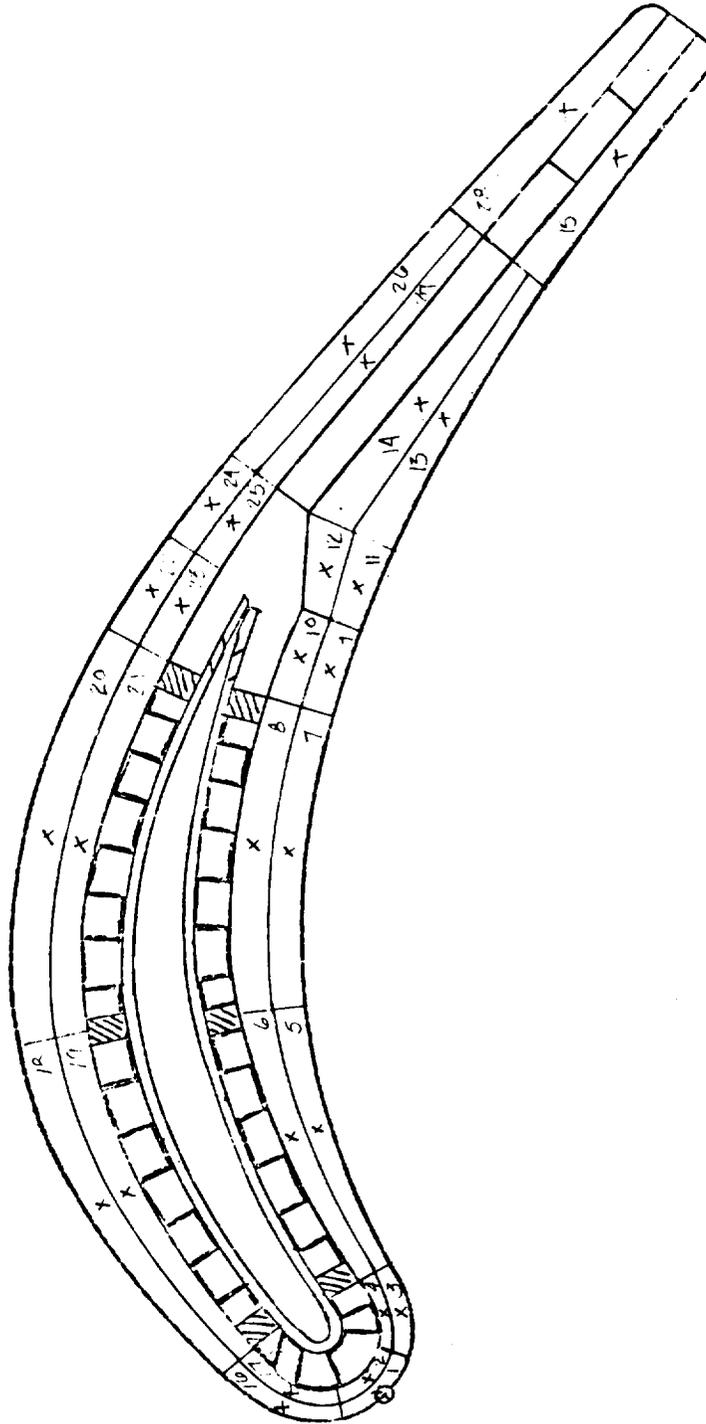
Trailing Edge W_{CTE} = 0.00293 lb/sec/blade (0.74 percent of hot gas flow)

248

Figure I-II. Scheme A-3 Convection Cooled Fabricated Radial Flow Plate Fin Blade--Node Element Numbers

Mean Section (50 percent span)
0.75 in. (0.01905 m) chord
10 x size

S-67895

249

TABLE I-11

SCHEME A-3 CONVECTION COOLED FABRICATED RADIAL FLOW PLATE
FIN BLADE, 0.75 IN. (0.01905 M) CHORD, MEAN SECTION

ELEMENT NO.	TEMPERATURE	STRESS	LIFE(HRS)
1	1772.0	-7767.6	43247.6480
2	1750.0	-2407.8	10 YRS PLUS
3	1720.0	7439.8	10 YRS PLUS
4	1698.0	12845.4	21756.4990
5	1605.0	29044.1	2847.6297
6*	1585.0	32307.8	2360.9156
7	1599.0	17920.6	55706.5290
8	1579.0	19553.4	55094.7280
9	1512.0	38711.4	4036.0058
10	1471.0	46087.6	3312.0235
11	1528.0	34369.3	6938.9921
12	1489.0	40875.8	4904.6873
13	1565.0	26829.6	13512.7570
14	1527.0	34263.7	7305.5142
15	1639.0	13022.2	10 YRS PLUS
16	1724.0	-1884.2	10 YRS PLUS
17	1702.0	5523.4	10 YRS PLUS
18	1583.0	16205.7	10 YRS PLUS
19	1542.0	29149.0	15218.0982
20	1550.0	6279.8	10 YRS PLUS
21	1503.0	22282.9	10 YRS PLUS
22	1491.0	23581.6	10 YRS PLUS
23	1441.0	40177.4	21982.1590
24	1519.0	19043.7	10 YRS PLUS
25	1482.0	31666.3	47541.5900
26	1578.0	10883.0	10 YRS PLUS
27	1543.0	22955.0	59222.2320
28	1638.0	6653.5	10 YRS PLUS

Trailing Edge W_{CTE} = 0.00293 lb/sec/blade (0.74 percent of hot gas flow)
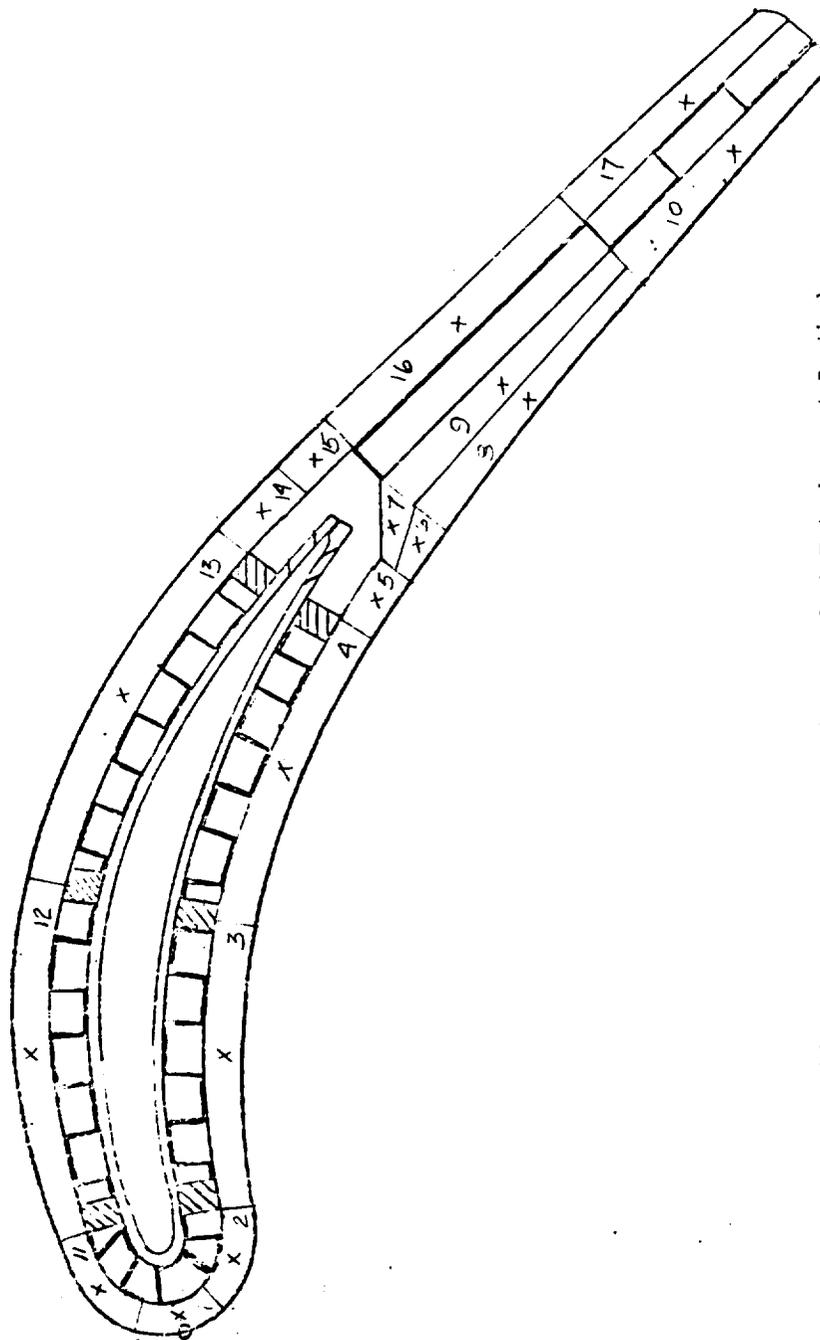
Figure I-12. Scheme A-3 Convection Cooled Fabricated Radial
Flow Plate Fin Blade--Node Element Numbers

Tip Section (83.3 percent span)
0.75 in. (0.01905 m) chord
10 x size

S-67896

251

TABLE I-12

SCHEME A-3 CONVECTION COOLED FABRICATED RADIAL FLOW PLATE
FIN BLADE, 0.75 IN. (0.01905 M) CHORD, TIP SECTION

ELEMENT NO.	TEMPERATURE	STRESS	LIFE(HRS)
1	1828.0	-13587.8	366.2828
2	1797.0	-2156.2	1835.7014
3*	1686.0	8152.4	8090.4435
4	1714.0	-23487.8	830.1404
5	1518.0	28893.0	45129.9820
6	1537.0	23062.2	86765.6910
7	1505.0	26469.2	10 YRS PLUS
8	1575.0	12759.9	10 YRS PLUS
9	1537.0	17832.9	10 YRS PLUS
10	1627.0	650.4	10 YRS PLUS
11	1779.0	-12941.1	1252.2301
12	1590.0	6289.5	10 YRS PLUS
13	1532.0	-4628.7	10 YRS PLUS
14	1465.0	14219.7	10 YRS PLUS
15	1503.0	6805.7	10 YRS PLUS
16	1574.0	-7316.5	10 YRS PLUS
17	1640.0	-15852.0	22246.9490

Trailing Edge W_{CTE} = 0.00293 lb/sec/blade (0.74 percent of hot gas flow)
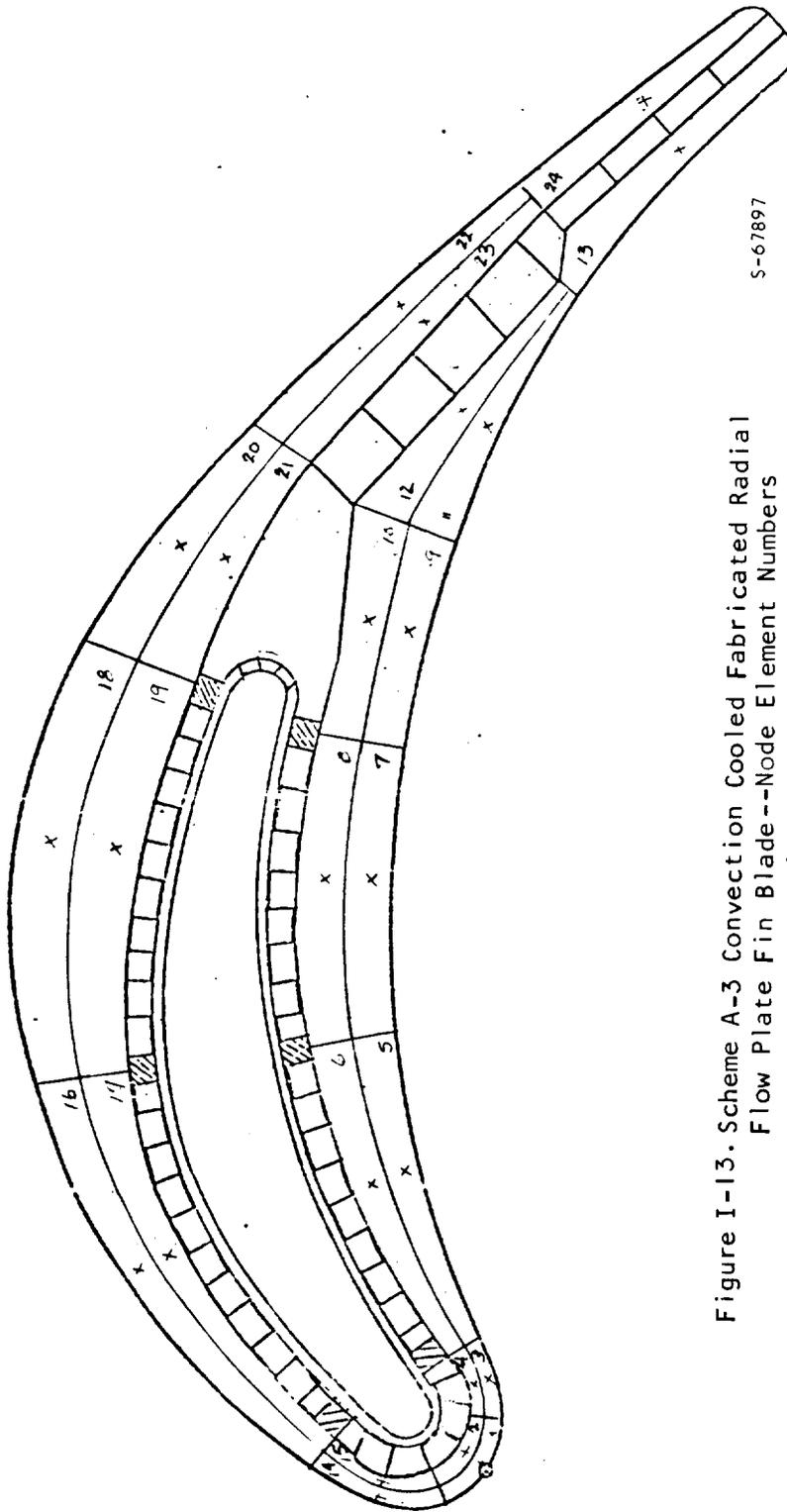
Figure I-13. Scheme A-3 Convection Cooled Fabricated Radial Flow Plate Fin Blade--Node Element Numbers Hub Section (16.7 percent span) 1.0 in. (0.0254 m) chord 10 x size

S-67897

253

TABLE I-13

SCHEME A-3 CONVECTION COOLED FABRICATED RADIAL FLOW PLATE FIN BLADE,
1.0 IN. (0.0254 M) CHORD, HUB SECTION,
23183 RPM, TIT = 2400°F (1588.9°K), WCA = 0.02203 LB/SEC/BLADE
(4.25 PERCENT OF HOT GAS FLOW) TCA = 900°F (755.6°K)

ELEMENT NO.	TEMPERATURE	STRESS	LIFE(HRS)
1	1669.0	-14559.0	26321.4460
2	1619.0	75.3	10 YRS PLUS
3	1583.0	11414.3	10 YRS PLUS
4	1549.0	20118.5	10 YRS PLUS
5	1471.0	38775.9	12608.3952
6	1423.0	50206.1	6346.0369
7	1485.0	34357.0	23421.2240
8	1436.0	45719.5	9603.3671
9	1470.0	40047.6	9684.1773
10*	1412.0	53852.8	4569.9091
11	1515.0	31132.1	20769.4400
12	1485.0	38269.9	9502.8161
13	1538.0	31984.3	9003.7988
14	1595.0	4145.5	10 YRS PLUS
15	1560.0	13821.3	10 YRS PLUS
16	1501.0	21542.2	10 YRS PLUS
17	1441.0	38413.9	32967.2410
18	1508.0	17377.1	10 YRS PLUS
19	1406.0	46325.8	20935.2210
20	1495.0	25716.2	10 YRS PLUS
21	1419.0	47259.5	12038.1291
22	1570.0	13539.0	10 YRS PLUS
23	1533.0	24314.5	58069.1000
24	1551.0	27400.7	17516.1430

Leading Edge W_{CLE} = 0.002 lb/sec/blade (0.385 percent of hot gas flow)

Pressure Side WCAP = 0.00181 lb/sec/blade (0.349 percent of hot gas flow)

Suction Side W_{CAS} = 0.00652 lb/sec/blade (1.25 percent of hot gas flow)

Trailing Edge W_{CTE} = 0.0039 lb/sec/blade (0.752 percent of hot gas flow)
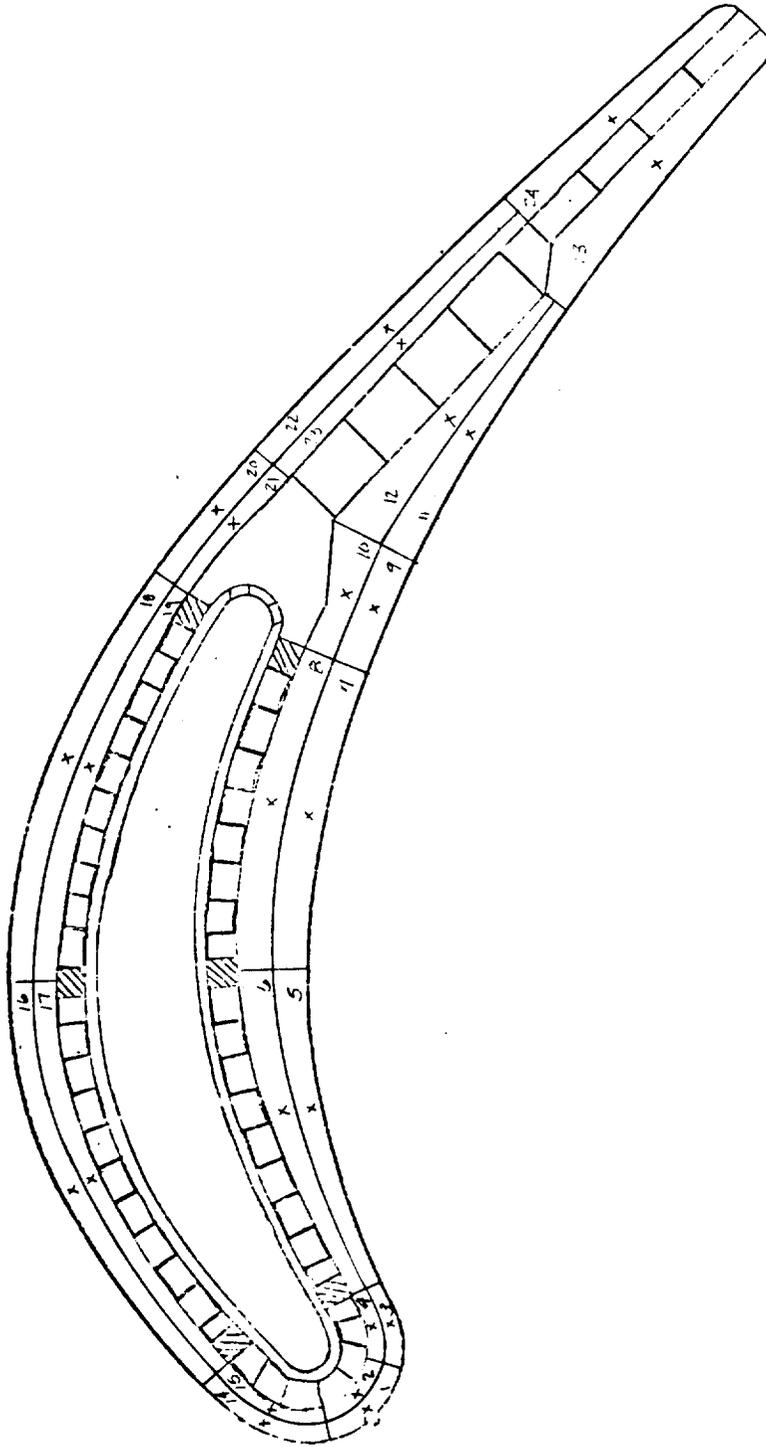
Figure I-14. Scheme A-3 Convection Cooled Fabricated Radial Flow Plate Fin Blade--Node Element Numbers Mean Section (50 percent span) 1.0 in. (0.0254 m) chord 10 x size

S-67898

255

TABLE I-14

SCHEME A-3 CONVECTION COOLED FABRICATED RADIAL FLOW PLATE
FIN BLADE, I.0 IN. (0.0254 M), CHORD, MEAN SECTION

ELEMENT NO.	TEMPERATURE	STRESS	LIFE(HRS)
1	1782.0	-4674.1	10 YRS PLUS
2	1742.0	6009.2	10 YRS PLUS
3	1720.0	17006.2	3177.1240
4	1690.0	20559.0	2085.4890
5	1625.0	27852.9	2191.5814
6 *	1600.0	33673.0	1185.3167
7	1655.0	6179.6	10 YRS PLUS
8	1628.0	11184.1	10 YRS PLUS
9	1540.0	35431.6	3933.8093
10	1488.0	46756.1	1841.0897
11	1581.0	24131.6	15812.6137
12	1547.0	31173.4	8427.3979
13	1598.0	21937.2	16097.2810
14	1714.0	9501.5	53218.1330
15	1687.0	17761.0	5683.3891
16	1612.0	17894.1	39317.8650
17	1574.0	29622.6	5709.1508
18	1571.0	10863.9	10 YRS PLUS
19	1528.0	24421.8	65420.7520
20	1492.0	32583.9	28781.6210
21	1453.0	44639.8	7098.0806
22	1609.0	5630.4	10 YRS PLUS
23	1581.0	15201.4	10 YRS PLUS
24	1602.0	15476.0	10 YRS PLUS

Trailing Edge W_{CTE} = 0.0039 lb/sec/blade (0.752 percent of hot gas flow)
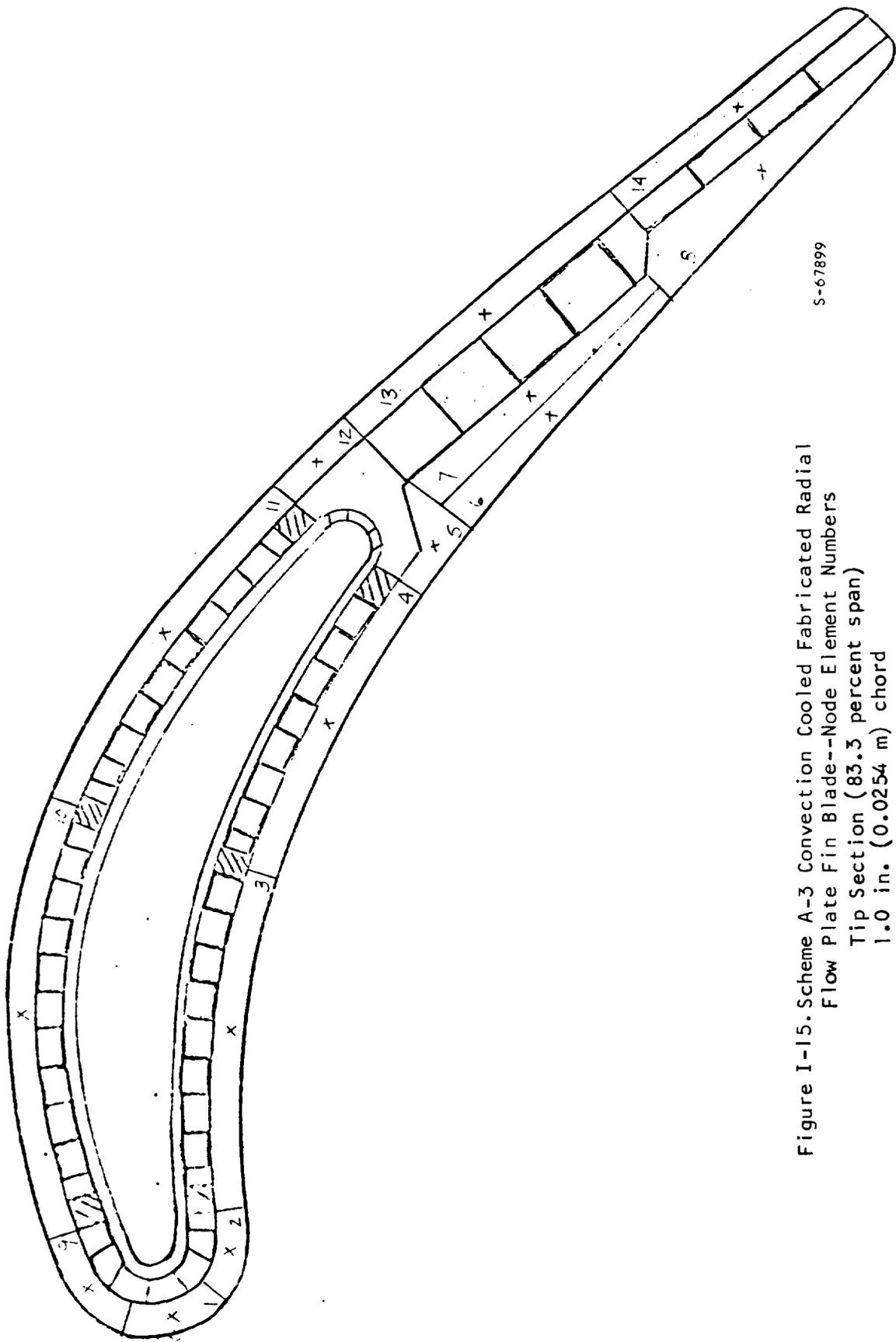
Figure I-15. Scheme A-3 Convection Cooled Fabricated Radial Flow Plate Fin Blade--Node Element Numbers Tip Section (83.3 percent span) 1.0 in. (0.0254 m) chord 10 x size

S-67899

257

TABLE I-15

SCHEME A-3 CONVECTION COOLED FABRICATED RADIAL FLOW PLATE
FIN BLADE, 1.0 IN. (0.0254 M) CHORD, TIP SECTION

ELEMENT NO.	TEMPERATURE	STRESS	LIFE(HRS)
1	1830.0	-4017.0	603.7542
2*	1786.0	9052.6	617.0595
3	1720.0	5465.9	5998.7054
4	1785.0	-28625.5	64.1427
5	1504.0	28633.1	70644.9710
6	1589.0	12604.9	10 YRS PLUS
7	1555.0	17238.7	10 YRS PLUS
8	1609.0	4225.9	10 YRS PLUS
9	1779.0	-1273.0	3325.6627
10	1621.0	7305.8	51829.9150
11	1561.0	-2302.5	10 YRS PLUS
12	1488.0	17661.0	10 YRS PLUS
13	1605.0	-12430.2	10 YRS PLUS
14	1614.0	-7681.0	57760.3820

Trailing Edge W_{CTE} = 0.0039 lb/sec/blade (0.752 percent of hot gas flow)

258
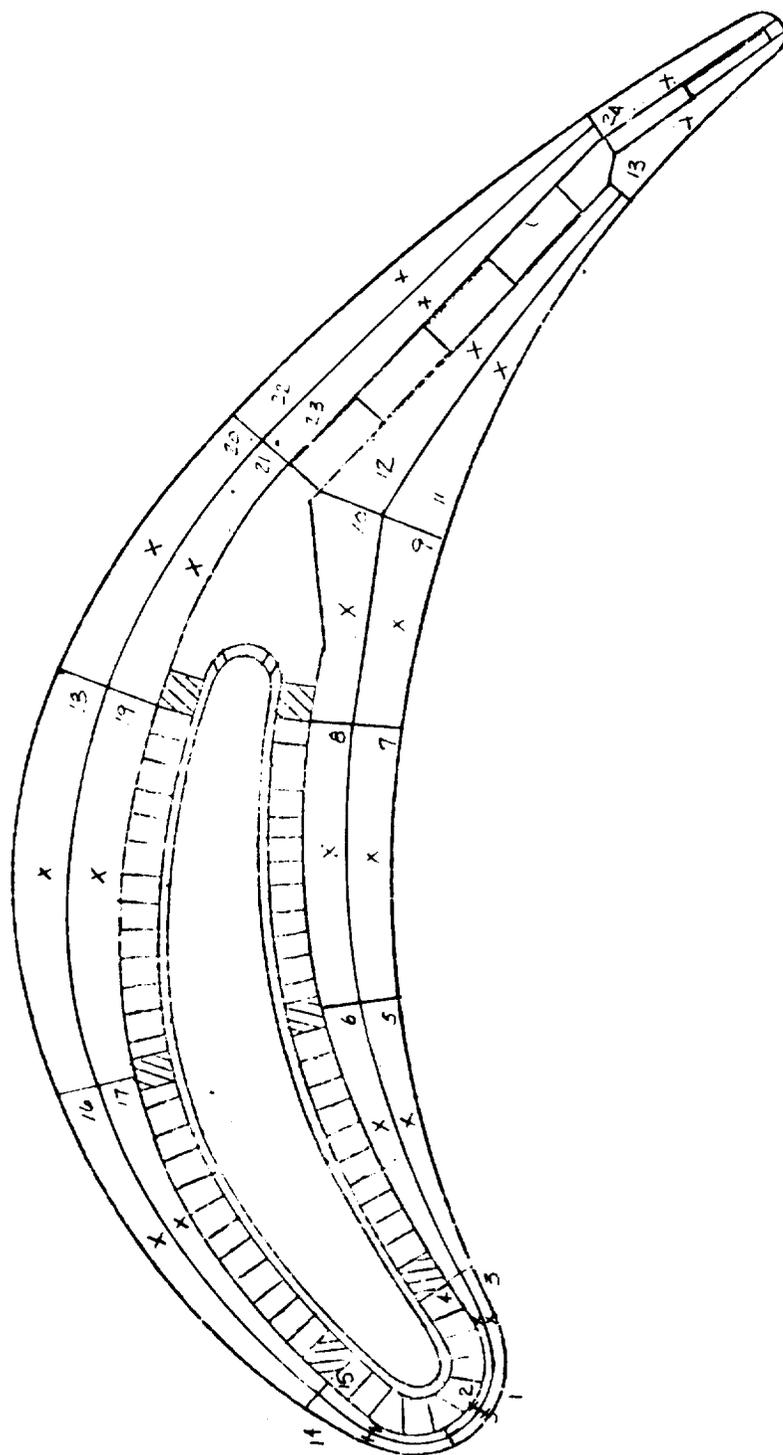
Figure I-16. Scheme A-3 Convection Cooled Fabricated Radial Flow Plate Fin Blade--Node Element Numbers Hub Section (16.7 percent span) 1.5 in. (0.0381 m) chord 5 x size

S-67901

259

TABLE I-16

SCHEME A-3 CONVECTION COOLED FABRICATED RADIAL FLOW PLATE FIN BLADE,
1.5 IN. (0.0381 M) CHORD, HUB SECTION,
23183 RPM, TIT = 2400°F (1588.9°K), WCA = 0.02946 LB/SEC/BLADE
(3.82 PERCENT OF HOT GAS FLOW) TCA = 900°F (755.6°K)

ELEMENT NO.	TEMPERATURE	STRESS	LIFE(HRS)
1	1623.0	4856.5	10 YRS PLUS
2	1587.0	14853.1	10 YRS PLUS
3	1537.0	29345.9	16738.0010
4	1504.0	37579.2	6521.7969
5	1533.0	26220.3	37820.9170
6	1465.0	37474.8	11414.5140
7	1574.0	13380.2	10 YRS PLUS
8	1511.0	28157.2	45781.5540
9	1511.0	31666.1	20606.9040
10	1428.0	50936.5	4823.5998
11	1527.0	32681.3	10440.8610
12	1490.0	41270.0	4458.1719
13	1558.0	34101.0	3256.5895
14	1542.0	21716.0	80422.9920
15	1509.0	30785.7	26655.4180
16	1497.0	22889.8	10 YRS PLUS
17	1421.0	43977.6	20321.1400
18	1509.0	13858.6	10 YRS PLUS
19	1383.0	49585.5	23331.0840
20	1504.0	20939.7	10 YRS PLUS
21	1406.0	48708.6	13668.4348
22	1577.0	14269.4	10 YRS PLUS
23	1526.0	29212.5	23494.3300
24*	1559.0	32658.1	4368.0120

Leading Edge W_{CLE} = 0.00376 lb/sec/blade (0.487 percent of hot gas flow)

Pressure Side W_{CAP} = 0.00295 lb/sec/blade (0.382 percent of hot gas flow)

Suction Side W_{CAS} = 0.00905 lb/sec/blade (1.17 percent of hot gas flow)

Trailing Edge W_{CTE} = 0.005 lb/sec/blade (0.648 percent of hot gas flow)

260
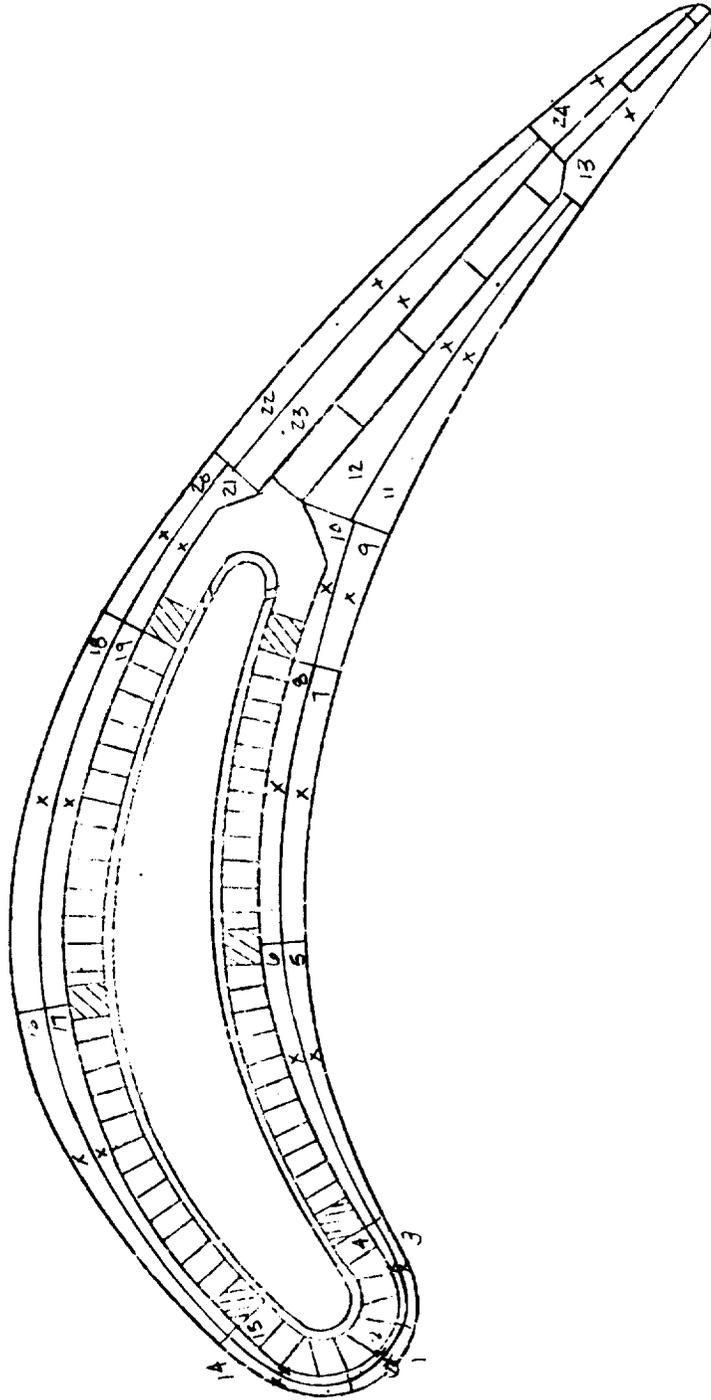
Figure I-17. Scheme A-3 Convection Cooled Fabricated Radial
Flow Plate Fin Blade--Node Element Numbers

Mean Section (50 percent span)
1.5 in. (0.0381 m) span
5 x size

S-67902

TABLE I-17

SCHEME A-3 CONVECTION COOLED FABRICATED RADIAL FLOW PLATE
FIN BLADE, 1.5 IN. (0.0381 M) CHORD, MEAN SECTION

ELEMENT NO.	TEMPERATURE	STRESS	LIFE(HRS)
1	1718.0	-11472.4	20368.3510
2	1688.0	-2953.6	10 YRS PLUS
3	1644.0	11153.7	10 YRS PLUS
4	1619.0	18366.1	27644.6900
5	1575.0	24149.0	18564.5180
6	1547.0	30528.8	9732.7206
7	1579.0	19759.3	51274.3740
8	1547.0	26796.5	22406.5460
9	1487.0	45569.0	2319.6806
10*	1430.0	58994.6	1096.7243
11	1602.0	19515.7	29566.6310
12	1562.0	29041.8	8984.4438
13	1650.0	11989.7	10 YRS PLUS
14	1646.0	4021.8	10 YRS PLUS
15	1621.0	12019.9	10 YRS PLUS
16	1590.0	6724.4	10 YRS PLUS
17	1543.0	20644.0	10 YRS PLUS
18	1567.0	7124.1	10 YRS PLUS
19	1503.0	25966.6	10 YRS PLUS
20	1518.0	25190.5	73366.8620
21	1464.0	40812.9	10073.6791
22	1640.0	1488.2	10 YRS PLUS
23	1590.0	18278.3	63183.7310
24	1635.0	14259.3	72585.8140

Trailing Edge W_{CTE} = 0.00435 lb/sec/blade (0.564 percent of hot gas flow)
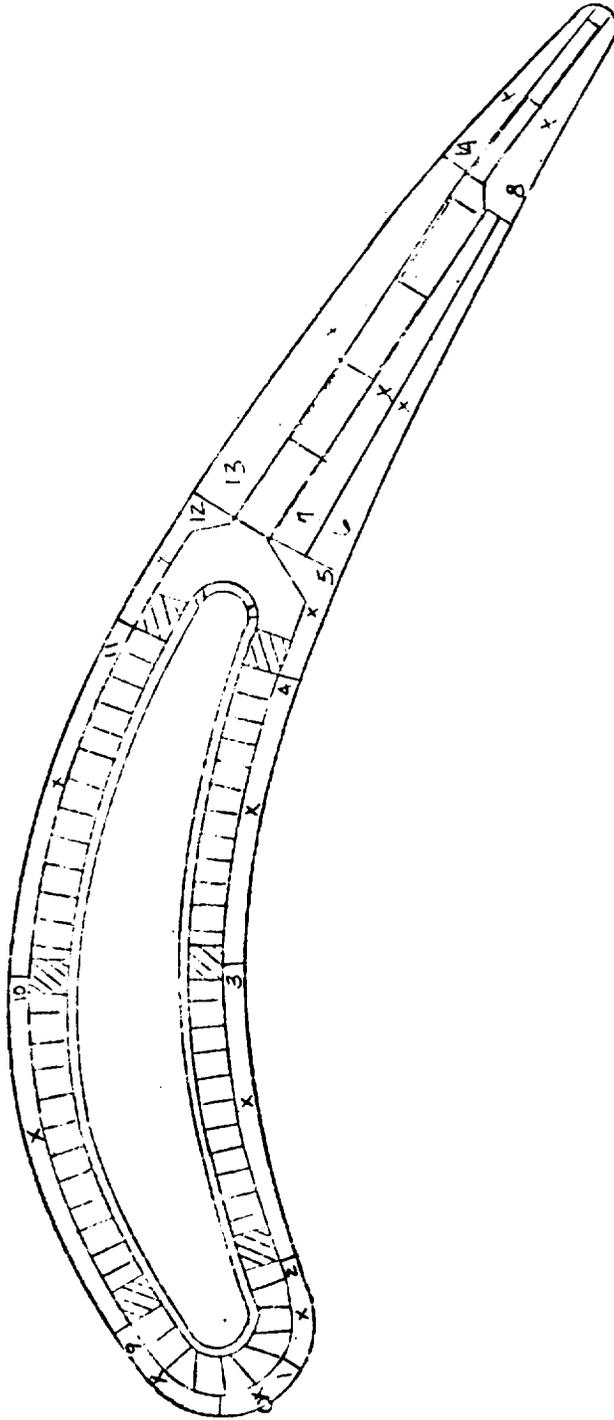
Figure I-18. Scheme A-3 Convection Cooled Fabricated Radial
Flow Plate Fin Blade--Node Element Numbers

Tip Section (83.3 percent span)
1.5 in. (0.0381 m) chord
5 x size

S-67903

TABLE I-18

SCHEME A-3 CONVECTION COOLED FABRICATED RADIAL FLOW PLATE FIN BLADE, 1.5 IN. (0.0381 M) CHORD, TIP SECTION

ELEMENT NO.	TEMPERATURE	STRESS	LIFE(HRS)
1	1768.0	-9508.0	854.0415
2	1736.0	1741.6	8542.3086
3	1673.0	2319.0	37214.8550
4	1702.0	-19479.3	2342.5043
5*	1452.0	50356.9	3270.8296
6	1613.0	5390.4	96251.2290
7	1572.0	13759.4	10 YRS PLUS
8	1656.0	-2165.1	59896.0730
9	1701.0	-3216.1	15154.4791
10	1596.0	-2036.2	10 YRS PLUS
11	1524.0	2656.7	10 YRS PLUS
12	1504.0	11246.2	10 YRS PLUS
13	1622.0	-10925.7	93056.8400
14	1645.0	-5700.4	38406.6420

Trailing Edge W_{CTE} = 0.00435 lb/sec/blade (0.564 percent of hot gas flow)
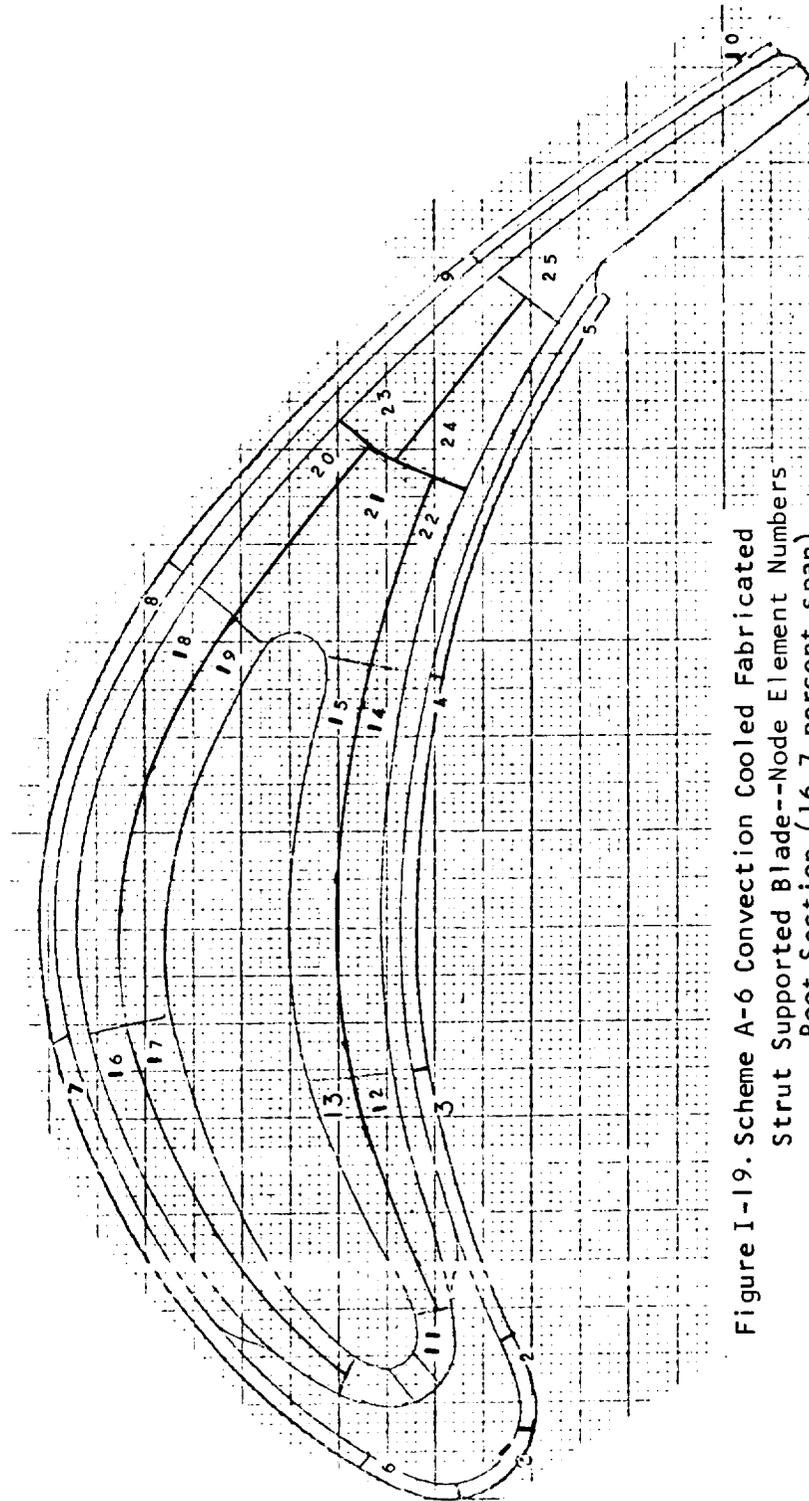
Figure I-19. Scheme A-6 Convection Cooled Fabricated
Strut Supported Blade--Node Element Numbers
Root Section (16.7 percent span)
0.75 in. (0.01905 m) chord
10 x size

S-67904

265

TABLE I-19

SCHEME A-6 STRUT SUPPORTED BLADE, 0.75 IN. (0.01905 M) CHORD,
HUB SECTION, 23384 RPM, TIT = 2450°F (1616.7°K),
WCA = 0.015 LB/SEC/BLADE (3.9 PERCENT OF HOT GAS FLOW),
TCA = 900°F (755.6°K)

ELEMENT NO.	TEMPERATURE	STRESS	LIFE(HRS)
1	1505.0	-11712.8	10 YRS PLUS
2	1495.0	-5387.1	10 YRS PLUS
3	1462.0	12373.3	10 YRS PLUS
4	1462.0	28569.3	10 YRS PLUS
5	1590.0	11200.1	10 YRS PLUS
6	1492.0	-7437.9	10 YRS PLUS
7	1559.0	-12838.4	10 YRS PLUS
8	1573.0	7376.1	10 YRS PLUS
9	1640.0	2890.7	10 YRS PLUS
10	1635.0	11544.3	10 YRS PLUS
11	1223.0	67391.3	10 YRS PLUS
12	1345.0	44129.7	10 YRS PLUS
13	1353.0	41783.8	10 YRS PLUS
14	1356.0	56337.4	15528.2077
15	1360.0	56788.5	12647.7022
16	1417.0	26909.7	10 YRS PLUS
17	1423.0	25696.9	10 YRS PLUS
18	1451.0	38197.0	25815.4820
19	1451.0	37001.4	34175.8260
20 *	1491.0	39029.3	6734.5827
21	1489.0	36825.7	11828.5494
22	1468.0	40555.6	9391.5451
23	1531.0	33732.8	7372.7018
24	1526.0	32860.1	10310.8941
25	1581.0	25526.4	11639.2080

Hub Section Cooling Flow

Pressure Side W_{CAP} = 0.0025 lb/sec/blade (0.65 percent of hot gas flow)

Suction Side W_{CAS} = 0.0025 lb/sec/blade (0.65 percent of hot gas flow)

266
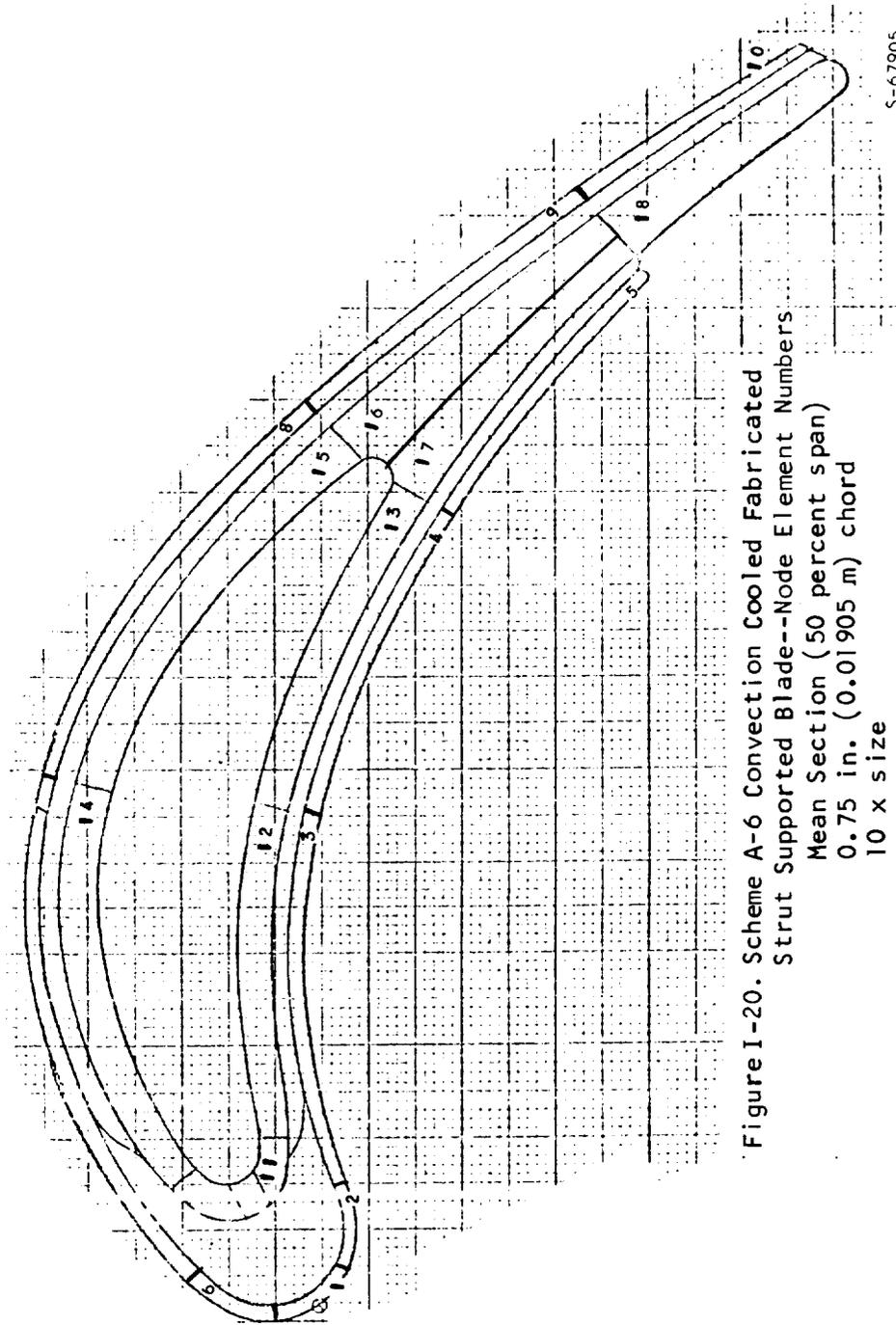
Figure I-20. Scheme A-6 Convection Cooled Fabricated
Strut Supported Blade--Node Element Numbers...
Mean Section (50 percent span)
0.75 in. (0.01905 m) chord
10 x size

S-67905

267

TABLE I-20

SCHEME A-6 STRUT SUPPORTED BLADE, 0.75 IN. (0.01905 M) CHORD,
MEAN SECTION

ELEMENT NO.	TEMPERATURE	STRESS	LIFE(HRS)
1	1558.0	-20427.2	73237.8490
2	1527.0	-8827.9	10 YRS PLUS
3	1507.0	16009.4	10 YRS PLUS
4	1528.0	31529.9	13165.6031
5	1689.0	-4979.0	10 YRS PLUS
6	1537.0	-10808.4	10 YRS PLUS
7	1663.0	-18812.0	7415.3464
8	1657.0	12375.8	75421.9710
9	1712.0	-96.2	10 YRS PLUS
10	1699.0	3456.5	10 YRS PLUS
11	1309.0	56012.4	72524.1970
12	1438.0	38471.3	35558.9250
13	1471.0	49981.1	1689.3784
14	1565.0	13091.6	10 YRS PLUS
15	1579.0	32028.9	2940.9876
16	1622.0	23224.3	6416.8622
17	1618.0	20852.0	12122.8848
18	1635.0	19058.0	14219.1140

Mean Section Cooling Flow

Pressure Side W_{CAP} = 0.0025 lb/sec/blade (0.65 percent of hot gas flow)

Suction Side W_{CAS} = 0.0025 lb/sec/blade (0.65 percent of hot gas flow)
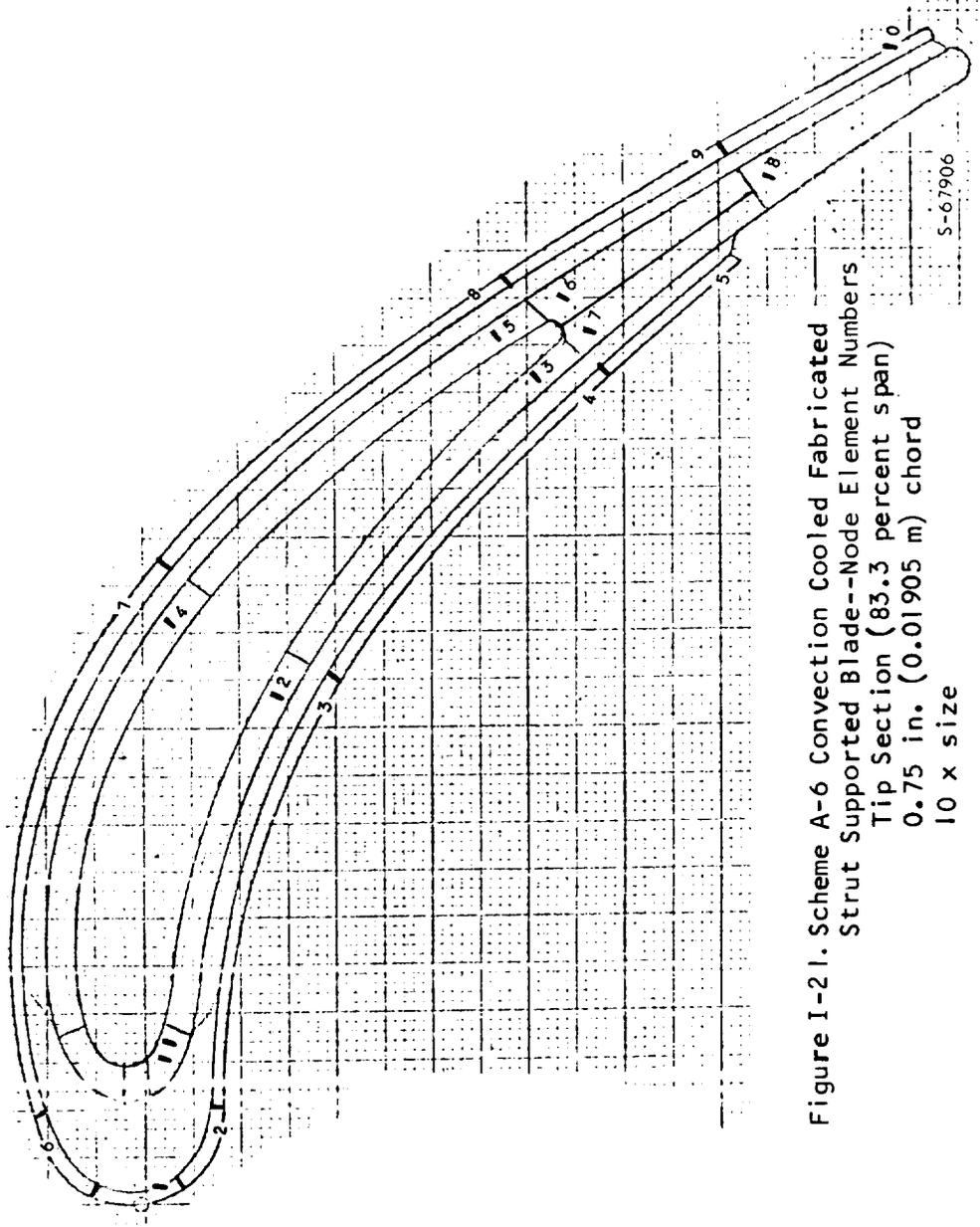
Figure I-21. Scheme A-6 Convection Cooled Fabricated
Strut Supported Blade--Node Element Numbers
Tip Section (83.3 percent span)
0.75 in. (0.01905 m) chord
10 x size

S-67906

TABLE I-21

SCHEME A-6 STRUT SUPPORTED BLADE, 0.75 IN. (0.01905 M) CHORD, TIP SECTION

ELEMENT NO.	TEMPERATURE	STRESS	LIFE (HRS)
1	1572.0	-38285.2	1594.5934
2	1546.0	-32848.4	9384.1541
3	1535.0	-3191.9	10 YRS PLUS
4	1622.0	627.0	10 YRS PLUS
5	1720.0	-17072.3	2372.6690
6	1566.0	-26052.3	21414.2383
7	1716.0	-19176.7	1766.0599
8	1730.0	-1846.4	9695.1717
9	1754.0	-8977.4	1314.9548
10	1739.0	-10100.3	5443.0073
11	1390.0	18385.9	10 YRS PLUS
12	1487.0	17395.2	10 YRS PLUS
13	1575.0	17713.5	38127.8125
14	1649.0	-4545.2	43957.6875
15 *	1680.0	4043.5	21796.0459
16	1678.0	2022.1	34752.3393
17	1674.0	-994.5	47593.7773
18	1685.0	-4077.5	19071.2461

Tip Section Cooling Flow

Pressure Side W_{CAP} = 0.0025 lb/sec/blade (0.65 percent of hot gas flow)

Suction Side W_{CAS} = 0.0025 lb/sec/blade (0.65 percent of hot gas flow)
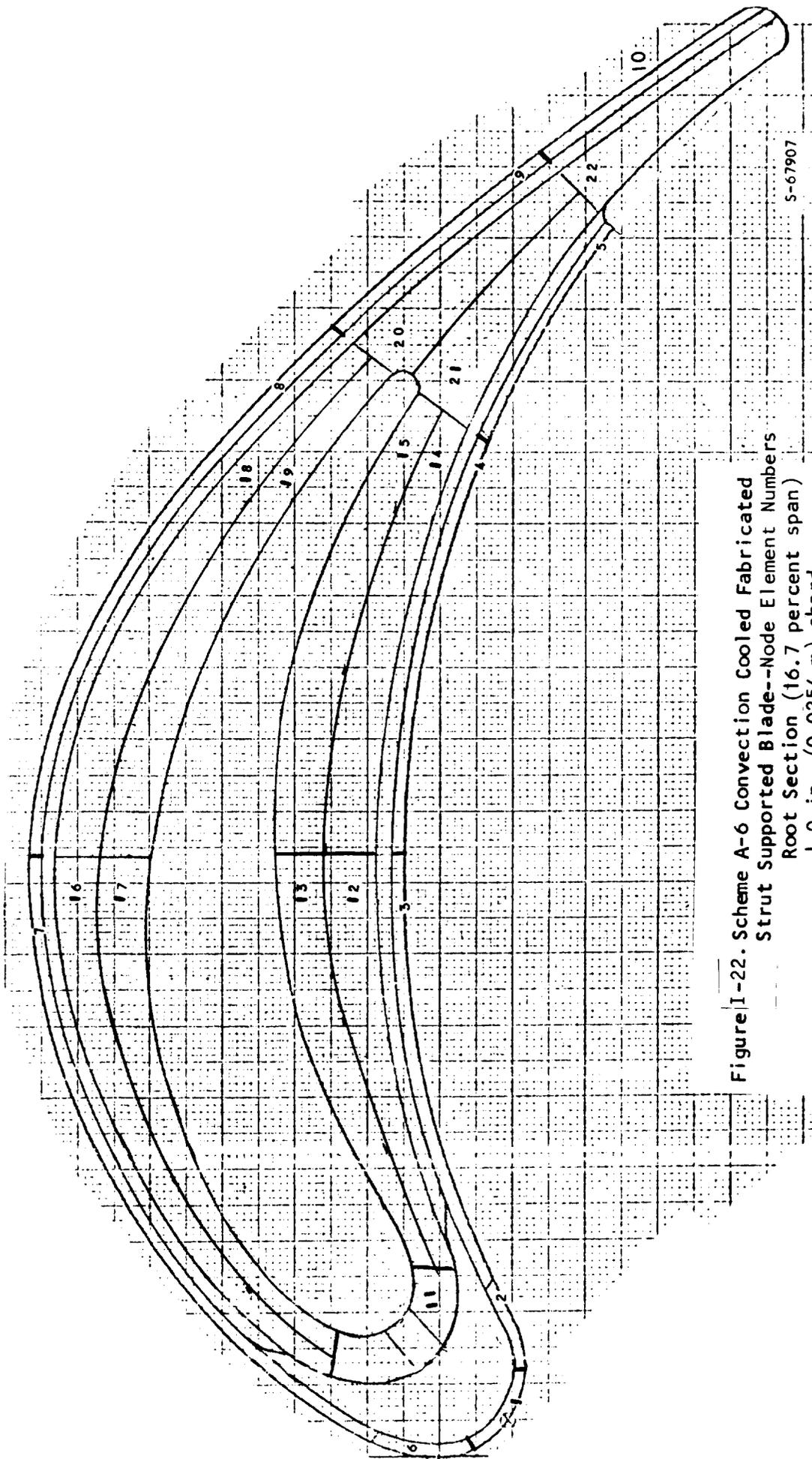
Figure I-22. Scheme A-6 Convection Cooled Fabricated
Strut Supported Blade--Node Element Numbers
Root Section (16.7 percent span)
1.0 in. (0.0254 m) chord
10 x size

S-67907

271

TABLE I-22

SCHEME A-6 STRUT SUPPORTED BLADE, 1.0 IN. (0.0254 M) CHORD,
HUB SECTION, 23585 RPM, TIT = 2500°F (1633.3°K),
WCA = 0.02 LB/SEC/BLADE (3.9 PERCENT OF HOT GAS FLOW),
TCA = 900°F (755.6°K)

ELEMENT NO.	TEMPERATURE	STRESS	LIFE(HRS)
1	1576.0	-14481.7	10 YRS PLUS
2	1559.0	-6864.0	10 YRS PLUS
3	1490.0	20594.1	10 YRS PLUS
4	1523.0	26923.5	42915.4460
5	1631.0	7991.5	10 YRS PLUS
6	1562.0	-9453.7	10 YRS PLUS
7	1533.0	3779.6	10 YRS PLUS
8	1561.0	18269.9	10 YRS PLUS
9	1633.0	10200.3	10 YRS PLUS
10	1608.0	24448.6	7131.9737
11	1153.0	85845.3	26771.9340
12	1376.0	50245.1	25630.0280
13	1362.0	48500.3	29280.9810
14	1414.0	55494.8	3218.1568
15	1418.0	54891.4	3192.4415
16	1415.0	36665.4	10 YRS PLUS
17	1426.0	34208.5	10 YRS PLUS
18	1456.0	46262.7	4908.7982
19	1461.0	44232.6	6061.0212
20	1550.0	32841.3	5350.4752
21	1551.0	31563.9	6922.8401
22*	1570.0	34178.9	2324.3245

Hub Section Cooling Flow

Pressure Side W_{CAP} = 0.00266 lb/sec/blade (0.52 percent of hot gas flow)

Suction Side W_{CAS} = 0.004 lb/sec/blade (0.78 percent of hot gas flow)

272
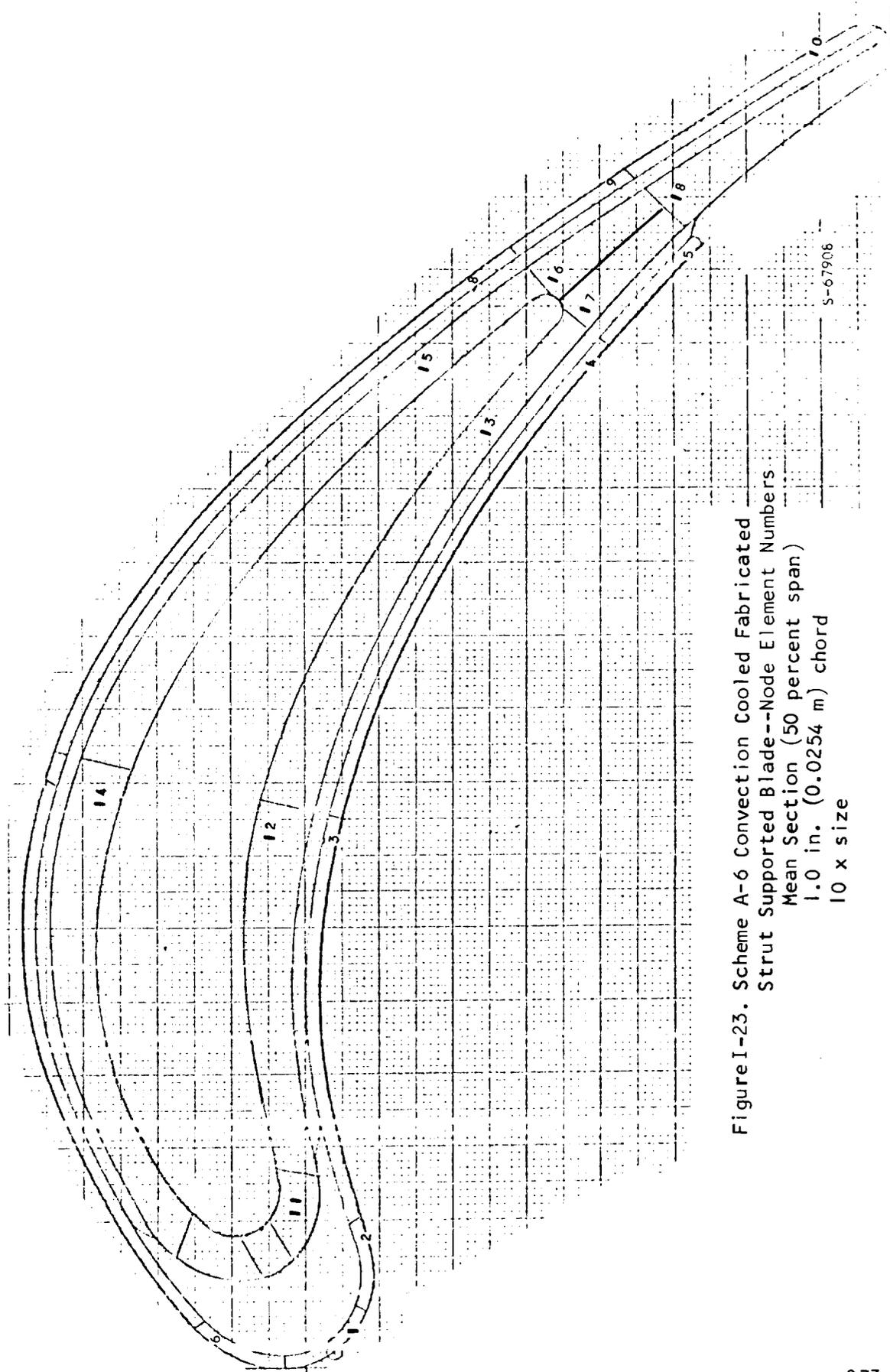
Figure I-23. Scheme A-6 Convection Cooled Fabricated
Strut Supported Blade--Node Element Numbers
Mean Section (50 percent span)
1.0 in. (0.0254 m) chord
10 x size

S-67908

273

TABLE I-23

SCHEME A-6 STRUT SUPPORTED BLADE, 1.0 IN. (0.0254 M) CHORD, MEAN SECTION

ELEMENT NO.	TEMPERATURE	STRESS	LIFE(HRS)
1	1597.0	-11786.9	10 YRS PLUS
2	1588.0	-5745.0	10 YRS PLUS
3	1550.0	17865.4	10 YRS PLUS
4	1615.0	21406.6	11434.6963
5	1719.0	-1164.5	10 YRS PLUS
6	1591.0	-8429.1	10 YRS PLUS
7	1617.0	2740.8	10 YRS PLUS
8	1642.0	21928.9	5021.2859
9	1713.0	6088.0	10 YRS PLUS
10	1688.0	16066.2	9714.7467
11	1276.0	75368.5	4283.8451
12	1497.0	34855.4	14811.2528
13	1569.0	35614.5	1737.9048
14	1550.0	23636.9	41701.1640
15 *	1593.0	34335.5	1229.3220
16	1647.0	24871.5	2358.3288
17	1650.0	21918.4	4091.8918
18	1648.0	26817.1	1519.7936

Mean Section Cooling Flow

Pressure Side W_{CAP} = 0.00266 lb/sec/blade (0.52 percent of hot gas flow)

Suction Side W_{CAS} = 0.004 lb/sec/blade (0.78 percent of hot gas flow)
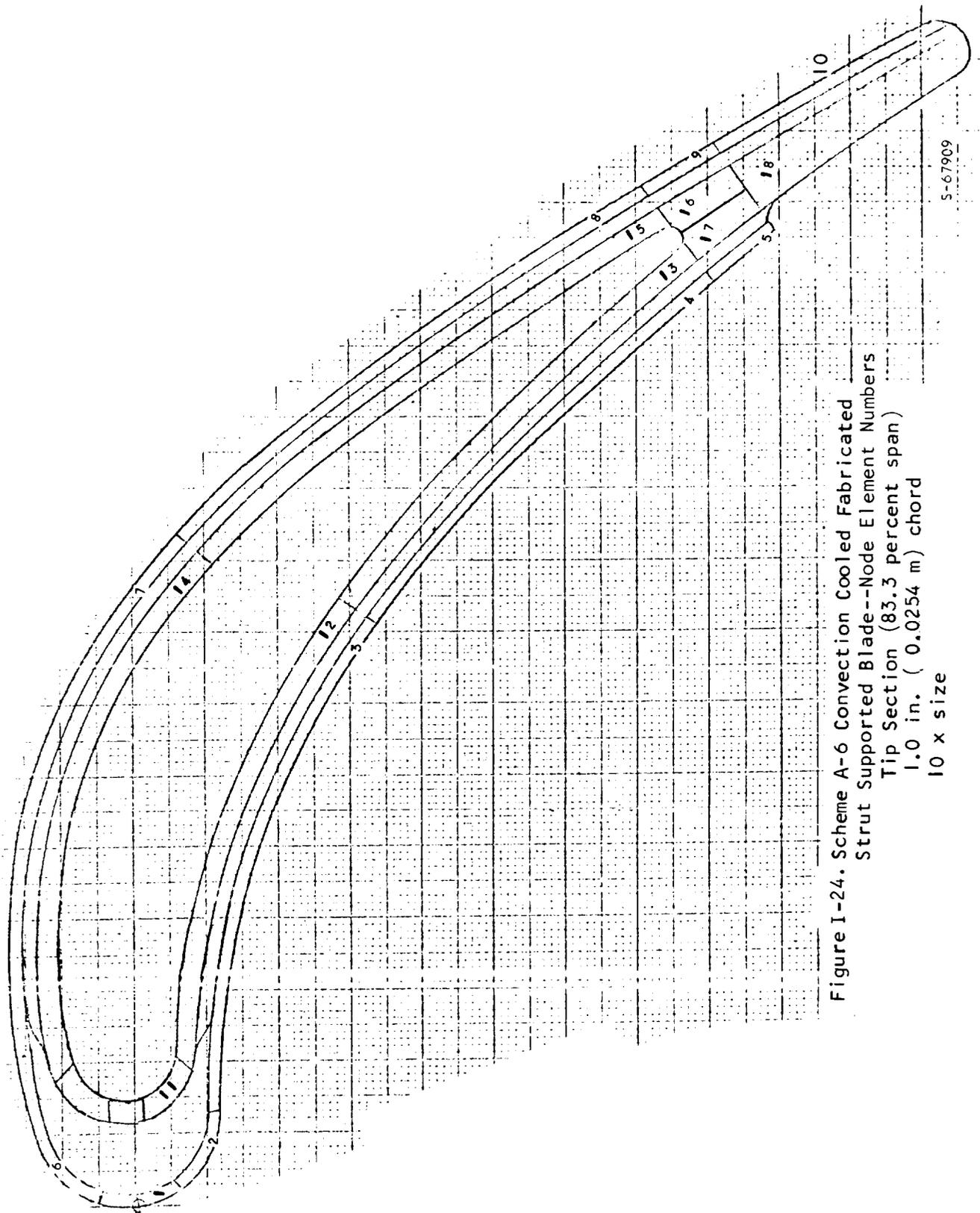
Figure I-24. Scheme A-6 Convection Cooled Fabricated Strut Supported Blade--Node Element Numbers Tip Section (83.3 percent span) 1.0 in. (0.0254 m) chord 10 x size

S-67909

TABLE I-24

SCHEME A-6 STRUT SUPPORTED BLADE, 1.0 IN. (0.0254 M) CHORD,
TIP SECTION

ELEMENT NO.	TEMPERATURE	STRESS	LIFE(HRS)
1	1626.0	-52642.1	25.5000
2	1614.0	-52456.0	34.9348
3	1570.0	-18964.6	78936.3125
4	1663.0	-10358.0	35046.6250
5	1740.0	-29764.5	141.9580
6	1625.0	-48258.4	61.1150
7	1665.0	-14633.8	14730.3164
8 *	1699.0	4760.0	11649.6719
9	1744.0	-16121.8	1593.4219
10	1717.0	-7044.3	4699.5586
11	1278.0	21207.6	10 YRS PLUS
12	1434.0	19482.4	10 YRS PLUS
13	1638.0	500.4	10 YRS PLUS
14	1628.0	-7300.7	43063.4219
15	1671.0	6465.4	16711.1445
16	1679.0	1282.7	39404.8437
17	1679.0	-3544.9	24791.4180
18	1670.0	291.7	61039.7422

Tip Section Cooling Flow

Pressure Side W_{CAP} = 0.00266 lb/sec/blade (0.52 percent of hot gas flow)

Suction Side W_{CAS} = 0.004 lb/sec/blade (0.78 percent of hot gas flow)
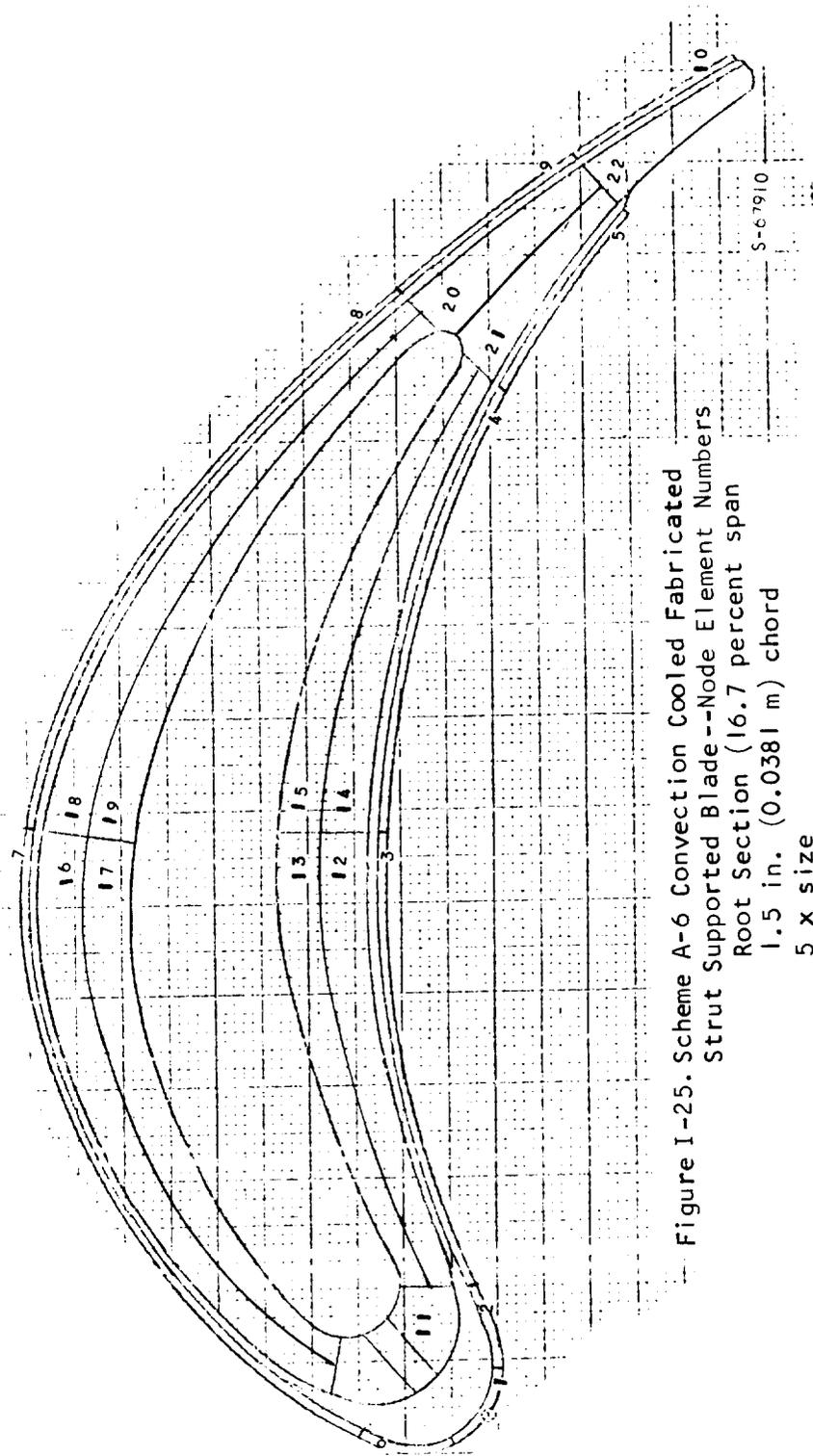
Figure I-25. Scheme A-6 Convection Cooled Fabricated
Strut Supported Blade--Node Element Numbers
Root Section (16.7 percent span
1.5 in. (0.0381 m) chord
5 x size

S-67910

277

TABLE I-25

SCHEME A-6 STRUT SUPPORTED BLADE, 1.5 IN. (0.0381 M) CHORD
HUB SECTION, 23783 RPM, TIT = 2550°F (1505.6°K)
WCA = 0.0312 LB/SEC/BLADE (4.16 PERCENT OF HOT GAS FLOW),
TCA = 900°F (755.6°K)

ELEMENT NO.	TEMPERATURE	STRESS	LIFE(HRS)
1	1539.0	-43005.1	878.2194
2	1516.0	-30929.4	21139.4180
3	1413.0	17702.3	10 YRS PLUS
4	1479.0	29998.2	76346.1170
5	1601.0	7819.0	10 YRS PLUS
6	1519.0	-34549.7	8550.1961
7	1543.0	-3323.7	10 YRS PLUS
8	1598.0	19563.0	32453.4740
9	1640.0	5673.2	10 YRS PLUS
10	1629.0	5801.8	10 YRS PLUS
11	1097.0	78308.6	10 YRS PLUS
12	1295.0	52103.6	10 YRS PLUS
13	1313.0	49098.4	10 YRS PLUS
14	1376.0	59393.7	4855.4148
15	1390.0	58376.9	3860.7958
16	1394.0	36943.6	10 YRS PLUS
17	1414.0	30834.9	10 YRS PLUS
18*	1494.0	44820.6	2174.0036
19	1504.0	39092.3	4616.8064
20	1532.0	33002.6	8453.4709
21	1517.0	31622.3	17560.3160
22	1581.0	17011.9	10 YRS PLUS

Hub Section Cooling Flow

Pressure Side W_{CAP} = 0.0052 lb/sec/blade (0.69 percent of hot gas flow)

Section Side W_{CAS} = 0.0052 lb/sec/blade (0.69 percent of hot gas flow)

278
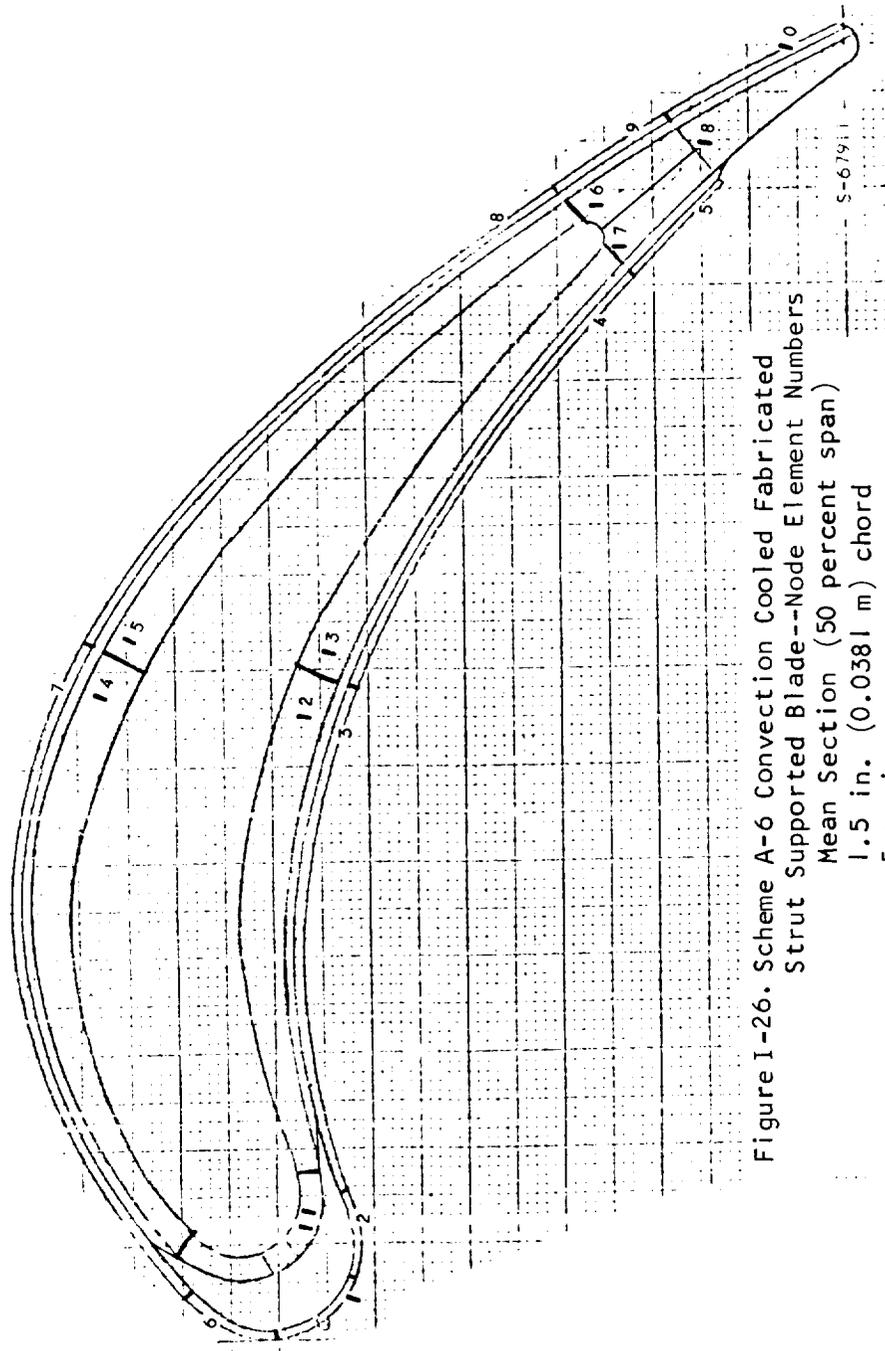
Figure I-26. Scheme A-6 Convection Cooled Fabricated
Strut Supported Blade--Node Element Numbers
Mean Section (50 percent span)
1.5 in. (0.0381 m) chord
5 x size

TABLE I-26

SCHEME A-6 STRUT SUPPORTED BLADE, 1.5 IN. (0.0381 M) CHORD
MEAN SECTION

ELEMENT NO.	TEMPERATURE	STRESS	LIFE(HRS)
1	1421.0	-18387.2	10 YRS PLUS
2	1426.0	-13912.3	10 YRS PLUS
3	1455.0	17886.1	10 YRS PLUS
4	1523.0	35734.7	5852.3702
5	1685.0	-4372.0	10 YRS PLUS
6	1441.0	-14169.3	10 YRS PLUS
7	1595.0	688.8	10 YRS PLUS
8	1662.0	19519.0	6003.3475
9	1713.0	1050.8	10 YRS PLUS
10	1706.0	-722.9	10 YRS PLUS
11	1118.0	68621.0	10 YRS PLUS
12	1386.0	40690.7	10 YRS PLUS
13 *	1475.0	52214.8	1028.7871
14	1522.0	24292.0	80093.3820
15	1608.0	31938.1	1405.8723
16	1611.0	28130.3	2967.9784
17	1597.0	27103.6	5363.1294
18	1652.0	10763.4	10 YRS PLUS

Mean Section Cooling Flow

Pressure Side W_{CAP} = 0.0052 lb/sec/blade (0.69 percent of hot gas flow)

Suction Side W_{CAS} = 0.0052 lb/sec/blade (0.69 percent of hot gas flow)

280
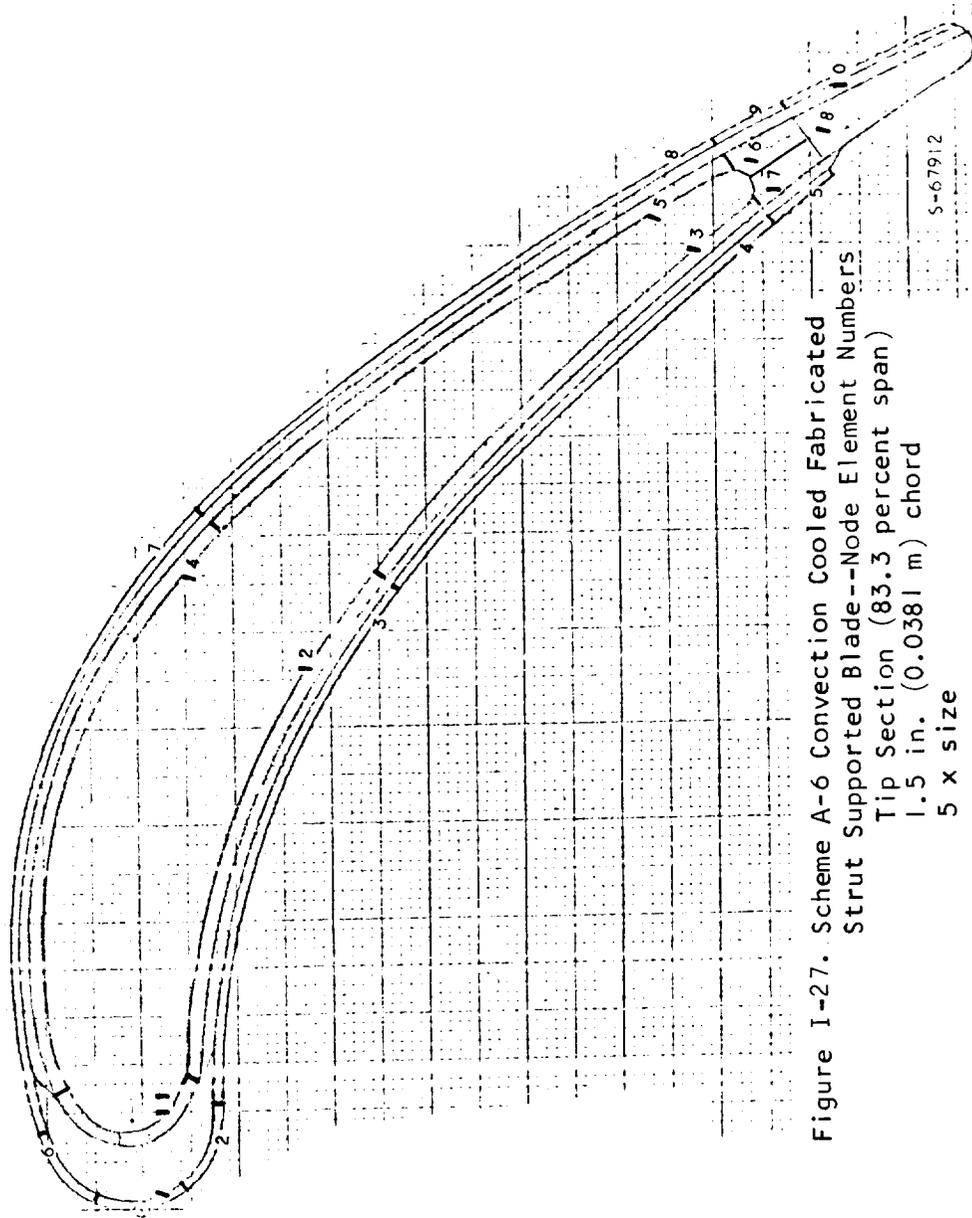
Figure I-27. Scheme A-6 Convection Cooled Fabricated
Strut Supported Blade--Node Element Numbers
Tip Section (83.3 percent span)
1.5 in. (0.0381 m) chord
5 x size

S-67912

TABLE I-27

SCHEME A-6 STRUT SUPPORTED BLADE, 1.5 IN. (0.0381 M) CHORD
TIP SECTION

ELEMENT NO.	TEMPERATURE	STRESS	LIFE(HRS)
1	1549.0	-62401.3	22.5906
2	1554.0	-61888.5	22.2292
3	1427.0	5342.4	10 YRS PLUS
4	1582.0	-1143.5	10 YRS PLUS
5	1707.0	-27477.3	465.1433
6	1557.0	-56750.6	57.9897
7	1623.0	-15687.3	35909.1562
8	1686.0	-591.5	37882.9844
9	1736.0	-17560.8	1477.9050
10	1726.0	-18958.3	1447.9397
11	1212.0	21632.1	10 YRS PLUS
12	1401.0	18083.2	10 YRS PLUS
13	1555.0	11332.2	10 YRS PLUS
14	1587.0	-7025.7	10 YRS PLUS
15 *	1661.0	2079.7	53454.0469
16	1650.0	-1831.9	75205.5625
17	1638.0	-4107.6	64404.0156
18	1674.0	-11909.0	19642.4922

Tip Section Cooling Flow

Pressure Side W_{CAP} = 0.0052 lb/sec/blade (0.69 percent of hot gas flow)

Suction Side W_{CAS} = 0.0052 lb/sec/blade (0.69 percent of hot gas flow)
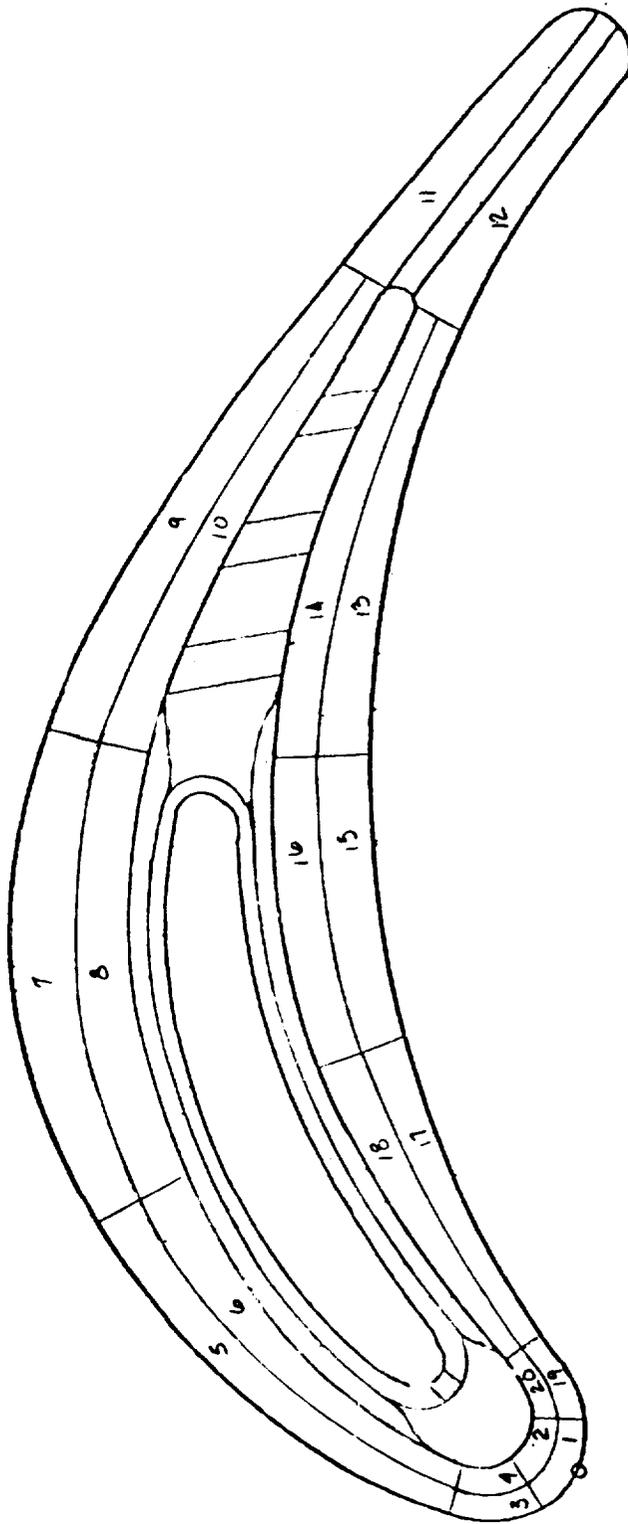
Figure I-28. Scheme A-7 Convection Cooled Cast Impingement Tube Blade
Node Element Numbers
Hub Section (16.7 percent span)
0.75 in. (0.01905 m) chord
10 x size

S-67913

TABLE I-28

SCHEME A-7 CONVECTION COOLED CAST IMPINGEMENT TUBE BLADE,
0.75 IN. (0.01905 M) CHORD HUB SECTION,
23183 RPM, TIT = 2400°F (1888.9°K),
WCA = .0186 LB/SEC/BLADE (4.77 PERCENT OF HOT GAS FLOW),
TCA = 900°F (755.6°K)

ELEMENT NO.	TEMPERATURE	STRESS	LIFE(HRS)
1	1665.0	9210.7	10 YRS PLUS
2	1595.0	33294.8	1901.4782
3	1676.	6763.8	10 YRS PLUS
4	1617.	24626.7	5409.4137
5	1615.0	22395.8	9234.0929
6	1571.0	34467.0	2124.0728
7	1604.0	15860.8	10 YRS PLUS
8	1540.0	33246.2	6421.0134
9	1500.0	32383.2	23945.3480
10	1452.0	45468.5	6320.6872
11	1587.0	624.7	10 YRS PLUS
12	1553.0	10560.0	10 YRS PLUS
13	1429.0	52137.2	3790.2853
14	1385.0	63623.1	1657.8633
15	1539.0	31777.9	9173.8590
16	1478.0	48271.6	1869.5182
17	1556.0	34869.0	2896.6828
18*	1505.0	49011.1	789.5833
19	1627.0	19019.3	17831.4760
20	1568.0	36373.9	1508.5842

Hub Section Cooling Flow

Pressure Side W_{CAP} = 0.0025 lb/sec/blade (0.665 percent of hot gas flow)

Suction Side W_{CAS} = 0.0061 lb/sec/blade (1.56 percent of hot gas flow)
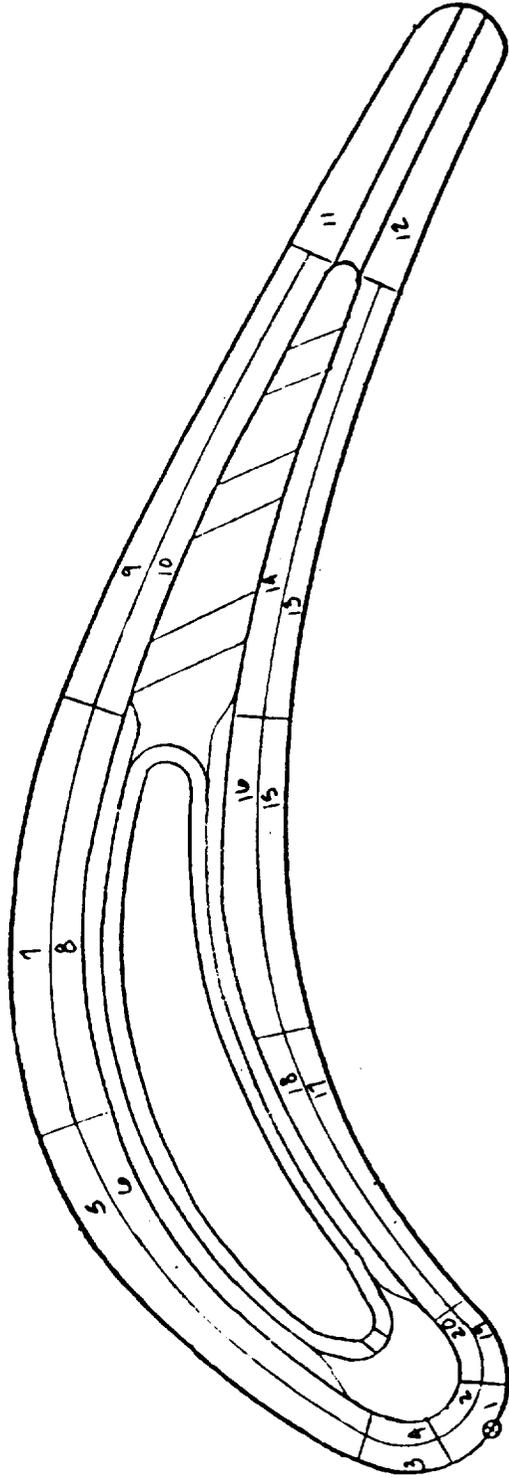
S-6791:4

Figure I-29.   Scheme A-7 Convection Cooled Cast Impingement Tube Blade
Node Element Numbers
Mean Section (50 percent span)
0.75 in. (0.01905 m) chord
10 x size

TABLE I-29

SCHEME A-7 CONVECTION COOLED CAST IMPINGEMENT TUBE BLADE, 0.75 IN. (0.01905 M) CHORD, MEAN SECTION

ELEMENT NO.	TEMPERATURE	STRESS	LIFE(HRS)
1	1726.0	2729.0	10 YRS PLUS
2	1658.0	22362.7	3033.0991
3	1717.0	7099.9	10 YRS PLUS
4	1666.0	23302.1	2029.8909
5	1741.0	4219.9	10 YRS PLUS
6	1706.0	14427.7	10517.2291
7	1742.0	5444.8	10 YRS PLUS
8	1705.0	16231.9	5962.3708
9	1640.0	33174.3	479.2672
10	1611.0	41929.3	166.4448
11	1792.0	-18173.4	389.4466
12	1792.0	-19302.3	272.5818
13	1594.0	44733.9	161.1374
14 *	1570.0	49981.2	124.4338
15	1658.0	26669.8	1218.6355
16	1620.0	39543.1	200.6289
17	1653.0	27349.0	1196.4898
18	1624.0	37090.5	308.1518
19	1679.0	16857.0	9420.8078
20	1636.1	30973.2	847.9430

Mean Section Cooling Flow

Pressure Side W_{CAP} = 0.0020 lb/sec/blade (0.512 percent of hot gas flow)

Suction Side W_{CAS} = 0.0030 lb/sec/blade (0.768 percent of hot gas flow)
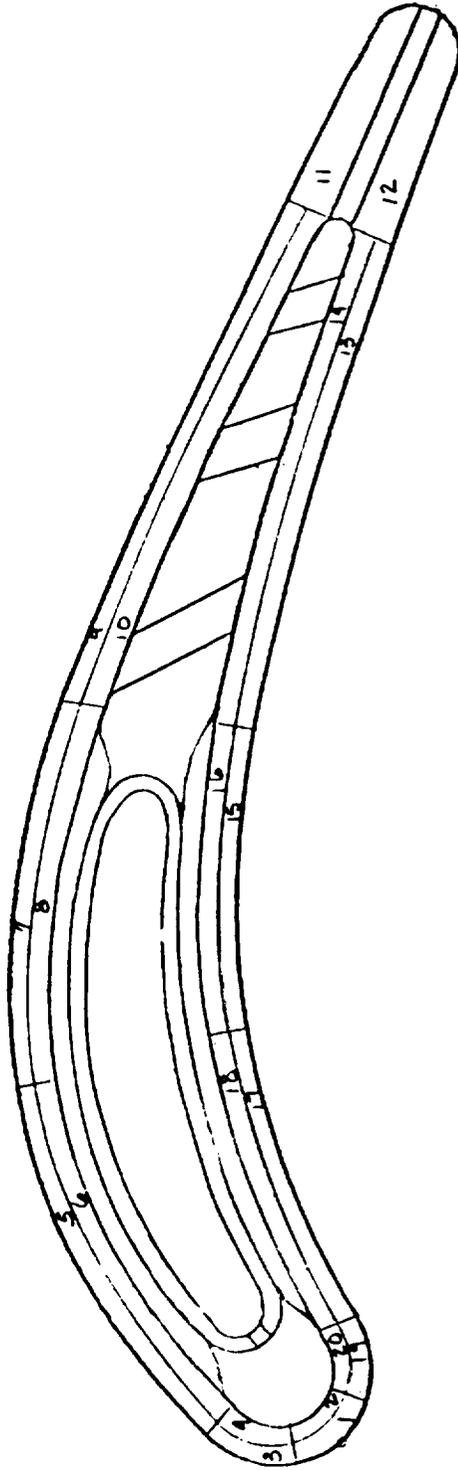
S-67915

Figure I-30. Scheme A-7 Convection Cooled Cast Impingement Tube Blade
Node Element Numbers
Tip Section (83.3 percent span)
0.75 in. (0.01905 m) chord
10 x size

TABLE I-30

SCHEME A-7 CONVECTION COOLED CAST IMPINGEMENT TUBE BLADE, 0.75 IN. (0.01905 M) CHORD, TIP SECTION

ELEMENT NO.	TEMPERATURE	STRESS	LIFE(HRS)
1	1600.0	-6379.0	13525.8853
2	1628.0	-1787.7	10 YRS PLUS
3	1650.0	-6707.6	12645.7317
4	1642.0	-3223.9	69626.8540
5	1725.0	-16097.0	2521.0600
6	1691.0	-4458.8	15151.4173
7	1725.0	-10253.3	7451.0156
8 *	1696.0	868.6	27706.1030
9	1663.0	10466.9	34327.9310
10	1642.0	12168.0	42932.8370
11	1596.0	-24677.5	82.4621
12	1607.0	-24859.3	78.1044
13	1626.0	12923.7	56705.5040
14	1607.0	14873.5	64565.1240
15	1642.0	5555.6	42833.3720
16	1621.0	7478.5	49979.7220
17	1611.0	3670.4	10 YRS PLUS
18	1547.0	9564.5	80451.9600
19	1663.0	-3856.3	35157.9550
20	1547.0	6744.1	10 YRS PLUS

Pressure Side W_{CAP} = 0.0020 lb/sec/blade (0.512 percent of hot gas flow)

Suction Side W_{CAS} = 0.0030 lb/sec/blade (0.768 percent of hot gas flow)

Figure I-31. Scheme A-7 Convection Cooled Cast Impingement Tube Blade
Node Element Numbers
Hub Section (16.7 percent span)
1.0 in. (0.0254 m) chord
10 x size

TABLE I-31

SCHEME A-7 CONVECTION COOLED CAST IMPINGEMENT TUBE BLADE, 1.0 IN. (0.0254 M) CHORD HUB SECTION, 23183 RPM, TIT = 2400°F (1888.9°K) WCA = 0.0260 LB/SEC/BLADE (5.07 PERCENT OF HOT GAS FLOW), TCA = 900°F (755.6°K)

ELEMENT NO.	TEMPERATURE	STRESS	LIFE(HRS)
1	1730.0	-10546.5	20250.0130
2	1618.0	23410.1	6850.8142
3	1718.0	-5660.9	10 YRS PLUS
4	1640.0	17404.1	21816.4210
5	1664.0	-1399.4	10 YRS PLUS
6	1623.0	16532.6	46423.8950
7	1596.0	8261.4	10 YRS PLUS
8	1498.0	34779.1	14649.9966
9	1486.0	21409.3	10 YRS PLUS
10	1437.0	34838.9	66451.0830
11	1629.0	-28097.5	1876.1477
12	1576.0	-12010.2	10 YRS PLUS
13	1402.0	44426.2	33193.6840
14	1365.0	53793.0	18792.3380
15	1474.0	39208.3	10464.9453
16	1396.0	59627.6	2586.5246
17	1533.0	37059.0	3301.2316
18*	1479.0	51912.7	971.5030
19	1653.0	9876.3	10 YRS PLUS
20	1583.0	31453.3	3002.0155

Hub Section Cooling Flow

Pressure Side W_{CAP} = 0.00353 lb/sec/blade (0.69 percent of hot gas flow)

Suction Side W_{CAS} = 0.00910 lb/sec/blade (1.78 percent of hot gas flow)

290

Figure I-31. Scheme A-7 Convection Cooled Cast Impingement Tube Blade
Node Element Numbers
Hub Section (16.7 percent span)
1.0 in. (0.0254 m) chord
10 x size

TABLE I-31

SCHEME A-7 CONVECTION COOLED CAST IMPINGEMENT TUBE BLADE, 1.0 IN. (0.0254 M) CHORD HUB SECTION, 23183 RPM, TIT = 2400°F (1888.9°K) WCA = 0.0260 LB/SEC/BLADE (5.07 PERCENT OF HOT GAS FLOW), TCA = 900°F (755.6°K)

ELEMENT NO.	TEMPERATURE	STRESS	LIFE(HRS)
1	1730.0	-10546.5	20250.0130
2	1618.0	23410.1	6850.8142
3	1718.0	-5660.9	10 YRS PLUS
4	1640.0	17404.1	21816.4210
5	1664.0	-1399.4	10 YRS PLUS
6	1623.0	16532.6	46423.8950
7	1596.0	8261.4	10 YRS PLUS
8	1498.0	34779.1	14649.9966
9	1486.0	21409.3	10 YRS PLUS
10	1437.0	34838.9	66451.0830
11	1629.0	-28097.5	1876.1477
12	1576.0	-12010.2	10 YRS PLUS
13	1402.0	44426.2	33193.6840
14	1365.0	53793.0	18792.3380
15	1474.0	39208.3	10464.9453
16	1396.0	59627.6	2586.5246
17	1533.0	37059.0	3301.2316
18*	1479.0	51912.7	971.5030
19	1653.0	9876.3	10 YRS PLUS
20	1583.0	31453.3	3002.0155

Hub Section Cooling Flow

Pressure Side W_{CAP} = 0.00353 lb/sec/blade (0.69 percent of hot gas flow)

Suction Side W_{CAS} = 0.00910 lb/sec/blade (1.78 percent of hot gas flow)

290

Figure I-32. Scheme A-7 Convection Cooled Cast Impingement Tube Blade
Node Element Numbers
Mean Section (50 percent span)
1.0 in.(0.0254 m) chord
10 x size

TABLE I-32

SCHEME A-7 CONVECTION COOLED CAST IMPINGEMENT TUBE BLADE, 1.0 IN. (0.0254 M) CHORD MEAN SECTION

ELEMENT NO.	TEMPERATURE	STRESS	LIFE(HRS)
1	1698.0	-13513.9	17451.7940
2	1609.0	14353.6	10 YRS PLUS
3	1682.0	-7210.8	10 YRS PLUS
4	1616.0	13370.9	10 YRS PLUS
5	1705.0	-6620.2	10 YRS PLUS
6	1654.2	8614.9	10 YRS PLUS
7	1673.0	10606.1	1C YRS PLUS
8	1627.0	24268.5	4496.2759
9	1649.0	17450.8	16907.8310
10	1624.0	24895.5	4249.2577
11	1742.0	-12962.5	6836.4851
12	1742.0	-14364.8	4345.1282
13	1611.0	26007.8	4699.4171
14	1588.0	33191.0	1798.3244
15	1576.0	34297.6	1932.3417
16 *	1538.0	45430.5	601.2629
17	1543.0	37977.7	2050.8561
18	1506.0	48413.3	850.8279
19	1658.0	-687.7	10 YRS PLUS
20	1593.0	19523.0	37754.4510

Mean Section Cooling Flow

Pressure Side W_{CAP} = 0.00270 lb/sec/blade (0.528 percent of hot gas flow)

Suction Side W_{CAS} = 0.00400 lb/sec/blade (0.78 percent of hot gas flow)
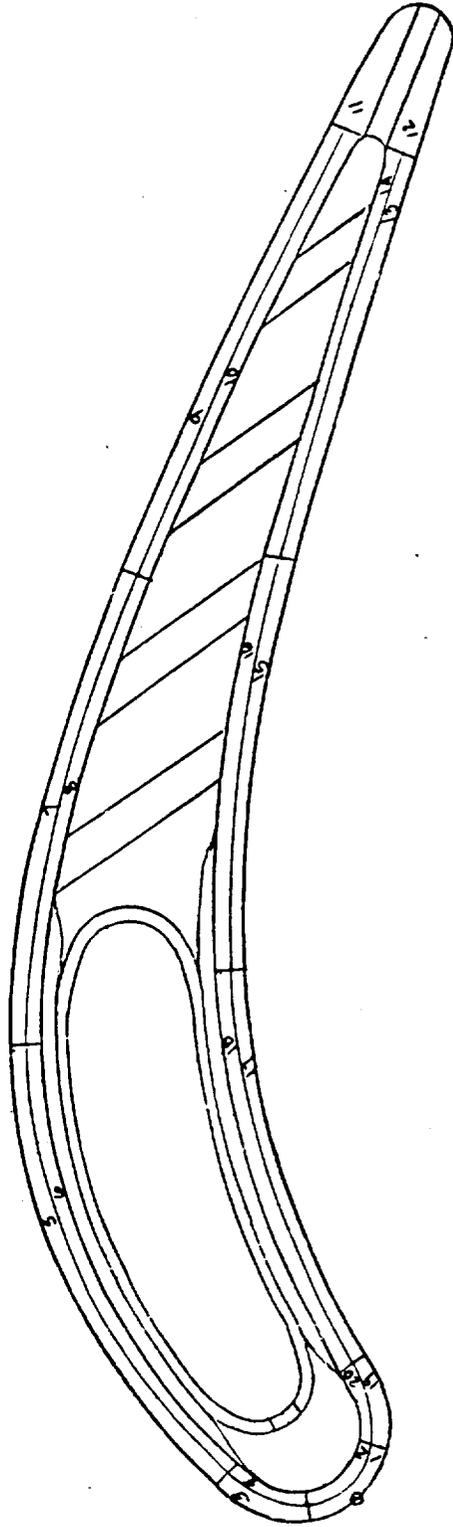
S-67916

Figure I-33. Scheme A-7 Convection Cooled Cast Impingement Tube Blade
Node Element Numbers
Tip Section (83.3 percent span)
1.0 in. (0.0254 m) chord
10 x size

TABLE I-33

SCHEME A-7 CONVECTION COOLED CAST IMPINGEMENT TUBE BLADE, 1.0 IN. (0.0254 M) CHORD TIP SECTION

ELEMENT NO.	TEMPERATURE	STRESS	LIFE(HRS)
1	1546.0	-18879.8	10 YRS PLUS
2	1494.0	1855.4	10 YRS PLUS
3	1492.0	7334.8	10 YRS PLUS
4	1455.0	21371.0	10 YRS PLUS
5	1701.0	-20220.0	2089.0365
6	1673.0	-18236.3	6062.0523
7	1664.0	2940.9	41374.2900
8	1641.0	3779.6	63682.9920
9 *	1658.0	8153.3	16468.7980
10	1639.0	8844.3	23342.7940
11	1753.0	-17828.9	942.5066
12	1754.0	-22054.2	424.8161
13	1630.0	2428.1	10 YRS PLUS
14	1612.0	4915.6	10 YRS PLUS
15	1578.0	774.8	10 YRS PLUS
16	1569.0	9390.2	10 YRS PLUS
17	1553.0	-4024.0	10 YRS PLUS
18	1533.0	4584.3	10 YRS PLUS
19	1473.0	10586.8	10 YRS PLUS
20	1435.0	25358.6	10 YRS PLUS

Tip Section Cooling Flow

Pressure Side W_{CAP} = 0.00270 lb/sec/blade (0.528 percent of hot gas flow)

Suction Side W_{CAS} = 0.00400 lb/sec/blade (0.78 percent of hot gas flow)
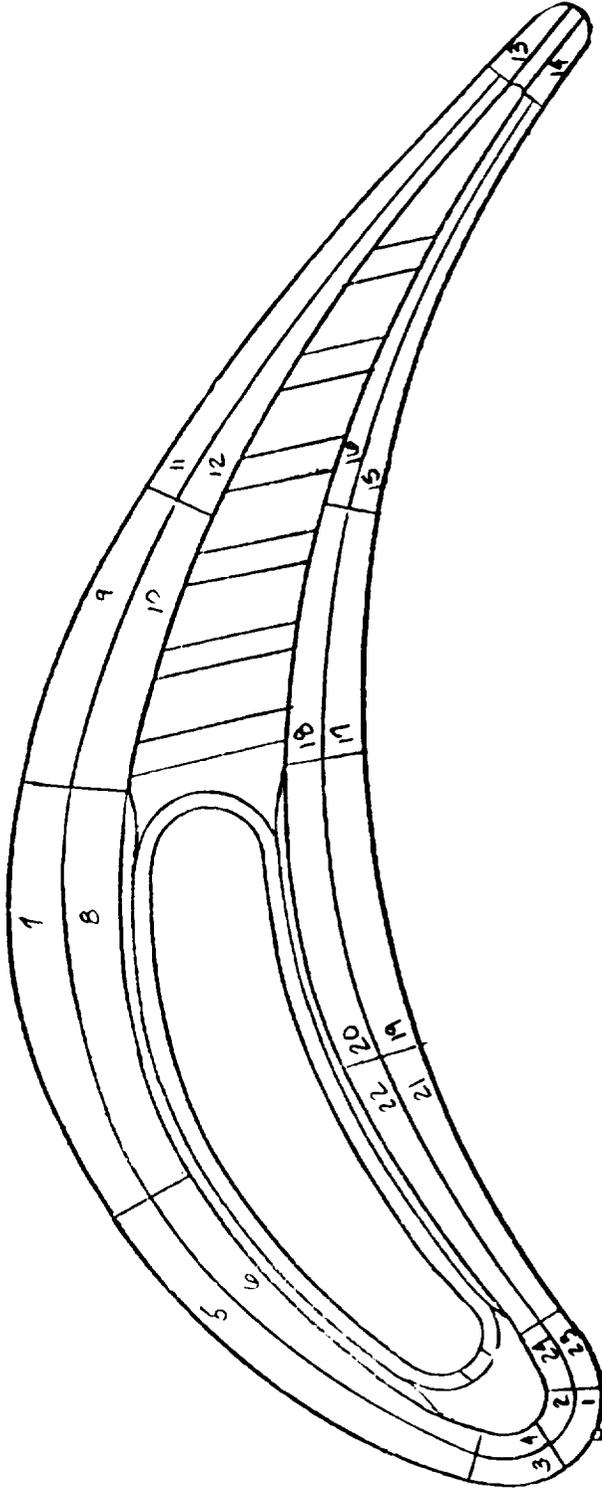
S-67919

Figure I-34. Scheme A-7 Convection Cooled Cast Impingement Tube Blade
Node Element Numbers
Hub Section (16.7 percent span)
1.5 in. (0.0381 m) chord
5 x size

TABLE I-34

SCHEME A-7 CONVECTION COOLED CAST IMPINGEMENT TUBE BLADE,
1.5 IN. (0.0381 M) CHORD HUB SECTION
23884 RPM, TIT = 2450°F (1611.1°K)
WCA = 0.0411 LB/SEC/BLADE (5.43 PERCENT OF HOT GAS FLOW),
TCA = 900°F (755.6°K)

ELEMENT NO.	TEMPERATURE	STRESS	LIFE(HRS)
1	1720.0	-21430.9	789.3827
2	1596.0	17472.0	70706.3150
3	1695.0	-8890.8	10 YRS PLUS
4	1601.0	19968.5	25987.1650
5	1694.0	4892.2	10 YRS PLUS
6	1610.0	29109.2	2464.4043
7	1683.0	15138.7	15037.3472
8 *	1577.0	43964.1	280.1070
9	1652.0	13277.1	63750.6460
10	1566.0	35861.7	1781.0600
11	1594.0	6016.4	10 YRS PLUS
12	1551.0	17343.1	10 YRS PLUS
13	1567.0	-5360.3	10 YRS PLUS
14	1501.0	10301.6	10 YRS PLUS
15	1444.0	39994.9	20784.8600
16	1418.0	47430.6	12027.4799
17	1528.0	31756.4	12509.7540
18	1468.0	50150.0	1783.0694
19	1545.0	32758.9	6245.4487
20	1461.0	58153.0	539.2774
21	1531.0	36463.1	3986.4027
22	1463.0	56767.8	649.5606
23	1651.0	-1972.7	10 YRS PLUS
24	1558.0	27116.9	15371.8652

Hub Section Cooling Flow

Pressure Side W_{CAP} = 0.0051 lb/sec/blade (0.67 percent of hot gas flow)

Suction Side W_{CAS} = 0.01905 lb/sec/blade (1.43 percent of hot gas flow)

296
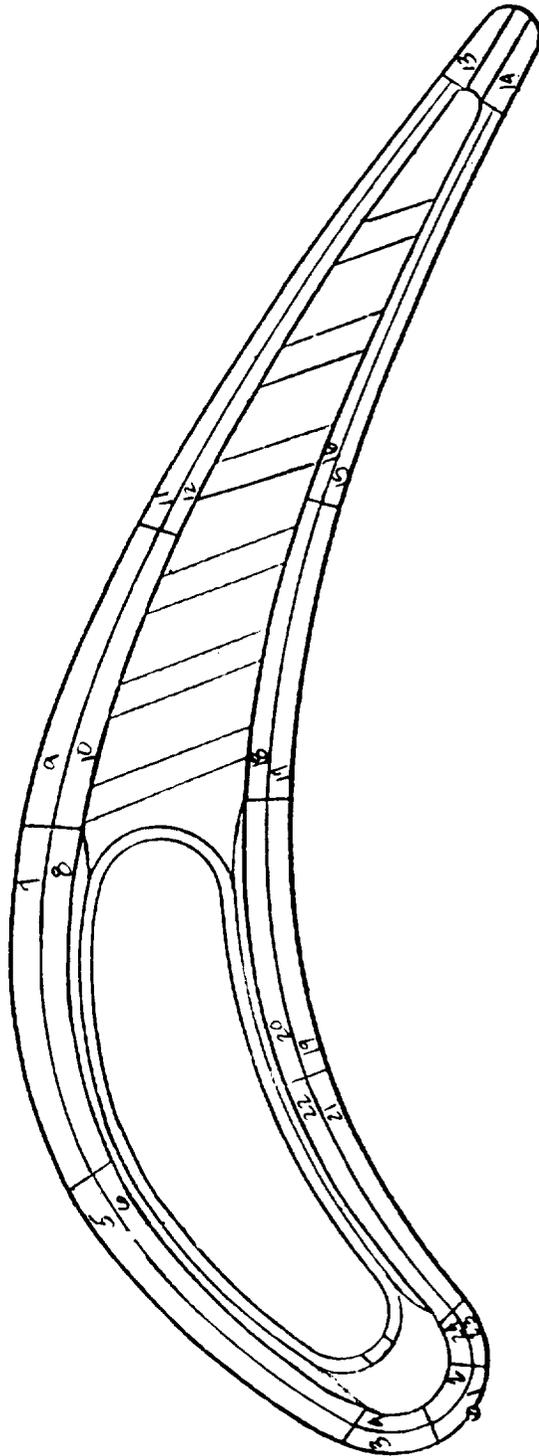
S-67920

Figure I-35. Scheme A-7 Convection Cooled Cast Impingement Tube Blade
Node Element Numbers
Mean Section (50 percent span)
1.5 in. (0.0381 m) chord
5 x size

TABLE I-35

SCHEME A-7 CONVECTION COOLED CAST IMPINGEMENT TUBE BLADE, 1.5 (0.0381 M) CHORD MEAN SECTION

ELEMENT NO.	TEMPERATURE	STRESS	LIFE(HRS)
1	1711.0	-22971.2	714.5741
2	1619.0	5575.4	10 YRS PLUS
3	1691.0	-16013.4	9153.0167
4	1630.0	3352.0	10 YRS PLUS
5	1666.0	3511.6	10 YRS PLUS
6	1600.0	24183.4	9352.0275
7	1690.0	13571.7	21073.1750
8	1621.0	34633.7	563.7486
9	1763.0	1552.0	10 YRS PLUS
10	1718.0	14275.6	8149.5655
11	1759.0	8936.4	25453.9970
12	1736.0	15440.7	3557.5344
13	1725.0	22367.3	577.3483
14	1728.0	19263.3	1251.0152
15	1729.0	13854.6	7086.3380
16	1706.0	21869.0	1013.6621
17	1680.0	20441.8	2786.8611
18	1645.0	32459.8	492.9471
19	1593.0	37436.0	624.5603
20*	1548.0	50146.0	211.4051
21	1567.0	26667.1	7706.6325
22	1544.0	38605.4	1735.0364
23	1671.0	-8750.7	10 YRS PLUS
24	1610.0	10286.8	10 YRS PLUS

Mean Section Cooling Flow

Pressure Side W_{CAP} = 0.00416 lb/sec/blade (0.552 percent of hot gas flow)

Suction Side W_{CAS} = 0.00624 lb/sec/blade (0.825 percent of hot gas flow)
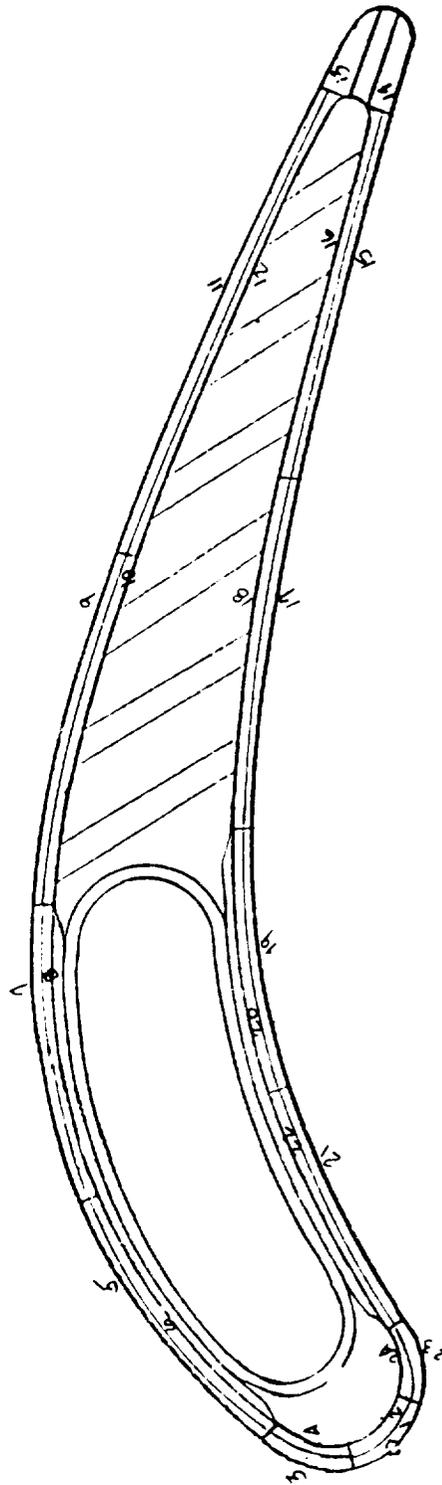
Figure I-36. Scheme A-7 Convection Cooled Cast Impingement Tube Blade
Node Element Numbers
Tip Section (83.3 percent span)
1.5 in. (0.0381 m) chord
5 x size

S-67921

TABLE I-36

SCHEME A-7 CONVECTION COOLED CAST IMPINGEMENT TUBE BLADE, 1.5 IN. (0.0381 M) CHORD TIP SECTION

ELEMENT NO.	TEMPERATURE	STRESS	LIFE(HRS)
1	1556.0	-28805.9	6907.8489
2	1545.0	-17599.9	10 YRS PLUS
3	1577.0	-18252.4	75026.7230
4	1546.0	-10438.3	10 YRS PLUS
5	1634.0	-8480.2	28711.5520
6	1606.0	-2315.8	10 YRS PLUS
7	1673.0	8112.0	11322.6765
8	1647.0	13291.0	30337.3850
9	1709.0	-16412.0	531.4459
10	1773.0	-11397.2	1905.9575
11	1734.0	-6608.0	1041.6393
12	1769.0	-1446.0	4075.0946
13	1746.0	10433.5	4321.3756
14 *	1750.0	4191.0	3734.8094
15	1752.0	-5634.5	2673.9621
16	1736.0	2865.4	6825.5121
17	1718.0	-2954.1	10445.8097
18	1703.0	3885.4	12583.2400
19	1563.0	19471.7	86562.6930
20	1545.0	25130.4	45720.0450
21	1530.0	4359.2	10 YRS PLUS
22	1511.0	9662.5	10 YRS PLUS
23	1556.0	-21386.3	54361.2360
24	1535.0	-13307.8	10 YRS PLUS

Tip Section Cooling Flow

Pressure Side W_{CAP} = 0.00416 lb/sec/blade (0.552 percent of hot gas flow)

Suction Side W_{CAS} = 0.00624 lb/sec/blade (0.825 percent of hot gas flow)
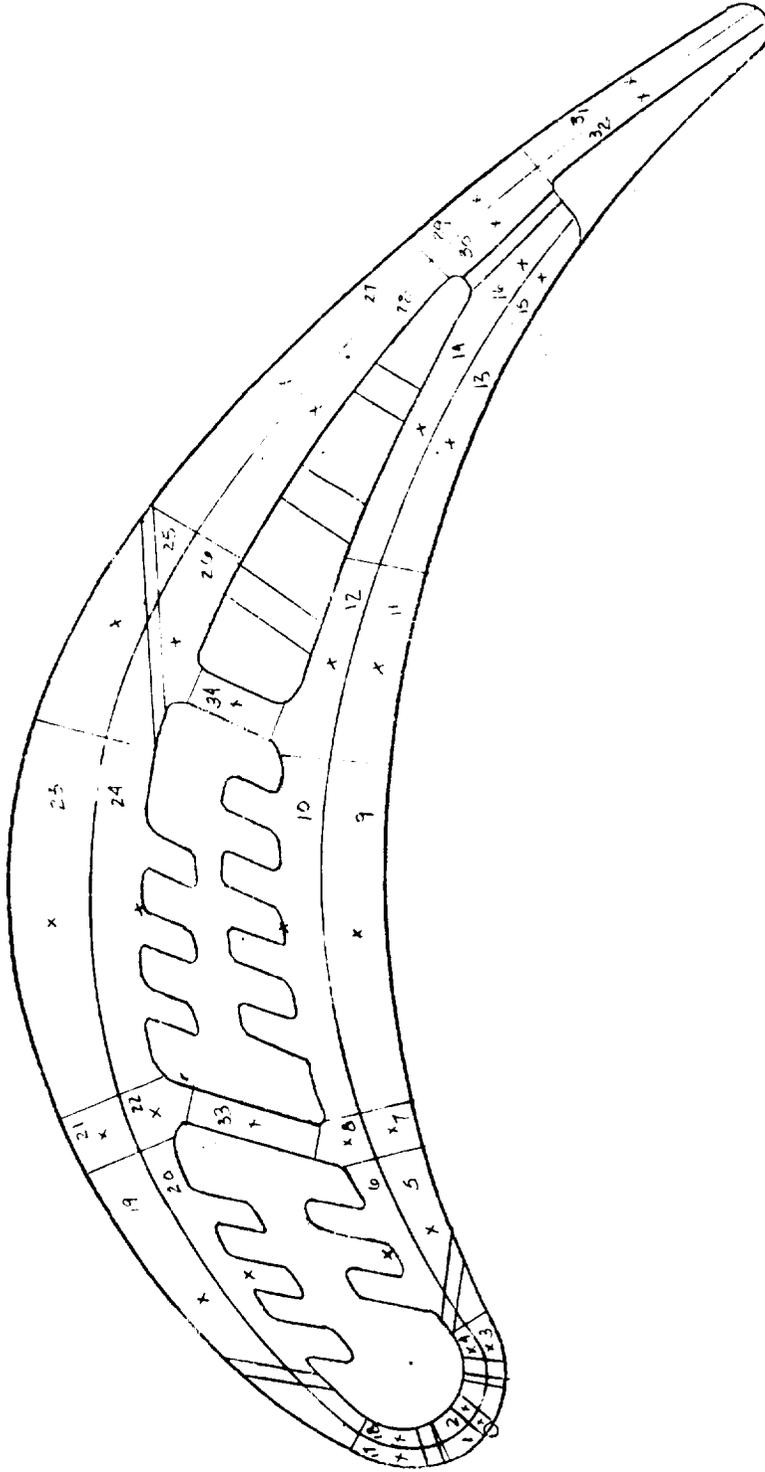
Figure I-37. Scheme B-I Film-Convection Cooled Cast Three Cavity Blade
Node Element Numbers
Hub Section (16.7 percent span)
0.75 in. (0.01905 m) chord
10 x size

S-67922

TABLE I-37

SCHEME B-I FILM-CONVECTION COOLED CAST THREE CAVITY BLADE, 0.75 IN.
(0.01905 M) CHORD, HUB SECTION, 23585 RPM, TIT = 2450°F
(1616.7°K), WCA = 0.02209 LB/SEC/BLADE (5.76 PERCENT OF
HOT GAS FLOW), TCA = 900°F (755.6°K)

ELEMENT NO.	TEMPERATURE	STRESS	LIFE(HRS)
1	1499.0	-1709.1	10 YRS PLUS
2	1479.0	3498.3	10 YRS PLUS
3	1470.0	4475.7	10 YRS PLUS
4	1453.0	9205.8	10 YRS PLUS
5	1368.0	29441.4	10 YRS PLUS
6	1320.0	42857.1	10 YRS PLUS
7	1387.0	23414.8	10 YRS PLUS
8	1345.0	34925.7	10 YRS PLUS
9	1420.0	12036.9	10 YRS PLUS
10	1357.0	28894.1	10 YRS PLUS
11	1343.0	26508.7	10 YRS PLUS
12	1282.0	42829.7	10 YRS PLUS
13	1272.0	39704.7	10 YRS PLUS
14	1231.0	50568.4	10 YRS PLUS
15	1312.0	25145.0	10 YRS PLUS
16	1285.0	32057.8	10 YRS PLUS
17	1480.0	4972.0	10 YRS PLUS
18	1466.0	8310.9	10 YRS PLUS
19	1356.0	36871.3	10 YRS PLUS
20	1296.0	51488.7	10 YRS PLUS
21	1397.0	24863.2	10 YRS PLUS
22	1354.0	34681.5	10 YRS PLUS
23	1477.0	2395.8	10 YRS PLUS
24	1404.0	18587.9	10 YRS PLUS
25	1347.0	28326.3	10 YRS PLUS
26	1275.0	46434.6	10 YRS PLUS
27	1217.0	55419.4	10 YRS PLUS
28	1183.0	64132.0	10 YRS PLUS
29	1306.0	26166.7	10 YRS PLUS
30	1282.0	32443.8	10 YRS PLUS
31	1469.0	-19090.6	10 YRS PLUS
32	1458.0	-16126.4	10 YRS PLUS
33*	1202.0	73876.1	66498.2800
34	1145.0	77678.6	10 YRS PLUS

Leading edge W_{CLE} = 0.00191 lb/sec/blade (0.498 percent of hot gas flow)

Suction side W_{CAS} = 0.00165 lb/sec/blade (0.43 percent of hot gas flow)

Pressure side W_{CAP} = 0.00025 lb/sec/blade (0.065 percent of hot gas flow)

Trailing edge W_{CTE} = 0.00306 lb/sec/blade (0.798 percent of hot gas flow)
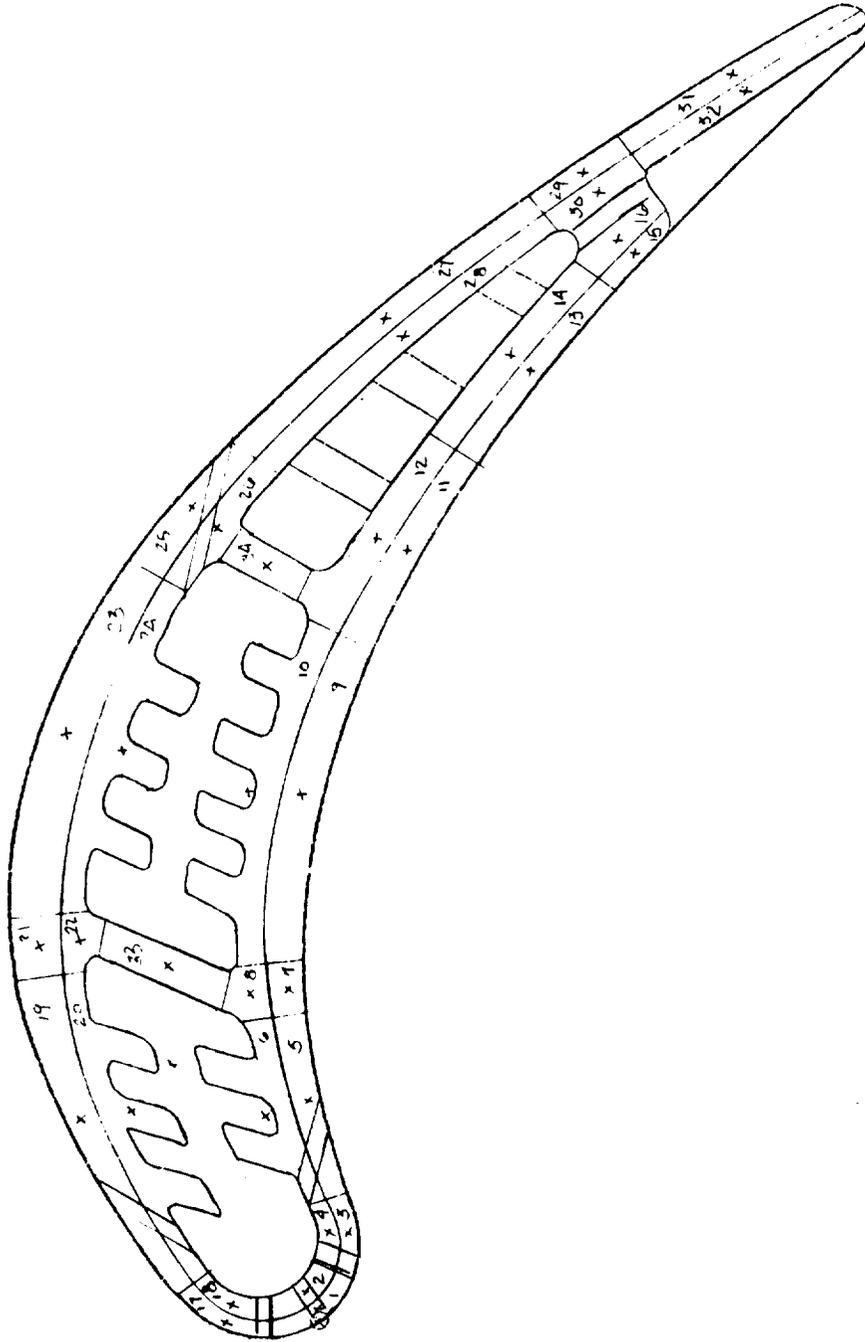
Figure I-38. Scheme B-I Film-Convection Cooled Cast Three Cavity Blade
Node Element Numbers
Mean Section (50 percent span)
0.75 in. (0.01905 m) chord
10 x size

S-67923

303

TABLE I-38

SCHEME B-I FILM-CONVECTION COOLED CAST THREE CAVITY BLADE, 0.75 IN. (0.01905 M) CHORD, MEAN SECTION

ELEMENT NO.	TEMPERATURE	STRESS	LIFE(HRS)
1	1590.0	-3162.1	10 YRS PLUS
2	1577.0	-174.1	10 YRS PLUS
3	1567.0	1836.0	10 YRS PLUS
4	1556.0	4533.3	10 YRS PLUS
5	1477.0	22577.3	10 YRS PLUS
6	1446.0	30541.0	10 YRS PLUS
7	1492.0	16137.5	10 YRS PLUS
8	1466.0	22620.4	10 YRS PLUS
9	1506.0	8584.1	10 YRS PLUS
10	1469.0	17659.0	10 YRS PLUS
11	1482.0	11082.5	10 YRS PLUS
12	1445.0	20191.6	10 YRS PLUS
13	1452.0	16624.3	10 YRS PLUS
14	1424.0	23362.0	10 YRS PLUS
15	1484.0	6969.4	10 YRS PLUS
16	1459.0	13098.8	10 YRS PLUS
17	1580.0	-1257.1	10 YRS PLUS
18	1570.0	1189.4	10 YRS PLUS
19	1482.0	19114.1	10 YRS PLUS
20	1438.0	31016.7	10 YRS PLUS
21	1527.0	3265.0	10 YRS PLUS
22	1499.0	10994.1	10 YRS PLUS
23	1601.0	-20615.1	20786.9240
24	1560.0	-8674.6	10 YRS PLUS
25	1474.0	9930.2	10 YRS PLUS
26	1438.0	20047.0	10 YRS PLUS
27	1358.0	38210.8	10 YRS PLUS
28	1341.0	43196.8	10 YRS PLUS
29	1464.0	10035.8	10 YRS PLUS
30	1447.0	15018.0	10 YRS PLUS
31	1597.0	-25561.8	7505.3996
32	1587.0	-22431.3	19490.4370
33*	1368.0	46632.2	63409.3880
34	1337.0	47552.6	10 YRS PLUS

Leading edge W_{CLE} = 0.00191 lb/sec/blade (0.498 percent of hot gas flow)

Suction side W_{CAS} = 0.00165 lb/sec/blade (0.43 percent of hot gas flow)

Pressure side W_{CAP} = 0.00025 lb/sec/blade (0.065 percent of hot gas flow)

Trailing edge W_{CTE} = 0.002812 lb/sec/blade (0.733 percent of hot gas flow)
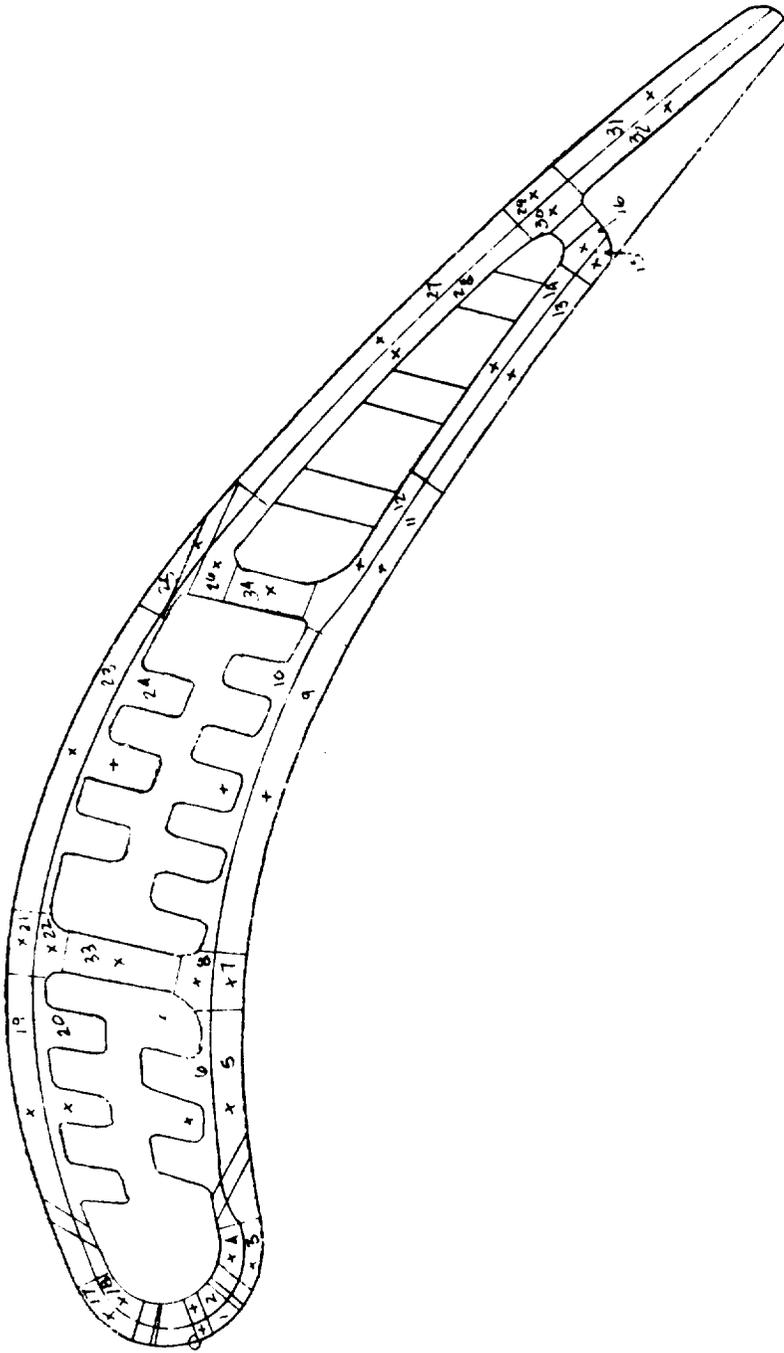
Figure I-39. Scheme B-I Film-Convection Cooled Cast Three Cavity Blade
Node Element Numbers
Tip Section (83.3 percent span)
0.75 in. (0.01905 m) chord
10 x size

S-67924

TABLE I-39

SCHEME B-1 FILM-CONVECTION COOLED CAST THREE CAVITY BLADE, 0.75 IN.
(0.01905 M) CHORD, TIP SECTION

ELEMENT NO.	TEMPERATURE	STRESS	LIFE(HRS)
1	1682.0	-26646.0	150.0989
2	1675.0	-23585.1	291.9681
3	1679.0	-25100.9	207.2842
4	1673.0	-22523.2	364.4053
5	1628.0	-3976.3	24315.5470
6	1613.0	1469.3	55191.5440
7	1604.0	7623.5	24794.9720
8	1596.0	11084.5	17036.6890
9	1549.0	27950.8	3238.0010
10	1535.0	33201.7	1869.8467
11	1665.0	-1824.6	13333.2378
12	1656.0	1738.2	17036.4270
13	1711.0	-13066.4	688.5182
14	1699.0	-8737.5	1848.4797
15	1715.0	-13144.8	618.5525
16	1702.0	-8355.5	1828.5953
17	1668.0	-25237.9	164.2459
18	1683.0	-25772.4	169.1348
19	1657.0	-6838.3	7146.4630
20	1640.0	-2780.3	21692.5630
21	1674.0	-6338.2	5058.6627
22	1660.0	-3116.5	12243.7496
23	1733.0	-19204.5	154.2490
24	1716.0	-15764.2	396.3610
25	1802.0	-26130.6	11.4824
26	1785.0	-26119.6	16.4731
27*	1595.0	27430.9	1083.7545
28	1589.0	28057.0	1133.3790
29	1702.0	-5153.6	3071.0880
30	1693.0	-3611.8	4921.6261
31	1776.0	-24802.7	24.5426
32	1771.0	-24962.8	26.6616
33	1572.0	20433.6	6489.3328
34	1666.0	468.0	16248.9370

Leading edge W_{CLE} = 0.00191 lb/sec/blade (0.498 percent of hot gas flow)

Suction side W_{CAS} = 0.00165 lb/sec/blade (0.43 percent of hot gas flow)

Pressure side W_{CAP} = 0.00025 lb/sec/blade (0.065 percent of hot gas flow)

Trailing edge W_{CTE} = 0.001916 lb/sec/blade (0.5 percent of hot gas flow)

Tip discharge W_{CTD} = 0.00287 lb/sec/blade (0.748 percent of hot gas flow)

306
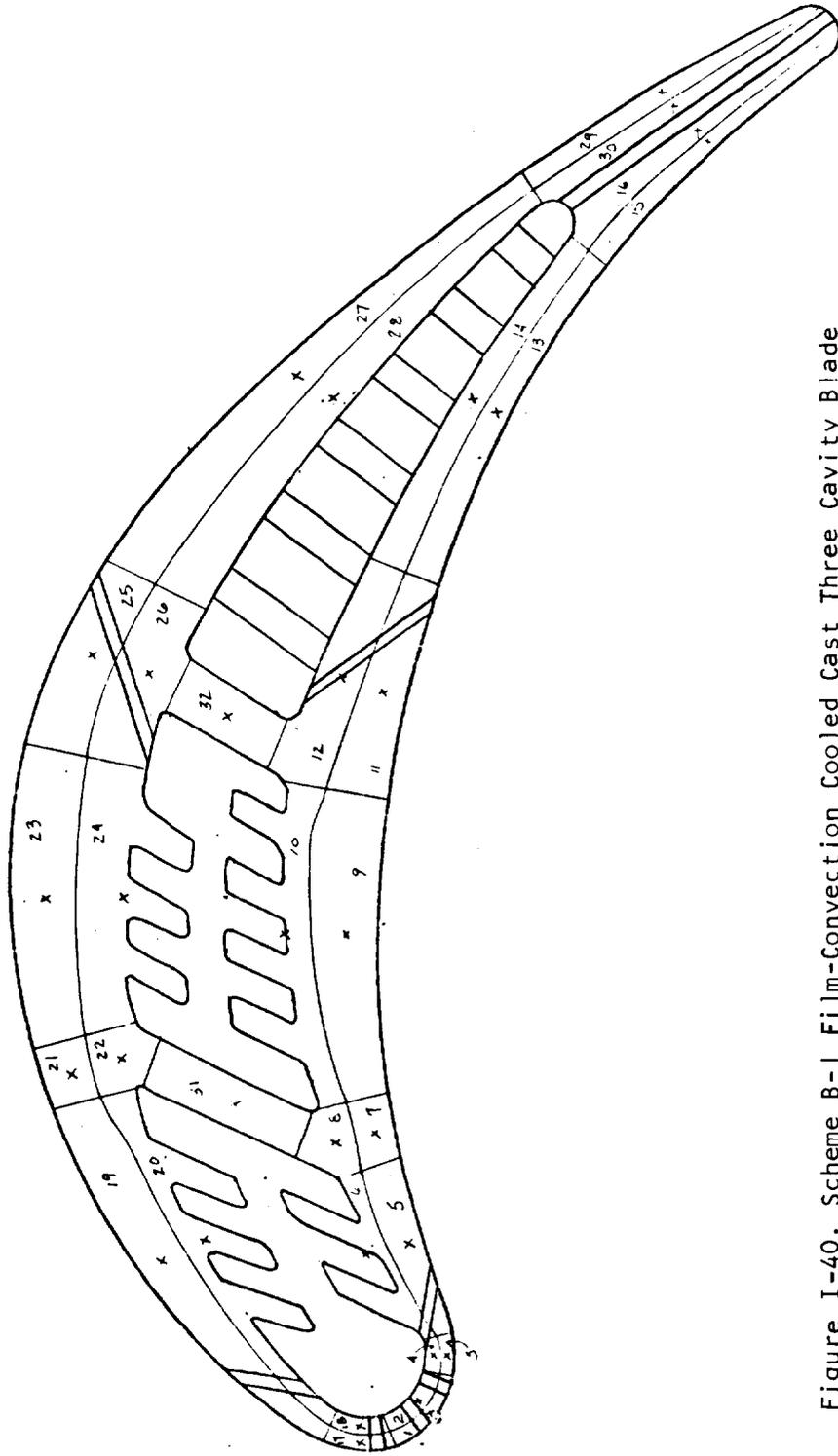
Figure I-40. Scheme B-I Film-Convection Cooled Cast Three Cavity Blade
Node Element Numbers
Hub Section (16.7 percent span)
1.0 in. (0.0254 m) chord
10 x size

S-67925

TABLE I-40

SCHEME B-I   FILM-CONVECTION COOLED CAST THREE CAVITY BLADE, 1.0 IN.
(0.0254 M) CHORD, HUB SECTION, 23585 RPM, TIT = 2500°F
(1644.4°K), WCA = 0.02818 LB/SEC/BLADE (5.53 PERCENT OF
HOT GAS FLOW), TCA = 900°F (755.6°K)

ELEMENT NO.	TEMPERATURE	STRESS	LIFE(HRS)
1	1436.0	21123.3	10 YRS PLUS
2	1419.0	25456.7	10 YRS PLUS
3	1419.0	23617.9	10 YRS PLUS
4	1407.0	27003.7	10 YRS PLUS
5	1415.0	22502.2	10 YRS PLUS
6	1364.0	36797.5	10 YRS PLUS
7	1439.0	14040.7	10 YRS PLUS
8	1390.0	27770.8	10 YRS PLUS
9	1450.0	6509.3	10 YRS PLUS
10	1374.0	27221.2	10 YRS PLUS
11	1363.0	21364.5	10 YRS PLUS
12	1290.0	40530.3	10 YRS PLUS
13	1189.0	55757.2	10 YRS PLUS
14	1165.0	61735.1	10 YRS PLUS
15	1338.0	5498.7	10 YRS PLUS
16	1321.0	9656.2	10 YRS PLUS
17	1436.0	23388.0	10 YRS PLUS
18	1422.0	26650.4	10 YRS PLUS
19	1394.0	33646.2	10 YRS PLUS
20	1327.0	49596.6	10 YRS PLUS
21	1455.0	14687.6	10 YRS PLUS
22	1408.0	25423.5	10 YRS PLUS
23	1510.0	-3858.3	10 YRS PLUS
24	1418.0	18510.7	10 YRS PLUS
25	1412.0	14235.4	10 YRS PLUS
26	1326.0	35318.2	10 YRS PLUS
27	1256.0	41926.5	10 YRS PLUS
28	1213.0	52986.2	10 YRS PLUS
29	1347.0	2922.3	10 YRS PLUS
30	1329.0	7481.6	10 YRS PLUS
31	1269.0	60535.5	10 YRS PLUS
32	1210.0	65402.0	10 YRS PLUS

Leading edge W_{CLE} = 0.00308 lb/sec/blade (0.605 percent of hot gas flow)

Suction side W_{CAS} = 0.00154 lb/sec/blade (0.302 percent of hot gas flow)

Pressure side W_{CAP} = 0.00101 lb/sec/blade (0.198 percent of hot gas flow)

Trailing edge W_{CTE} = 0.00272 lb/sec/blade (0.534 percent of hot gas flow)
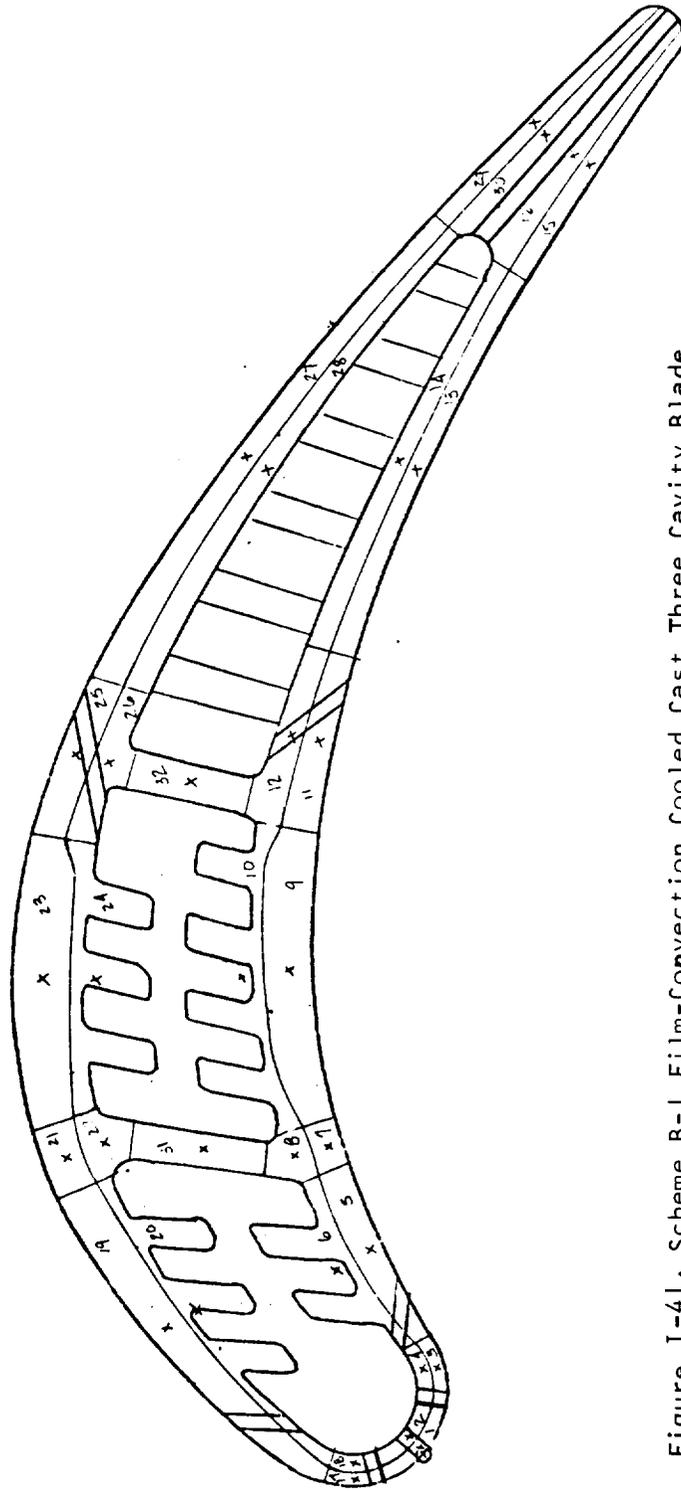
S-67926

Figure I-41. Scheme B-1 Film-Convection Cooled Cast Three Cavity Blade
Node Element Numbers
Mean Section (50 percent span)
1.0 in. (0.0254 m) chord
10 x size

TABLE I-41

SCHEME B-I FILM-CONVECTION COOLED CAST THREE CAVITY BLADE, I.O IN.
(0.0254 M) CHORD, MEAN SECTION

ELEMENT NO.	TEMPERATURE	STRESS	LIFE(HRS)
1	1588.0	2408.3	10 YRS PLUS
2	1578.0	5024.6	10 YRS PLUS
3	1580.0	2419.8	10 YRS PLUS
4	1572.0	4818.1	10 YRS PLUS
5	1522.0	16273.5	10 YRS PLUS
6	1487.0	26549.4	10 YRS PLUS
7	1527.0	13232.4	10 YRS PLUS
8	1497.0	21863.7	10 YRS PLUS
9	1522.0	11084.2	10 YRS PLUS
10	1475.0	24314.8	10 YRS PLUS
11	1482.0	15889.8	10 YRS PLUS
12	1441.0	26921.0	10 YRS PLUS
13	1367.0	37999.7	10 YRS PLUS
14	1352.0	41989.6	10 YRS PLUS
15	1496.0	-5016.6	10 YRS PLUS
16	1480.0	-798.7	10 YRS PLUS
17	1574.0	7824.6	10 YRS PLUS
18	1565.0	9910.4	10 YRS PLUS
19	1521.0	21323.9	10 YRS PLUS
20	1478.0	31883.5	50837.6320
21	1570.0	5822.0	10 YRS PLUS
22	1535.0	14273.3	10 YRS PLUS
23	1616.0	-10887.6	10 YRS PLUS
24	1561.0	3675.6	10 YRS PLUS
25	1519.0	10090.8	10 YRS PLUS
26	1475.0	21368.1	10 YRS PLUS
27	1392.0	33837.1	10 YRS PLUS
28	1372.0	38986.6	10 YRS PLUS
29	1490.0	-3591.2	10 YRS PLUS
30	1476.0	187.6	10 YRS PLUS
31*	1407.0	46672.8	19094.0620
32	1345.0	54608.4	30022.1320

Leading edge W_{CLE} = 0.00208 lb/sec/blade (0.408 percent of hot gas flow)

Suction side W_{CAS} = 0.00154 lb/sec/blade (0.302 percent of hot gas flow)

Pressure side W_{CAP} = 0.00101 lb/sec/blade (0.198 percent of hot gas flow)

Trailing edge W_{CTE} = 0.00272 lb/sec/blade (0.534 percent of hot gas flow)
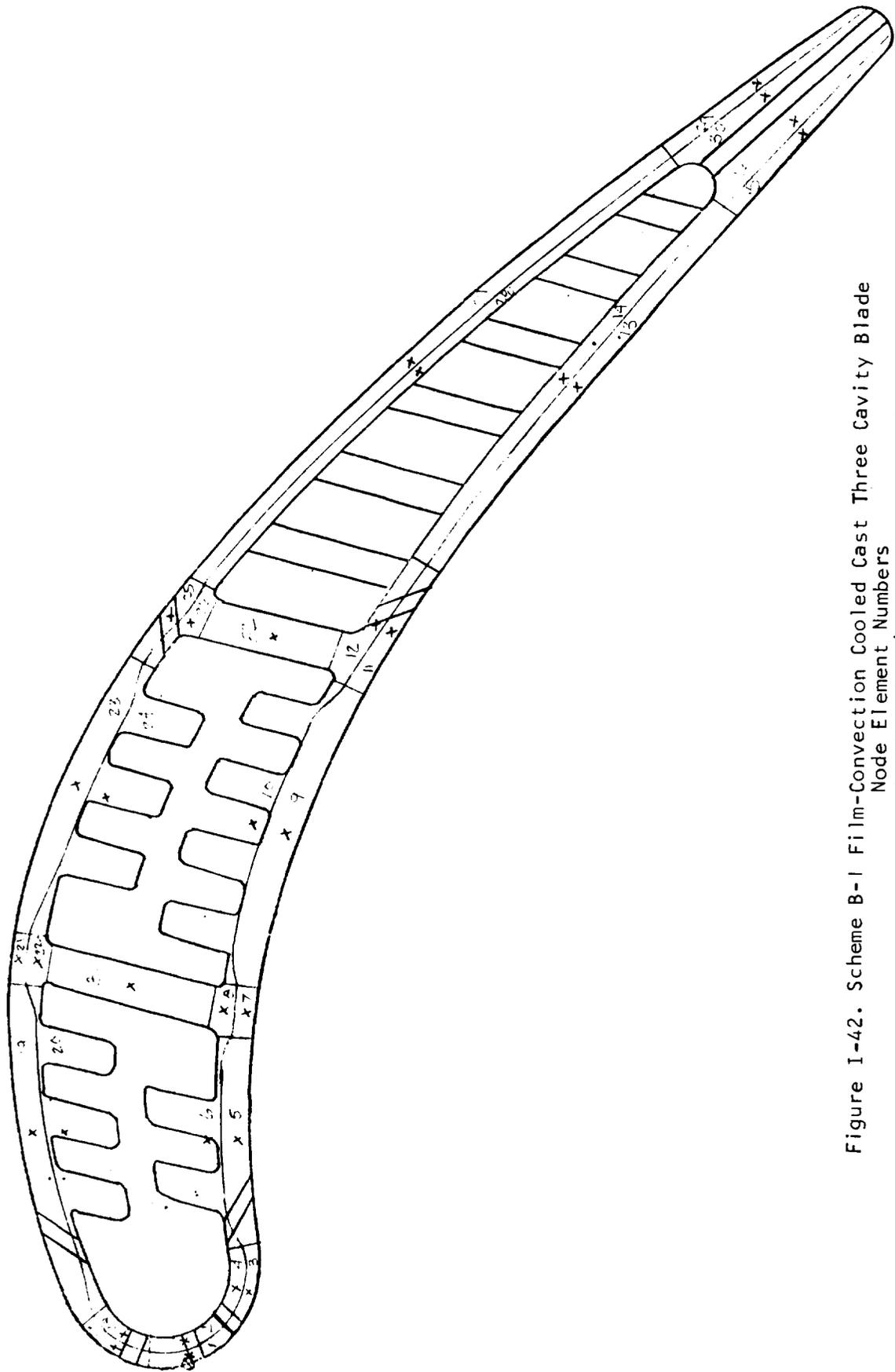
Figure I-42. Scheme B-I Film-Convection Cooled Cast Three Cavity Blade
Node Element Numbers
Tip Section (83.3 percent span)
1.0 in. (0.0254 m) chord
10 x size

S-67927

TABLE I-42

SCHEME B-I FILM-CONVECTION COOLED CAST THREE CAVITY BLADE, I.0 IN. (0.0254 M) CHORD, TIP SECTION

ELEMENT NO.	TEMPERATURE	STRESS	LIFE(HRS)
1	1662.0	-132.1	19031.3440
2	1656.0	1443.7	17886.8200
3	1695.0	-9603.7	1769.7422
4	1692.0	-9042.2	2085.7076
5	1683.0	-8083.1	3040.7901
6	1670.0	-4800.6	7198.5092
7	1652.0	-21.1	25104.9580
8	1642.0	2507.3	21548.8020
9	1601.0	14416.3	8481.6831
10	1582.0	18731.7	6682.2288
11	1667.0	-12012.3	1452.2031
12	1675.0	-8843.8	3271.9594
13	1652.0	-265.0	24110.4980
14	1645.0	1470.5	23680.4700
15	1707.0	-14965.6	557.0093
16	1696.0	-12043.2	1162.4005
17	1665.0	-8881.8	2540.8734
18	1681.0	-7645.7	3431.4384
19	1677.0	-10939.7	2209.1436
20	1658.0	-4474.7	10296.3230
21	1663.0	-15134.6	961.1785
22	1665.0	-9306.3	3889.0541
23	1697.0	-20153.5	304.2722
24	1677.0	-13383.4	1480.5286
25	1653.0	-6920.2	7804.0262
26	1623.0	2802.5	33779.1760
27	1610.0	8573.9	18013.0320
28	1603.0	11060.8	14218.7242
29	1697.0	-13598.7	881.5896
30	1668.0	-10574.7	1791.5695
31	1547.0	27404.5	3753.5454
32*	1528.0	31433.4	3066.9904

Leading edge W_{CLE} = 0.00208 lb/sec/blade (0.408 percent of hot gas flow)

Suction side W_{CAS} = 0.00154 lb/sec/blade (0.302 percent of hot gas flow)

Pressure side W_{CAP} = 0.00101 lb/sec/blade (0.198 percent of hot gas flow)

Trailing Edge W_{CTE} = 0.00272 lb/sec/blade (0.534 percent of hot gas flow)

Tip discharge W_{CTD} = 0.00513 lb/sec/blade (1.007 percent of hot gas flow)
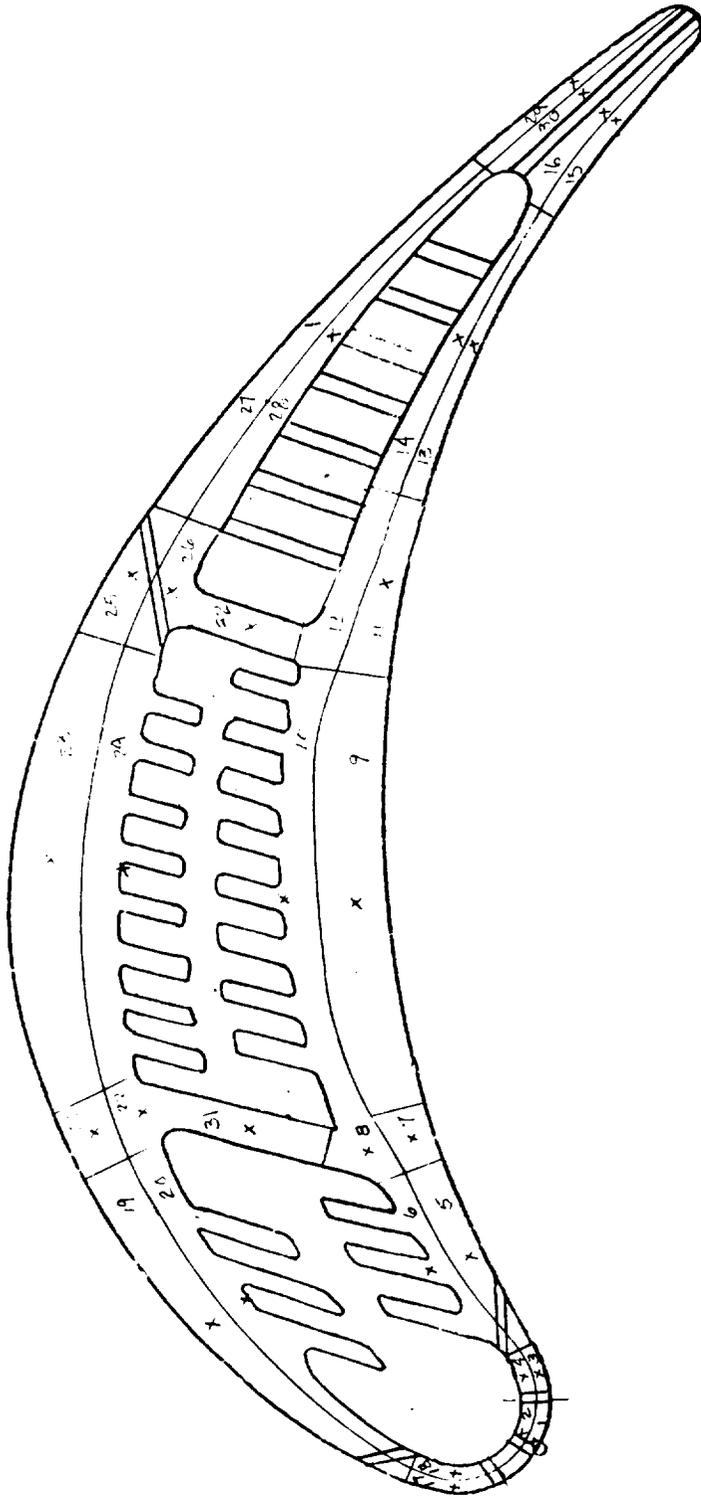
Figure I-43. Scheme B-1 Film-Convection Cooled Cast Three Cavity Blade
Node Element Numbers
Hub Section (16.7 percent span)
1.5 in. (0.0381 m) chord
5 x size

S-67926

TABLE I-43

SCHEME B-I   FILM-CONVECTION COOLED CAST THREE CAVITY BLADE, 1.5 IN.
(0.0381 M) CHORD, HUB SECTION, 23585 RPM, TIT = 2500°F
(1644.4°K), WCA = 0.04585 LB/SEC/BLADE (6.05 PERCENT OF
HOT GAS FLOW), TCA = 900°F (755.6°K)

ELEMENT NO.	TEMPERATURE	STRESS	LIFE(HRS)
1	1420.0	37461.9	77725.0620
2	1402.0	42157.0	49861.5240
3	1428.0	34432.0	10 YRS PLUS
4	1415.0	38021.7	79214.3190
5	1463.0	24621.4	10 YRS PLUS
6	1412.0	38635.3	74966.3230
7	1498.0	14683.5	10 YRS PLUS
8	1444.0	29623.7	10 YRS PLUS
9	1510.0	9190.5	10 YRS PLUS
10	1400.0	38830.1	10 YRS PLUS
11	1475.0	13884.8	10 YRS PLUS
12	1410.0	31123.9	10 YRS PLUS
13	1483.0	7569.7	10 YRS PLUS
14	1446.0	17363.7	10 YRS PLUS
15	1475.0	4899.5	10 YRS PLUS
16	1445.0	12779.5	10 YRS PLUS
17	1470.0	26034.7	10 YRS PLUS
18	1458.0	28971.4	10 YRS PLUS
19	1482.0	23867.7	10 YRS PLUS
20	1420.0	39367.3	49339.6490
21	1513.0	14764.4	10 YRS PLUS
22	1454.0	29371.7	10 YRS PLUS
23	1552.0	1380.4	10 YRS PLUS
24	1431.0	32495.2	10 YRS PLUS
25	1362.0	46482.3	78660.5000
26	1293.0	64579.2	22586.5100
27	1301.0	56865.6	80014.5370
28	1274.0	63997.1	47053.3400
29	1423.0	18518.0	10 YRS PLUS
30	1405.0	23135.9	10 YRS PLUS
31*	1286.0	71489.9	6915.1182
32	1221.0	78368.3	13466.2130

Leading edge W_{CLE} = 0.00478 lb/sec/blade (0.631 percent of hot gas flow)

Suction side W_{CAS} = 0.00265 lb/sec/blade (0.35 percent of hot gas flow)

Pressure side W_{CAP} = 0.0005 lb/sec/blade (0.066 percent of hot gas flow)

Trailing edge W_{CTE} = 0.00302 lb/sec/blade (0.399 percent of hot gas flow)
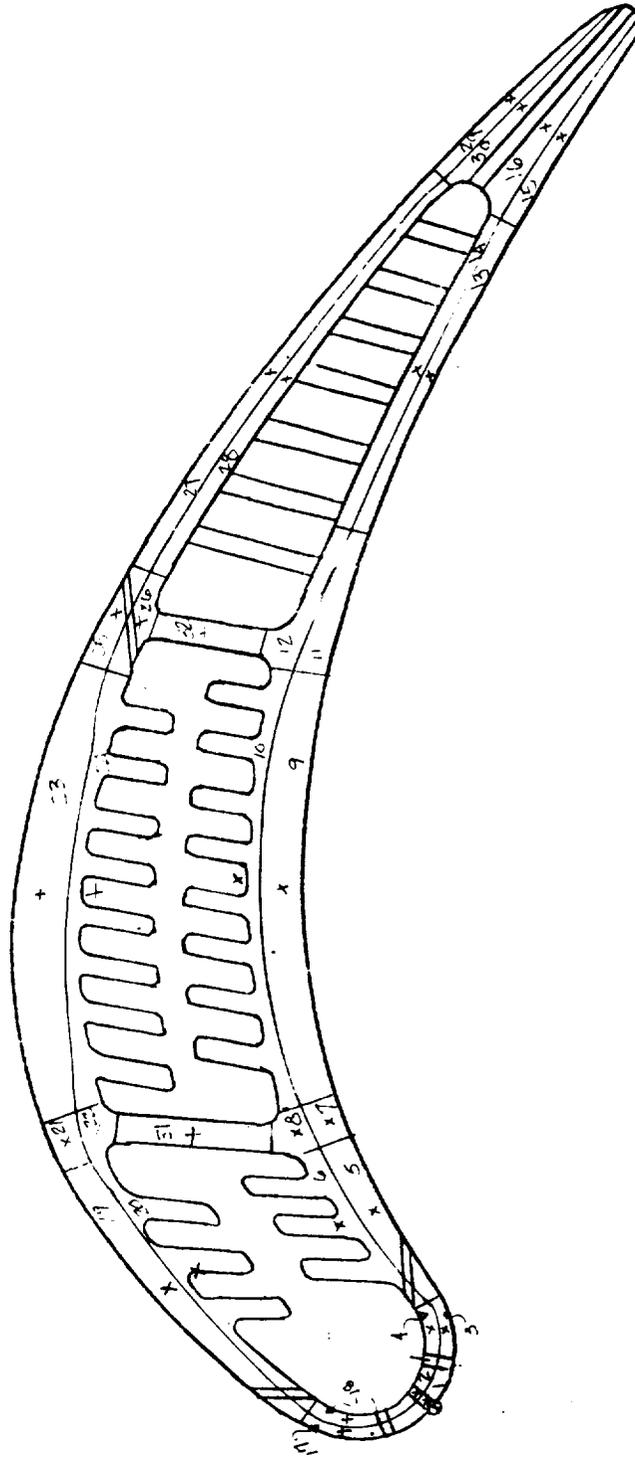
Figure I-44. Scheme B-I Film-Convection Cooled Cast Three Cavity Blade
Node Element Numbers
Mean Section (50 percent span)
1.5 in. (0.0381 m) chord
5 x size

S-67929

TABLE I-44

SCHEME B-1 FILM-CONVECTION COOLED CAST THREE CAVITY BLADE, 1.5 IN.
(0.0381 M) CHORD, MEAN SECTION

| ELEMENT NO.	TEMPERATURE	STRESS	LIFE(HRS)
1	1568.0	11711.1	10 YRS PLUS
2	1555.0	15018.6	10 YRS PLUS
3	1576.0	10075.5	10 YRS PLUS
4	1567.0	12301.5	10 YRS PLUS
5	1542.0	18333.3	10 YRS PLUS
6	1505.0	27582.2	62083.4570
7	1546.0	16741.6	10 YRS PLUS
8	1507.0	26547.2	74170.7320
9	1540.0	18291.9	10 YRS PLUS
10	1477.0	34278.1	30074.0600
11	1608.0	1525.2	10 YRS PLUS
12	1566.0	12831.9	10 YRS PLUS
13	1682.0	-18397.4	5226.6948
14	1657.0	-11150.7	10 YRS PLUS
15	1634.0	-852.3	10 YRS PLUS
16	1608.0	6858.0	10 YRS PLUS
17	1598.0	1962.1	10 YRS PLUS
18	1589.0	4556.1	10 YRS PLUS
19	1562.0	9030.8	10 YRS PLUS
20	1520.0	20820.5	10 YRS PLUS
21	1575.0	4138.7	10 YRS PLUS
22	1539.0	14407.6	10 YRS PLUS
23	1616.0	-7125.5	10 YRS PLUS
24	1537.0	15740.4	10 YRS PLUS
25	1465.0	36123.9	27800.7630
26	1422.0	47750.5	10100.5197
27	1447.0	44454.0	8715.8646
28	1432.0	48657.8	6425.9294
29	1582.0	13711.8	10 YRS PLUS
30	1566.0	18193.2	10 YRS PLUS
31	1363.0	62619.9	3844.2016
32*	1342.0	68355.6	2332.0738

Leading edge W_{CLE} = 0.00328 lb/sec/blade (0.433 percent of hot gas flow)

Suction side W_{CAS} = 0.00265 lb/sec/blade (0.35 percent of hot gas flow)

Pressure side W_{CAP} = 0.0005 lb/sec/blade (0.066 percent of hot gas flow)

Trailing edge W_{CTE} = 0.00302 lb/sec/blade (0.399 percent of hot gas flow)

316
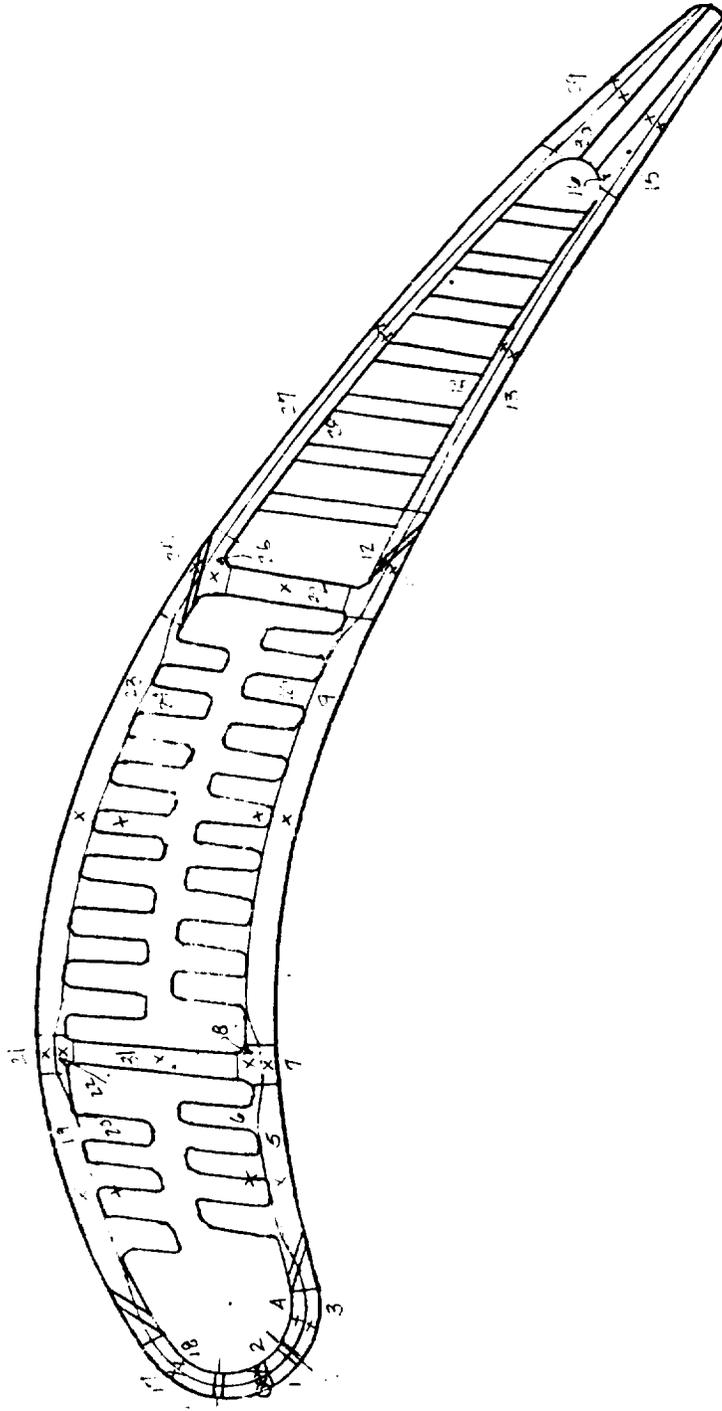
Figure I-45. Scheme B-I Film-Convection Cooled Cast Three Cavity Blade
Node Element Numbers
Tip Section (83.3 percent span)
1.5 in. (0.0381 m) chord
5 x size

S-67930

TABLE I-45

SCHEME B-1 FILM-CONVECTION COOLED CAST THREE CAVITY BLADE, 1.5 IN.
(0.0381 M) CHORD, TIP SECTION

| ELEMENT NO.	TEMPERATURE	STRESS	LIFE(HRS)
1	1624.0	4563.1	24480.3720
2	1616.0	6721.3	21022.4610
3	1647.0	-1173.4	23616.4530
4	1642.0	-152.4	31889.4540
5	1678.0	-12865.2	1572.7615
6	1661.0	-8962.7	4549.1411
7	1627.0	1261.1	39349.4120
8	1612.0	5033.1	31065.9580
9	1564.0	12558.6	18228.1320
10	1555.0	19122.9	12792.8190
11	1689.0	-16641.8	650.8402
12	1678.0	-13754.7	1359.6366
13	1672.0	-8671.8	3625.7606
14	1665.0	-6942.5	5739.8984
15	1721.0	-19398.9	196.7961
16	1705.0	-15172.7	564.7476
17	1703.0	-22849.2	170.9309
18	1695.0	-20322.8	310.2543
19	1661.0	-15489.9	1549.6911
20	1641.0	-8180.3	8599.5952
21	1640.0	-11771.0	4850.8988
22	1625.0	-6467.7	17323.2490
23	1647.0	-14468.2	2596.7956
24	1614.0	-2717.2	43534.4480
25	1531.0	20661.6	18757.2020
26	1508.0	27957.1	9715.1948
27	1619.0	1991.6	43050.7750
28	1613.0	4116.5	35310.8790
29	1661.0	-9591.1	2496.6379
30	1669.0	-5524.2	6554.4703
31*	1430.0	50325.6	1439.8304
32	1446.0	47336.2	1609.2421

Leading edge W_{CLE} = 0.00328 lb/sec/blade (0.433 percent of hot gas flow)

Suction side W_{CAS} = 0.00265 lb/sec/blade (0.35 percent of hot gas flow)

Pressure side W_{CAP} = 0.00162 lb/sec/blade (0.214 percent of hot gas flow)

Trailing edge W_{CTE} = 0.00302 lb/sec/blade (0.399 percent of hot gas flow)

Tip discharge W_{CTD} = 0.01488 lb/sec/blade (1.96 percent of hot gas flow)
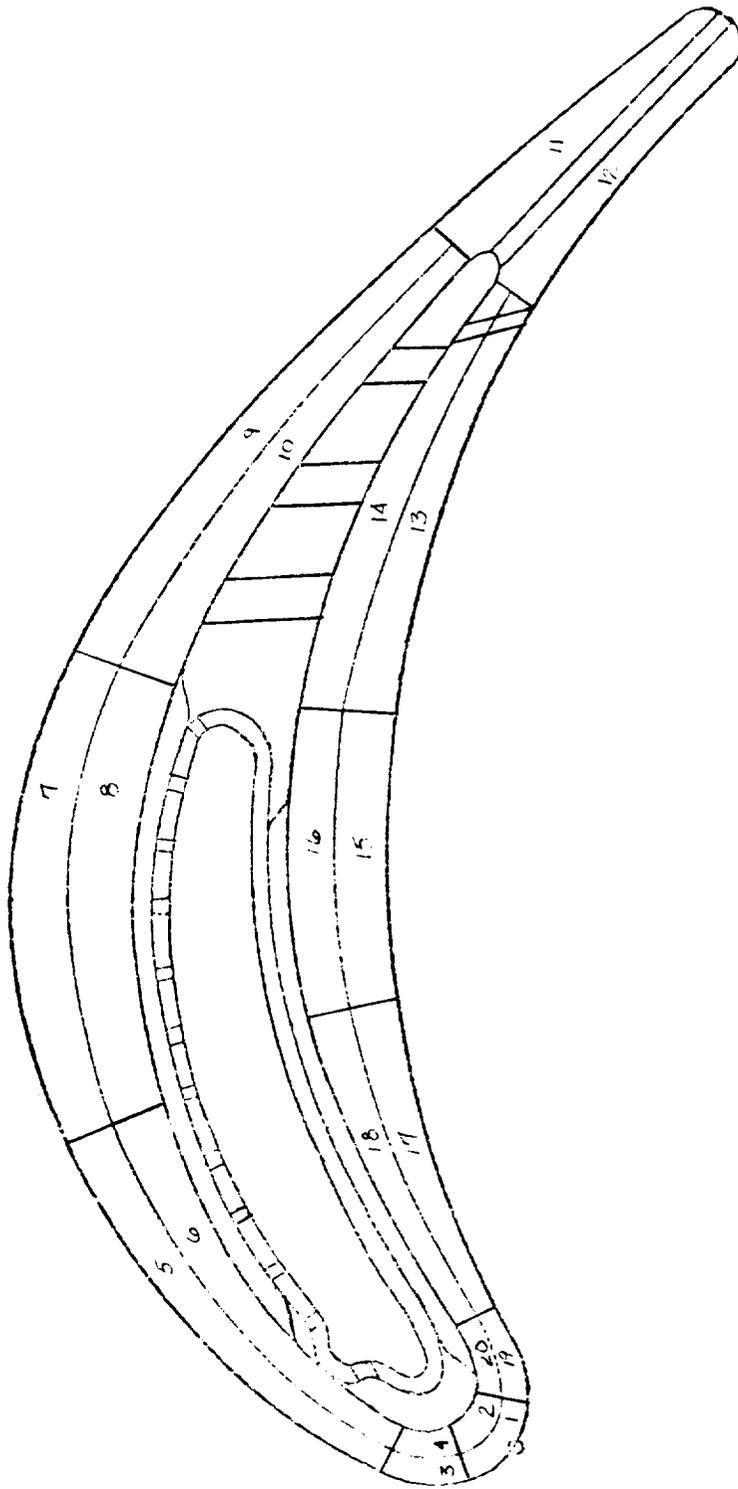
S-67931

Figure I-46.   Scheme B-4 Film-Convection Cooled Cast Impingement
Tube Blade with Crossflow Impingement and Sharp
Corner Flow Leading Edge--Node Element Numbers

Hub Section (16.7 percent span)
0.75 in. (0.01 05 m) chord
10 x size

TABLE I-46

SCHEME B-1   FILM-CONVECTION COOLED CAST IMPINGEMENT TUBE BLADE WITH CROSS-
FLOW IMPINGEMENT AND SHARP CORNER FLOW LEADING EDGE, 0.75 IN.
(0.01905 M) CHORD, HUB SECTION, 22567 RPM, TIT = 2250°F
(1505.6°K), WCA = 0.01728 LB/SEC/BLADE (4.27 PERCENT OF HOT
GAS FLOW), TCA = 900°F (755.6°K)

ELEMENT NO.	TEMPERATURE	STRESS	LIFE(HRS)
1	1502.0	32042.3	24445.8300
2	1432.0	49193.9	5845.8681
3	1465.0	38729.3	15152.8317
4*	1394.0	56840.3	4528.5495
5	1475.0	23097.8	10 YRS PLUS
6	1433.0	35333.9	86805.0460
7	1423.0	25442.1	10 YRS PLUS
8	1362.0	44031.9	10 YRS PLUS
9	1455.0	23251.1	10 YRS PLUS
10	1418.0	34813.8	10 YRS PLUS
11	1531.0	16263.8	10 YRS PLUS
12	1485.0	31645.9	43758.1200
13	1400.0	46903.1	22611.4860
14	1367.0	53752.6	17807.9490
15	1532.0	11660.1	10 YRS PLUS
16	1491.0	20387.4	10 YRS PLUS
17	1521.0	20397.1	10 YRS PLUS
18	1487.0	28136.3	10 YRS PLUS
19	1473.0	38945.2	11446.4416
20	1420.0	52167.2	4889.1167

Leading Edge and Pressure Side W_{CLE} = 0.0019 lb/sec/blade (0.469 percent
of hot gas flow)

Suction Side W_{CAS} = 0.00404 lb/sec/blade (0.998 percent of hot gas flow)
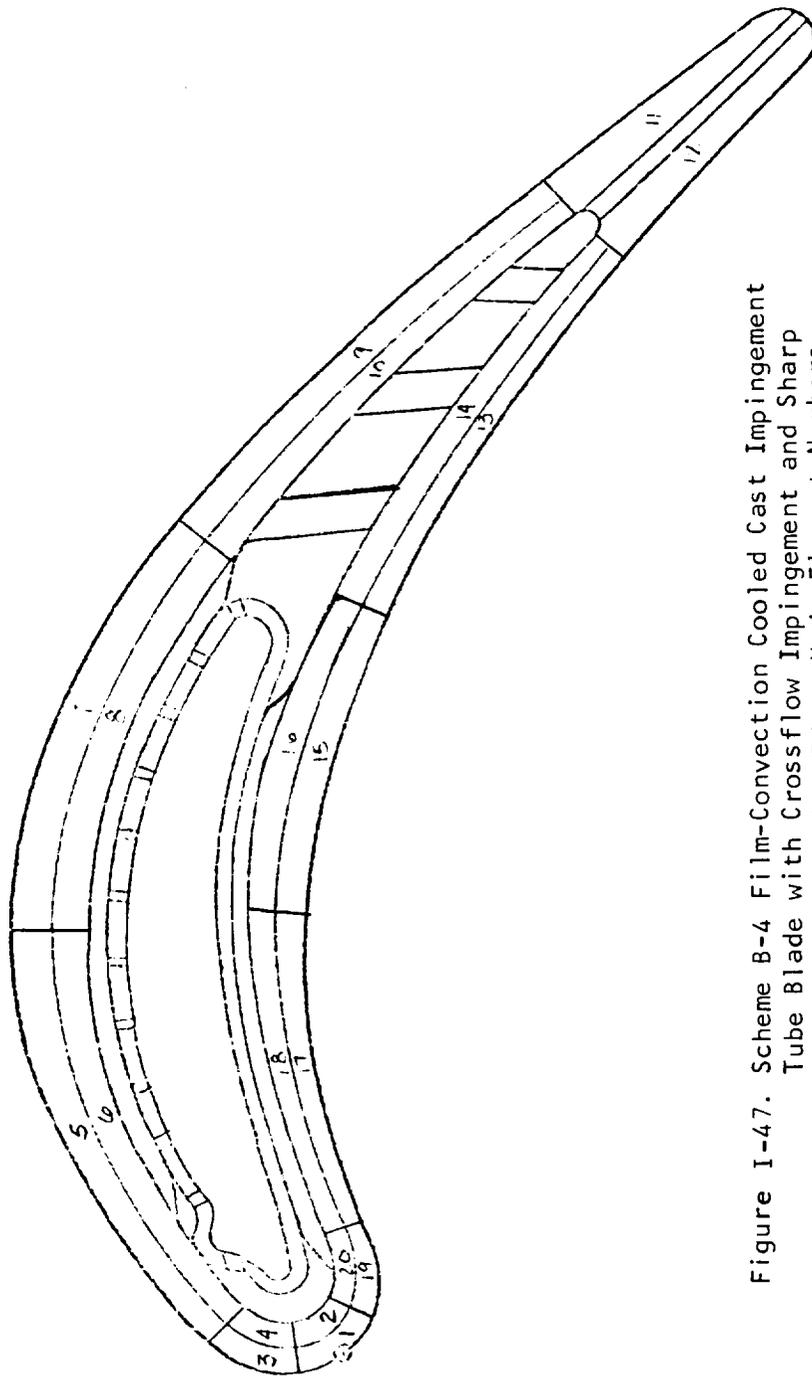
Figure I-47. Scheme B-4 Film-Convection Cooled Cast Impingement
Tube Blade with Crossflow Impingement and Sharp
Corner Flow Leading Edge--Node Element Numbers
Mean Section (50 percent span)
0.75 in. (0.01905 m) chord
10 x size

S-67932

TABLE I-47

SCHEME B-4 FILM-CONVECTION COOLED CAST IMPINGEMENT TUBE BLADE WITH CROSSFLOW IMPINGEMENT AND SHARP CORNER FLOW LEADING EDGE, 0.75 IN. (0.01905 M) CHORD, MEAN SECTION

| ELEMENT NO.	TEMPERATURE	STRESS	LIFE(HRS)
1	1587.0	26884.7	7347.7869
2*	1525.0	48636.3	494.3954
3	1523.0	39041.3	2770.8096
4	1460.0	54970.0	963.9131
5	1561.0	11758.0	10 YRS PLUS
6	1518.0	25403.2	69912.7000
7	1499.0	19202.1	10 YRS PLUS
8	1450.0	34679.2	60719.4800
9	1548.0	17041.5	10 YRS PLUS
10	1518.0	26913.4	49645.3960
11	1657.0	-367.5	10 YRS PLUS
12	1597.0	22411.1	14916.2212
13	1502.0	39050.8	4926.9680
14	1478.0	43975.7	3918.7859
15	1665.0	-10544.6	10 YRS PLUS
16	1633.0	-3111.0	10 YRS PLUS
17	1623.0	8009.3	10 YRS PLUS
18	1599.0	13946.5	10 YRS PLUS
19	1561.0	34846.4	2547.0057
20	1520.0	44392.3	1153.9239

Leading Edge and Pressure Side W_{CLE} = 0.0019 lb/sec/blade (0.469 percent of hot gas flow)

Suction Side W_{CAS} = 0.00404 lb/sec/blade (0.998 percent of hot gas flow)

322
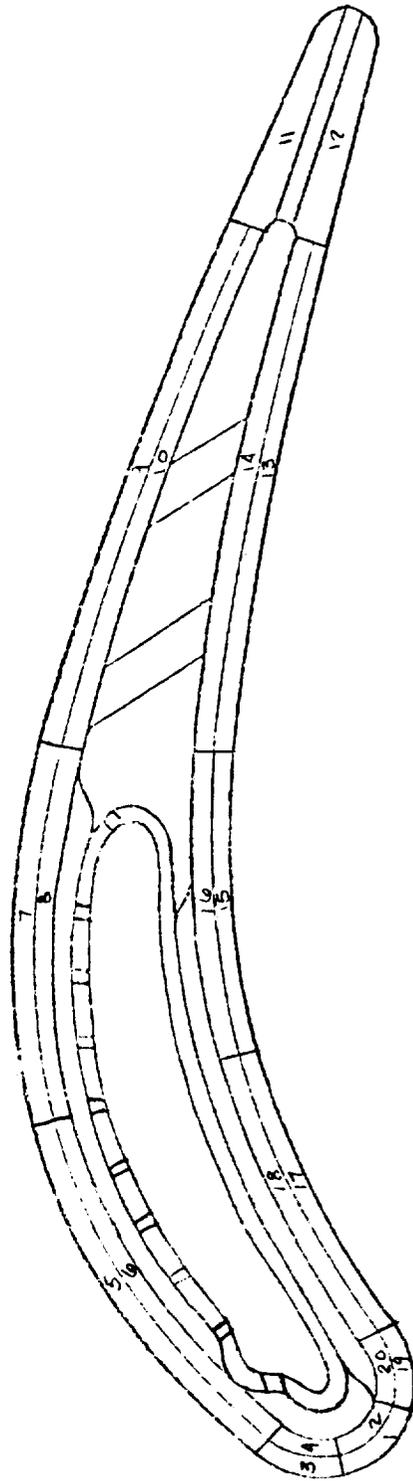
S-67933

Figure I-48. Scheme B-4 Film-Convection Cooled Cast Impingement
Tube Blade with Crossflow Impingement and Sharp
Corner Flow Leading Edge--Node Element Numbers
Tip Section (83.3 percent span)
0.75 in. (0.01905 m) chord
10 x size

323

TABLE I-48

SCHEME B-4   FILM-CONVECTION COOLED CAST IMPINGEMENT TUBE BLADE WITH
CROSSFLOW IMPINGEMENT AND SHARP CORNER FLOW LEADING EDGE,
0.75 IN. (0.01905 M) CHORD, TIP SECTION

ELEMENT NO.	TEMPERATURE	STRESS	LIFE(HRS)
1	1652.0	2856.4	57673.3730
2	1618.0	11521.3	92320.9120
3	1592.0	12004.4	10 YRS PLUS
4	1558.0	22187.5	57709.0050
5	1596.0	-8007.5	87716.1730
6	1570.0	832.4	10 YRS PLUS
7	1514.0	6875.5	10 YRS PLUS
8	1490.0	15536.0	10 YRS PLUS
9	1626.0	-10597.9	89046.3110
10	1607.0	-3101.9	10 YRS PLUS
11	1634.0	-10327.4	20523.3040
12 *	1637.0	9685.3	20633.7100
13	1591.0	12743.8	10 YRS PLUS
14	1573.0	16215.5	10 YRS PLUS
15	1706.0	-26505.1	544.8582
16	1691.0	-23746.3	1372.4957
17	1642.0	-1593.9	97787.0950
18	1625.0	2028.3	10 YRS PLUS
19	1653.0	5263.1	34107.7350
20	1627.0	11021.6	79845.8640

Leading Edge and Pressure Side W_{CLE} = 0.0019 lb/sec/blade (0.469 percent
of hot gas flow)

Suction Side W_{CAS} = 0.0035 lb/sec/blade (0.864 percent of hot gas flow)
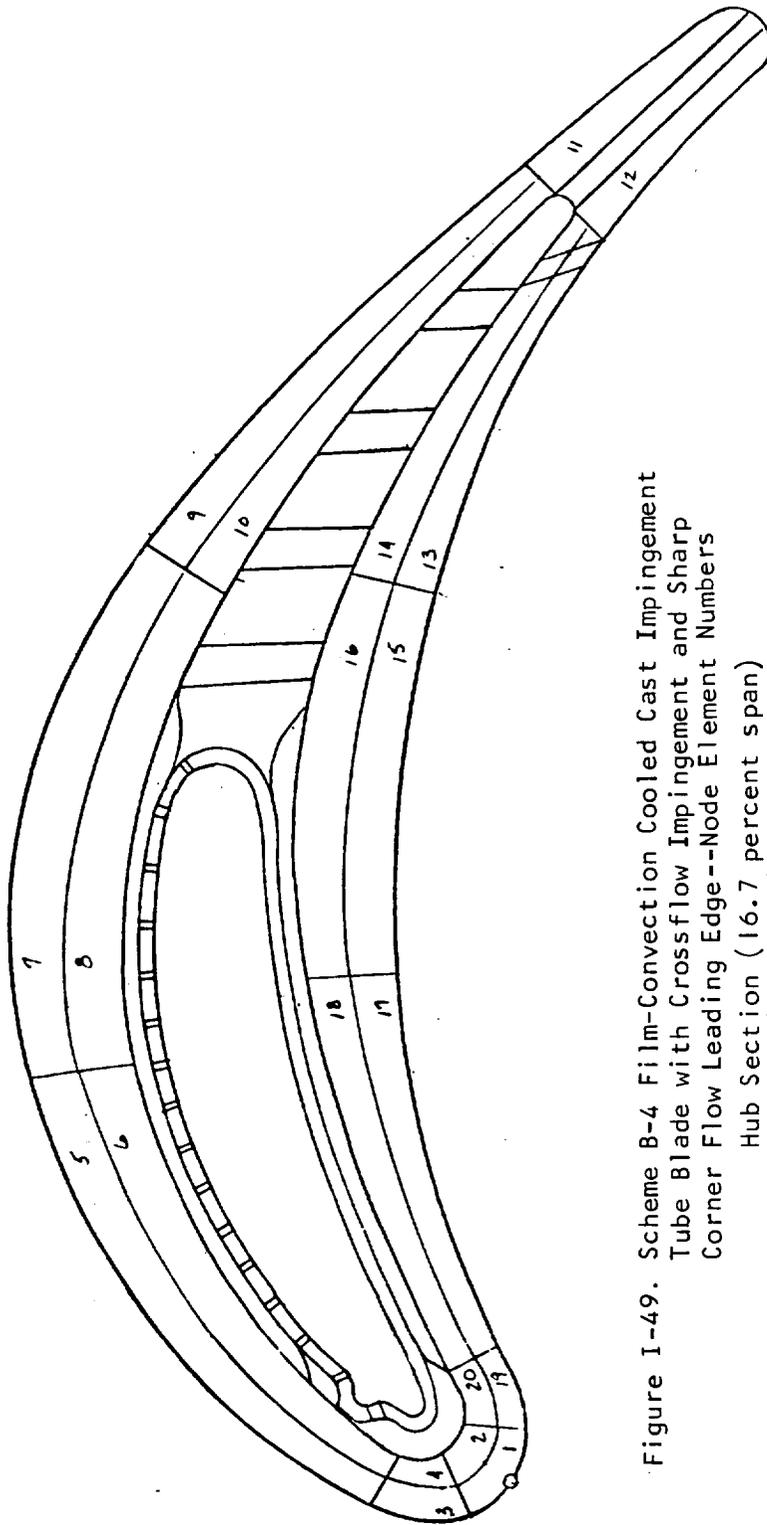
324

Figure I-49. Scheme B-4 Film-Convection Cooled Cast Impingement Tube Blade with Crossflow Impingement and Sharp Corner Flow Leading Edge--Node Element Numbers

Hub Section (16.7 percent span)
1.0 in. (0.0254 m) chord
10 x size

S-67934

TABLE I-49

SCHEME B-4   FILM-CONVECTION COOLED CAST IMPINGEMENT TUBE BLADE WITH CROSS-
FLOW IMPINGEMENT AND SHARP CORNER FLOW LEADING EDGE, 1.0 IN.
(0.0254 M) CHORD, HUB SECTION, 22774 RPM, TIT = 2300°F
(1533.3°K), WCA = 0.02583 LB/SEC/BLADE (4.89 PERCENT OF HOT
GAS FLOW), TCA = 900°F (755.6°K)

ELEMENT NO.	TEMPERATURE	STRESS	LIFE(HRS)
1	1682.0	-2193.8	10 YRS PLUS
2	1570.0	29835.8	6066.3667
3	1629.0	12965.7	10 YRS PLUS
4*	1542.0	36483.7	2943.7693
5	1561.0	14826.1	10 YRS PLUS
6	1496.0	32599.1	25560.9660
7	1487.0	9378.5	10 YRS PLUS
8	1394.0	35926.5	10 YRS PLUS
9	1453.0	10075.0	10 YRS PLUS
10	1409.0	23075.8	10 YRS PLUS
11	1561.0	-18327.1	10 YRS PLUS
12	1406.0	25302.6	10 YRS PLUS
13	1327.0	50408.7	10 YRS PLUS
14	1260.0	66749.9	42272.8390
15	1470.0	24767.0	10 YRS PLUS
16	1405.0	39742.2	71229.3870
17	1572.0	14952.1	10 YRS PLUS
18	1536.0	23899.5	58507.8980
19	1628.0	11183.7	10 YRS PLUS
20	1570.0	27552.5	10045.3484

Leading Edge and Pressure Side W_{CLE} = 0.00304 lb/sec/blade (0.575 percent
of hot gas flow)

Suction Side W_{CAS} = 0.00582 lb/sec/blade (1.102 percent of hot gas flow)

326
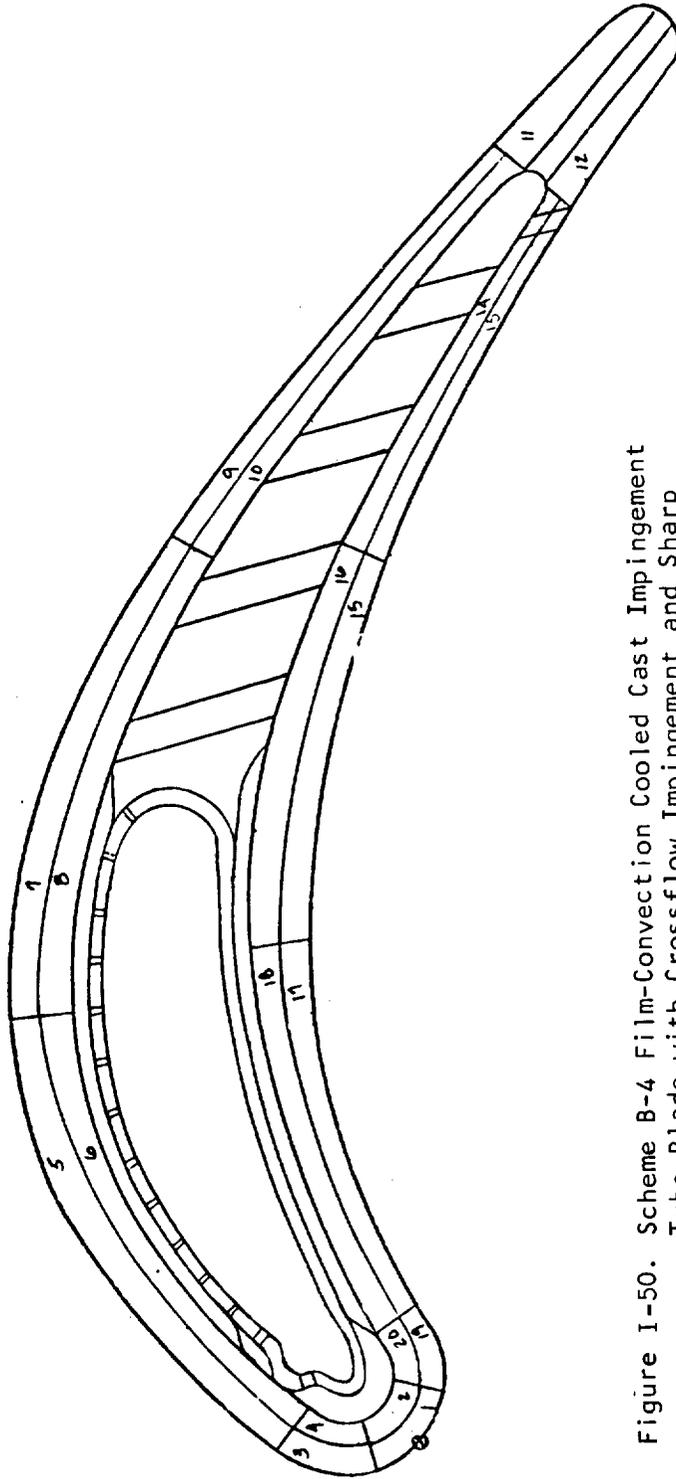
Figure I-50. Scheme B-4 Film-Convection Cooled Cast Impingement Tube Blade with Crossflow Impingement and Sharp Corner Flow Leading Edge--Node Element Numbers

Mean Section (50 percent span)
1.0 in. (0.0254 m) chord
10 x size

S-67935

TABLE I-50

SCHEME B-4 FILM-CONVECTION COOLED CAST IMPINGEMENT TUBE BLADE WITH CROSS-FLOW IMPINGEMENT AND SHARP CORNER FLOW LEADING EDGE, 1.0 IN. (0.0254 M) CHORD, MEAN SECTION

ELEMENT NO.	TEMPERATURE	STRESS	LIFE(HRS)
1	1608.0	2809.3	10 YRS PLUS
2	1527.0	24519.9	65855.0650
3	1527.0	24822.4	61509.8880
4*	1446.0	45881.2	6987.0339
5	1544.0	15193.9	10 YRS PLUS
6	1490.0	29542.9	61360.7490
7	1534.0	9043.5	10 YRS PLUS
8	1485.0	22403.8	10 YRS PLUS
9	1522.0	6963.0	10 YRS PLUS
10	1494.0	14633.2	10 YRS PLUS
11	1569.0	-8300.2	10 YRS PLUS
12	1478.0	16731.4	10 YRS PLUS
13	1413.0	37208.3	10 YRS PLUS
14	1344.0	55051.4	28536.8270
15	1491.0	22324.3	10 YRS PLUS
16	1454.0	31715.0	10 YRS PLUS
17	1603.0	-1367.8	10 YRS PLUS
18	1574.0	6551.2	10 YRS PLUS
19	1593.0	5884.9	10 YRS PLUS
20	1530.0	22821.8	10 YRS PLUS

Leading Edge and Pressure Side W_{CLE} = 0.00304 lb/sec/blade (0.575 percent of hot gas flow)

Suction Side W_{CAS} = 0.00582 lb/sec/blade (1.102 percent of hot gas flow)
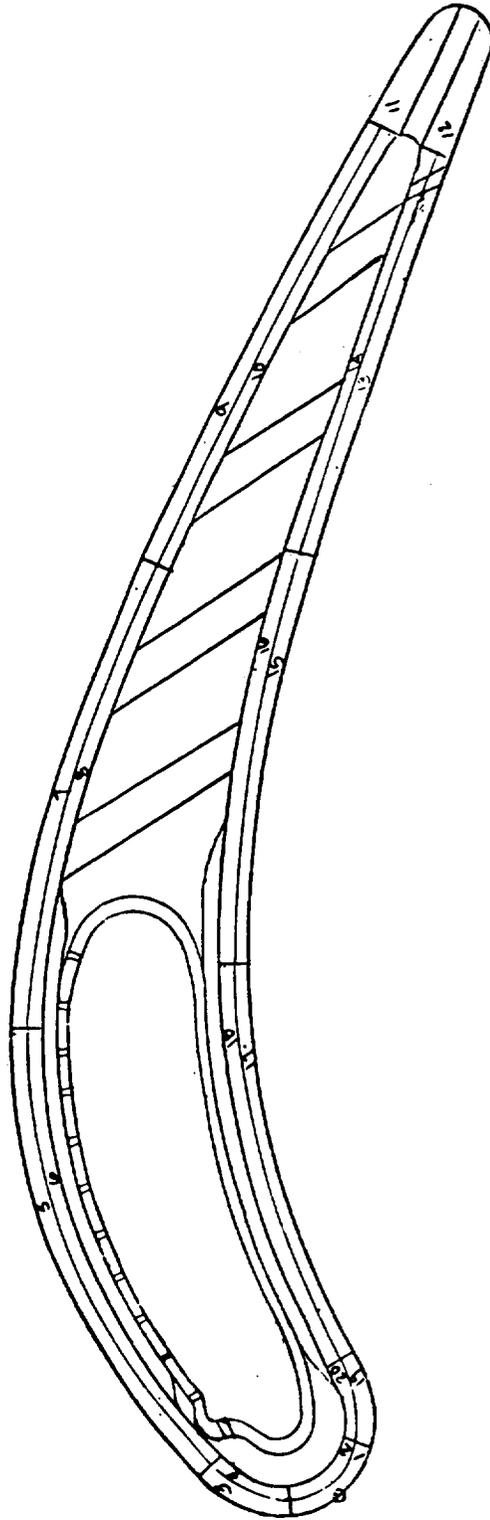
5-67936

Figure I-51. Scheme B-4 Film-Convection Cooled Cast Impingement
Tube Blade with Crossflow Impingement and Sharp
Corner Flow Leading Edge--Node Element Numbers

Tip Section (83.3 percent span)
1.0 in. (0.0254 m) chord
10 x size

TABLE I-51

SCHEME B-4   FILM CONVECTION COOLED CAST IMPINGEMENT TUBE BLADE WITH CROSS-
FLOW IMPINGEMENT AND SHARP CORNER FLOW LEADING EDGE, 1.0 IN.
(0.0254 M) CHORD, TIP SECTION

ELEMENT NO.	TEMPERATURE	STRESS	LIFE(HRS)
1	1522.0	-799.6	10 YRS PLUS
2	1477.0	12235.4	10 YRS PLUS
3	1470.0	19619.3	10 YRS PLUS
4	1438.0	28083.6	10 YRS PLUS
5	1643.0	-13955.4	29642.4780
6	1619.0	-7832.0	48939.8020
7	1605.0	3813.0	10 YRS PLUS
8	1585.0	8573.3	10 YRS PLUS
9	1607.0	-4337.1	10 YRS PLUS
10	1549.0	12.3	10 YRS PLUS
11	1670.0	-29028.6	839.9279
12	1590.0	-10112.9	10 YRS PLUS
13	1527.0	10843.4	10 YRS PLUS
14	1470.0	27615.2	10 YRS PLUS
15	1569.0	956.4	10 YRS PLUS
16	1553.0	6811.8	10 YRS PLUS
17	1606.0	-16361.6	49560.8430
18	1592.0	-11486.3	10 YRS PLUS
19	1464.0	14151.0	10 YRS PLUS
20	1432.0	23620.5	10 YRS PLUS

Leading Edge and Pressure Side W_{CLE} = 0.00254 lb/sec/blade (0.481 percent of
hot gas flow)

Suction Side W_{CAS} = 0.00557 lb/sec/blade (1.054 percent of hot gas flow)
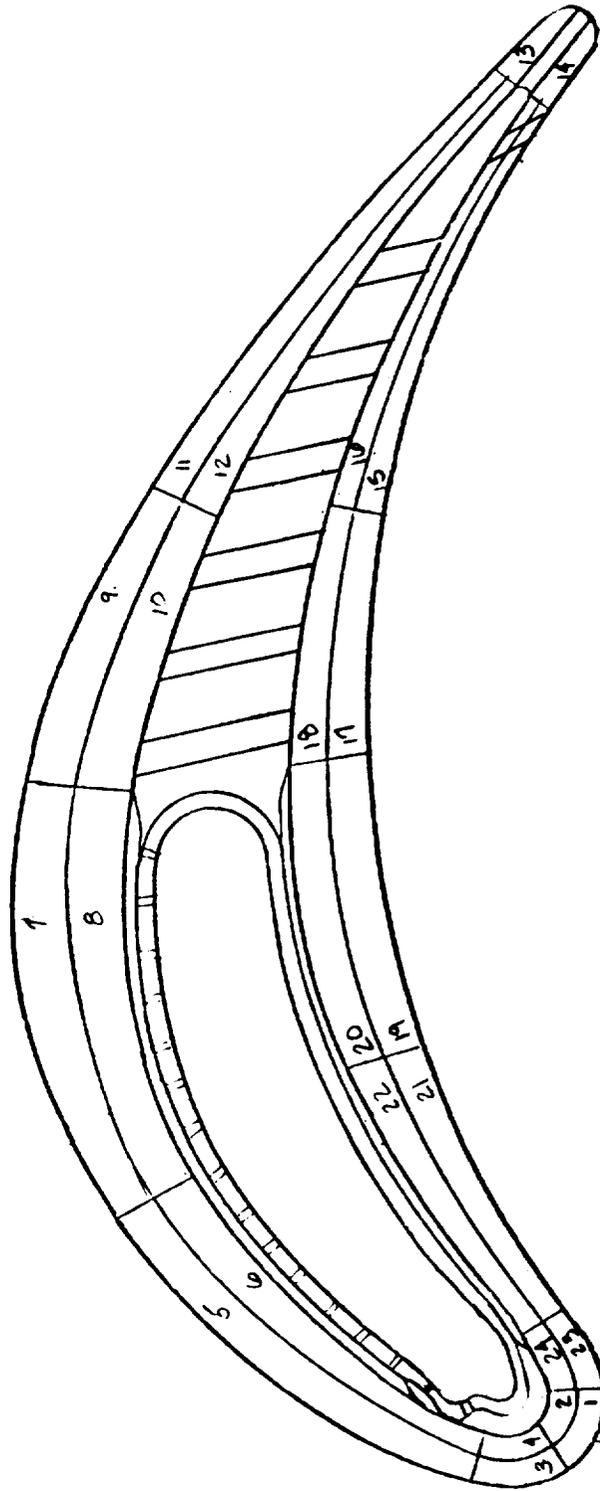
S-67937

Figure 1-52. Scheme B-4 Film-Convection Cooled Cast Impingement Tube Blade with Crossflow Impingement and Sharp Corner Flow Leading Edge Node Element Numbers
Hub Section (16.7 percent span)
1.5 in. (0.0381 m) chord
5 x size

TABLE I-52

SCHEME B-4 FILM-CONVECTION COOLED CAST IMPINGEMENT TUBE BLADE WITH CROSSFLOW IMPINGEMENT AND SHARP CORNER FLOW LEADING EDGE, 1.5 IN. (0.0381 M) CHORD, HUB SECTION, 22774 RPM, TIT = 2300°F (1533.3°K), WCA = 0.03192 LB/SEC/BLADE (4.06 PERCENT OF HOT GAS FLOW), TCA = (755.6°K)

ELEMENT NO.	TEMPERATURE	STRESS	LIFE(HRS)
1	1623.0	1408.8	10 YRS PLUS
2	1519.0	29743.8	25402.8620
3	1547.0	22043.0	64803.9340
4	1443.0	49261.3	4210.5476
5	1530.0	20958.1	10 YRS PLUS
6	1438.0	45481.7	9447.4347
7	1496.0	22459.8	10 YRS PLUS
8	1378.0	54318.4	11503.8240
9	1563.0	2463.0	10 YRS PLUS
10	1484.0	24486.0	10 YRS PLUS
11	1535.0	11069.5	10 YRS PLUS
12	1498.0	21249.4	10 YRS PLUS
13	1472.0	29691.5	10 YRS PLUS
14*	1331.0	67821.6	3608.6372
15	1410.0	46238.7	18863.0470
16	1388.0	51698.3	13604.3079
17	1483.0	28439.2	10 YRS PLUS
18	1428.0	42288.2	22262.2100
19	1603.0	-1255.7	10 YRS PLUS
20	1541.0	14837.6	10 YRS PLUS
21	1569.0	12268.4	10 YRS PLUS
22	1520.0	25033.5	71750.4180
23	1581.0	12782.5	10 YRS PLUS
24	1500.0	34108.6	16135.7325

Leading Edge and Pressure Side W_{CLE} = 0.00416 lb/sec/blade (0.529 percent of hot gas flow)

Suction Side W_{CAS} = 0.00744 lb/sec/blade (0.947 percent of hot gas flow)
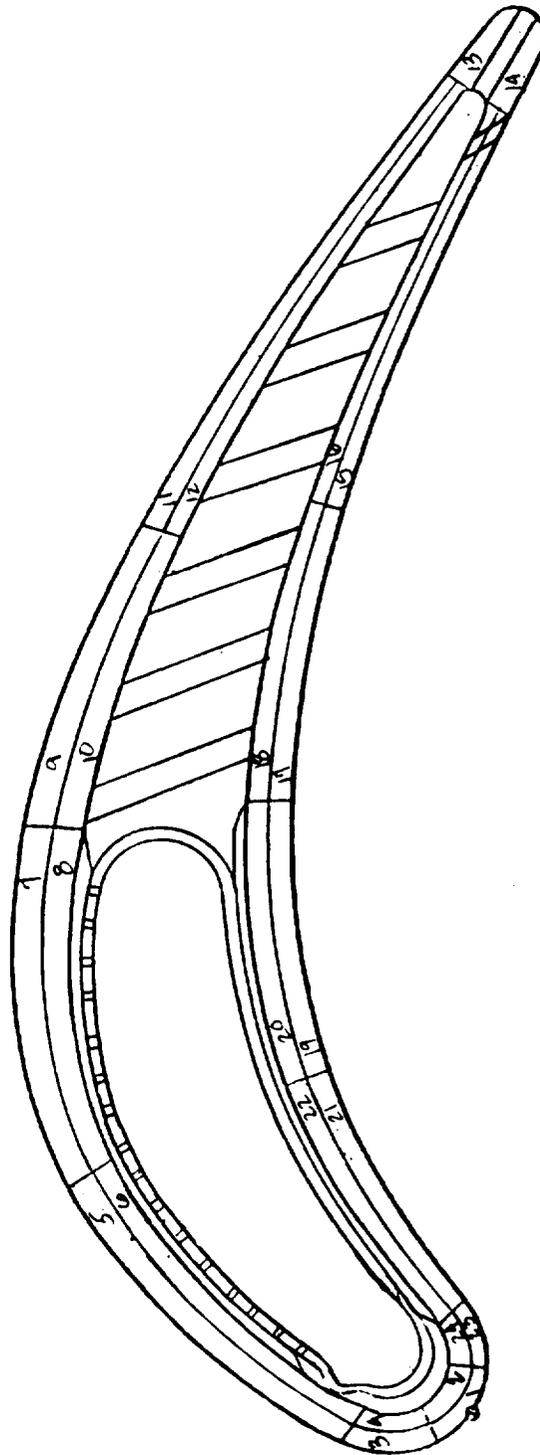
S-67938

Figure I-53. Scheme B-4 Film-Convection Cooled Cast Impingement
Tube Blade with Crossflow Impingement and Sharp
Corner Flow Leading Edge--Node Element Numbers
Mean Section (50 percent span)
1.5 in. (0.0381 m) chord
5 x size

333

TABLE I-53

SCHEME B-4 FILM-CONVECTION COOLED CAST IMPINGEMENT TUBE BLADE
WITH CROSSFLOW IMPINGEMENT AND SHARP CORNER FLOW LEADING EDGE,
1.5 IN. (0.0381 M) CHORD, MEAN SECTION

ELEMENT NO.	TEMPERATURE	STRESS	LIFE(HRS)
1	1587.0	3707.3	10 YRS PLUS
2	1501.0	26830.7	82828.5810
3	1501.0	25677.2	10 YRS PLUS
4	1425.0	45898.2	12841.8982
5	1558.0	10855.0	10 YRS PLUS
6	1497.0	27489.5	80085.2860
7	1531.0	21529.3	10 YRS PLUS
8	1462.0	40044.3	12194.0504
9	1623.0	1084.7	10 YRS PLUS
10	1576.0	14788.9	10 YRS PLUS
11	1623.0	7483.2	10 YRS PLUS
12	1599.0	14898.8	10 YRS PLUS
13	1559.0	30731.1	6701.1369
14*	1427.0	63142.5	552.2042
15	1581.0	20514.6	37265.2110
16	1557.0	27032.2	16102.6990
17	1557.0	21377.9	56598.9710
18	1521.0	30948.4	18273.6600
19	1610.0	2580.3	10 YRS PLUS
20	1573.0	12734.0	10 YRS PLUS
21	1598.0	3348.6	10 YRS PLUS
22	1564.0	12219.2	10 YRS PLUS
23	1569.0	9681.2	10 YRS PLUS
24	1425.0	47622.7	9461.7281

Leading Edge and Pressure Side W_{CLE} = 0.00416 lb/sec/blade
(0.529 percent of hot gas flow)

Suction Side W_{CAS} = 0.00648 lb/sec/blade (0.824 percent of hot gas flow)

334
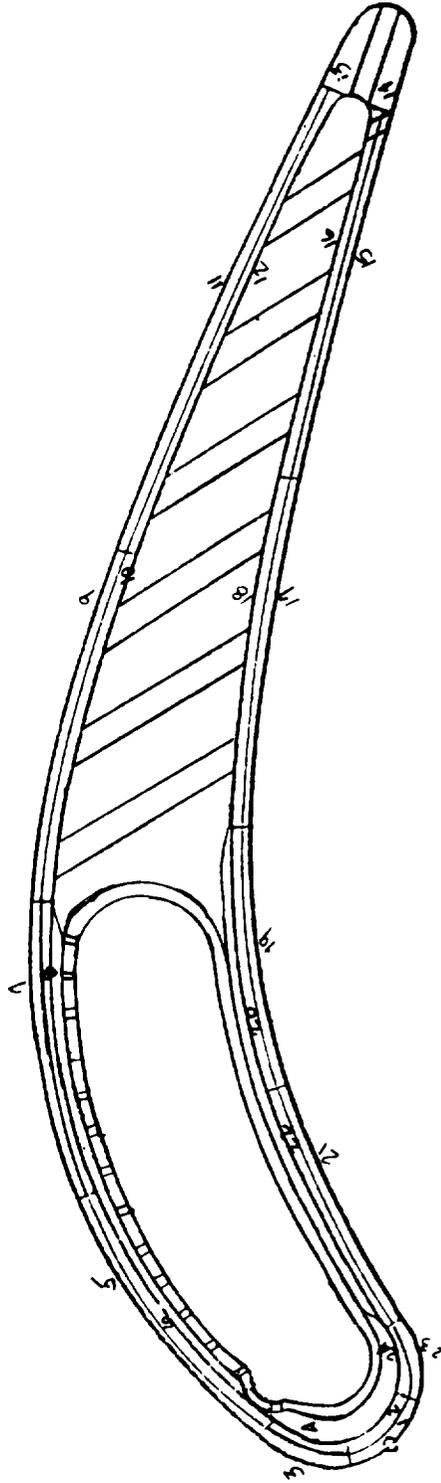
S-67939

Figure I-54. Scheme B-4 Film-Convection Cooled Cast Impingement Tube Blade with Crossflow Impingement and Sharp Corner Flow Leading Edge—Node Element Numbers

Tip Section (83.3 percent span)
1.5 in. (0.0381 m) chord
5 x size

TABLE I-54

SCHEME B-4   FILM-CONVECTION COOLED CAST IMPINGEMENT TUBE BLADE WITH CROSS-
FLOW IMPINGEMENT AND HARP CORNER FLOW LEADING EDGE, 1.5 IN.
(0.0381 M) CHORD, TIP SECTION

ELEMENT NO.	TEMPERATURE	STRESS	LIFE(HRS)
1	1445.0	4352.7	10 YRS PLUS
2	1401.0	16118.9	10 YRS PLUS
3	1435.0	10657.1	10 YRS PLUS
4	1402.0	19265.4	10 YRS PLUS
5	1549.0	-8002.7	10 YRS PLUS
6	1524.0	-931.9	10 YRS PLUS
7	1523.0	15156.7	10 YRS PLUS
8	1498.0	21952.2	10 YRS PLUS
9	1668.0	-14878.3	13023.9218
10	1651.0	-10745.4	44534.2130
11	1671.0	-7540.7	13397.2469
12	1656.0	-3671.8	43846.6590
13	1608.0	14810.3	63629.5620
14*	1475.0	52290.3	1230.6596
15	1630.0	-1043.0	10 YRS PLUS
16	1615.0	4316.9	10 YRS PLUS
17	1605.0	-2903.0	10 YRS PLUS
18	1590.0	1985.3	10 YRS PLUS
19	1577.0	-6755.3	10 YRS PLUS
20	1565.0	-2152.1	10 YRS PLUS
21	1567.0	-17403.6	10 YRS PLUS
22	1552.0	-12854.6	10 YRS PLUS
23	1435.0	8539.0	10 YRS PLUS
24	1404.0	17123.1	10 YRS PLUS

Leading Edge and Pressure Side W_{CLE} = 0.00378 lb/sec/blade (0.481 percent
of hot gas flow)

Suction Side W_{CAS} = 0.00590 (lb/sec/blade (0.751 percent of hot gas flow)
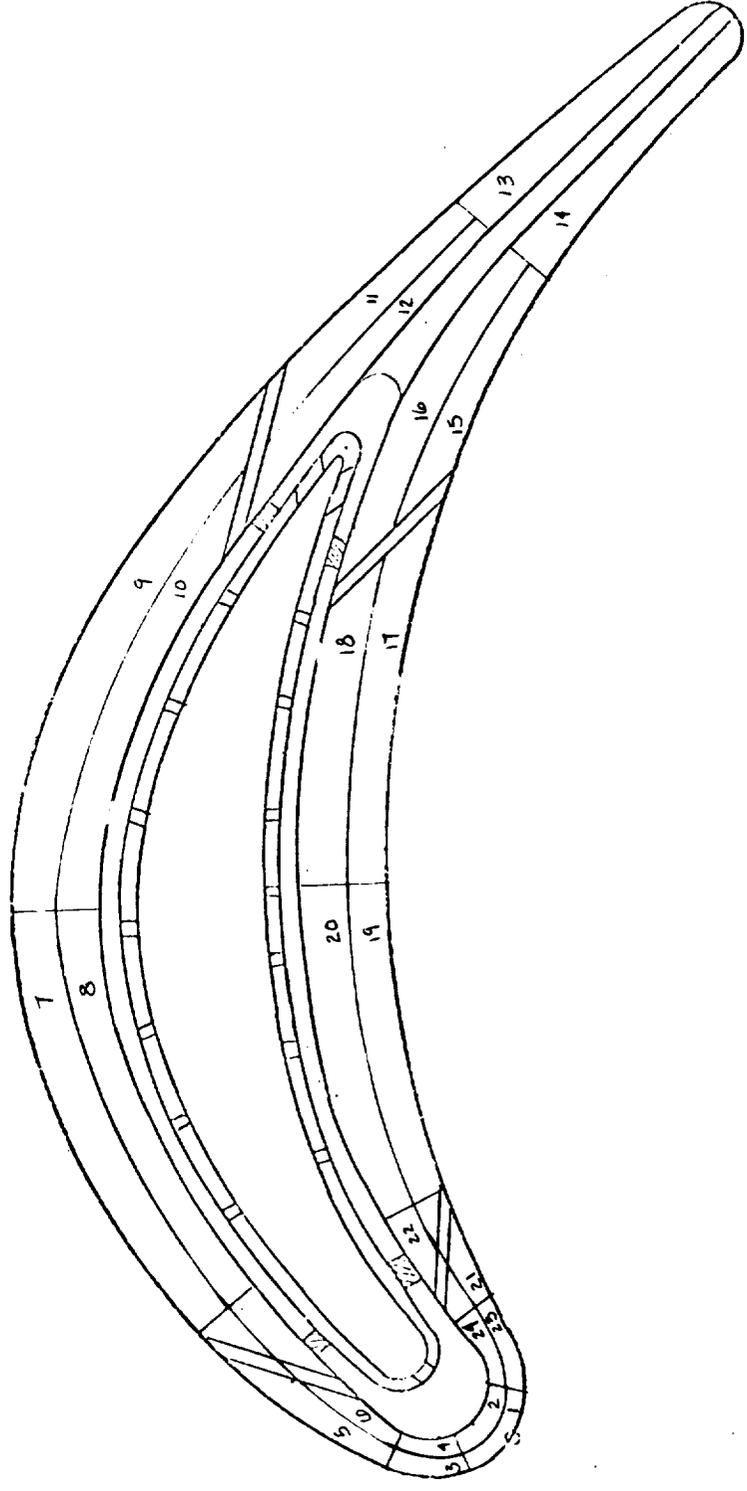
Figure 1-55. Scheme B-5 Film-Convection Cooled Fabricated
Impingement Tube Blade--Node Element Numbers
Hub Section (16.7 percent span)
0.75 in. (0.01905 m) chord
10 x size

S-67940

337

TABLE I-55

SCHEME B-5 FILM-CONVECTION COOLED FABRICATED IMPINGEMENT TUBE BLADE,
0.75 IN. (0.01905 M) CHORD, HUB SECTION, 23980 RPM, TIT = 2600°F
(1700°K), WCA = 0.0242 LB/SEC/BLADE (6.43 PERCENT OF HOT GAS FLOW),
TCA = 900°F (755.6°K)

ELEMENT NO.	TEMPERATURE	STRESS	LIFE(HRS)
1	1650.0	11274.8	10 YRS PLUS
2*	1567.0	34272.4	2465.4258
3	1647.0	8962.6	10 YRS PLUS
4	1572.0	30829.4	4616.3657
5	1655.0	-4038.2	10 YRS PLUS
6	1588.0	16979.1	10 YRS PLUS
7	1408.0	42982.3	35840.1750
8	1376.0	54610.1	11588.2666
9	1475.0	12052.8	10 YRS PLUS
10	1433.0	26000.2	10 YRS PLUS
11	1378.0	42665.2	10 YRS PLUS
12	1365.0	47313.9	61483.5550
13	1509.0	15500.1	10 YRS PLUS
14	1507.0	19867.9	10 YRS PLUS
15	1313.0	68941.9	4998.6281
16	1308.0	67863.9	7246.1715
17	1465.0	32974.1	57902.6760
18	1423.0	41862.4	27861.5740
19	1472.0	41251.9	7427.6023
20	1437.0	49432.7	4852.3475
21	1557.0	29799.7	8703.6949
22	1549.0	30789.4	8691.4188
23	1627.0	15947.9	50822.7570
24	1556.0	35537.6	2496.4076

Leading Edge W_{CLE} = 0.00254 lb/sec/blade   (0.675 percent of hot gas flow)

Pressure side W_{CAP} = 0.00191 lb/sec/blade   (0.507 percent of hot gas flow)

Suction side W_{CAS} = 0.00254 lb/sec/blade   (0.675 percent of hot gas flow)

Trailing edge W_{CTE} = 0.00127 lb/sec/blade   (0.337 percent of hot gas flow)

338
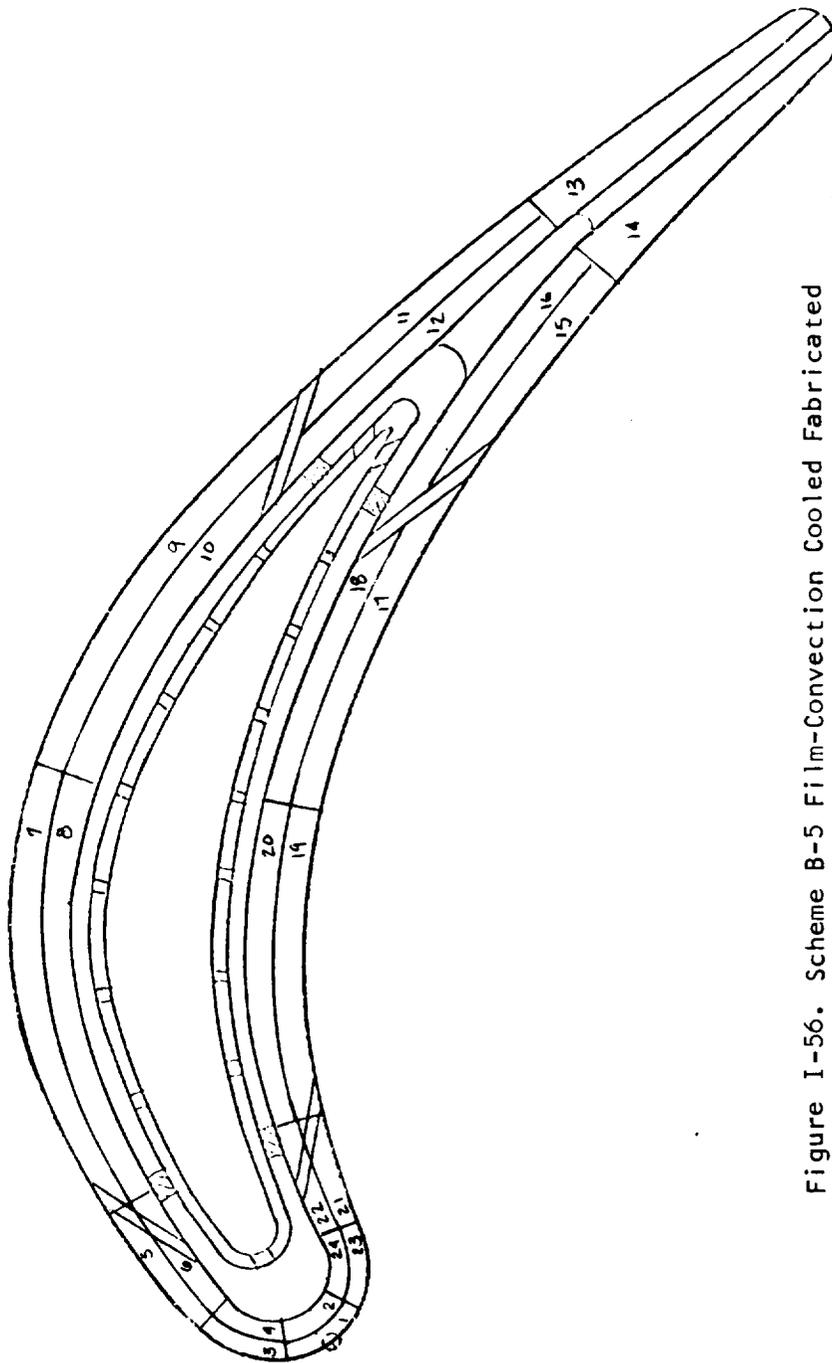
Figure I-56. Scheme B-5 Film-Convection Cooled Fabricated Impingement Tube Blade--Node Element Numbers Mean Section (50 percent span) 0.75 in. (0.01905 m) Chord 10 x Size

S-67941

339

TABLE I-56

SCHEME B-5 FILM-CONVECTION COOLED FABRICATED IMPINGEMENT TUBE BLADE,
0.75 IN. (0.01905 M) CHORD, MEAN SECTION

ELEMENT NO.	TEMPERATURE	STRESS	LIFE(HRS)
1	1684.0	-9547.2	10 YRS PLUS
2	1600.0	14839.7	10 YRS PLUS
3	1664.0	-8459.8	10 YRS PLUS
4	1603.0	10114.7	10 YRS PLUS
5	1621.0	-3971.4	10 YRS PLUS
6	1569.0	11493.3	10 YRS PLUS
7	1446.0	24431.1	10 YRS PLUS
8	1422.0	33654.5	10 YRS PLUS
9	1503.0	2845.7	10 YRS PLUS
10	1466.0	14930.0	10 YRS PLUS
11	1437.0	28133.5	10 YRS PLUS
12	1424.0	32875.8	10 YRS PLUS
13	1568.0	3183.8	10 YRS PLUS
14	1566.0	7973.1	10 YRS PLUS
15	1361.0	57875.6	10051.1734
16	1356.0	56542.2	14954.4042
17	1491.0	22696.0	10 YRS PLUS
18	1462.0	28463.5	10 YRS PLUS
19	1465.0	35727.6	30489.4880
20	1441.0	41294.1	18067.4240
21	1573.0	17764.8	10 YRS PLUS
22	1529.0	28285.7	26603.4940
23	1643.0	2450.9	10 YRS PLUS
24	1581.0	19877.1	46542.9380

Leading edge W_{CLE} = 0.00254 lb/sec/blade   (0.675 percent of hot gas flow)

Pressure side W_{CAP} = 0.00191 lb/sec/blade   (0.507 percent of hot gas flow)

Suction side W_{CAS} = 0.00254 lb/sec/blade   (0.675 percent of hot gas flow)

Trailing edge W_{CTE} = 0.00127 lb/sec/blade   (0.337 percent of hot gas flow)
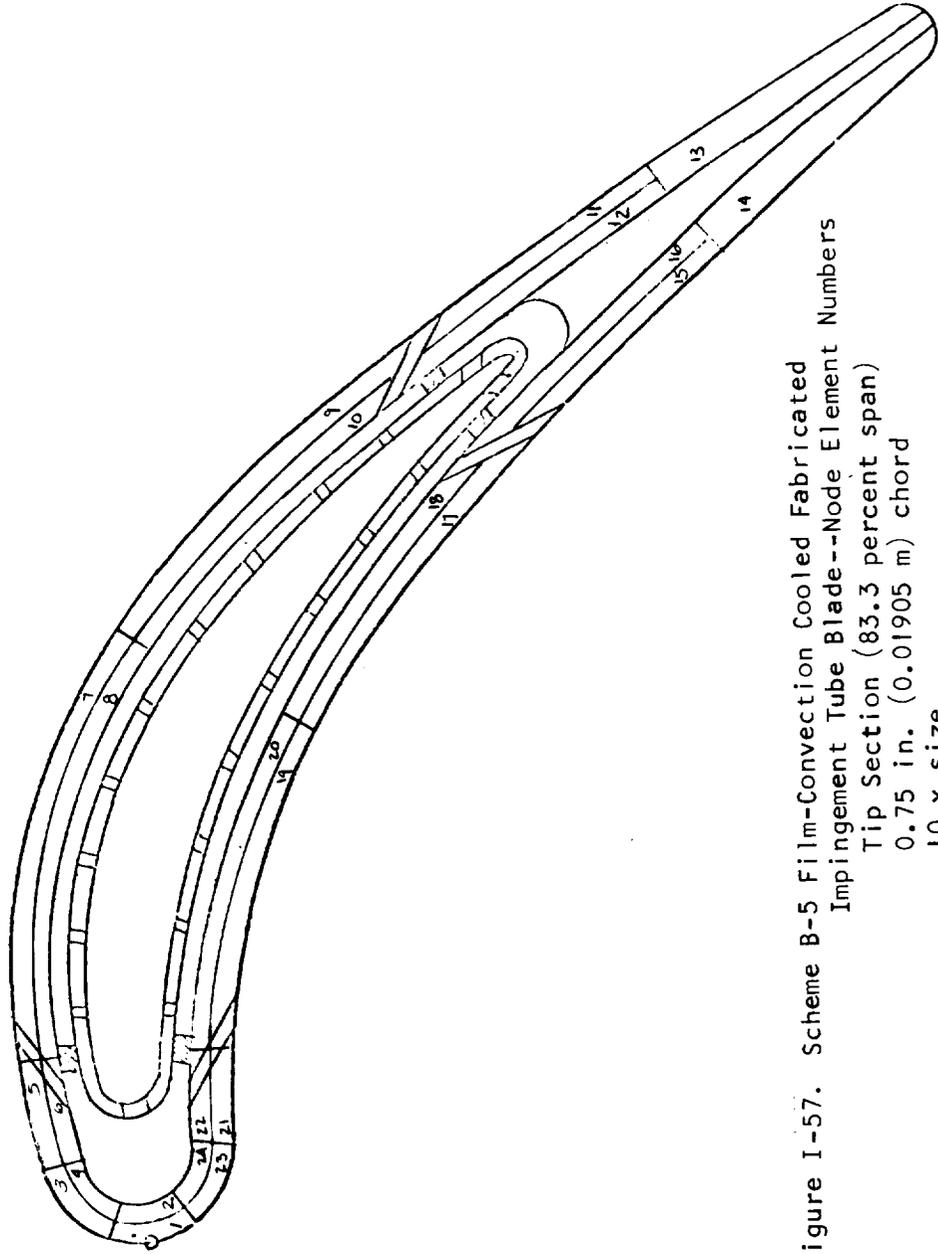
Figure I-57. Scheme B-5 Film-Convection Cooled Fabricated
Impingement Tube Blade--Node Element Numbers
Tip Section (83.3 percent span)
0.75 in. (0.01905 m) chord
10 x size

S-67942

341

TABLE I-57

SCHEME B-5 FILM-CONVECTION COOLED FABRICATED IMPINGEMENT TUBE BLADE,
0.75 IN. (0.01905 M) CHORD, TIP SECTION

ELEMENT NO.	TEMPERATURE	STRESS	LIFE(HRS)
1	1774.0	-29396.8	71.0211
2	1720.0	-24438.2	603.6319
3	1744.0	-31068.0	102.0383
4	1705.0	-24240.9	893.4638
5	1726.0	-34607.0	79.6241
6	1696.0	-30926.3	315.6566
7	1470.0	7623.2	10 YRS PLUS
8	1452.0	16106.8	10 YRS PLUS
9	1562.0	-27766.8	16933.7570
10	1538.0	-18007.8	10 YRS PLUS
11	1462.0	7660.8	10 YRS PLUS
12	1452.0	12112.5	10 YRS PLUS
13	1601.0	-20460.8	25357.2190
14	1601.0	-15298.5	69867.8090
15	1397.0	37467.7	10 YRS PLUS
16	1393.0	35306.5	10 YRS PLUS
17	1561.0	-7402.0	10 YRS PLUS
18	1541.0	-3766.3	10 YRS PLUS
19	1456.0	31112.3	10 YRS PLUS
20	1442.0	34186.5	10 YRS PLUS
21	1698.0	-23700.7	1169.1587
22	1672.0	-17999.7	6501.8561
23	1754.0	-29457.9	109.5384
24	1715.0	-23383.5	826.5874

Leading edge W_{CLE} = 0.00191 lb/sec/blade   (0.507 percent of hot gas flow)

Pressure side W_{CAP} = 0.00191 lb/sec/blade   (0.507 percent of hot gas flow)

Suction side W_{CAS} = 0.00254 lb/sec/blade   (0.675 percent of hot gas flow)

Trailing edge W_{CTE} = 0.00127 lb/sec/blade   (0.337 percent of hot gas flow)
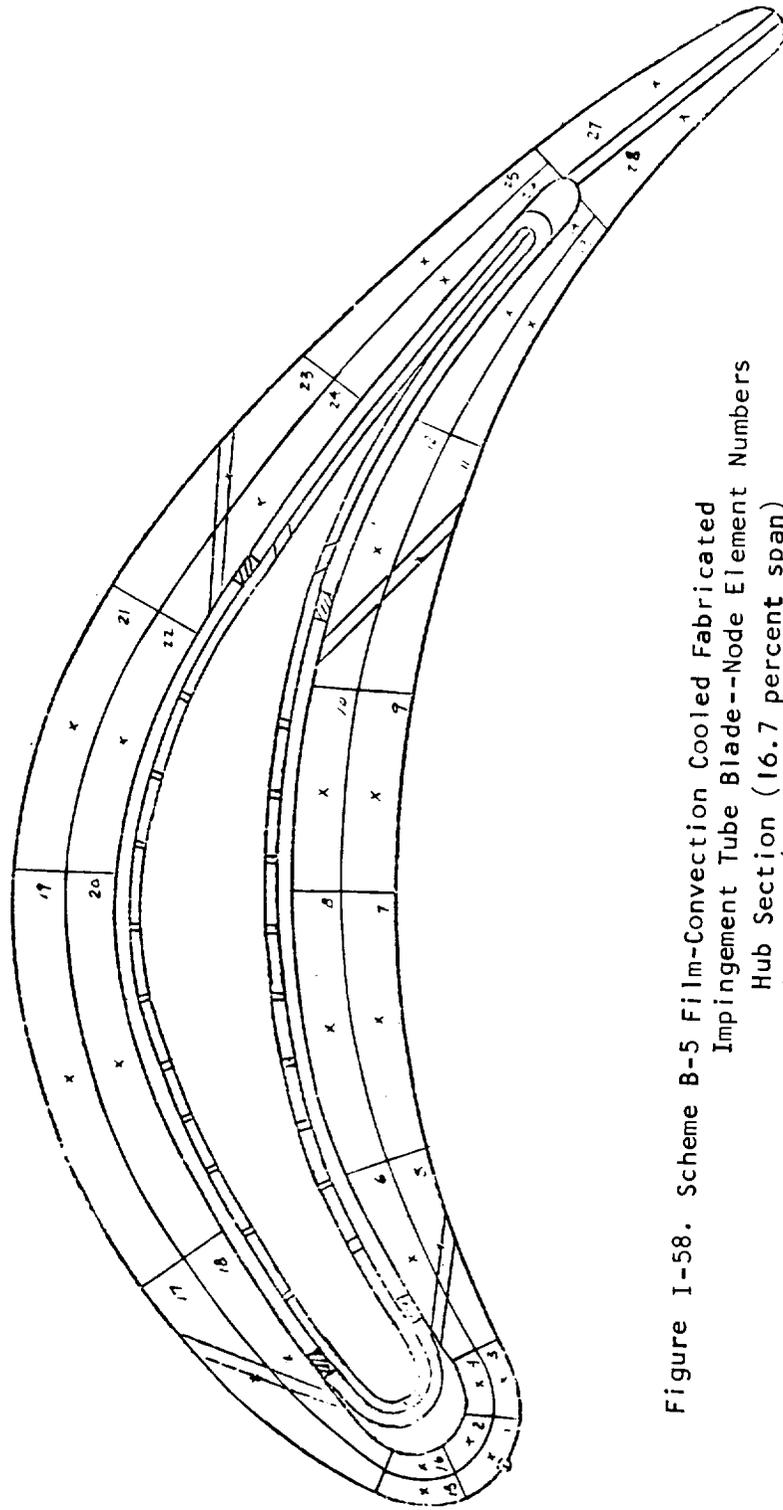
Figure I-58. Scheme B-5 Film-Convection Cooled Fabricated
Impingement Tube Blade--Node Element Numbers
Hub Section (16.7 percent span)
1.0 in. (0.0254 m) chord
10 x size

S-67943

TABLE I-58

SCHEME B-5 FILM-CONVECTION COOLED FABRICATED IMPINGEMENT TUBE BLADE
1.0 IN. (0.0254 M) CHORD, HUB SECTION, 23980 RPM, TIT = 2600°F (1700°K),
WCA = 0.0279 LB/SEC/BLADE (5.58 PERCENT OF HOT GAS FLOW) TCA = 900°F (755.6°K)

ELEMENT NO.	TEMPERATURE	STRESS	LIFE(HRS)
1	1651.0	-10176.9	10 YRS PLUS
2	1550.0	18281.0	10 YRS PLUS
3	1598.0	5910.3	10 YRS PLUS
4	1531.0	23438.1	74911.0780
5	1591.0	5743.6	10 YRS PLUS
6	1489.0	32372.1	32955.4610
7	1508.0	25540.7	10 YRS PLUS
8	1451.0	39438.6	19291.1940
9	1516.0	22360.9	10 YRS PLUS
10	1452.0	37983.1	26357.0620
11	1430.0	45076.0	12821.1868
12	1388.0	54981.5	7561.5875
13	1404.0	53565.3	6078.7316
14	1398.0	54549.6	6078.5483
15	1594.0	5555.3	10 YRS PLUS
16	1528.0	23165.4	86853.9940
17	1450.0	39340.1	20329.1310
18	1367.0	61953.4	3886.4267
19	1460.0	30981.5	10 YRS PLUS
20	1401.0	47456.5	19866.3950
21	1524.0	12684.6	10 YRS PLUS
22	1454.0	32407.0	10 YRS PLUS
23	1519.0	16654.1	10 YRS PLUS
24	1446.0	36818.5	41377.9600
25	1570.0	6838.8	10 YRS PLUS
26	1559.0	10387.3	10 YRS PLUS
27	1488.0	33544.7	25899.4050
28	1486.0	34897.3	20092.0720

Leading edge W_{CLE} = 0.00169 lb/sec/blade   (0.338 percent of hot gas flow)

Pressure side W_{CAP} = 0.00254 lb/sec/blade   (0.508 percent of hot gas flow)

Suction side W_{CAS} = 0.00338 lb/sec/blade   (0.676 percent of hot gas flow)

Trailing edge W_{CTE} = 0.00169 lb/sec/blade   (0.338 percent of hot gas flow)
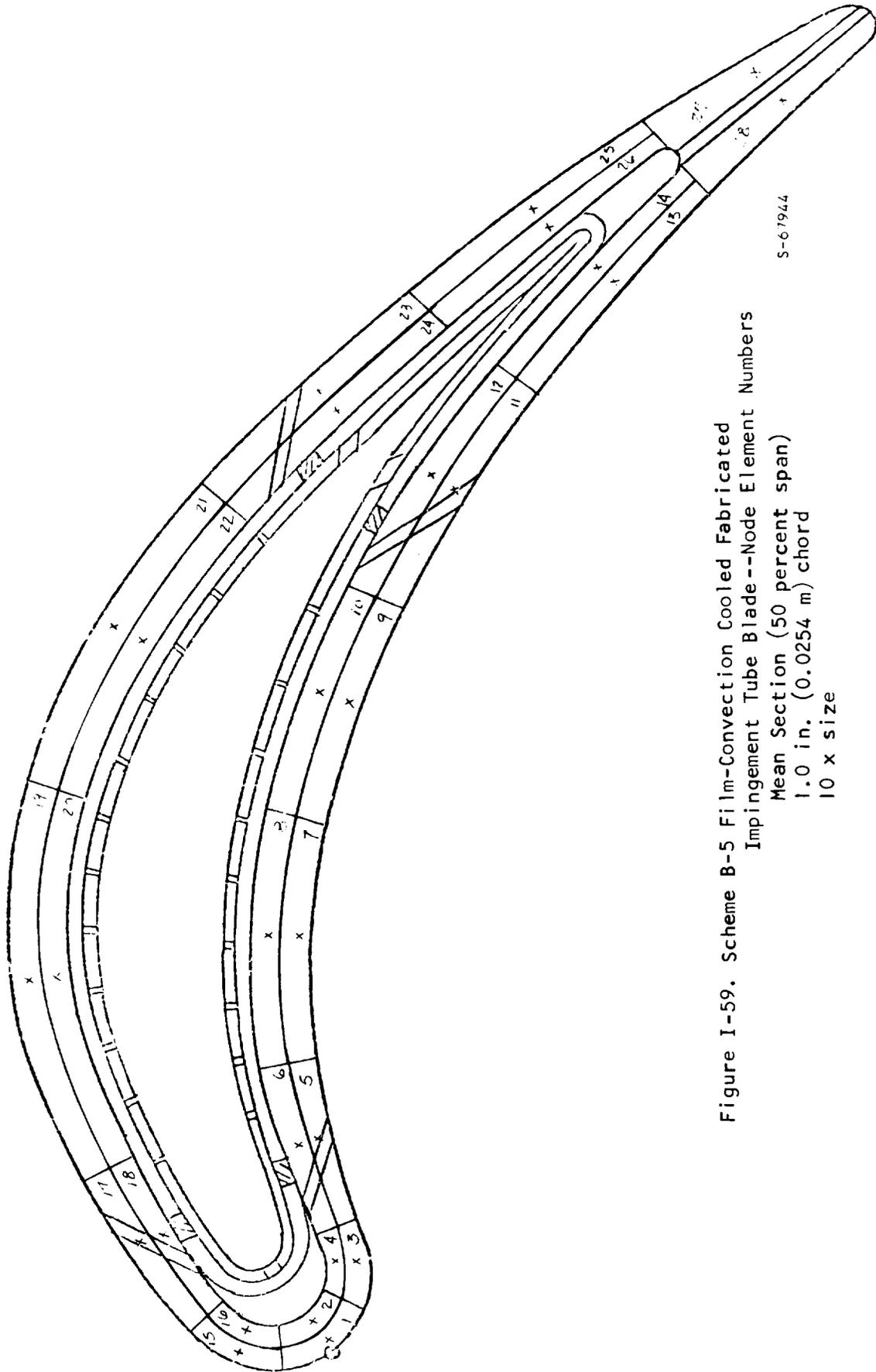
Figure I-59. Scheme B-5 Film-Convection Cooled Fabricated Impingement Tube Blade--Node Element Numbers Mean Section (50 percent span) 1.0 in. (0.0254 m) chord 10 x size

S-67944

345

TABLE I-59

SCHEME B-5 FILM-CONVECTION COOLED FABRICATED IMPINGEMENT TUBE BLADE,
1.0 IN. (0.0254 M) CHORD, MEAN SECTION

ELEMENT NO.	TEMPERATURE	STRESS	LIFE(HRS)
1	1617.0	-247.4	10 YRS PLUS
2	1545.0	19487.9	10 YRS PLUS
3	1590.0	7918.7	10 YRS PLUS
4	1537.0	21836.3	10 YRS PLUS
5	1598.0	4798.5	10 YRS PLUS
6	1530.0	22818.3	10 YRS PLUS
7	1504.0	29212.3	44052.3700
8	1468.0	38231.6	15600.6043
9	1527.0	23342.5	85898.8570
10	1488.0	33204.4	28009.7030
11	1465.0	41024.4	9435.9069
12	1418.0	52880.5	4564.4233
13	1500.0	33843.3	17145.4340
14	1493.0	35419.6	14582.7295
15	1605.0	1975.0	10 YRS PLUS
16	1551.0	16805.8	10 YRS PLUS
17	1654.0	-14764.9	36599.9180
18	1570.0	10085.7	10 YRS PLUS
19	1513.0	22463.5	10 YRS PLUS
20	1474.0	33224.3	41906.2350
21	1564.0	9351.0	10 YRS PLUS
22	1519.0	21903.0	10 YRS PLUS
23	1597.0	3238.6	10 YRS PLUS
24	1548.0	16773.5	10 YRS PLUS
25	1635.0	-5249.6	10 YRS PLUS
26	1627.0	-2490.8	10 YRS PLUS
27	1558.0	20135.0	81188.8340
28	1559.0	20389.0	72157.0010

Leading edge W_{CLE} = 0.00169 lb/sec/blade   (0.338 percent of hot gas flow)

Pressure side W_{CAP} = 0.00254 lb/sec/blade   (0.508 percent of hot gas flow)

Suction side W_{CAS} = 0.00338 lb/sec/blade   (0.676 percent of hot gas flow)

Trailing edge W_{CTE} = 0.00169 lb/sec/blade   (0.338 percent of hot gas flow)
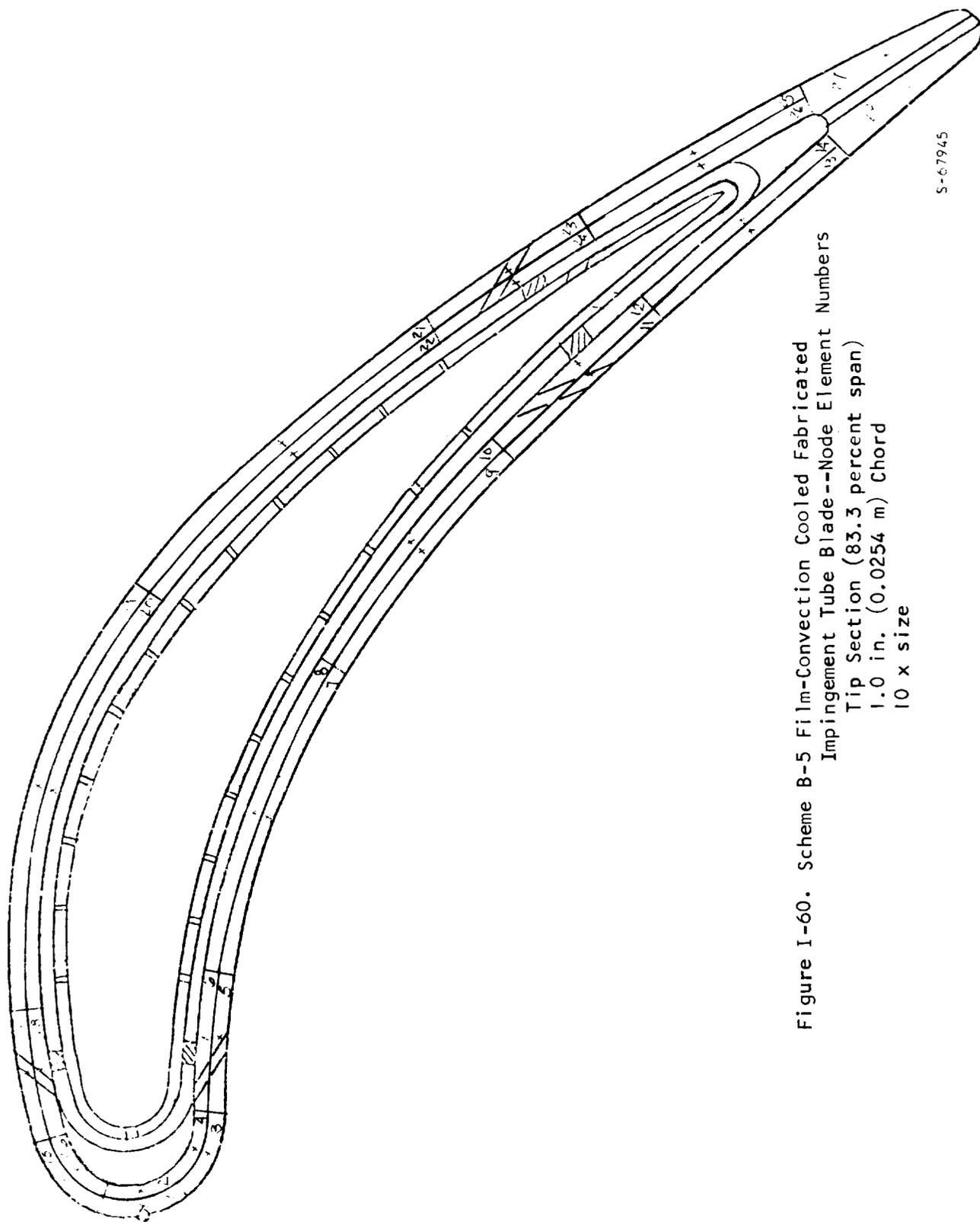
Figure I-60. Scheme B-5 Film-Convection Cooled Fabricated Impingement Tube Blade--Node Element Numbers Tip Section (83.3 percent span) 1.0 in. (0.0254 m) Chord 10 x size

S-67945

347

TABLE I-60

SCHEME B-5 FILM-CONVECTION COOLED FABRICATED IMPINGEMENT TUBE BLADE,
1.0 IN. (0.0254 M) CHORD, TIP SECTION

ELEMENT NO.	TEMPERATURE	STRESS	LIFE(HRS)
1	1564.0	-14776.0	10 YRS PLUS
2	1518.0	-2362.4	10 YRS PLUS
3	1538.0	-7726.8	10 YRS PLUS
4	1506.0	1103.5	10 YRS PLUS
5	1610.0	-24247.4	9527.8902
6	1548.0	-7976.4	10 YRS PLUS
7	1480.0	14381.2	10 YRS PLUS
8	1465.0	18862.3	10 YRS PLUS
9	1560.0	-3862.9	10 YRS PLUS
10	1541.0	1535.7	10 YRS PLUS
11	1512.0	10687.4	10 YRS PLUS
12	1474.0	21775.9	10 YRS PLUS
13	1481.0	20430.2	10 YRS PLUS
14	1477.0	21881.9	10 YRS PLUS
15	1556.0	-11231.8	10 YRS PLUS
16	1523.0	-2495.7	10 YRS PLUS
17	1628.0	-27918.6	2937.8831
18	1563.0	-10574.2	10 YRS PLUS
19	1541.0	1095.9	10 YRS PLUS
20	1520.0	6548.9	10 YRS PLUS
21	1580.0	-5228.2	10 YRS PLUS
22	1557.0	473.2	10 YRS PLUS
23	1601.0	-9956.9	50602.3470
24	1564.0	-650.9	10 YRS PLUS
25	1648.0	-23566.6	4107.0917
26	1642.0	-22125.2	6308.6542
27	1579.0	-4446.9	10 YRS PLUS
28	1571.0	-3237.8	10 YRS PLUS

Leading edge W_{CLE} = 0.00169 lb/sec/blade   (0.338 percent of hot gas flow)

Pressure side W_{CAP} = 0.00254 lb/sec/blade   (0.508 percent of hot gas flow)

Suction side W_{CAS} = 0.00338 lb/sec/blade   (0.676 percent of hot gas flow)

Trailing edge W_{CTE} = 0.00169 lb/sec/blade   (0.338 percent of hot gas flow)
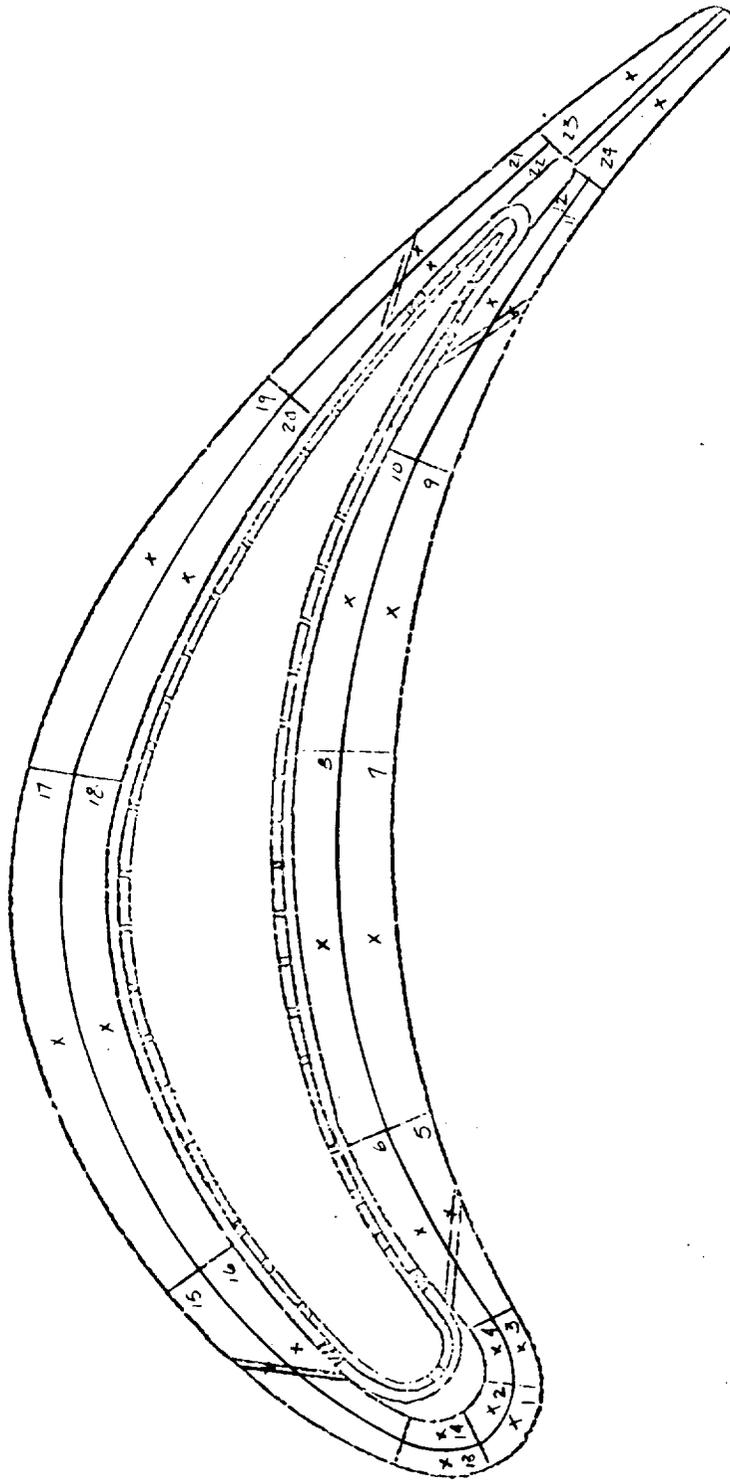
Figure I-61. Scheme B-5 Film-Convection Cooled Fabricated
Impingement Tube Blade--Node Element Numbers
Hub Section (16.7 percent span)
1.5 in. (0.0381 m) chord
5 x size

S-67946

TABLE I-6I

SCHEME B-5 FILM CONVECTION COOLED FABRICATED IMPINGEMENT TUBE BLADE,
I.5 IN. (0.038I M) CHORD, HUB SECTION, 23980 RPM, TIT = 2600°F (I700°K),
WCA = 0.040I7 LB/SEC/BLADE (5.40 PERCENT OF HOT GAS FLOW), TCA = 900°F (755.6°K)

ELEMENT NO.	TEMPERATURE	STRESS	LIFE(HRS)
1	1693.0	-16490.2	7427.6102
2	1531.0	30346.5	15806.7901
3	1601.0	10554.7	10 YRS PLUS
4	1501.0	37546.6	7145.5413
5	1582.0	13974.1	10 YRS PLUS
6	1454.0	48413.7	3570.8946
7	1540.0	21637.1	86690.1760
8	1468.0	40943.8	8780.9356
9	1553.0	13775.0	10 YRS PLUS
10	1484.0	32068.5	40869.1900
11	1471.0	31381.2	70209.2760
12	1448.0	37332.7	34552.6010
13	1628.0	3836.5	10 YRS PLUS
14	1512.0	35821.3	7786.6385
15	1589.0	14358.8	10 YRS PLUS
16*	1447.0	52034.4	2311.6780
17	1529.0	26330.5	41340.0400
18	1462.0	43885.7	6256.6980
19	1560.0	11414.8	10 YRS PLUS
20	1494.0	29287.7	57886.1190
21	1535.0	13686.1	10 YRS PLUS
22	1444.0	37949.0	33650.8010
23	1427.0	39584.8	37944.2020
24	1420.0	41739.0	31155.4370

Leading edge W_{CLE} = 0.00338 lb/sec/blade   (0.455 percent of hot gas flow)

Pressure side W_{CAP} = 0.00420 lb/sec/blade   (0.565 percent of hot gas flow)

Suction side W_{CAS} = 0.00562 lb/sec/blade   (0.756 percent of hot gas flow)

Trailing edge W_{CTE} = 0.00225 lb/sec/blade   (0.303 percent of hot gas flow)

350
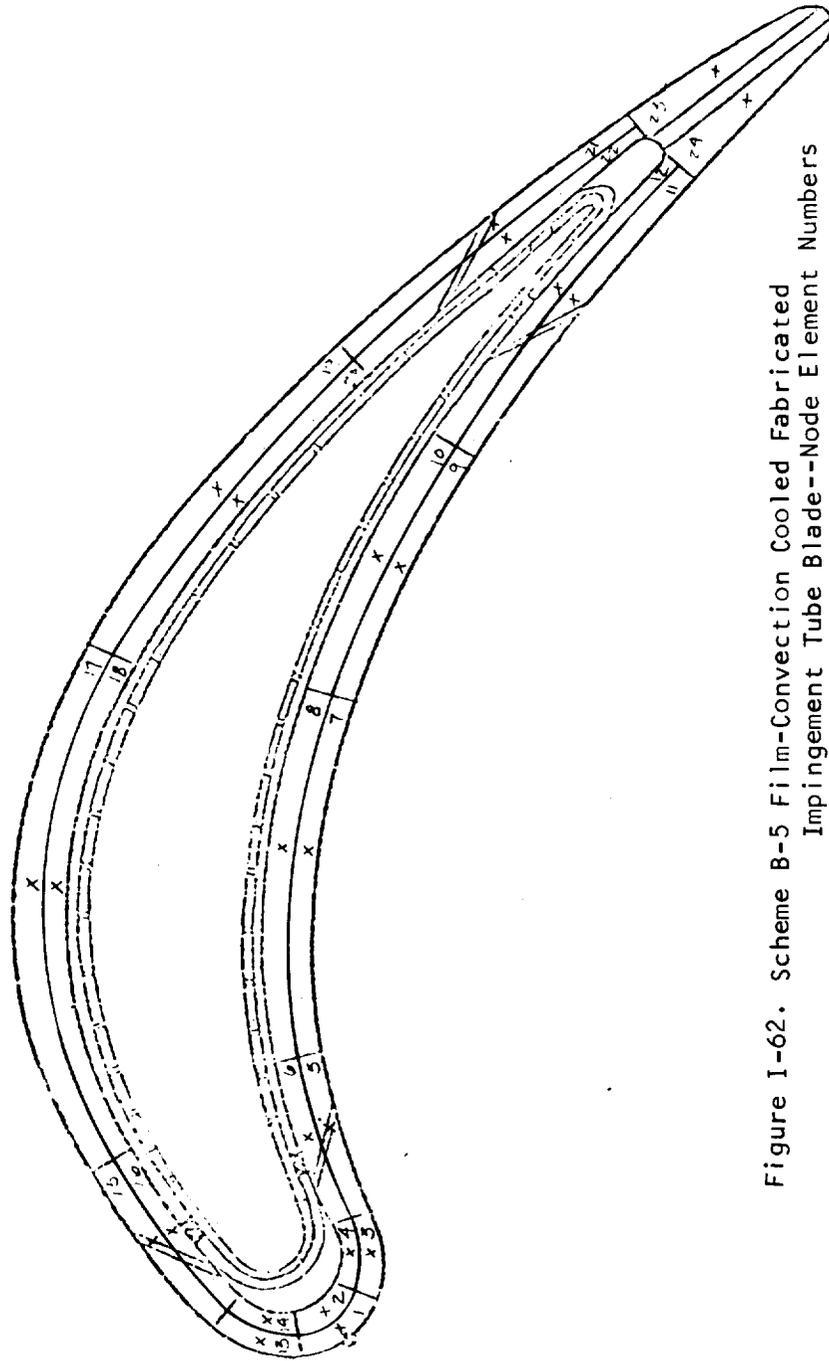
Figure I-62. Scheme B-5 Film-Convection Cooled Fabricated
Impingement Tube Blade--Node Element Numbers
Mean Section (50 percent span)
1.5 in. (0.0381 m) Chord
5 x size

5-67947

TABLE I-62

SCHEME B-5 FILM-CONVECTION COOLED FABRICATED IMPINGEMENT TUBE BLADE,
1.5 IN. (0.0381 M) CHORD, MEAN SECTION

ELEMENT NO.	TEMPERATURE	STRESS	LIFE(HRS)
1	1703.0	-11514.6	29614.2410
2	1569.0	24253.6	12385.8011
3	1635.0	7499.9	10 YRS PLUS
4	1566.0	28981.1	8166.5748
5	1663.0	2219.0	10 YRS PLUS
6	1565.0	32815.5	3590.0869
7	1601.0	24477.5	8540.5736
8	1565.0	36130.7	1723.0347
9	1650.0	4063.2	10 YRS PLUS
10	1611.0	17839.0	41181.5520
11	1559.0	19442.1	10 YRS PLUS
12	1482.0	41149.6	5695.9118
13	1657.0	7966.6	10 YRS PLUS
14	1586.0	29112.2	4632.4661
15	1705.0	1081.1	10 YRS PLUS
16	1679.0	7752.1	10 YRS PLUS
17	1675.0	20438.3	3166.0764
18	1631.0	32669.2	668.7168
19	1702.0	951.6	10 YRS PLUS
20	1661.0	12345.0	68403.0290
21	1642.0	1582.7	10 YRS PLUS
22	1548.0	27660.9	17964.7030
23	1504.0	25041.4	10 YRS PLUS
24	1500.0	23760.5	10 YRS PLUS

Leading edge W_{CLE} = 0.00225 lb/sec/blade   (0.303 percent of hot gas flow)

Pressure side W_{CAP} = 0.00336 lb/sec/blade   (0.452 percent of hot gas flow)

Suction side W_{CAS} = 0.0045 lb/sec/blade   (0.605 percent of hot gas flow)

Trailing edge W_{CTE} = 0.00225 lb/sec/blade   (0.303 percent of hot gas flow)
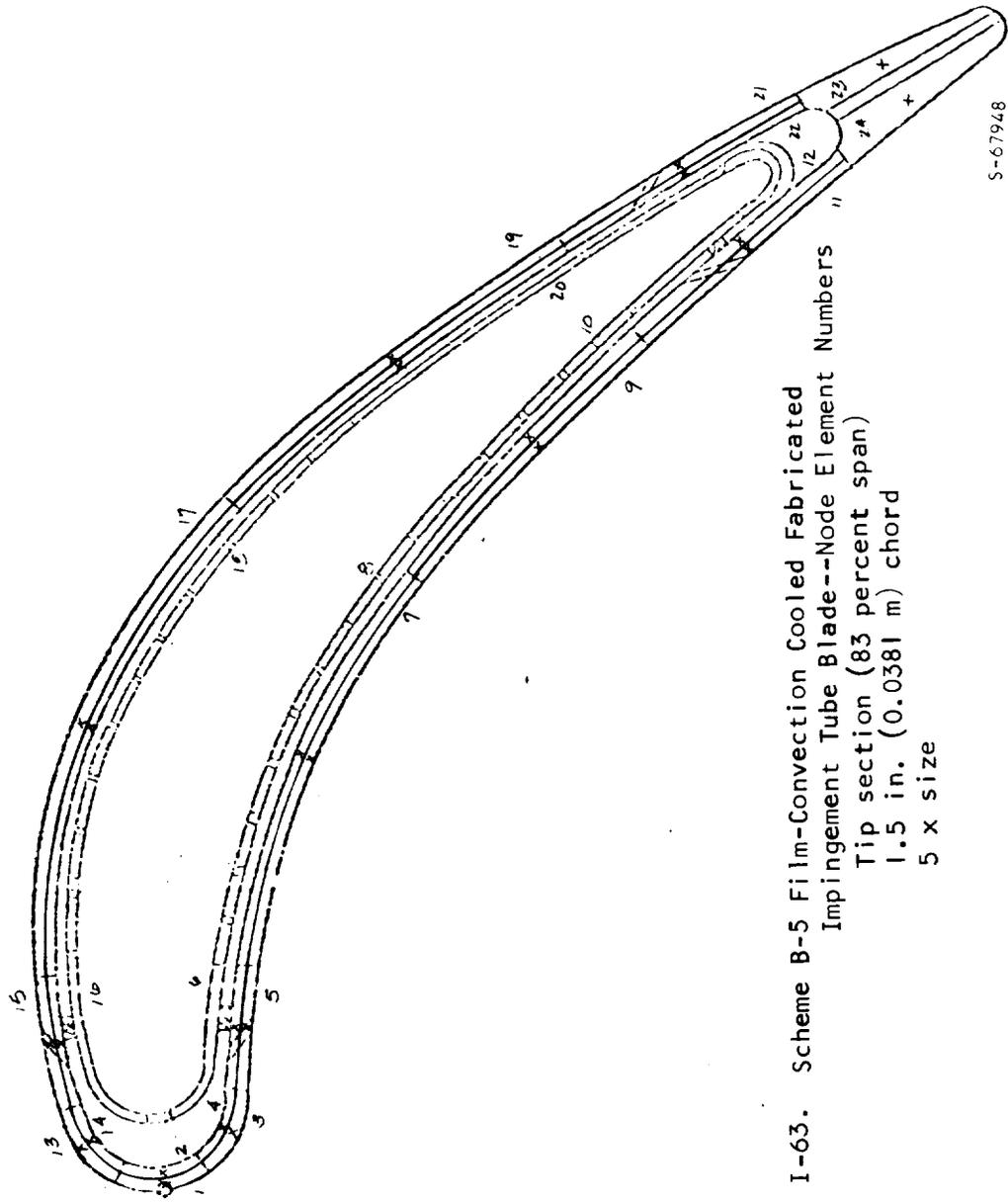
Figure I-63. Scheme B-5 Film-Convection Cooled Fabricated
Impingement Tube Blade--Node Element Numbers
Tip section (83 percent span)
1.5 in. (0.0381 m) chord
5 x size

S-67948

TABLE I-63

SCHEME B-5 FILM-CONVECTION COOLED FABRICATED IMPINGEMENT TUBE BLADE,
1.5 IN. (0.0381 M) CHORD, TIP SECTION

ELEMENT NO.	TEMPERATURE	STRESS	LIFE(HRS)
1	1505.0	20085.2	10 YRS PLUS
2	1461.0	32839.4	10 YRS PLUS
3*	1266.0	79458.4	1066.2702
4	1263.0	79785.0	1080.6148
5	1599.0	-2116.2	10 YRS PLUS
6	1530.0	16358.5	10 YRS PLUS
7	1574.0	8912.1	10 YRS PLUS
8	1561.0	12369.7	10 YRS PLUS
9	1686.0	-15755.8	7000.8181
10	1669.0	-10828.5	27429.1350
11	1583.0	20655.8	39555.7980
12	1519.0	39034.1	5529.2015
13	1507.0	18353.7	10 YRS PLUS
14	1475.0	27696.4	10 YRS PLUS
15	1686.0	-31343.0	369.4153
16	1601.0	-6280.6	10 YRS PLUS
17	1679.0	-25182.0	1400.5339
18	1663.0	-20365.7	5196.1599
19	1708.0	-23837.0	897.0344
20	1691.0	-18875.4	3434.4950
21	1686.0	-10078.1	20442.7910
22	1618.0	10231.0	10 YRS PLUS
23	1524.0	17644.3	10 YRS PLUS
24	1521.0	22856.9	10 YRS PLUS

Leading edge W_{CLE} = 0.00225 lb/sec/blade   (0.303 percent of hot gas flow)

Pressure side W_{CAP} = 0.00336 lb/sec/blade   (0.452 percent of hot gas flow)

Suction side W_{CAS} = 0.0045 lb/sec/blade   (0.605 percent of hot gas flow)

Trailing edge W_{CTE} = 0.00225 lb/sec/blade   (0.303 percent of hot gas flow)

Surface Number
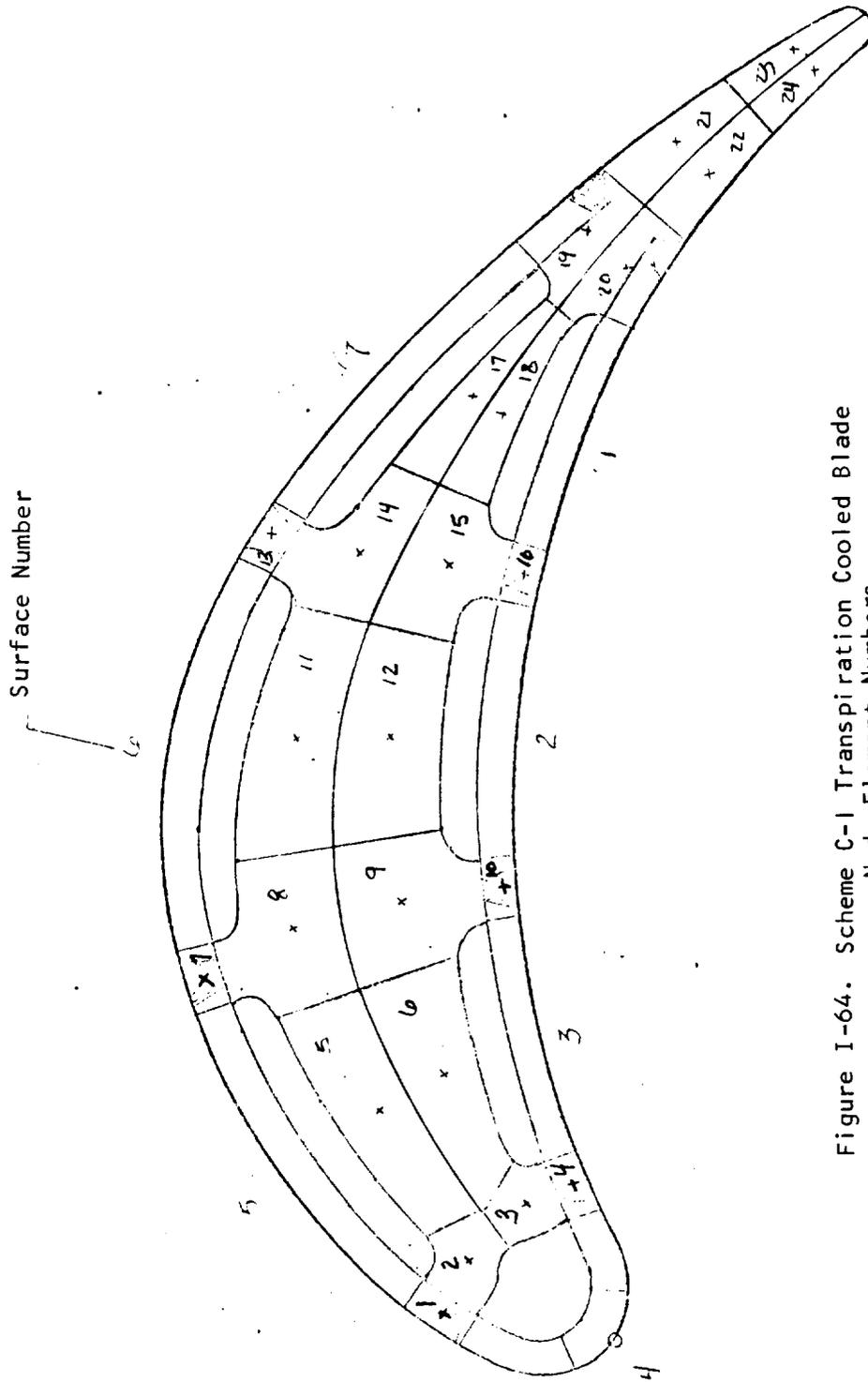
Figure I-64. Scheme C-I Transpiration Cooled Blade
Node Element Numbers
Hub Section (16.7 percent span)
0.75 in. (0.01905 m) chord
10 x size

S-67949

355

TABLE I-64

SCHEME C-1   TRANSPIRATION COOLED BLADE 0.75 IN. (0.01905 M) CHORD
HUB SECTION, 23370 RPM, TIT 2450°F (1616°K),
WCA = 0.01505 LB/SEC/BLADE (3.89 PERCENT OF HOT GAS FLOW)
TCA = 900°F (755.6°K), PTOT = 150 PSIA (1.034x10^6 NEWTONS/SQ M)

ELEMENT NO.	TEMPERATURE	STRESS	LIFE(HRS)
1	1569.0	-6142.6	1 YRS PLUS
2	1456.0	28964.9	10 YRS PLUS
3	1455.0	42133.5	10375.3810
4	1556.0	26107.5	20334.1750
5	1262.0	53190.7	10 YRS PLUS
6	1263.0	68961.1	24257.7480
7	1516.0	-55029.1	212.9772
8	1263.0	25842.3	10 YRS PLUS
9	1260.0	54327.0	10 YRS PLUS
10	1453.0	29039.7	10 YRS PLUS
11	1188.0	40345.7	10 YRS PLUS
12	1184.0	66354.7	10 YRS PLUS
13	1455.0	-37424.4	27507.7630
14	1190.0	52111.3	10 YRS PLUS
15	1187.0	76159.8	68326.4710
16	1362.0	50354.4	38690.3430
17	1076.0	88232.8	10 YRS PLUS
18	1075.0	90543.6	10 YRS PLUS
19	1399.0	47770.6	19941.7010
20*	1400.0	58139.8	3008.4644
21	1573.0	21231.9	37323.5400
22	1574.0	30438.5	4769.2864
23	1715.0	4489.9	10 YRS PLUS
24	1716.0	9331.3	57405.9170

| Surface No.	Cooling Air Flow lbs/sec/blade	Percent of Hot Gas Flow	Surface Temperature °F
1	0.00077	0.1991	1460
2	0.000385	0.0996	1402
3	0.000262	0.0678	1572
4	0.000423	0.1094	1768
5	0.000456	0.1179	1614
6	0.00039	0.1009	1660
7	0.001076	0.2783	1529
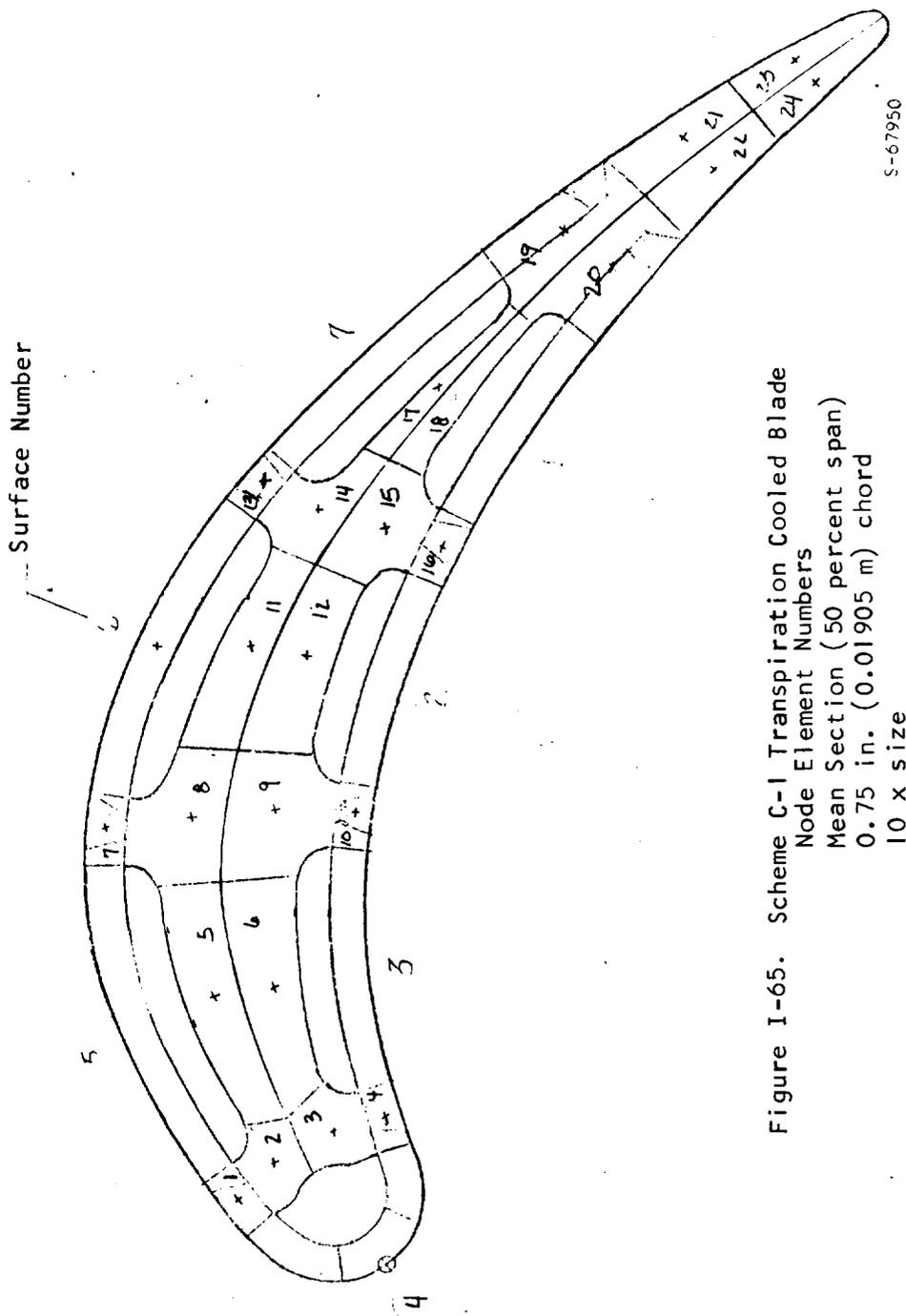
Figure I-65. Scheme C-I Transpiration Cooled Blade
Node Element Numbers
Mean Section (50 percent span)
0.75 in. (0.01905 m) chord
10 x size

357

TABLE I-65

SCHEME C-I   TRANSPIRATION COOLED BLADE, 0.75 IN. (0.01905)
             CHORD MEAN SECTION

ELEMENT NO.	TEMPERATURE	STRESS	LIFE(HRS)
1	1590.0	-5636.3	10 YRS PLUS
2	1519.0	19533.8	10 YRS PLUS
3	1504.0	36192.7	8950.4847
4	1554.0	34396.6	3395.3176
5	1382.0	30607.1	10 YRS PLUS
6	1383.0	44452.7	59123.6390
7	1587.0	-52474.5	54.3035
8	1396.0	10077.1	10 YRS PLUS
9	1407.0	27410.4	10 YRS PLUS
10	1482.0	27237.8	10 YRS PLUS
11	1335.0	29471.0	10 YRS PLUS
12	1332.0	44632.5	10 YRS PLUS
13	1548.0	-29592.2	11671.5011
14	1358.0	31959.1	10 YRS PLUS
15	1356.0	49485.2	54732.3450
16	1426.0	46545.8	11118.6714
17	1215.0	82475.3	6862.1182
18	1214.0	84080.7	5029.3469
19	1520.0	31384.7	17028.1250
20*	1520.0	45323.3	986.2756
21	1674.0	9554.4	10 YRS PLUS
22	1675.0	18308.3	6440.0199
23	1798.0	-7317.5	31192.8640
24	1799.0	-2196.4	10 YRS PLUS

Surface No.	Cooling Air Flow lbs/sec/blade	Percent of Hot Gas Flow	Surface Temperature °F
1	0.00108	0.2793	1608
2	0.000538	0.1391	1371
3	0.000367	0.0949	1582
4	0.000594	0.1536	1703
5	0.000638	0.165	1671
6	0.000546	0.1412	1684
7	0.001504	0.389	1667

Surface Number
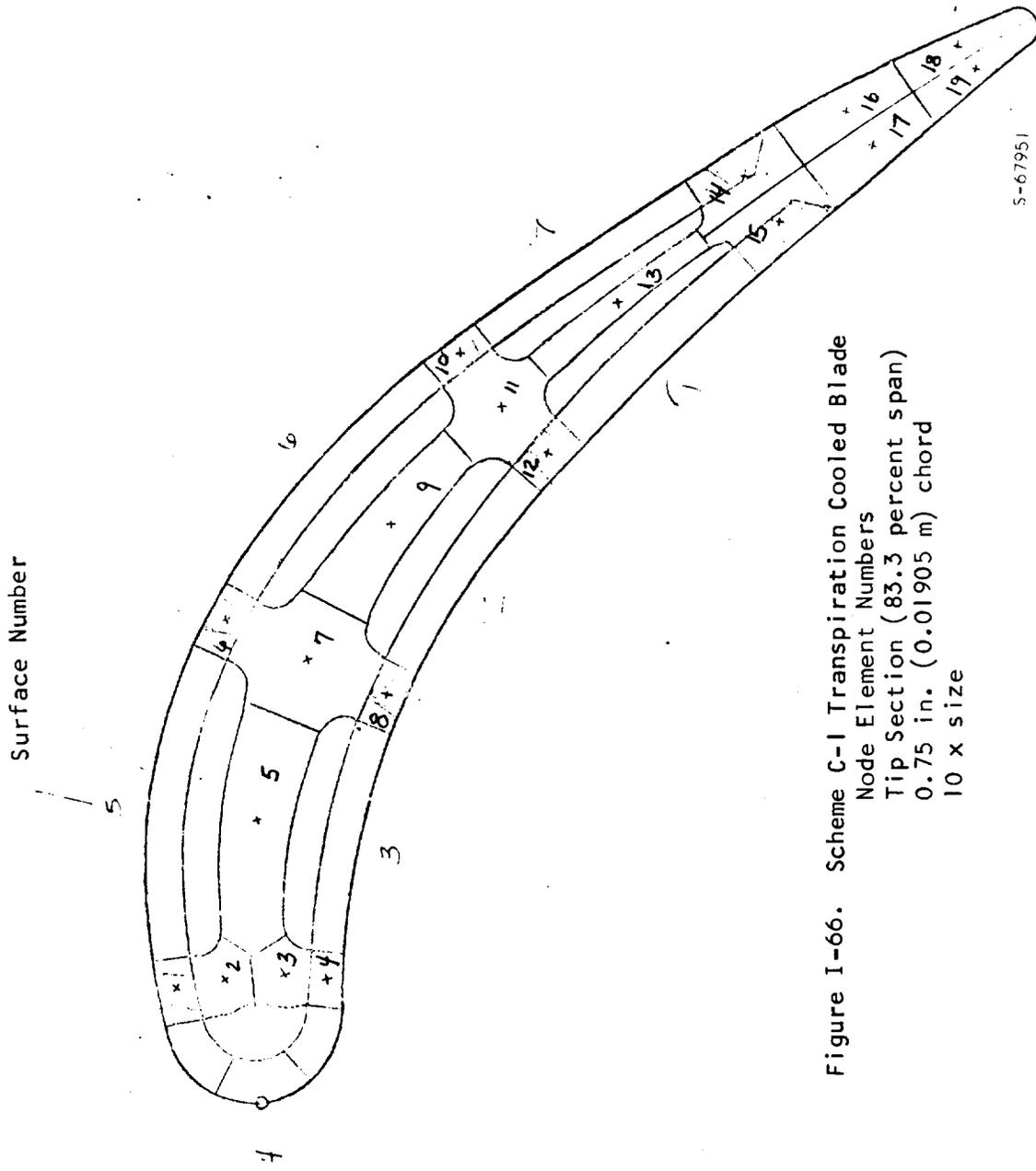


Figure I-66. Scheme C-I Transpiration Cooled Blade
Node Element Numbers
Tip Section (83.3 percent span)
0.75 in. (0.01905 m) chord
10 x size

S-67951

359

TABLE I-66

SCHEME C-I   TRANSPIRATION COOLED BLADE, 0.75 IN.
(0.01905 M) CHORD, TIP SECTION

ELEMENT NO.	TEMPERATURE	STRESS	LIFE(HRS)
1	1692.0	-19210.0	3099.5706
2	1664.0	-7146.2	10 YRS PLUS
3	1649.0	1975.9	10 YRS PLUS
4	1659.0	2460.5	10 YRS PLUS
5	1613.0	5742.3	10 YRS PLUS
6	1747.0	-32807.2	41.0552
7	1670.0	-12908.2	44504.5400
8	1695.0	-12934.3	22840.7340
9	1600.0	17444.7	63869.2200
10	1744.0	-29102.2	93.3568
11	1673.0	-6675.9	10 YRS PLUS
12	1713.0	-13408.7	12287.4701
13*	1431.0	63426.7	468.5651
14	1674.0	5034.3	10 YRS PLUS
15	1676.0	8638.2	10 YRS PLUS
16	1753.0	-12775.5	5526.9496
17	1755.0	-10527.5	10832.8815
18	1836.0	-21158.2	58.0216
19	1838.0	-20512.6	66.6211

Surface No.	Cooling Air Flow lbs/sec/blade	Percent of Hot Gas Flow	Surface Temperature °F
1	0.001235	0.3194	1841
2	0.000615	0.159	1752
3	0.00042	0.1086	1663
4	0.000681	0.1761	1735
5	0.00073	0.1888	1798
6	0.000624	0.1614	1805
7	0.00172	0.4448	1843
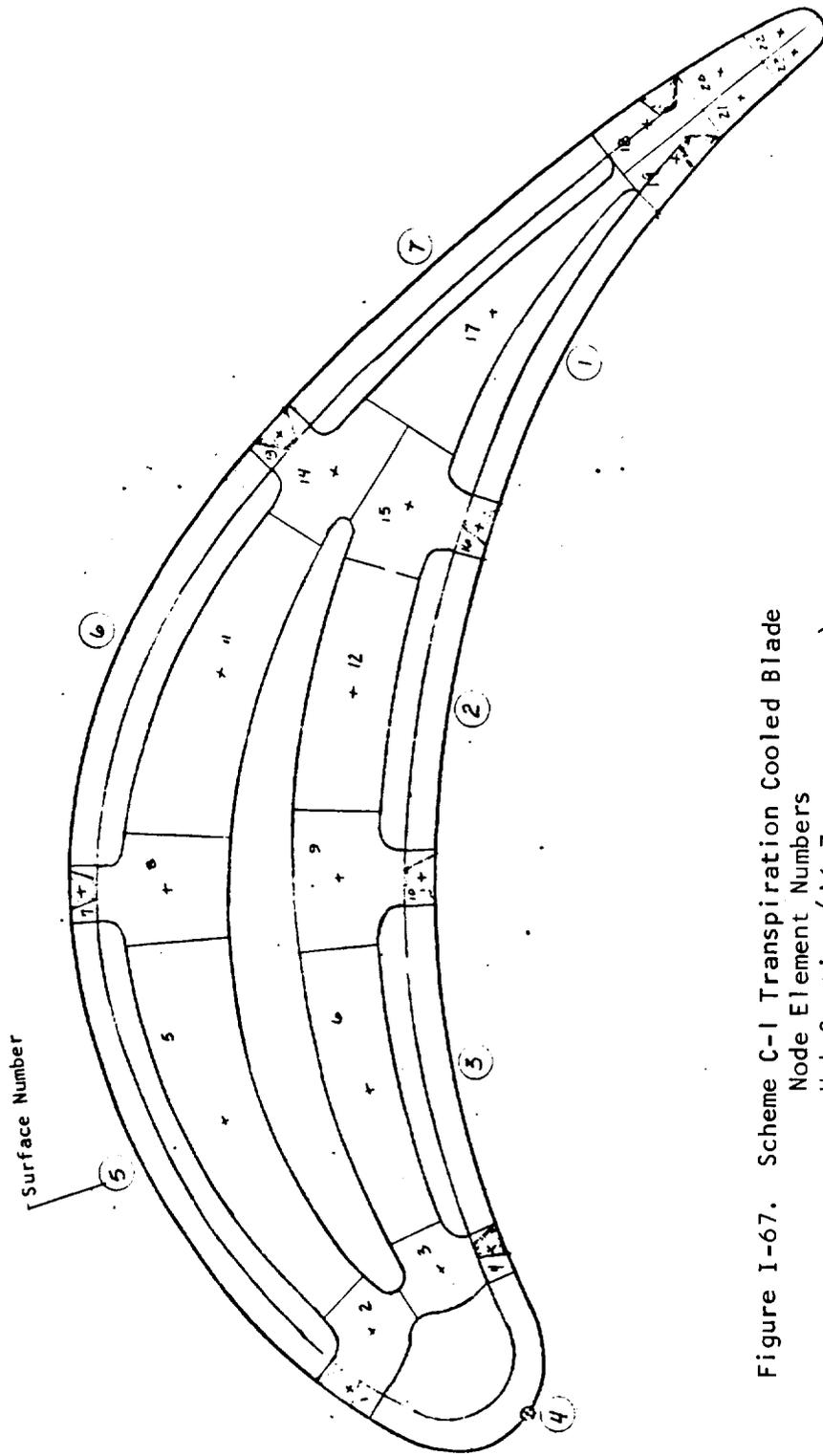
Figure I-67. Scheme C-I Transpiration Cooled Blade
Node Element Numbers
Hub Section (16.7 percent span)
1.0 (0.0254 m) chord
10 x size

Surface Number

S-67952

TABLE I-67

SCHEME C-1   TRANSPIRATION COOLED BLADE, 1.0 IN. (0.0254 M) CHORD
HUB SECTION, 23183 RPM, TIT 2500°F (1644.4°K)
WCA = 0.02235 LB/SEC/BLADE (4.31 PERCENT OF HOT GAS FLOW)
TCA = 900°F (755.6°K) PTOT = 150 PSIA (1.034x10^6 NEWTONS/SQ M)

ELEMENT NO.	TEMPERATURE	STRESS	LIFE(HRS)
1	1521.0	-17751.9	10 YRS PLUS
2	1374.0	25478.6	10 YRS PLUS
3	1420.0	29639.3	10 YRS PLUS
4	1583.0	-374.8	10 YRS PLUS
5	1080.0	50498.6	10 YRS PLUS
6	1186.0	66122.4	10 YRS PLUS
7	1376.0	-65073.3	1626.6626
8	1179.0	3625.3	10 YRS PLUS
9	1246.0	35808.7	10 YRS PLUS
10	1388.0	22328.8	10 YRS PLUS
11	1069.0	38503.3	10 YRS PLUS
12	1143.0	77824.7	10 YRS PLUS
13	1291.0	-4676.7	10 YRS PLUS
14	1160.0	44163.3	10 YRS PLUS
15	1171.0	64371.6	10 YRS PLUS
16	1295.0	51644.3	10 YRS PLUS
17	1010.0	91207.8	10 YRS PLUS
18	1586.0	12820.2	10 YRS PLUS
19	1588.0	17102.5	10 YRS PLUS
20	1722.0	-14469.4	6915.9723
21	1724.0	-9262.7	49047.3890
22	1793.0	-20883.6	161.6588
23	1796.0	-18460.2	324.4127

| Surface No.	Cooling Air Flow lb/sec/blade	Percent of Hot Gas Flow	Surface Temperature °F
1	0.000832	0.1606	1259
2	0.000417	0.0805	1500
3	0.000474	0.0915	1542
4	0.000767	0.14806	1644
5	0.000823	0.1589	1536
6	0.000714	0.1378	1503
7	0.001163	0.2245	1222

Surface Number
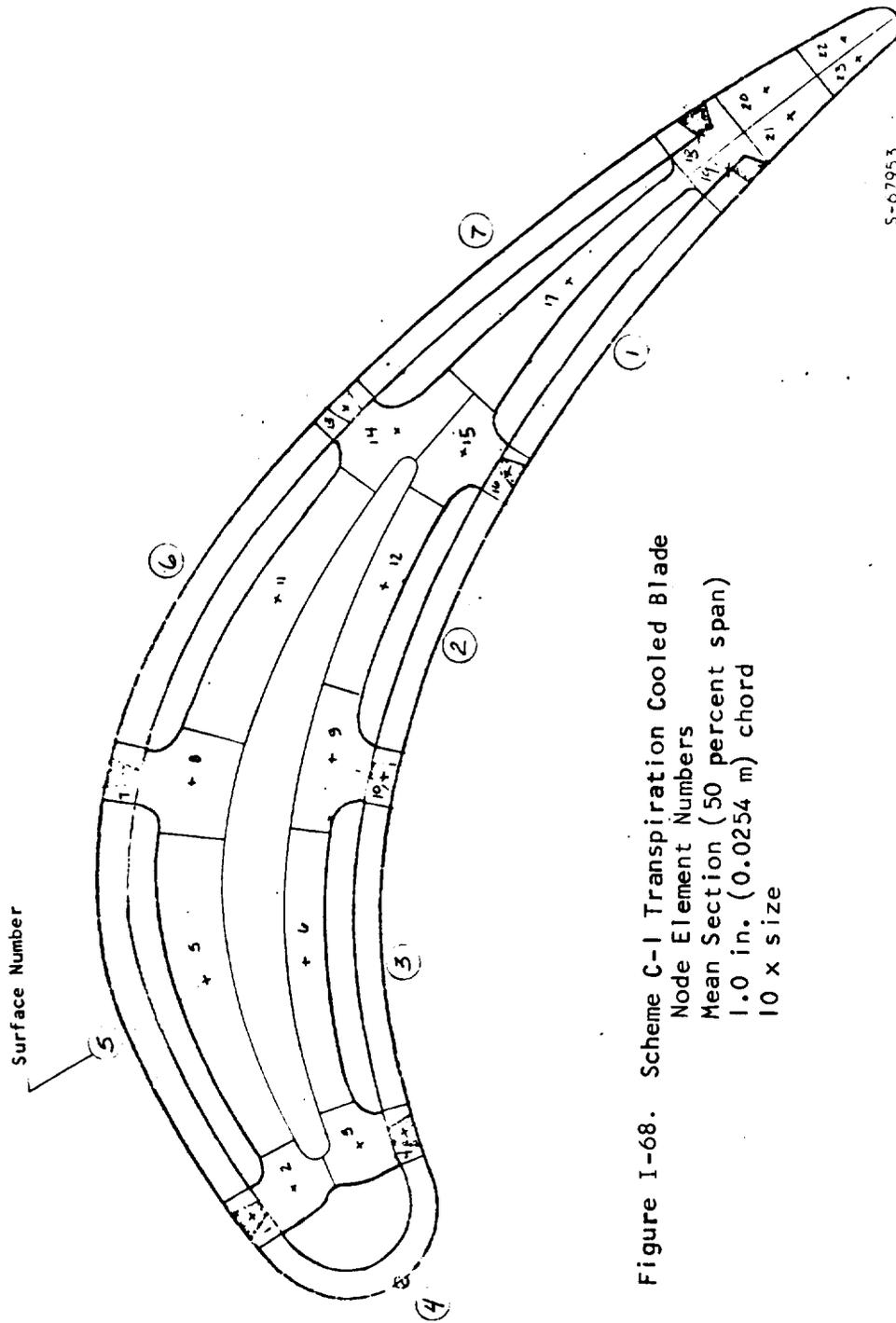
Figure I-68. Scheme C-I Transpiration Cooled Blade
Node Element Numbers
Mean Section (50 percent span)
1.0 in. (0.0254 m) chord
10 x size

S-67953

TABLE I-68

SCHEME C-1   TRANSPIRATION COOLED BLADE, 1.0 IN. (0.0381 M)
CHORD MEAN SECTION

ELEMENT NO.	TEMPERATURE	STRESS	LIFE(HRS)
1	1594.0	-47280.2	106.5234
2	1487.0	-20276.8	10 YRS PLUS
3	1463.0	-13501.7	10 YRS PLUS
4	1524.0	-29279.9	24485.5990
5	1221.0	50524.7	10 YRS PLUS
6	1301.0	28508.4	10 YRS PLUS
7	1460.0	-8575.3	10 YRS PLUS
8	1332.0	24539.0	10 YRS PLUS
9	1387.0	11044.0	10 YRS PLUS
10	1453.0	-6060.8	10 YRS PLUS
11	1197.0	62212.8	10 YRS PLUS
12	1268.0	43601.3	10 YRS PLUS
13	1367.0	20650.8	10 YRS PLUS
14	1278.0	43171.0	10 YRS PLUS
15	1292.0	39179.7	10 YRS PLUS
16	1364.0	20482.5	10 YRS PLUS
17	1108.0	80713.3	10 YRS PLUS
18	1603.0	-37487.1	478.9019
19	1606.0	-38794.7	334.2412
20	1738.0	-41747.2	8.8990
21	1741.0	-41649.1	8.4577
22	1848.0	-31350.2	6.1729
23	1850.0	-31113.9	6.2002

| Surface No.	Cooling Air Flow lb/sec/blade	Percent of Hot Gas Flow	Surface Temperature °F
1	0.001168	0.2255	1308
2	0.000584	0.1127	1544
3	0.000663	0.128	1556
4	0.001071	0.2067	1516
5	0.00115	0.222	1587
6	0.000986	0.1903	1550
7	0.00163	0.3147	1274
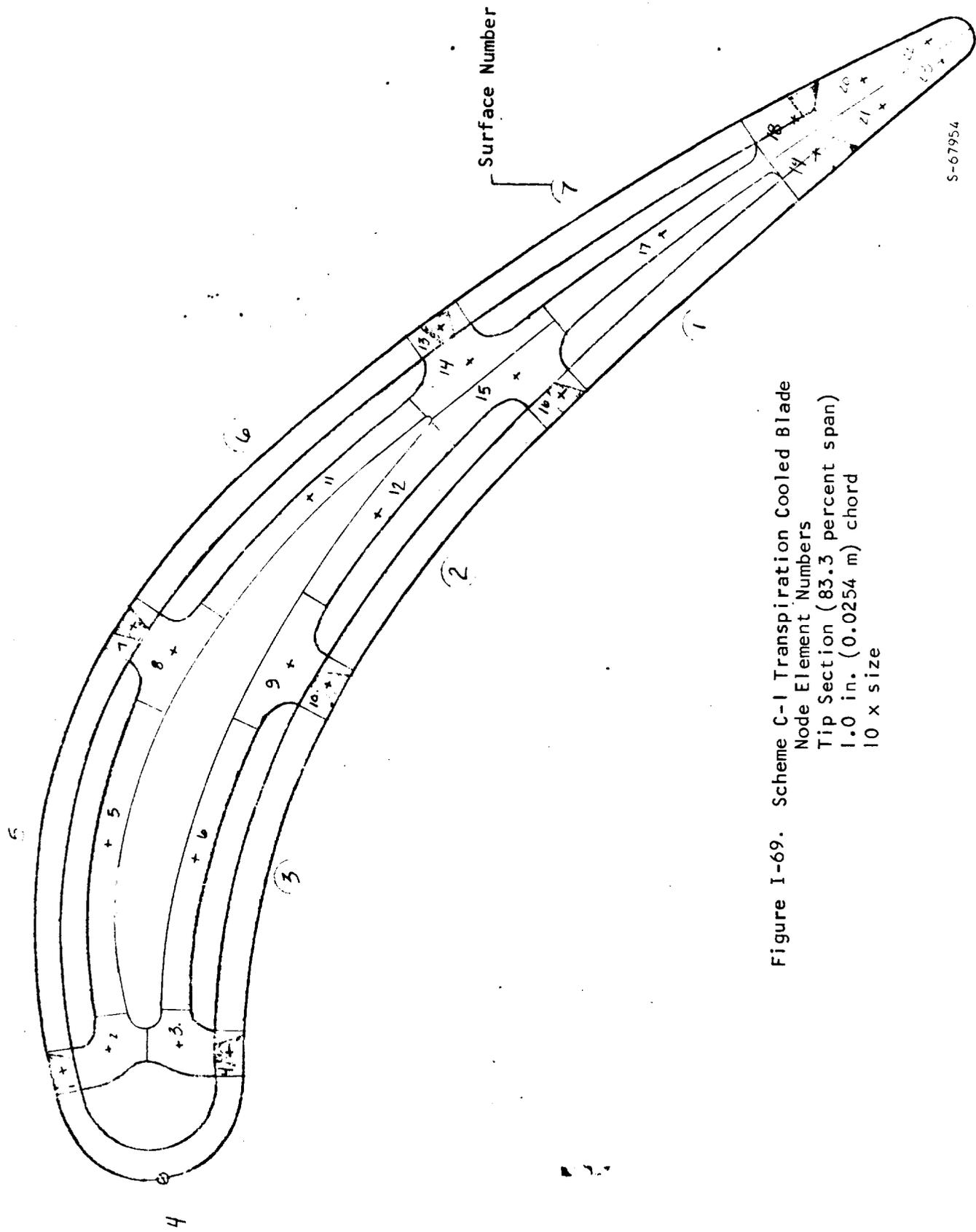
Figure I-69. Scheme C-I Transpiration Cooled Blade
Node Element Numbers
Tip Section (83.3 percent span)
1.0 in. (0.0254 m) chord
10 x size

TABLE I-69

SCHEME C-1   TRANSPIRATION COOLED BLADE, 1.0 IN. (0.0254 M)
CHORD TIP SECTION

ELEMENT NO.	TEMPERATURE	STRESS	LIFE(HRS)
1	1454.0	-13795.3	10 YRS PLUS
2	1421.0	562.3	10 YRS PLUS
3	1432.0	8737.6	10 YRS PLUS
4	1461.0	10127.2	10 YRS PLUS
5	1341.0	3818.6	10 YRS PLUS
6	1389.0	7602.7	10 YRS PLUS
7	1524.0	-53577.2	221.0066
8	1461.0	-35589.5	19777.7170
9	1523.0	-26818.8	43943.9190
10	1557.0	-27984.3	13030.8869
11	1340.0	9945.0	10 YRS PLUS
12	1420.0	2530.8	10 YRS PLUS
13	1462.0	-12783.3	10 YRS PLUS
14	1432.0	2525.1	10 YRS PLUS
15	1440.0	8998.0	10 YRS PLUS
16	1493.0	3788.4	10 YRS PLUS
17	1195.0	79949.3	22944.5290
18	1680.0	-32257.7	218.8012
19	1683.0	-27378.8	565.1092
20	1780.0	-32608.2	20.5239
21	1782.0	-31326.6	25.3843
22	1852.0	-26119.4	15.6709
23	1854.0	-25511.1	16.9033

| Surface No.	Cooling Air Flow lb/sec/blade	Percent of Hot Gas Flow	Surface Temperature °F
1	0.00145	0.2799	1343
2	0.000667	0.1288	1713
3	0.000756	0.1459	1579
4	0.001227	0.2369	1385
5	0.002070	0.3996	1508
6	0.00166	0.3204	1512
7	0.002075	0.4006	1303
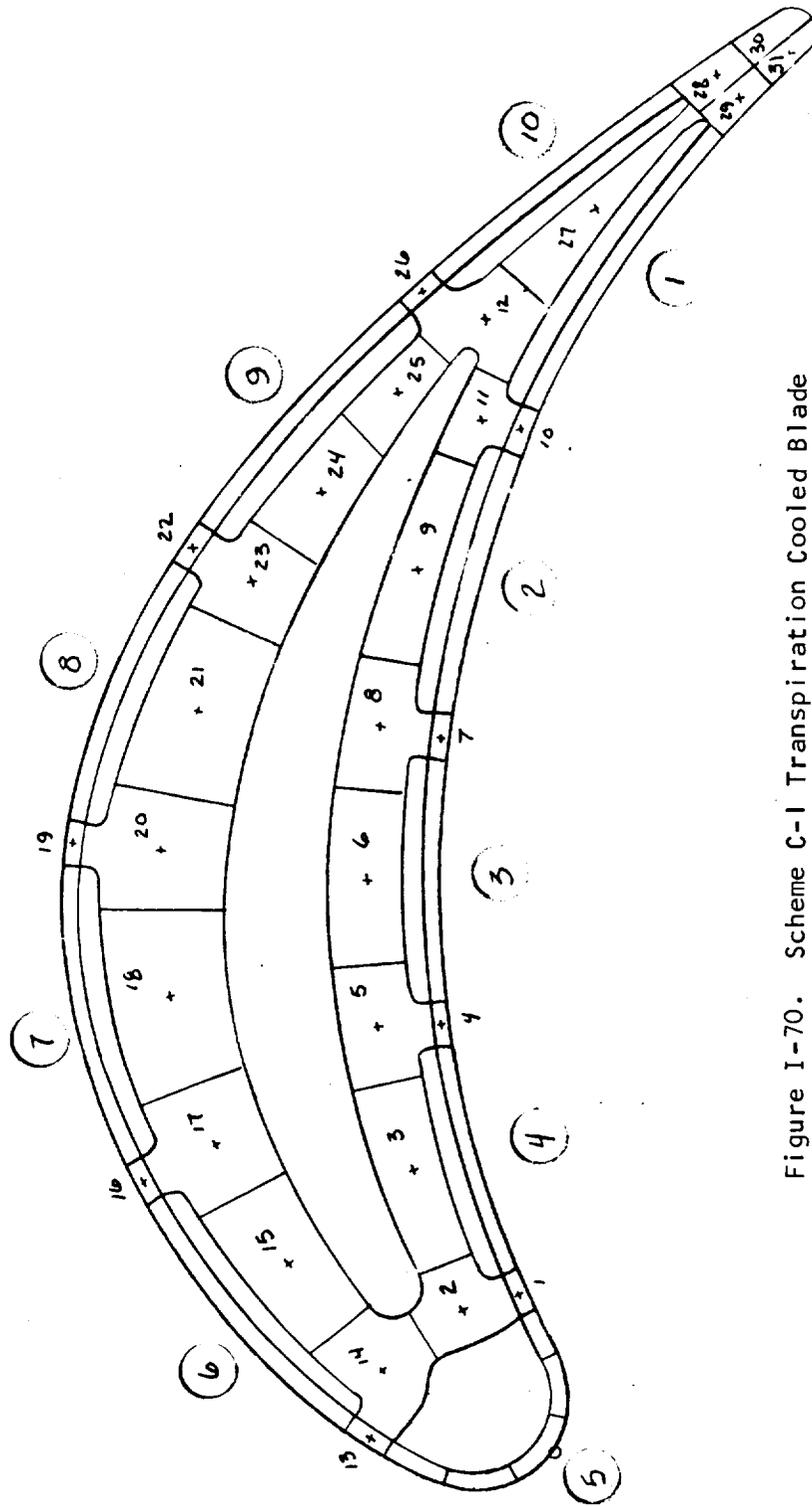
Figure I-70. Scheme C-I Transpiration Cooled Blade
Node Element Numbers
Hub Section (16.7 percent span)
1.5 in. (0.0381 m) chord
5 x size

TABLE I-70

SCHEME C-I TRANSPIRATION COOLED BLADE, 1.5 IN. (0.0381 M) CHORD
HUB SECTION, 24750 RPM, TIT 2800°F (1811.1°K)
WCA = 0.0380 LB/SEC/BLADE (5.29 PERCENT OF HOT GAS FLOW)
TCA = 900°F (755.6°K), PTOT = 150 PSIA (1.034x10^6 NEWTONS/SQ M)

ELEMENT NO.	TEMPERATURE	STRESS	LIFE(HRS)
1	1376.0	13129.0	10 YRS PLUS
2	1226.0	47434.1	10 YRS PLUS
3	1166.0	58019.4	10 YRS PLUS
4	1453.0	-13222.1	10 YRS PLUS
5	1270.0	26245.1	10 YRS PLUS
6	1192.0	46689.0	10 YRS PLUS
7	1414.0	-4698.0	10 YRS PLUS
8	1253.0	31095.4	10 YRS PLUS
9	1120.0	66029.3	10 YRS PLUS
10	1328.0	20615.3	10 YRS PLUS
11	1223.0	44669.3	10 YRS PLUS
12	1118.0	70346.7	10 YRS PLUS
13	1420.0	-7548.7	10 YRS PLUS
14	1203.0	47790.8	10 YRS PLUS
15	1128.0	58159.9	10 YRS PLUS
16	1438.0	-29092.3	10 YRS PLUS
17	1196.0	35861.4	10 YRS PLUS
18	1142.0	44398.5	10 YRS PLUS
19	1457.0	-40453.6	13122.3446
20	1195.0	30270.3	10 YRS PLUS
21	1142.0	44901.0	10 YRS PLUS
22	1414.0	-22747.6	10 YRS PLUS
23	1199.0	34698.1	10 YRS PLUS
24	1111.0	60459.1	10 YRS PLUS
25	1073.0	74874.4	10 YRS PLUS
26	1335.0	11255.1	10 YRS PLUS
27	993.0	88472.5	10 YRS PLUS
28	1525.0	-17752.6	10 YRS PLUS
29	1528.0	-17004.8	10 YRS PLUS
30	1676.0	-43378.4	27.9697
31	1679.0	-42967.8	27.8257

| Surface No.	Cooling Air Flow lb/sec/blade	Percent of Hot Gas Flow	Surface Temperature °F
1	0.001668	0.2370	1194
2	0.000693	0.0964	1572
3	0.00052	0.0723	1600
4	0.00052	0.0723	1634
5	0.001701	0.2366	1768
6	0.00104	0.1446	1542
7	0.000867	0.1206	1580
8	0.00078	0.1085	1577
9	0.00078	0.1085	1567
10	0.00222	0.3088	1084

Figure I-7I. Scheme C-I Transpiration Cooled Blade
Node Element Numbers
Mean Section (50 percent span)
1.5 in. (0.0381 m) chord
5 x size

S-67956

TABLE I-71

SCHEME C-1 TRANSPIRATION COOLED BLADE, 1.5 IN. (0.0381 M) CHORD MEAN SECTION

ELEMENT NO.	TEMPERATURE	STRESS	LIFE(HRS)
1	1415.0	10562.4	10 YRS PLUS
2	1335.0	28982.9	10 YRS PLUS
3	1287.0	38304.9	10 YRS PLUS
4	1498.0	-15732.0	10 YRS PLUS
5	1400.0	7903.0	10 YRS PLUS
6	1307.0	30380.3	10 YRS PLUS
7	1473.0	-9682.0	10 YRS PLUS
8	1390.0	10043.0	10 YRS PLUS
9	1236.0	50455.9	10 YRS PLUS
10	1387.0	15253.9	10 YRS PLUS
11	1305.0	34547.0	10 YRS PLUS
12	1238.0	52505.8	10 YRS PLUS
13	1462.0	-6573.7	10 YRS PLUS
14	1325.0	28919.5	10 YRS PLUS
15	1256.0	42664.2	10 YRS PLUS
16	1493.0	-23280.2	10 YRS PLUS
17	1325.0	21764.2	10 YRS PLUS
18	1280.0	31539.1	10 YRS PLUS
19	1530.0	-35051.1	5631.4795
20	1344.0	15097.5	10 YRS PLUS
21	1285.0	31306.8	10 YRS PLUS
22	1503.0	-24191.3	10 YRS PLUS
23	1376.0	10149.3	10 YRS PLUS
24	1280.0	36447.7	10 YRS PLUS
25	1265.0	42784.5	10 YRS PLUS
26	1377.0	14467.5	10 YRS PLUS
27	1101.0	81473.5	10 YRS PLUS
28	1573.0	-27875.3	8622.3478
29	1578.0	-28261.5	6918.2358
30	1697.0	-42932.0	18.5310
31	1701.0	-42662.8	17.6439

Surface No.	Cooling Air Flow lb/sec/blade	Percent of Hot Gas Flow	Surface Temperature °F
1	0.001668	0.2320	1379
2	0.000972	0.1352	1556
3	0.000729	0.1014	1600
4	0.000729	0.1014	1638
5	0.001701	0.2366	1634
6	0.001668	0.2320	1623
7	0.001215	0.1690	1660
8	0.001083	0.1506	1638
9	0.001083	0.1506	1606
10	0.00222	0.3088	1157
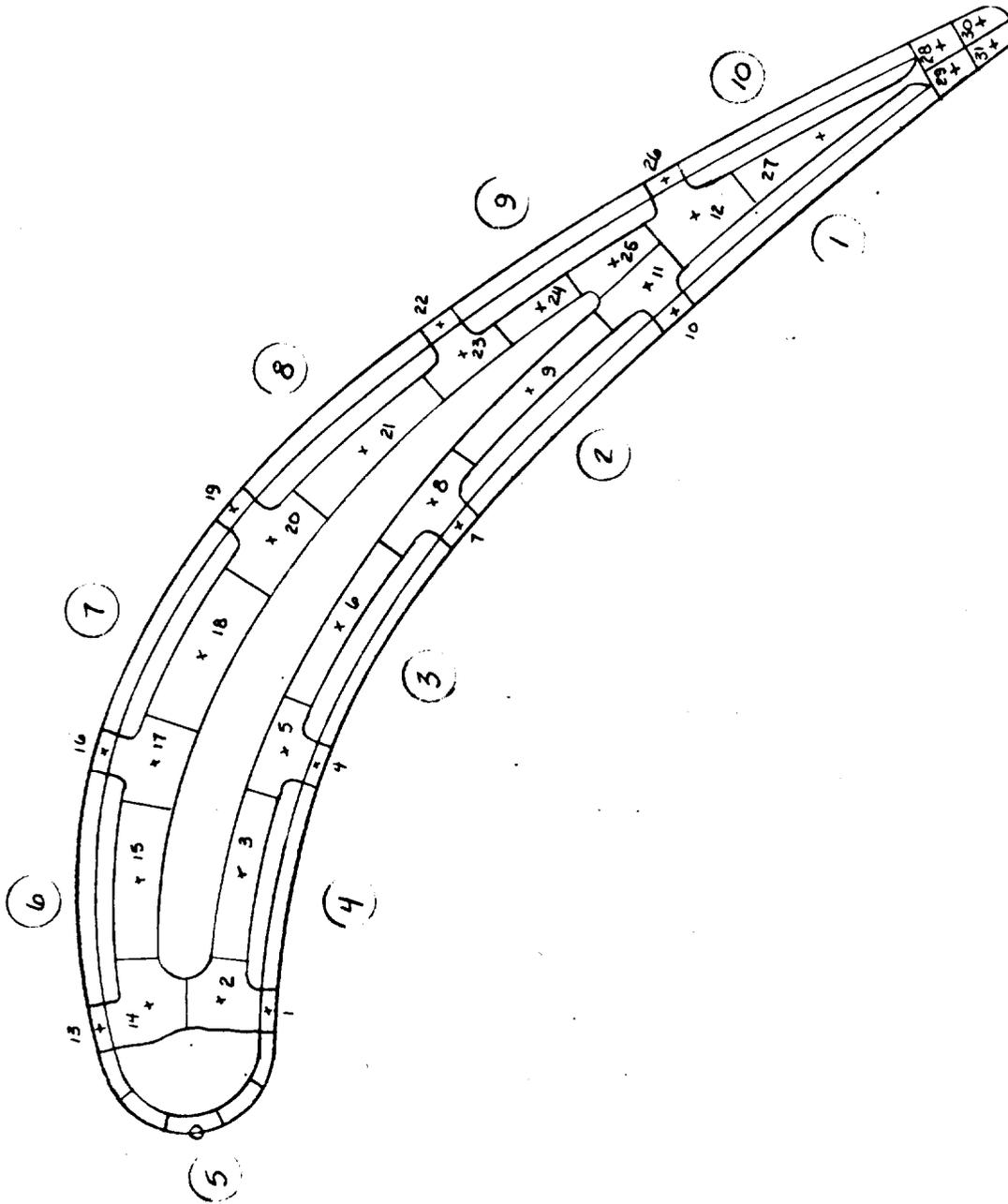
Figure I-72. Scheme C-I Transpiration Cooled Blade
Node Element Numbers
Tip Section (83.3 percent span)
1.5 in. (0.0381 m) chord
5 x size

S-67957

TABLE I-72

SCHEME C-1 TRANSPIRATION COOLED BLADE, 1.5 IN. (0.0381 M) CHORD TIP SECTION

ELEMENT NO.	TEMPERATURE	STRESS	LIFE(HRS)
1	1474.0	-17342.3	10 YRS PLUS
2	1430.0	-2571.0	10 YRS PLUS
3	1416.0	7037.6	10 YRS PLUS
4	1542.0	-24071.8	47448.7920
5	1502.0	-10829.9	10 YRS PLUS
6	1454.0	5774.4	10 YRS PLUS
7	1615.0	-38393.6	291.0816
8	1562.0	-21073.7	52588.5240
9	1426.0	15641.0	10 YRS PLUS
10	1545.0	-19402.4	10 YRS PLUS
11	1468.0	3875.9	10 YRS PLUS
12	1432.0	14583.9	10 YRS PLUS
13	1442.0	-525.8	10 YRS PLUS
14	1416.0	4864.3	10 YRS PLUS
15	1421.0	11212.4	10 YRS PLUS
16	1597.0	-25773.7	7166.6173
17	1507.0	-5392.5	10 YRS PLUS
18	1486.0	3663.1	10 YRS PLUS
19	1662.0	-37726.8	106.5749
20	1572.0	-16670.7	10 YRS PLUS
21	1496.0	3261.8	10 YRS PLUS
22	1645.0	-34709.7	305.2563
23	1575.0	-17786.9	10 YRS PLUS
24	1482.0	5040.5	10 YRS PLUS
25	1458.0	9802.6	10 YRS PLUS
26	1530.0	-7442.4	10 YRS PLUS
27	1291.0	50746.9	10 YRS PLUS
28	1652.0	-43675.7	46.7724
29	1658.0	-44541.7	35.4257
30	1758.0	-40472.0	6.9792
31	1764.0	-40298.1	6.2938

Surface No.	Cooling Air Flow lb/sec/blade	Percent of Hot Gas Flow	Surface Temperature °F
1	0.001668	0.2320	1608
2	0.001112	0.1547	1730
3	0.000834	0.1160	1691
4	0.000834	0.1160	1562
5	0.001943	0.2702	1547
6	0.00146	0.2031	1585
7	0.00139	0.1933	1742
8	0.00139	0.1933	1711
9	0.00125	0.1739	1693
10	0.00222	0.3088	1306